The Northern Sky Optical Cluster Survey: Galaxy Clusters From Five Thousand Square Degrees of DPOSS

Thesis by

Roy R. Gal

In Partial Fulfillment of the Requirements

for the Degree of

Doctor of Philosophy

California Institute of Technology

Pasadena, California

2001

(Submitted 22 January 2001)

© 2001

Roy R. Gal

All Rights Reserved

Acknowledgements

As with all theses, the people to be thanked far outnumber the interesting facts contained within. This is especially true for a large survey, which would not have been possible without the assistance of myriad individuals, contributing in manners both great and small. I will try to remember everyone, in some vaguely historical order.

First, I must thank Mike Rich, for taking me on as a high school senior, and supporting me through my undergraduate years. Neil Tyson was a great friend during that time, and made my first real observing run a pleasure. Once I arrived at Caltech, my advisor, George Djorgovski, provided me with all the resources (and perhaps even too many!) to pursue my research interests, go observing and travel to conferences that I ever needed. The free rein I have been given during my graduate years has allowed the exploration of diverse research areas, and a most extensive thesis. This work would certainly have been impossible without the guidance and support of the always-ready-to-listen Reinaldo de Carvalho. Our chats, both scientific and otherwise, helped me find my way through the early, murky stages of the thesis, and kept up my faith in astronomy as an interesting field. Stephen Odewahn proved a great companion for ranting in bad times and rejoicing in good times. His effort in the thankless task of writing DPOSS code, and constantly modifying it to meet our ever-changing whims, has made this project not only doable, but much simpler as well. The spectroscopic data presented here was all processed by Sandra Castro, who not only makes good spectra, but a fine squash partner and caipirinha drinker as well! Robert Brunner's tireless work on our servers has allowed us to process vast areas of sky in a reasonable amount of time. I can only say that the headaches he has endured have, in the end, provided a great resource to all of us in the DPOSS group. He has also provided me with insights and hints on photometric redshift estimation. In the last few months, Paulo Lopes has suffered with me, as we struggled to produce the final, calibrated catalogs from DPOSS. Ashish Mahabal has also been very helpful, producing code to perform some of the more mundane but important tasks in the survey. Vera Margoniner has been very helpful with the photo-z's as well, and did most of the work on the Butcher-Oemler analysis of the CCD data.

Many others have engaged in the data taking, for both POSS-II and this thesis. The Palomar Oschin Schmidt observers are perhaps the most important, for without them, there would be no survey to write about. Jean Mueller, Kevin Rykosi, Dave Mendenhall, Jeff Phinney (and others who were before even my time) have spent countless hours in the darkest of domes, hypering, loading, exposing, and developing the venerable plates. I have especially enjoyed Jean's enthusiasm for the survey as a whole, and helping her confirm just a few of her semi-infinite number of supernovae and comets. During my three hundred (or more) nights and days on the mountain, the day crew and night assistants have been more than a great help; they made me feel like a member of the Palomar family. Bob Thicksten, Mike Doyle, Steve, Dave, Greg, Merle, Nancy, and everyone else have helped me out of many sticky situations, from getting stuck on a fire road with my truck, to calling out an ambulance for a bad case of road rash. At night, Rick, Karl and the unforgettable Skip have helped keep me up through many long observing runs, and saved me a few ruined exposures along the way. And, perhaps most importantly, Dipali and Rose have provided more great food than one could ever wish for.

Over the years, a large group of undergraduates has helped keep DPOSS afloat, processing plates, observing at the P60, and performing many menial tasks, with an occassional bit of science tossed in. Vandana Desai, Juna Kollmeier, Anne Kelly, Rebecca Stob, Brian Stalder, Vit Hradecky, Jason Meltzer, and many others have all participated in DPOSS, and some have even continued work in astronomy afterwards!

Of course, money and resources count too. I was supported in part by an NSF Fellowship, NASA GSRP NGT5-50215, and a Kingsley Fellowship. I also thank the Norris Foundation for their generous support of the DPOSS project, as well as the Palomar TAC and Directors for generous time allocations for the DPOSS calibration effort. This work was made possible in part through the NPACI sponsored Digital Sky project and a generous equipment grant from SUN Microsystems. Access to the POSS-II image data stored on the HPSS, located at the California Institute of Technology, was provided by the Center for Advanced Computing Research.

Even with all these people helping on the scientific front, this thesis would be nothing without those who kept me nourished, both physically and emotionally, over the past seven years. Many of my astronomical comrades have been good friends and a great pleasure to be with. The other guys in my year made a great group to suffer through problem sets

and enjoy big parties at OVRO, Mammoth, and even home at Robinson. John Yamasaki provided great meat and a spark of fun and enthusiasm that made everything more bearable. The soccer team, and lately pick-up basketball, have been a fun way to relax and get in some exercise.

From the very start, my parents, Eva and Steve, while pushing me hard to achieve, let me choose my own path in life. They never once forced me to be a doctor, lawyer, or to follow in their footsteps, always allowing me to pursue my interests and supporting me wholeheartedly. Last, but certainly not least, my companion over many more years than she probably cares to remember, Pensri, has provided love, caring, and balance (nutritional as well as spiritual!) without which I could not be where I am today.

Abstract

Clusters of galaxies are the largest bound systems in the Universe and, as such, have been used to study how matter is distributed over extremely large scales. They provide fundamental constraints for theories of large-scale structure formation and evolution, and are valuable samples for studying galaxy evolution in dense environments. Despite their importance, the last large-area Northern sky cluster catalog was produced over forty years ago, via visual inspection of photographic plates of POSS-I, presented in George Abell's seminal 1958 paper and thesis. To remedy the limitations of this earlier work, we present a modern, objectively generated catalog of galaxy clusters drawn from the object catalogs of the three-band Digitized Second Palomar Observatory Sky Survey (DPOSS). In this thesis we have undertaken the following:

1) We have created a uniform, calibrated catalog of galaxies over ten thousand square degrees, covering the entire high galactic latitude northern sky.

2) From the input DPOSS galaxy catalogs, we used a simple adaptive kernel technique to create galaxy density maps, combined with a bootstrap technique to make significance maps, from which candidate galaxy clusters were selected in a model-independent fashion.

3) We performed complete follow-up imaging and multislit spectroscopy for candidates from two sky survey plates (totalling $\sim 60\square^\circ$) to assess the contamination of our catalog by spurious clusters, and to estimate the redshift distribution of the true clusters.

4) We derived a robust photometric redshift estimator for the clusters, using the plate photometry in conjunction with redshifts culled from the literature as well as our own observations.

5) We used our compilation of clusters with redshifts to measure the cluster-cluster correlation function to very large angular scales, in various photometric redshift shells.

6) We used the large library of CCD images of Abell clusters taken for DPOSS calibration to provide photometric redshifts for these clusters, and study the evolution of the galaxy populations in clusters for $0.05 < z < 0.3$.

Additionally, future scientific projects using this data are discussed.

Contents

Acknowledgements iii

Abstract vi

1 Introduction 1

1.1 A Brief History of Cluster Catalogs 1

1.2 Limitations of Existing Catalogs 3

1.3 DPOSS: A Brief Overview 4

2 DPOSS Plate Processing 6

2.1 Overview of SKICAT 6

2.2 Post-SKICAT Procedures 7

2.2.1 Creation of a Matched Catalog 7

2.2.2 Vignetting Correction 7

2.2.3 Improved Object Classification 8

2.2.4 Photometric Calibration 8

2.2.5 Catalog Quilting 9

3 DPOSS Photometry 10

3.1 CCD Data 10

3.1.1 Telescope and Detectors 10

3.1.2 CCD Observations 11

3.1.3 Image Reduction 13

3.1.4 Photometric Calibration 13

3.1.5 Object Detection and Photometry 14

3.2 Plate Overlap Analysis 16

3.3 Calibration to the Gunn *gri* System 19

3.3.1 Color Terms 21

3.3.2 Photometric Accuracy 22

4 Star-Galaxy Separation in DPOSS **26**

4.1 Object Parameters for Classification 26

4.2 Classifier Induction 27

4.2.1 Decision Trees and The Ruler System 27

4.2.2 Artificial Neural Networks 28

4.3 Classification Attributes 28

4.3.1 Plate-Dependent Image Parameter Variations 29

4.3.2 A Source of High Confidence Image Classifications 32

4.4 Classification Results with Training and Testing Data 34

4.4.1 Image Classification Probability Estimates 37

4.5 More Stringent Assessments of Classification Quality 37

4.5.1 Plate Overlap Comparisons 38

4.5.2 Classification Success Rates from CCD Comparisons 39

4.5.3 Catalog Contamination Rates from CCD Comparisons 40

5 Creating the Cluster Catalog **46**

5.1 Input DPOSS Data 46

5.1.1 Selecting Cluster Galaxies Using Colors 46

5.2 Galaxy Density Maps and Cluster Detection 53

5.2.1 Density and Significance Maps 53

5.2.2 Selecting Cluster Candidates 55

5.3 Extinction 60

6 Spectroscopy and Imaging of Cluster Candidates **63**

6.1 Spectroscopic Data 66

6.1.1 Observations 66

6.1.2 Data Reduction 68

6.1.3 Redshift Measurement 68

6.1.4 Are Redshift Peaks Real Clusters? 71

6.1.5 Spectroscopic *vs.* Photometric Redshifts 90

6.2 CCD Imaging of Cluster Candidates 91

7 Photometric Redshifts and Richnesses for Cluster Candidates **93**

7.1 Photometric and Spectroscopic Data 93

7.2 The Photometric Redshift Estimator 95

7.3 Richness 97

7.4 Consistency Between NGP and SGP 99

8 Physical Properties of Abell Clusters **102**

8.1 Photometric Redshifts 102

8.1.1 Redshift Estimation Technique 103

8.1.2 Redshift Errors 106

8.1.3 Redshifts for 431 Abell Clusters 107

8.2 The Butcher-Oemler Effect 108

8.2.1 Analysis of the Butcher-Oemler Effect 110

9 The Cluster-Cluster Correlation Function **116**

9.1 A Brief History 116

9.2 The Correlation Function from DPOSS 117

9.3 Richness Dependence 121

10 Future Scientific Studies with the Cluster Catalog **124**

10.1 Selection Effects in Optical vs. X-ray Cluster Catalogs 124

10.2 Clusters at Intermediate Redshift 126

10.3 Morphological Properties of Butcher-Oemler Galaxies 126

10.4 Dependence of the Butcher-Oemler Effect on Cluster Properties 127

10.5 Cluster Substructure 127

10.6 The Luminosity Function of Galaxy Clusters 128

10.7 A Comparison of Optical Cluster Detection Techniques 130

10.8 Other Cluster-related Projects 130

A Galaxy Distributions **138**

B Properties of Galaxy Clusters **158**

C Imaging of Candidate Galaxy Clusters **217**

List of Figures

2.1 The data processing flow for DPOSS. 9

3.1 The POSS-II *JFN* and Gunn *gri* bandpasses. 11
3.2 The distribution of sky survey plates and CCD pointings. 12
3.3 Night-to-night photometric comparisons. 15
3.4 A typical plate overlap analysis. 18
3.5 Deriving the mean photometric transformations. 19
3.6 Results of the photometric overlap analysis. 20
3.7 A transformation from DPOSS F to Gunn r magnitude. 21
3.8 Calibrated plate and CCD magnitudes as a function of color. 23
3.9 A test of photometric accuracy for stars and galaxies. 24

4.1 The *MTotJ-MCoreJ vs. MTotJ* parameter space. 30
4.2 Mean stellar loci measured on 25 different DPOSS J plates. 31
4.3 The *MTotF-MCoreF* DPOSS image parameter space. 33
4.4 The image parameter spaces used by the ANN and DTREE pattern classifiers. 35
4.5 The ANN and DTREE classifier success rates. 38
4.6 Classification agreement in overlapping plate areas. 40
4.7 Agreement between plate and CCD classifications. 42
4.8 Star and galaxy number counts from the Palomar 60″ CCD fields. 43
4.9 Contamination by misclassified objects in DPOSS catalogs. 44
4.10 Results of a 36 field DPOSS survey of the NGP. 45

5.1 The areas masked in the NGP region due to saturated objects. 47
5.2 The areas masked in the SGP region due to saturated objects. 48
5.3 The $(g-r)$ *vs.* $(r-i)$ diagram for galaxies in Field 475. 50
5.4 The $(g-r)$ *vs.* $(r-i)$ diagram for P60-observed Abell clusters. 51
5.5 Plates used in the NGP area. 52
5.6 Adaptive kernel density map for the NGP region. 56

5.7 Adaptive kernel density map for the SGP region. 57
5.8 Density maps with different kernels. 59
5.9 Detected clusters in part of the NGP area. 60
5.10 100μ IRAS map and DPOSS galaxy density map for Field 479. 61

6.1 Density maps for DPOSS fields 447 and 475. 65
6.2 Significance maps for DPOSS fields 447 and 475. 65
6.3 Locations of new clusters and slitmasks for Field 475 66
6.4 A typical slitmask used for cluster observations with COSMIC. 67
6.5 Sample COSMIC spectra of galaxies in a cluster at $z = 0.18$. 69
6.6a Redshift and galaxy color distributions for candidates from Field 447. . . . 73
6.6b Redshift and galaxy color distributions for candidates from Field 447. . . . 74
6.6c Redshift and galaxy color distributions for candidates from Field 447. . . . 75
6.6d Redshift and galaxy color distributions for candidates from Field 447. . . . 76
6.6e Redshift and galaxy color distributions for candidates from Field 447. . . . 77
6.7a Redshift and galaxy color distributions for candidates from Field 475. . . . 78
6.7b Redshift and galaxy color distributions for candidates from Field 475. . . . 79
6.7c Redshift and galaxy color distributions for candidates from Field 475. . . . 80
6.7d Redshift and galaxy color distributions for candidates from Field 475. . . . 81
6.7e Redshift and galaxy color distributions for candidates from Field 475. . . . 82
6.7f Redshift and galaxy color distributions for candidates from Field 475. . . . 83
6.8 Redshift histogram for all galaxies with spectra in Field 447. 83
6.9 Redshift histogram for all galaxies with spectra in Field 475. 84
6.10 Redshift histogram for clusters in both fields. 84
6.11 Photometric *vs.* spectroscopic redshifts for Fields 447 and 475. 90
6.12 Mean CCD $g - r$ color *vs.* z_{spec}. 92

7.1 The color distribution of galaxies in Abell 115. 94
7.2 Photometric *vs.* spectroscopic redshift for calibrating clusters. 96
7.3 The redshift distribution of candidate clusters. 97
7.4 The richness distribution of candidate clusters. 99
7.5 Comparison of NGP and SGP photo-z distributions. 100
7.6 Comparison of NGP and SGP richness distributions. 101

8.1 The background correction procedure for photometric redshifts. 104
8.2 Estimating redshifts with colors only, magnitudes only, and both. 105
8.3 Comparison of photometric and spectroscopic redshifts. 107
8.4 Bootstrap errors on photometric redshifts. 108
8.5 The blue galaxy fraction in 295 Abell clusters. 113
8.6 Fitting the Butcher-Oemler effect with redshift and richness. 114

9.1 Cluster-cluster correlation functions, all clusters. 119
9.2 Cluster-cluster correlation functions with z, N cuts. 121
9.3 Cluster-cluster correlation functions with b cuts. 122
9.4 Cluster-cluster correlation functions with richness. 123

10.1 Redshift distributions of DPOSS and NORAS detected clusters. 125
10.2 Cluster substructure maps for A1062. 128
10.3 Background correction used to determine cluster LFs. 129
10.4 Composite cluster luminosity function. 129

A.1 Galaxies in NGP Area 13. 139
A.2 Galaxies in NGP Area 14. 140
A.3 Galaxies in NGP Area 15. 141
A.4 Galaxies in NGP Area 18. 142
A.5 Galaxies in NGP Area 19. 143
A.6 Galaxies in NGP Area 20. 144
A.7 Galaxies in NGP Area 21. 145
A.8 Galaxies in NGP Area 22. 146
A.9 Galaxies in NGP Area 23. 147
A.10 Galaxies in NGP Area 27. 148
A.11 Galaxies in NGP Area 31. 149
A.12 Galaxies in SGP Area 2. 150
A.13 Galaxies in SGP Area 3. 151
A.14 Galaxies in SGP Area 4. 152
A.15 Galaxies in SGP Area 5. 153
A.16 Galaxies in SGP Area 8. 154

A.17 Galaxies in SGP Area 9. 155
A.18 Galaxies in SGP Area 10. 156
A.19 Galaxies in SGP Area 11. 157

C.1 Candidate NSC0104+2627. 218
C.2 Candidate NSC0103+2703. 219
C.3 Candidate NSC0118+2248. 220
C.4 Candidate NSC0105+2438. 221
C.5 Candidate NSC0112+2427. 222
C.6 Candidate NSC0104+2230. 223
C.7 Candidate NSC0120+2452. 224
C.8 Candidate NSC0104+2719. 225
C.9 Candidate NSC0108+2653. 226
C.10 Candidate NSC0108+2438. 227
C.11 Candidate NSC0106+2459. 228
C.12 Candidate NSC0102+2503. 229
C.13 Candidate NSC0110+2507. 230
C.14 Candidate NSC0113+2513. 231
C.15 Candidate NSC0112+2747. 232

List of Tables

3.1 CCD13 Extinction and Color Terms 14
3.2 CCD Photometric Residuals at $m_r = 20.0$ 16
3.3 Plate Photometric Errors 22

4.1 DPOSS Classification Attributes in J 29
4.2 DPOSS Classifier Training Statistics 37

6.1 Candidate Spectroscopy Results 72

Chapter 1

Introduction

Clusters of galaxies are the largest bound systems in the Universe and, as such, have been used to study how matter is distributed over extremely large scales. They provide useful constraints for theories of large scale structure formation and evolution, and are valuable (possibly coeval) samples for studying galaxy evolution in dense environments. Studies of the cluster two-point correlation function and power spectrum are important probes of large scale structure and the scenarios of its formation. Correlations between optically and X-ray selected (*e.g.*, ROSAT, Chandra, etc.) clusters are also of considerable scientific interest, and will help us better understand the various selection effects present in both types of cluster samples.

1.1 A Brief History of Cluster Catalogs

Surveys for galaxy clusters have only recently benefited from the automation afforded by computers. The earliest surveys relied on visual inspection of vast numbers of photographic plates, usually by a single astronomer. As early as 1938, Zwicky discussed such a survey based on plates from the 18″ Schmidt telescope at Palomar, and results were presented in 1942 by both Zwicky and Katz & Mulders. Even then, Zwicky, with his typical prescience, noted that elliptical galaxies are much more strongly clustered than late-type galaxies. However, the true pioneering work in this field did not come until 1957, upon the publication of a catalog of galaxy clusters produced by George Abell as his Caltech Ph.D. thesis, which appeared in the literature the following year (Abell 1958). Zwicky followed suit a decade later, with his voluminous Catalogue of Galaxies and of Clusters of Galaxies (Zwicky, Herzog & Wild 1968).

Abell used the red plates of the first National Geographic-Palomar Observatory Sky Survey. In selecting clusters, Abell applied a number of criteria in an attempt to produce a fairly homogeneous catalog. He required a minimum number of galaxies within two magnitudes of the third brightest galaxy in a cluster, a fixed physical size within which

galaxies were to be counted, a maximum and minimum distance to the clusters, and a minimum galactic latitude to avoid obscuration by interstellar dust. The resulting catalog, consisting of 1,682 clusters in the statistical sample, remained the only such resource until 1989. In that year, Abell, Corwin & Olowin (hereafter ACO) published an improved and expanded catalog, now including the Southern sky. These catalogs have been the foundation for many cosmological studies over the last four decades, despite serious questions about their reliability (which are addressed in the next section). Some other catalogs based on plate material have also been produced, such as Shectman (1985), from the galaxy counts of Shane & Wirtanen (1954), and a search for more distant clusters carried out on plates from the Palomar 200″ by Gunn, Hoessel & Oke (1986).

Only in the past ten years has it become possible to utilize the objectivity of computational algorithms in the search for galaxy clusters. These more modern studies required that plates be digitized, so that the data are in machine readable form. Alternatively, the data had to be digital in origin, coming from CCD cameras. Unfortunately, this latter option provided only small area coverage, so the hybrid technology of digitized plate surveys blossomed into a cottage industry, with numerous catalogs being produced in the past decade. All such catalogs relied on two fundamental data sets: the Southern Sky Survey plates, scanned with the Automatic Plate Measuring (APM) machine (Maddox *et al.* 1990) or COSMOS scanner (to produce the Edinburgh/Durham Southern Galaxy Catalog / EDSGC, Heydon-Dumbleton, Collins & MacGillivray 1989), and the POSS-I, scanned by the APS group (Pennington *et al.* 1993). The first objective catalog produced was the Edinburgh/Durham Cluster Catalog (EDCC, Lumsden *et al.* 1992), which covered 0.5 sr ($\sim 1,600$ square degrees) around the South Galactic Pole (SGP). Later, the APM cluster catalog was created by applying Abell-like criteria to select overdensities from the galaxy catalogs, and is discussed in detail in Dalton *et al.* (1997). The work by Odewahn & Aldering (1995), based on the POSS-I, provided a Northern sky example of such a catalog, while utilizing additional information (namely galaxy morphology). Some initial work on this problem, using higher quality POSS-II data, was performed by Picard (1991) in his thesis.

In addition to these hybrid photo-digital surveys, smaller areas, to much higher redshift, have been covered by numerous deep CCD imaging surveys. Notable examples include the Palomar Distant Cluster Survey (PDCS, Postman *et al.* 1996), the ESO Imaging Survey (EIS, Lobo *et al.* 2000), Zaritsky *et al.* (1997), and many others. None of these surveys

provide the angular coverage necessary for large-scale structure and cosmology studies, and are designed to find rich clusters at high redshift. Only the Sloan Digital Sky Survey (SDSS, York *et al.* 2000) will provide large area, moderately deep CCD coverage.

Despite these efforts, one thing was missing: a catalog of galaxy clusters, produced by objective means, that was at least as deep as the Southern surveys, but which covered the Northern sky. This thesis is intended to provide such a catalog.

There have also been many surveys for galaxy clusters at other wavelengths, most notably in the X-ray. All-sky surveys, such as RASS (Collins *et al.* 2000, Ebeling *et al.* 2000, Böhringer *et al.* 2000) and EMSS (Gioia & Luppino 1994), as well as pointed ROSAT observations (Scharf *et al.* 1997, Romer *et al.* 2000), have been used to produce cluster catalogs at X-ray wavelengths. However, the relationship between optically and X-ray selected clusters is still not fully understood, so that a Northern, optically selected catalog is essential.

1.2 Limitations of Existing Catalogs

Most of the optical studies to date have been limited by the statistical quality of the available cluster samples. For instance, the Abell catalog suffers from a non-objective selection process, poorer plate material, a bias towards centrally-concentrated clusters (especially those with cD galaxies), a relatively low redshift cutoff ($z \sim 0.15$; Bahcall & Soneira 1983), and strong plate-to-plate sensitivity variations. Still, many far-reaching cosmological conclusions have been drawn from it (*i.e.*, Bahcall & West 1992), although later studies have sometimes shown these to be flawed. Photometric errors and other inhomonogeneieties in the Abell catalog (Sutherland 1988, Efstathiou *et al.* 1992), as well as projection effects (Lucey 1983, Katgert *et al.* 1996) are a serious and difficult-to-quantify issue. These effects resulted in early findings of excess large-scale power in the angular correlation function (Bahcall & Soneira 1983), and later attempts to disentangle these issues relied on models to decontaminate the catalog (Sutherland 1988, Olivier *et al.* 1990). The extent of these effects is also surprisingly unknown; measures of completeness and contamination in the Abell catalog disagree by factors of a few. For instance, Miller, Batuski & Slinglend (1999) claim that under- or over-estimation of richness is not a significant problem, whereas van Haarlem, Frenk & White (1997) suggest that one-third of Abell clusters have incorrect richnesses, and that one-third of rich ($R \geq 1$) clusters are missed. Unfortunately, some of these

problems will plague any optically selected cluster sample, including our own, but objective selection criteria and a strong statistical understanding of the catalog can mitigate their effects.

Even some of the other objective catalogs preceding ours have their drawbacks. The APM group, for instance, used digitized J (blue) plates from the Southern Sky Survey; the use of a single blue band provides no color information to distinguish galaxy types, and is a poor choice for cluster detection because clusters are better delineated by redder, early-type galaxies in the redshift range probed ($z < 0.3$). Comparable surveys, such as the EDCC, already find a factor of two higher space density of clusters than Abell, and more sensitive CCD surveys find as many as five times more clusters than Abell.

More recent surveys, such as the EDCCII (Bramel, Nichol & Pope 2000) have not yet achieved the area coverage of DPOSS, and perhaps more importantly, are not nearly as deep. For instance, the EDCCII's limiting magnitude is $b_J = 20.5$. For an L_* elliptical this corresponds to a limiting redshift of $z \sim 0.23$. The survey presented here utilizes F plates, with a limiting magnitude of $m_r = 20$. This corresponds to a limiting redshift of 0.33 for an L_* elliptical. Because of the increase in $g - r$ color with redshift, the APM would have to go as deep as $b_J = 22.0$ to reach the same redshift from their data for early type galaxies. Similarly, even at lower redshift, this implies that DPOSS can see $\sim 0.5^m - 1^m$ deeper in the cluster luminosity functions. Additionally, the survey presented here utilizes at least one color (two filters), and a significantly increased amount of CCD photometric calibration data.

1.3 DPOSS: A Brief Overview

The POSS-II (Reid *et al.* 1991) covers the entire northern sky ($\delta > -3°$) with 897 overlapping fields (each 6.5° square, with 5° spacings), and, unlike the old POSS-I, has no gaps in the coverage. Approximately half of the survey area is covered at least twice in each band, due to plate overlaps. Plates are taken in three bands: blue-green, IIIa-J + GG395, $\lambda_{\rm eff} \sim 480nm$; red, IIIa-$F$ + RG610, $\lambda_{\rm eff} \sim 650nm$; and very near-IR, IV-$N$ + RG9, $\lambda_{\rm eff} \sim 850nm$. Typical limiting magnitudes reached are $B_J \sim 22.5$, $R_F \sim 20.8$, and $I_N \sim 19.5$, *i.e.*, $\sim 1^m - 1.5^m$ deeper than POSS-I. The image quality is improved relative to POSS-I, and is comparable to the southern photographic sky surveys.

The original survey plates are digitized at STScI, using modified PDS scanners (Lasker 1996). The plates are scanned with 15μ ($1.0''$) pixels, in rasters of 23,040 square, giving ~ 1 GB/plate, or ~ 3 TB of pixel data total for the entire digital survey (DPOSS). Currently, astrometric solutions are good to $rms \sim 0.5''$.

Our ongoing effort at Caltech and the sites in Italy (Osservatorio Astronomico di Capodimonte and Osservatorio Astronomico di Roma) and Brazil (Observatório Nacional) is to process, calibrate, and catalog the scans, with the detection of all objects down to the survey limit, and star/galaxy classifications accurate to 90% or better down to $\sim 1^m$ above the detection limit. Object detection and photometry is performed by SKICAT, a software system developed for this purpose (Weir *et al.* 1995abc; hereafter W95abc), incorporating standard astronomical image processing packages, a commercial Sybase database, as well as a number of artificial intelligence (AI) and machine learning (ML) modules. Using this code, we measure ~ 60 attributes per object on each plate. Currently, all plates at $b > 10°$ have been processed into catalogs. The catalogs then undergo a series of procedures, described in Chapter 2, to produce large-area photometrically calibrated catalogs.

The final product of DPOSS will be the Palomar-Norris Sky Catalog (PNSC), expected to contain $> 5 \times 10^7$ galaxies, and $> 2 \times 10^9$ stars. The catalog will be made available to the community via the World Wide Web in 2001.

This thesis utilizes all plates at $b > 30°$, a total of 450 fields, covering π steradians ($\sim 10,000$ square degrees).

Chapter 2

DPOSS Plate Processing

The general procedure for the processing of DPOSS plates via the SKICAT software system has been outlined in W95abc. Since that time, a number of additional post-processing steps and software modules have been added to the reduction pipeline. This chapter provides a brief overview of SKICAT and the newer procedures used to produce the final catalogs.

2.1 Overview of SKICAT

The initial processing of the plate scans involves the determination of the plate density-to-intensity transformation via a set of densitometry spots exposed on each POSS-II plate, estimation of the plate density saturation level, and measurement of the mean sky level. Next, a robust background mapping algorithm is applied to filter out discrete image sources and produce a map of the mean level and standard deviation of the sky background across the plate.

The FOCAS image detection system (Valdes *et al.* 1982) is used to process the entire plate in a grid of 13×13 partially overlapping subregions we refer to as *footprints*. The sky level and noise maps for each footprint are used to set an image detection threshold which is some fraction of the local background noise. FOCAS detects objects in the form of groups of connected image pixels whose values lie above the local threshold level. Next, a series of rough classification rules are applied to the FOCAS catalog of each footprint to establish a set of stars for that region, and these sources are used by FOCAS to automatically model the two-dimensional local stellar point spread function (PSF) for the footprint. Having established the mean PSF, a FOCAS analysis stage is run where each detected object is scaled in the intensity and spatial domains to best match this PSF model. Finally, FOCAS determines which detected images are actually a merged set of overlapping detections and an algorithm is applied to deblend these cases and determine the positions, image classes, and photometric parameters of each constituent. The initial set of FOCAS runs are applied to spatially overlapping plate regions. Following FOCAS treatment of all these areas, SKICAT

conducts an automated overlap comparison to bring the photometric properties of each footprint onto a common mean system. The final set of homogenized image parameters are organized by plate footprint into a Sybase database catalog which may be queried with SQL commands to perform subsequent analysis.

2.2 Post-SKICAT Procedures

Once a set of plates has been processed, the catalogs contain only instrumental magnitudes, with inhomogeneous parameters from plate to plate, and are not merged between the three bandpasses. A number of procedures are applied to generate a final, calibrated, stitched object catalog.

2.2.1 Creation of a Matched Catalog

The first step in the post-SKICAT processing is the merging of individual J, F, and N catalogs for a given field into a single catalog, which we refer to as an *MCAT* (**M**atched **CAT**alog). We query the Sybase database for a subset of image parameters from each of the three catalogs for a given field, forming individual binary catalogs (called *FCAT*s) on the local disk. These are then positionally cross-matched in a two stage process. First, for each F plate footprint, rough positional matches for a subset of objects are found in the J and N catalogs, using a large ($15''$) search radius. The mean offset in RA and Dec is calculated and applied, and a more comprehensive cross-match with a smaller search radius of $3''$ is performed. Finally, all objects, detected on one, two or all three plates are written out to the MCAT. This binary file still contains only uncalibrated, uncorrected magnitudes, and the original SKICAT object classifications.

2.2.2 Vignetting Correction

Next, we apply a correction for telescope vignetting to all three bands in each MCAT. The same correction is applied to all fields. The vignetting pattern is determined by median stacking 100 plate images in each band (binned at 8×8 pixels), discarding the 10 highest and lowest values in each pixel. This provides an accurate measurement of the mean large scale sensitivity variations due to telescope vignetting and filter throughput. The vignetting

correction is applied to all measured magnitudes contained in the MCATs. A more detailed description of this procedure can be found in Mahabal *et al.* (2001).

2.2.3 Improved Object Classification

The next three steps are designed to provide improved star/galaxy classification based on new neural networks and decision trees, trained from a much larger sample of plates and CCD data than presented in W95a. A lengthy description of the issues and procedures involved is provided in Chapter 4; here we present a very brief overview of the actual processing steps.

First, the locus of compact (stellar) objects in three parameter spaces (total area, second moment of the light distribution, and a concentration index, all as a function of magnitude) are visually mapped for the central region of each plate, a total of 9 loci per field. These loci, whose positions and shapes vary from plate to plate, are then subtracted from the corresponding parameters in all footprints, creating normalized versions of each parameter, which are stored in the MCATs. This ensures that the star/galaxy separation parameters are the same for all plates. Finally, these normalized parameters are used by a set of neural networks and decision trees to classify all of the detected objects.

2.2.4 Photometric Calibration

We calibrate the photometry by transforming sets of 9 plates onto a common instrumental system, and then using all of the available CCD data for this 9-plate area to derive the mapping between JFN and gri. This is described in detail in the next chapter. All steps are performed separately for stars and galaxies. We first match the overlapping areas of neighboring plates, map the magnitude offset as a function of magnitude between plate pairs, and average the resulting splines from various multi-plate paths to derive a transformation between the magnitudes from a given plate to those of the fiducial plate. Next, all of the CCD data for this area are matched to the plate data, and a spline transformation from instrumental to calibrated magnitudes is derived and applied. Finally, we apply an extinction correction based on the maps of Schlegel, Finkbeiner & Davis (1998).

2.2.5 Catalog Quilting

To create a seamless catalog of objects over areas larger than a single field, we join individual catalogs, applying linear cuts in right ascension and declination to each catalog so that it does not overlap its neighbors. Additionally, we ensure that the area of each plate containing the densitometry spots (and therefore no astronomical objects) is filled in with objects from neighboring plates which also contain the same region.

The entire processing flow is diagrammed in Figure 2.1.

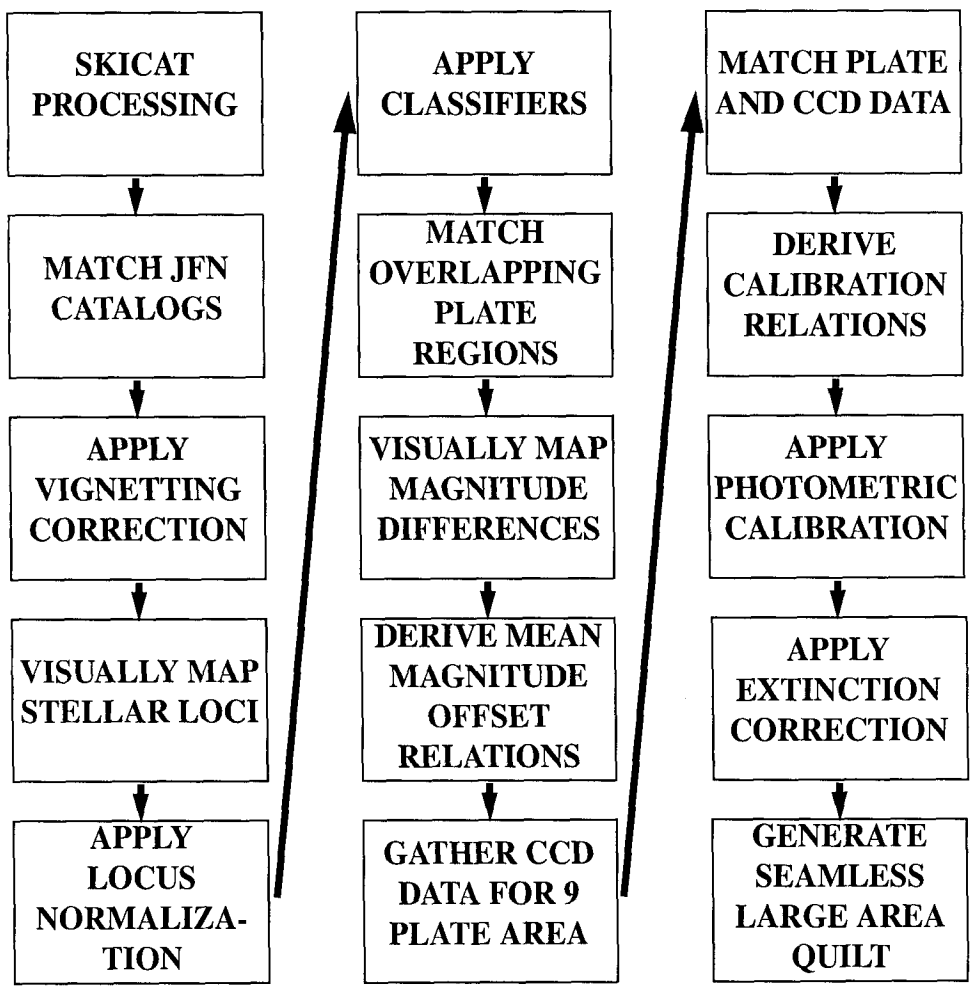

Figure 2.1: The data processing flow for DPOSS.

Chapter 3

DPOSS Photometry

The two most crucial aspects of any large sky survey are the photometry of objects and their classification (star, galaxy, unknown). Although these issues have been previously addressed for DPOSS (Weir *et al.* 1995abc), we now have available a much larger database of processed plates and CCD imaging. This allows us to produce accurate classification and calibration over the entire high-galactic-latitude northern sky, with robust measures of our accuracy. This chapter describes the details of the CCD data obtained for photometric calibration and used as our classification training set, and the generation of uniform, calibrated object catalogs.[1] Object classification is described in the following chapter.

3.1 CCD Data

Nearly all of the CCD data utilized in this thesis were obtained at the Palomar Observatory 60″ telescope. A small number of equatorial clusters were observed at the Cerro Tololo Inter-American Observatory 0.9-meter telescope, and are described in Margoniner & de Carvalho (2000). The data processing for the CTIO imaging was performed identically to that described here.

3.1.1 Telescope and Detectors

The Palomar 60″ telescope is an $f/8.75$ Ritchey-Chretien design, with the CCD imaging cameras placed at Cassegrain focus. From the initial data through June 1996, and on rare occasions thereafter, we used CCD16, a SITe 1024^2, thinned, AR coated array, with 24μ pixels. The pixel scale is 0.376″/pixel, providing a $6.4' \times 6.4'$ field of view. CCD16 has a gain of $2.5e^-/DN$ and a read noise of $8.2e^-$. Starting in July 1996, a new, larger detector was made available at the Palomar 60″. This detector, CCD13, is a SITe 2048^2 thinned, AR coated array, also with 24μ pixels. The pixel scale at this detector is 0.368″/pixel,

[1] A majority of this chapter is adapted from the articles "Photometric Calibration of DPOSS," Gal *et al.* 2001, *in prep.*, and Gal *et al.* 2000b.

providing a $12.56' \times 12.56'$ FOV. CCD13 has a gain of $1.63e^{-}/DN$ and a read noise of $6.3e^{-}$. In addition to the factor of four increase in area over CCD16, this detector also provides extremely good blue sensitivity ($\sim 55\%$ QE at 4000Å). All objects were observed in the Gunn *gri* filters, which are well matched to the DPOSS JFN passbands, as shown in Figure 3.1.

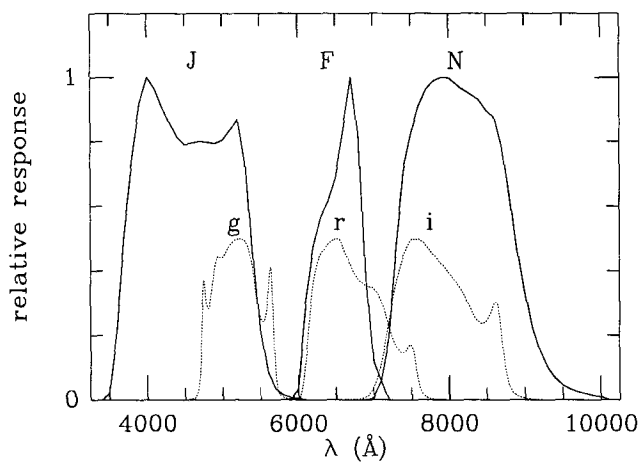

Figure 3.1: The POSS-II JFN (solid lines) and Gunn *gri* (dashed lines) bandpasses.

3.1.2 CCD Observations

The imaging targets are selected from the list of northern Abell clusters (ACO89). Because the CCD survey was designed to provide photometric calibration and star-galaxy separation data for DPOSS, we attempted to observe at least two Abell clusters per DPOSS field. Priority was given to the richest clusters closest to the plate centers; therefore, our sample is biased toward richer Abell clusters. Nevertheless, many plates have only one or two known clusters; in such cases, whatever clusters were available were observed. Approximately fifty clusters were observed twice, sometimes with both detectors. This allows us to check our photometric accuracy, as well as consistency between detectors.

Data were taken only on photometric nights with seeing better than $2''$. The mean seeing for our data is $\sim 1.5''$; the best seeing is $0.9''$. Integration times were fixed for each filter/CCD combination, regardless of sky brightness or seeing. The vast majority of nights allocated for this program were $> 75\%$ dark. For CCD16, we integrated for 1200 seconds in g, and 900 seconds each in r and i. When using CCD13, the integration times were

shortened to 900 seconds in g, and 600 seconds each in r and i. These exposures yielded limiting magnitudes of $m_{lim,gri} \sim 22$ for CCD13 observations, with limiting magnitudes for CCD16 observations ~ 0.5 magnitude brighter. With the typical observational overhead, we usually observed between seven and eleven clusters in a single night. Figure 3.2 shows our current CCD coverage.

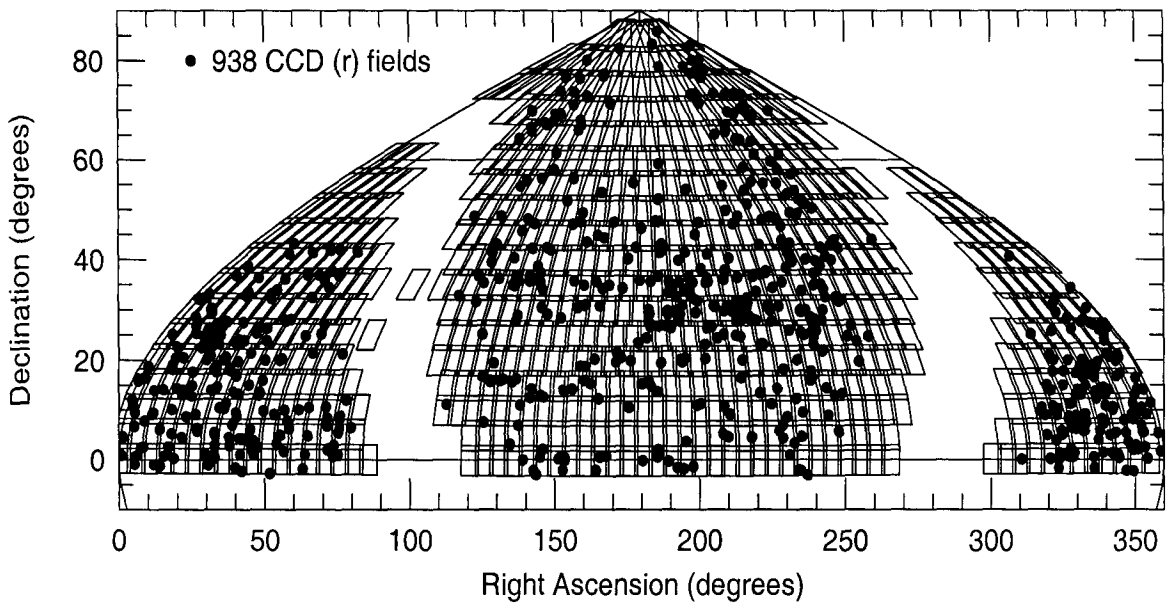

Figure 3.2: The distribution of sky survey plates (squares) with currently available CCD calibration pointings (dots).

For every night that was deemed photometric, we observed a set of Gunn standards. Between 5 and 12 observations of available Gunn standards were made each night, at a variety of airmasses. Each star observed at each pointing was imaged three times on a single frame by closing the shutter, offsetting the telescope, and reopening the shutter. This was done to increase the S/N of our photometric measurements, as well as avoid excessive time loss due to the long ($\sim 180s$) readout time for CCD13. In addition to the standard stars, we also took nine bias frames, nine dome flats in each filter, and three sky flats in each filter on every night of observing.

3.1.3 Image Reduction

Data were processed using the IRAF data reduction package (Tody 1986). First, a single bias value, determined from the median of the overscan region of each image, was subtracted from all object and calibration frames. The bias frames were median filtered and fit with a smooth two-dimensional polynomial, which was subtracted from all object and flat field images. Individual dome and sky flats in each filter were median stacked, and the resulting sky flats processed with the dome flats. The remaining large scale structure was smoothed, and this smooth correction was recombined with the dome flats to create a master flat field image for each filter.

These master flat field corrections were applied to all target and standard star frames. After this procedure there were still noticeable large scale gradients in the CCD illumination pattern, especially in the g frames. To remove this, we generated dark sky flat field frames (also known as illumination corrections) by median filtering all of the unregistered target frames in each filter. On those nights when too few targets were observed to generate such an illumination correction, data were combined with an adjacent night. These combined images were smoothed with a large (50 pixel) boxcar, and the resulting correction applied to both the target and standard star frames. This procedure results in images that are flat to approximately the 1% level. Finally, for CCD13, it was necessary to apply a fringe correction to the i images. This was generated by median stacking the completely flat-fielded i-band target images, and smoothing the result with a small 9 pixel boxcar. The resulting image was used as the fringe correction for the target frames.

3.1.4 Photometric Calibration

Standard star photometry was performed using the *apphot* package in IRAF. Stars were photometered in numerous apertures up to 50 pixels (18.5″) in radius, and the local sky was determined using a 10 pixel wide annulus centered on each star, starting at a radius of 50 pixels. The convergence magnitudes for all three exposures of each star on each frame were measured, and the three values averaged to provide a mean instrumental magnitude.

The resulting collection of between five and twelve measured instrumental magnitudes were used to determine the zero-point offset, airmass term, and color term in each filter.

We used the IRAF *fitparams* task to fit the relation

$$m_{true} = m_{inst} + A + Bsec(z) + C(color) \tag{3.1}$$

for each filter. On some nights, not enough standards were observed to robustly determine values for all three unknowns. In these cases, we only determined the zero point, using airmass and color terms derived from the mean of nights with sufficient standards; these values are given in Table 3.1. Typical *rms* deviations in the fit of the calibration relation are 0.01 magnitude. In addition, on two nights, over twenty Gunn standards were observed to test our measurements of the airmass and color terms. In both cases, the derived terms were within 10% of the mean values obtained from other nights with many fewer standards.

Table 3.1: CCD13 Extinction and Color Terms

Filter	**Extinction**	**Color**
g	-0.152	$0.150 \times (g-r)$
r	-0.094	$0.068 \times (g-r)$
i	-0.070	$-0.013 \times (g-i)$

3.1.5 Object Detection and Photometry

Object detection on the target frames was done using the FOCAS package (Jarvis & Tyson 1979, Valdes 1982). The g, r, and i frames were processed independently, using detection parameters of 2.5σ per pixel, a 25 pixel minimum area, and a sky value estimated individually for each image. Object classification was also performed by FOCAS, and the classifications were visually inspected. Bright objects with incorrect classifications (usually due to saturated pixels) were corrected by hand. The photometric coefficients derived from the standard star observations were used to determine object magnitudes. Color terms were applied only after objects were detected in multiple filters, and matched together at a later stage. For objects detected in only one filter, default colors of $g - r = 0.5$ and $g - i = 0.5$ were used when applying the color correction.

In order to properly study such a large collection of imaging data, we must establish photometric consistency between many observing nights, and in our case, two different detectors. Photometric accuracy is also a necessary condition for using this data to calibrate DPOSS. To examine this question, we observed 51 clusters on two or more occasions. In

some cases, both sets of observations were taken with the same CCD, and in others, with both CCDs.

We have compared the photometry of numerous, multiply-observed clusters in three scenarios: *(1)* both observations with CCD16, *(2)* one observation with CCD16 and one with CCD13, and *(3)* both observations with CCD13. We find that there are no systematic night-to-night or CCD-to-CCD photometric offsets greater than 0.05^m, and the residuals are typically 0.05^m at $m_{gri} = 19.0$, rising to no more than 0.15^m for objects within one magnitude of the detection limit. Table 3.2 presents the typical residuals at $m_r = 20.0$ for the various comparisons, while Figure 3.3 shows a typical set of photometric comparisons. The left plot is a comparison of photometry for the cluster A31, where both nights of data were taken with CCD16, 14 months apart. The center plot compares photometry for the cluster A98, with one night of CCD16 data, and one night of CCD13 data. In this case, the data were taken almost four years apart. Finally, the right plot shows photometry for A2562, with both nights of data taken with CCD13, taken only 3 months apart. The bottom panels show the magnitude differences between each pair of observations.

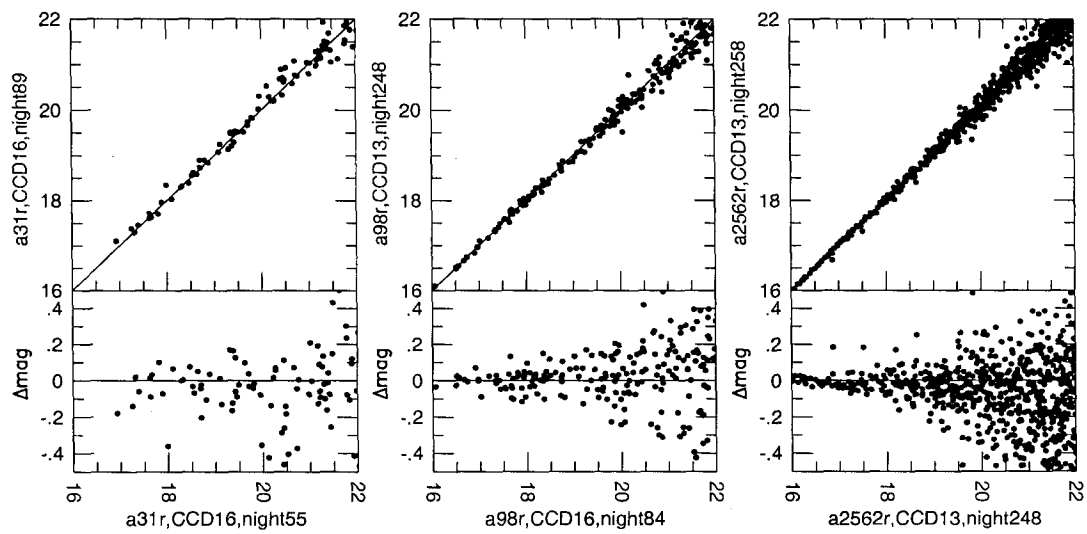

Figure 3.3: Typical photometric comparisons. The left plot is a comparison of photometry for the cluster A31, where both nights of data were taken with CCD16. The center plot compares photometry for the cluster A98, with one night of CCD16 data, and one night of CCD13 data. Finally, the right plot shows photometry for A2562, with both nights of data taken with CCD13. The bottom panels show the magnitude differences between each pair of observations.

Table 3.2: CCD Photometric Residuals at $m_r = 20.0$

Comparison	σ_g	σ_r	σ_i
CCD16 *vs.* CCD16	0.19	0.13	0.09
CCD13 *vs.* CCD16	0.10	0.09	0.10
CCD13 *vs.* CCD13	0.12	0.10	0.16

3.2 Plate Overlap Analysis

A great advantage of POSS-II over earlier surveys is the extensive overlap between neighboring plates. Adjacent plates overlap each other by 1.5° along edges covering 6.5°, providing $\sim 9\square^\circ$ of duplicated area for each plate pair. These areas each contain thousands of objects which can be used to derive the transformation of one plate's instrumental magnitude system to that of its neighbor. These transformations can be propagated across multiple plate overlaps to tie a contiguous set of plates onto a common photometric system.

In practice, this instrumental magnitude transformation must be mapped independently for stars and galaxies, especially for brighter magnitudes ($m_{\rm inst} < 19.0$). Although the density-to-intensity (D-I) transformation has been linearized using the densitometry spots on each plate, stars and galaxies nevertheless display distinct photometric behaviors. This is because the brighter pixels in stellar images populate the highly nonlinear part of the D-I relation, where small errors in the polynomial fit (mostly due to the small number of points characterizing the "shoulder" of the curve) can result in large variations in the derived intensity. Pixels within galaxies occupy the more linear part of the D-I transformation, resulting in more stable and linear photometry.

Additionally, propagating the photometric transformations across a large number of plates (as would be necessary to knit the whole sky) can result in the unacceptable accumulation of (possibly systematic) errors. This issue was addressed by Groth & Peebles (1986), and their technique utilized by Maddox, Efstathiou & Sutherland (1990; hereafter MES90) to estimate the extent of such errors in the APM. A similar approach was also taken by Odewahn & Aldering (1995; hereafter OA95) in an analysis of galaxy counts at the North Galactic Pole, but that study was limited by the small overlap regions and poorer quality of POSS-I. An early attempt to address the problem of plate inhomogeneities in POSS-II is discussed in Picard (1991). To avoid this issue entirely, we have elected to stitch and calibrate "small" areas of 8 to 10 plates ($\sim 250\square^\circ$). These smaller areas can be combined with

no additional offsets because they are already on a calibrated, rather than instrumental, magnitude system. Unlike MES90 and OA95, we are afforded this luxury by the enormous quantity of available CCD calibration data.

First, we determine which plate pairs have overlap regions larger than $5\square^\circ$, thereby eliminating pairs where only the heavily vignetted corners overlap. The overlap regions are matched, and the outermost 10% of the matched area is clipped on all four sides, to avoid the most heavily vignetted regions. A spline is fit to the magnitude difference between the matched objects as a function of the instrumental magnitude on the fiducial plate, $\Delta m = m_{\rm fid} - m_{\rm slave} = f(m_{\rm fid})$. This fit is performed independently for stars and galaxies in each filter (JFN). At faint magnitudes ($m_{\rm inst} > 19.0$) we use both stars and galaxies in the independent fits, to avoid biases due to possible differences in classification between plates. At these faint magnitudes, there are no bright pixels (which populate the highly nonlinear part of the D-I relation) in the stellar images, resulting in identical photometric properties for both stars and galaxies. There are typically between 5,000 and 30,000 objects used to determine the transformation between a given pair of plates. Although significant scatter is present, especially at faint magnitudes, the mean is nevertheless well determined. At the bright end ($m < 16$), where the number of objects is small and classification problems exist, the spline fit is constrained with points located visually. At intermediate magnitudes (typically $16 < m < 20$), a robust locus mapping algorithm is used. Finally, at the faint end ($m > 20$), where incompleteness is a factor, the fit is fixed at a constant Δm. These objects are in any case too faint to be photometered and classified properly, and are therefore of limited scientific use from the current survey. Figure 3.4 shows a typical pair of plate overlaps, for galaxies (top) and stars (bottom) matched between plates 392 and 333. The resulting spline fits are also shown.

In contrast, MES90 defined a single coefficient, T_{ij}, to match the magnitudes between adjacent plates. While they state that the rms of a linear fit to the magnitude differences (in their case, $(m_i - m_j)$ *vs.* $(m_i + m_j)/2$) is nearly as good as a higher order polynomial, we find that this is not always the case, and is certainly not true for stars (which they do not treat). We therefore have elected to utilize our procedure as described above, which is more general, but requires a great deal more interaction and inspection. This process also permits us to find individual plates which behave abnormally, either due to their intrinsic properties or processing failures, which can then be corrected.

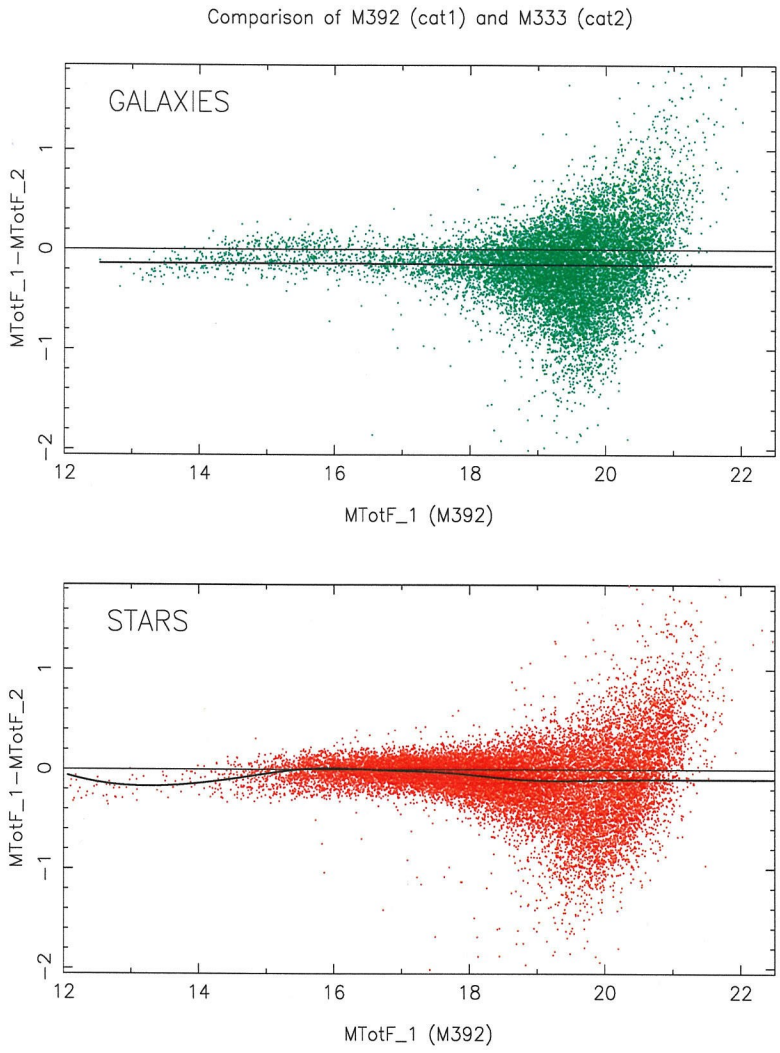

Figure 3.4: A typical plate overlap analysis, for F plates in fields 333 and 392. We show the magnitude difference between plates for galaxies (top) and stars (bottom), along with the spline fits to unify the photometric systems.

To actually transform a specific plate's instrumental system to that of the reference plate for a given area, we propagate magnitude transformations through sets of up to five plates connecting the plate being transformed to the fiducial plate. This is illustrated in Figure 3.5, where arrows represent the transformation paths used to tie plates 392 and 452 to the center (fiducial) plate 391. A plate directly adjacent to the center plate can be tied to it by up to three paths (the green/solid arrows), while a plate diagonally away from the center can be tied by four paths (the red/dashed arrows). Figure 3.6 shows the four photometric transformations derived between plates 333 and 391. The ordinate shows the fiducial plate magnitude m_f, while the abscissa shows the difference between the magnitude on the plate

to be transformed, m_p, and m_f. Rather satisfyingly, all possible convolution paths provide similar transformations for a given plate, especially for galaxies. These transformations are averaged for each plate to generate a spline $\Delta m_{pf} = m_p - m_f$ as a function of m_f, also shown in Figure 3.6. These plots are visually inspected for each plate pair, and instances of abnormal behavior, such as highly variable transformations, are flagged and treated by hand. The transformations for stars are highly nonlinear, reflecting their saturated cores, and show much more variance than those for galaxies. This contributes to the large errors in stellar photometric calibration discussed later.

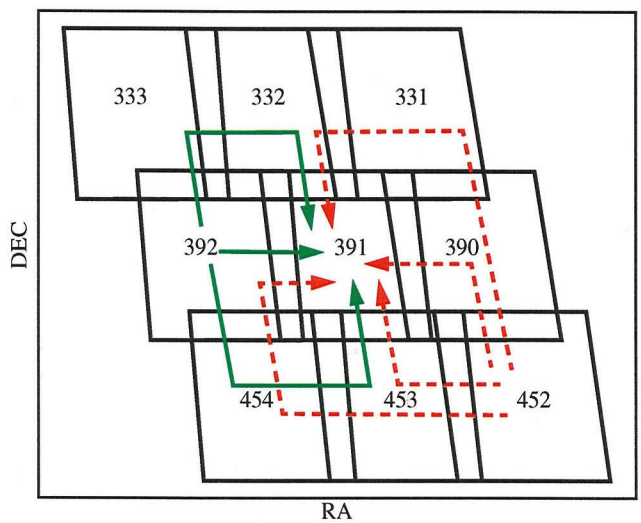

Figure 3.5: An illustration of the derivation of mean photometric transformations. Arrows represent the transformation paths used to tie plates 392 and 452 to the center (fiducial) plate 391. A plate directly adjacent to the center plate can be tied to it by up to three paths (the green/solid arrows), while a plate diagonally away from the center can be tied by four paths (the red/dashed arrows).

3.3 Calibration to the Gunn *gri* System

Once a set of plates has been transformed to a common instrumental system, we match our CCD catalogs to the plate catalogs for that area. Typically, we have between 5 and 15 CCD pointings, in the three filters (*gri*), for a given nine plate area. This provides between 1,000 and 5,000 matched galaxies and a similar number of matched stars from which to derive photometric calibration.

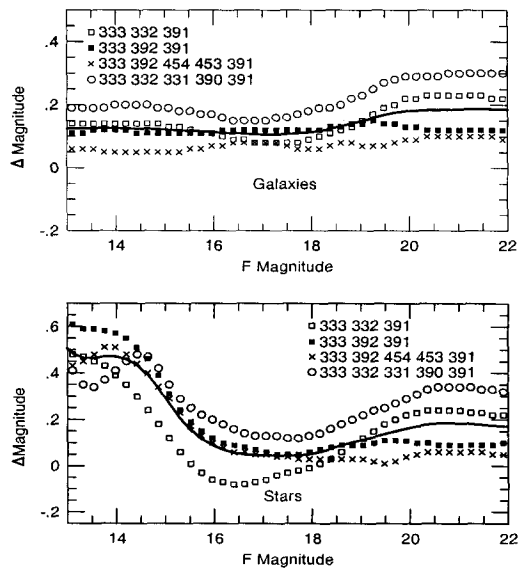

Figure 3.6: The results of the overlap analysis illustrated in Figure 3.4. The ordinate shows the fiducial plate magnitude m_f, while the abscissa shows the difference between the magnitude on the plate to be transformed m_p and m_f. The solid line is the mean of the four different paths. Rather satisfyingly, all possible convolution paths provide similar transformations for a given plate.

The CCD and plate data are matched, allowing for an overall offset, scale change, and rotation between the CCD-derived celestial coordinates and the plate celestial coordinates. After the mean CCD-plate offset is derived, a search radius of $3''$ is used, and the search process iterated until the RA,Dec offsets converge. Typical coordinate residuals are $0.4''$, which both confirms the stated astrometric accuracy of DPOSS, and implies that false matches are not a significant source of added noise. A spline is fit to the difference between the CCD calibrated magnitude $m_{\rm CCD}$ and the plate instrumental magnitude $m_{\rm inst}$, in a manner identical to the plate overlap analysis. Once again, this is done independently for stars and galaxies. Figure 3.7 shows a typical set of points and the resulting transformations between plate F and CCD r magnitudes, for both stars and galaxies, in a nine plate area.

This method differs sharply from that employed by MES90, who obtained only magnitude zero points from their CCD data. Their frames, at $2' \times 3'$ in size, cover only 6% of the area of our CCD images, providing a factor of 17 fewer calibrating objects from detector area alone; considering our deeper exposures and more numerous CCD fields (over

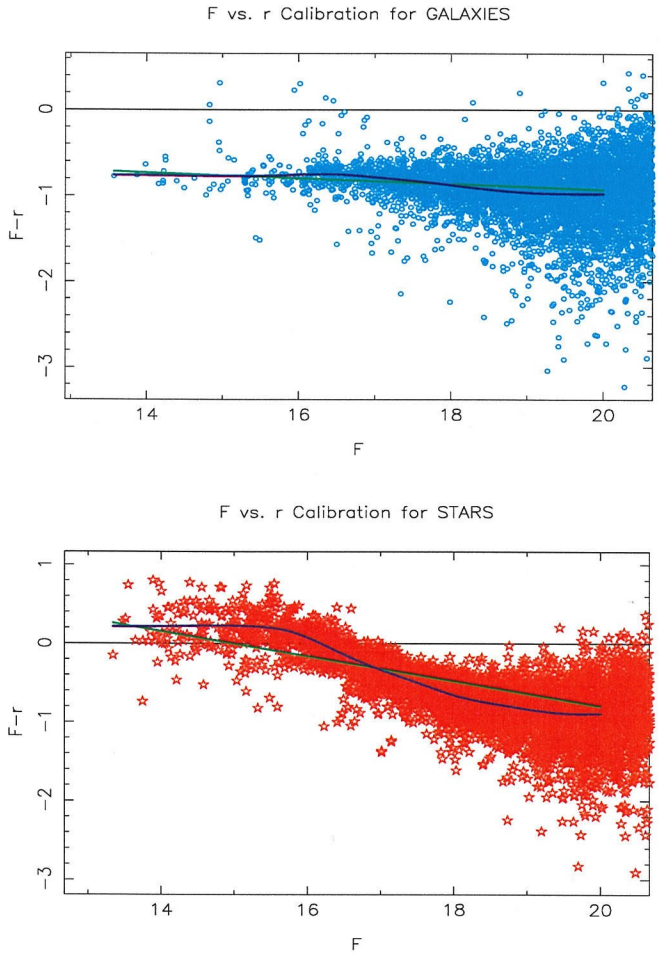

Figure 3.7: The transformation from DPOSS F to Gunn r magnitude derived for a set of 9 plates, for galaxies (top) and stars (bottom). A single zero point offset is clearly insufficient.

700 *vs.* 69), we have a factor of approximately one thousand more calibration objects. The nonlinearities in the transformations to calibrated magnitudes, if not treated, can lead to incorrect number count slopes and correlation functions.

3.3.1 Color Terms

An examination of the filter curves in Figure 3.1 shows that the $F - r$ and $N - i$ transformations are likely to be free of color terms, as the plate and CCD filter systems are well matched. However, the J filter is significantly broader and bluer than the corresponding CCD g filter, and we may expect a color correction to be necessary. In the left panels of Figure 3.7, we show the difference between calibrated plate magnitude and CCD magnitude,

$g_0(J) - g_{\rm CCD}$ as a function of $g - r$ color, for both galaxies and stars. A strong color term is evident, especially for the stars. The galaxies do not span a significant range in $g - r$, making the color term impossible to discern in the noise.

To estimate the color correction, we calculated the median $g_0(J) - g_{\rm CCD}$ in bins of $\Delta(g - r) = 0.1$, shown as the filled squares in Figure 3.8. We fit a linear relation to these points , resulting in a corrected magnitude

$$g_{\rm corr}(J) = g_0(J) - 0.373 \times [g_0(J) - r_0(F)] + 0.177 \tag{3.2}$$

We apply this correction to both stars and galaxies, with the results shown in the right panels of Figure 3.8. The correction both removes the slope and reduces the scatter in the relations, as expected. Inspection of the corresponding data for $r(F)$ and $i(N)$ shows that no color terms are needed for those filters.

3.3.2 Photometric Accuracy

The errors in our photometry can be estimated in two ways. First, we compare the calibrated plate magnitudes from a set of plates with the corresponding CCD data. The results are shown in Figure 3.9. The 1σ errors for galaxies are $0.19^m, 0.23^m, 0.37^m$ at $m = 19.0$ in the g, r and i filters, respectively. Table 3.3 provides the average photometric errors for galaxies and stars as a function of magnitude for the three bandpasses.

Table 3.3: Plate Photometric Errors

		Calibrated Magnitude						
Band	**Class**	**17.0**	**18.0**	**18.5**	**19.0**	**19.5**	**20.0**	**20.5**
g	galaxy	0.31	0.22	0.19	0.19	0.21	0.28	0.33
g	star	0.20	0.18	0.18	0.19	0.18	0.21	0.26
r	galaxy	0.16	0.21	0.22	0.23	0.28	0.31	0.34
r	star	0.28	0.20	0.21	0.21	0.25	0.30	0.34
i	galaxy	0.21	0.29	0.35	0.37	0.40	0.43	0.43
i	star	0.31	0.31	0.33	0.37	0.38	0.38	0.35

This scatter is an accurate reflection of our accumulated errors. Because the CCD data cover many plates, and come from many independent nights, all sources of error are present in this calibration. This includes errors in the zero points of the CCD sequences, star/galaxy separation errors, inhomogeneities within individual plates, and errors in transforming all

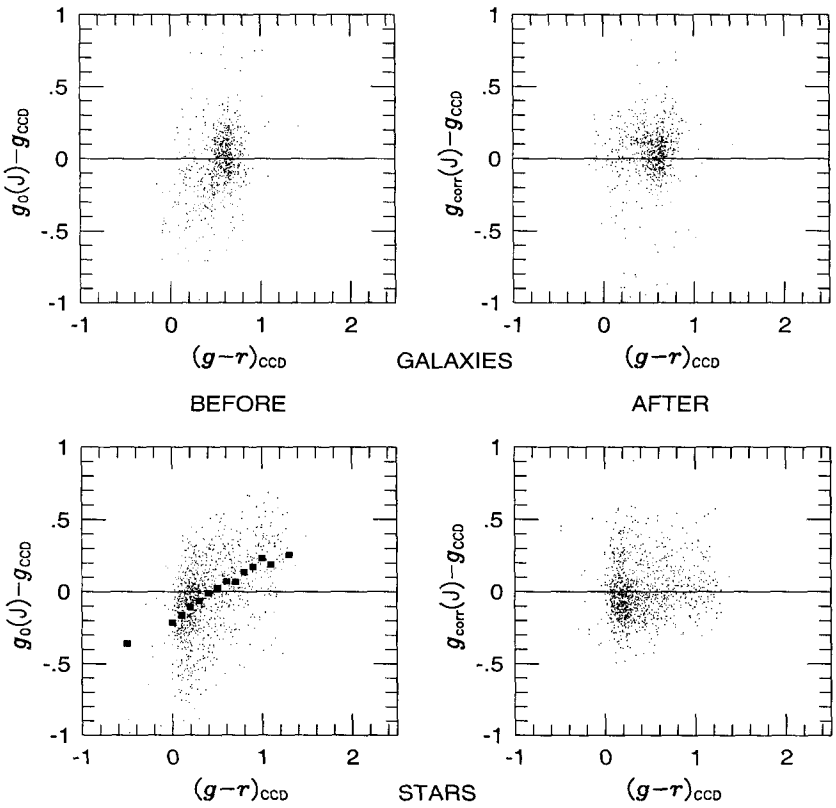

Figure 3.8: The difference between CCD and calibrated plate magnitudes, $(g(J) - g_{CCD})$, as a function of $g - r$ color, for galaxies (top) and stars (bottom), before and after a color correction has been applied. The filled squares show the median points used to derive the color correction.

the plates to the fiducial instrumental system. Although the scatter is larger than those typically reported in the literature, it is the true combination of all possible errors. There are no additional effects to model or theoretical considerations to account for. These errors can therefore be used in any future work with no modification.

The second test of photometric accuracy is a comparison of calibrated magnitudes from the overlap regions of two or more plates. This test is especially useful for examining possible pistoning between the individually calibrated nine plate areas. Unfortunately, this test reveals that areas with the smallest amount of CCD calibration have systematically incorrect photometry, especially at faint magnitude levels ($m_r = 19.5$). Zero-point offsets as high as 0.3^m are measured between neighboring 9-plate areas; the largest offsets are found where we have the least CCD calibration (as expected).

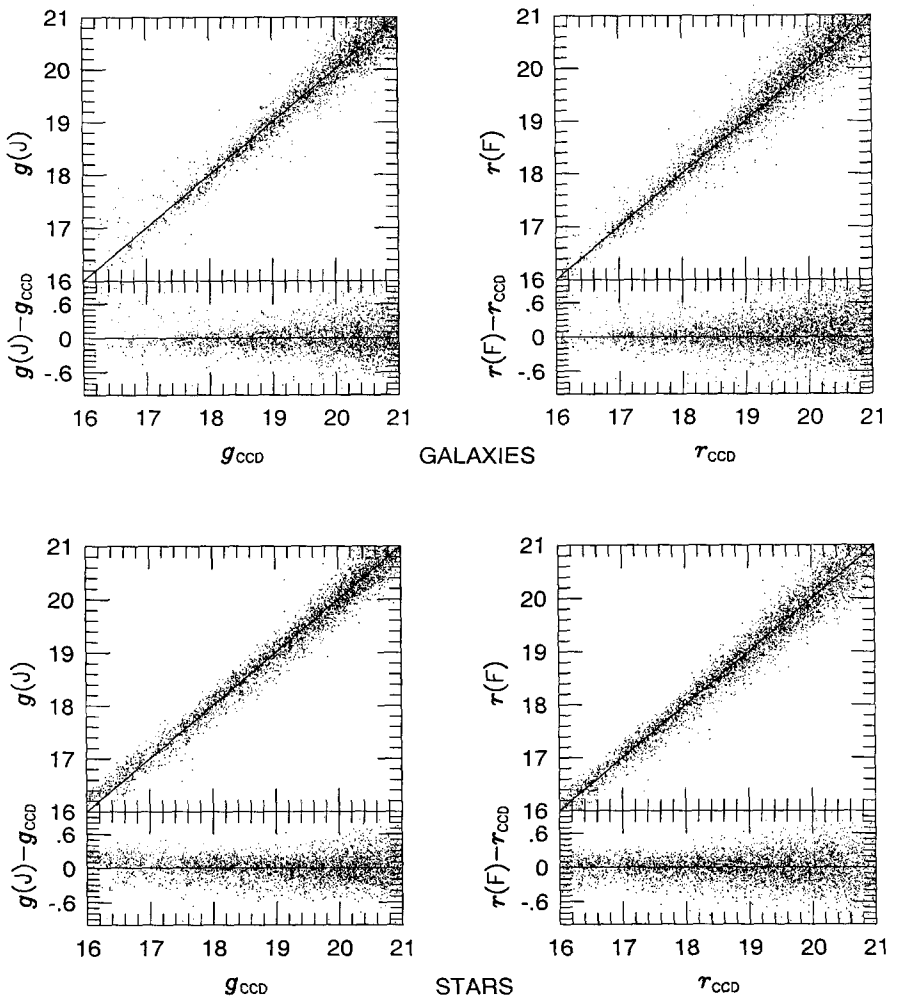

Figure 3.9: Comparison of the DPOSS g and r magnitudes derived from the transformation shown in Figure 3.7, *vs.* the corresponding CCD magnitudes, for galaxies (top) and stars (bottom).

This photometry problem precludes any measurements on large angular scales. We are currently attempting to address this issue in two ways. First, and simplest, we are obtaining more CCD calibration data in the most affected regions. Second, we are developing a different technique to derive photometric transformations. Briefly, every plate will be calibrated using CCD photometry from itself and the surrounding 15 plates (a 4×4 plate area). The plate overlaps are mapped as they have been for our current calibration, but rather than calibrating fixed sets of plates, each individual plate is calibrated. This provides two advantages over the current method: first, a much larger area (16 plates rather than 9) is used, so more CCD calibration is available; and second, because of the sliding calibration

area, there will be no sharp boundaries. Based on measurements from our current photometry, we anticipate that this method will provide calibration with offsets of less than 0.07^m between plates.

Chapter 4

Star-Galaxy Separation in DPOSS

For the preparation of a catalog of galaxy clusters, we must first produce a catalog of individual galaxies. Thus, star/galaxy classification is an issue of great importance for this project, as well as for most other scientific endeavors utilizing DPOSS. Here we describe the details of classification for the survey.[1]

4.1 Object Parameters for Classification

As described earlier, during plate processing a FOCAS analysis stage is run where each detected object is scaled in the intensity and spatial domains to best match a local PSF model. The outputs of this stage include two parameters describing the fit of each object to the PSF, *scale* and *frac*. In addition to *scale* and *frac*, the parameters utilized for refining star/galaxy separation are the total magnitude (*MTot*), the isophotal image area (*Area*), which is just the number of pixels constituting each object, the core magnitude (*MCore*), which is the integrated magnitude of the central 3×3 set of pixels in each image, and the second moment of the intensity-weighted radii of all pixels composing each image (*IR*2). As we shall discuss later, all of these photometric parameters are used in some magnitude range to perform star/galaxy classification.

The classical FOCAS approach using *scale* and *frac* rules is superior to more basic techniques in the regime of faint sources where density saturation is not an issue. However, for bright, compact sources (*i.e.*, stars with $g \leq 17$) the core saturation in DPOSS images is substantial, and two-dimensional PSF fitting alone is not applicable for image classification. Parameter spaces may be formed using photometric parameters like *Area*, *MTot*, *MCore*, and *IR*2 that provide substantial segregation between stellar and extended sources (*i.e.*, stars and galaxies), and this is used in SKICAT to provide bright object image classes via a set of parameter-based classification rules. Similarly, at faint magnitudes, the use of these

[1] A majority of this chapter is adapted from the article "Star-Galaxy Separation in DPOSS," Odewahn *et al.* 2001, *in prep.*

additional parameters in a set of classification rules can produce significantly improved results compared to FOCAS. The derivation of these rules, as well as the application of another such supervised learning approach, are reviewed briefly in the next section.

4.2 Classifier Induction

In the last two decades several different methods have been suggested for automatic object classification (*e.g.*, Sebok 1979, Heydon-Dumbleton *et al.* 1989, Odewahn *et al.* 1992, W95a). Modern classifiers use the non-parametric approach, where a set of classification rules is built based on examples of accurate classification (from deep CCD imaging, for example). The main advantage of such an approach is that the rules are created in an objective and reproducible way. One such technique, using decision trees and related methods, is presented in Fayyad 1991 and Fayyad & Irani 1990. Another approach is to use artificial neural networks to map sets of input image parameter vectors to output image classes. This method, applied to star/galaxy separation by Odewahn *et al.* 1992, has the advantage that quite complicated nonlinear mappings are able to solve complicated problems using even overlapping parameter spaces. This method lends itself well to work in the faint regime of photographic analysis where nonlinear effects and low S/N are profound.

4.2.1 Decision Trees and The Ruler System

The essence of the machine learning approach is to extract rules from a given dataset, consisting of a set of attributes, that can be applied to similar data. One of these methods is a decision tree (Quinlan 1986). For a given set of attributes this method creates nodes which represent tests applied to the attribute values. The outgoing branches of a node correspond to the possible outcomes of the test at the node. For a detailed discussion about decision tree methodology and its application to a restricted set of the DPOSS data, we refer the reader to W95a.

There are several algorithms for generating decision trees (Quinlan 1986, 1990). A basic problem with decision tree generation algorithms is the fact that even in a good tree there are leaves that are over-specialized or predict the wrong class. If there are measurement errors in the attributes, the decision tree will tend to fit to the noise and, hence, not generalize well to data that are out of the sample. In decision trees the data are partitioned

quickly into smaller subsets and this speeds up the learning process. At the same time this creates over-specialization of the leaves in the tree. The RULER system, used here in this paper, was designed to extract only the best rules from a set of multiple trees trained on the same data set.

4.2.2 Artificial Neural Networks

It is clear that one wishes to combine as much quantitative information as possible when assigning classifications. An artificial neural network (ANN), discussed by Rumelhardt & McClelland (1988), provides a means of mapping a large amount of input information defining a complicated nonlinear space to derive a best-guess classification. Neural networks are systems of weight vectors, whose component values are established through various machine learning algorithms, which take as input a linear set of pattern inputs and produce an output numerical pattern encoding a classification. This technique has been applied with great success to the problem of star/galaxy separation by Odewahn *et al.* (1992, 1993). In these studies, neural network classifiers were trained using the backpropagation algorithm. The networks consisted of an input node layer of image parameters, two hidden layers, and an output layer consisting of two nodes (a star node and a non-star node) for encoding the classifications. Systematic experiments were conducted to determine the optimum network architecture, weight-update parameters, and input image parameters (Odewahn & Nielsen 1995). Statistical comparisons of the ANN-classified photographic image surveys with more reliable (but less extensive) CCD surveys have proven this classification method to be very robust.

4.3 Classification Attributes

The input patterns fed to the ANN and DTREE classifiers just discussed consist, for DPOSS detections, of a set of FOCAS image parameters that have been shown to segregate the compact (star) and extended (galaxy) populations. In practice, we combine some of our parameters to produce single star/galaxy separation parameters. In one such case we calculate the difference between *MTot* and *MCore* to form a crude concentration index, *i.e.*, a single number that indicates the amount of flux contained in the central area of the image relative to the flux in the total area (the extrapolated isophotal area). An example of this

very effective parameter space is shown in Figure 4.1. The tight locus of points running in a roughly horizontal pattern across the plot is composed of stars. Compared to stars, extended objects have a smaller percentage of flux in the central 3×3 pixel area relative to the total area and thus produce a more negative value for *MTot-MCore*. Hence, the diffuse cloud of points extending below the stellar locus in Figure 4.1 at all magnitudes is attributed to galaxies. In a similar fashion, we have combined the FOCAS *scale* and *frac* parameters in a series of simple rules to form a single parameter that is linearly correlated with image compactness. This parameter is referred to as the composite stellar function (hereafter *csf*), and provides a simple way of using the *scale* and *frac* information for pattern classification. Decision trees are well adapted to discrete, irregular data spaces (like that produced in the *scale-frac* domain); however, ANN classifiers are best used with continuous, smoothly varying input parameters, and so we have opted to use the csf parameter as inputs for both the ANN and DTREE classifiers developed for DPOSS. The complete set of basic image parameters is summarized in Table 4.1.

Table 4.1: DPOSS Classification Attributes in J

Attribute	**Description**
MTotJ	Total FOCAS magnitude
MTotJ-MCoreJ	concentration index from FOCAS core magnitude
IR2J	intensity weighted second spatial moment
AreaJ	number of pixels above isophotal threshold
csfJ	linear composite of FOCAS *scale*, *frac* estimates
n_MTotJ-MCoreJ	stellar locus corrected *MTotJ-MCoreJ*
n_IR2J	stellar locus corrected *IR2J*
n_AreaJ	stellar locus corrected *AreaJ*
Class_ann_J	classification from ANN classifier
prob_ann_J	probability of ANN class estimate
Class_dtree_J	classification from DTREE classifier
prob_dtree_J	probability of DTREE class estimate

The classification-related image attributes in a DPOSS record are shown here for a J plate detection. Each of these attributes is also tabulated for F and N detected sources.

4.3.1 Plate-Dependent Image Parameter Variations

As discussed in Odewahn *et al.* (1993), the dominant source of error in the classification of images in Schmidt plate surveys derives from large systematic differences in the plate

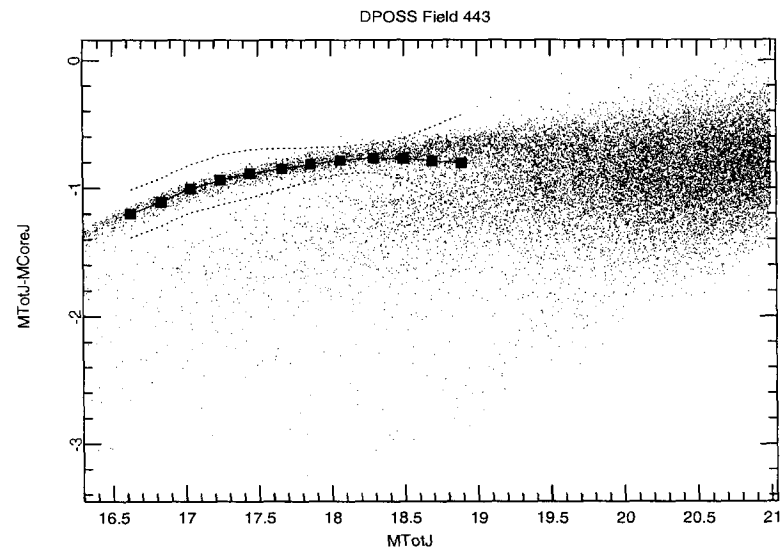

Figure 4.1: The *MTotJ-MCoreJ vs. MTotJ* parameter space from a single DPOSS J plate.

densitometry. These differences produce substantial variations in the shape and placement of the stellar loci for key classification parameter spaces. We have studied variations in stellar locus placement for all DPOSS image parameters useful for star/galaxy separation (*MTot-MCore*, *IR2*, *csf*, *Area*) for a large number of DPOSS fields in order to assess this problem. In Figure 4.2 we summarize one such study by showing the mean stellar loci in *MTot-MCore* on 25 different DPOSS J plates. We map the stellar locus in each parameter space using a robust median filtering technique in overlapping *MTot* bins (the x-axis of each parameter space). At faint levels (roughly $g \geq 19.5$), all differences between extended and compact images disappear, so to increase the contrast of the faint end stellar locus we have used a *csf* filter to isolate FOCAS-classified stars. In this way, we are able to better describe the properties of the faint stellar loci in the *MTot-MCore*, *IR2*, and *Area* parameter spaces. Having isolated each stellar locus in this manner, we can map the location and width of the locus as a function of magnitude, *MTot*. In the top panel of Figure 4.2 we show the mean loci, while in the bottom panel we plot the locus widths as a function of apparent magnitude for 25 different DPOSS plates. Locus width changes are relatively small, but the mean placement of the locus is highly plate dependent. For the development of a universal pattern classifier based on these image parameters, such plate-dependent variations must be removed prior to classification.

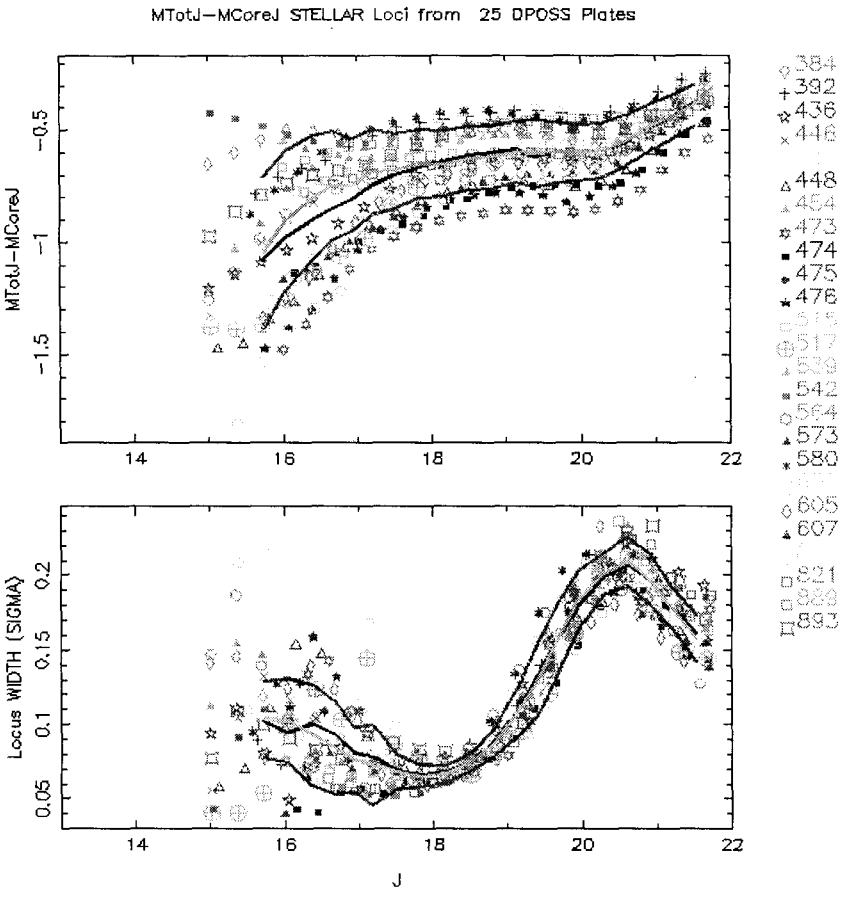

Figure 4.2: Mean stellar loci measured on 25 different DPOSS J plates.

One empirical way to remove these variations is to map the stellar locus in each parameter space and then subtract it, as a function of magnitude. For the DPOSS reductions, this procedure is performed for each footprint using a robust locus mapper for each classification parameter. An example of such a mean locus fit is plotted as the solid curve in Figure 4.1 for the *MTot-MCore* parameter space. Particularly bright sources ($MTot < 18$) are normally too rare in a single footprint to provide a useful locus map. To work around this problem, we create a set of plate-wide mean loci for each parameter. These loci are computed using many footprints covering the central portion of each field. Moreover, a graphical software package is used to guide the (human) DPOSS reducer in mapping and verifying each plate-wide mean locus. In addition to providing a more reliable fit to each stellar locus, this step insures that each important parameter space in each DPOSS plate catalog is inspected.

This quality control step has been extremely useful in identifying catalogs with previously undetected processing problems. Having subtracted the stellar locus from each parameter space on each plate, we are able to combine data from many different fields to formulate a training and testing data set for the ANN and DTREE pattern classifiers. An example of such a data set is summarized in Figure 4.3 using locus-subtracted *MTot-MCore* parameters from 31 different DPOSS F plates spread across many declinations and observing seasons. A stellar locus subtraction is applied to the *MTot-MCore*, *Area*, and *IR2* image parameters from the J, F, and N plate catalogs. No such normalization is required for the *csf* parameter, since the *scale* and *frac* values from FOCAS are estimated relative to the mean stellar PSF adopted for each plate. To denote these locus-corrected image parameters, we add the "*n_*" prefix to each parameter name (see Table 4.1).

4.3.2 A Source of High Confidence Image Classifications

As discussed in Chapter 3 and Gal *et al.* (2000b), we conducted a long-term CCD observing program with the Palomar 60″ to collect calibration and image classification material for DPOSS. Our initial classifier training/testing set comprised 79 CCD fields, located on 31 DPOSS fields (listed in Figure 4.3), to assign image classes to the objects measured in DPOSS. This provided a set of 14,370 training patterns (*i.e.*, detected sources with image parameters and classes). We also collected a totally independent classification quality assessment sample; a set of 14,304 patterns from 46 CCD fields located on a completely different set of 21 DPOSS fields. This quality assessment set was drawn from half the number of CCD fields as used in the initial training set sample, yet contains nearly the same number of objects. This is due to the slightly more stringent seeing and image class agreement criteria applied to the CCD catalogs when selecting the classifier training data (as explained below). Hence, only the highest quality image parameter sets were assembled for classifier development. These restrictions were relaxed in assembling the data set for a final quality check, both to increase the number of objects used, as well as to more faithfully reflect the properties of the average DPOSS plate and CCD material.

All CCD fields have quantitative mean seeing estimates for each of the three filters (*gri*), and we are able to grade the CCD fields by seeing quality. Seeing is measured on each image by computing the median FWHM of FOCAS-classed stars in a magnitude range of approximately $17.5 \leq g \leq 19.75$. This range was chosen to produce reliable star/galaxy

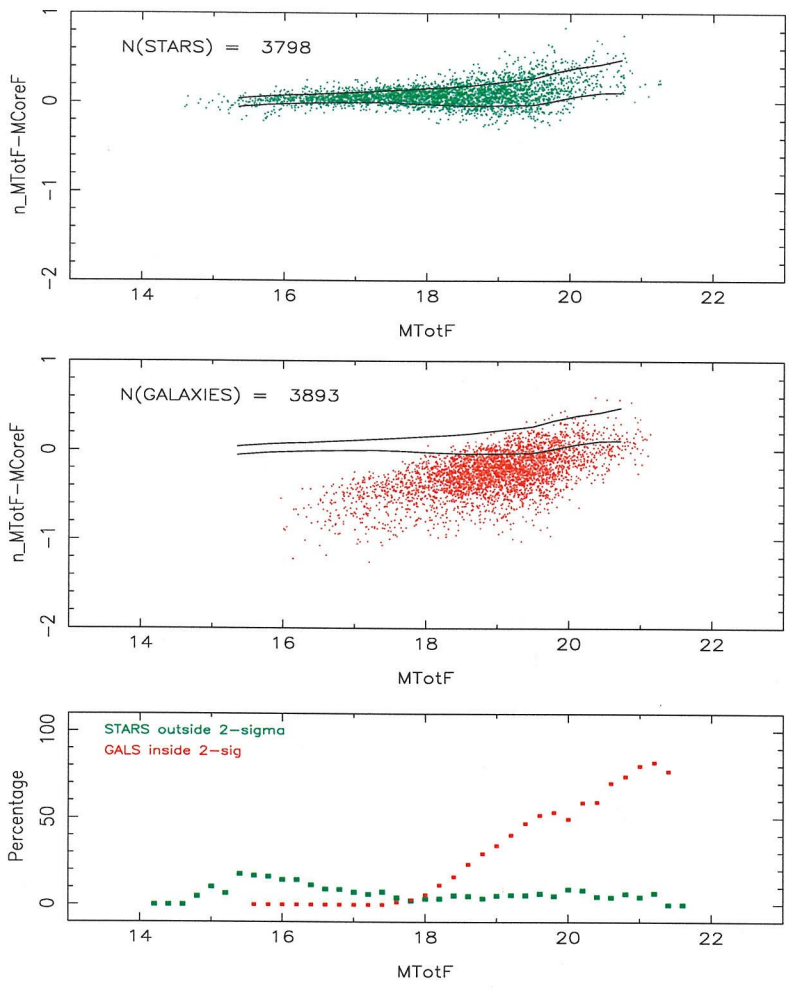

Figure 4.3: The *MTotF-MCoreF* DPOSS image parameter s̄pace, used as one of the inputs to the star/galaxy classifiers, with the stellar locus subtracted for each DPOSS plate.

separation and images with S/N high enough to allow accurate estimates of the FWHM. For the image classifications used in Figure 4.3, and for all of our training/testing data sets, we have selected only objects from CCD fields that have superior seeing.

These seeing estimates are confirmed by comparing the agreement between FOCAS estimated image classes in g, r, and i as a function of apparent magnitude. To measure classification quality, we fit a polynomial relation to the percentage agreement between comparisons of the $g-r$, $g-i$, and $r-i$ CCD FOCAS class pairs as function of magnitude. From these relations, we estimate the Gunn r magnitude at which the level of agreement falls below 90%. From a study of 100 Palomar 60″ CCD fields we found these class quality measures to be well correlated with our quantitative mean seeing estimates. The systematically better classification agreement to fainter magnitudes and smaller seeing measured in

the redder CCD bandpasses (r, i) also suggest that our classification quality measures are robust. These effects are expected for a ground-based survey using a CCD detector with a peak quantum efficiency around 7000Å.

Only CCD catalogs having a high classification agreement rating and superior seeing measures have been used to establish training and testing samples for the DPOSS image classifiers. In establishing the final image parameter training sets, we have applied one more constraint before assigning classifications to sources used in the initial training/testing set. Only objects having CCD classes that agree in the g, r, and i bandpasses are allowed into the classifier training data set. This seemingly heavy constraint was imposed to avoid one last problem involved with image misclassification in crowded regions. In heavily crowded parts of a CCD image, even under the best seeing conditions, FOCAS may be unable to assign a reliable image class. Under the assumption that image merging will be handled differently in different bandpasses, we reasoned that severe crowding problems would result in variations in class estimate for different bands. By taking only those sources with class agreement in g, r, and i, we avoid the bulk of such crowding-induced class mistakes. Following the application of this final quality constraint, we were left with approximately 7600 training patterns.

We should stress that the training and testing image parameter sets collected using this CCD database have been assembled in a rigorous, automated, well-defined way. These image parameters form a highly reliable "truth set" for the development of star/galaxy classifiers. This data set is summarized for our F-band training/testing material in Figure 4.4, where we plot locus-subtracted image parameters as a function of apparent magnitude for stars and galaxies for all of the relevant classification parameters.

4.4 Classification Results with Training and Testing Data

Using the testing/training data sets described in the previous section, we have trained ANN and DTREE star/galaxy classifiers in each of the 3 DPOSS bandpasses. The details of training supervised classifiers of these types are discussed in Odewahn 1997 (for ANNs) and Weir *et al.* 1995 (for DTREEs). Briefly, we use some fraction of the data sample as a training set. For both classifiers, an iterative training algorithm is used to establish the final classifier. In the case of an ANN, we use backpropagation training to adjust the

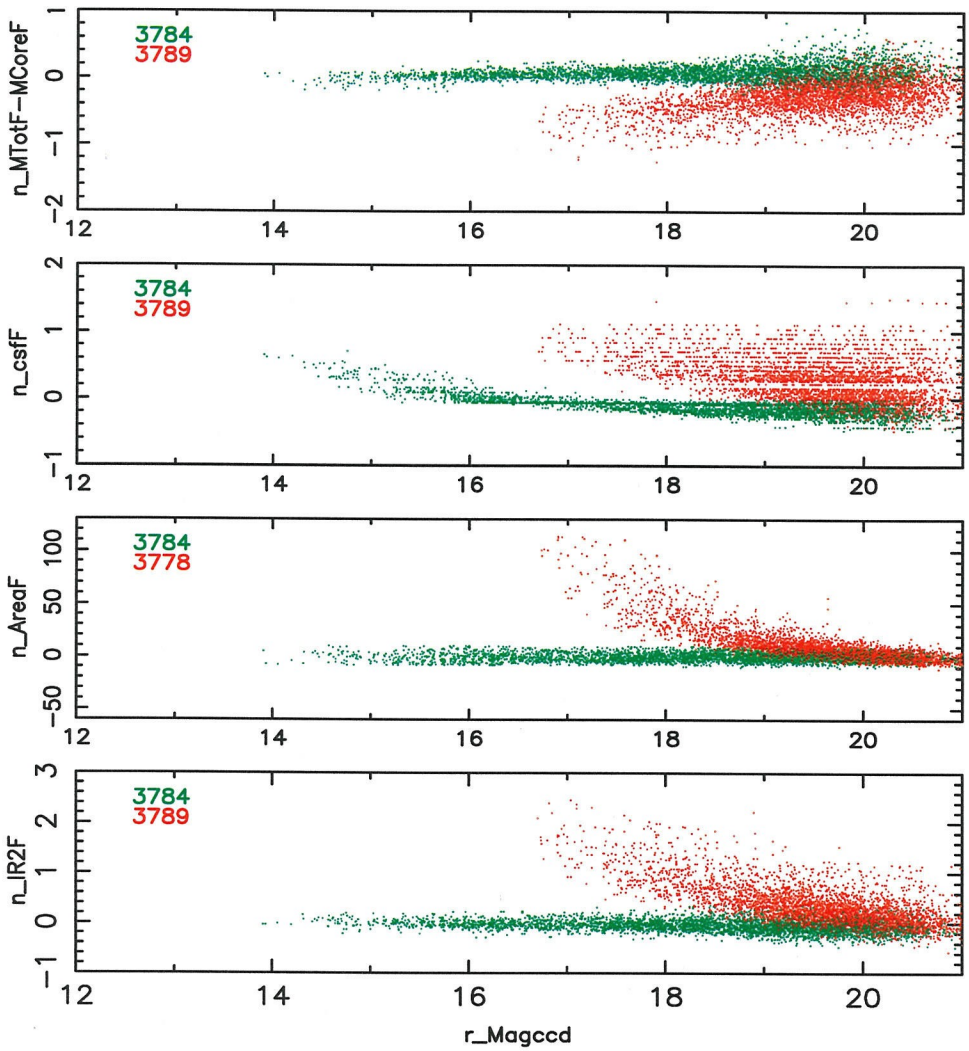

Figure 4.4: The image parameter spaces used as inputs for the ANN and DTREE pattern classifiers used for DPOSS star/galaxy separators. Green points are stars; red points are galaxies.

weight values in each node of the network to minimize the mean error function, which in this case is the difference between the network output pattern and the target pattern (determined by whether the object is a star or a galaxy). As discussed in Section 3.1, the DTREE code establishes a series of decision rules that map the input parameter sets to class memberships. These rules are gradually pruned in order to optimize the percentage of successful class outcomes.

For training both the ANN and DTREE classifiers, we used the following image parameters as classifier inputs for each bandpass: *MTot*, *n_MTot-MCore*, *n_IR2*, *n_Area*, and *n_csf*. We split the initial data set into training and testing samples by simply dividing the avail-

able data into stars and galaxies in a series of magnitude bins. Each set was then combined into two interleaved samples of stars and galaxies: one for training and one for testing. Some classifier builders support the notion that one should train a pattern classifier using training samples that have the same class frequency distribution as that expected when the classifier is used in classification mode. We view this as a risky prospect at best, especially in our own astronomical problem. The ratio of star to galaxy numbers will change systematically with galactic latitude, and this is in fact one of the very things we will measure in the completed DPOSS survey. By splitting the samples into roughly equal numbers of stars and galaxies in 0.5 magnitude bins spanning our range of interest, we avoid building in any classifier predisposition for class assignment on the basis of class frequency in the training sample.

At each step in the iterative training process for each classifier, we present the classifiers with the testing patterns to attain an independent assessment of classifier performance. Although our data sets are quite large, one can achieve an apparently high success rate for the training sample alone by overtraining. We used classification success rate statistics computed using only the testing data to guard against this. No changes to the ANN weights or the DTREE rules were applied on the basis of these test sample statistics. For each bandpass, we summarize in Table 4.2 the sample sizes, the magnitude range covered, and the overall success rates achieved for each classifier, using both the training and testing samples. A more meaningful assessment of classifier performance is shown in Figure 4.5, where we plot the percentage of successful classification as function of apparent *gri* magnitude. We used the following relations to compute the success rates for star and galaxy classification in each magnitude bin:

$$S_{star} = \frac{N(CCD = star \bigcap Plate = star)}{N(CCD = star)} \tag{4.1}$$

$$S_{gal} = \frac{N(CCD = gal \bigcap Plate = gal)}{N(CCD = gal)} \tag{4.2}$$

Table 4.2: DPOSS Classifier Training Statistics

Class	Band	N(stars)	N(gals)	S(Train)	S(Test)	Mag Range
ANN	J	1182	1182	92.3	92.1	$16.0 \leq g \leq 21.0$
DTREE	J	1182	1182	91.0	90.4	$16.0 \leq g \leq 21.0$
ANN	F	1188	1187	94.5	93.7	$16.0 \leq r \leq 20.5$
DTREE	F	1188	1187	94.9	92.9	$16.0 \leq r \leq 20.5$
ANN	N	918	918	92.5	93.4	$15.0 \leq r \leq 20.0$
ANN	N	918	918	94.0	91.4	$15.0 \leq r \leq 20.0$

4.4.1 Image Classification Probability Estimates

The ANN and DTREE image classifiers each produce, in addition to a "best guess" class estimate, a probability estimate which can be used to measure classification confidence. The node values in the output vector of an artificial neural network are in some sense the Bayesian *a posteriori* probability that the input vector is drawn from the class associated with that node (Richard & Lippmann 1991). The use of this probability as a measure of classification confidence in the star/galaxy separation problem is demonstrated in Odewahn (1995). Similarly, the decision tree classifier evaluates the probability that an output class assignment (averaged over all class conditions in the rules set) is due to chance. For both ANN and DTREE classifiers, we have renormalized these probabilities to be a number in the range 0.5 to 1.0, where values near 1.0 indicate a high degree of classification confidence and values near 0.5 indicate large uncertainty. As summarized in Table 4.1, we catalog the probability associated with the image class predicted by these two types of pattern classifiers.

4.5 More Stringent Assessments of Classification Quality

We have applied a series of checks to verify the quality of the final DPOSS image catalogs. On the basis of our estimated success rate functions derived during classifier training, we found little evidence for preferring one pattern classifier over the other. Indeed, the two methods appear to be very similar in quality and this would imply that our ability to estimate correct image classes is limited by the quality of the image parameters and not the pattern classification algorithm. To verify the quality of our final catalogs, we have

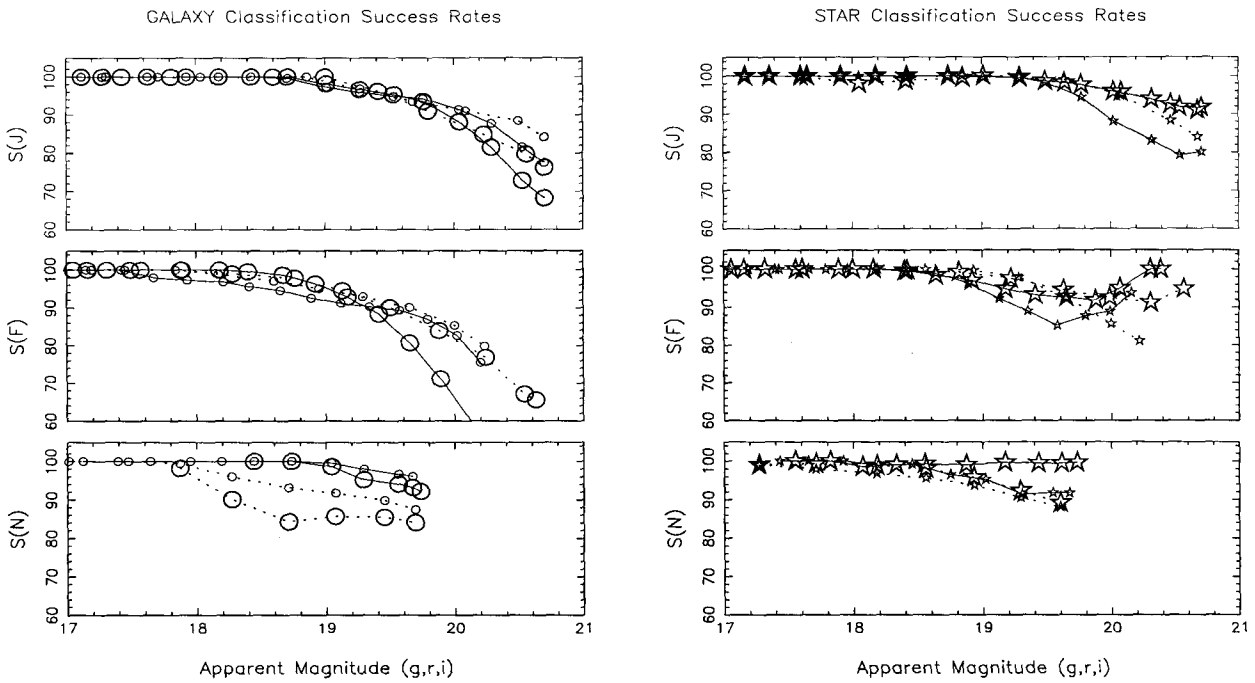

Figure 4.5: The ANN and DTREE classifier success rates as a function of apparent magnitude. Each panel represents a different set of bandpass-specific classifiers. Training data are connected with solid lines, and the independent test samples are connected with dashed lines. Galaxy relations are shown on the left, stars on the right.

conducted several verification exercises. These tests break down into two categories: (1) comparisons between image classifications from more than one plate for sources located in plate overlap zones, and (2) comparisons between DPOSS image classes and those from CCD images in DPOSS fields not used in classifier training. In the first case, we wish to confirm that classifier performance is consistent with that predicted by the success rate relations of Figure 4.5, and not severely degraded by optical distortions near the plate edges. In the second case, we use a completely independent test sample that excludes all of the DPOSS fields used in classifier training to confirm the success rate functions and to investigate the contamination of star/galaxy catalogs drawn from DPOSS.

4.5.1 Plate Overlap Comparisons

Following OA95, we perform a consistency check that is not limited by the availability of CCD calibration fields, and which involves a large number of sources. The spatially overlapping sections of neighboring plate catalogs are positionally cross-matched, and the

image classes assigned to each cross-matched source are then compared, as a function of DPOSS magnitude, in the same manner as the CCD test described above. In reality, this approach represents a significantly more rigorous comparison; in the CCD test, we can consider the much higher weight CCD samples to be essentially error free in the magnitude ranges where the tests are conducted. In the plate overlap analysis, we are comparing two class samples that are characterized by the same level of misclassification, and hence our errors added in quadrature will produce a roughly $\sqrt{2}$ increase in class comparison scatter. Additionally, this analysis is more subject to errors caused by positional cross-matching in crowded fields since we have no straightforward way of excluding such cases from the analysis. Finally, as discussed by Mahabal *et al.* 2001, photometric errors near the plate boundaries due to optical vignetting are significant. We expect classifier performance to degrade near the plate edges due to decreased relative S/N in the images for each magnitude bin used in our analysis, as well as possible optical distortions. On the other hand, we might consider this overlap analysis a worst-case assessment of the errors resulting from many different sources. These results, based on a large percentage of the catalogs, can be considered a good consistency check and an honest upper limit to the expected classification errors. In Figure 4.6 we summarize the results of our classification comparisons from 43 overlap zones in a 36 field area at the North Galactic Pole (NGP).

4.5.2 Classification Success Rates from CCD Comparisons

For a final DPOSS classification quality assessment, we cross-matched 46 P60 CCD catalogs on 21 DPOSS fields that were **not** used in classifier development. This procedure allowed us to gather a large testing set, with the advantage that we were testing DPOSS plate catalogs that were *in no way* involved in the development of the DTREE and ANN image classifiers. Using these CCD *gri* samples, we were able to rederive our classification success rate functions in each DPOSS bandpass. As with our initial classifier training sets, the ground truth classifications were those where the g, r, and i CCD classifications agreed. We stress that no data cleaning was applied (*i.e.*, no attempt was made to interactively reject outliers in classification parameter spaces) prior to calculating the success rate functions. Hence, this final analysis reflects more faithfully the quality of data samples drawn from a typical DPOSS catalog query. The success rates derived in this way are summarized in Figure 4.7. The J and F plate catalogs produce superior classification results compared

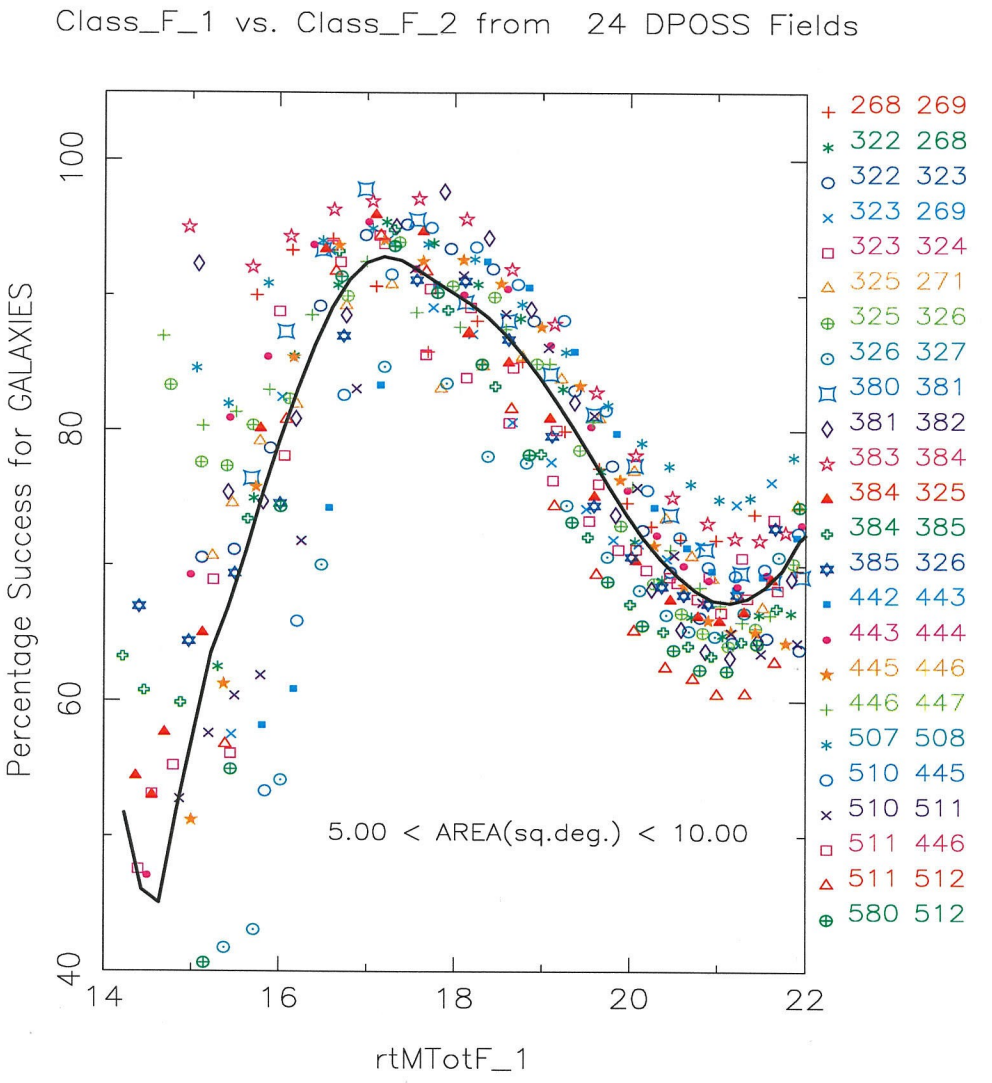

Figure 4.6: The percentage agreement in classification for galaxies in 36 overlapping regions of DPOSS plate pairs.

to the lower S/N and shallower N plate material. However, we rely exclusively on J and F classifications in our final catalogs (except for N-plate only detections), so the poor N performance is of no consequence.

4.5.3 Catalog Contamination Rates from CCD Comparisons

Since the surface density of stars varies strongly with galactic latitude, while the surface density of galaxies remains roughly constant, the contamination signal (*e.g.*, stars misclassified as galaxies) can vary greatly across the sky. Therefore, any single estimate of the contamination (as presented in Weir *et al.* 1995a, for instance) is insufficient. This is a

major, but solvable problem for many projects, and for *any* sky survey, yet it is seldom addressed with the care it requires.

In our analysis of the classification success, we also suffer from the opposite problem. Because most of our CCD imaging targets are Abell clusters, the relative frequency of galaxies compared to stars is higher than in the average field. Therefore, we will overestimate the contamination rate of true stars by galaxies misclassified as stars.

To alleviate this problem, we have compared the galaxy counts in our Abell CCD fields with those in some blank fields that were observed under the same conditions. As shown in Figure 4.8, we find that our Abell fields have approximately twice as many galaxies as those in blank fields that were observed under the same conditions, a trend that persists at all magnitudes of interest.

Based on this, we chose to apply a correction factor, β ($\approx 1/2$), to the stellar contamination rate (*i.e.*, we divide the rate of "false" galaxies by two), and increase the galaxy contamination rate by the same factor (since the number of real galaxies in a typical field will be half that in our CCD pointings).

Following Weir *et al.* 1995 we assess the contamination in magnitude bins for each classifier trained in each bandpass. Stellar contamination (misclassified galaxies contaminating stars) is given by

$$C_{star} = \frac{\beta N(CCD = star \bigcap Plate = gal)}{N(CCD = star)} \tag{4.3}$$

Galaxy contamination (misclassified stars contaminating galaxies) is given by

$$C_{gal} = \frac{N(CCD = gal \bigcap Plate = star)}{\beta N(CCD = gal)} \tag{4.4}$$

Galaxy catalog contamination functions estimated for each classifier are shown in Figure 4.9 where we plot percentage contamination as function of apparent magnitude. The contamination function is similarly dependent on the true density of contaminators on the sky, and hence the galaxy contamination function will be strongly dependent on galactic latitude. The sample of fields used for this exercise has $\langle b \rangle = 43°$. Strictly speaking, one must derive a contamination function for the range of b used to construct a given catalog. We include the functions shown in Figure 4.9 as a purely illustrative example.

In Figure 4.10 we show the distribution of stars and galaxies, as classified with DPOSS

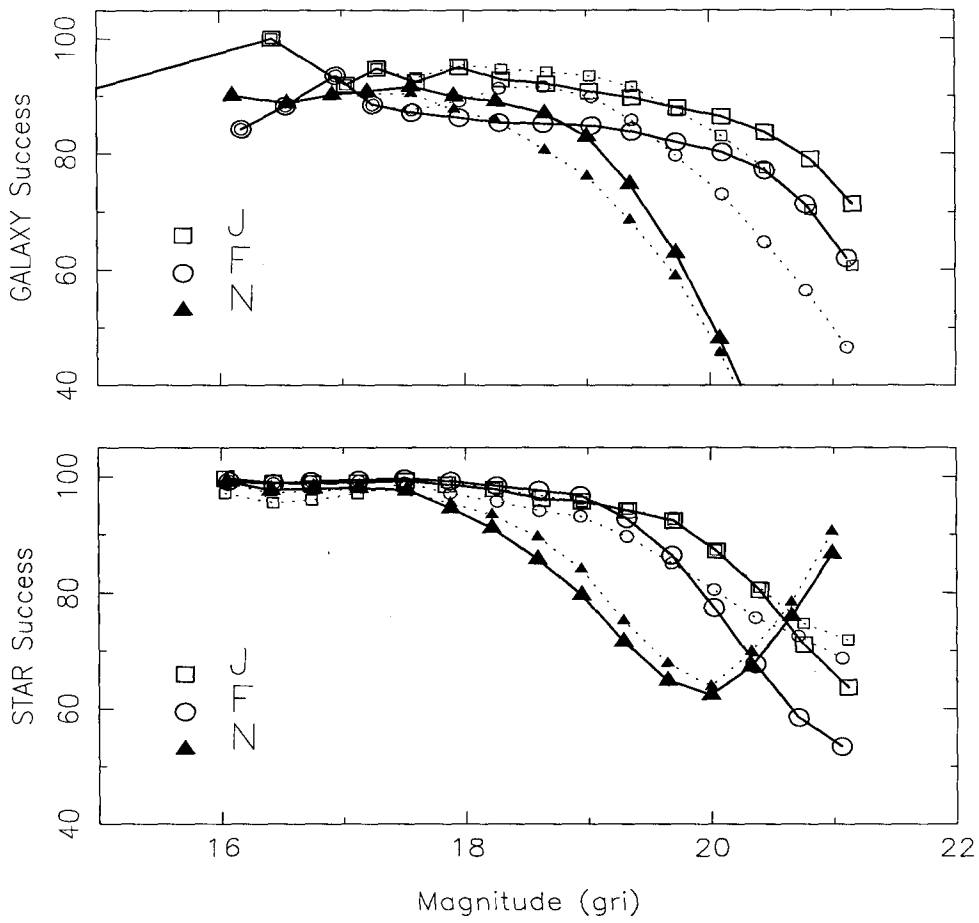

Figure 4.7: The agreement between DPOSS J, F, and N image classes and those derived from deep CCD images of the same objects, as a function of gri magnitude, for galaxies (top) and stars (bottom). In all panels we use solid lines to indicate ANN estimates, and dashed lines for DTREE estimates. The poor N performance (due to much lower S/N plate material) is of no consequence, since we utilize only J and F classes in our final catalogs.

classifiers described here, for two different faint magnitude cuts. Even as we approach our estimated 10% error level in classification quality at $r \approx 19.5$, we see little evidence for plate-dependent properties in the survey.

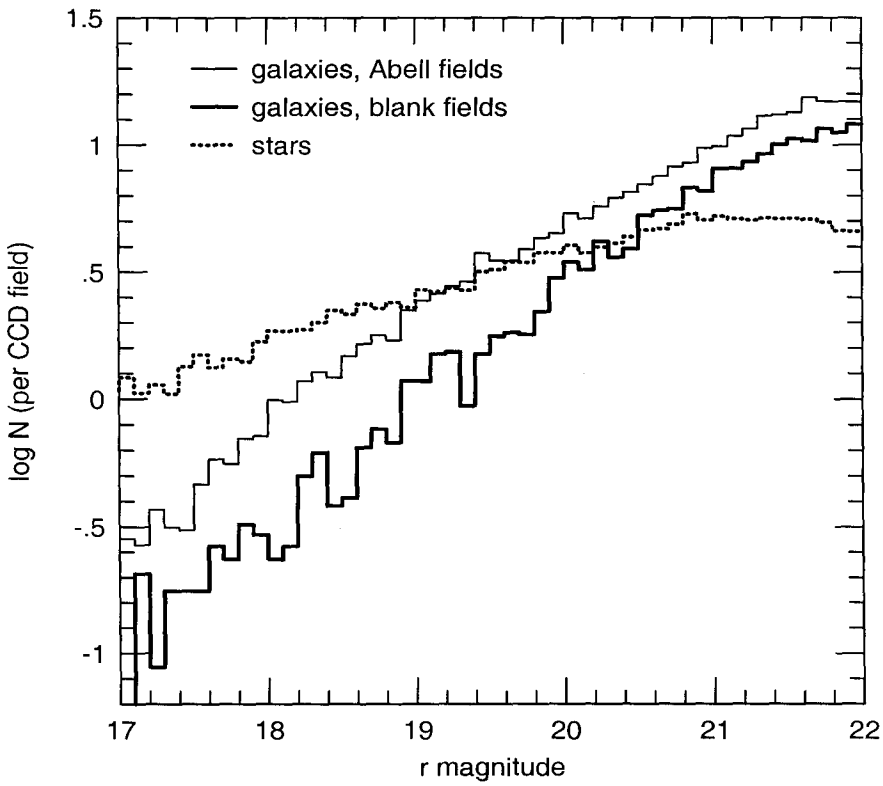

Figure 4.8: Star and galaxy number counts from the Palomar 60″ CCD fields.

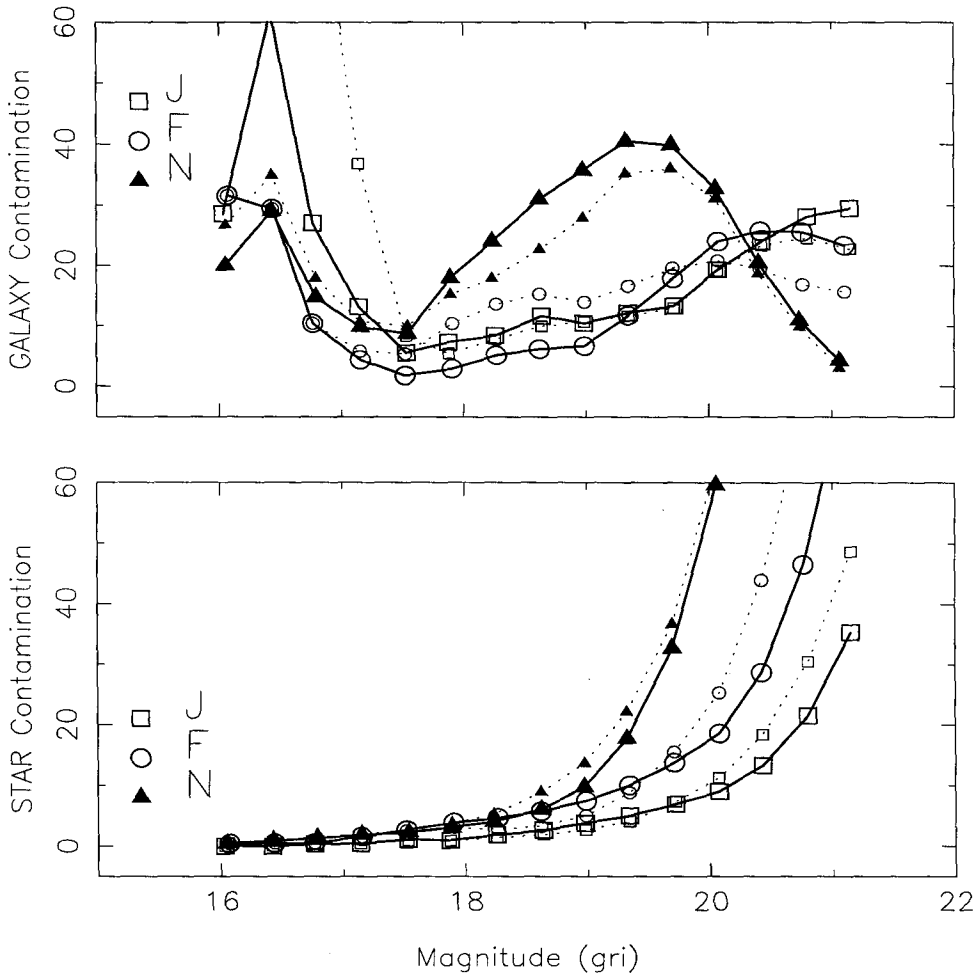

Figure 4.9: As a function of Gunn *gri* magnitudes we plot the percentage contamination in DPOSS J, F, and N image catalogs. As with Figure 4.7, ground truth image classes are those derived from FOCAS analysis of deep CCD images. In all panels we use solid lines to indicate ANN estimates, and dashed lines for DTREE estimates.

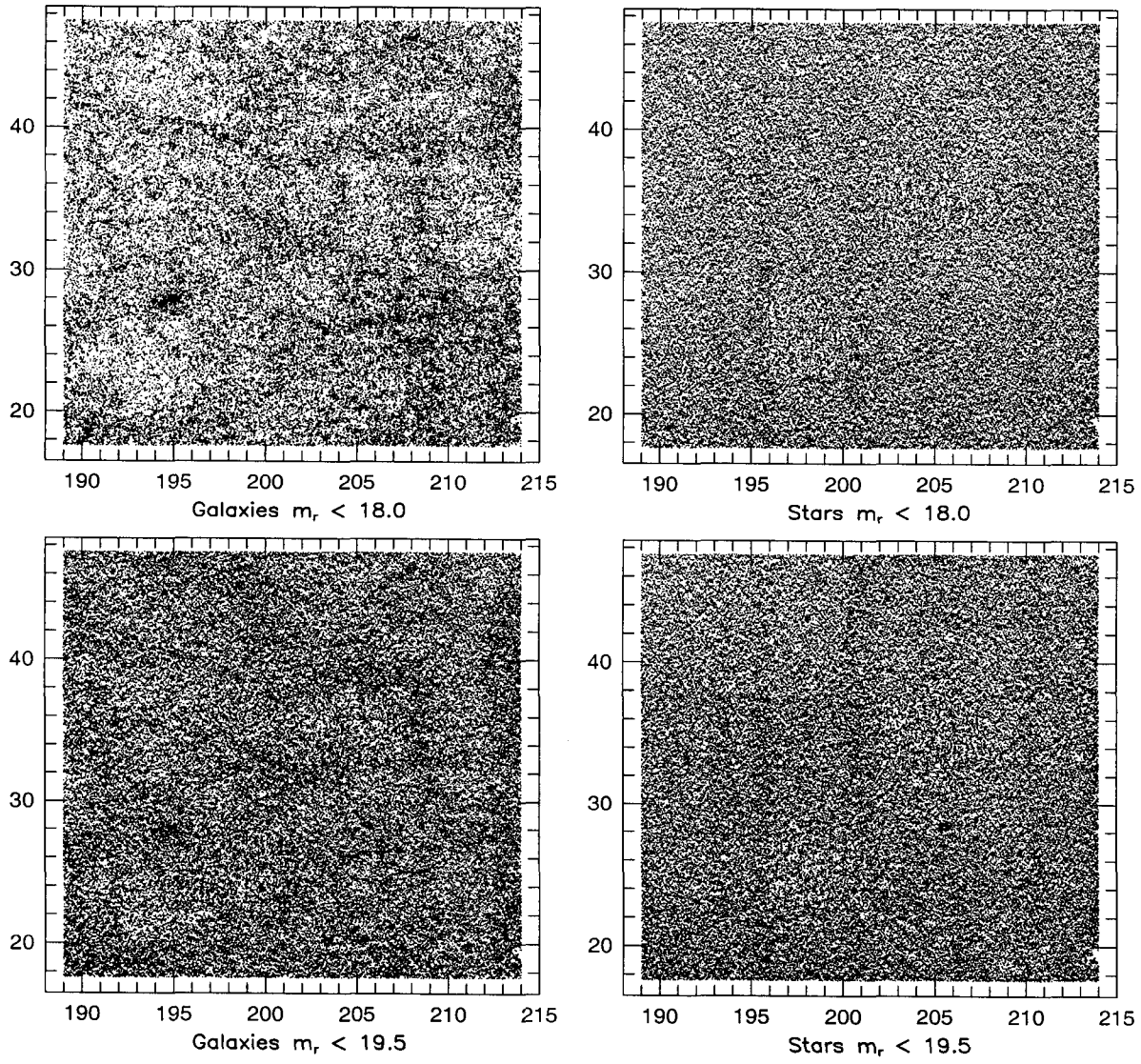

Figure 4.10: Results of a 36 field (1000□°) DPOSS survey of the NGP. In the top panels we plot all sources having $r \leq 18.0$, with galaxies on the left and stars on the right. The same is true for the bottom panels except we use $r \leq 19.5$.

Chapter 5

Creating the Cluster Catalog

Provided with a catalog of photometrically calibrated objects, which have been classified as galaxies, we are ready to detect galaxy clusters.[1] Point plots of the galaxy distributions in the 19 nine plate areas used in this thesis, along with the final contiguous areas from the North Galactic Pole (NGP) and South Galactic Pole (SGP), are provided in Appendix A.

5.1 Input DPOSS Data

For the cluster survey, we require a detection in both the J and F bands so we can measure at least one color. N-plate detections are not required because these plates are not as deep as the other two bands, and suffer from large plate sensitivity variations. In practice, however, the relatively bright r magnitude limit ($m_r = 20.0$) imposed to maintain accurate classification results in most objects ($\sim 98\%$) being detected in all three bands. Those areas on the plate containing saturated objects are masked. These areas often contain large numbers of falsely identified galaxies, as the plate processing software handles large, bright objects improperly. The masked areas, on average, cover 7% of the total area. Figure 5.1 shows the entire NGP area with the masked areas enclosed in boxes, while Figure 5.2 shows the same for the SGP area. These areas are not used in cluster detection.

5.1.1 Selecting Cluster Galaxies Using Colors

The morphology-density relation (Dressler 1980) has been observed in galaxy clusters at low redshift for nearly two decades. Late-type galaxies are dominant in the field population, whereas early-type galaxies are preferentially seen in high density regions. Therefore, any technique that can eliminate field (*i.e.*, late-type) galaxies on the basis of some simple observable parameter will enhance the contrast of galaxy clusters relative to the background.

[1] Portions of this chapter have appeared in Gal *et al.* 2000a.

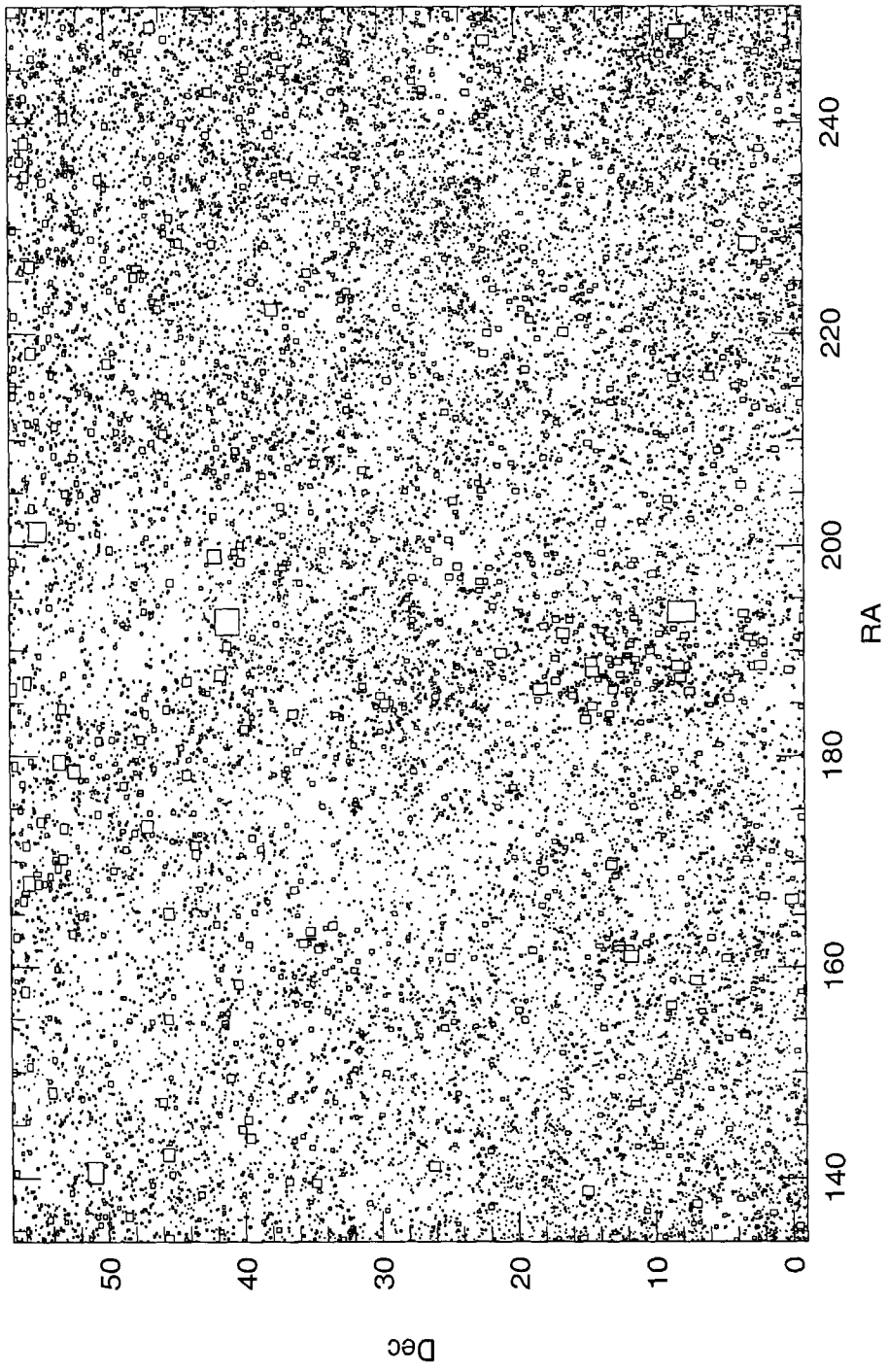

Figure 5.1: The areas masked in the NGP region due to saturated objects.

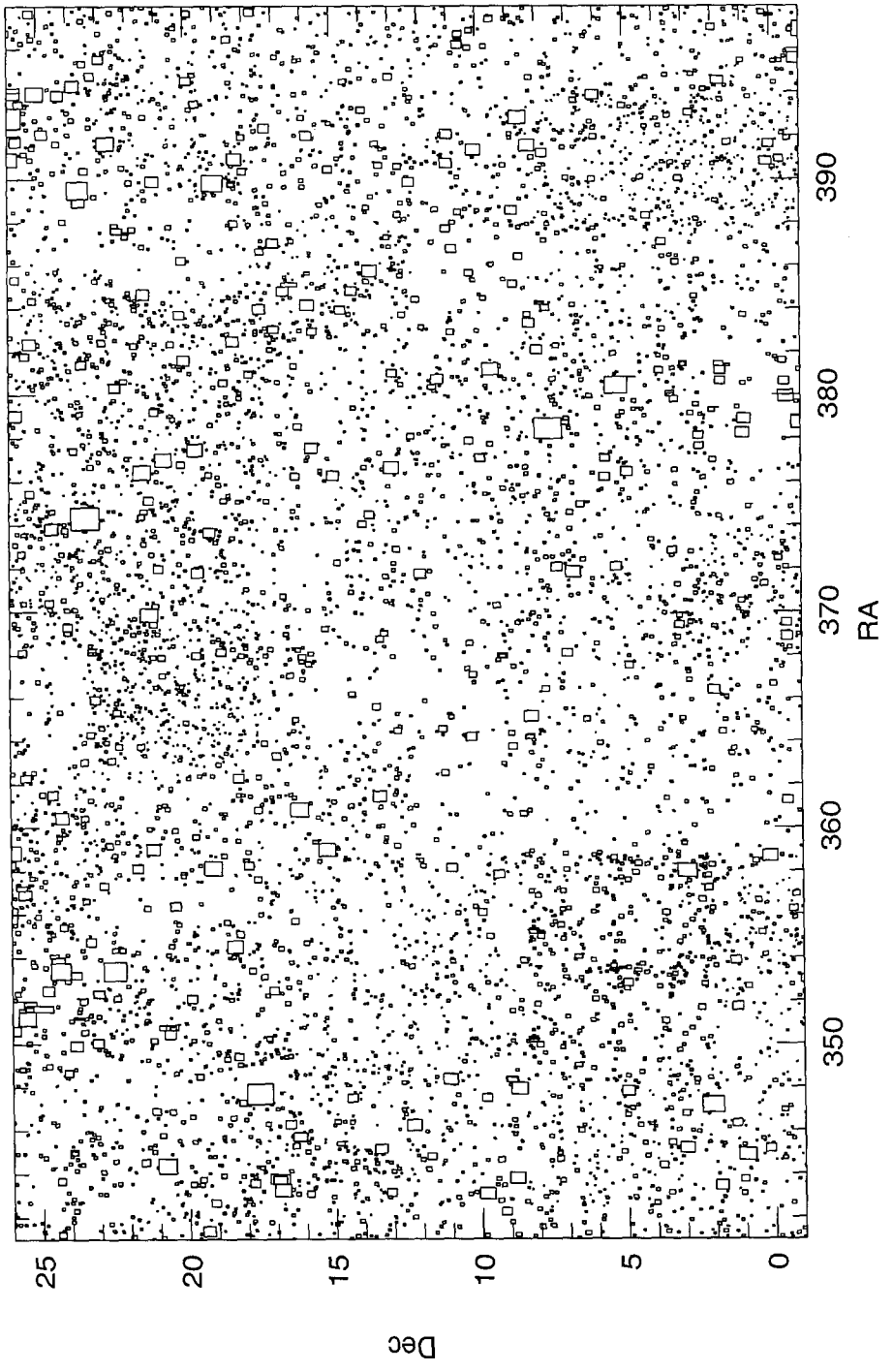

Figure 5.2: The areas masked in the SGP region due to saturated objects.

Dressler & Gunn (1992) presented photometric data for seven rich clusters. They show that cluster galaxies follow a well-defined sequence in the $(g-r)$ *vs.* $(r-i)$ color-color space, whereas field galaxies occupy a much larger area in this space. By defining a locus of "cluster galaxies", and using only those objects which satisfy this color criterion, it is possible to preferentially discard field galaxies from the sample. Such a procedure was utilized effectively by Odewahn & Aldering (1995) in their cluster detection program. The Palomar Distant Cluster Survey (Postman *et al.* 1995), using deep, multi-color CCD data, also employed colors to detect clusters and estimate their redshifts. However, no other large (all-sky), systematic cluster survey has been able to use color information for this purpose, as the data simply did not exist.

Figure 5.3 shows the $(g-r)$ *vs.* $(r-i)$ diagram for galaxies which are matched in the three plate catalogs (JFN) for Field 475. We use only objects classified as galaxies on the F plate with calibrated magnitudes $m_r < 20.0$, where our classification accuracy is $> 90\%$ (see Chapter 4). In practice, this imposes an approximate redshift limit of $z \sim 0.3$ on our cluster detection.

Initially, we defined a strict locus of cluster galaxies in the $(g-r)$ *vs.* $(r-i)$ space, similar to the prescription given by Dressler & Gunn (1992). However, inspection of our color-color diagrams shows that the i photometry is poor, resulting in large scatter in the $r-i$ color. We have therefore chosen to make color cuts in the $g-r$ space only. The chosen cuts in $g-r$ have two motivations. On the blue side, $(g-r) < 0.3$, we are excluding blue field galaxies at low z. On the red side, $(g-r) > 1.3$, we are excluding objects that have a high likelihood of being either misclassified stars, or at high redshift. These color limits are marked in Figure 5.3. Clearly, a significant fraction ($\sim 30\%$) of galaxies in our catalog lie outside our chosen $g-r$ range. We have also tested different color selection criteria, and find that only the lowest significance clusters, usually near the plate edges, are affected. In addition, the k-corrected no-evolution colors for both E and Scd galaxies are shown, for the redshift range $0.0 < z < 0.8$, for the Gunn filters used to calibrate the data. The differences between the actual plate filter/emulsion combination and the CCD filters used for calibration do not introduce any significant effects. The sharp turn in the k-correction curves occur at $z = 0.4$, where the 4000Å break passes from the g to the r band. We see clear evidence for the locus of cluster galaxies along the k-correction track for early-type galaxies, albeit with large scatter. From this figure, it is clear that we are seeing galaxies

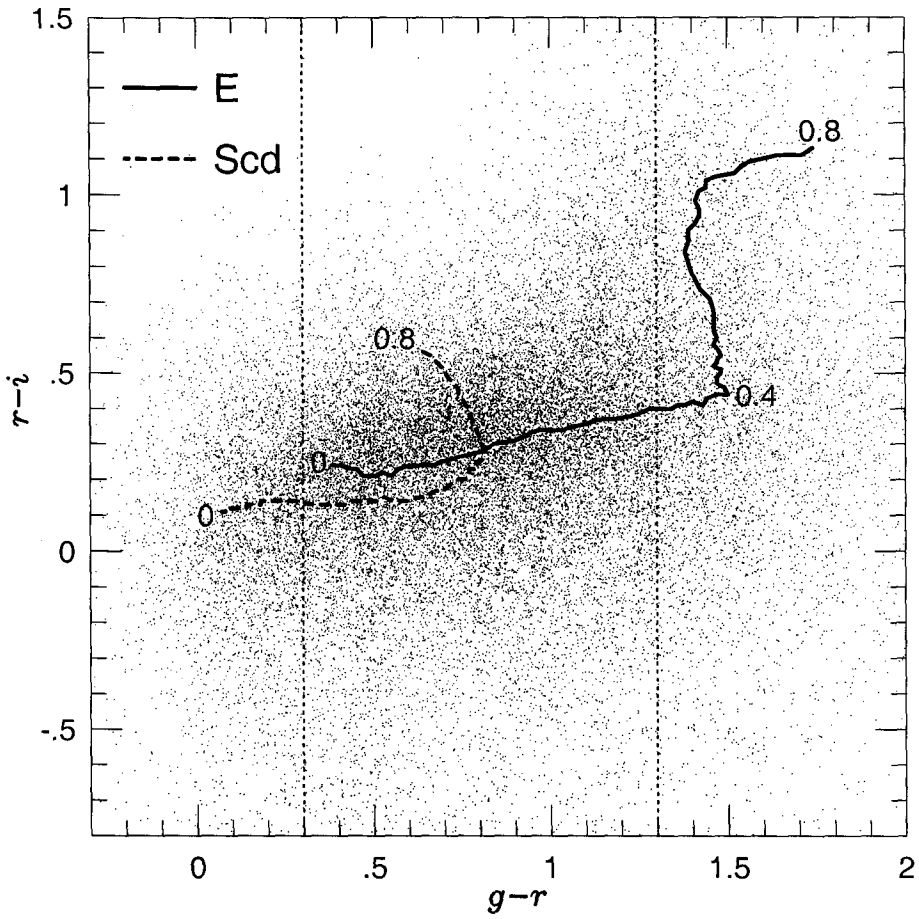

Figure 5.3: The $(g-r)$ *vs.* $(r-i)$ diagram for galaxies in Field 475. The k-correction curve for E galaxies is shown as the solid line, and for Scd galaxies as the dashed line, with some redshifts marked. The vertical dotted lines denote our color cuts, which enclose $\sim 70\%$ of the objects.

out to $z = 0.4$, although we are very incomplete above $z = 0.25-0.3$. This is not surprising, as an $L_\star$ early-type galaxy will have $m_r \sim 20$ at $z \sim 0.3$ for any reasonable cosmology.

For comparison, Figure 5.4 shows the results of a similar analysis of a number of Abell clusters imaged at the Palomar 60″ telescope. The cluster galaxy sequence is very well delineated, but is clearly truncated for $z > 0.2$, as is well known (ACO89).

Unfortunately, because there are areas where we have little or no CCD calibration data, we are currently unable to impose the limits described above. While they are appropriate for the two individual plates used for follow-up studies, we have been forced to relax the color criteria. For the time being, we are using limits of $0.0 < g-r < 1.6$. Additionally, while we have created a cluster catalog for objects with $m_r < 20$, here we report only a catalog

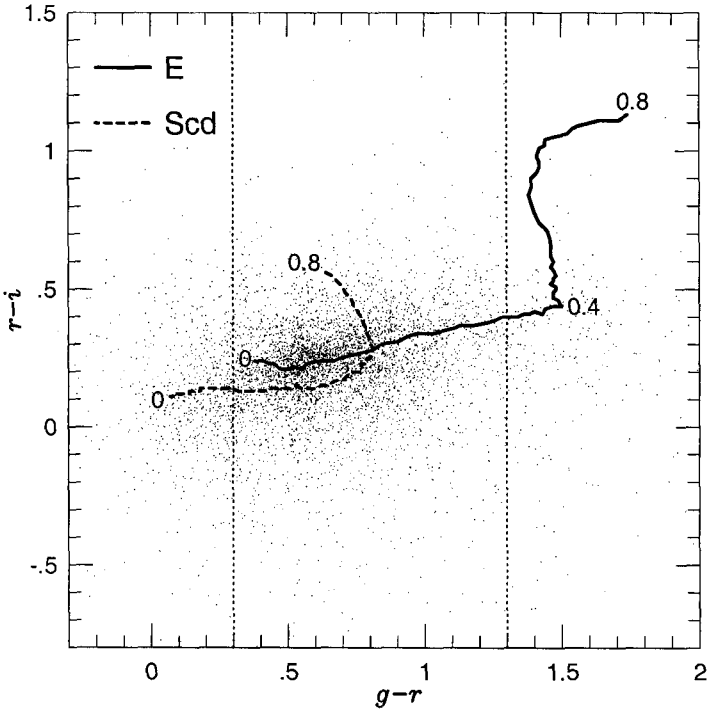

Figure 5.4: The $(g-r)$ *vs.* $(r-i)$ diagram for galaxies in Abell clusters observed at the Palomar 60″ telescope. The k-correction tracks from Figure 5.3 are shown for comparison.

utilizing objects with $m_r < 19.5$. This is approximately one-half magnitude fainter than the limit imposed by the APM survey. The use of such a magnitude limit by the APM may be reflective of their experience with the difficulty of calibration at fainter magnitudes. Nevertheless, as we anticipate the acquisition of further CCD data, we will generate a larger cluster catalog, utilizing more stringent color criteria and fainter galaxies. Additionally, we have imposed somewhat more stringent limits on the area used for cluster detection, to avoid areas of poor calibration, high extinction and contamination by misclassified stars. We have also excised certain individual plates which exhibited unusual photometric properties during the calibration process. The current areas mapped therefore have unusual geometries; we show the layout of plates for the final NGP area in Figure 5.5.

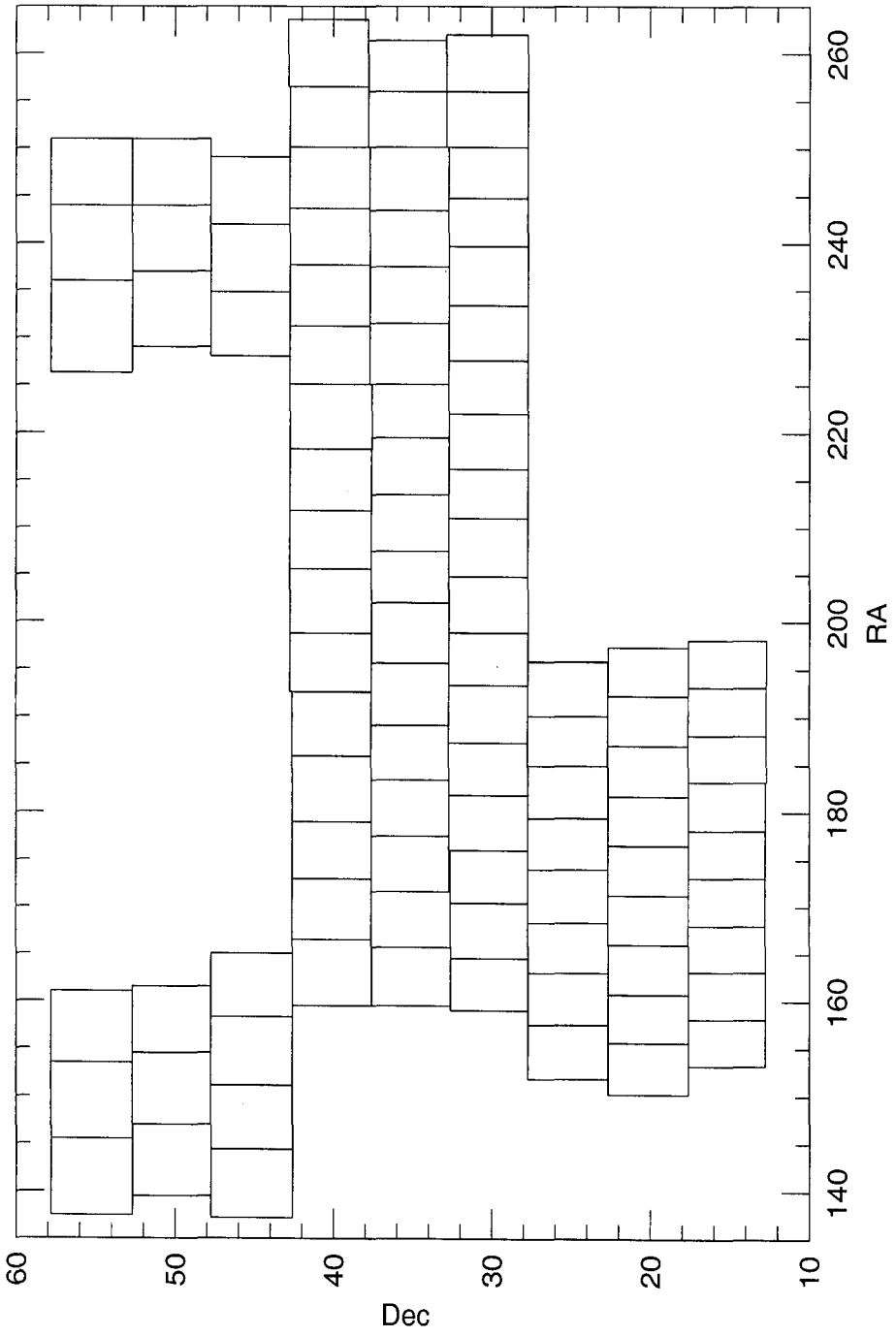

Figure 5.5: The distribution of well-calibrated plates used for cluster detection in the NGP region.

5.2 Galaxy Density Maps and Cluster Detection

5.2.1 Density and Significance Maps

Once a catalog of galaxies meeting our classification, magnitude, and color criteria has been created, we proceed to detecting candidate clusters. First, we linearize the coordinates of individual galaxies using an equal-area projection. For generating the galaxy density field, we use the Adaptive Kernel (AK) technique (Silverman 1986), detailed below. This technique possesses many advantages over methods used by other surveys. First, the two-step process significantly smoothes the low density regions, without affecting the high density peaks. The smaller kernel size at high density means that multiple clusters in high density regions (*e.g.*, filaments) are still separated. The AK may be more robust than percolation or friends-of-friends algorithms, which can link clusters in regions of high galaxy density, since they employ a fixed linking length. Second, the AK is model-independent; it does not require an assumed luminosity function or radial profile for the cluster, as did the matched filter of the PDCS. With our plate data, the range in magnitude covered is small ($16 \leq m_r \leq 19.5$), so that fitting a luminosity function is a precarious endeavor. More importantly, perhaps, visual inspection of our candidate clusters shows that many (perhaps most) do not appear symmetric, so that any radially symmetric profile, assumed by some techniques like the matched filter (Postman *et al.* 1996), may produce biased results (although there is some evidence that this may not be true). We are attempting to avoid any bias towards rich, relaxed, evolved clusters (which may also occur if clusters are selected from X-ray surveys). This results in a catalog in which some clusters will likely have different physical properties than those discovered by other techniques and at other wavelengths.

The adaptive kernel uses a two-stage process to produce a density map. First, at each point t, it produces a pilot estimate $f(t)$ of the galaxy density. We use a fixed Epanechnikov kernel,

$$K(t) = \begin{cases} \frac{3}{4\sqrt{5}}\left(1 - \frac{1}{5}t^2\right) & -\sqrt{5} \leq t \leq \sqrt{5}; \\ 0 & \text{otherwise.} \end{cases} \tag{5.1}$$

of $7.5'$ width. Based on this pilot estimate, it then applies a smoothing kernel whose size changes as a function of the local density, with a smaller kernel at higher density. This is

achieved by defining a *local bandwidth factor*:

$$\lambda_i = [f(t)/g]^{-\alpha}, \tag{5.2}$$

where g is the geometric mean of $f(t)$. We use a sensitivity parameter $\alpha = 0.5$, which results in a minimally biased final density estimate, and is simultaneously more sensitive to local density variations than a fixed-width kernel (Silverman 1986). This is then used to construct the adaptive kernel estimate:

$$\hat{f}(t) = n^{-1} \sum_{i=1}^{n} h^{-2} \lambda_i^{-2} K\{h^{-2} \lambda_i^{-2} (t - X_i)\} \tag{5.3}$$

where h is the bandwidth. The choice of bandwidth is discussed below.

Our density maps are created using $1'$ pixels, resulting in a final map size of 360×360 pixels for individual plates; the maps for the large, contiguous areas are of course much bigger. This pixel size maintains a reasonable number of galaxies per pixel, while keeping a significant number of pixels per smoothing kernel, and the output maps, at a modest size. Changes in pixel size do not effect the final catalog significantly; the area required for a cluster to be detected can be scaled appropriately. The kernel itself has a bandwidth comparable to half of the Abell radius of a cluster at $z \sim 0.15$, which is expected to be the median redshift of our cluster candidates. This combination of pixel size and bandwidth prevents us from over-resolving clusters into structural components, while maintaining a reasonable number of galaxies per pixel. Previous surveys, including the APM, have suggested that larger kernels become inefficient for cluster detection. Once a density map has been constructed, we use the *bootstrap* technique (Press *et al.* 1992) to build a significance map. This technique uses the input data set, $C^S_{(0)}$, containing N points, to generate synthetic data sets $C^S_{(1)}$, $C^S_{(2)}$, ... with the same number of points N as the input set. These N points are selected at random from the input set, with replacement. This means that the same point can be selected more than once for each synthetic data set. We generate 200 synthetic data sets, each resulting in a density map $D^S_i(j,k)$, with map number $i = 1, 200$ and pixels $j, k = 1, 360$. We define a mean map, $\mathcal{M}$, as:

$$\mathcal{M}(j,k) = \frac{1}{200} \sum_{i=1}^{200} D^S_i(j,k) \tag{5.4}$$

and an analogous map $\mathcal{M}2$:

$$\mathcal{M}2(j,k) = \frac{1}{200}\sum_{i=1}^{200}[D_i^S(j,k)]^2 \tag{5.5}$$

From these, we form a final significance map $\mathcal{S}$:

$$\mathcal{S}(j,k) = \mathcal{M}(j,k) - 3(\mathcal{M}^2(j,k) - \mathcal{M}2(j,k))^{\frac{1}{2}} \tag{5.6}$$

To quantify the robustness of our cluster candidates, we generate six density maps, with slightly different kernel sizes, and different magnitude limits. We use catalogs limited at $m_r = 19.0$ and $m_r = 19.5$, and kernels with widths of $420'', 450''$, and $480''$. For the time being, we have restricted our density maps to only those nine plate regions with adequate photometric calibration. The final density maps for the NGP and SGP regions, using the $450''$ kernel, and a limiting magnitude of $m_r = 19.0$, are shown in Figures 5.6 and 5.7. Every dark speck in the maps is a candidate galaxy cluster.

5.2.2 Selecting Cluster Candidates

The six density maps constructed using the various kernel sizes and magnitude limits are then used to identify peaks in the galaxy distribution, which we mark as candidate galaxy clusters. We utilize SExtractor (Bertin & Arnout 1996) to detect enhancements with a minimum area of ~ 15 pixels with $\geq 1.8\sigma_F$ significance, where σ_F is the rms of the background in the density map. The exact minimum area used for detection is scaled to account for the varying kernel width. In practice, this is a very liberal detection threshold, in the sense that we accept a larger number of possibly false detections in return for enhanced completeness both at higher redshift and lower richness. Finally, we have set the deblending threshold at 0.007; while there is no physical basis for choosing this value, we found it to produce reasonable results through visual inspection of the catalogs produced with different settings.

The resulting catalogs from the six separate density maps in each area are then cross-correlated. Candidates within $7'$ of each other in any pair of maps are considered matched. We build a list of candidates identified in n maps, with $1 \leq n \leq 6$. Candidates found in all 6 maps are considered extremely robust. This yields 5,987 robust candidate clusters in the 96-plate NGP area, and 2,826 candidates in the 68-plate SGP area.

Figure 5.6: The adaptive kernel density map for the NGP region, for galaxies with $m_r < 19$.

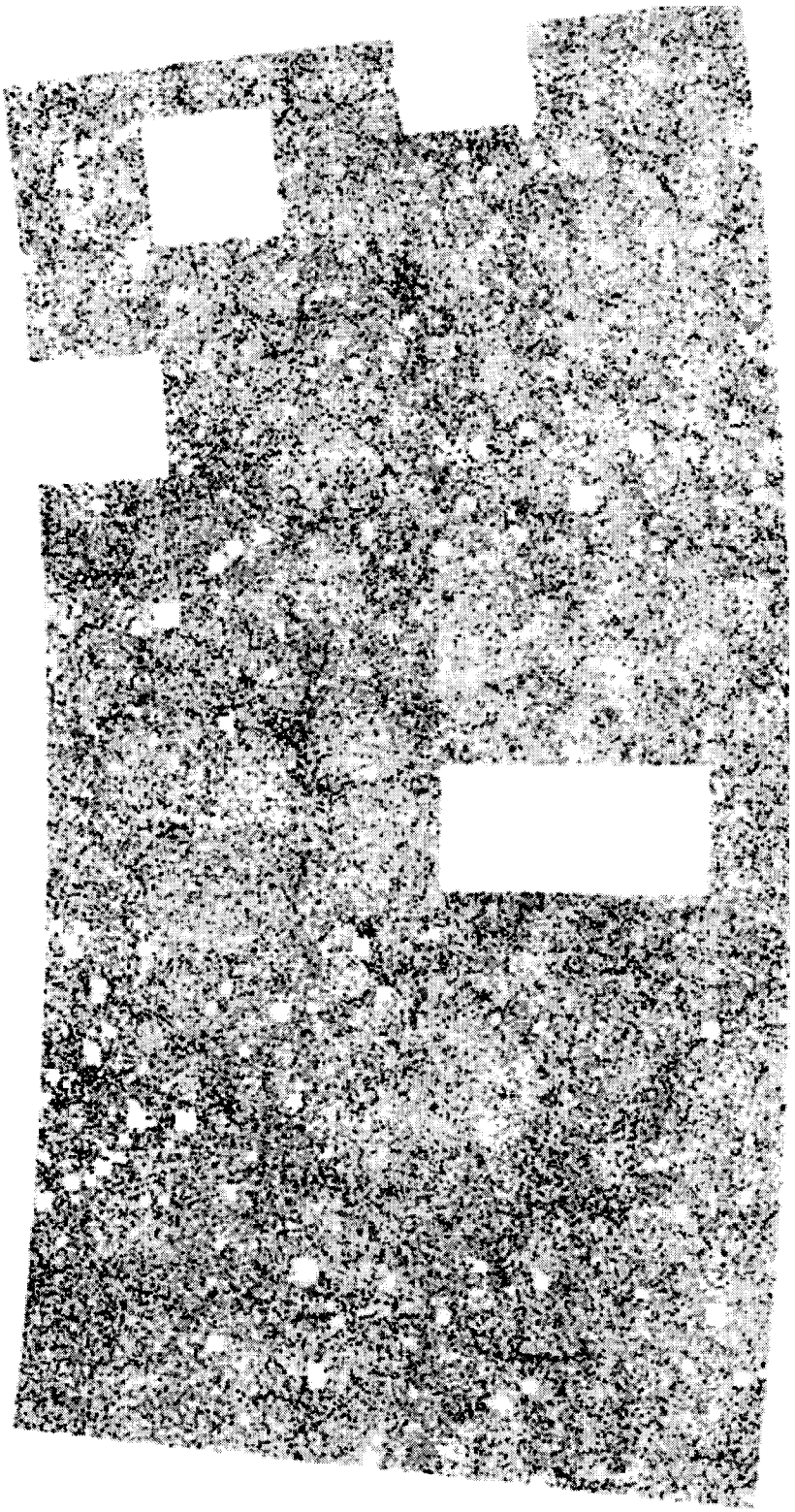

Figure 5.7: The adaptive kernel density map for the SGP region for galaxies with $m_r < 19$.

Additionally, there are a large number of candidates detected in all three $m_r < 19$ maps, or all three $m_r < 19.5$ maps, but not in all six maps. This is likely due to a combination of effects. The brighter catalog has lower photometric errors, and fewer objects, reducing the *rms* scatter in the pixel-to-pixel values in the density maps. Thus, weaker density enhancements may be detected. The fainter catalog, on the other hand, is likely to pick up more clusters at higher redshifts.

In Figure 5.8 we demonstrate the effect of varying the magnitude limit and kernel size on a $12^\circ \times 12^\circ$ area from the NGP density map. Maps on the left are for a catalog with $m_r < 19$, and on the right for $m_r < 19.5$. The upper maps use a kernel of $450''$ width, the middle maps $420''$, and the lower maps $480''$. While changing the kernel size does not produce significant changes, varying the depth of the catalog produces large numbers of new peaks in the deeper maps, as expected.

Figure 5.9 shows an expanded view of the upper left map from Figure 5.8 (constructed using galaxies with $m_r < 19.5$ and the $450''$ kernel). Each detected cluster is now marked with a circle of $6'$ radius ($\sim 0.75 \times R_{Abell}$ at $z = 0.15$). Blue circles are robust candidates, appearing in all six density maps. Red circles mark candidates appearing in five maps, yellow are in four maps, green in the three $m_r < 19$ maps, and magenta in the three $m_r < 19.5$ maps. To quantify our false detection rate (which may be large at low significance), we have undertaken a spectroscopic follow-up campaign to measure redshifts for all cluster candidates in two single sky survey plate areas. The results of the spectroscopy, as well as follow-up CCD imaging of the same candidates, are presented in the next chapter.

After detection, some simple properties (such as size and ellipticity) of the clusters are measured from the original density map. Properties of the galaxy population of each cluster (photometric redshift and richness, described in Chapter 7) are derived from the DPOSS galaxy catalogs. This helps eliminate spurious detections, and allows us to compare our catalog with pre-existing catalogs.

In Tables B.1 and B.2 we provide the relevant information for the robust cluster candidates for the NGP and SGP regions. Column (1) gives the name of the candidate; columns (2) and (3) show the right ascension and declination for J2000.0; column (4) shows the redshift estimated from our photometric technique (see Chapter 7); column (5) provides a background-corrected galaxy count within an Abell radius, and column (6) identifies which are Abell clusters.

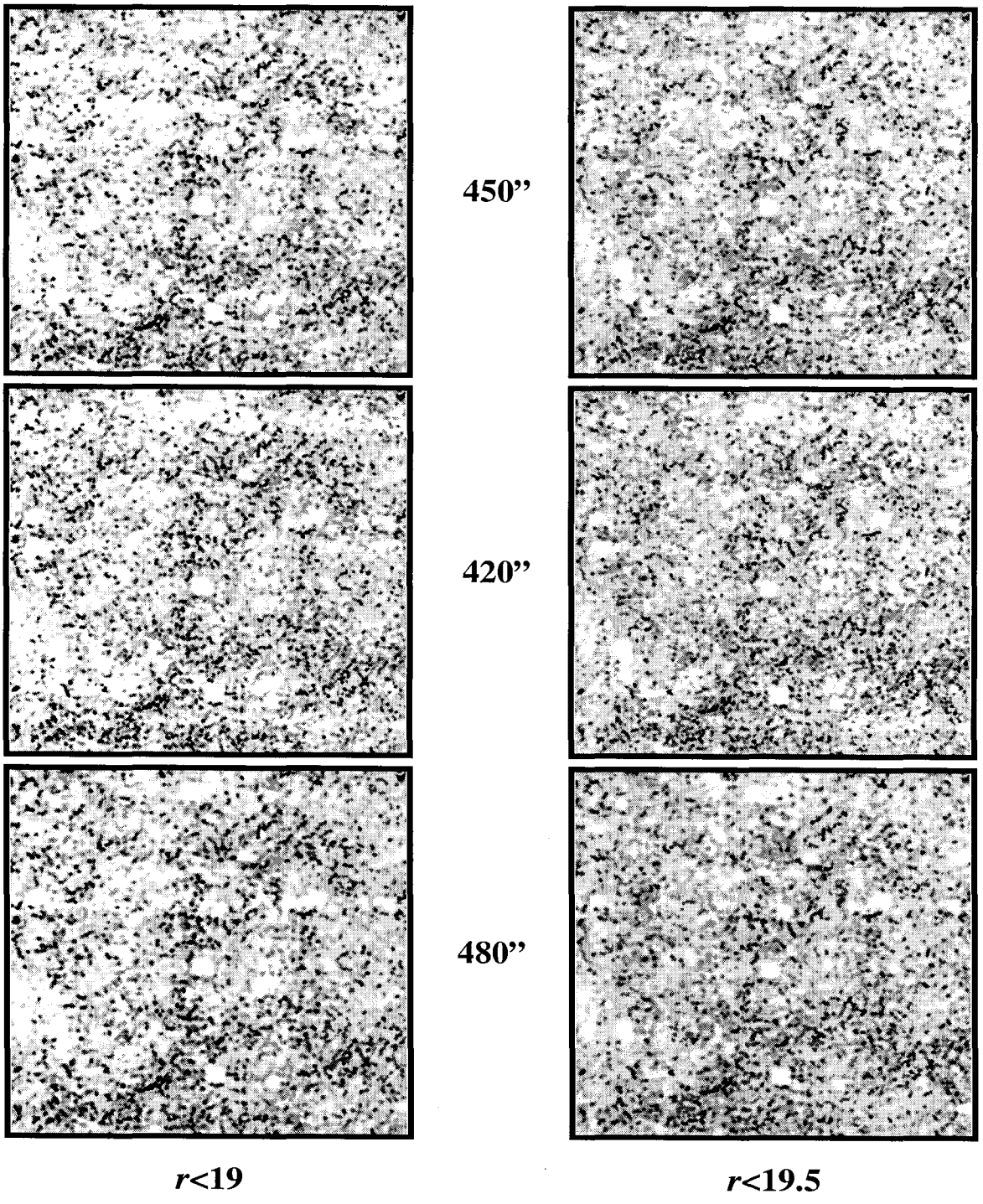

Figure 5.8: The adaptive kernel density map for a $12^\circ \times 12^\circ$ region of the NGP. Maps on the left are for a catalog with $m_r < 19$, and on the right for $m_r < 19.5$. The upper maps use a kernel of $450''$ width, the middle maps $420''$, and the lower maps $480''$.

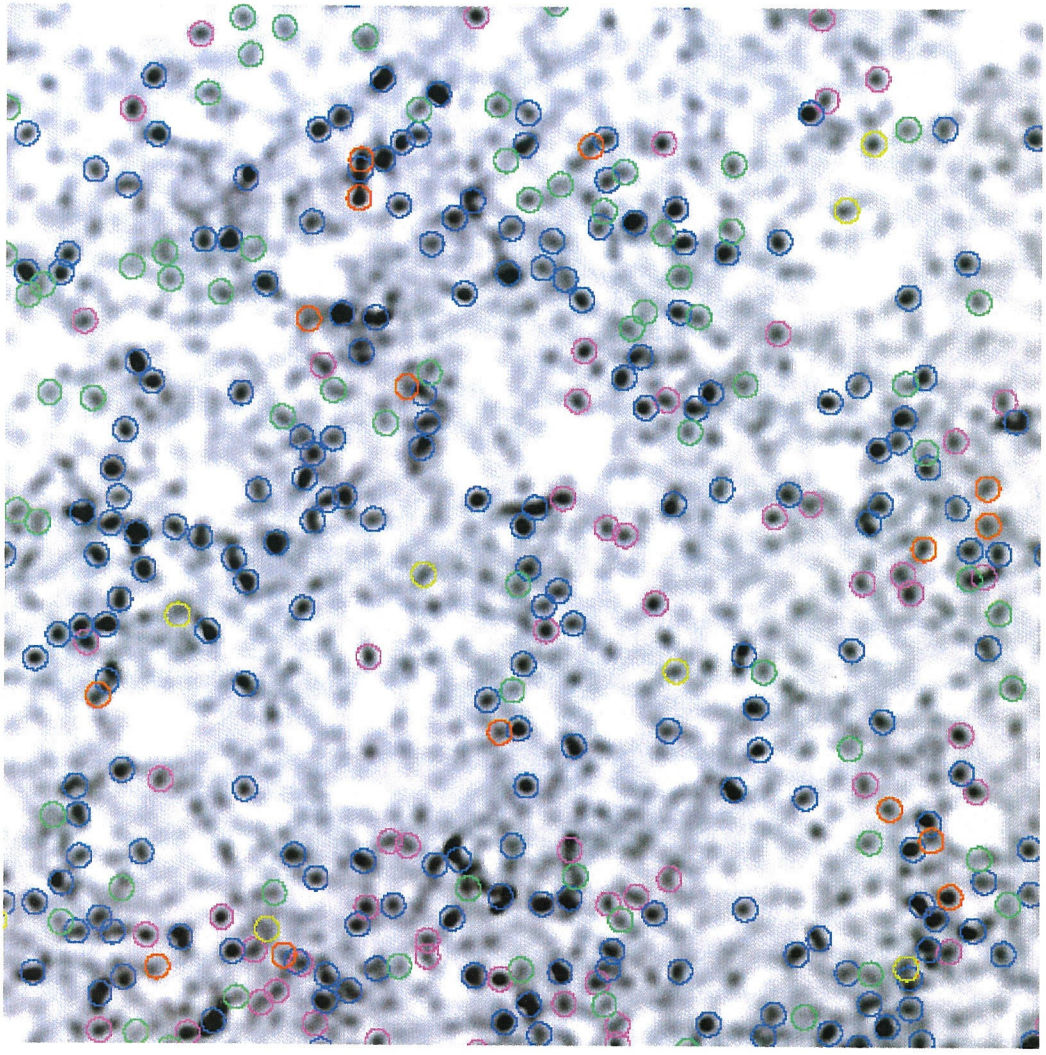

Figure 5.9: A $12^\circ \times 12^\circ$ region of the NGP $m_r < 19.5$ density map, with detected clusters marked. Blue circles are robust candidates, appearing in all six density maps. Red circles mark candidates appearing in five maps, yellow are in four, green in the three $m_r < 19$, and magenta in the three $m_r < 19.5$ maps.

5.3 Extinction

An important consideration in the construction of an all-sky cluster catalog is extinction by dust in our Galaxy. Because the two fields used for the pilot studies and follow-up spectroscopy are at high galactic latitude, the extinction correction is negligible. The mean reddening E($g-r$) derived from the Schlegel *et al.* (1998) maps is only 0.01^m and 0.05^m for fields 447 and 475, respectively. Nevertheless, our final all-sky maps use extinction-corrected magnitudes and colors to derive cluster properties. It is also instructive to compare the 100μ

IRAS map and the galaxy surface density map for an example DPOSS field, number 479 $(l, b = 150, -32)$, shown in Figure 5.10. This field is an area not covered by our current cluster survey. It is clear that galaxies are extincted out of our detection threshold, creating false large-scale structure. This cannot be avoided; it is impossible to correct the color of a galaxy that is not detected. This effect has been largely ignored by past cluster surveys, which only corrected magnitudes of detected galaxies, or were restricted to areas of low extinction (Maddox, Efstathiou & Sutherland 1996). This can have dire consequences for measurements of large scale structure, introducing false power on all scales. Clusters are detected where the galactic extinction is low, and lost where the extinction is high. This non-uniform detection threshold across the sky must be accounted for when measuring the cluster-cluster correlation function, for instance.

In our survey, we have cut the catalogs sufficiently bright that at least 1.5^m of extinction would be necessary to make them undetectable. The areas currently used for the cluster survey are all at $|b| > 30$, such that extinction should not be a significant issue. However, as our photometric errors increase rapidly as objects become fainter on the plates, we might be concerned that even at reasonably high b, we will observe the effects of extinction. The impact of extinction on the cluster-cluster correlation function is discussed in Chapter 9.

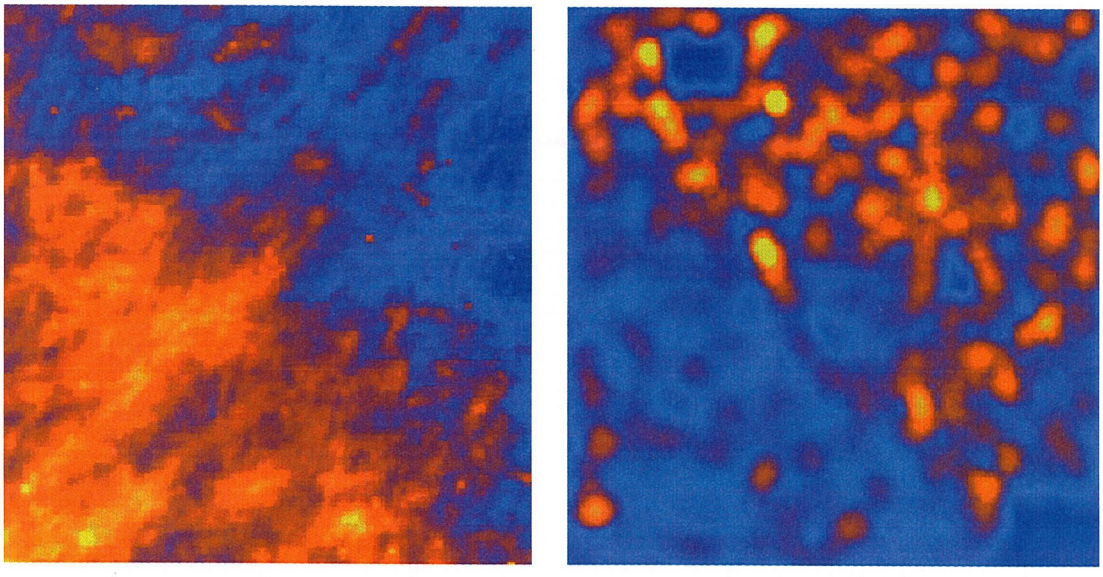

Figure 5.10: The 100μ IRAS map (left), and DPOSS galaxy density map (right), for Field 479 $(l, b = 150, -32)$. The strong correlation between high IR-flux and low observed galaxy density is evident.

Finally, we note that the next large-area galaxy cluster catalogs will not be produced for

some years. These will likely be redshift-selected samples from the 2dF and SDSS redshift surveys. Until then, we hope that this catalog will serve as a replacement for the Abell catalog. The next complete photometrically selected sample, from the SDSS imaging survey, is in the somewhat more distant future. Additionally, our catalog of galaxy clusters will be useful in broad-ranging, multi-wavelength studies by ourselves and other investigators. Upcoming and recent space missions, such as the Chandra X-ray Observatory (CXO) and the X-Ray Multi-Mirror (XMM) satellite, will also benefit greatly from this new resource.

Chapter 6

Spectroscopy and Imaging of Cluster Candidates

The weakest aspect of optical imaging surveys for galaxy clusters is the lack of distance information. The two-dimensional projection of the galaxy distribution can produce many apparent overdensities which may be identified as clusters but are not actual physical associations. This issue has been discussed in some detail for the Abell catalog (see the overview in Chapter 1), where rates of false clusters due to projection effects as high as 40% have been claimed. Other types of surveys (*e.g.*, X-ray, SZ) are not as strongly affected by projection, but suffer from other selection effects or observational difficulties. Therefore, redshifts are needed to validate the existence of a given cluster.

X-ray cluster surveys (REFLEX, Collins *et al.* 2000; NORAS, Böhringer *et al.* 2000) are extremely effective at cluster detection, even out to higher redshifts. However, only the ROSAT All Sky Survey (RASS, Voges 1993) covers very large angular scales in a systematic fashion, but it is not very deep and suffers from positionally variable effective exposure times. X-ray surveys also require that a cluster contain hot (keV) gas (Jones & Forman 1978); while this may provide an operational definition of a galaxy cluster for some observers, it may require that a cluster be sufficiently massive and relaxed. This is also true for surveys which utilize the Sunyaev-Z'eldovich effect (Holder *et al.* 2000), which requires the presence of gas to scatter the CMB photons. To detect poorer, unrelaxed clusters, or those which may have low gas fractions, optical surveys may be necessary.

A variety of X-ray surveys based on deeper pointed exposures have also been conducted (SHARC, Romer *et al.* 2000; RIXOS, Mason *et al.* 2000; etc.), searching for serendipitous clusters in targeted observations of other objects. These have provided some of the best candidates for clusters at high redshifts ($z \sim 0.7$), but they are not useful for studying the distribution of clusters at large angular scales, nor do they detect many poor clusters.

In the optical, redshift surveys provide definitive evidence for the reality of cluster candidates. Unfortunately, to achieve coverage of large areas, depth must be sacrificed (LCRS, Lin *et al.* 1996), or conversely, deep surveys can only cover relatively small angular

scales (CNOC, Borgani *et al.* 1999; CNOC2, Yee *et al.* 2000; CFGRS, Cohen *et al.* 2000). Without dedicated telescopes and instrumentation, moderately deep, large angular scale redshift surveys are impossible. Such a data set will exist when the Sloan Digital Sky Survey is complete; nevertheless, the magnitude limit of their spectroscopic sample will still be brighter than that of DPOSS, much less the SDSS imaging survey.

To address the issue of projection effects in our own cluster catalog, as well as to calibrate our photometric redshift estimator (see the next chapter and Gal *et al.* 2000a) and examine the redshift distribution of our clusters, we have undertaken a complete spectroscopic survey of candidates in two DPOSS fields: 447 ($14^h30^m, +30°$) and 475 ($01^h, +25°$). These fields were chosen because they are at relatively high galactic latitude ($+67°$ and $+40°$) where the effects of dust are expected to be small (but see the discussion in section 5.3), and because scans in all three bands were available when this project was started. Density maps and corresponding significance maps for these two fields are shown in Figures 6.1 and 6.2. The original candidate clusters in the two individual (single-plate) fields are marked with Abell clusters shown in green, and new clusters in white.

These maps were generated, and cluster detection performed, using the methodology discussed in Gal *et al.* (2000a), which differs significantly from the final technique used in this thesis. The smoothing kernel was a factor of two larger, and different software (FOCAS) was used to perform object detection. Additionally, the *rms* galaxy density fluctuations were measured locally on each plate. Therefore, the sample with follow-up spectroscopy is only a subset of the final cluster catalog in these areas. Figure 6.3 demonstrates the magnitude of this effect for Field 475, plotting the locations of slitmasks taken of the originally detected clusters with asterisks, the newly detected 'robust' clusters with open circles, and the less robust detections (those detected in 3,4, or 5 maps) with filled squares. Although there is a clear correspondence between the different samples, our spectroscopic survey does not cover all of the new robust candidates. The exact magnitude of this effect is discussed in the next section.

In addition to spectroscopy at the Palomar 5m Hale Telescope, we have obtained deep CCD imaging of these clusters in *gri* at the Palomar 60″ telescope. In this chapter, we discuss the data obtained, the data reduction for the spectroscopy, and the results of these follow-up surveys.

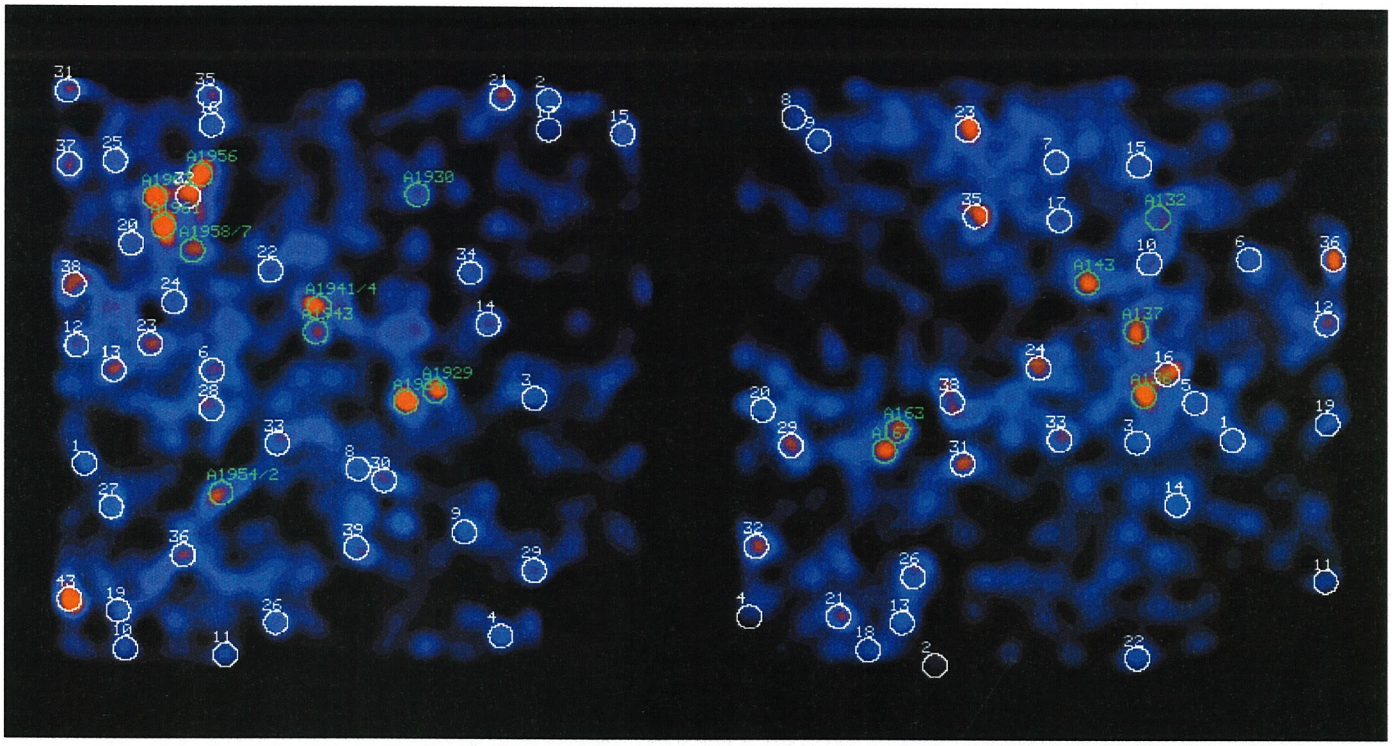

Figure 6.1: Density maps for DPOSS Fields 447 (left) and 475 (right). Abell clusters are marked in green, and new candidate clusters in white.

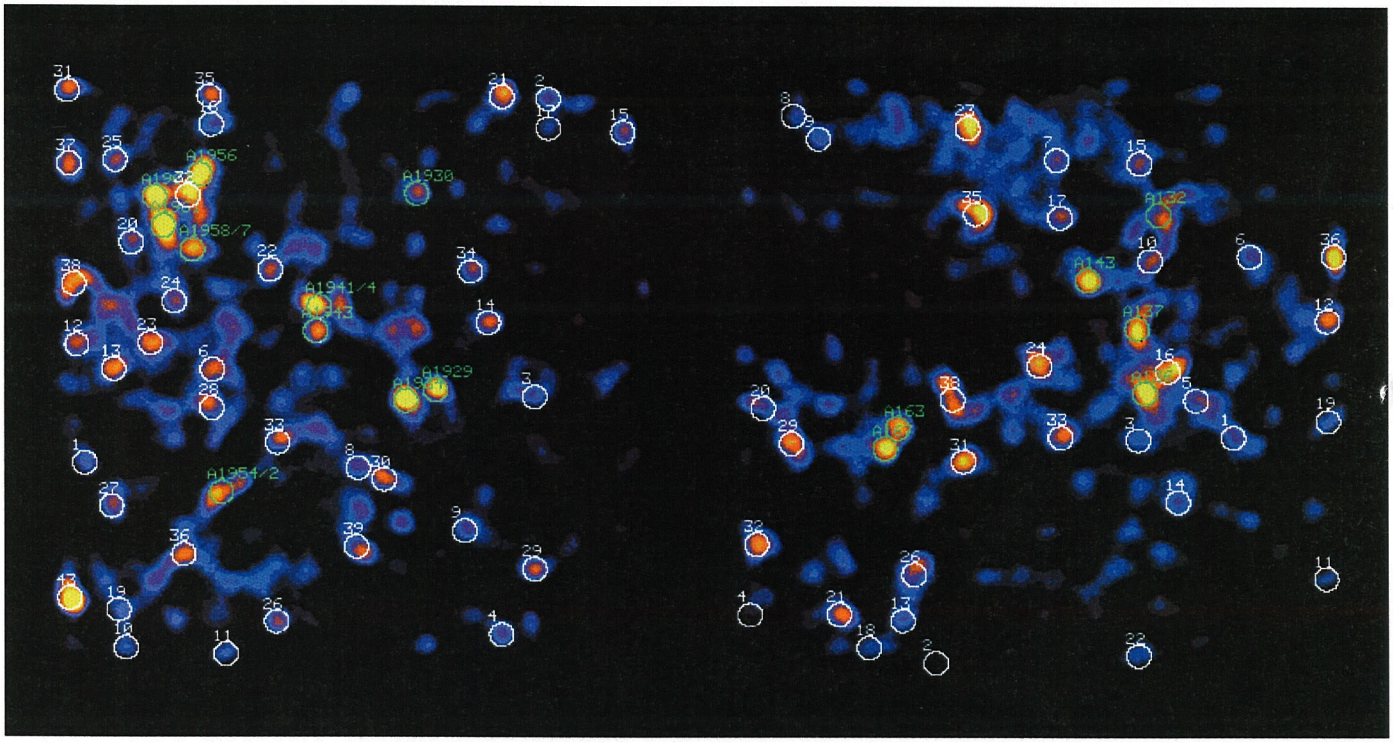

Figure 6.2: Significance maps for DPOSS fields 447 and 475.

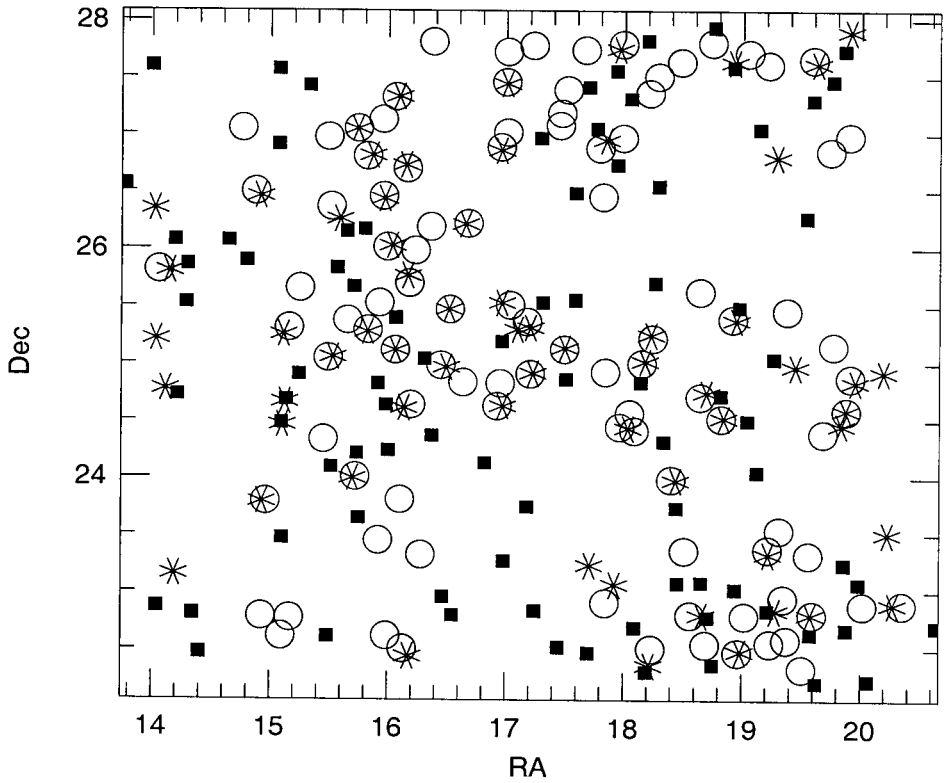

Figure 6.3: The locations of slitmasks (asterisks), the final robust clusters (open circles), and less robust clusters (filled squares).

6.1 Spectroscopic Data

6.1.1 Observations

Spectra of the cluster candidates were obtained between April 1996 and April 2000 with the COSMIC instrument (Dressler, Kells & Sivaramakrishnan 1998) in re-imaged mode, mounted at the prime focus of the Hale 5m Telescope at Palomar Observatory. Targets for each mask were chosen from the DPOSS catalog for the appropriate field, selecting only galaxies with $m_r \leq 20$ to maintain reasonable exposure times. No color selection was applied; this was done to maximize the number of possible objects which could have slits placed on them. Multislit masks, made of photographic film negatives, with 1.5″ slit widths, were mounted at the focal plane. The reimaged pixel scale is 0.399″/pixel; the slits therefore correspond to ~ 3.75 pixels. The available field for spectroscopy is theoretically $8' \times 12'$,

with the long dimension corresponding to the spatial axis. The field is further limited by the lack of an accurate distortion map in the slitmask production software; this requires that slits be placed within $\sim 3'$ of the central axis in the direction perpendicular to the slits.

Slitmasks were designed using the *cosmicslitmask* program, written by M. Pahre. This software simply takes an input list of coordinates, and allows the user to interactively select objects for slit assignment. There is no automated slit optimization algorithm, so objects were selected visually for each mask, to maximize the number of targets observed per mask. This often resulted in densely packed slitmasks, with as many as 45 slits on a single mask, some as short as $10''$. An example slitmask layout is shown in Figure 6.4.

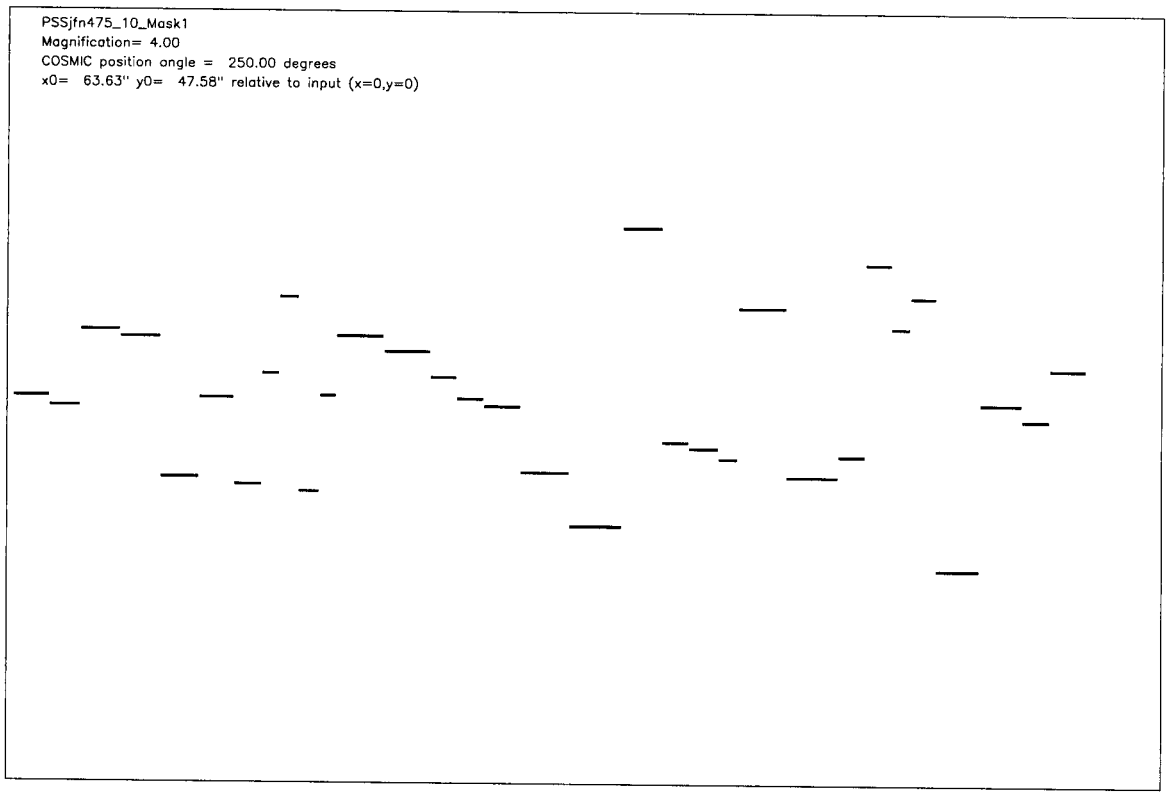

Figure 6.4: A typical slitmask used for cluster observations with COSMIC.

Spectra were taken using a grism with 300 l/mm, blazed at 5500Å, which produced a dispersion of 3.03Å pixel^{-1}. The spectra typically cover a wavelength range $\sim$3000Å to $\sim$9000Å, with a central wavelength of $\sim$6000Å. Since the dispersing element is a grism and cannot be tilted, the wavelength range is fixed and varies only as a result of the vertical displacement of the slits from the mask center. Therefore, nearly all spectra are observed from blueward of the 4000Å break (for $z = 0$), through the redshifted Na lines (5890Å rest frame, 7950Å at our highest expected $z = 0.35$). The COSMIC CCD has a gain of

$3.1e^-/DN$ and a relatively high read noise of $13e^-$. Exposure times varied greatly from night to night, depending largely on the seeing (which ranged from $0.8''$ to as high as $2.0''$) and spectrograph focus changes (due to temperature fluctuations). Exposures ranged from a single 1800s exposure up to two 3600s exposures per slitmask, with most consisting of two 1800s exposures.

6.1.2 Data Reduction

All data reduction was performed using the IRAF package. The object spectra were overscan subtracted, and flattened using spectra of a halogen lamp reflected off the dome interior. Cosmic rays were removed using the *szap* task (written by M. Dickinson), and night sky emission removed by subtraction in the spatial direction on the two-dimensional images, using the *background* task to perform median filtering and sigma clipping. Because the slits were typically very narrow, we used only a second order fit along the spatial direction. After sky subtraction, each spectrum was traced and optimally extracted in the individual exposures. The extracted spectra were wavelength calibrated using spectra of an arc lamp, taken immediately before or after the object spectra, to minimize the effects of instrument flexure. The individual extracted, wavelength-calibrated spectra were then combined to produce the final spectrum for each object, used to measure the redshifts. Some sample spectra are shown in Figure 6.5. It should be noted that the spectra seen here are among the higher S/N ones obtained.

6.1.3 Redshift Measurement

All redshifts were measured by RRG using the IRAF task *redshift*, written by T. Small. This program allows the user to visually mark specific spectroscopic features, and input their rest wavelengths. The object's redshift is then calculated, and the positions of other common absorption and emission lines overplotted. In this way, the user can check the redshift assignments. Such visual measurement was necessitated by the poor S/N of the majority of our spectra; automated techniques (such as cross-correlations) were strongly affected by residuals from poor sky subtraction. To enable completion of the survey in a reasonable time, a tradeoff in exposure times *vs.* number of masks observed was made, since we were only interested in measuring redshifts and not any specific galaxy properties (such as velocity dispersions or line strengths). Comparison of redshifts obtained by different

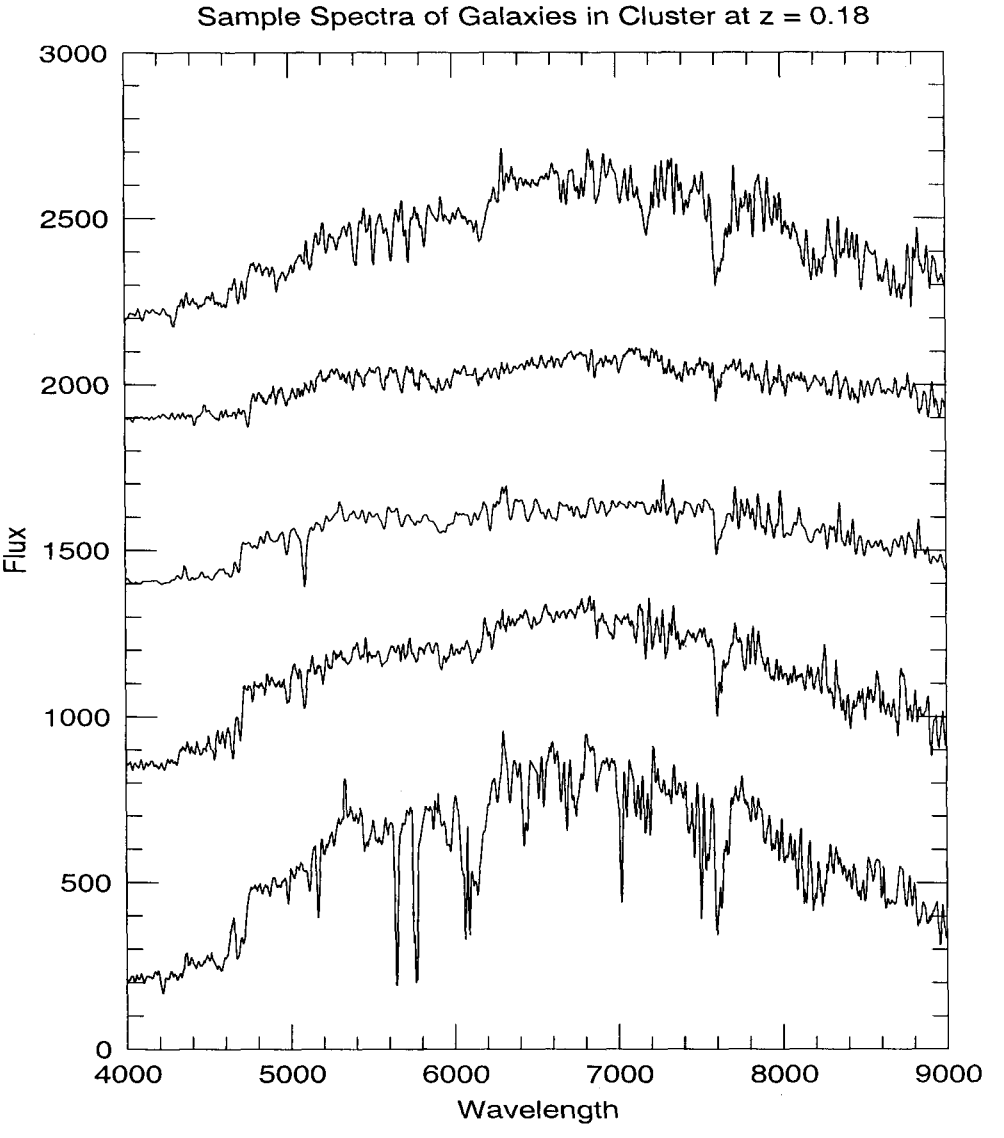

Figure 6.5: Sample COSMIC spectra of galaxies in a cluster at $z = 0.18$.

reducers and at different times suggests the redshifts are accurate to $\sim \Delta z = 0.002$, or approximately 600 km s^{-1}.

In addition, over the course of the survey, our list of candidate galaxy clusters changed as the photometric calibration and sample selection improved. This resulted in a significant number of targets being observed which are not included in the final cluster sample. This extraneous data is actually useful in assessing the rate at which we miss real clusters and is discussed later in the chapter. A total of 3249 individual spectra were visually inspected; of these, 1655 (51%) were identified as galaxies, and 326 (10%) as stars. Thus, a total of 1981 spectra were identifiable, a 61% success rate. Of the galaxies, 1245 (75%) had securely

measured redshifts. We also note that the 10% stellar contamination is consistent with the results of Chapter 4, and should be taken as an upper limit on misclassification, as extended sources (*i.e.*, galaxies) tend to have lower S/N spectra, making identification more difficult. This large spectroscopic sample constitutes a significant survey in its own right, with other applications in addition to those discussed here.

The results of the spectroscopic survey are summarized in Tables 6.2 (for Field 447) and 6.3 (for Field 475). Column (1) provides the candidate name, columns (2) and (3) give the coordinates in J2000.0, column (4) notes whether or not spectroscopy exists, columns (5) and (6) provide the spectroscopic redshift and the number of galaxies at that redshift (if spectra were obtained), column (7) lists whether or not imaging was obtained at the Palomar 60″, and column (8) notes if the candidate is also an Abell cluster, or for those masks with no current candidates, whether or not the mask is near an excised area.

Clearly, many candidates in both fields lack spectroscopy, and a similar number lack imaging. This is due to the constant changing of the candidate list as photometry, classification, and stitching improves. The original list of cluster candidates in these two fields was drawn from the individually calibrated plates, using galaxies to $m_r = 20$. The density and significance maps were produced for the individual plate areas ($\sim 36\square^\circ$), so measurements of the background galaxy density and its fluctuations were significantly compromised by local large scale structure. In Field 447, there are 96 new candidates, only 24 of which have usable spectroscopy (due to inclement weather). In addition, 2 slitmasks are associated with less robust candidates, and 3 do not correspond to any current candidates, of which two are near bad areas. Similarly, Field 475 has 100 new, robust candidates, of which 44 have corresponding slitmasks with usable spectra. Additionally, 4 less robust candidates have associated masks, and there are 12 masks not associated with any new candidates. Of these last 12 masks, seven are within 10′ of an excised bad area.

We show the spectroscopic redshift histograms for the cluster candidates in the top panels Figures 6.6a–e (for Field 447) and 6.7a–f (for Field 475). Each bin spans a redshift range $\Delta z = 0.005$. From these redshift distributions, we can clearly see strong clustering in redshift space, providing evidence for true galaxy clusters in most of the slitmasks. In a few cases, the seeing was so poor that hardly any spectra were obtained. Where no redshifts are shown, there were no spectra taken.

In addition, redshift histograms for all galaxies with secure redshifts in the individual

fields are shown in Figures 6.8 and 6.9. Evidence for clusters and possible superclusters, filaments, or walls is clearly seen.

The median redshift of our spectroscopically confirmed cluster candidates is $z_{med} \sim 0.2$. This value is in keeping with the photometric redshifts presented in the following chapter, and with our earlier estimates of the depth of our galaxy catalogs. The redshift distribution of our cluster candidates (for both fields combined) is shown in Figure 6.10.

6.1.4 Are Redshift Peaks Real Clusters?

Although the peaks in the redshift distributions provide evidence for clustering, we would like to quantify the likelihood that a given peak is a real structure. Certainly, large peaks (as in candidate NSC0105+2542, with 15 galaxies) are undoubtedly clusters. However, many of the masks show peaks with only 3 or 4 members. Individual galaxies are assigned as members of a peak if they fall within $\Delta z = 0.005$ (± 1500 km s^{-1}) of the peak center. Increasing this range does not change the results significantly, since most redshift peaks are well isolated.

A rough estimate of the likelihood for such small peaks being real can be made following the argument of Zaritsky *et al.* (1997). If the underlying redshift distribution of galaxies were smooth, the formal probability of a pair of galaxies within $\Delta z = 0.005$ would be negligible, much less for three or more galaxies. However, because galaxies are correlated, the likelihood of pairs, triplets, etc., is increased. If we assume that *all* slitmasks where the richest clump has only three or four members correspond to spurious detections (there are 18 such masks out of 95 total masks), the probability of finding a single false peak is 18/95, or $\sim 20\%$. We might then expect a comparable fraction of our histograms to show a second redshift peak with similarly few members, but there are only eight ($\sim 8\%$). In fact, some of the distributions with multiple peaks may be projections of multiple poorer clusters which we detect as a single candidate. Additionally, there is only one mask with a secondary peak containing five members. An additional argument in favor of the reality of three-or-more galaxy clumps is that if peaks with three members were often spurious, we expect to find many more such peaks than those containing four galaxies. However, we find an almost identical number of peaks with three and four galaxies, supporting the idea that even three-galaxy peaks are often real. Therefore, we conservatively identify all peaks with four or more members as real clusters, and peaks with only three members

as tentative. The number of clumps with two clusters is much higher (nearly every mask contains one); we therefore ignore those completely. Furthermore, while Zaritsky *et al.* follow similar arguments for only two galaxies, their spectroscopy covers a significantly larger magnitude range ($m_r < 22$ compare to our $m_r < 20$), thereby greatly increasing their likely contamination rate. These results are summarized in Table 6.1, where we provide the number of robust candidates in each field, the number of these with usable spectroscopy, and the fraction of spectroscopically observed candidates with confirmed clusters (using both 3 and 4 redshifts as the minimum), and the fraction with multiple peaks of 3 or more galaxies. Conservatively, we estimate that at least 80% of our robust candidates are true clusters.

We also note that there are six slitmasks associated with less robust candidates, of which 5 have good data. All five show peaks of four or more galaxies, suggesting that *(a)*, the more robust candidates should have a high likelihood of being true clusters, and *(b)*, even the less robust candidates (those detected on 3, 4, or 5 maps) may often be real. The masks not associated with current candidates, and not near excised bad areas, also show evidence for real structures (in 5 of 6 masks). Three of these clusters are at higher redshifts ($z > 0.2$) and may be missed in our current survey due to the brighter magnitude cut ($m_r < 19$ as opposed to $m_r < 20$). One appears to be a very large structure at $z = 0.117$; this is likely missed because it is much bigger than the kernel size. Nevertheless, these missed apparently real clusters suggest that our catalog is not less than $\sim 10\%$ incomplete at $z < 0.2$.

Table 6.1: Candidate Spectroscopy Results

Field	$\mathbf{N_{cand}}$	$\mathbf{N_{spec}}$	% Real,$\mathbf{N(z) \geq 4}$	% Real,$\mathbf{N(z) \geq 3}$	% Multiple
447	96	24	83%	100%	8%
475	100	44	95%	100%	7%
Total	196	68	91%	100%	7%

The 2dF redshift survey (Drinkwater *et al.* 2000) and the SDSS redshift survey will provide excellent magnitude-redshift distributions with which we can compare our histograms. Inspection of an early 2dF redshift distribution for background galaxies in their Fornax field shows the typical, clumpy redshift distribution seen in earlier surveys. The fraction of these peaks corresponding to true structures is unknown.

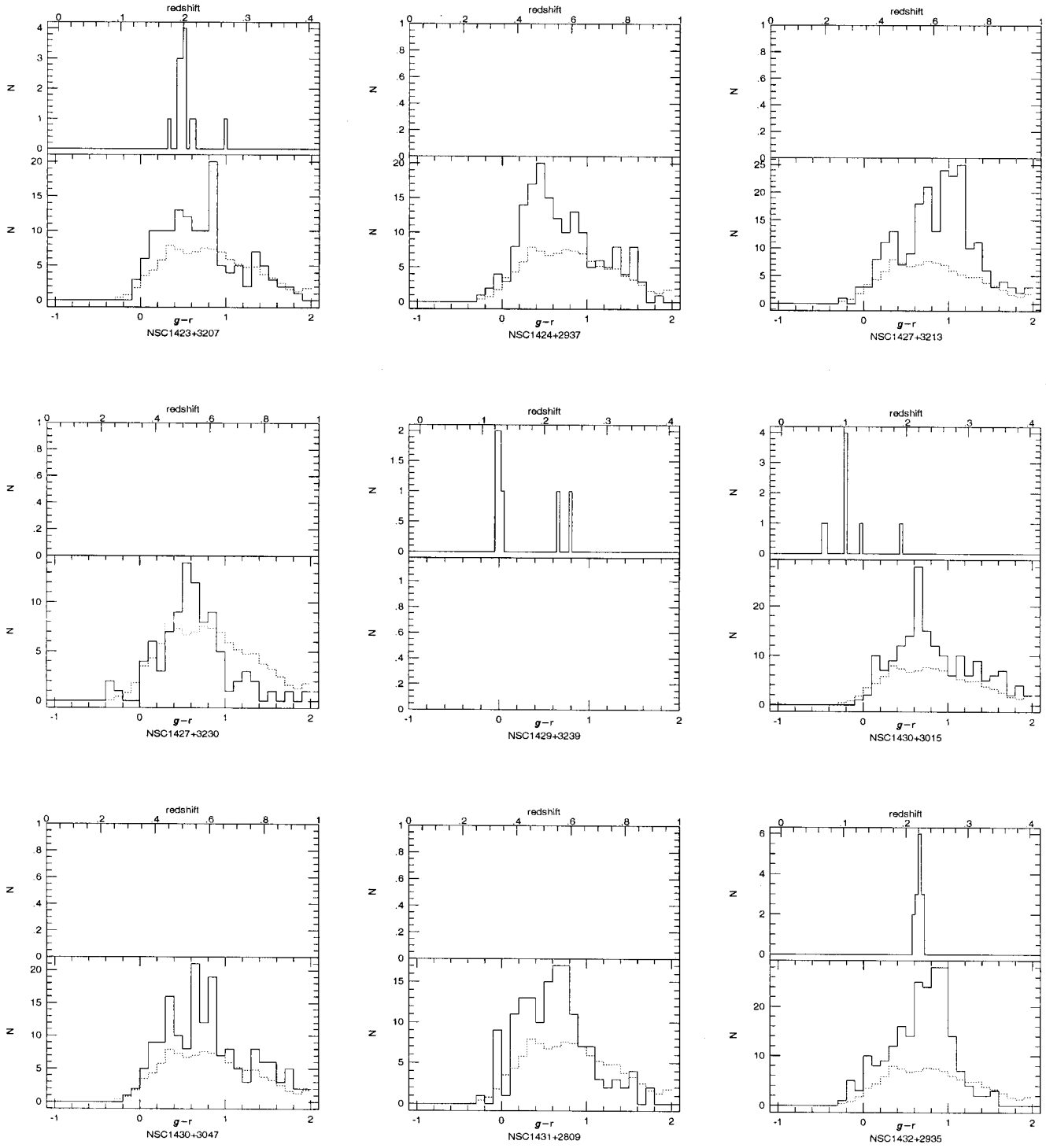

Figure 6.6a: Redshift and galaxy color distributions for candidates from Field 447.

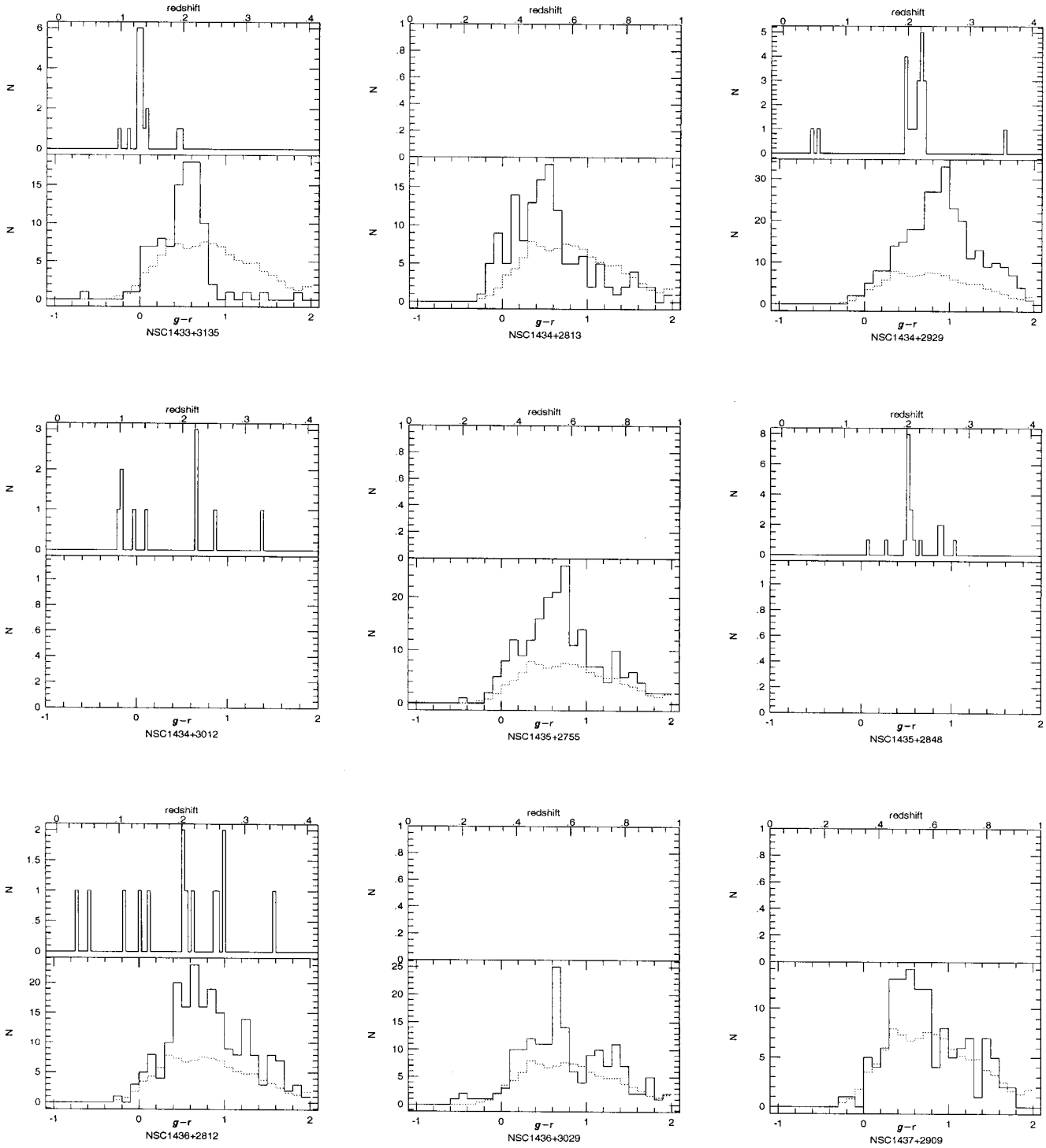

Figure 6.6b: Redshift and galaxy color distributions for candidates from Field 447.

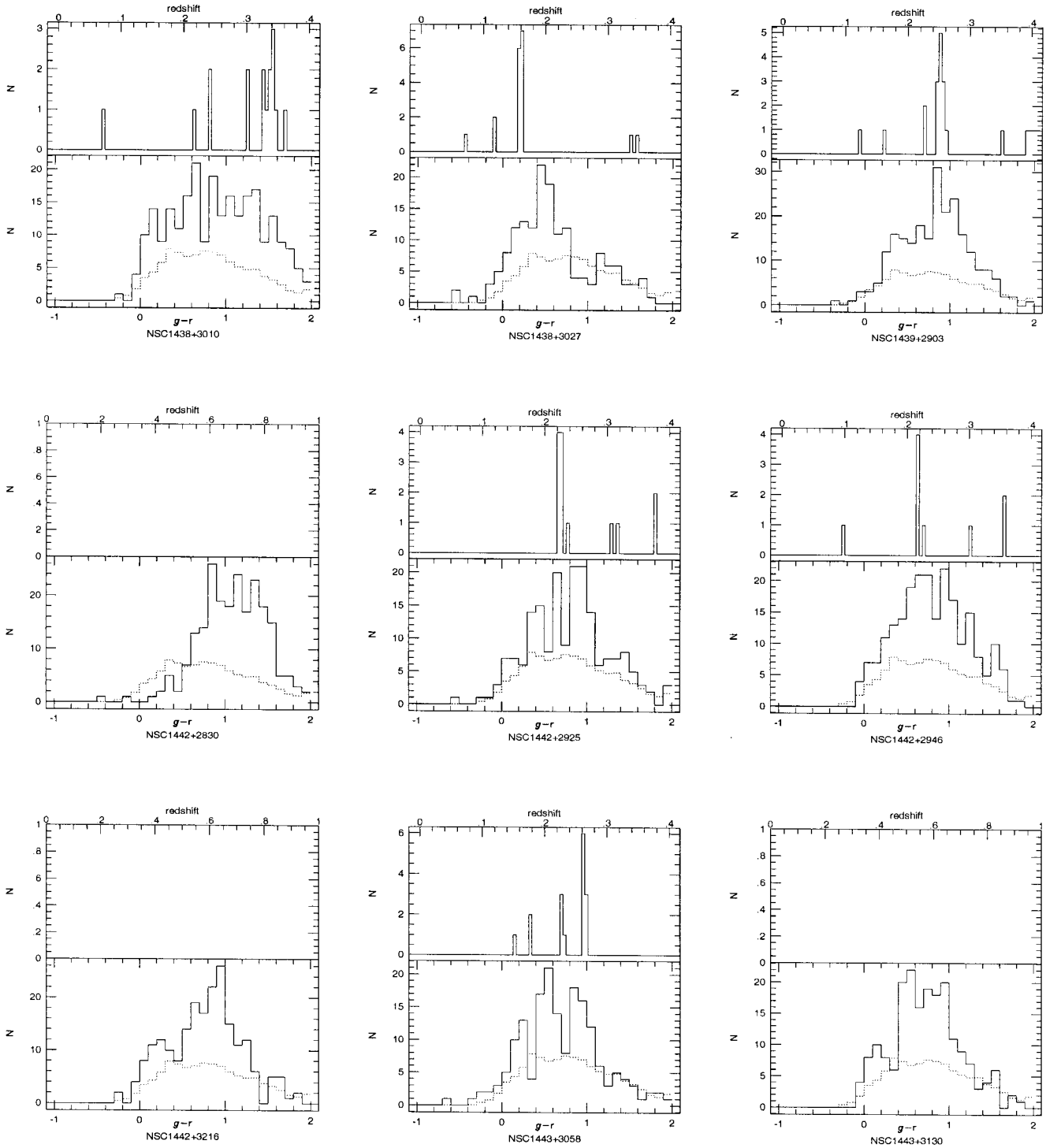

Figure 6.6c: Redshift and galaxy color distributions for candidates from Field 447.

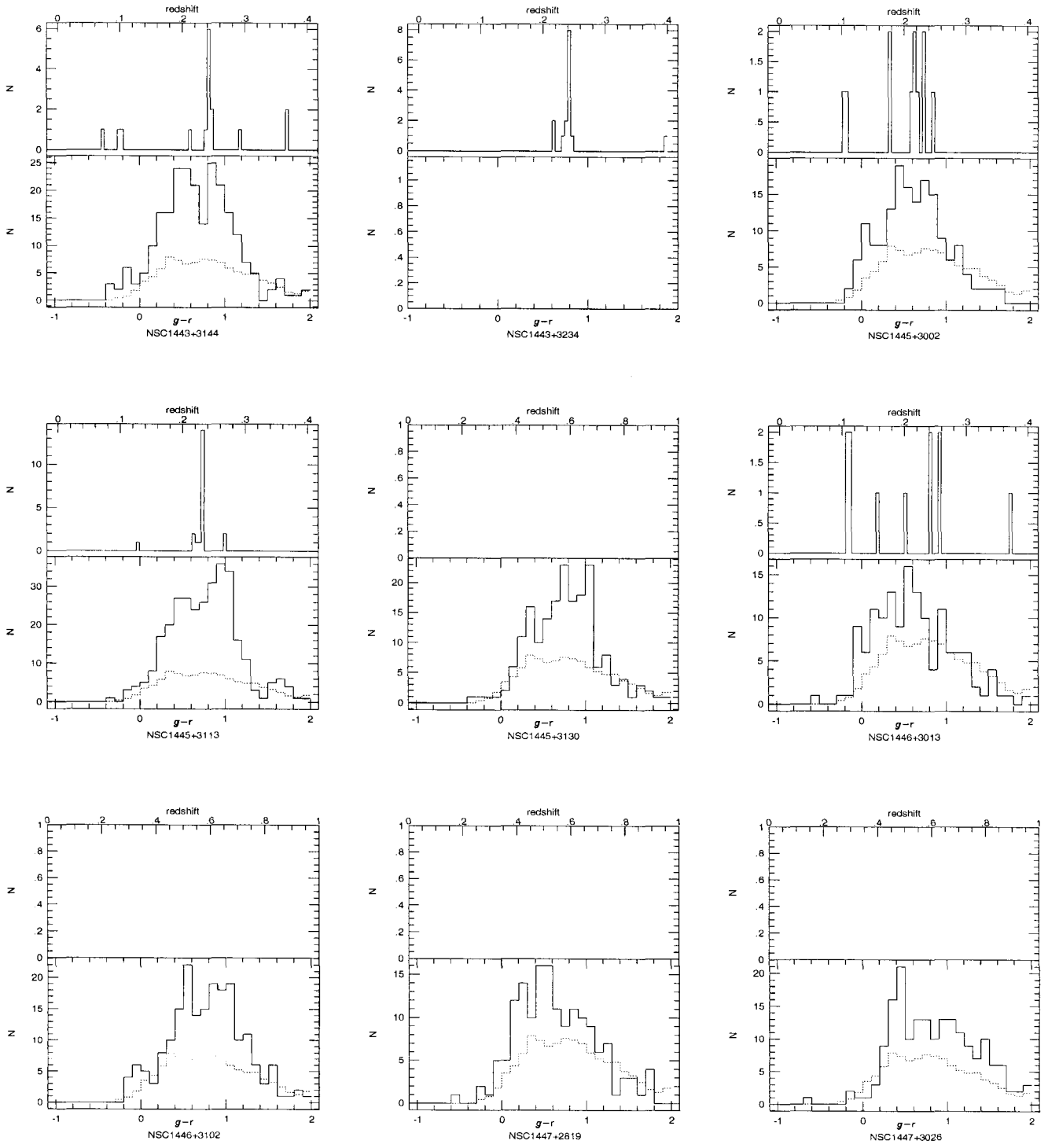

Figure 6.6d: Redshift and galaxy color distributions for candidates from Field 447.

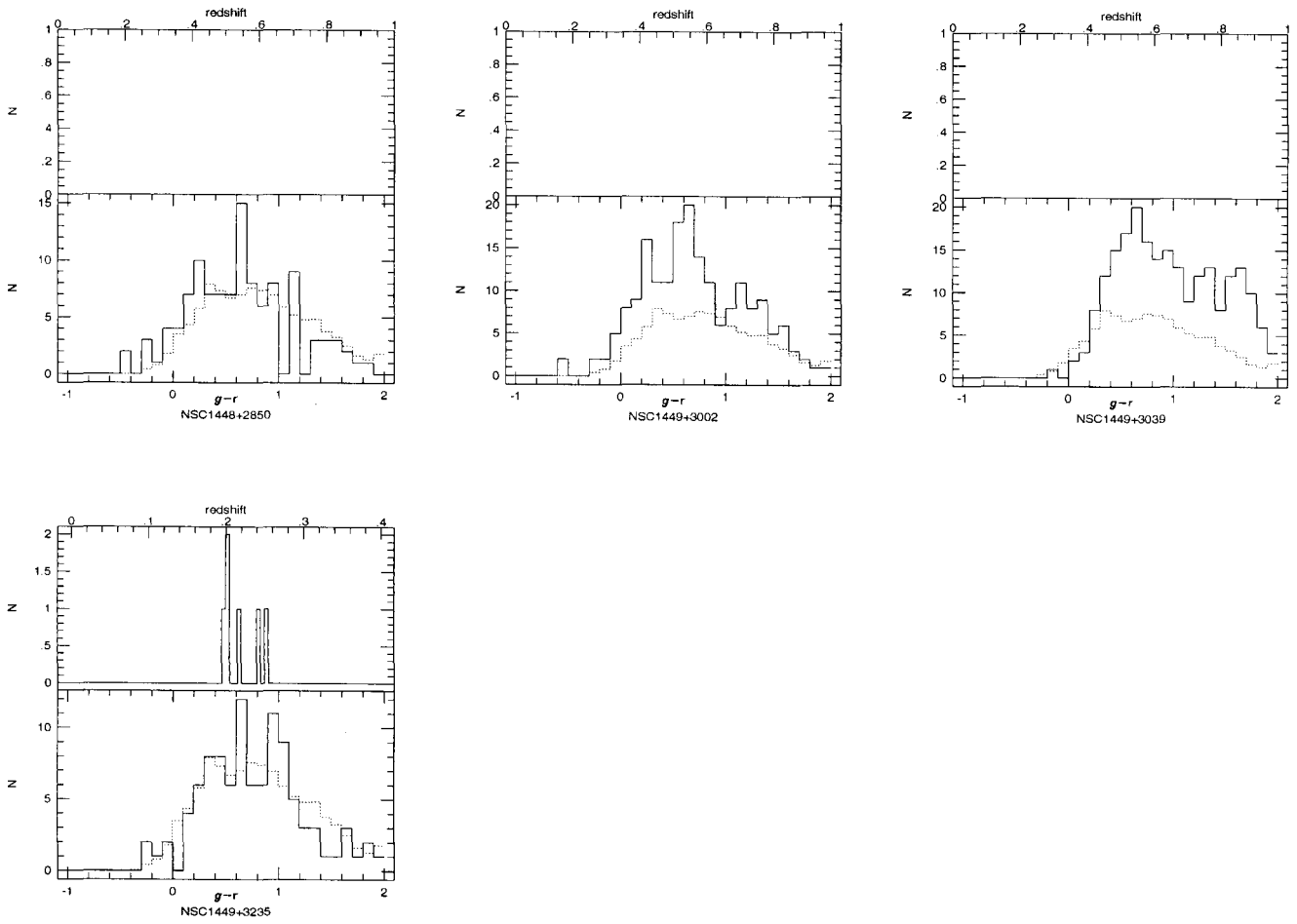

Figure 6.6e: Redshift and galaxy color distributions for candidates from Field 447.

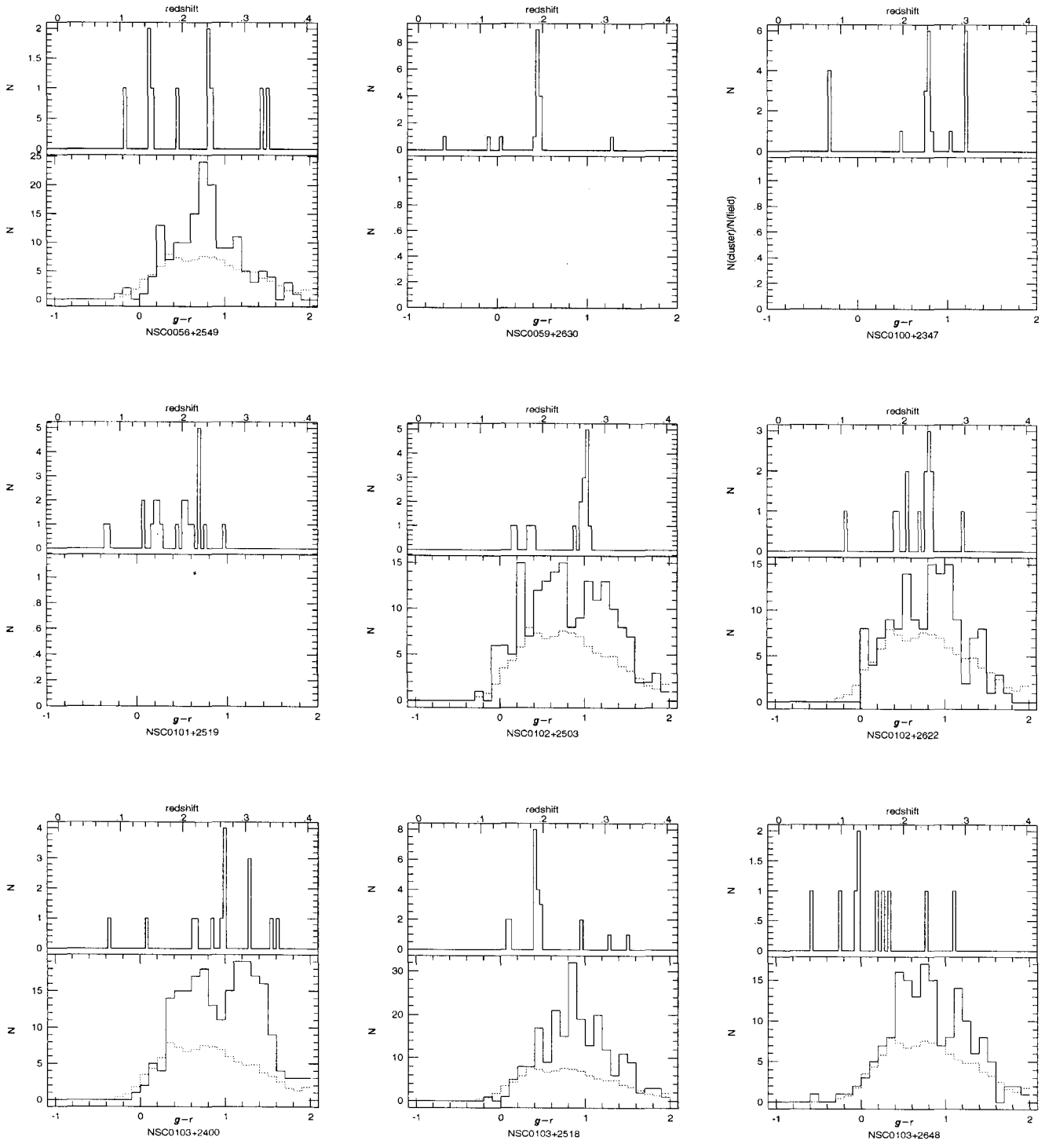

Figure 6.7a: Redshift and galaxy color distributions for candidates from Field 475.

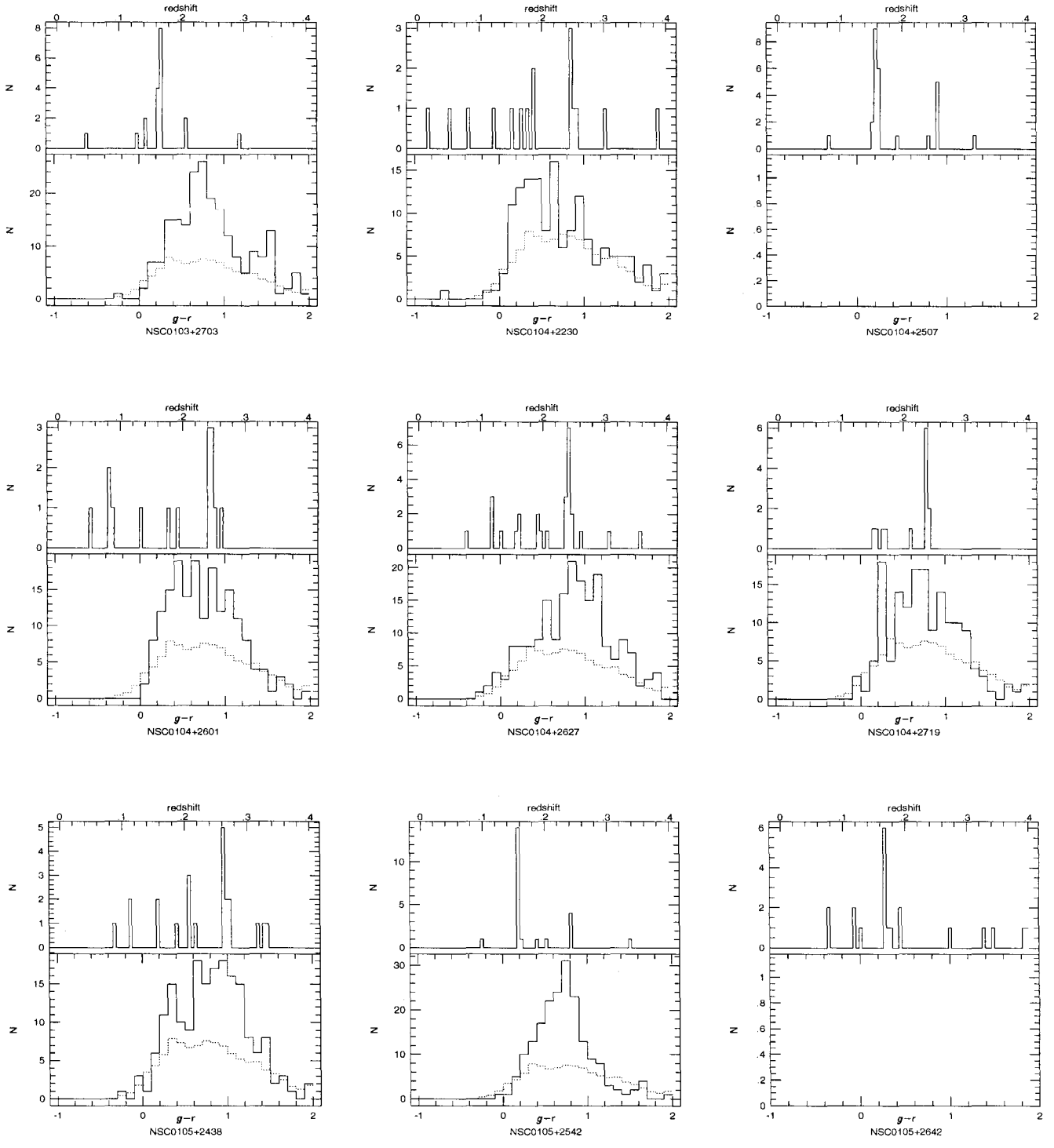

Figure 6.7b: Redshift and galaxy color distributions for candidates from Field 475.

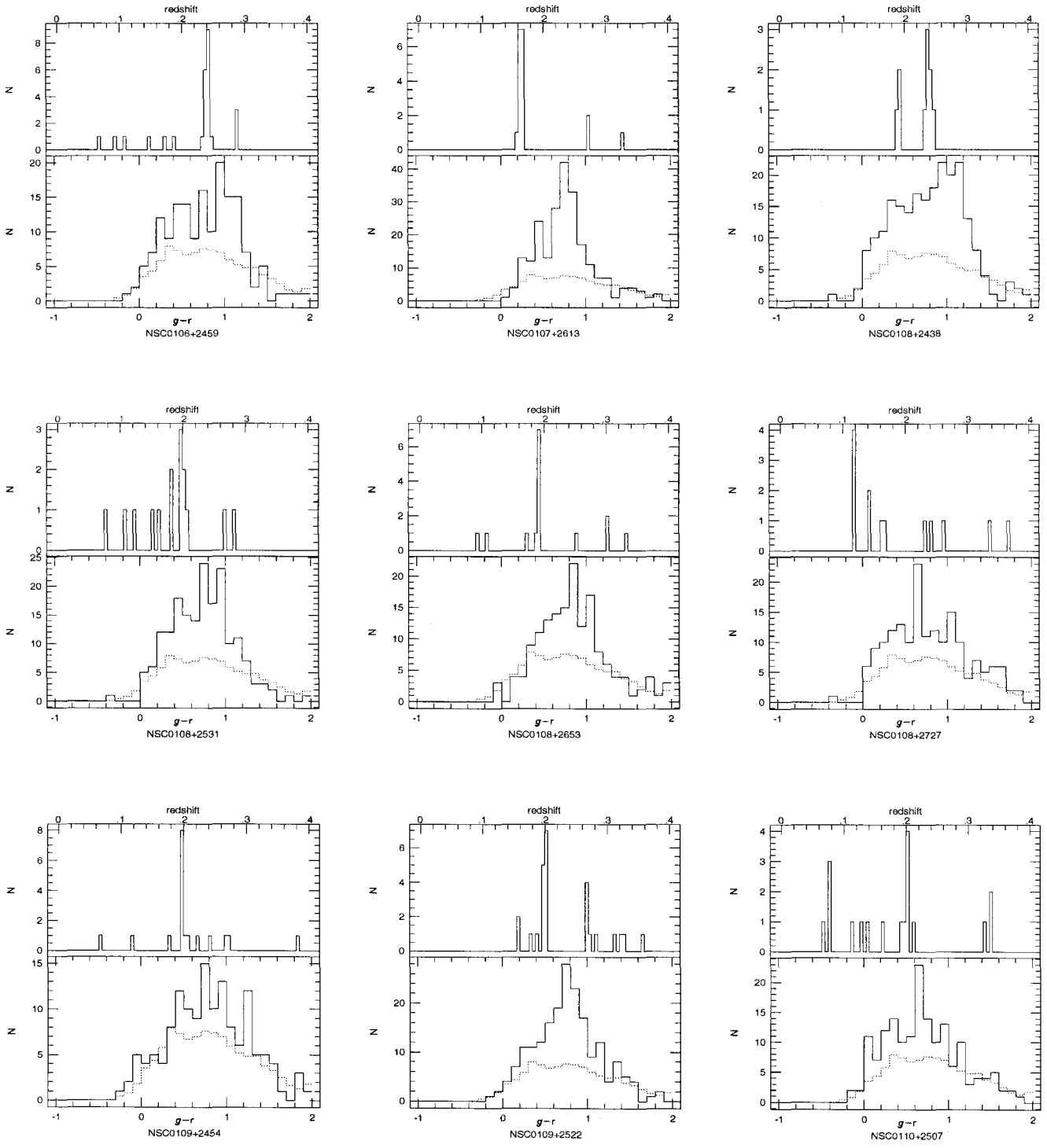

Figure 6.7c: Redshift and galaxy color distributions for candidates from Field 475.

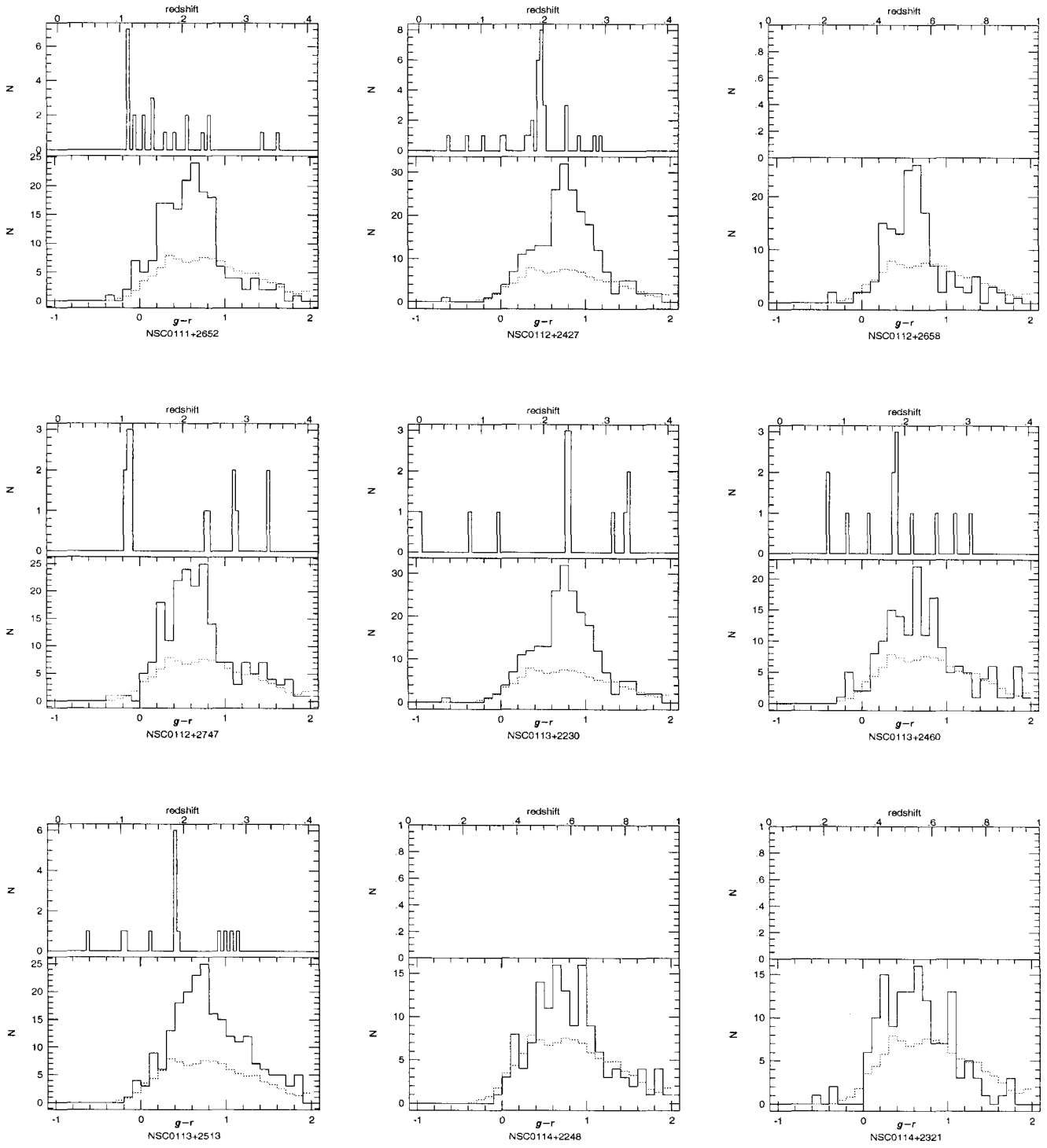

Figure 6.7d: Redshift and galaxy color distributions for candidates from Field 475.

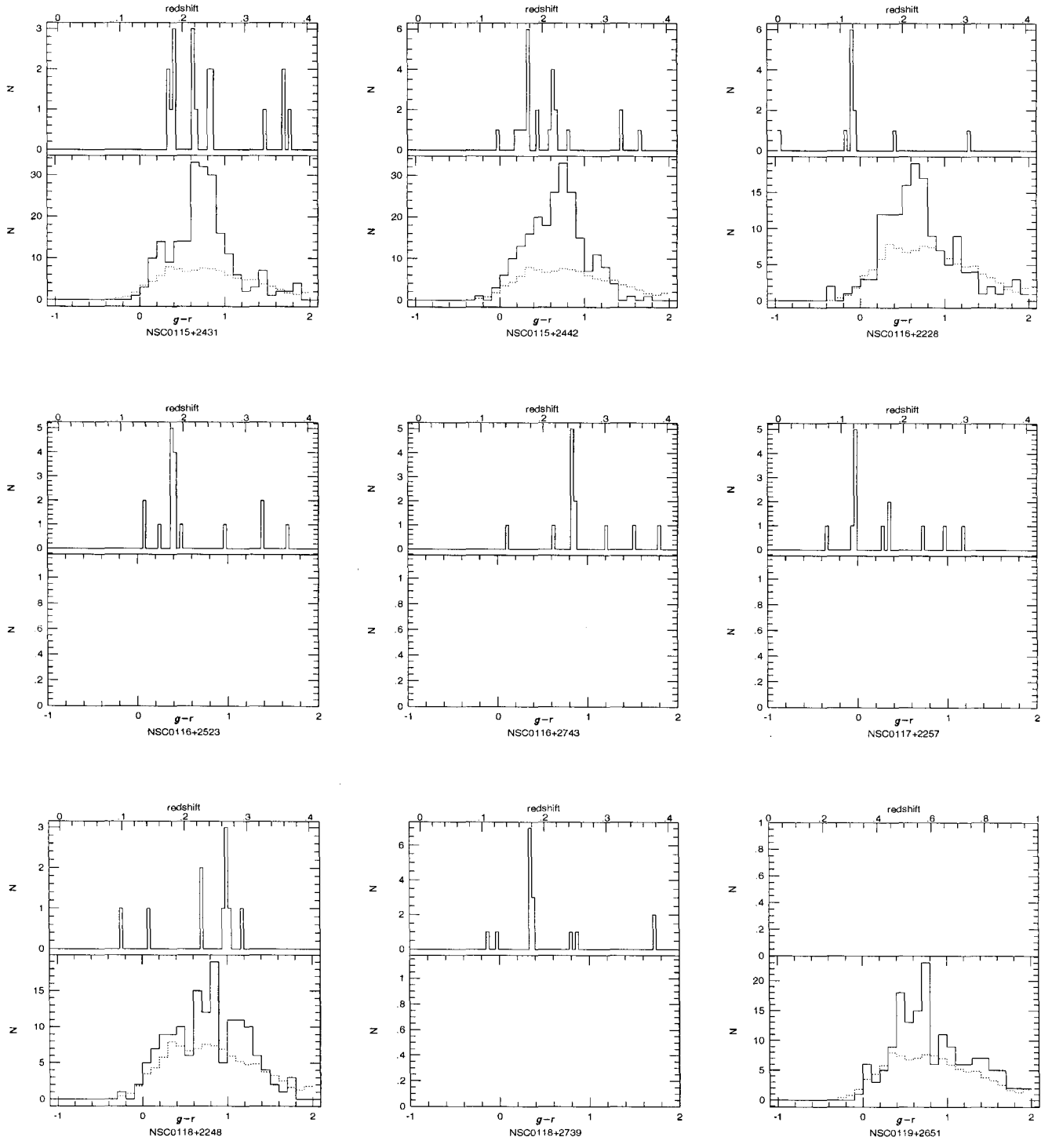

Figure 6.7e: Redshift and galaxy color distributions for candidates from Field 475.

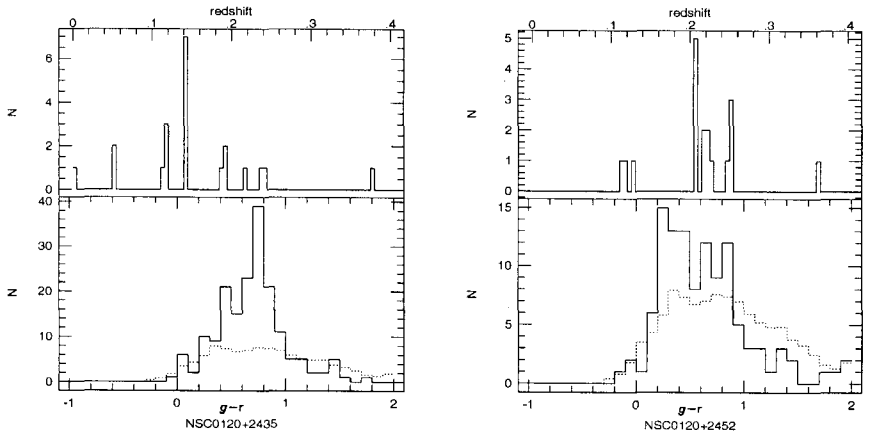

Figure 6.7f: Redshift and galaxy color distributions for candidates from Field 475.

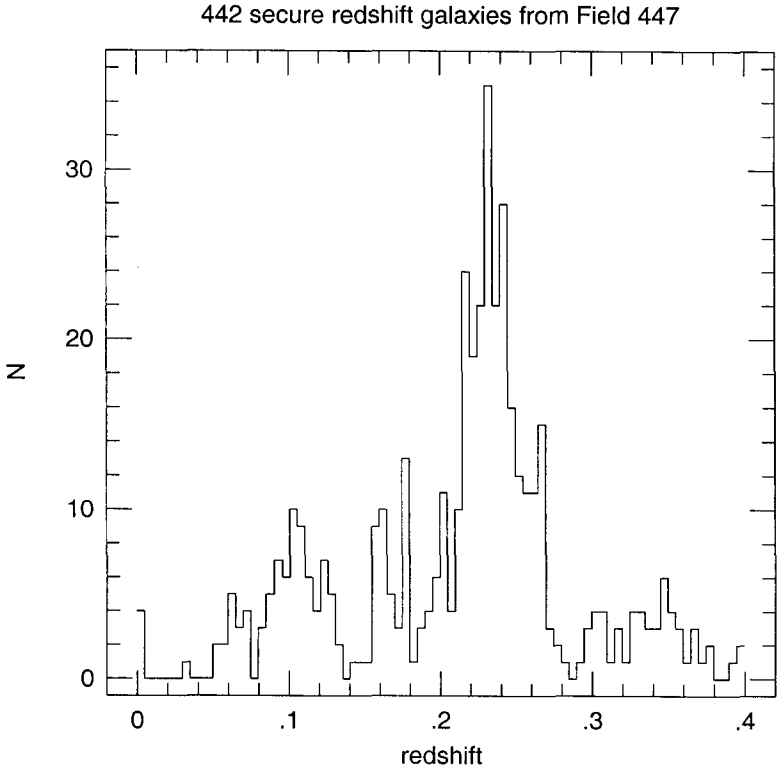

Figure 6.8: Redshift histogram for all galaxies with spectra in Field 447.

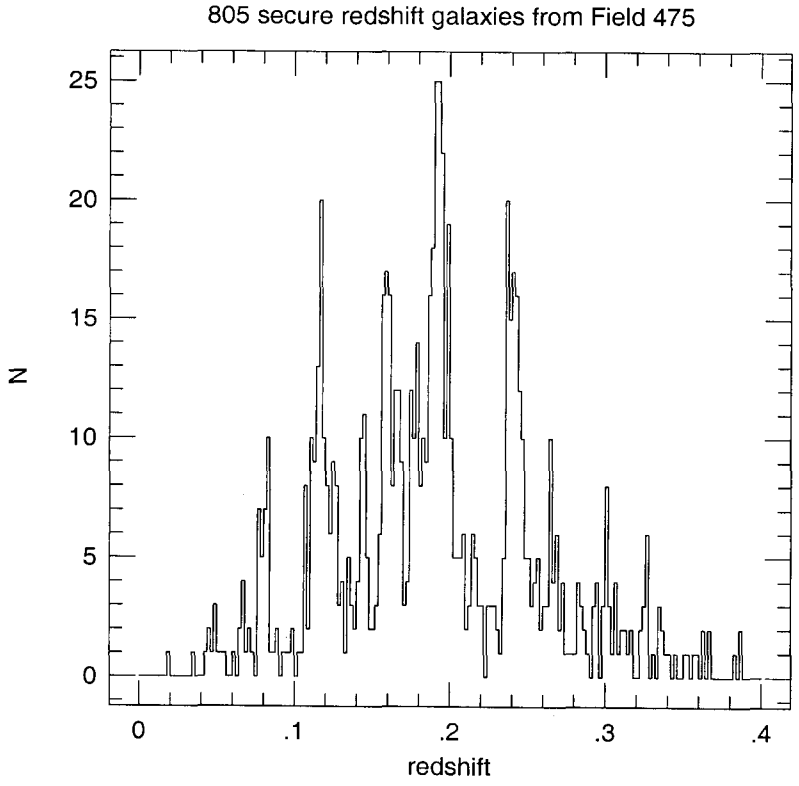

Figure 6.9: Redshift histogram for all galaxies with spectra in Field 475.

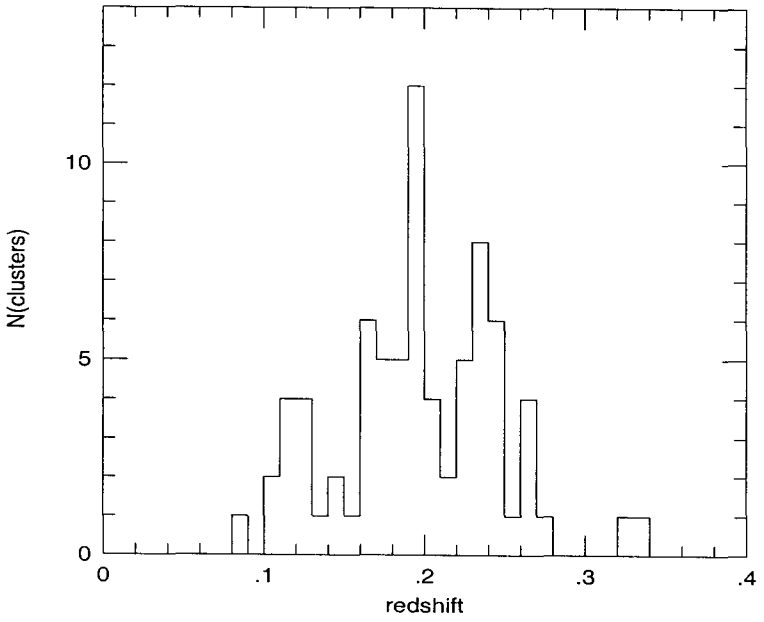

Figure 6.10: Redshift histogram for clusters in both fields.

Table 6.2 - Field 447 Clusters

Candidate	RA	Dec	Spec?	z_{spec}	N(z)	P60?	Abell
NSC1449+2804	222.3417	28.0654	N	–	–	N	
NSC1449+2856	222.3156	28.9373	N	–	–	N	
NSC1449+2910	222.2000	29.1733	N	–	–	N	
NSC1447+2741	221.8080	27.6809	N	–	–	N	
NSC1450+3047	222.4709	30.7793	N	–	–	N	
NSC1448+2850	221.9750	28.8303	Y	BAD	–	Y	
NSC1449+3002	222.1765	30.0259	N	–	–	Y	
NSC1448+2936	222.0569	29.6018	N	–	–	N	
NSC1447+2832	221.7164	28.5370	N	–	–	N	
NSC1447+2819	221.6519	28.3100	Y	.229	4[12]	Y	
NSC1449+3039	222.1434	30.6579	Y	BAD	–	Y	
NSC1448+3003	221.9341	30.0479	N	–	–	N	
NSC1449+3226	222.3223	32.4378	N	–	–	N	
NSC1447+2945	221.6488	29.7513	N	–	–	Y	
NSC1447+3026	221.7954	30.4405	Y	.170	4	Y	
NSC1448+3143	222.0207	31.7102	N	–	–	N	
NSC1449+3235	222.2117	32.5762	Y	.200	3	Y	
NSC1447+3105	221.7711	31.0900	N	–	–	N	
NSC1446+3013	221.5139	30.2147	Y	.109	5	Y	
NSC1444+2753	220.8876	27.8806	Y	BAD	–	Y	
NSC1448+3233	221.9212	32.5537	N	–	–	N	
NSC1447+3208	221.7778	32.1255	N	–	–	N	
NSC1447+3152	221.7032	31.8707	N	–	–	N	1968
NSC1446+3102	221.4965	31.0401	N	–	–	Y	
NSC1444+2905	220.9979	29.0860	N	–	–	N	
NSC1445+3002	221.2218	30.0317	Y	.177	3	Y	
NSC1444+2918	220.9847	29.3048	N	–	–	N	
NSC1447+3222	221.6432	32.3623	N	–	–	N	
NSC1446+3136	221.4211	31.6081	N	–	–	N	
NSC1445+3130	221.2435	31.4942	N	–	–	Y	1963[1]
NSC1442+2830	220.5133	28.4998	Y	BAD	–	Y	1954[2]
NSC1445+3113	221.1274	31.2196	Y	.233	14	Y	1961[3]
NSC1442+2902	220.5395	29.0254	N	–	–	N	
NSC1442+2925	220.6039	29.4147	Y	.224	8	Y	
NSC1442+2946	220.5735	29.7715	Y	.216	4	Y	
NSC1443+3058	220.8022	30.9713	Y	.263	7	Y	1958[4]
NSC1442+2915	220.4086	29.2543	N	–	–	N	
NSC1441+2837	220.2553	28.6168	N	–	–	N	1952[5]
NSC1443+3112	220.8053	31.2021	N	–	–	N	1957[6]
NSC1443+3130	220.8248	31.5009	Y	.240	11	Y	
NSC1442+2959	220.4270	29.9913	N	–	–	N	
NSC1443+3058	220.6434	30.9720	N	–	–	Y	
NSC1442+3034	220.5042	30.5586	N	–	–	N	
NSC1442+3018	220.4380	30.3026	N	–	–	N	
NSC1443+3144	220.6974	31.7289	Y	.243	9	Y	1956

Continued...

Table 6.2 - Continued

Candidate	RA	Dec	Spec?	z_{spec}	N(z)	P60?	Abell
NSC1440+2849	219.9955	28.8154	N	–	–	N	
NSC1441+3008	220.2384	30.1305	N	–	–	N	
NSC1442+3132	220.4672	31.5342	N	–	–	N	
NSC1442+3216	220.6051	32.2728	N	–	–	Y	
NSC1443+3234	220.6313	32.5671	Y	.243	11	Y	
NSC1439+2903	219.7966	29.0466	Y	.253	11	Y	
NSC1439+2846	219.6934	28.7718	N	–	–	N	
NSC1440+3046	219.9519	30.7667	N	–	–	Y	
NSC1439+3054	219.8502	30.8930	N	–	–	N	
NSC1437+2909	219.3085	29.1459	N	–	–	Y	
NSC1437+2839	219.1546	28.6481	N	–	–	N	
NSC1438+3010	219.3956	30.1592	Y	.338	9	Y	1943
NSC1438+3027	219.4339	30.4472	Y	.160	13	Y	1944[7,8]
NSC1436+2903	219.1063	29.0533	N	–	–	N	
NSC1436+2812	218.9122	28.1924	Y	.203	3	Y	
NSC1435+2755	218.8714	27.9128	Y	BAD	–	Y	
NSC1436+2847	218.9558	28.7852	N	–	–	Y	
NSC1438+3104	219.3898	31.0683	N	–	–	N	
NSC1435+2822	218.8183	28.3748	N	–	–	N	
NSC1436+3029	219.1001	30.4830	N	–	–	Y	
NSC1435+2848	218.7577	28.8073	Y	.205	11	N	
NSC1434+2753	218.4789	27.8775	N	–	–	N	
NSC1435+2952	218.8587	29.8593	N	–	–	N	
NSC1434+2813	218.4751	28.2096	N	–	–	Y	
NSC1434+2836	218.4283	28.6075	N	–	–	N	
NSC1436+3144	219.0156	31.7323	N	–	–	N	
NSC1434+2955	218.5401	29.9235	N	–	–	N	
NSC1434+2929	218.3777	29.4794	Y	.219	12	Y	1934[9]
NSC1434+3012	218.4903	30.2058	Y	.222	3	N	
NSC1433+2958	218.3492	29.9683	N	–	–	N	
NSC1433+3005	218.2199	30.0786	N	–	–	N	
NSC1433+3014	218.2141	30.2352	N	–	–	N	
NSC1433+3030	218.2092	30.5073	N	–	–	N	
NSC1432+2935	218.0154	29.5763	Y	.221	14	Y	1929[10]
NSC1431+2809	217.7386	28.1486	N	–	–	Y	
NSC1433+3135	218.1798	31.5752	Y	.131	13	Y	1930[11]
NSC1430+3047	217.6005	30.7774	N	–	–	Y	
NSC1431+3133	217.7154	31.5581	N	–	–	N	
NSC1430+3015	217.3824	30.2510	Y	.103	4	Y	
NSC1431+3235	217.8072	32.5752	N	–	–	N	
NSC1428+2932	216.9938	29.5294	N	–	–	N	
NSC1429+3146	217.2310	31.7695	N	–	–	N	
NSC1426+2801	216.5137	28.0186	N	–	–	N	
NSC1427+2935	216.7032	29.5758	N	–	–	N	
NSC1429+3239	217.1939	32.6452	Y	.127	5	Y	
NSC1425+2943	216.3517	29.7131	N	–	–	N	
NSC1424+2811	216.0424	28.1774	N	–	–	N	
NSC1427+3213	216.6561	32.2128	N	–	–	Y	1915

Continued...

Table 6.2 - Continued

Candidate	RA	Dec	Spec?	z_{spec}	N(z)	P60?	Abell
NSC1427+3230	216.6701	32.5076	N	–	–	Y	
NSC1424+2937	216.0298	29.6128	N	–	–	Y	
NSC1423+3207	215.8099	32.1174	Y	.200	10	Y	
Masks Associated with Less Robust Clusters							
P447_23	220.9651	30.4564	Y	.320	4	Y	
P447_46	222.3688	31.8079	Y	BAD	–	N	
Masks Not Associated with New Clusters							
P447d_2	221.2399	31.4966	Y	.233	6	Y	Excl.
P447d_14	221.7048	30.4947	Y	.170	4	Y	Excl.
P447_39	217.3539	327.0682	Y	.268	6	Y	

[1]SR99 gives $z = 0.221$
[2]SR99 gives $z = 0.181$
[3]SR99 gives $z = 0.232$
[4]4 at $z = 0.228$; SR99 gives $z = 0.227$
[5]SR99 gives $z = 0.248$
[6]SR99 gives $z = 0.241$
[7]SR99 gives $z = 0.162$
[8]Also A1941, $z = 0.088$
[9]SR99 gives $z = 0.2194$
[10]SR99 gives $z = 0.2191$
[11]SR99 gives $z = 0.1313$
[12]Also 4 at $z = 0.098$

Table 6.3 - Field 475 Clusters

Candidate	RA	Dec	Spec?	z_{spec}	N(z)	P60?	Abell
NSC0056+2549	14.0570	25.8159	Y	.150[1]	3	Y	
NSC0059+2703	14.7630	27.0495	N	–	–	N	
NSC0059+2630	14.8740	26.4963	Y	.193	14	N	
NSC0060+2247	14.9250	22.7871	N	–	–	N	
NSC0060+2347	14.9610	23.7911	Y	.240[2]	10	Y	
NSC0100+2237	15.0940	22.6130	N	–	–	N	
NSC0101+2519	15.1600	25.3121	Y	.227	5	N	
NSC0101+2246	15.1660	22.7724	N	–	–	N	
NSC0101+2539	15.2510	25.6583	N	–	–	N	
NSC0102+2420	15.4510	24.3342	N	–	–	N	
NSC0102+2503	15.4900	25.0473	Y	.273	11	Y	
NSC0102+2658	15.4930	26.9713	N	–	–	N	
NSC0102+2622	15.5150	26.3645	Y	.239	7	Y	
NSC0103+2523	15.6550	25.3774	N	–	–	N	
NSC0103+2400	15.7220	24.0059	Y	.266	6	Y	
NSC0103+2703	15.7430	27.0480	Y	.166	12	Y	132
NSC0103+2648	15.8220	26.8037	Y	.127	3	Y	
NSC0103+2518	15.8280	25.2934	Y	.189	15	Y	
NSC0104+2327	15.9180	23.4472	N	–	–	N	
NSC0104+2532	15.9260	25.5274	N	–	–	N	
NSC0104+2708	15.9530	27.1260	N	–	–	N	
NSC0104+2627	15.9590	26.4543	Y	.242	12	Y	
NSC0104+2237	15.9850	22.6149	N	–	–	N	
NSC0104+2601	15.9920	26.0146	Y	.245	7	Y	
NSC0104+2507	16.0600	25.1162	Y	.160	17	N	136[3]
NSC0104+2719	16.0640	27.3246	Y	.239	8	Y	
NSC0104+2348	16.1020	23.8046	N	–	–	N	
NSC0104+2230	16.1250	22.5032	Y	.250	5	Y	
NSC0105+2642	16.1600	26.6942	Y	.168	7	N	
NSC0105+2542	16.1790	25.6998	Y	.158	15	Y	137

Continued...

Table 6.3 - Continued

Candidate	RA	Dec	Spec?	z_{spec}	N(z)	P60?	Abell
NSC0105+2438	16.1920	24.6375	Y	.266	9	Y	
NSC0105+2559	16.2300	25.9836	N	–	–	N	
NSC0105+2319	16.2790	23.3215	N	–	–	N	
NSC0105+2611	16.3610	26.1886	N	–	–	N	
NSC0106+2749	16.3790	27.8109	N	–	–	N	
NSC0106+2459	16.4480	24.9832	Y	.241	17	Y	
NSC0106+2528	16.5240	25.4727	Y	BAD	0	N	
NSC0107+2450	16.6350	24.8342	N	–	–	N	
NSC0107+2613	16.6780	26.2176	Y	.164	15	Y	143
NSC0108+2438	16.9250	24.6257	Y	.238	7	Y	
NSC0108+2450	16.9510	24.8251	N	–	–	N	
NSC0108+2653	16.9560	26.8824	Y	.192	8	Y	
NSC0108+2727	17.0000	27.4569	Y	.117	4	Y	
NSC0108+2701	17.0110	27.0130	N	–	–	N	
NSC0108+2743	17.0120	27.7232	N	–	–	N	
NSC0108+2531	17.0350	25.5087	Y	.200	6	Y	
NSC0109+2522	17.1800	25.3629	Y	.200	12	Y	
NSC0109+2454	17.2050	24.9073	Y	.197	10	Y	
NSC0109+2747	17.2300	27.7781	N	–	–	N	
NSC0110+2704	17.4560	27.0745	N	–	–	N	
NSC0110+2711	17.4680	27.1822	N	–	–	N	
NSC0110+2507	17.4950	25.1228	Y	.200	6	Y	
NSC0110+2723	17.5200	27.3897	N	–	–	N	
NSC0111+2744	17.6710	27.7398	N	–	–	N	
NSC0111+2652	17.7930	26.8732	Y	.113	7	Y	
NSC0111+2627	17.8210	26.4498	N	–	–	N	
NSC0111+2254	17.8420	22.9026	N	–	–	N	
NSC0111+2456	17.8430	24.9250	N	–	–	N	
NSC0112+2427	17.9650	24.4436	Y	.196	17	Y	
NSC0112+2747	17.9880	27.7913	Y	.115	8	Y	
NSC0112+2658	17.9890	26.9652	N	–	–	Y	
NSC0112+2434	18.0480	24.5626	N	–	–	N	
NSC0113+2460	18.1520	24.9994	Y	.183	5	Y	
NSC0113+2722	18.2140	27.3610	N	–	–	N	
NSC0113+2230	18.2320	22.5042	Y	.240	6	Y	
NSC0113+2513	18.2440	25.2189	Y	.189	7	Y	
NSC0113+2730	18.2880	27.5081	N	–	–	N	
NSC0114+2359	18.4000	23.9813	Y	BAD	–	N	
NSC0114+2738	18.4800	27.6358	N	–	–	N	
NSC0114+2321	18.5110	23.3575	N	–	–	Y	
NSC0114+2248	18.5620	22.7965	Y	BAD	–	Y	
NSC0115+2538	18.6430	25.6268	N	–	–	N	
NSC0115+2442	18.6450	24.7081	Y	.178	8	Y	163
NSC0115+2232	18.6910	22.5416	N	–	–	N	
NSC0115+2748	18.7410	27.8025	N	–	–	N	
NSC0115+2431	18.8220	24.5174	Y	.189	6	Y	167

Continued...

Table 6.3 - Continued

Candidate	RA	Dec	Spec?	z_{spec}	N(z)	P60?	Abell
NSC0116+2523	18.9180	25.3868	Y	.185	9	N	
NSC0116+2228	18.9610	22.4712	Y	.120	8	Y	
NSC0116+2247	19.0200	22.7895	N	–	–	N	
NSC0116+2743	19.0510	27.7129	Y	.248	7	N	
NSC0117+2322	19.2140	23.3689	Y	BAD	–	Y	
NSC0117+2737	19.2170	27.6110	N	–	–	N	
NSC0117+2233	19.2320	22.5516	N	–	–	N	
NSC0117+2332	19.3110	23.5364	N	–	–	N	
NSC0117+2257	19.3460	22.9425	Y	.123	6	N	
NSC0117+2235	19.3710	22.5827	N	–	–	N	
NSC0118+2527	19.3760	25.4580	N	–	–	N	
NSC0118+2220	19.5040	22.3318	N	–	–	N	
NSC0118+2319	19.5580	23.3199	N	–	–	N	
NSC0118+2248	19.5910	22.8024	Y	.267	5	Y	
NSC0118+2739	19.5930	27.6571	Y	.177	10	N	
NSC0119+2423	19.6800	24.3870	N	–	–	N	
NSC0119+2651	19.7390	26.8482	N	–	–	Y	
NSC0119+2509	19.7660	25.1532	N	–	–	N	
NSC0120+2435	19.8760	24.5849	Y	.142	7	Y	
NSC0120+2659	19.9000	26.9806	N	–	–	N	
NSC0120+2452	19.9100	24.8743	Y	.207	5	Y	
NSC0120+2253	20.0160	22.8804	N	–	–	N	
NSC0121+2253	20.3490	22.8878	Y	BAD	–	Y	
Masks Associated with Less Robust Clusters							
P475_3	14.1141	24.7734	Y	–	0	Y	
P475_8	15.1020	24.4621	Y	.125	10	Y	
P475_10	15.1229	24.6635	Y	.082	7	Y	
P475_54	19.4469	24.9682	Y	.145	11	N	
Masks Not Associated with New Clusters							
P475_1	14.0018	26.3886	Y	.194	24	Y	Excl.
P475_2	14.0350	25.2111	Y	.175	8	N	Excl.
P475_5	14.1880	23.1530	Y	.180	6	Y	
P475_32	17.0982	25.2951	Y	.160	7	N	
P475_36	17.7102	23.2286	Y	.115	5	Y	Excl.
P475_38	17.9226	23.0602	Y	.195	7	N	
P475_53	19.2902	26.7921	Y	.238	3	N	
P475_57	19.8351	24.4567	Y	.117	4	Y	Excl.
P475_59	19.9105	27.8991	Y	.099[4]	3	Y	Excl.
P475_61	20.1903	24.9209	Y	.190	4	Y	Excl.
P475_62	20.2235	23.5025	Y	.117	21	Y	
P475_63	20.2289	24.9657	Y	.190	5	N	Excl.

[1]Also 3 at $z = 0.240$
[2]Also 6 at $z = 0.302$
[3]SR99 gives $z = 0.157$
[4]Also 3 at $z = 0.249$ and 3 at $z = 0.335$

6.1.5 Spectroscopic *vs.* Photometric Redshifts

An additional test of the reality of our cluster candidates is a comparison of our plate photometric redshift estimator (discussed in the next chapter) with the spectroscopic redshifts measured for the candidate clusters. Although our own spectroscopy was used for the calibration of the photometric redshift estimator, we would expect increased scatter in $z_{spec} - z_{phot}$ if a significant fraction of our clusters were spurious. The results of this test are shown in Figure 6.11. Filled boxes represent the 60 clusters with four or more redshifts in the most significant peak, and the five open boxes are clusters with only three redshifts. Although the total sample is small (65 clusters), the photometric redshift estimates agree well. The *rms* scatter of $z_{spec} - z_{phot}$ for the whole sample is 0.04, consistent with the errors in the calibration of the photometric redshift estimator. The candidates with only three redshifts in a peak show comparable (in fact, even less) scatter than the larger sample, but they are very few in number.

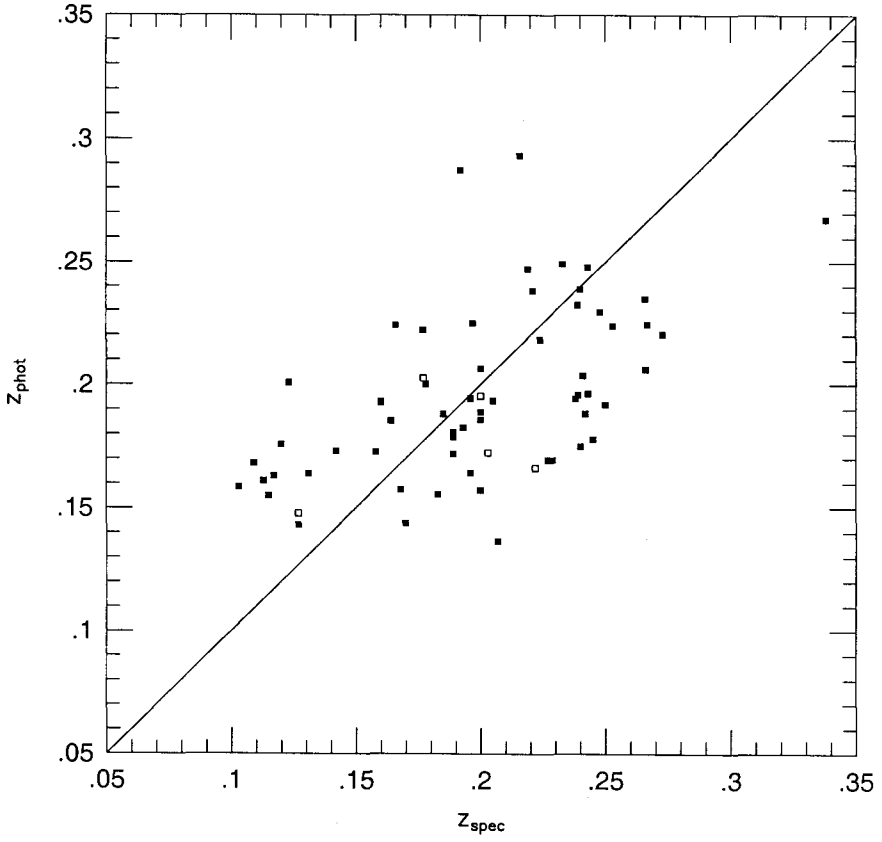

Figure 6.11: Photometric *vs.* spectroscopic redshifts for Fields 447 and 475.

6.2 CCD Imaging of Cluster Candidates

In addition to obtaining spectra of the cluster candidates in our two follow-up fields, we have also imaged them with CCD13 at the Palomar 60″. These images are intended to provide visual confirmation of the cluster candidates, as well as significantly deeper photometry than the plates. With this data, we can construct luminosity functions, improved photometric redshifts, substructure maps, and study galaxy evolution to somewhat higher redshifts than with the Abell cluster sample.

Data were taken, processed, and calibrated in a manner identical to that described in Chapter 3, except for longer exposure times: 1200s in g, and 900s in r and i. Unfortunately, due to time constraints we have not yet observed any blank fields with these longer exposure times, so we cannot generate appropriate background corrections for the various scientific projects.

Color images of selected cluster candidates are provided in Appendix C. The gri images have been mapped to RGB output; therefore, redder (typically early-type) galaxies appear yellow in these images. In most cases, the candidate clusters are apparent.

In addition to peaks in the redshift distributions from our Palomar 200″ spectroscopy, we utilize the existence of an overall galaxy excess, as well as the difference between cluster and field galaxy color distributions to test our candidates. The bottom panels of Figures 6.6a-e and 6.7a-f show the distribution of galaxy colors for each candidate from the Palomar 60″ observations (solid line), and the mean background color distribution from 22 shorter blank field exposures (dashed line). Both data sets have been limited at $m_r < 21$ to mitigate the effects of shorter exposures for the blank fields. Nevertheless, the excess galaxy population and, more specifically, excess red galaxies, which indicate the presence of a cluster, are visible.

Even before we obtain deep blank fields to generate a proper CCD photometric redshift estimate for these candidates, we can make a very rough estimate using only the mean $g-r$ color as a proxy for redshift, since they are so well correlated (see Fig 5.4). In Figure 6.12, we plot the mean $g-r$ color of the galaxies in our CCD-observed candidates against the spectroscopic redshift for the candidate. We also show the expected trend based on a simple no-evolution k-correction model. Despite the large scatter, the candidates clearly follow the prediction. Because these CCD data were taken at the positions of the original

candidates, they can be a few arcminutes away from the final cluster centers, contributing to the scatter. Also, at lower redshifts, the CCD field is not large enough to cover most of the cluster. Nevertheless, this correlation provides additional evidence that a majority of the cluster candidates are real.

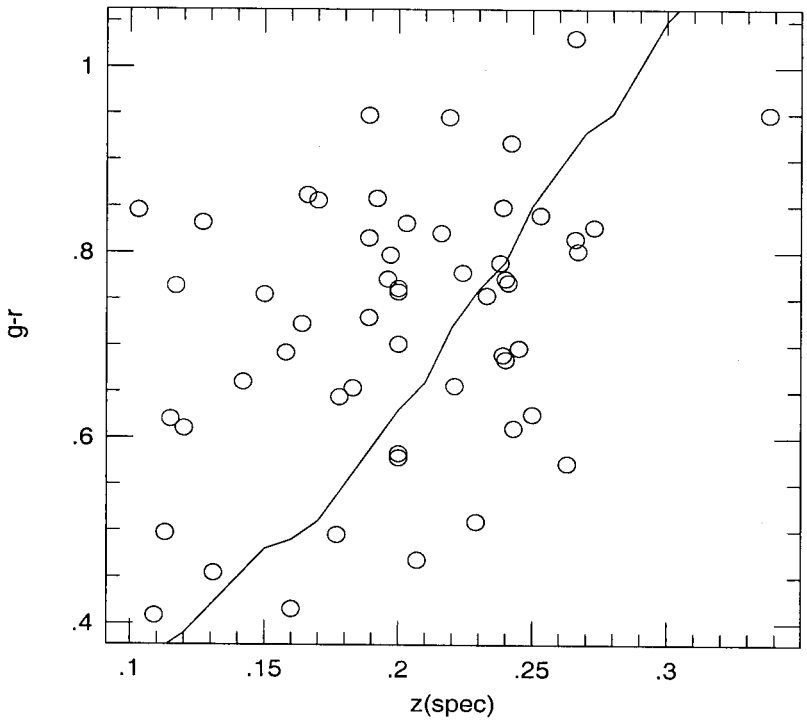

Figure 6.12: The background-corrected mean $g-r$ colors of galaxies in P60 observed cluster candidates *vs.* their spectroscopic redshift. The expected trend from a k-correction model is also shown.

Once we have obtained the necessary deeper blank field images, we will perform a more detailed analysis of the 60″ data. For a detailed description of some of the potential projects, utilizing the shallower Abell cluster observations, the reader is referred to Chapter 8. Other future studies are described in Chapter 10.

Chapter 7

Photometric Redshifts and Richnesses for Cluster Candidates

After detection from the significance map, some basic properties (angular extent, ellipticity, PA) of the clusters are measured from the original density map. Properties of the galaxy population of each cluster are derived from the input DPOSS galaxy catalogs. This helps eliminate spurious detections, and allows us to compare our catalog with pre-existing catalogs. In this chapter, we describe our methodology for estimating cluster photometric redshifts and richnesses directly from the plate data.

7.1 Photometric and Spectroscopic Data

Our photometric redshift estimator is based on the assumptions that each candidate is a single cluster, at one redshift, and the cluster galaxy population is dominated by early-type galaxies. The $g-r$ color of elliptical galaxies evolves rapidly at $z < 0.4$ due to a strong k-correction, as the 4000Å break passes through the g filter. Similarly, the r magnitudes of these galaxies fade rapidly with redshift, and the r band measurements are more accurate due to the red colors of the galaxies. For these reasons, we have chosen to use the $g-r$ colors and r magnitudes of the cluster galaxies in our plate photometric redshift estimator.

We count the number of galaxies as a function of color, N_{g-r}, and the number as a function of r magnitude, N_r, inside a radius of 1 Mpc ($0.67 \times R_{Abell}$). The background galaxy color and magnitude distributions, $N_{bg,g-r}$ and $N_{bg,r}$, are determined from a large ($\sim 3940 \square^\circ$) galaxy catalog around the North Galactic Pole, constructed from DPOSS data. This distribution, scaled to the appropriate area, is then subtracted from the color and magnitude distributions of each candidate cluster, and the median $g-r$ color and mean r magnitude of the remaining galaxies calculated.

Figure 7.1 shows the N_{g-r} distribution for a typical candidate before subtraction, the scaled $N_{bg,g-r}$ background distribution, and the final $N_{corr,g-r}$ distribution after background correction. As expected, the background galaxy counts are clearly bluer than the cluster

galaxies. We also experimented with the use of locally derived background estimates. We found that the closer to the cluster the local background was determined, the lower the estimated cluster richness. This effect continues out to very large radii, and prompted the use of a global background estimate, which has been questioned in the past (Lumsden *et al.* 1992). This procedure was also performed for known Abell clusters with measured redshifts $z_{spect} > 0.05$, setting the radius to two-thirds of the Abell radius (1 Mpc; $R = 0.67 \times 1.7'/z_{spect}$) to measure the mean and median colors and magnitudes.

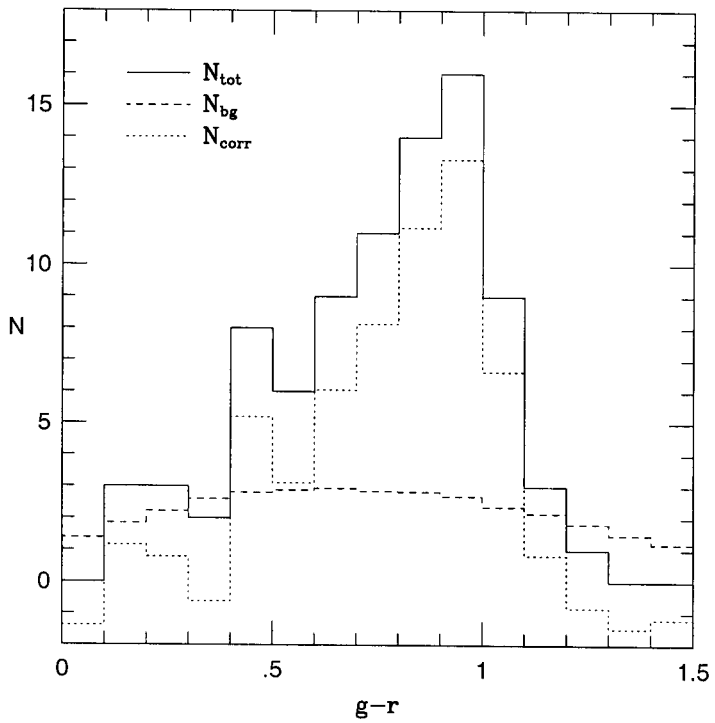

Figure 7.1: The color distribution of galaxies in Abell 115. The solid line is the uncorrected N_{g-r}. The dashed line shows the background correction, $N_{bg,g-r}$, and the dotted line is the corrected counts, $N_{corr,g-r}$.

Spectroscopic redshifts for the clusters used to derive our empirical photometric redshift estimator were taken from Struble & Rood (1999, hereafter SR99). These are culled from diverse sources in the literature, and are of highly variable quality. A majority of the cluster redshifts, especially those at $z > 0.1$, are based on very few (one or two) individual galaxy redshifts, and may therefore be incorrect. Nevertheless, this catalog is the largest, somewhat homogenized resource currently available. In order to minimize the number of incorrect cluster distances, we use only those clusters with two or more galaxies defining their

redshift. We supplant the catalog of SR99 with our own spectroscopic catalog, described in the previous chapter. The addition of our own clusters significantly increases the number of available clusters at $z \sim 0.2$. Our final sample comprises 176 clusters, taken from 3940$\square^\circ$ around the NGP, and 1412$\square^\circ$ around the SGP.

7.2 The Photometric Redshift Estimator

We find that both the colors and magnitudes are equally well correlated with measured spectroscopic redshifts. We derive an empirical relation between redshift, median $g-r$ color, and mean r magnitude using a bivariate least-squares fit:

$$log(z_{phot}) = 0.22269 \times r_{mean} + 1.474925 \times (g-r)_{med} - 0.9420 \times (g-r)^2_{med} - 5.4116 \quad (7.1)$$

The rms of $z_{spect} - z_{phot}$ is $\Delta z = 0.025$.

In practice, this must be an iterative procedure, because we do not initially know the redshift, and therefore the Abell radius, for our cluster candidates. Once a redshift is estimated, we then calculate the angular radius equivalent to 1 Mpc ($R_{phot} = 0.67 \times 1.7'/z_{phot}$) for each candidate, and re-center on the median location of galaxies inside this radius. We then repeat the background correction and color and magnitude measurements inside R_{phot}, centered on the new location, and estimate the redshift anew. These steps are repeated until the redshift converges; $\Delta z_{phot} < 0.005$. This threshold was chosen to be a small fraction of our final redshift errors.

The complete iterative procedure was also performed on the 176 clusters with measured redshifts. As expected, starting the process with the incorrect radius increases our errors, although not significantly. The final rms of $z_{spect}-z_{phot}$ is $\Delta z = 0.028$. This error includes all random and systematic errors, such as plate-to-plate photometry, classification, background correction, and even incorrectly measured spectroscopic redshifts. Figure 7.2 shows the final photometrically estimated redshift against the spectroscopically measured redshift for all 176 clusters. Clusters from the NGP region are shown as filled squares, while those from the SGP are open squares. The two samples are clearly consistent with each other, suggesting that any systematic differences (*i.e.*, calibration, classification) between the two areas are very small.

We have tested various cluster radii for calculating the mean colors and magnitudes of the galaxies in each cluster, and find no significant changes in the photometric redshift estimator. Using a somewhat smaller radius ($0.67 \times R_{Abell}$ instead of R_{Abell}) results in slightly lower scatter; this is probably because we are sampling the more homogeneous core galaxy population in each cluster. Making the radius much smaller significantly reduces the number of galaxies used to derive the mean properties for each cluster, resulting in larger errors. Additionally, we have ignored clusters with $z_{spect} < 0.05$, as these are too extended for our technique to handle properly, and our photometric calibration for bright galaxies is currently too poor.

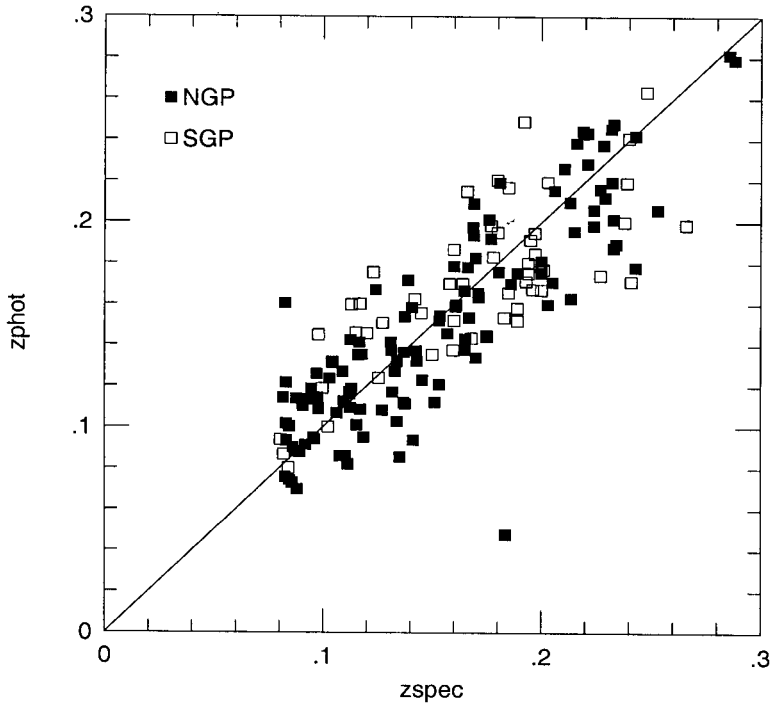

Figure 7.2: The photometrically estimated redshift against the spectroscopically measured redshift for 176 Abell and DPOSS clusters. Filled squares are clusters from the NGP region; open squares are from the SGP region.

We find the small errors from this photometric redshift technique to be remarkable, particularly in light of the data we are using. The data is taken from many plates in various parts of the sky, and therefore encompasses all of our photometric and classification errors. Additionally, we span a large range of galactic latitude, and thus varying amounts of extinction. Although we apply a correction to each galaxy, this can introduce added uncertainties in galaxy colors as well as small modulations in catalog depth. The photom-

etry is taken from photographic plates, where the quality is much lower than for CCDs. Additionally, the galaxy populations of these clusters must also vary; the fraction of bluer, late-type galaxies is not constant with richness or redshift. In comparison, the APM group, utilizing a richness-dependent, magnitude-based redshift estimator, achieved similar errors over only a much smaller redshift range ($0.04 < z < 0.1$, Dalton *et al.* 1994).

The photometric redshift estimates for the candidate clusters are provided in the fourth column of Tables B.1 through B.4. The mean redshift for our sample is $< z_{phot} >= 0.170$, which is comparable to our original estimate of $< z > \sim 0.15$, based on the magnitude range covered. Our highest redshift clusters are at $z = 0.3$, with many at $z > 0.2$. The redshift distribution of our robust sample is shown in Figure 7.3.

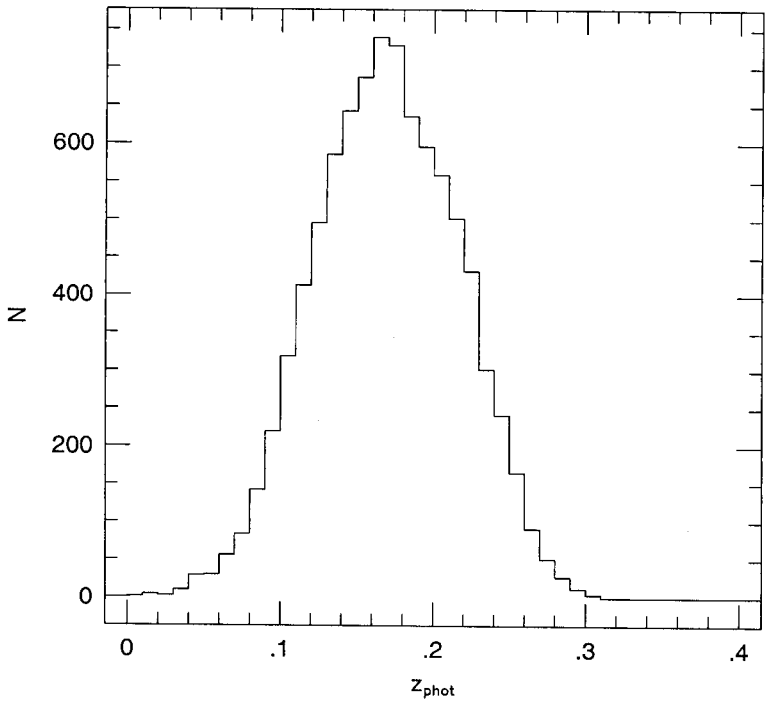

Figure 7.3: The redshift distribution of candidate clusters.

7.3 Richness

We have attempted to estimate the richness of our cluster candidates in numerous ways. First, we tested Abell's prescription (counting galaxies between m_3 and $m_3 + 2$, where m_3 is the magnitude of the third brightest galaxy), with and without a background correction applied, as well as simply counting all galaxies in the range $16.0 < m_r < 20.0$. The richnesses

of clusters with spectroscopic redshifts was measured from our catalog data, and compared directly to the data from Abell (1958). Rather than use richness class (which has a small range, is not continuous, and is dominated by poor clusters), we used the number of galaxies in the cluster. We find that there is a good correlation between our richness measures and those from Abell for clusters at $z<0.1$, but at higher z, we consistently underestimate the richness. This effect is certainly not new; Scott (1953) demonstrated the redshift dependence of such a simple-minded richness measure. As expected, the degree of underestimation worsens as z increases. This is due to the $m_r=20.0$ cut imposed due to classification. By $z=0.1$, we are no longer able to sample a reasonable part of the luminosity function of the cluster, and at $z=0.25$, only the very brightest cluster members are visible.

To alleviate these problems, we use a richness estimator which is dependent on the cluster redshift. We compute the richness in a fixed absolute magnitude interval, $M_* - 1 < M < M* +2$, using the r-band data, and assuming $M_{*,r} = -21.3$, taken from the cluster luminosity functions derived by Garilli *et al.* (1999; hereafter G99) based on CCD imaging of Abell clusters. For clusters at low redshift ($z<0.119$), we measure the richness by directly summing the background-corrected number of galaxies in the appropriate magnitude interval. Only at these low redshifts is this entire magnitude range contained within our data. For more distant clusters ($z>0.119$), we directly sum the galaxies with $M_* - 1 < M < M_{20}$, where M_{20} is the absolute magnitude limit corresponding to our catalog limit $m_r = 20.0$. We then calculate a correction factor β for the richness, defined as

$$\beta = \frac{\int_{M_*-1}^{M_*+2} \Phi(M)dM}{\int_{M_*-1}^{M_{20}} \Phi(M)dM} \tag{7.2}$$

We set the exponent in the luminosity function to $\alpha=-0.87$ (G99); the correction factor is slightly larger for lower α (by $\sim 5\%$ for $\alpha=-1.0$). Typical values of β are 1.15 for $z=0.2$ and 1.46 at $z=0.3$. The final richness for each cluster is listed in column 5 of Tables B.1 through B.4.

We show the richness distribution of our robust cluster candidates in Figure 7.4. The mean richness for our clusters is $<N_{gal}>= 29$, which corresponds to the poorest end of Abell's richness class 0. We therefore expect that our catalog contains many very poor clusters (or even groups).

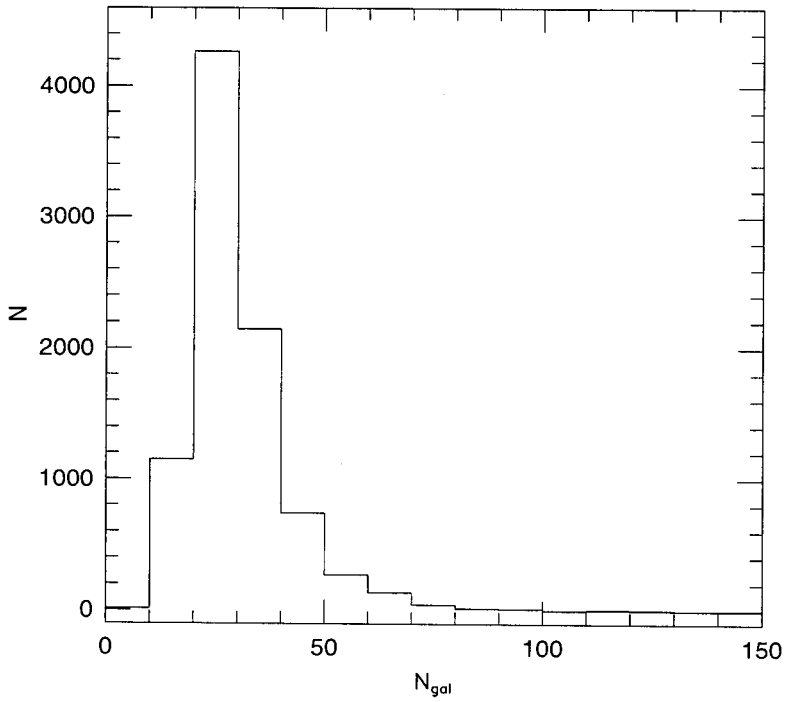

Figure 7.4: The richness distribution of candidate clusters.

An alternative method for computing richness could use objects fainter than $m_r = 20.0$, ignoring classification, as was done by Croft *et al.* (1997). At such faint magnitudes, the objects in a putative cluster should be predominantly galaxies, so that including them in a richness estimate may be feasible. This would force us to increase the limiting richness for a complete sample at higher redshift. It should be noted that the APM survey did not require a correction for their measured richnesses because they were limited to $z < 0.1$ for estimating both richness and redshift.

7.4 Consistency Between NGP and SGP

The photometric redshift and richness estimators provide tests for systematic errors between the NGP and SGP regions. If there are any significant photometric or classification differences between the two areas, the cluster redshift and richness distributions should reflect this. Similarly, if the detection criteria for clusters were systematically different (*i.e.*, threshold offsets, background correction errors) we should see evidence in these distributions.

We compare the distributions of photometric redshifts for the two areas in Figure 7.5. The SGP is plotted with solid lines; the NGP, scaled to the same total number of clusters as the SGP, is shown with dotted lines. For both the NGP and SGP, the mean redshift is $< z_{phot} >= 0.17$, and the *rms* scatter is also identical; $\sigma_N = 0.05$.

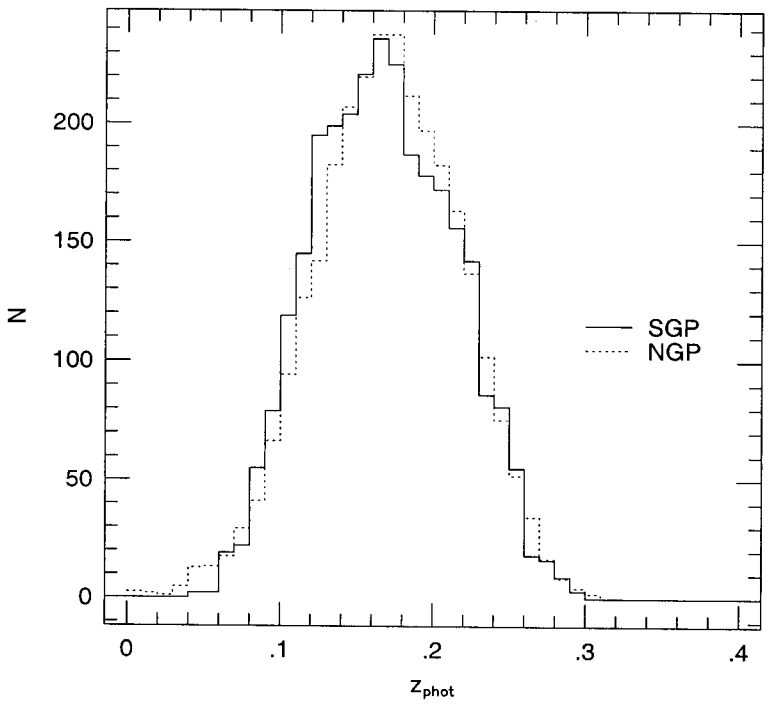

Figure 7.5: The distribution of photometric redshifts from the SGP region (solid lines) and the NGP region (scaled, dotted lines).

Similarly, Figure 7.6 compares the distributions of richnesses for the two areas. This may be a more sensitive test of systematics, as the photometric redshift depends on average properties of the cluster galaxies, which are less susceptible to small errors in the background correction or photometry. Richness, however, is a direct sum of galaxy counts, and could therefore be effected rather strongly by photometric zero-point errors, for instance. In both regions, the mean richness as well as the richness distributions are extremely similar, further demonstrating consistency.

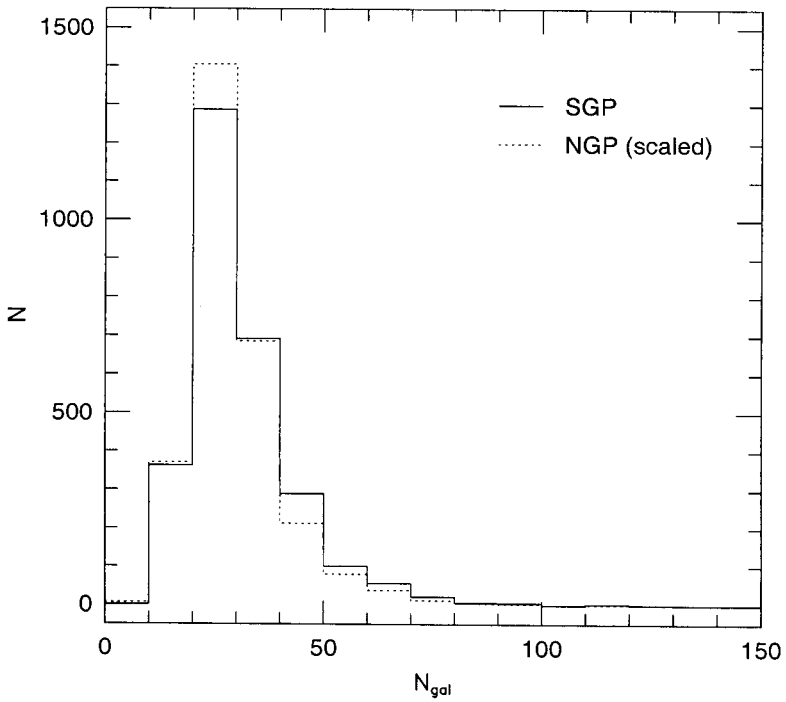

Figure 7.6: The distribution of cluster richnesses from the SGP region (solid lines) and the NGP region (scaled, dotted lines).

Chapter 8

Physical Properties of Abell Clusters

In addition to the cluster catalog generated from DPOSS, our extensive collection of CCD imaging of Abell clusters provides a unique resource to examine the basic properties of these systems. In this chapter we present photometric redshifts for 431 Abell clusters imaged as part of the Palomar Abell Cluster Optical Survey (PACOS), of which 236 are new redshifts.[1] In addition, we briefly examine the Butcher-Oemler effect in a subset of these clusters.[2]

8.1 Photometric Redshifts

The data used here are the CCD images of Abell clusters, obtained for the photometric calibration of DPOSS. Details of the data acquisition, reduction, and photometric accuracy are presented in Chapter 3.

From the CCD data, we wish to measure the redshift of each cluster. This can be done either by estimating the redshift of each galaxy individually, and examining the resulting redshift distribution, or by using the properties of all the galaxies in the image. We have chosen to use the second method, for a number of reasons. First, we only have limited wavelength coverage. Having only three filters (and especially the lack of u images) makes it difficult to disentangle color-redshift degeneracies. Second, our photometric errors on individual objects are significant enough to pose a problem for an object-by-object redshift estimator. Finally, since we have performed object detection in the different filters independently (*i.e.*, we do not have matched apertures), there may be systematic effects in the relative colors of different galaxy types. We have therefore elected to use the average properties of the galaxies in each field. Spectroscopic redshifts are taken from Struble & Rood (1999).

[1] The photometric redshift discussion is taken from Gal *et al.* 2000b.
[2] The Butcher-Oemler analysis is taken from Margoniner *et al.* 2001.

8.1.1 Redshift Estimation Technique

The basis of our photometric redshift estimator from the CCD data is the same as for our plate data. However, here we use the g magnitudes (as opposed to r for the plates), because the g magnitudes fade more rapidly due to the k-correction, and S/N is not an issue (as it is for the plates). We also assume a single cluster per CCD field is reasonable, although projections are certain to occur. While it has been estimated that up to 35% of clusters in the Abell catalog with $R \geq 1$ may be the result of projections of poorer clusters (van Haarlem, Frenk & White 1997), our results will be dominated by the richest cluster in each field. Our redshift estimator will fail if there are two similarly rich clusters projected along the line of sight.

We count the number of galaxies as a function of color, N_{g-r}, and the number as a function of g aperture magnitude (where our aperture has a radius of 13 pixels, or $\sim 5''$), N_g, inside each CCD frame, imposing a magnitude limit of $m_r = 21.5$ for CCD 13 and $m_r = 21.0$ for CCD16, to avoid incompleteness. We use the whole CCD area (as opposed to a given physical radius), because the size of our field is comparable to the sizes of clusters in the redshift range we are examining, and the centers of many clusters are not well determined.

First, we apply an extinction correction to the magnitudes and colors of all objects in our fields, derived from the maps of Schlegel *et al.* (1998). A single correction is used for each CCD field, since the pixel size of the extinction maps is comparable to the CCD FOV, and the vast majority of our fields are at high galactic latitudes; the mean $E(B-V)$ for our sample is 0.075^m. A statistical background correction must then be applied to both galaxy color and magnitude distributions. These corrections, $N_{bg,g-r}$ and $N_{bg,g}$,are determined from a set of 22 observations of random fields taken with CCD13, during numerous observing runs. This distribution (scaled to the appropriate area for CCD16 data), is then subtracted from the color and magnitude distributions of each cluster, and the median $g-r$ color and mean g magnitude of the remaining galaxies calculated. An example showing this procedure is shown in Figure 8.1. The thin solid line is the distribution of all galaxy colors $(g-r)$ in CCD13 images of Abell 2063. The dotted line is the distribution of galaxy colors derived from our random field observations, while the thick solid line is the background-corrected distribution. A sharp peak at $(g-r) \sim 0.5$ is seen, corresponding to the early-type galaxy

population in this cluster.

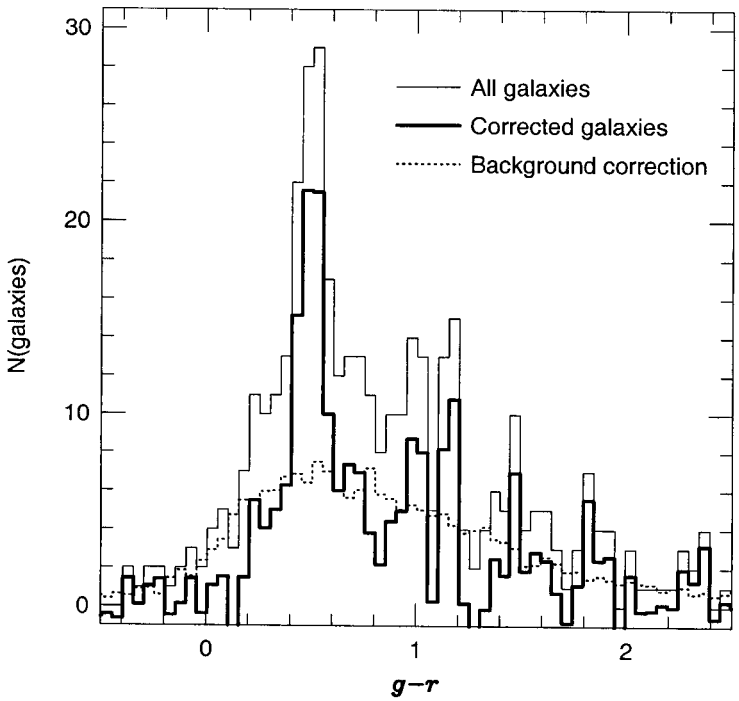

Figure 8.1: An example of the background correction procedure. The thin solid line is the distribution of all galaxy colors $(g-r)$ in CCD13 images of Abell 2063. The dotted line is the distribution of galaxy colors derived from our random field observations, while the thick solid line is the background-corrected distribution. A sharp peak at $(g-r) \sim 0.5$ is seen, corresponding to the early-type galaxy population in this cluster.

Empirical relations between our measured cluster properties and the spectroscopic redshifts were then derived independently for CCD13 and CCD16 data. For CCD13, 114 clusters with measured redshifts were used, while only 33 clusters were available for CCD16. Using the GAUSSFIT package (Jefferys *et al.* 1988), we performed a bivariate least-squares fit, deriving the following relations between redshift, median $g-r$ color, and mean g magnitude:

CCD13, with $\mathbf{m_{r,lim} = 21.5}$:

$$log(z) = 3.2619 \times (g-r)_{med} - 1.6687 \times (g-r)^2_{med} + 0.1190 \times g_{mean} - 4.6532 \qquad (8.1)$$

CCD16, with $m_{r,lim} = 21.0$:

$$log(z) = 3.2151 \times (g-r)_{med} - 1.6957 \times (g-r)^2_{med} + 0.0710 \times g_{mean} - 3.5983 \qquad (8.2)$$

The formal errors on each coefficient from the fit are very small (± 0.0002 or less). The above relations, although apparently dissimilar, should be universal, since we are using calibrated quantities. To test this, we applied the same magnitude cut ($m_r < 21.0$) used for the CCD16 data to the CCD13 data. The coefficients from the CCD16 fit were then used to estimate redshifts for the CCD13 clusters with spectroscopic redshifts. The rms value of $z_{spect} - z_{phot}$ was only marginally higher (0.025 *vs.* 0.024) than using the true CCD13 fit, although a slight systematic overestimate of the redshift does occur at $z < 0.1$. The effects of detector area, the background correction technique, and the sample used can all affect the fit; nevertheless, it appears that our derived relations should be applicable to other data sets treated in an identical fashion (*i.e.*, same filters, apertures, magnitude cuts, and background correction).

It is important to note that the combination of both color and magnitude information significantly improves our photometric redshift estimates. Figure 8.2 shows the photometric redshift estimates using magnitudes only, colors only, and the combination of colors and magnitudes for the CCD13 data. The scatter in redshift decreases from 0.034 for magnitudes only, to 0.031 for colors only, to 0.024 when both are used.

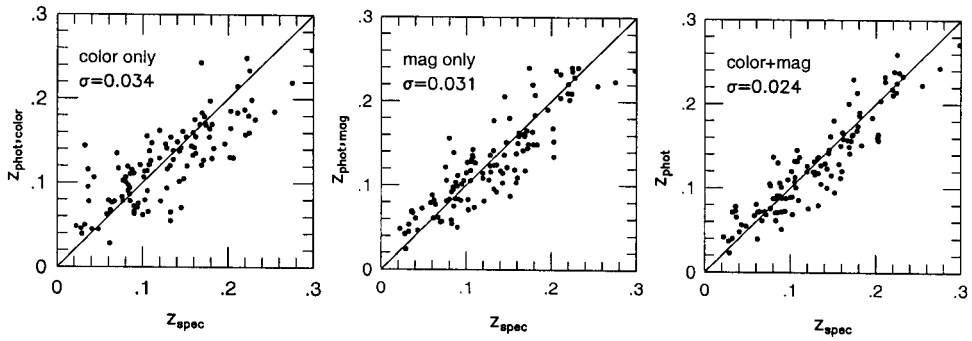

Figure 8.2: The photometric redshift estimates for the CCD13 data plotted against the spectroscopic redshifts, using magnitudes only, colors only, and the combination of colors and magnitudes to derive the estimates. The decrease in scatter is clearly seen.

8.1.2 Redshift Errors

The *rms* values of $z_{spect} - z_{phot}$ are $\sigma(z) = 0.024$ and 0.027 for CCD13 and CCD16, respectively. These figures represent the intrinsic scatter of our derived relationship between redshift and photometric properties. The scatter is larger for the CCD16 data due to the small number of clusters with spectroscopic redshifts used in the derivation. The error on any individual cluster redshift depends not only on the scatter of the relation, but also on the number of clusters in the local redshift range used to determine the relation. For instance, at the high redshift end ($z \sim 0.3$), there are only four clusters which constrain the relation for the CCD13 data. Therefore, we expect the errors in this redshift range to be larger than at $0.05 < z < 0.1$, where there are 29 clusters.

To estimate the magnitude of this effect, we have performed bootstrap simulations of our training samples. We randomly select clusters from our training sample, with replacement (allowing the same object to be selected more than once), until we have built a new training sample of the same size as the original (114 for CCD13, 33 for CCD 16). This new sample is used to derive a new redshift estimator, which is then applied to the original sample. We repeat this procedure 500 times, and calculate the mean redshift estimate, and the standard deviations about this estimate, for each cluster. Figure 8.3 shows the photometrically estimated redshift against the spectroscopically measured redshift for both CCDs. Error bars on individual redshifts represent the one-sigma redshift limits from the bootstrap procedure.

Clearly, the errors are smallest in the redshift bins with the largest number of calibrating clusters. Figure 8.4 shows the errors on each cluster redshift derived from the bootstrap procedure. Solid circles show the mean redshift errors in bins of $\Delta z = 0.05$. For CCD13, the errors are largest at $z \sim 0.3$, where there are only 3 clusters. The redshift distribution for CCD16 clusters is more even, yielding nearly equal errors over the entire redshift range. To estimate the true redshift error on any given measurement, we add in quadrature the intrinsic scatter of our z_{phot} *vs.* z_{spec} relation, and the error from the appropriate bin from our bootstrap simulation. This error estimate then encompasses both the intrinsic errors of our fit, and the errors introduced from our sample selection. For 57 clusters, we have multiple observations from which to estimate their redshifts. Comparing these redshift estimates, we find *rms* $\Delta z = 0.038$, which is exactly what we expect from the

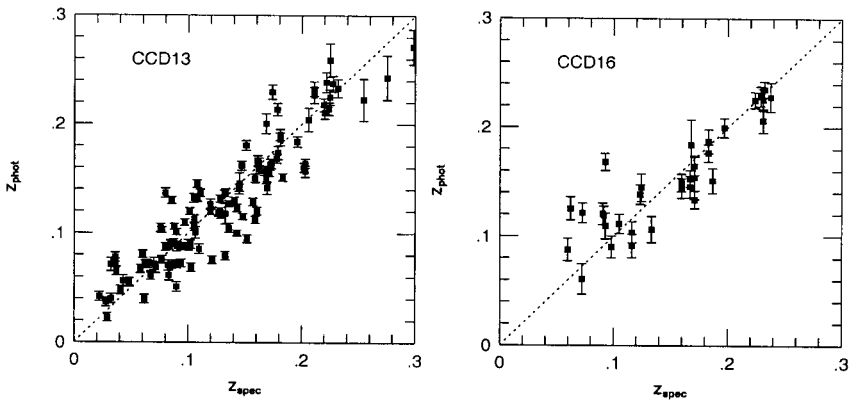

Figure 8.3: The photometrically estimated redshift against the spectroscopically measured redshift for both CCDs. Error bars on individual redshifts represent the one-sigma redshift limits from the bootstrap procedure. The 114 clusters used to derive the relation for CCD13 are on the left, while the 33 clusters used for CCD16 are on the right.

individual error estimates. Our redshift errors are not dominated by photometric errors, since a large number of galaxies contribute to the mean color and magnitude values in each cluster. The scatter is most likely due to inaccurate spectroscopic redshifts (less than 20% of the clusters have three or more galaxies with measured redshifts) and variance in the cluster properties (blue galaxy fraction, richness, etc.). For instance, Miller *et al.* (1999) have demonstrated that projection effects have resulted in significantly erroneous redshifts for 14% of clusters with single spectroscopic redshifts. These two effects cannot be disentangled without a larger sample of clusters with properly measured spectroscopic redshifts. Unfortunately, almost all of the clusters we studied that also have a significant number of spectroscopic redshifts are very nearby ($z < 0.05$), and therefore we cannot draw any significant conclusions about spectroscopic redshift errors for our sample as a whole.

8.1.3 Redshifts for 431 Abell Clusters

We present the photometric redshifts in Table B.3. Clusters are arranged in numerical order. The first column gives the Abell cluster number. The second column gives the CCD used for the observation. The next two columns provide the background-corrected median $(g-r)$ color and g magnitude for each cluster. The fifth column is the extinction $E(B-V)$. The sixth column provides the photometric redshift estimate, and the seventh column contains

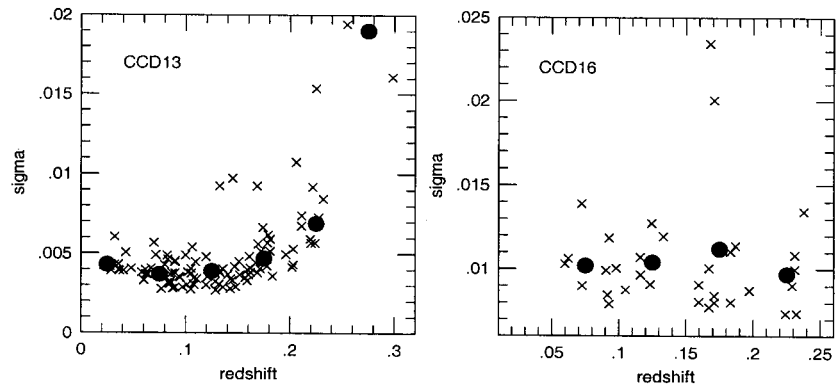

Figure 8.4: Crosses show the error of each cluster redshift, as determined by our bootstrap simulation. Solid circles show the mean redshift errors in redshift bins of $\Delta z = 0.05$. The left panel shows the 114 clusters from CCD13, while the right panel shows the 33 clusters from CCD16.

the estimated error, as described above. The final column gives the spectroscopic redshift, if it is available. For clusters with very low spectroscopic redshifts ($z_{spec} < 0.03$), we usually obtain a significantly higher photometric redshift. For these clusters, our CCD field covers only a small physical area, and we are likely seeing through the lower redshift cluster and measuring a background cluster.

8.2 The Butcher-Oemler Effect

The Butcher-Oemler (BO) effect provided some of the first evidence for the evolution of galaxies and clusters. Butcher & Oemler (1978, 1984) found an excess of blue galaxies in high redshift clusters in comparison with the typical early-type population observed in the central region of local clusters (Dressler 1980). The BO effect has also been observed in more recent studies, which indicate an even stronger evolution of the fraction of blue galaxies in clusters (Rakos & Schombert 1995, Margoniner & de Carvalho 2000, hereafter MdC00).

The BO effect is an indicator of evolution in the cluster galaxy population, which may result from changes in the morphology and star-formation rates of member galaxies with redshift. The fact that blue galaxies are more commonly found at higher redshifts, and the observation of an apparent excess of S0 galaxies in low redshift clusters, lead to the

suggestion by Larson *et al.* (1980) of an evolutionary connection between S0 and spiral galaxies. This idea can explain the population of blue galaxies observed by Butcher & Oemler as spiral galaxies seen just before running out of gas, and the disappearance of this population in more evolved, low redshift rich clusters (Dressler *et al.* 1997, Couch *et al.* 1998). In the last decade, high-resolution HST images have allowed the determination of the morphology of these high redshift blue galaxies. Dressler *et al.* (1994), Couch *et al.* (1994, 1998), and Oemler *et al.* (1997) found that the Butcher-Oemler galaxies are predominantly normal late-type spirals, and that dynamical interactions and mergers between galaxies may be a secondary process responsible for the enhanced star formation. A recent study by Fasano *et al.* (2000) indicates that as the redshift decreases, the S0 cluster population increases while the number of spiral galaxies decreases, supporting Larson's original idea of spirals evolving into S0s.

A second factor affecting the number of blue galaxies may be their environment. The fraction of blue galaxies seems to be correlated with local galaxy density, and with the degree of substructure in the cluster. Many studies have shown that the blue galaxies lie preferentially in the outer, lower density cluster regions (Butcher & Oemler 1984, Rakos *et al.* 1997, Margoniner & de Carvalho 2000). Also, Smail *et al.* (1998) studied 10 massive clusters and found that the fraction of blue galaxies in these clusters is smaller than observed in BO84 clusters at the same redshift range. However, an opposite trend is found in non-relaxed clusters with a high degree of substructure, where the fraction of blue galaxies is higher than that observed in regular clusters (Caldwell & Rose 1997, Metevier *et al.* 2000).

The evolution of these galaxies is probably correlated with their environment in the sense that spirals might consume and/or lose their gas, evolving to SOs, while falling into the higher density cluster regions. Although the exact mechanism responsible for the Butcher-Oemler effect is not completely understood (Kodama & Bower 2000), most authors seem to agree that the effect is real. A different idea is presented by Andreon & Ettori (1999) who show that the mean X-ray luminosity and richness of Butcher & Oemler (1984) clusters increases with redshift, and argue that the increase in the fraction of blue galaxies with redshift may not represent the evolution of a single class of objects.

We present observations of the Butcher-Oemler effect in a large sample of 295 Abell (1958, 1989) clusters of all richnesses, with no further selection on the basis of morphology or X-ray luminosities. This is important because all previous studies were based on samples

biased toward richer clusters, with some samples being further selected according to morphology and/or X-ray luminosities, so that a combination of different selection effects could be mimicking the observed $f_B(z)$ relation. Although our sample inherits biases existent in the Abell catalog, it should contain a more representative variety of clusters (in terms of degree of substructure, richness, and mass) at each redshift than any previous sample, and because of its large size should allow a better determination of the relation. Any results driven by selection effects present in previous samples might become apparent when compared with this one.

The sample used in this analysis is also taken from the dataset described in Chapter 3. From this original sample we excluded 120 clusters observed with a small field of view CCD, and 31 very low redshift ($z < 0.05$) clusters, for which only the core region can be observed with our $13' \times 13'$ images. Also, 26 cluster fields which exhibited galaxy counts comparable to the mean background, and one cluster with a bright star occupying $\sim 25\%$ of the CCD region, were excluded from the analysis. Since 2 Abell clusters had repeated observations from Gal *et al.* 2000a and MdC00, our final sample comprises 295 clusters. It is important to note that at variance with previous studies, the sample presented in this work is representative of all richness class clusters (21% $R = 0$, 50% $R = 1$, 21% $R = 2$, and 8% $R \geq 3$). No further selection regarding richness, morphology or degree of sub-clustering was applied when determining our sample. Spectroscopic redshifts for 77 clusters were obtained from the literature, and for the remainder photometric redshifts were estimated with an *rms* accuracy of approximately 0.04 using the methodology described in MdC00.

8.2.1 Analysis of the Butcher-Oemler Effect

The BO effect can be measured by comparing the fraction of blue galaxies in clusters at different redshifts. The $(g-r)$ *vs.* r color-magnitude (CM) relation was determined by fitting a linear relation to the red galaxy envelope using the same prescription as in MdC00. Red envelopes were subjectively classified as well-defined or not by visual inspection. Galaxies were defined as *blue* if they had $(g-r)$ colors 0.2^m below the linear locus in the CM relation. We used the spectral energy distribution of a typical elliptical galaxy (Coleman *et al.* 1980) to derive $k(z)$ corrections for our sample, and also corrected the data for extinction using the maps of Schlegel *et al.* (1998). Because the main purpose of this work is to study the evolution of galaxy populations, fainter galaxies play a crucial role. Whereas Butcher &

Oemler were limited to brighter galaxies by their photographic data, our CCD sample allows us to probe significantly deeper, selecting galaxies with r magnitude between $M^* - 1$ and $M^* + 2$, inside a region of radius 0.7 Mpc from the cluster center. This fixed linear size was chosen because our CCD images cover a field of radius $\sim 0.5 - 4.0$ Mpc at $z = 0.03 - 0.38$, and we want to study the same physical region and the same galaxy luminosity range for the entire sample. We assume a cosmology with $H_\circ = 67$ km s^{-1} Mpc^{-1}, and $q_0 = 0.1$, in which $M_r^* = -20.16$ (Lin *et al.* 1996).

Most (61%) of the clusters in our sample are at $z = 0.1 - 0.2$, so that the 0.7 Mpc central region, and the entire luminosity range between $M^* - 1$ and $M^* + 2$ can be observed. Clusters at higher redshifts are limited at brighter absolute magnitudes and a correction was applied in order to compare the fraction of blue galaxies in these clusters with the rest of our sample. The lower redshift clusters suffer from the opposite problem, since the brighter galaxies will be saturated, and we are also limited by the field of view. Details about these corrections can be found in MdC00, the only difference being that in the present work we adopt a more conservative brighter limiting magnitude of $M^* + 2$ instead of $M^* + 3$.

The blue and total counts contain a mix of cluster members and background galaxies. Background variations place a fundamental limit on the accuracy of f_B measurements: no matter how well one determines the *mean* background from a number of control fields, the background estimate for any particular cluster is no more accurate than the *scatter* in the control fields. For each cluster, we measured the effect of this scatter by computing f_B using background corrections from the 22 individual control fields scaled to the area of the CCD and the CM relation appropriate to that cluster. The final f_B is given by the median and the *rms* is based on the central two quartiles of the distribution. Simple propagation of errors through the equation $f_B \equiv \frac{n_{blue,cluster} - n_{blue,background}}{n_{total,cluster} - n_{total,background}}$ would give an overestimate because $n_{blue,background}$ and $n_{total,background}$ are correlated. The usual assumption that the error in f_B is mainly due to Poisson statistics in the background-corrected cluster counts does not properly take into account the background variations, and errors thus derived are about three times smaller than ours when applied to the same data.

The final fractions of blue galaxies for the entire sample are shown in the upper panel of Figure 8.5. For those clusters with multiple observations, we have used the observation with smaller σ_{f_B}. Clusters with spectroscopic and photometric redshift measurements are indicated by solid and open circles respectively. The individual error bars are not presented

to avoid confusion in the plot, but the median σ_{f_B} is 0.071. The lower panel presents only clusters that have: (1) $\sigma_{f_B} < 0.071$, (2) spectroscopic redshift measurements, and (3) a well-defined CM relation. The 1-σ_{f_B} errors are indicated for these clusters. In both panels, the solid lines indicates a linear fit derived from the clusters with $z \leq 0.25$ ($f_B = (1.24 \pm 0.07)z - 0.01$, with an *rms* scatter of 0.1 for the entire sample shown in the upper panel, and $f_B = (1.34 \pm 0.11)z - 0.03$, with an *rms* of 0.07 for the sample shown in the lower panel). The fits were done with the GAUSSFIT program (Jefferys *et al.* 1988) taking into account the measurement errors in f_B. The dashed line indicates the *rms* scatter around the fit, and while the upper panel shows a larger scatter, the two derived relations are the same within the errors. A clear trend of strong evolution with redshift is seen. A χ_ν test applied to the fit presented in the upper panel yields a value of 1.36 if only f_B errors are considered, and 1.13 when the uncertainties in the photometric redshifts are also taken into account. Such small χ_ν is due, however, to large measurement errors in this sample. A higher χ_ν of 1.72 is obtained for the subsample of clusters with smaller σ_{f_B} and spectroscopic redshift (lower panel of Figure 8.5).

Richness is a natural second parameter which might cause the range in f_B at given redshift. The left upper panel of Figure 8.6 shows the $f_B(z)$ diagram with symbol sizes scaled by N, the number of galaxies between $M^* - 1$ and $M^* + 2$, inside 0.7 Mpc, after background correction. Only clusters from the lower panel in Figure 8.5 and at redshifts between 0.1 and 0.2, where no corrections needed to be applied to compute f_B, are presented in this figure. The solid line is the best-fit linear $f_B(z)$ relation for the 26 clusters shown, and the dashed lines indicate the relations obtained when the sample is subdivided in two 13 cluster samples according to richness. The slopes of the three relations are the same within the errors (0.86 ± 0.23 for the entire sample, 0.96 ± 0.26 for the subsample of richest clusters, and 0.86 ± 0.56 for the poorest ones). Although the uncertainties are large, the rate of evolution is approximately constant for all richnesses, and there is clearly an effect, with richer clusters tending to lower f_B. The suggestion by Andreon & Ettori (1999) that the observed increase of f_B with redshift is caused by missing poor clusters at higher redshift is therefore no longer tenable, because any such selection effects would serve to *decrease* the redshift evolution of f_B. The evolution in f_B is real, and takes place in all richness classes.

To ensure that richness and redshift are not correlated in this subsample, we plot N *vs.* z in the right upper panel of Figure 8.6. The best-linear fit ($N = -(38.2 \pm 106.2)z + (89.5 \pm$

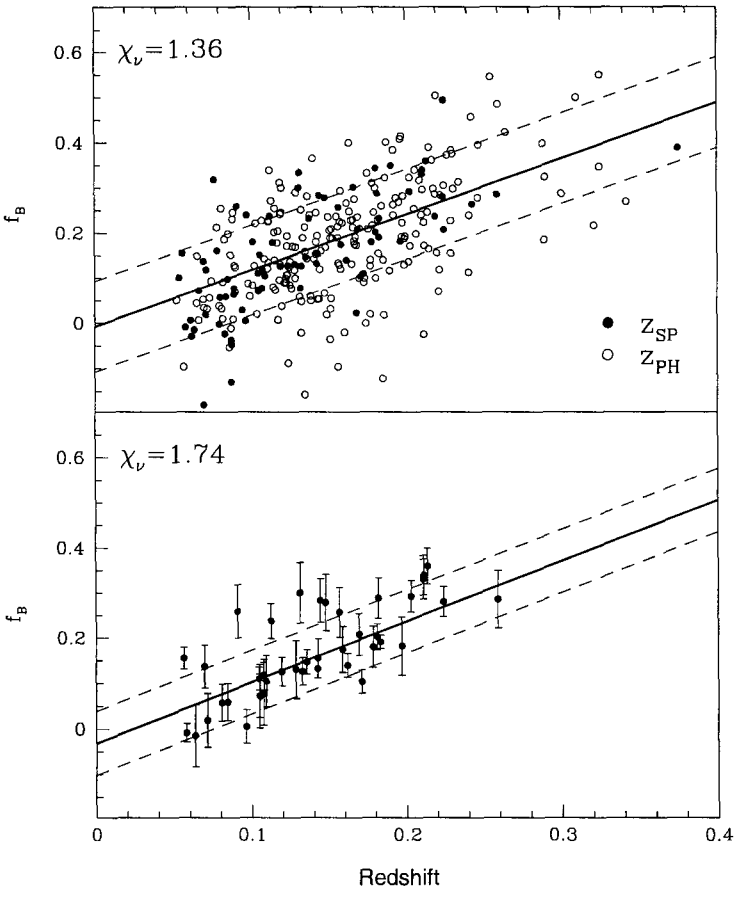

Figure 8.5: Fraction of blue galaxies in the magnitude range between $M^* - 1$ and $M^* + 2$, and within 0.7 Mpc from the center of the cluster. The entire 295-cluster sample is shown in the upper panel, and only clusters with (1) $\sigma_{f_B} < 0.071$, (2) spectroscopic redshift measurements, and (3) well-defined CM relation are presented in the lower panel. In each panel the solid line indicates a linear $f_B(z)$ fit derived from the clusters with $z \leq 0.25$, and the dashed line represents the *rms* scatter of the clusters around the fit.

14.5)) is indicated by the solid line, and the dashed lines represent adding/subtracting 1-σ uncertainties to its coefficients. Richness and redshift are uncorrelated in this sample.

To gauge the richness importance, we investigate $f_B(z, N)$ relations with various richness dependences (N^{-1}, $N^{-3/2}$, N^{-2}, and N^{-3}), and found that N^{-2} correlates slightly better with f_B. The final best-fit relation for the data, when both redshift and richness are considered, and taking into account the errors in f_B and N, is $f_B = (1.03 \pm 0.25)z + (388.3 \pm 111.4)N^{-2} - 0.04$, with $\chi_\nu = 0.99$. The F test indicates with $> 99\%$ confidence ($F_{\chi_\nu} = 23.8$, for 25 to 24 degrees of freedom) that richness is responsible for the improvement observed in χ_ν. Richness is therefore extremely important in determining f_B , and it is in fact enough to account for the scatter observed in a simple $f_B(z)$ relation. In the lower left

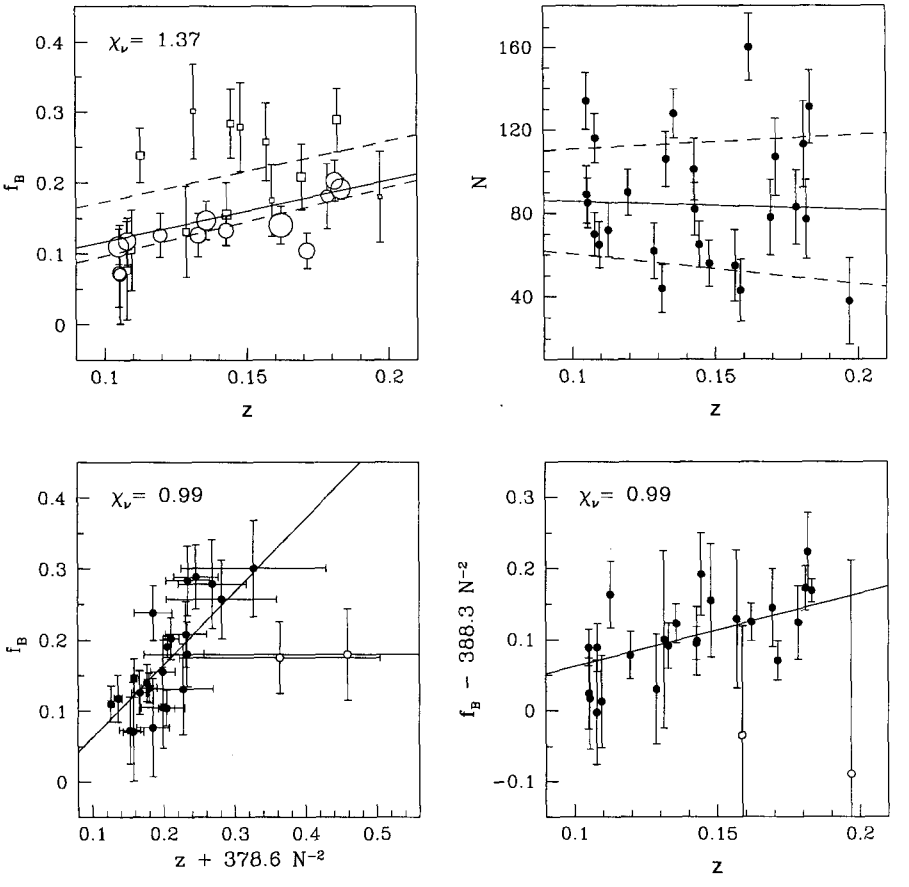

Figure 8.6: Subsample of clusters with $0.1 \leq z \leq 0.2$ from the lower panel in Figure 8.5. The solid line in each panel represents the best-fit to the entire sample. Left upper panel: $f_B(z)$ diagram with marker sizes scaled by N (galaxy counts). The dashed lines indicate the fits computed separately for the richest (circles) and poorest (squares) clusters. Right upper panel: N *vs.* z. The linear $N(z)$ fit is indicated by the solid line, and the dashed lines represent adding/subtracting 1-σ uncertainties to its coefficients. Lower left panel: f_B *vs.* $z+378.6N^{-2}$ (edge-on view of the best-fit plane $f_B = (1.03\pm0.25)z+(388.3\pm111.4)N^{-2}-0.04$ to the data). Lower right panel: richness-corrected f_B as a function of redshift.

panel of Figure 8.6 we plot f_B *vs.* $z + 378.6N^{-2}$, which represent an edge-on view of the best-fit plane $f_B(z, N)$, and in the lower right panel we present the redshift dependence of a richness-corrected-f_B: the redshift evolution is clear.

Although all 26 clusters shown in Figure 8.6 were used to compute the relations indicated by solid lines in the figure, the two clusters represented by open circles (Abell 520, and Abell 1081) seem to deviate from the trend. These clusters also have the largest σ_N (derived from the scatter in the 22 control regions), and if excluded from the fitting, the relation changes to $f_B = 1.13z + 480.56N^{-2} - 0.06$ ($\chi_\nu = 0.95$), indicating a slightly stronger redshift dependence.

Finally, we used 11 clusters with ROSAT X-ray luminosities to check for correlations with f_B, but this small sample did not allow any conclusions. There is a possible trend of increasing L_X with redshift in the sense found by Andreon & Ettori (1999) in BO's original sample. However, there is no clear trend of f_B with L_X, arguing against any contamination of the $f_B(z)$ relation by selection effects. A comparison of the X-ray luminosities of these clusters with their f_B could provide new insight to the BO effect, and we are in the process of obtaining X-ray fluxes and upper limits from the RASS (Rosat All Sky Survey) for all of these clusters, as well as a larger sample of new clusters generated from DPOSS-II.

We stress that these results are not to be directly compared with fractions of blue galaxies as originally defined in BO84. The most important reason for differences is the magnitude range used to calculate f_B. The number of blue galaxies increases at fainter magnitudes and it is therefore natural that our f_B measurements are in general higher. Also, the usage of a rigid physical scale for all clusters, instead of regions determined individually for each cluster according to its density profile, should yield different f_B estimates. When f_B is computed using the same absolute magnitude range used by BO84, we find signs of evolution that are stronger than originally suggested in their work, and which are consistent with recent works by Rakos & Schombert (1995) and MdC00. Limiting our sample at brighter absolute magnitudes, however, increases the σ_{f_B} (and σ_N) because of the smaller galaxy count statistics, and probes a smaller fraction of the cluster population.

This is the first sample large enough to allow the study of the f_B variations at a given redshift. A χ_ν test applied to a simple linear $f_B(z)$ relation shows that the scatter in f_B at a given redshift is consistently larger than the measurement error, indicating a real cluster-to-cluster variation. We investigate the richness dependence of the Butcher-Oemler effect, and find a strong correlation between f_B and galaxy counts in the sense that poorer clusters tend to have larger f_B than richer clusters at the same redshift. The inclusion of poor clusters tends therefore to increase the slope of the $f_B(z)$ relation, and is another factor (together with the inclusion of fainter galaxies) responsible for the stronger evolution observed in this sample when compared to previous works based mostly on rich clusters.

Chapter 9

The Cluster-Cluster Correlation Function

9.1 A Brief History

The cluster-cluster correlation function is an essential cosmological probe. Despite the seeming simplicity of this measure, it is extremely difficult to carry out, especially at the largest scales. The correlation strength is a function of cluster richness (Bahcall & Soneira 1983), so any attempt to measure it requires a catalog with well-understood selection criteria. At large angular scales, catalog homogeneity is also an issue.

Bahcall & West (1992) used a "small" catalog of 200 clusters drawn from the APM survey to perform one of the first measures of the correlation function using an objectively generated cluster catalog. They attempt to measure a "universal" correlation function, where the dependences on richness and intracluster separation are taken out by a normalization. Their results ($r_0 = 13.2h^{-1}$ Mpc, $A = 135$) were consistent with the expectations for a catalog containing many poor clusters to $z \sim 0.1$. Croft *et al.* (1997) performed a similar analysis, using 165 clusters of varying richnesses, to measure the correlation function and test the universal scaling relation used by Bahcall & West, and find that the proposed scaling of the correlation length on mean intracluster distance ($r_0 = 0.4d_c$) is *not* valid. In fact, they believe it to be an artifact due to inhomogeneities in the Abell catalog, consistent with the earlier findings of Efstathiou *et al.* (1992). The question remains unsettled, however, with a more recent study (Lee & Park 1999), also utilizing the APM survey, finding a much longer correlation length and higher amplitude for rich APM clusters than Croft *et al.* Lee & Park also find a richness dependence nearly identical to that of Bahcall & West, and claim that using X-ray selected cluster samples reduces the projection effects found in optically selected cluster samples.

Without redshifts, however, one is reduced to measuring the angular correlation function $w(\theta)$. If a comparison with spatial results is desired, one must invert $w(\theta)$ via the Limber equation (Limber 1954) along with some estimate of the redshift distribution of the objects

studied. The Abell and Zwicky catalogs have been used to measure $w(\theta)$, for the statistical sample as a whole (Hauser & Peebles 1973), as well as for subsets of different richnesses and redshifts (Bahcall & Soneira 1983, hereafter BS83; Postman, Geller & Huchra 1986, hereafter PGH86; Olivier *et al.* 1990, hereafter O90). The samples used in these analyses were small compared to our catalog; for instance, BS83, O90 and PGH86 used ~ 1600 clusters with distance class $D \geq 5$ (over the entire high-latitude northern and southern sky), while PGH86's distance limited sample of only 152 clusters extends only to $z = 0.1$, due to a catalog magnitude limit of $m_{10} = 18$.

Intermediate to these two cases is the use of photometric redshifts, in combination with angular information, to measure the evolution of the correlation function (Brunner, Szalay & Connolly 2000). Although a full spatial measurement is impossible because of the redshift errors, subdivision of the observed sample into redshift shells significantly thicker than the errors allows one to directly measure the evolution of $w(\theta)$.

The disagreement on such fundamental measures is striking. The amplitude and length of the correlation function, as well as its richness dependence, are sensitive tests of cosmological models, so understanding selection effects and biases in the input cluster catalog are extremely important. The earlier studies have utilized rather small numbers of clusters, because the Abell catalog is an order of magnitude smaller than ours, and the spatial correlation functions require spectroscopic redshifts to enforce a uniform redshift limit. Our catalog, covering a larger area, and with photometric redshifts, allows us to perform the same measurements using much larger samples. However, we currently restrict ourselves to measuring only the angular correlation function, to minimize possible systematic errors due to our photometric redshifts.

9.2 The Correlation Function from DPOSS

We estimate the correlation function using the method described in Landy & Szalay (1993). This estimator has the form:

$$1 + \hat{w} = \frac{(DD - 2DR + RR)}{RR} \tag{9.1}$$

where D refers to a point in the actual data set, and R to a point in a randomly generated data set (with the same angular limits and bad area masking applied). This estimator reduces the variance in the measured correlation function in comparison to other methods (*e.g.*, Peebles 1975, Sharp 1979, Hewett 1982, and others).

First, we attempted to measure the correlation function using all of the robustly detected clusters in the NGP and SGP regions. These initial results are shown in Figure 9.1. Red circles denote the NGP sample, while blue squares are the SGP sample. Error bars show the Poisson errors derived from multiple realizations of the random catalog, scaled with the number of random-random pairs in each angular scale bin. This error measure is known to underestimate the true errors by a factor of ~ 1.5 (Croft *et al.* 1997). In addition, the results from the APM (Dalton *et al.* 1997) are shown as triangles, and the fit from PGH86 of $w(\theta) = 3\theta^{-1}$ as the dotted line.

The most striking result is the small size of our error bars. This is in stark contrast to previous work, where errors are not even shown (BS83) or are rather large (O90, D97). We have entered the regime where systematic errors, such as zero-point offsets between calibrated plate areas, are dominant over Poisson noise. The slope of the correlation function for $1^\circ < \theta < 5^\circ$ is very similar for the two samples; -0.96 for the NGP and -0.95 for the SGP. Additionally, the amplitude of the correlation function is nearly identical for both samples. We note that the two areas are calibrated, and the clusters selected, completely independently. Therefore, the excellent agreement between the two regions provides a constraint on certain systematic errors. We also note the apparently good agreement with the APM survey, especially at intermediate angular scales.

From Figure 9.1, we can see deviations of the correlation function from a pure power law. At small angular scales ($\theta < 3^\circ$), there appears to be a flattening of the correlation function. Similarly, at large angular scales ($\theta \sim 10^\circ$), there is a sharp drop in the correlation function, especially for the NGP. Some deviations of the correlation function from the expected smooth power law are likely due to small offsets in single plate and nine-plate area zero-points resulting in variable effective redshift and richness limits, adding and/or subtracting power at various scales. To address these issues, we have used the photometric redshifts and richnesses of our clusters to generate a more complete subsample. We take only those clusters with $N_{gal} > 30$ and $0.1 < z < 0.15$. We expect that only detection of the highest redshift clusters ($z \geq 0.2$) should be modulated by zero-point offsets. Similarly,

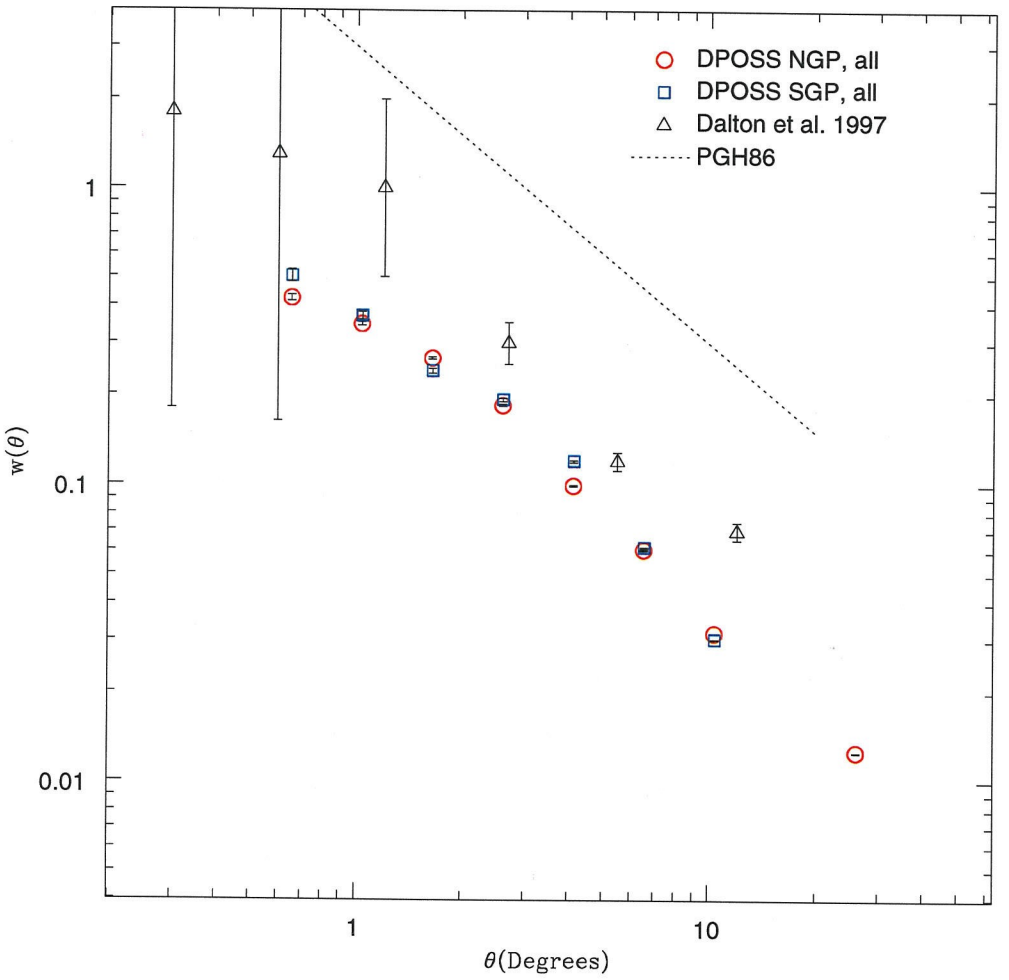

Figure 9.1: The cluster-cluster correlation function for all robust clusters in the NGP (red circles) and SGP (blue squares) samples, along with points from Dalton *et al.* (1997) as triangles, and the $w(\theta) = 3\theta^{-1}$ fit from PGH86 as the dotted line.

detection of the poorest clusters is most strongly effected by such errors. We show the results of this exercise in Figure 9.2. Here we compare the entire NGP sample (from Figure 9.1, filled circles), with the smaller but more complete sample from the NGP (red circles) and SGP (blue squares), after applying the richness and redshift cuts.

The application of these cuts produces significant improvement in the shape of the correlation function at small angles. The reasons for the improvement are unclear; it may be due to problems in the splitting of poor and rich clusters in high density regions. The error bars, however, are much larger, as the sample size is decreased by a factor of $\sim$10. Notably, the amplitudes and shapes of the correlation function are very similar for both regions, further supporting the homogeneity of the catalog discussed in Chapter 7. Additionally,

we note that the amplitude of $w(\theta)$ increases after we apply our selection criteria; this is the expected behavior as our cut sample has higher richness than the complete dataset. The sharp drop in the correlation function at large scales can still be seen, and is even exacerbated by these cuts. Our first assumption was that this may be due to the lack of an integral constraint. This constraint, typically applied to catalogs covering smaller areas, ensures that the mean density of clusters (or galaxies) in a given catalog is an accurate representation of the universal mean density. However, our survey covers such a large area that this constraint should be unnecessary. In fact, the magnitude of the correction due to the integral constraint is dependent on the cosmological model used, and can generate results that reflect the input model. Rough estimates of the magnitude of the integral constraint contribution to the correlation function for our sample at large angles are $\Delta w(\theta) \leq 0.01$ (M. Kerscher, *pvt. comm.*), much smaller than the measured amplitude. We therefore do not apply this correction.

An additional clue to the cause of the downturn at large θ is that it does not appear in the full SGP sample, and is smaller in the cut SGP sample than in the cut NGP sample. The NGP region spans a much larger range of galactic latitude than the SGP; this results in a larger gradient of contaminating objects due to misclassified stars. Such a gradient introduces an effective anti-correlation at large angular scales, reducing the power in the correlation function. To test this, we have generated a subsample of the NGP cluster catalog, applying the richness and redshift cuts described earlier, but also imposing a galactic latitude cut of $|b| > 60°$. The results are presented in Figure 9.3. We plot the cut NGP sample (from Figure 9.2) with filled circles, and the b-limited sample with red circles. The downturn at large angular scales is alleviated. However, this catalog covers only about $\sim$50% of the original area, so we are unable to make measurements at angular scales significantly larger than 10° without the application of a significant integral constrain correction. Indeed, at $\theta \sim 15°$, the correlation function becomes negative; the estimated integral constraint correction is $\delta w(\theta) \sim 0.01$.

The slope of the correlation function for the NGP galactic latitude, richness- and redshift-limited sample is -0.85; this value changes at the $\sim$ 10% level depending on the exact angular limits used in the calculation. We note that our results are similar to those of the APM group, although there is evidence for slightly more large scale power in our survey. The only similarity between the surveys is that both are based on plate material. The input

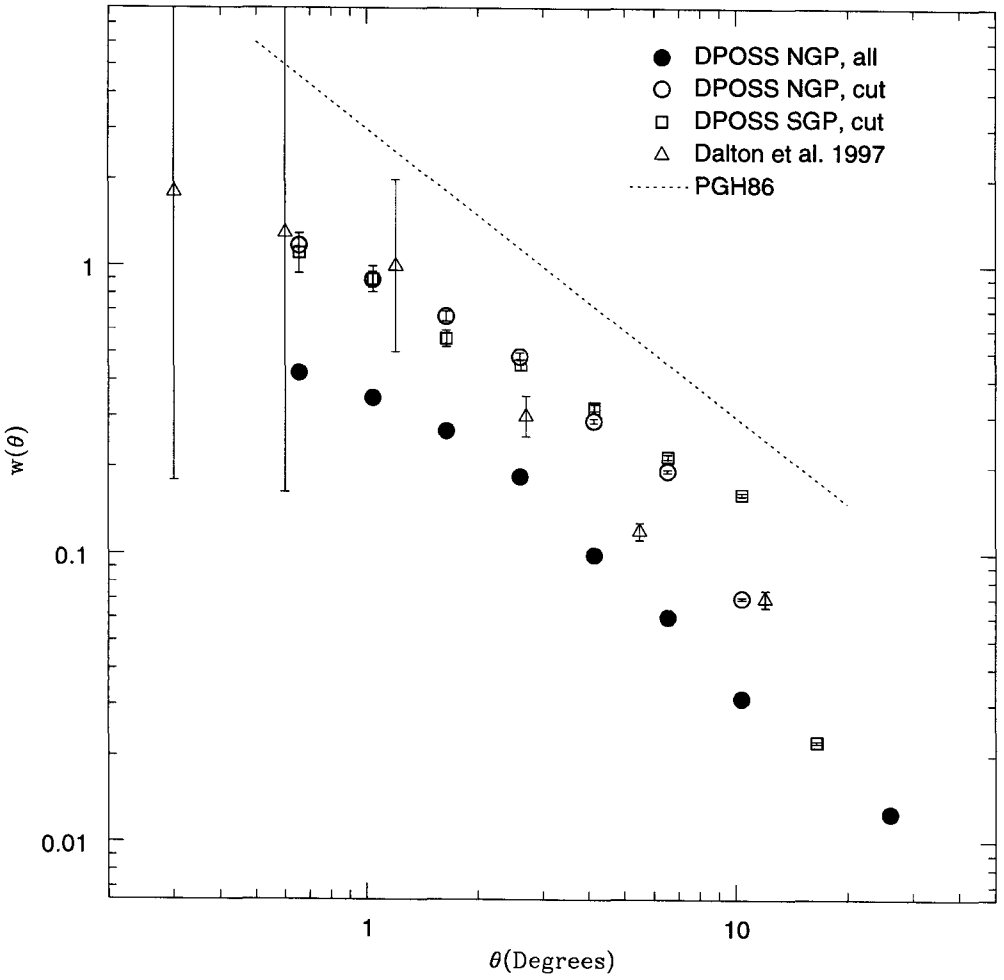

Figure 9.2: The cluster-cluster correlation function for the original NGP sample (filled circles), and the cut NGP (red circles) and SGP (blue squares) samples, along with points from Dalton *et al.* (1997) as triangles, and the $w(\theta) = 3\theta^{-1}$ fit from PGH86 as the dotted line.

galaxy catalogs come from plates with different filters, the plate scanning is done by separate machines, the image processing algorithms differ, and the cluster detection methods and criteria are quite distinct.

9.3 Richness Dependence

The amplitude of the cluster-cluster correlation function evolves with redshift, and increases with the mean richness of the clusters used in the measurement (Bahcall & Soneira 1983). Because our cluster catalog is reasonably complete over only a relatively modest range in redshift ($0.1 < z < 0.2$), and our photometric redshift errors are a significant fraction of this

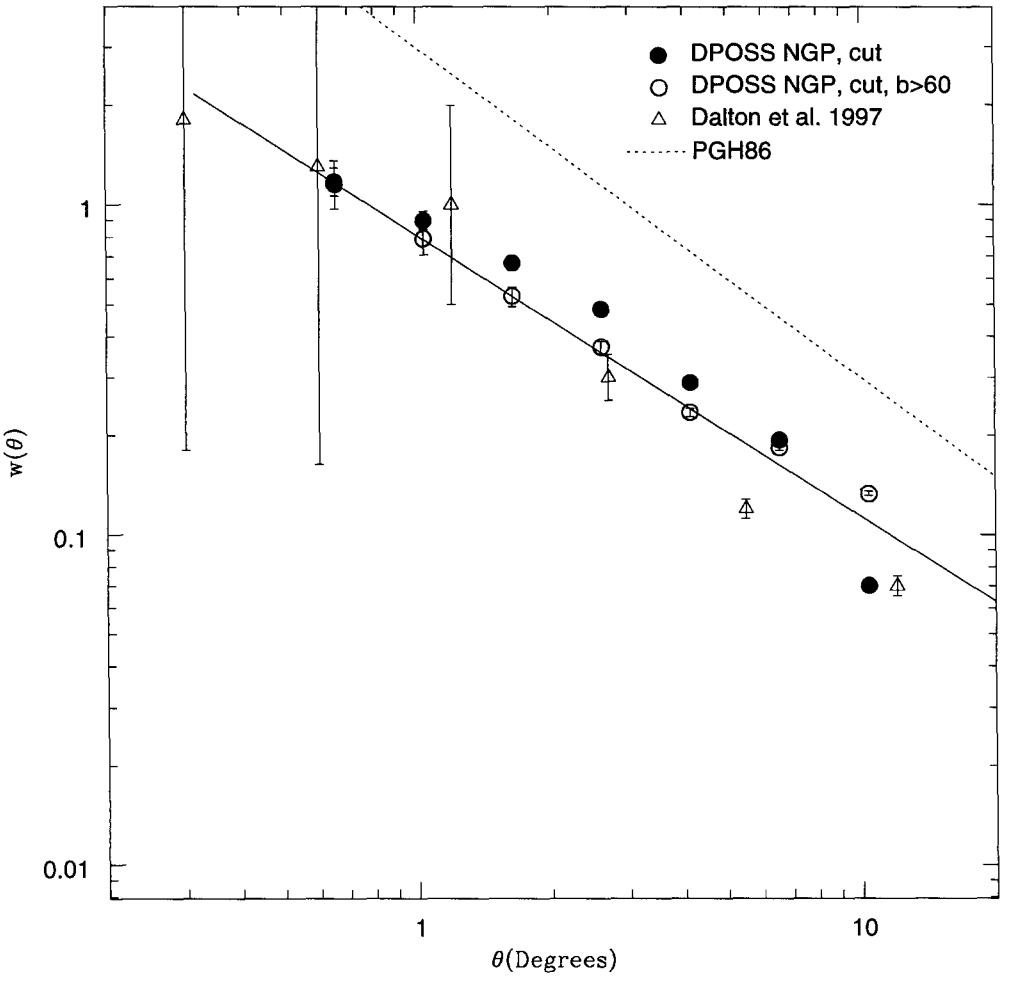

Figure 9.3: The cluster-cluster correlation function for the richness/redshift limited NGP sample (filled circles), and the same sample with a galactic latitude cut applied (red circles), along with points from Dalton *et al.* (1997) as triangles, and the $w(\theta) = 3\theta^{-1}$ fit from PGH86 as the dotted line.

range, it is difficult, if not impossible, to discern any redshift evolution. In addition, this redshift baseline is short enough that we would expect little or no evolution in $w(\theta)$ over this time.

However, in our redshift range, we have very good measures of the cluster richnesses. Therefore, we perform a preliminary examination of the dependence of $w(\theta)$ on cluster richness, using the NGP region. We take only those clusters with $0.1 < z < 0.15$ to ensure that our catalog is complete. The catalog is then divided into two richness ranges, $20 < N < 30$ and $N > 40$. The low-richness sample contains 2,855 clusters with a mean richness of $< N >= 25$. The high-richness sample is much smaller, consisting of 630 clusters with $< N >= 51$. The results are shown in Figure 9.4. We find that the expected trend of

increasing amplitude with richness is verified.

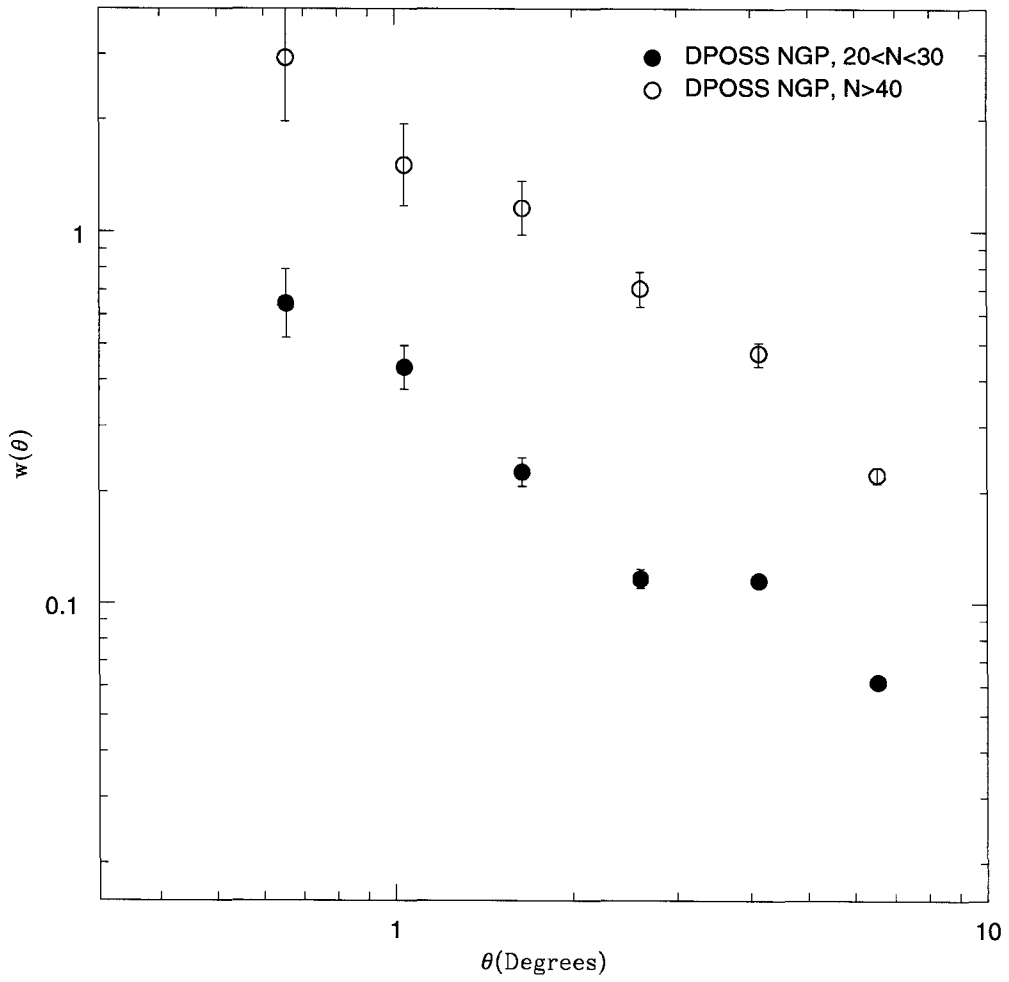

Figure 9.4: The cluster-cluster correlation function as a function of richness for the NGP sample. Filled circles are poor clusters ($< N >= 25$), while open red circles are richer clusters ($< N >= 51$).

In the future, once our final photometric calibration and even larger samples are available, we will perform more detailed analysis of the correlation function and its dependence on richness and redshift. In addition, bootstrap error estimation will be performed to provide a more realistic estimate of our errors; this is a computationally intensive and time-consuming process. Until then, we leave this chapter as a demonstration of the power of a large, systematic survey, and proceed to discussion of some other future prospects in the next chapter.

Chapter 10

Future Scientific Studies with the Cluster Catalog

In the time span of a graduate career (even a long one like mine), it is impossible to undertake, much less complete, many of the scientific projects for which the data in this thesis is useful. In this chapter, I hope to convey a sense of the many other directions we have begun to explore using this catalog of galaxy clusters culled from DPOSS.

10.1 Selection Effects in Optical vs. X-ray Cluster Catalogs

The production of cluster catalogs in both X-ray and optical wavelengths is plagued by selection effects. As discussed earlier, optical catalogs suffer from potentially high numbers of false clusters due to projection effects. The correctly detected clusters may have incorrect richnesses assigned due to projection effects as well, and multiple real clusters, separated in redshift, can appear as one along a single line of sight for the same reasons. X-ray catalogs, on the other hand, are akin to performing a mass and virialization selection. Poor clusters or unrelaxed systems, with little or no hot gas, or no bright central gas concentration, may be undetected. Current all-sky X-ray surveys are also not as deep as their optical counterparts. It would be very instructive to compare catalogs produced from these two complimentary wavelengths to study the biases that might be present in each. Some samples for such a study already exist: Abell, DPOSS, and soon SDSS in the optical; RASS (Collins *et al.* 2000, Ebeling *et al.* 2000, Böhringer *et al.* 2000), EMSS (Gioia & Luppino 1994), and catalogs from pointed ROSAT observations (Scharf *et al.* 1997, Romer *et al.* 2000) in X-rays. We are planning to conduct just such an exercise, taking into account the properties of the detected clusters as well.

As an example, we have cross-correlated our NGP cluster catalog with that of the Northern ROSAT All-Sky (NORAS) cluster survey (Böhringer *et al.* 2000). Their survey contains a total of 378 securely identified galaxy clusters; 135 of these are within our NGP area. Using a $5'$ search window, we find 73 of the NORAS clusters (54%) are also detected by DPOSS. Increasing the search window to $10'$, we find 93 of the NORAS clusters (69%).

Additionally, 26 NORAS clusters (19%) of NORAS clusters are in the areas of DPOSS excluded due to the presence of bright, extended objects. Therefore, nearly all NORAS clusters which we expect to find in DPOSS are indeed detected.

However, it is extremely interesting to examine the redshift distribution of the matched and unmatched clusters, shown in Figure 10.1. The most obvious feature is the lack of clusters detected in DPOSS at $z < 0.05$. This is exactly what we expect based on the size of our smoothing and detection kernels. The masking of extremely bright objects in DPOSS will also prevent us from finding low redshift clusters, which may contain bright, large cD galaxies. We also expect clusters at $z > 0.2$ to be rarely detected in the current DPOSS cluster catalog; this is because of our bright magnitude limit, $m_r < 19$. If we restrict ourselves to the redshift range $0.05 < z < 0.2$, then we detect 55/76 (72%) and 67/76 (88%) NORAS clusters in DPOSS using the $5'$ and $10'$ match radii, respectively. Interestingly, a comparison of X-ray luminosities for the detected and undetected clusters shows no obvious differences; the mean L_x is the same for both samples, within the uncertainties.

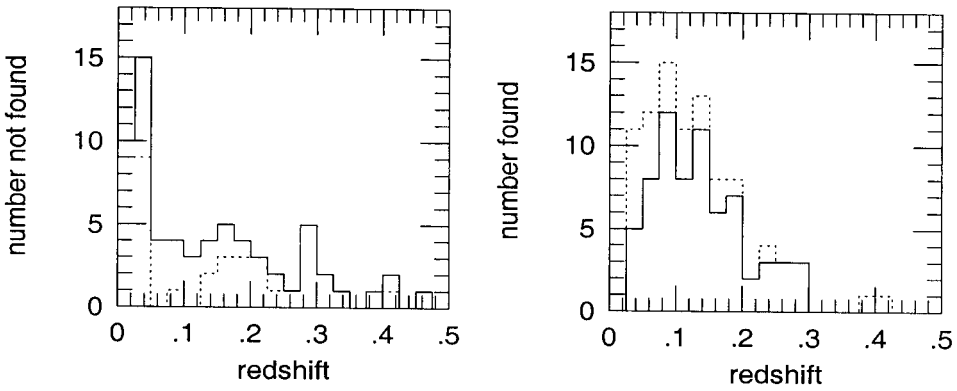

Figure 10.1: Redshift histograms for clusters detected in NORAS but not DPOSS (left), and in both surveys (right). The solid lines show the distributions for objects matched using a $5'$ radius; the dotted lines are using a $10'$ radius.

Unfortunately, we do not have a complete list of NORAS clusters, only those with follow-up completed and published. Nevertheless, there are vastly more (a factor of ~ 50) clusters detected in the NGP area of DPOSS. This suggests that current large-area X-ray cluster catalogs are severely incomplete, most likely missing the poorer clusters.

It should be noted that NORAS contains only very significant detections from the first processing of the RASS. It has been suggested that there are perhaps $\sim$ 3000 clusters

detected in RASS, with most at very low significance (Böhringer, *pvt. comm.*). Because the extended size and even the reality of these sources is so uncertain, they will not be published. A joint analysis of the X-ray and optical samples can provide strong evidence for the reality of such low-significance detections.

10.2 Clusters at Intermediate Redshift

While this thesis uses a magnitude-limited sample of galaxies from DPOSS to create a cluster catalog, the data we have available goes approximately 1.5 magnitudes deeper. At such faint magnitudes, the number counts of galaxies dominate those of stars (especially at high galactic latitude, Koo & Kron 1982). Thus, it is possible to search for clusters at higher redshifts ($z \sim 0.3 - 0.5$), by ignoring classification entirely. At these redshifts, our cluster catalogs will contain only the richest clusters, and the selection effects imposed by plate-dependent depth effects will be significant. Nevertheless, there has been no systematic survey for clusters at moderate redshift over large sky areas. Only deep photographic surveys, such as Gunn, Hoessel & Oke (1986), or even smaller area CCD surveys, like the PDCS (Postman *et al.* 1986) and EIS (Lobo *et al.* 2000), have searched for clusters at these distances. Therefore, we are currently using our catalogs of faint objects ($m_r > 20$) to search for rich, intermediate-redshift clusters using the same techniques presented in this thesis. We simply ignore classification, and impose no color cuts, due to the extremely poor photometry at the plate detection limits.

10.3 Morphological Properties of Butcher-Oemler Galaxies

Following the examination of the Butcher-Oemler effect in our extensive CCD sample, we are preparing a more detailed study combining morphological information with galaxy colors. Despite the relatively poor resolution of our CCD data, it may still be possible to separate disk-dominated and bulge-dominated galaxies on the basis of simple morphological quantities, such as concentration indices or radial light profiles. We can then study the question of whether the Butcher-Oemler galaxies in low redshift clusters are indeed late-type (spirals), and how their morphological type depends on the overall properties of the clusters (richness, substructure, merging, etc.). This has been done recently by Adami *et*

al. (2000), utilizing a far smaller sample of clusters. Ironically, this issue has been better studied at intermediate and high redshift, using high resolution imaging with HST (Dressler *et al.* 1997, Stanford, Eisenhardt & Dickinson 1998). As with many issues related to the evolution of galaxies and galaxy clusters, a proper low redshift baseline study is still sorely lacking.

10.4 Dependence of the Butcher-Oemler Effect on Cluster Properties

We have presented results showing that the Butcher-Oemler effect is indeed real, and shows a strong dependence on cluster richness. However, the physical basis for the BO effect is poorly understood (if at all; see the discussion in Chapter 8), and many other cluster properties may play important roles. We are therefore in the process of studying the BO effect in the context of global properties of the clusters: level of substructure, X-ray flux, mass, etc. Such a study was carried out by Smail *et al.* (1998) in a similar redshift range, using a sample of only 10 clusters, albeit with much deeper 5-band imaging. Using the CCD imaging library in conjunction with the plate data, we are producing surface density maps of hundreds of Abell clusters, to quantify the level of substructure in each cluster. In collaboration with Hans Böhringer, we are measuring the X-ray fluxes of both the Abell clusters and our new candidate clusters from the RASS. With our photometric redshifts, we can then derive X-ray luminosities, and from those, masses, using the mass-luminosity relation derived by Reiprich & Böhringer (*pvt. comm.*).

10.5 Cluster Substructure

Additionally, studies of cluster substructure (*e.g.*, Lopes *et al.* 2001) and the evolution of the cluster red sequence (*e.g.*, Gladders *et al.* 1998) are in progress. For example, we have made adaptive kernel maps of the galaxy distributions for each of our Abell cluster CCD fields. These maps are made using all galaxies in the field, those inside the "red sequence" (and therefore more likely cluster members), and those outside the red sequence. Figure 10.2 shows an example, using Abell 1062. The left map is for all galaxies in the CCD field; the cluster center is difficult to discern. The center map uses only galaxies inside

the red sequence. We see that this cluster either has two peaks, or is in fact two clusters in superposition. Finally, the right map is for galaxies outside the red sequence. In this map, the cluster disappears. Such studies are extremely powerful tools to help determine the reality of cluster candidates, find possible superpositions, and measure cluster substructure.

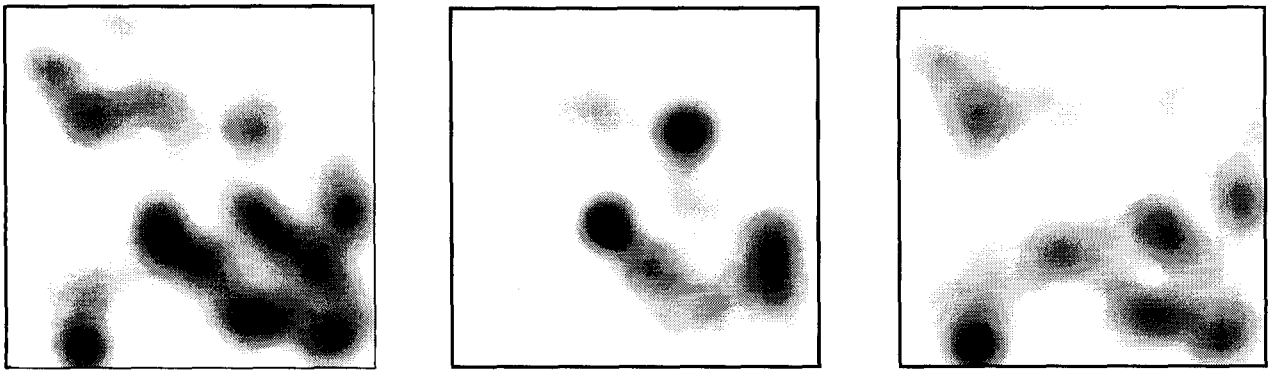

Figure 10.2: Cluster substructure maps for A1062. The left panel uses all galaxies in the field, the center panel is for red sequence galaxies only, and the right panel is for galaxies outside the red sequence. The segregation of galaxies by color is evident.

10.6 The Luminosity Function of Galaxy Clusters

Combining the depth and breadth of DPOSS data, as well as our CCD imaging, we will construct luminosity functions for galaxy clusters. Once again, with the large number of clusters at our disposal, we can examine systematic variations in the LF as a function of cluster properties. Early work on this using plate data has been done by our Italian collaborators (Paolillo *et al.* 2001), who study 39 Abell clusters from DPOSS data. They apply a local background correction, based on galaxy counts near each cluster, excluding nearby density peaks (illustrated in Figure 10.3), to remove any effects of underlying large scale structure, unlike using a universal background correction. A composite LF is shown in Figure 10.4, compared to the results of Trentham's 1997 CCD study. The DPOSS-derived LF agrees quite well with earlier studies, and the large area coverage allows accurate determinations of the bright end. The composite LFs are also similar to those of cluster cores observed by Garilli, Maccagni & Andreon (1999), suggesting that the LF does not vary strongly with cluster radius in the magnitude range studied.

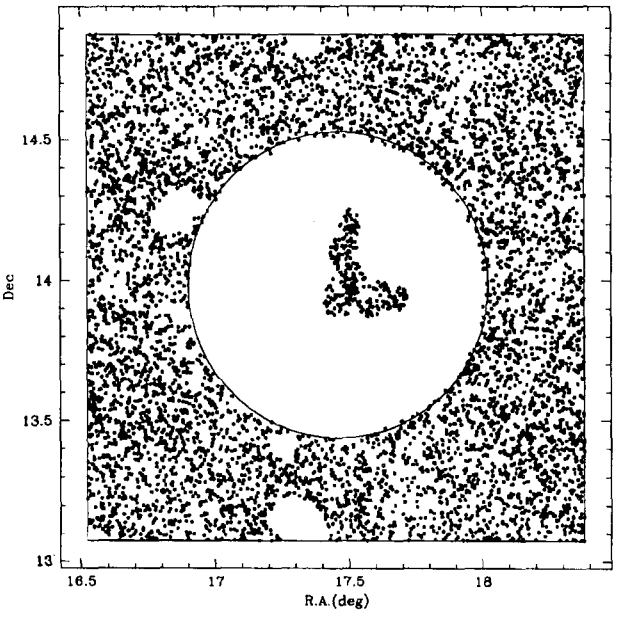

Figure 10.3: The cluster & background field for A152. The central points are galaxies inside a region with overdensity greater than 1.5σ; points outside the circle are galaxies used to estimate the background contribution.

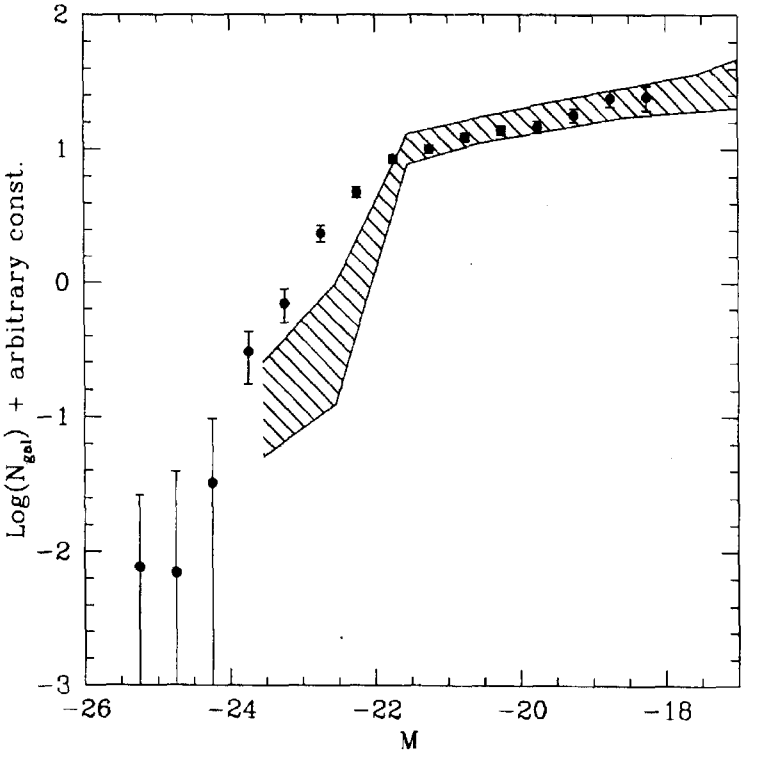

Figure 10.4: Cluster luminosity function in r from 39 Abell clusters (dots), and the Trentham 1997 CCD results (shaded area).

10.7 A Comparison of Optical Cluster Detection Techniques

Many cluster detections have been utilized recently to produce objective catalogs of galaxy clusters from a variety of surveys. Simple Gaussian filters (Puddu *et al.* 2001), the matched filter (Postman *et al.* 1996, Kawasaki *et al.* 1998), adaptive matched filter (Kepner *et al.* 1999), Voronoi tessellation (Kim *et al.* 2000), friends-of-friends (Tucker *et al.* 2000) and many other methods have been used. Although all of these methods have advantages and disadvantages, an objective comparison of the different techniques on the same data set has not been performed. Such a test would provide interesting data on the effectiveness and reliability of the different methods, and also provide a means of quantifying the robustness of cluster candidates.

10.8 Other Cluster-related Projects

There is an almost endless list of potential projects not discussed above, for which our data can (and hopefully will) be used. These include:

- Improved photometric redshift estimates using matched-aperture detections (as in Brunner & Lubin 2000).
- Searches for intracluster light; for a review see Vílchez-Gómez (1999).
- The color-magnitude relation as an evolutionary indicator in clusters, similar to the analysis of many fewer clusters by Gladders *et al.* (1998).
- The fundamental plane of galaxy clusters, which to date has been studied using only relatively few rich clusters (Adami *et al.* 1998). Combining our optical data with X-ray measurements, we can examine the dependence of clusters' scatter from the FP on cluster properties, along the lines of Miller, Melott & Gorman (1999).
- The Binggeli effect: are Brightest Cluster Members (BCMs) preferentially aligned with the major axes of clusters? What is the distribution of cluster ellipticities?
- Surface photometry of, and color gradients in BCMs, to study their star-formation and interaction history.

Bibliography

Abell, G. O. 1957, Ph.D. Thesis

Abell, G. O. 1958, ApJS, 3, 211

Abell, G. O., Corwin, H. G. & Olowin, R. P. 1989, ApJS, 70, 1

Adami, C., Mazure, A., Biviano, A., Katgert, P. & Rhee, G. 1998, A&A, 331, 493

Adami, C., Holden, B. P., Castander, F. J., Mazure, A., Nichol, R. C. & Ulmer, M. P. 2000, A&A, 362, 825

Bahcall, N. A. & Soneira, R. M. 1983, ApJ, 270, 20

Bahcall, N. A. & West, M. J. 1992, ApJ, 392, 419

Bertin, E. & Arnouts, S. 1996, A&AS, 117, 393

Böhringer, H. *et al.* 2000, ApJS, 129, 435

Borgani, S., Girardi, M., Carlberg, R. G., Yee, H. K. C. & Ellingson, E. 1999, ApJ, 527, 561

Bramel, D. A., Nichol, R. C. & Pope, A. C. 2000, ApJ, 533, 601

Brunner, R. J. & Lubin, L. M. 2000, AJ, 120, 2851

Brunner, R. J., Szalay, A. S. & Connolly, A. J. 2000, ApJ, 541, 527

Butcher, H. & Oemler, A. 1978, ApJ, 226, 559

Cohen, J. G., Hogg, D. W., Blandford, R., Cowie, L. L., Hu, E., Songaila, A., Shopbell, P. & Richberg, K. 2000, ApJ, 538, 29

Collins, C. A. et al. 2000, MNRAS, 319, 939

Croft, R. A. C., Dalton, G. B., Efstathiou, G., Sutherland, W. J. & Maddox, S. J. 1997, MNRAS, 291, 305

Dalton, G. B., Efstathiou, G., Maddox, S. J. & Sutherland, W. J. 1992, ApJ, 390, L1

Dalton, G. B., Efstathiou, G., Maddox, S. J. & Sutherland, W. J. 1994, MNRAS, 269, 151

Dalton, G. B., Maddox, S. J., Sutherland, W. J. & Efstathiou, G. 1997, MNRAS, 289, 263

Dalton, G. B., Croft, R. A. C., Efstathiou, G., Sutherland, W. J., Maddox, S. J. & Davis, M. 1994, MNRAS, 271, L47

Djorgovski, S. G., Odewahn, S. C., Gal, R. R., Brunner, R., de Carvalho, R. R., Longo, G. & Scaramella, R. 1999, American Astronomical Society Meeting, 194, 0414

Dressler, A. 1980, ApJ, 236, 351

Dressler, A. & Gunn, J. E. 1992, ApJS, 78, 1

Dressler, A. *et al.* 1997, ApJ, 490, 577

Drinkwater, M. J. et al. 2000, A&A, 355, 900

Ebeling, H., Edge, A. C., Allen, S. W., Crawford, C. S., Fabian, A. C. & Huchra, J. P. 2000, MNRAS, 318, 333

Efstathiou, G., Dalton, G. B., Sutherland, W. J. & Maddox, S. J. 1992, MNRAS, 257, 125

Fayyad, U. & Irani, K. 1990, Proc. of the Eighth National Conf. on Artificial Intelligence, AAAI-90, Boston, MA

Fayyad, U. 1991, Ph.D. Thesis, EECS Department, The University of Michigan

Gal, R. R., de Carvalho, R. R., Odewahn, S. C., Djorgovski, S. G. & Margoniner, V. E. 2000a, AJ, 119, 12

Gal, R. R., de Carvalho, R. R., Brunner, R., Odewahn, S. C. & Djorgovski, S. G. 2000b, AJ, 120, 540

Garilli, B., Maccagni, D. & Andreon, S. 1999, A&A, 342, 408

Gioia, I. M. & Luppino, G. A. 1994, ApJS, 94, 583

Gladders, M. D., Lopez-Cruz, O., Yee, H. K. C. & Kodama, T. 1998, ApJ, 501, 571

Groth, E. J. & Peebles, P. J. E. 1986, ApJ, 310, 499

Gunn, J. E., Hoessel, J. G. & Oke, J. B. 1986, ApJ, 306, 30

Hewett, P. C. 1982, MNRAS, 201, 867

Heydon-Dumbleton, N. H., Collins, C. A. & MacGillivray, H. T. 1989, MNRAS, 238, 379

Holder, G. P., Mohr, J. J., Carlstrom, J. E., Evrard, A. E. & Leitch, E. M. 2000, ApJ, 544, 629

Hradecky, V., Jones, C., Donnelly, R. H., Djorgovski, S. G., Gal, R. R. & Odewahn, S. C. 2000, ApJ, 543, 521

Infante, L. & Pritchet, C. J. 1995, ApJ, 439, 565

Jarvis, J. F. & Tyson, J. A. 1981, AJ, 86, 476

Jones, C. & Forman, W. 1978, ApJ, 224, 1

Katgert, P. *et al.* 1996, A&A, 310, 8

Katz, L. & Mulders, G. F. W. 1942, ApJ, 95, 565

Kawasaki, W., Shimasaku, K., Doi, M. & Okamura, S. 1998, A&AS, 130, 567

Kennefick, J. D., de Carvalho, R. R., Djorgovski, S. G., Wilber, M. M., Dickson, E. S., Weir, N., Fayyad, U. & Roden, J. 1995, AJ, 110, 78

Kennefick, J. D., Djorgovski, S. G. & de Carvalho, R. R. 1995, AJ, 110, 2553

Kennefick, J. D. 1996, Ph.D. Thesis, Caltech

Kent, S. M. 1985, PASP, 97, 165

Kepner, J., Fan, X., Bahcall, N., Gunn, J., Lupton, R. & Xu, G. 1999, ApJ, 517, 78

Kim, R., Strauss, M., Bahcall, N. & *et al.* 2000, ASP Conf. Ser. 200: Clustering at High Redshift, 422

Koo, D. C. & Kron, R. G. 1982, A&A, 105, 107

Koo, D. C. & Szalay, A. S. 1984, ApJ, 282, 390

Landy, S. D. & Szalay, A. S. 1993, ApJ, 412, 64

Lasker, B. M., Doggett, J., McLean, B., Sturch, C., Djorgovski, S., de Carvalho, R. R. & Reid, I. N. 1996, ASP Conf. Ser. 101: Astronomical Data Analysis Software and Systems V, 5, 88

Lee, S. & Park, C. 1999, astro-ph 9909008

Limber, D. N. 1954, ApJ, 119, 655

Lin, H., Kirshner, R. P., Shectman, S. A., Landy, S. D., Oemler, A., Tucker, D. L. & Schechter, P. L. 1996, ApJ, 471, 617

Lobo, C., Iovino, A., Lazzati, D. & Chincarini, G. 2000, A&A, 360, 896

Lopes, P. A. A., Gal, R. R., Djorgovski, S. G., de Carvalho, R. R. & Odewahn, S. C. 2000, American Astronomical Society Meeting, 197, 110611

Lucey, J. R. 1983, MNRAS, 204, 33

Lumsden, S. L., Nichol, R. C., Collins, C. A. & Guzzo, L. 1992, MNRAS, 258, 1

Maddox, S. J., Efstathiou, G. & Sutherland, W. J. 1990, MNRAS, 246, 433

Maddox, S. J., Efstathiou, G. & Sutherland, W. J. 1996, MNRAS, 283, 1227

Mahabal, A. A. *et al.* , 2001, *in prep.*

Margoniner, V. E. & de Carvalho, R. R. 2000, AJ, 119, 1562

Margoniner, V. E., de Carvalho, R. R., Gal, R. R., Djorgovski, S. G. & Odewahn, S. C. 2001, ApJ, *in press.*

Miller, C. J., Batuski, D. J., Slinglend, K. A. & Hill, J. M. 1999, ApJ, 523, 492

Miller, C. J., Melott, A. L. & Gorman, P. 1999, ApJ, 526, L61

Odewahn, S. C., Stockwell, E. B., Pennington, R. L., Humphreys, R. M. & Zumach, W. A. 1992, AJ, 103, 318

Odewahn, S. C., Humphreys, R. M., Aldering, G. & Thurmes, P. 1993, PASP, 105, 1354

Odewahn, S. C. & Nielsen, M. L. 1994, Vistas in Astronomy, 38, 281

Odewahn, S. C. 1995, PASP, 107, 770

Odewahn, S. C. & Aldering, G. 1995, AJ, 110, 2009

Odewahn, S. C., de Carvalho, R. R., Gal, R. R., Djorgovski, S. G., Stalder, B., 2001, *in prep.*

Olivier, S., Primack, J. R., Blumenthal, G. R., Dekel, A. & Stanhill, D. 1990, ApJ, 356, 1

Paolillo, M. *et al.* , 2001, Å, *in prep.*

Peebles, P. J. E. 1975, ApJ, 196, 647

Pennington, R. L., Humphreys, R. M., Odewahn, S. C., Zumach, W. & Thurmes, P. M. 1993, PASP, 105, 521

Picard, A. 1991, Ph.D. Thesis, Caltech

Postman, M., Lubin, L. M., Gunn, J. E., Oke, J. B., Hoessel, J. G., Schneider, D. P. & Christensen, J. A. 1996, AJ, 111, 615

Press, W. H., Teukolsky, S. A., Vetterling, W. T. & Flannery, B. P. 1992, *Numerical Recipes in Fortran*, Cambridge: University Press, 2nd ed.

Puddu, E. *et al.* 2001, *in prep.*

Quinlan, J. 1986, *Machine Learning: An Artifical Intelligence Approach*, vol. 1, San Mateo, CA, ed. Y. Kodratoff & R. Michalski (Morgan Kaufmann)

Quinlan, J. 1990, *Machine Learning: An Artifical Intelligence Approach*, vol. 3, San Mateo, CA, ed. Y. Kodratoff & R. Michalski (Morgan Kaufmann)

Reid, I. N. *et al.* 1991, PASP, 103, 661

Richard, M. D. & Lippmann, R. P. 1991, Neural Computation, 3, 461

Romer, A. K. *et al.* 2000, ApJS, 126, 209

Rumelhardt, D. E. & McClelland, J. L. 1988, *Explorations in Parallel Distributed Processing*, Cambridge, MA: MIT Press

Scharf, C. A., Jones, L. R., Ebeling, H., Perlman, E., Malkan, M. & Wegner, G. 1997, ApJ, 477, 79

Schlegel, D. J., Finkbeiner, D. P. & Davis, M. 1998, ApJ, 500, 525

Sebok, W. L. 1979, AJ, 84, 1526

Shane, C. D. & Wirtanen, C. A. 1954, AJ, 59, 285

Sharp, N. A. 1979, A&A, 74, 308

Shectman, S. A. 1985, ApJS, 57, 77

Silverman, B. W. 1986, *Monographs on Statistics and Applied Probability*, London: Chapman and Hall

Smail, I., Edge, A. C., Ellis, R. S. & Blandford, R. D. 1998, MNRAS, 293, 124

Stanford, S. A., Eisenhardt, P. R. & Dickinson, M. 1998, ApJ, 492, 461

Struble, M. F. & Rood, H. J. 1991, ApJS, 77, 363

Struble, M. F. & Rood, H. J. 1999, ApJS, 125, 35

Sutherland, W. 1988, MNRAS, 234, 159

Thuan, T. X. & Gunn, J. E. 1976, PASP, 88, 543

Tody, D. 1986, Proc. SPIE, 627, 733

Trentham, N. 1997, MNRAS, 290, 334

Tucker, D. L. *et al.* 2000, ApJS, 130, 237

Valdes, F. 1982, SPIE, 331, 465

van Haarlem, M. P., Frenk, C. S. & White, S. D. M. 1997, MNRAS, 287, 817

Vílchez-Gómez, R. 1999, ASP Conf. Ser. 170: The Low Surface Brightness Universe, 349

Voges, W. 1993, Advances in Space Research, 13, 391

Wade, R. A., Hoessel, J. G., Elias, J. H. & Huchra, J. P. 1979, PASP, 91, 35

Weir, N., Fayyad, U. M. & Djorgovski, S. 1995a, AJ, 109, 2401

Weir, N., Djorgovski, S. & Fayyad, U. M. 1995b, AJ, 110, 1

Weir, N., Fayyad, U. M., Djorgovski, S. G. & Roden, J. 1995c, PASP, 107, 1243

Worthey, G. 1994, ApJS, 95, 107

Yee, H. K. C. et al. 2000, ApJS, 129, 475

York, D. G. *et al.* 2000, AJ, 120, 1579

Zaritsky, D., Nelson, A. E., Dalcanton, J. J. & Gonzalez, A. H. 1997, ApJ, 480, L91

Zwicky, F. 1938, PASP, 50, 218

Zwicky, I. F. 1942, ApJ, 95, 555

Zwicky, F., Herzog, E. & Wild, P. 1968, Catalogue of Galaxies and of Clusters of Galaxies, Pasadena: California Institute of Technology (CIT), 1961-1968

Appendix A

Galaxy Distributions

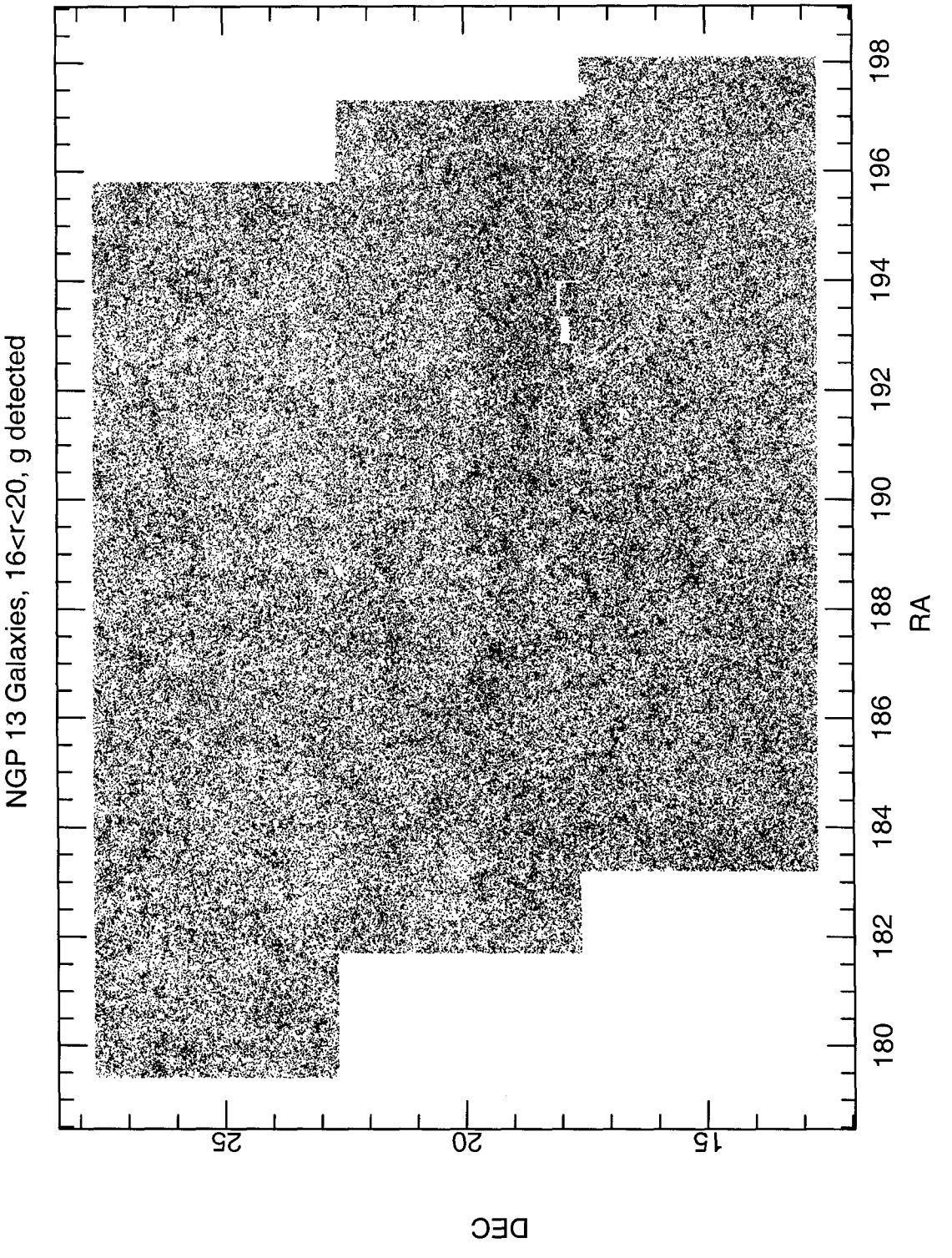

Figure A.1: Galaxies in NGP Area 13.

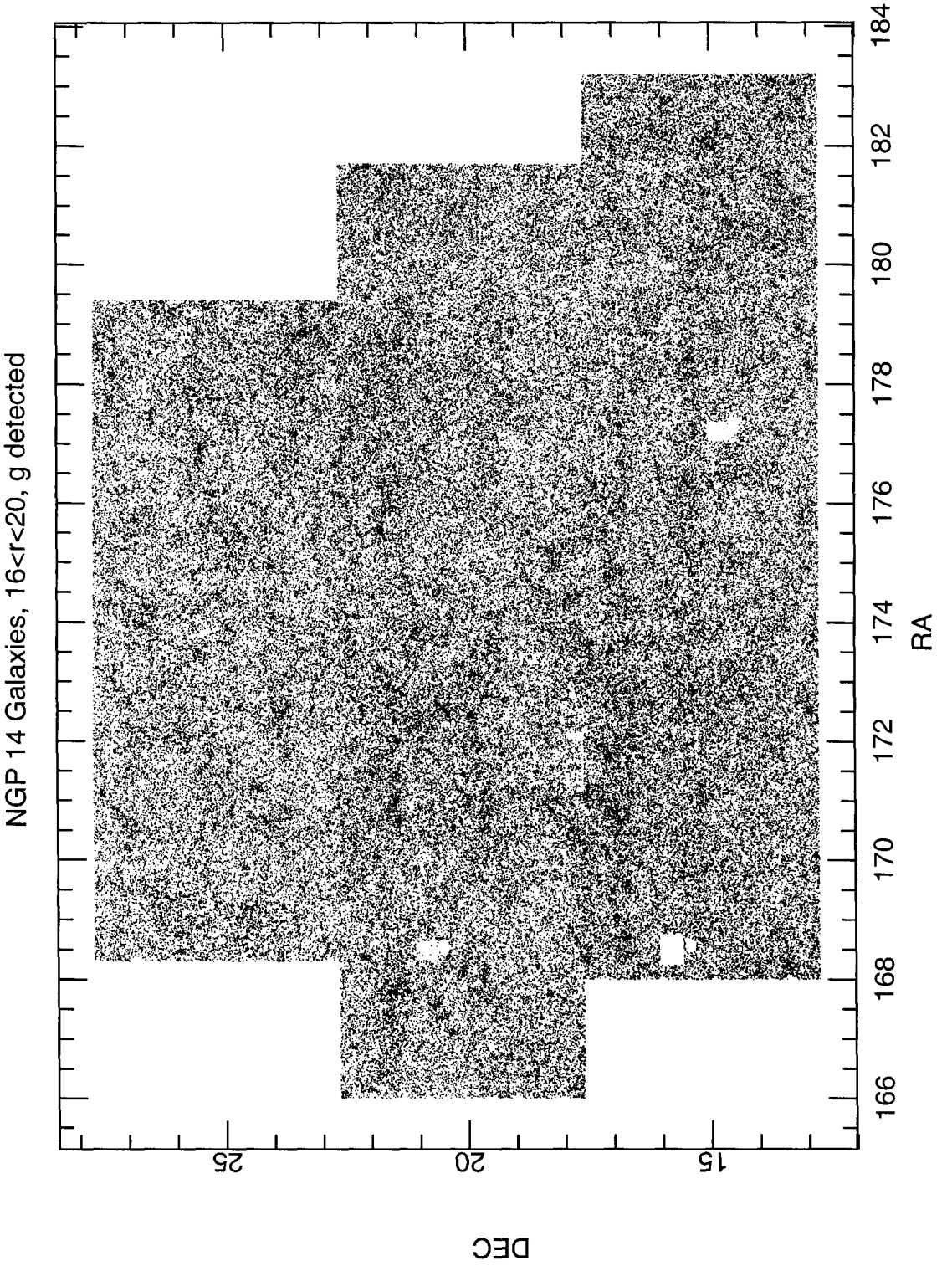

Figure A.2: Galaxies in NGP Area 14.

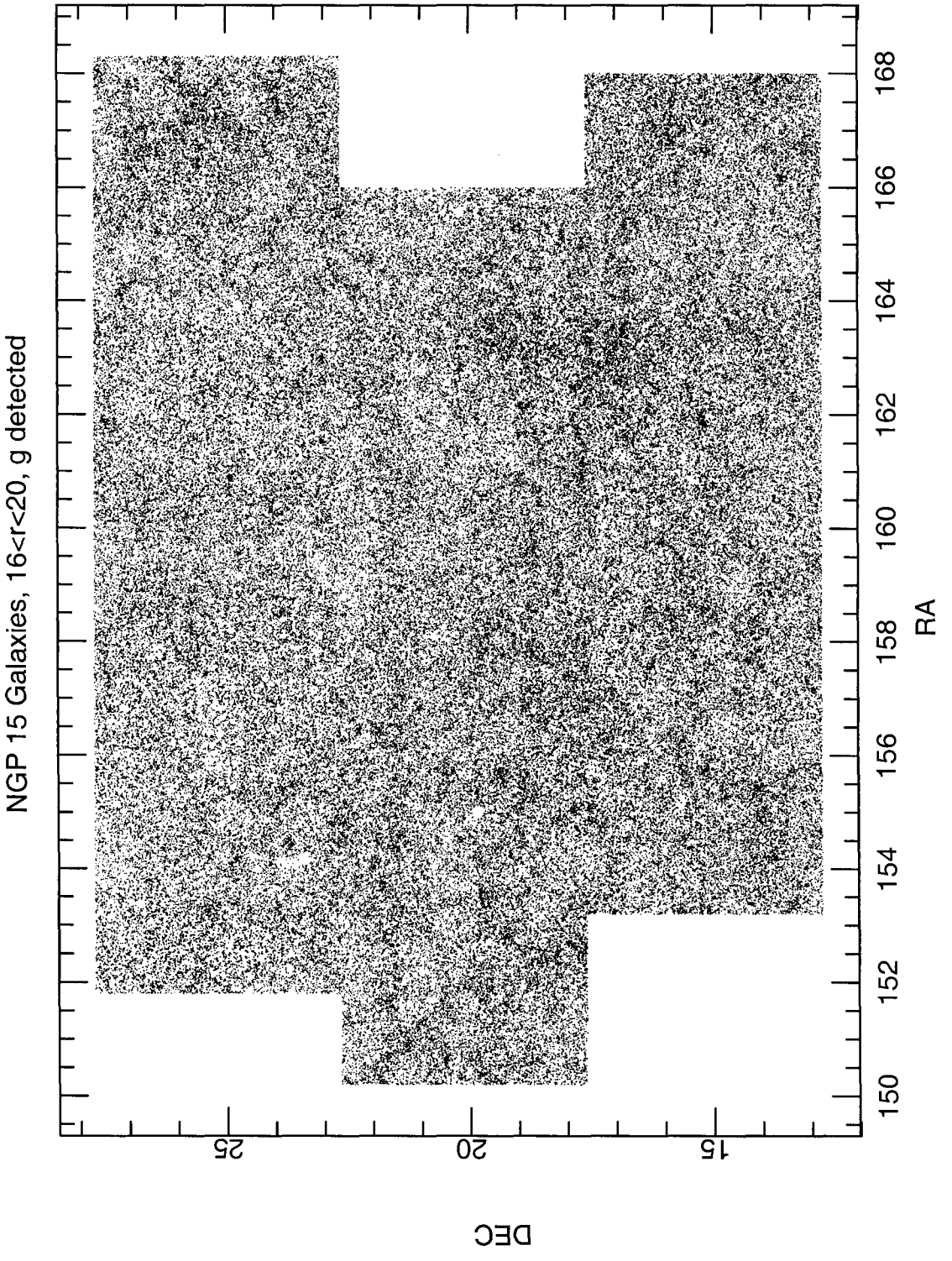

Figure A.3: Galaxies in NGP Area 15.

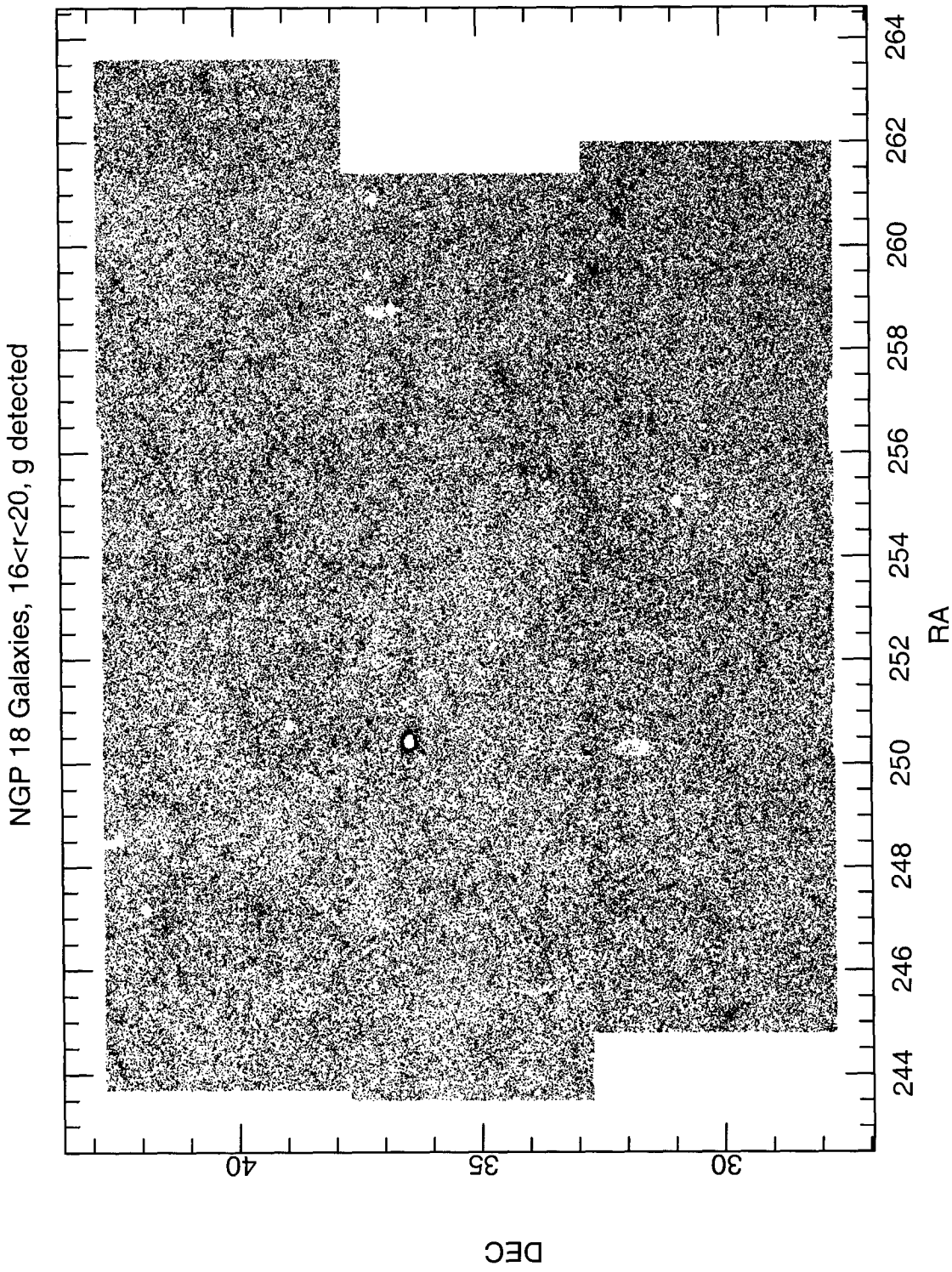

Figure A.4: Galaxies in NGP Area 18.

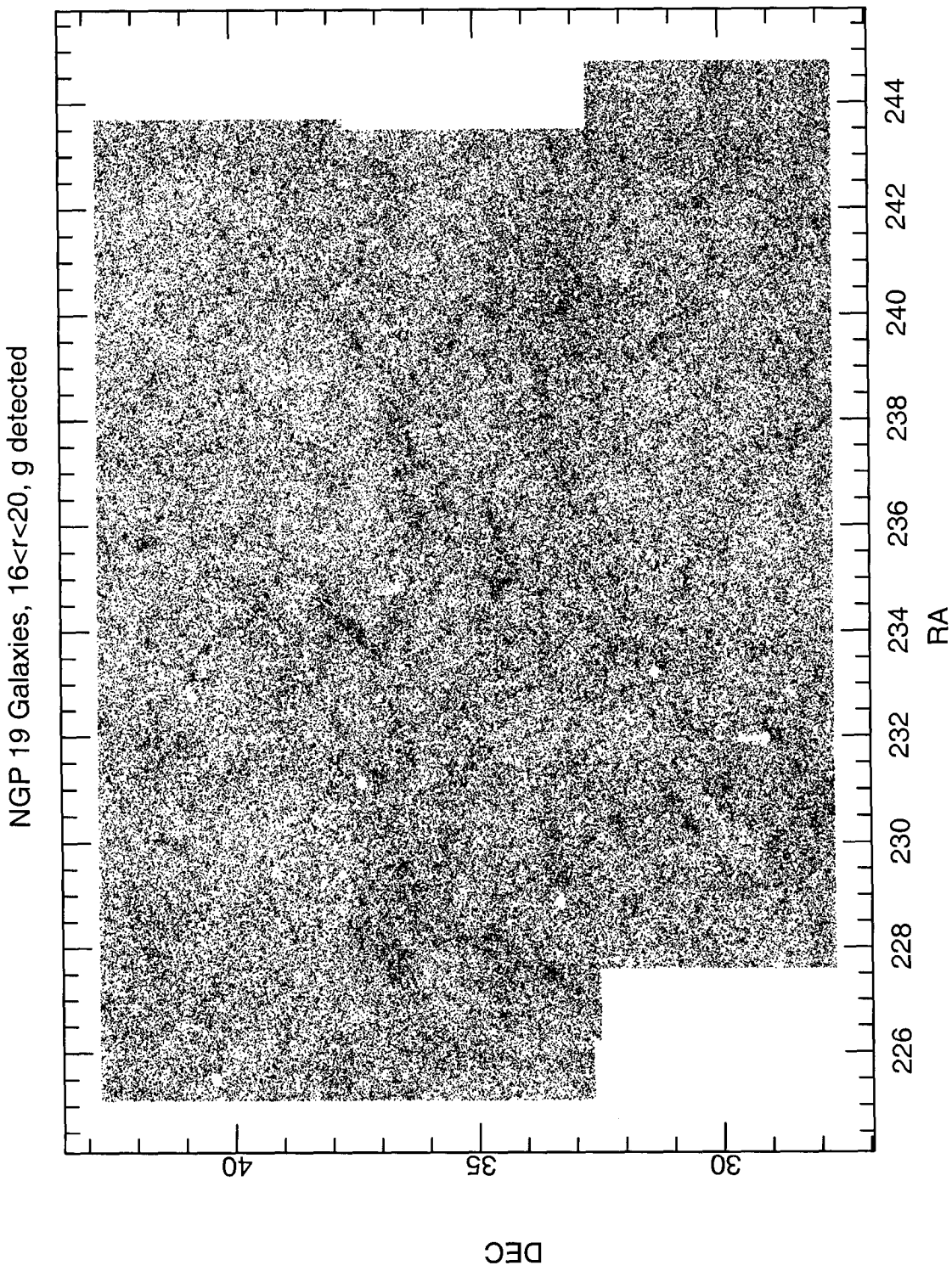

Figure A.5: Galaxies in NGP Area 19.

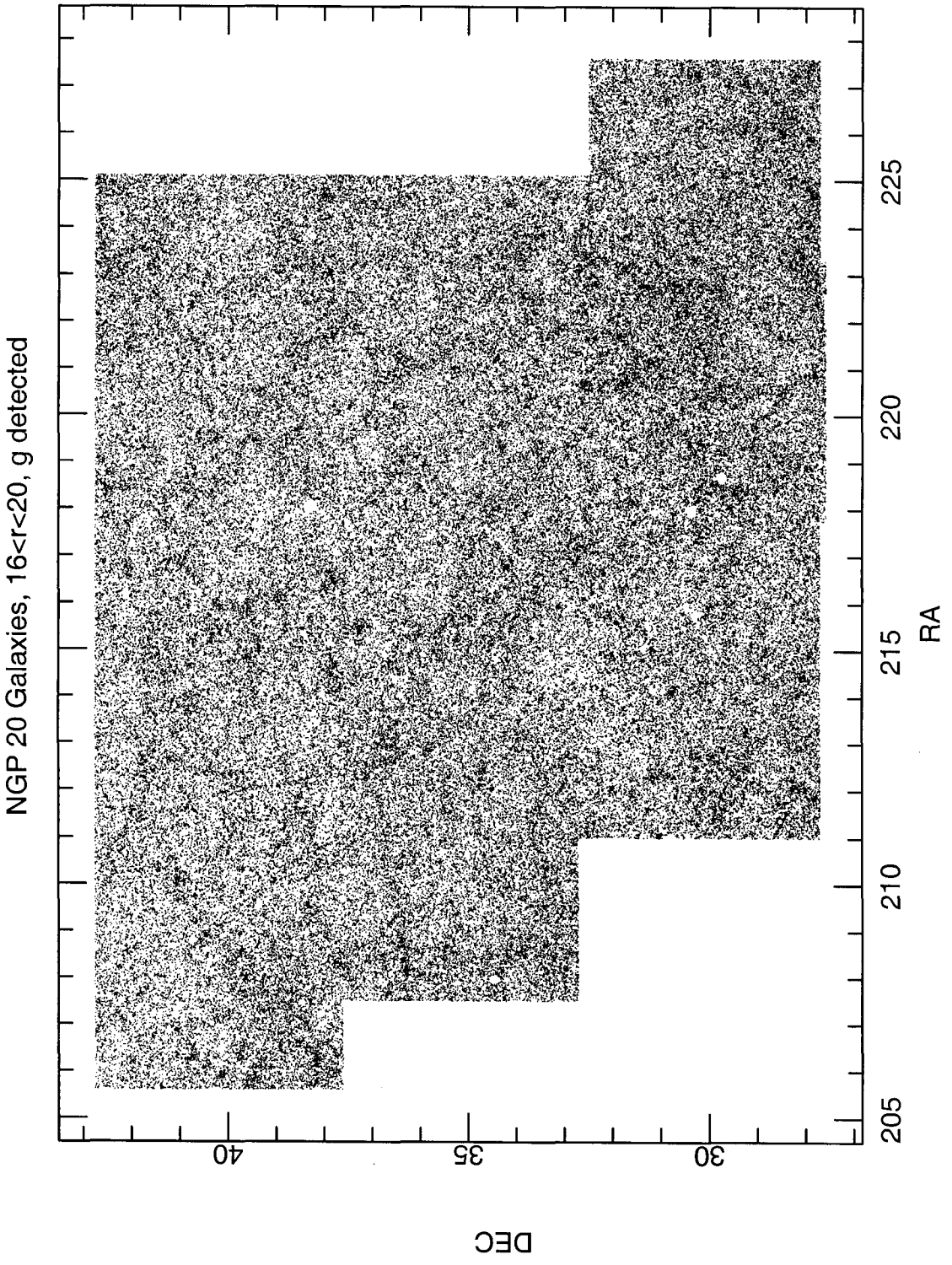

Figure A.6: Galaxies in NGP Area 20.

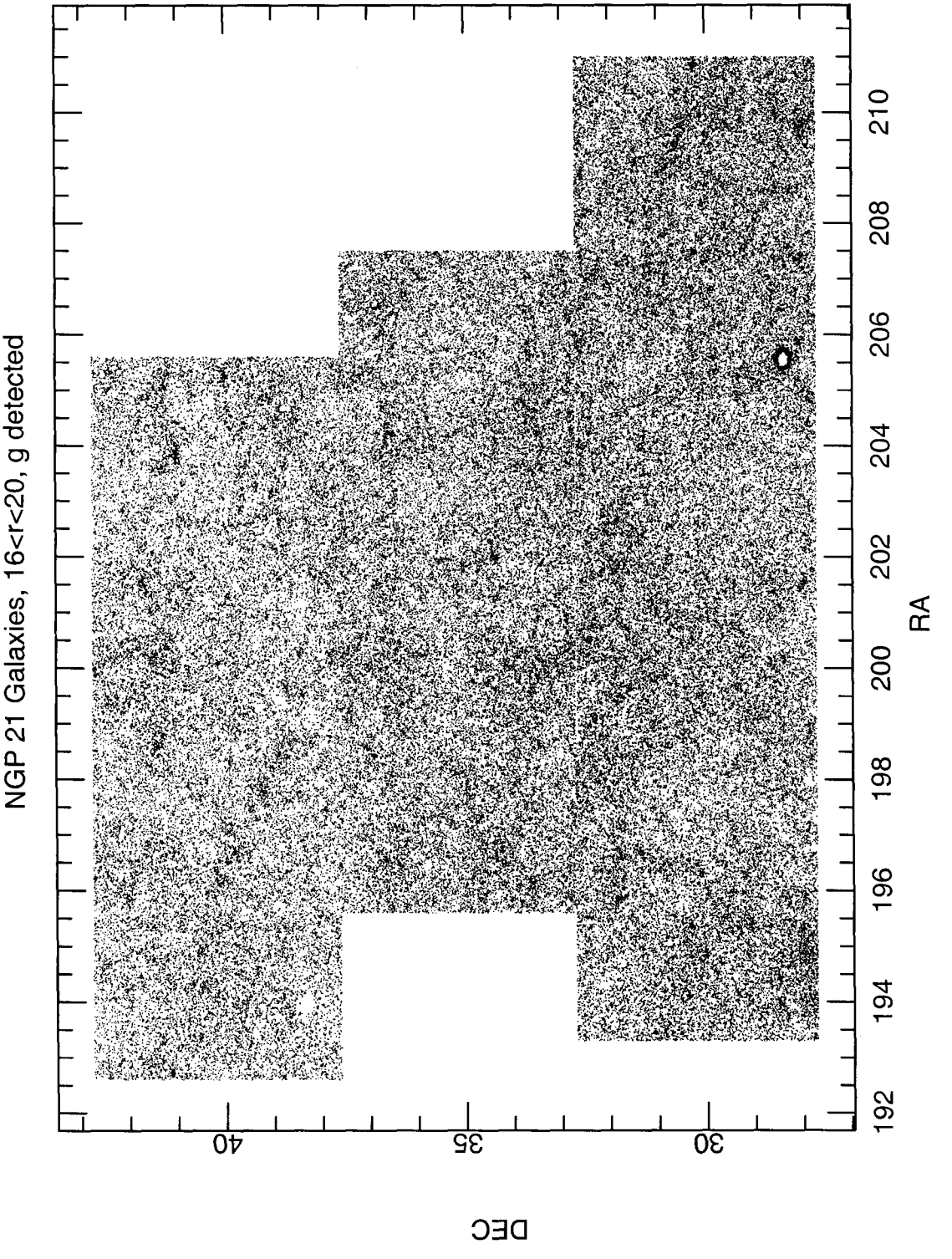

Figure A.7: Galaxies in NGP Area 21.

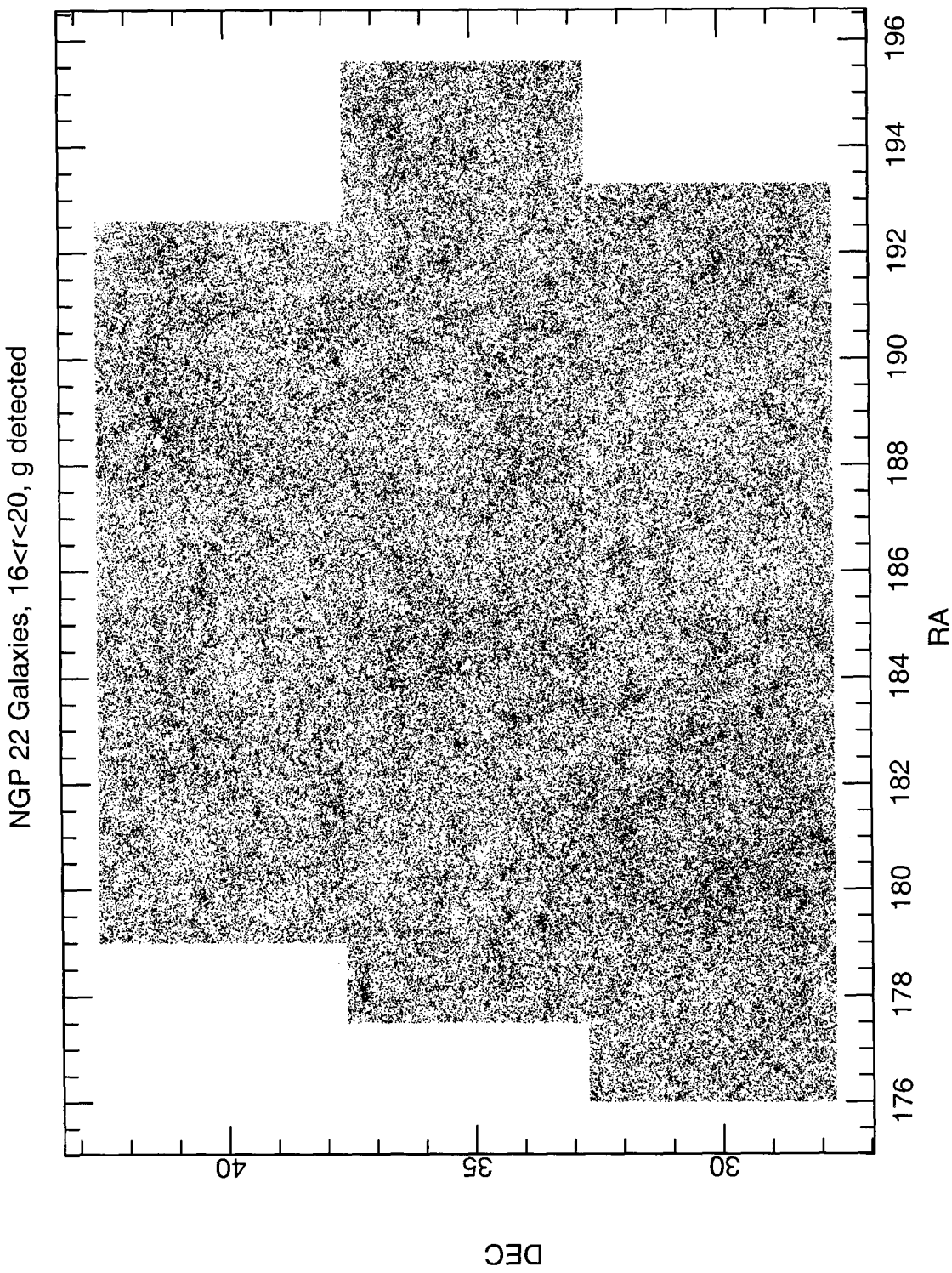

Figure A.8: Galaxies in NGP Area 22.

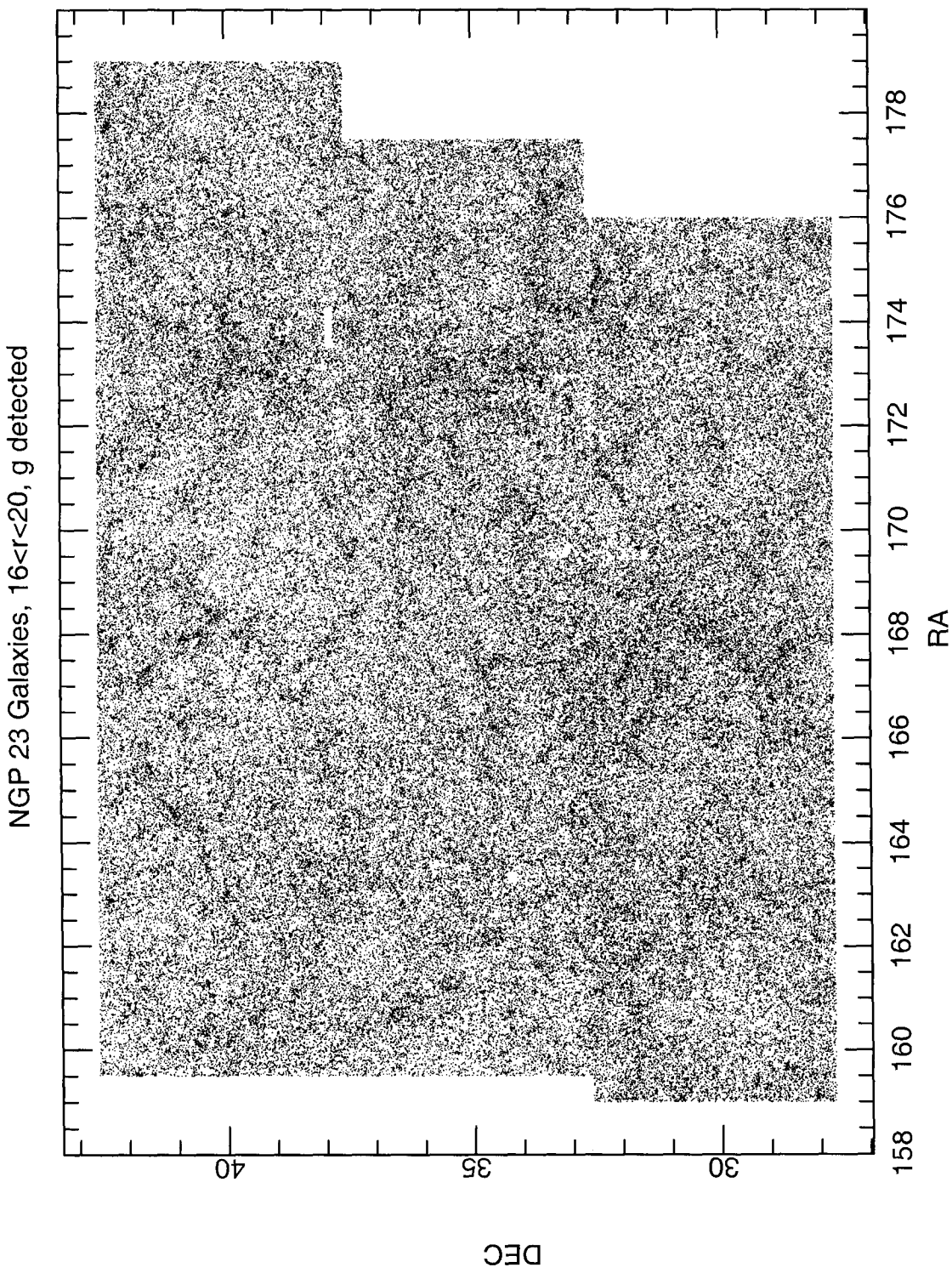

Figure A.9: Galaxies in NGP Area 23.

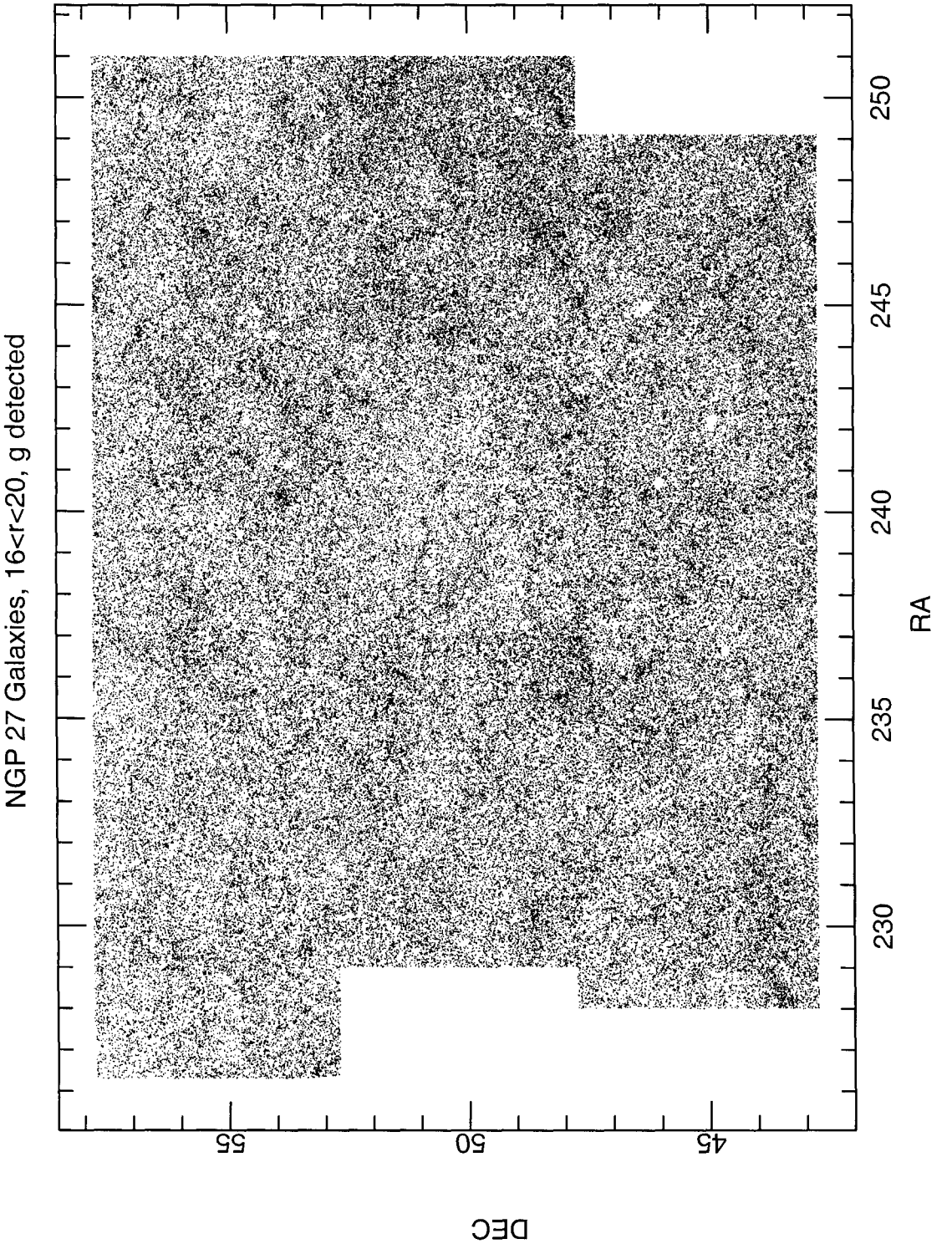

Figure A.10: Galaxies in NGP Area 27.

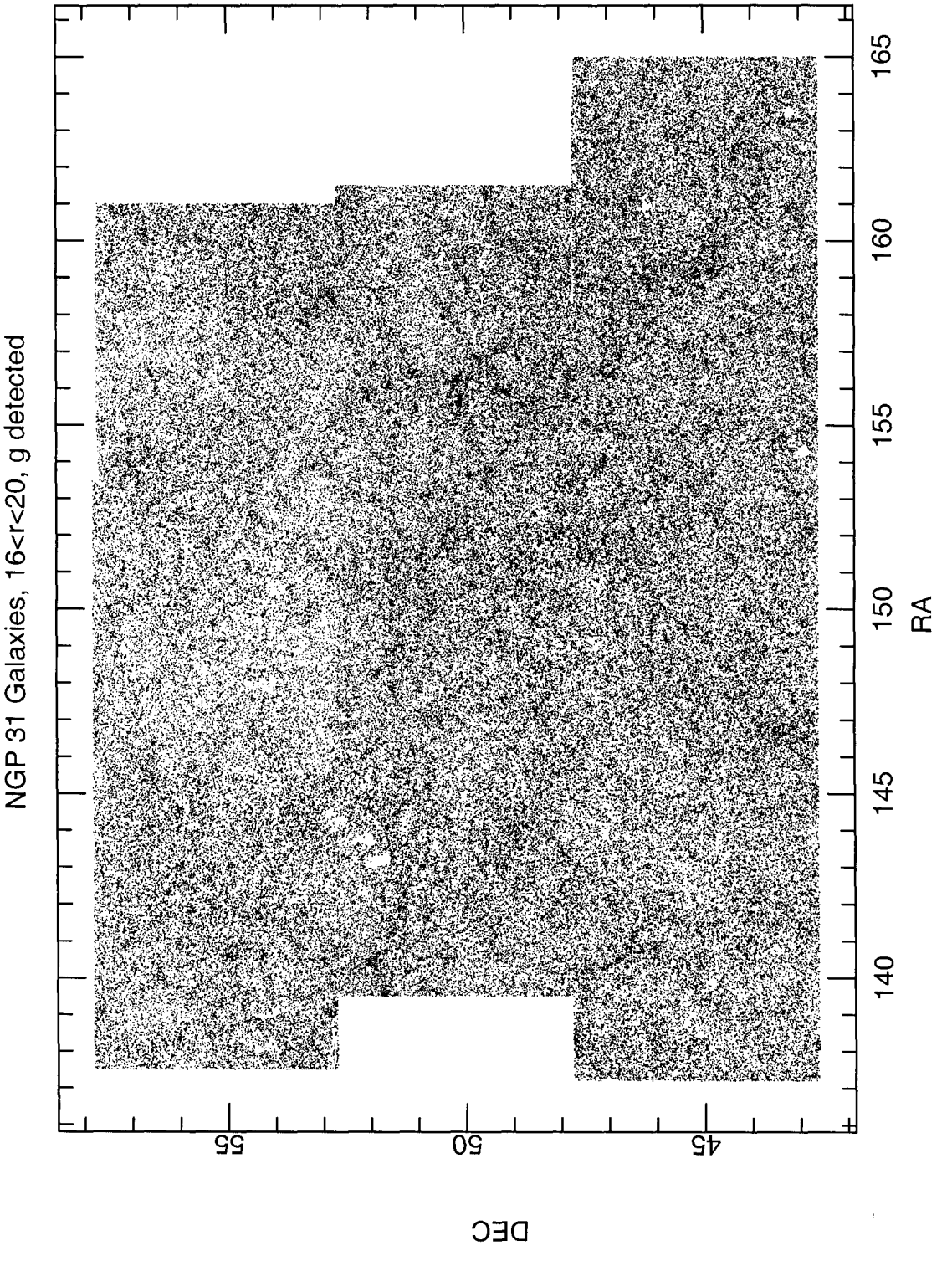

Figure A.11: Galaxies in NGP Area 31.

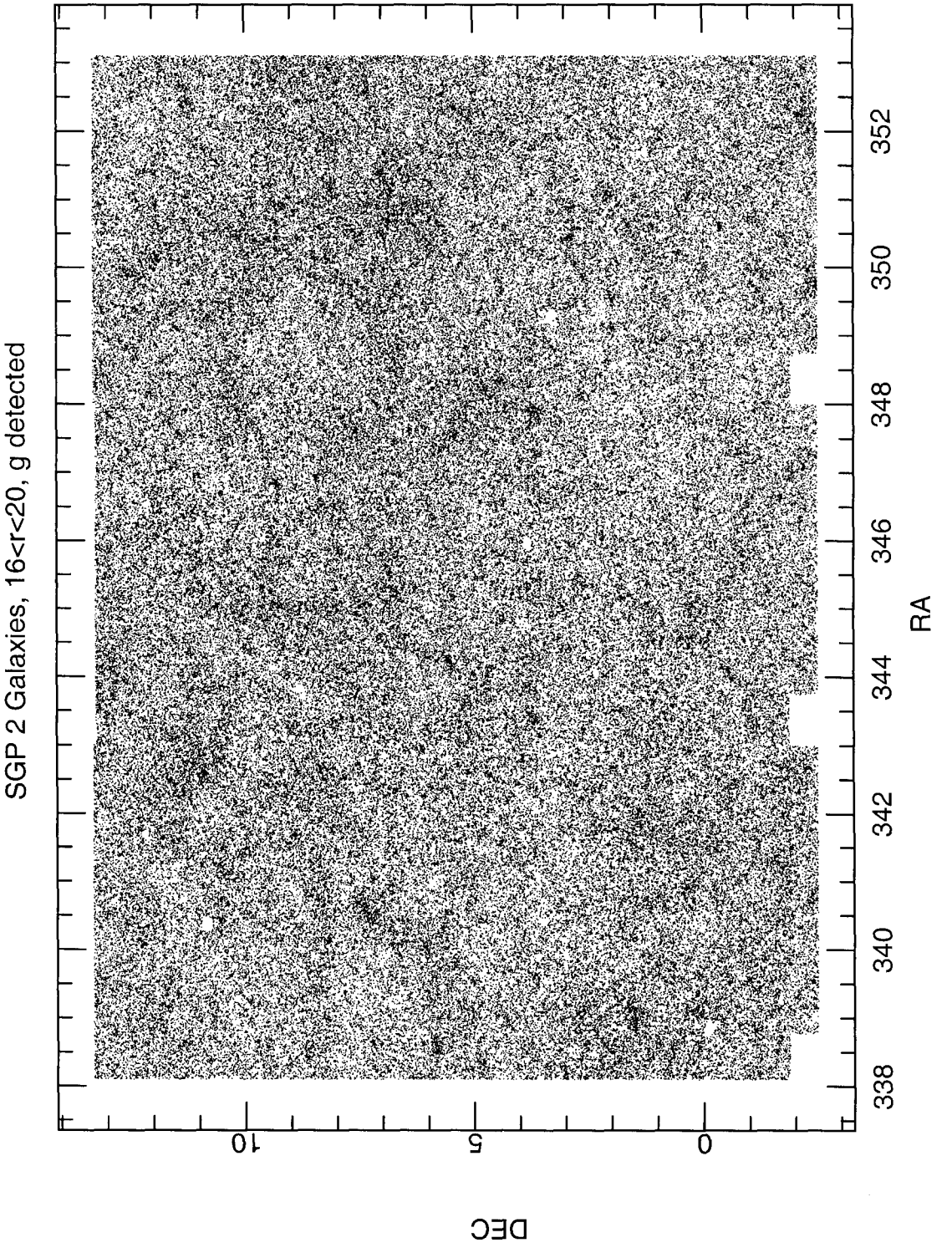

Figure A.12: Galaxies in SGP Area 2.

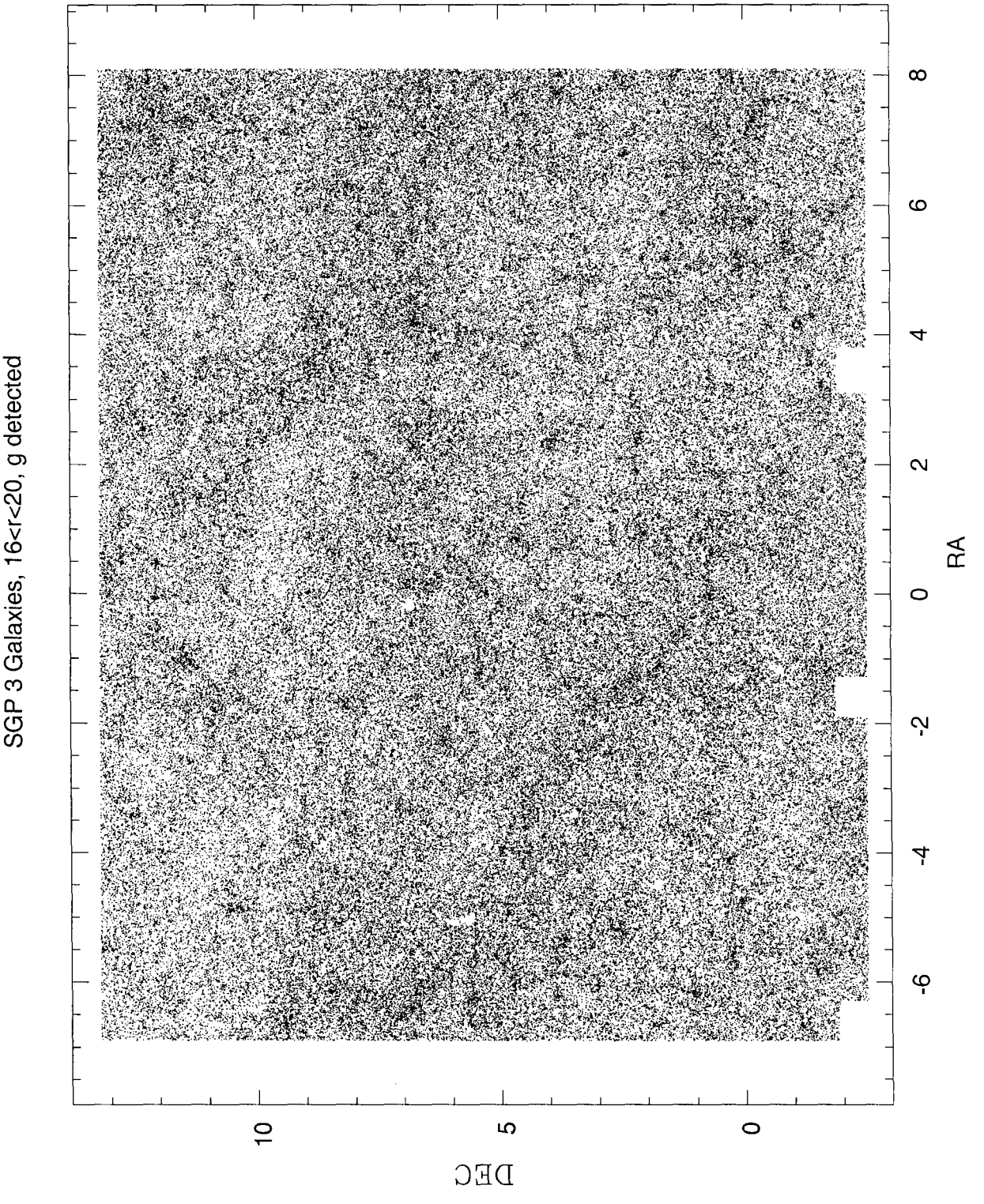

Figure A.13: Galaxies in SGP Area 3.

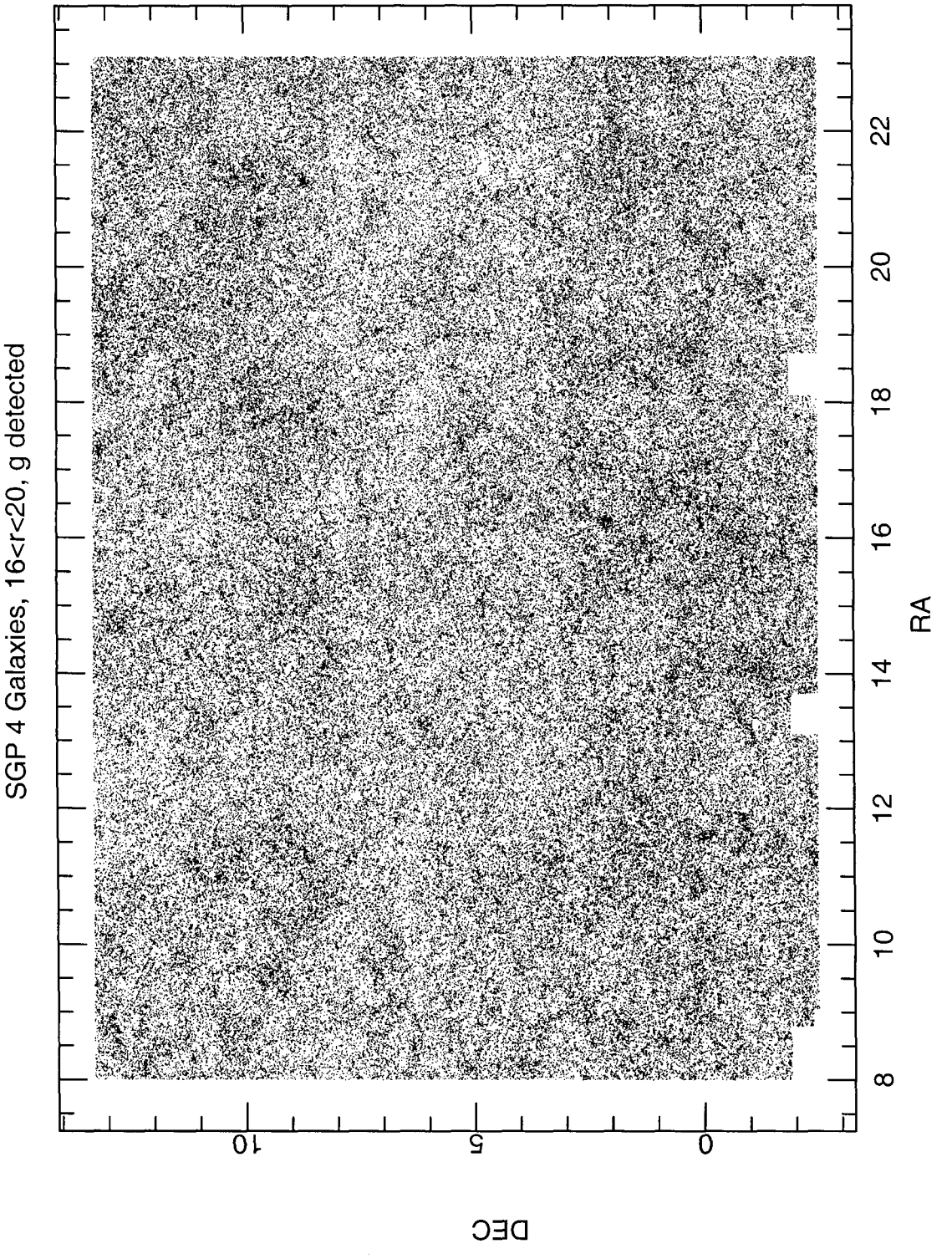

Figure A.14: Galaxies in SGP Area 4.

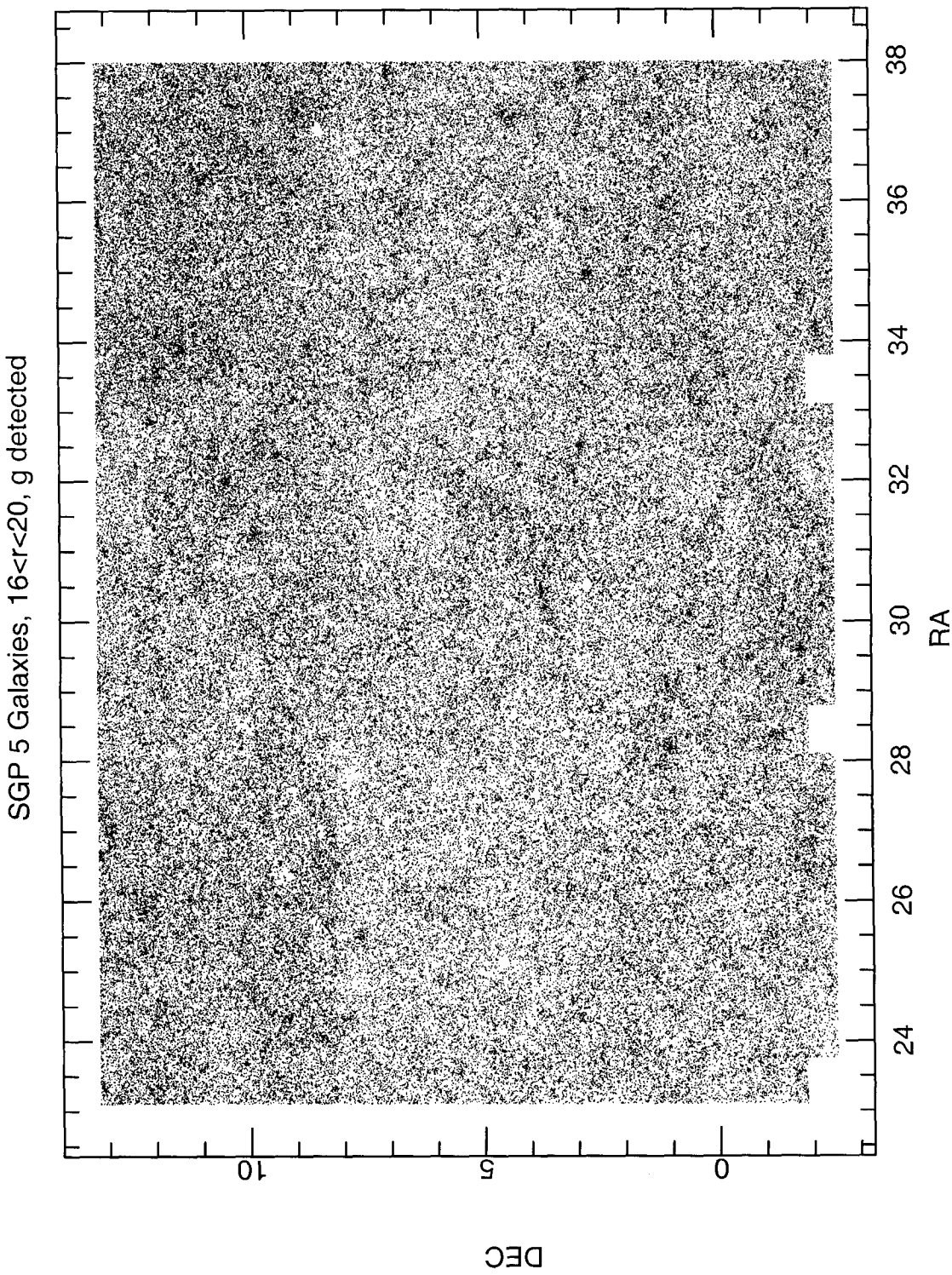

Figure A.15: Galaxies in SGP Area 5.

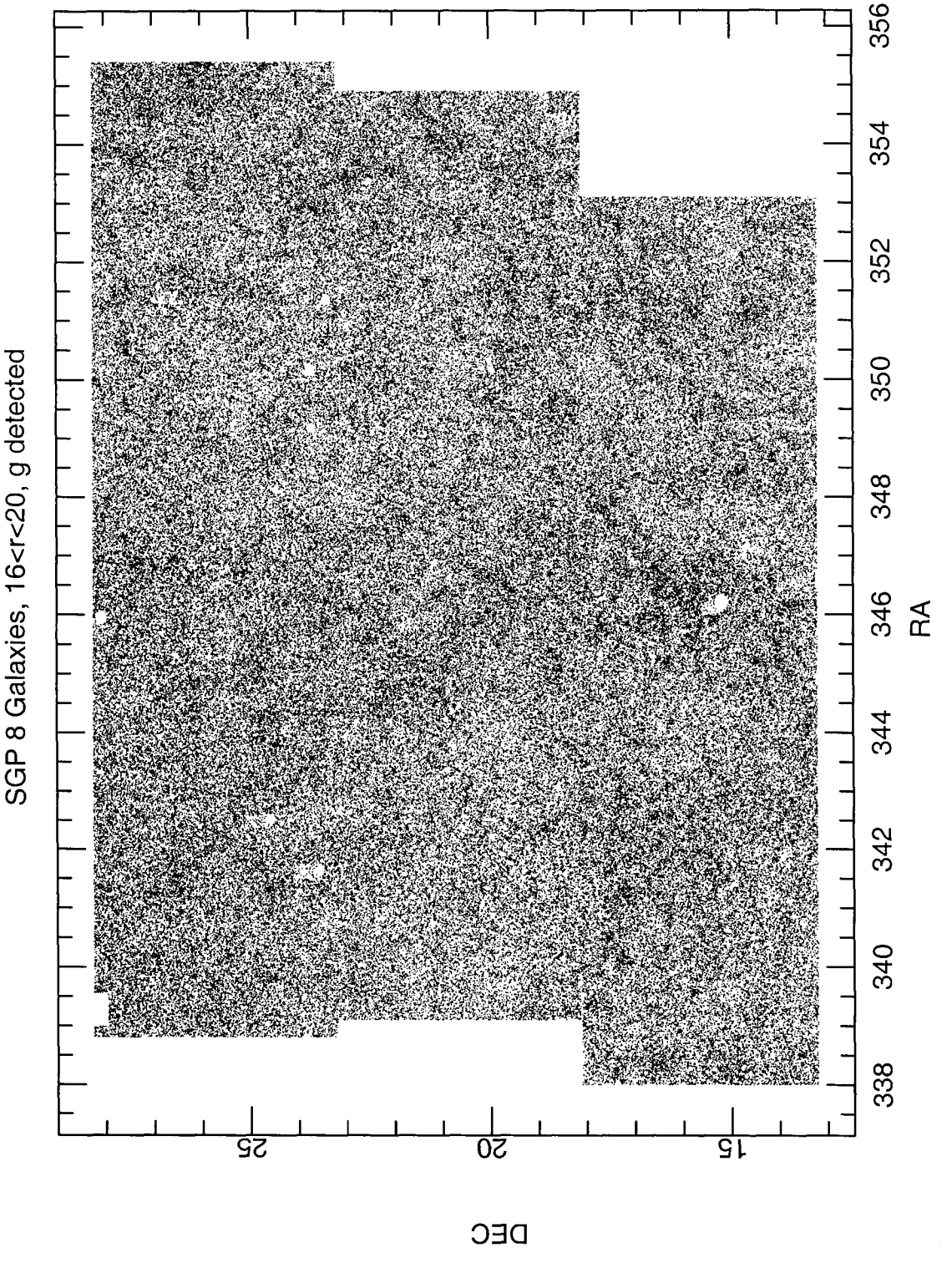

Figure A.16: Galaxies in SGP Area 8.

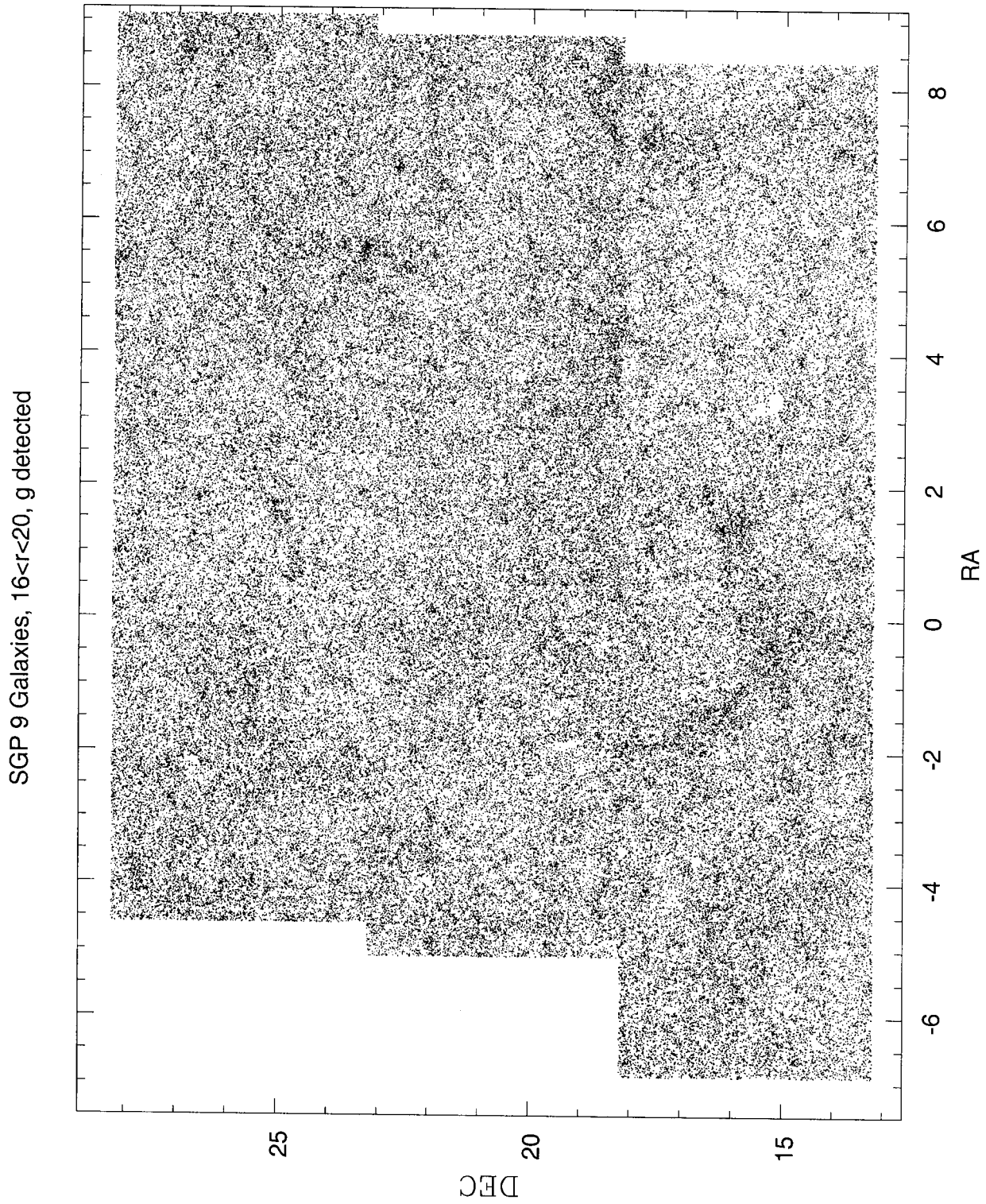

Figure A.17: Galaxies in SGP Area 9.

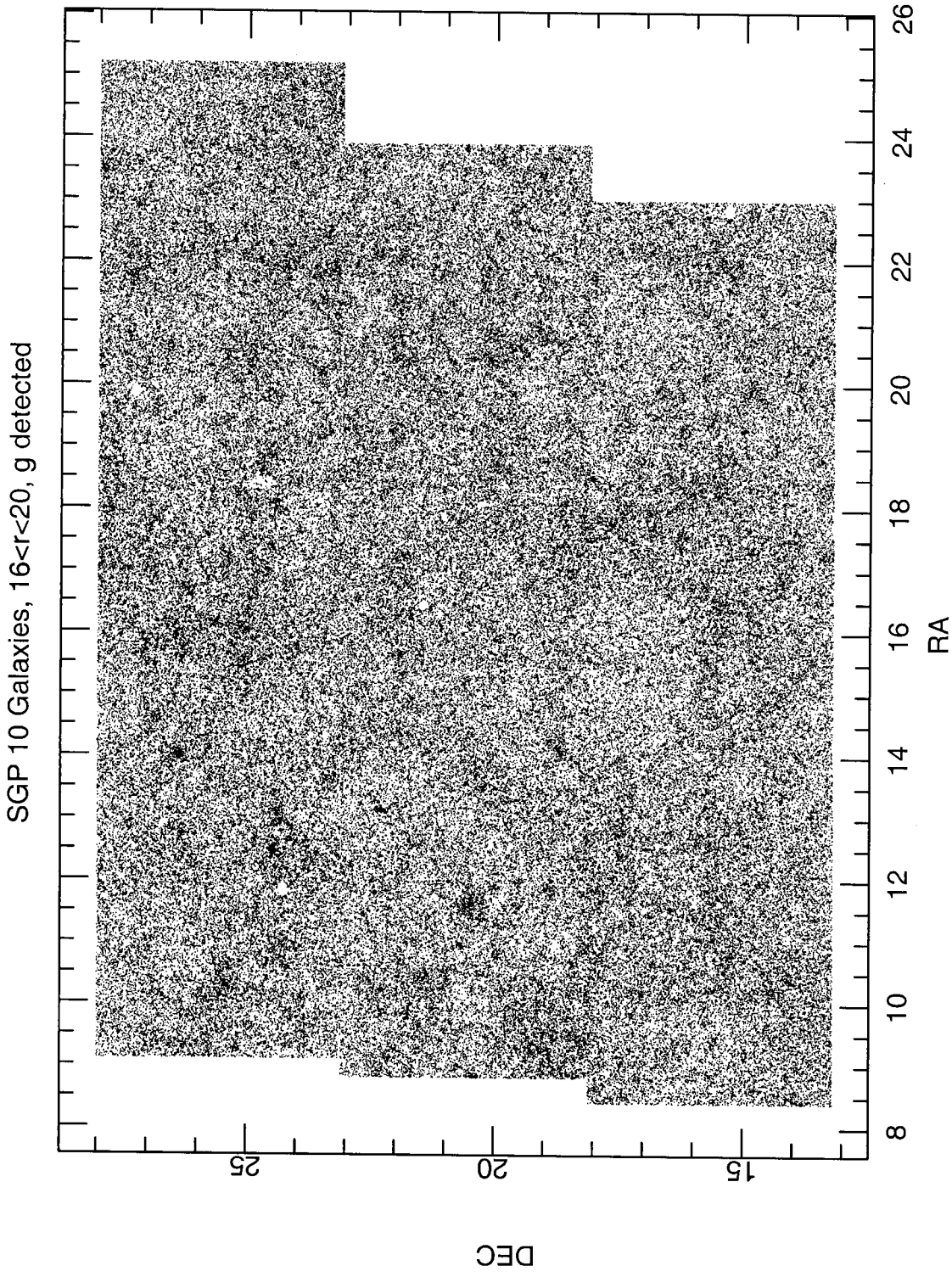

Figure A.18: Galaxies in SGP Area 10.

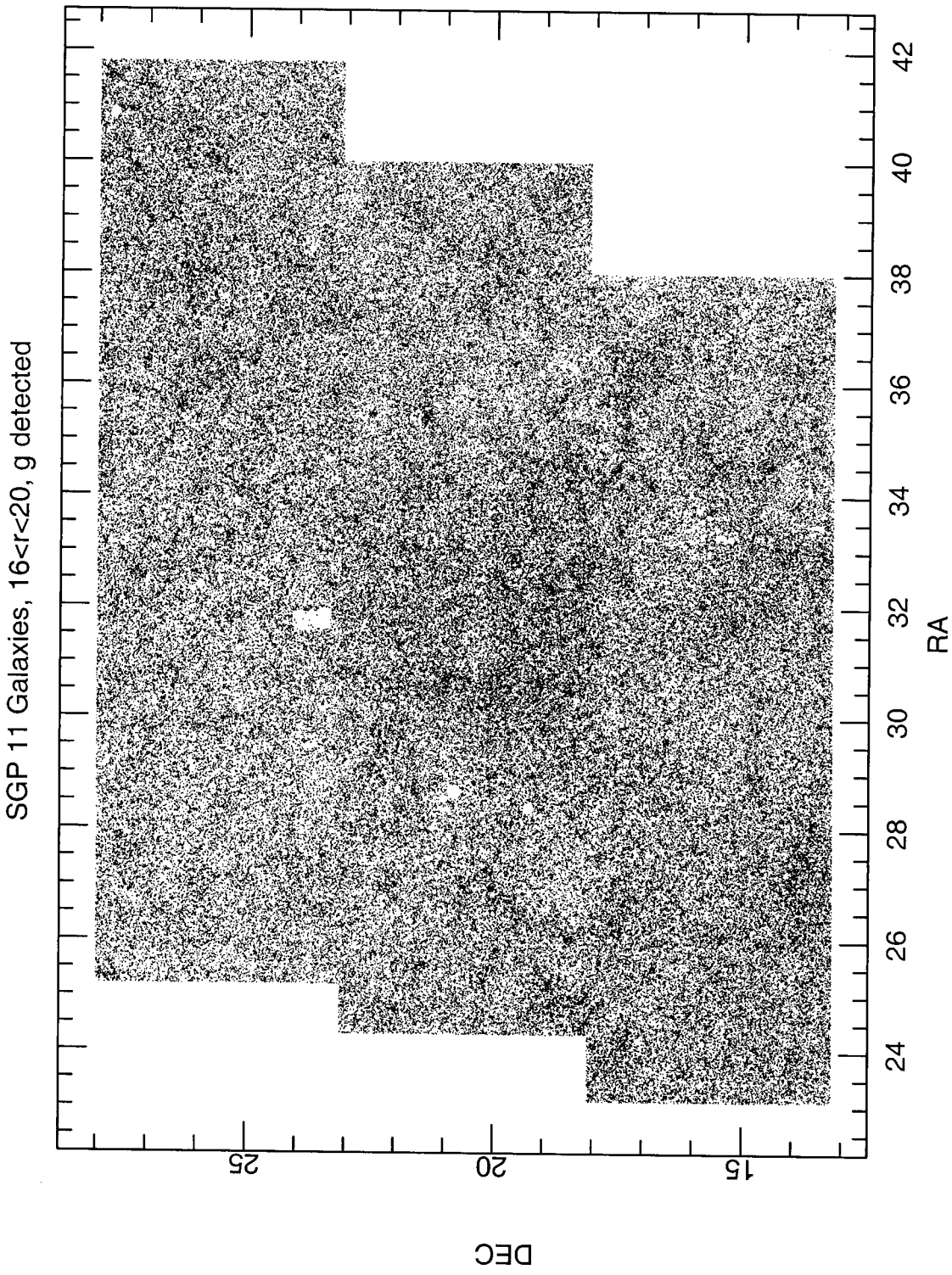

Figure A.19: Galaxies in SGP Area 11.

Appendix B

Properties of Galaxy Clusters

This appendix contains tables listing the basic properties of the galaxy clusters studied in this thesis. Tables B.1 and B.2 provide the names, coordinates, photometric redshifts, and richnesses for the candidate clusters in the NGP and SGP regions, respectively. Table B.3 gives the photometric redshifts for the Abell clusters imaged at the Palomar 60″.

Table B.1 - NGP Robust Candidate Galaxy Clusters

Name	RA	Dec	z_{phot}	N_{gal}
NSC0909+4243	137.304	42.723	0.1740	27
NSC0909+4649	137.364	46.815	0.1489	22
NSC0912+4604	137.984	46.067	0.1316	21
NSC0912+4739	138.012	47.643	0.1174	31
NSC0913+4741	138.248	47.681	0.0888	48
NSC0913+4603	138.273	46.045	0.1322	23
NSC0916+5739	139.037	57.648	0.2095	30
NSC0916+5253	139.058	52.890	0.1870	44
NSC0917+5246	139.257	52.775	0.1902	50
NSC0917+5510	139.306	55.172	0.1438	25
NSC0918+5144	139.579	51.730	0.2049	91
NSC0918+4814	139.583	48.235	0.2002	19
NSC0919+5306	139.670	53.103	0.1885	24
NSC0920+5535	139.894	55.584	0.1275	42
NSC0920+5627	140.063	56.445	0.1855	26
NSC0921+4539	140.233	45.652	0.1880	26
NSC0921+4727	140.233	47.454	0.1548	20
NSC0922+5203	140.387	52.045	0.2223	39
NSC0922+5154	140.495	51.903	0.2401	56
NSC0922+4649	140.516	46.819	0.1992	21
NSC0922+5458	140.569	54.964	0.1905	52
NSC0922+5418	140.614	54.303	0.1193	41
NSC0923+4408	140.646	44.129	0.1953	25
NSC0923+5232	140.707	52.528	0.1207	25
NSC0923+4621	140.738	46.346	0.2019	18
NSC0923+5451	140.806	54.856	0.1570	38
NSC0923+4635	140.834	46.587	0.1830	24
NSC0923+5244	140.834	52.728	0.1308	33
NSC0924+5602	140.924	56.039	0.1555	26
NSC0924+5335	140.929	53.591	0.1654	38
NSC0924+4630	141.119	46.499	0.1640	35
NSC0925+4250	141.250	42.842	0.1152	35
NSC0926+4613	141.537	46.218	0.2115	19
NSC0927+5048	141.676	50.792	0.1224	38
NSC0927+5326	141.720	53.434	0.2066	33
NSC0927+5424	141.746	54.397	0.1350	36
NSC0927+5125	141.818	51.421	0.1866	30
NSC0927+5545	141.833	55.749	0.2185	28
NSC0929+4415	142.334	44.252	0.1606	20
NSC0930+5717	142.504	57.289	0.1762	27
NSC0930+4358	142.554	43.967	0.1661	23
NSC0930+5126	142.562	51.431	0.2296	33
NSC0932+5113	142.934	51.220	0.2026	24
NSC0932+5052	143.024	50.863	0.2334	23
NSC0932+4448	143.061	44.794	0.1072	21
NSC0932+5558	143.071	55.975	0.1570	28
NSC0933+5018	143.242	50.304	0.2307	21
NSC0933+4757	143.336	47.950	0.2007	24
NSC0934+5421	143.489	54.352	0.1302	29
NSC0934+4806	143.577	48.099	0.1732	17
NSC0934+5114	143.589	51.239	0.2067	22
NSC0934+4934	143.609	49.570	0.1577	28
NSC0935+4305	143.780	43.085	0.1603	16
NSC0935+5344	143.868	53.733	0.1830	31
NSC0936+5325	143.954	53.419	0.1713	33
NSC0936+5105	143.973	51.085	0.2710	14
NSC0936+4858	143.982	48.966	0.1854	29
NSC0936+5139	144.058	51.654	0.1755	23
NSC0936+4844	144.094	48.730	0.1968	23
NSC0937+5022	144.214	50.366	0.1641	27
NSC0938+5331	144.383	53.516	0.1863	22
NSC0938+5129	144.412	51.483	0.1650	26
NSC0938+4257	144.545	42.954	0.1838	18
NSC0939+5117	144.688	51.280	0.2371	21
NSC0939+4251	144.746	42.846	0.1781	22
NSC0941+5046	145.222	50.773	0.1873	24
NSC0941+5112	145.256	51.204	0.1557	23
NSC0942+5633	145.416	56.551	0.2041	33
NSC0944+5228	145.918	52.470	0.1790	27
NSC0944+5207	145.957	52.125	0.2182	26
NSC0945+5621	146.264	56.347	0.1370	19
NSC0945+5633	146.342	56.553	0.1301	29
NSC0946+4303	146.467	43.048	0.0868	70
NSC0946+4254	146.474	42.899	0.0884	55
NSC0947+5427	146.668	54.456	0.0595	29
NSC0947+4405	146.687	44.080	0.1412	32
NSC0947+4327	146.720	43.445	0.1022	61
NSC0947+4306	146.762	43.100	0.1584	31
NSC0948+5005	146.882	50.088	0.1741	19
NSC0948+5117	146.915	51.277	0.2219	24
NSC0948+5031	146.951	50.519	0.1640	33
NSC0948+4820	147.006	48.334	0.2289	17
NSC0949+4251	147.174	42.850	0.1883	28
NSC0949+4833	147.226	48.550	0.2252	30
NSC0950+4820	147.448	48.337	0.1751	27
NSC0950+4913	147.499	49.220	0.2103	23
NSC0950+5429	147.515	54.485	0.0318	13
NSC0951+4612	147.656	46.205	0.1276	22
NSC0952+4840	147.953	48.666	0.1500	32

Continued...

Table B.1 - NGP Robust, Continued

Name	RA	Dec	z_{phot}	N_{gal}
NSC0952+5626	147.963	56.435	0.1968	24
NSC0952+4448	147.989	44.801	0.2483	17
NSC0952+5741	147.996	57.678	0.1242	32
NSC0953+5152	148.198	51.871	0.2518	25
NSC0954+5711	148.425	57.188	0.0436	21
NSC0954+4429	148.446	44.488	0.1691	22
NSC0954+4814	148.518	48.236	0.1752	26
NSC0954+5510	148.569	55.169	0.1509	20
NSC0955+4346	148.760	43.769	0.1522	25
NSC0955+4409	148.773	44.143	0.1782	21
NSC0955+5132	148.819	51.530	0.1970	34
NSC0955+4319	148.849	43.308	0.1714	21
NSC0956+5120	148.912	51.329	0.1955	37
NSC0956+5505	149.124	55.087	0.1916	20
NSC0957+4545	149.132	45.749	0.1351	28
NSC0957+4930	149.135	49.493	0.2259	40
NSC0957+4806	149.312	48.104	0.2318	18
NSC0957+4645	149.335	46.743	0.2039	30
NSC0957+4918	149.354	49.304	0.2251	42
NSC0958+5517	149.531	55.282	0.1904	27
NSC0959+4336	149.655	43.598	0.1911	28
NSC0959+4835	149.683	48.584	0.1785	33
NSC0959+5414	149.806	54.231	0.0000	3
NSC1000+4346	149.883	43.770	0.1743	22
NSC1000+4921	149.957	49.350	0.2387	18
NSC1000+5729	150.000	57.480	0.1790	24
NSC1000+5317	150.018	53.290	0.1776	24
NSC1000+4408	150.040	44.139	0.1418	32
NSC1000+4748	150.073	47.805	0.2316	21
NSC1001+5044	150.167	50.738	0.1354	46
NSC1001+4540	150.232	45.662	0.1216	28
NSC1001+2232	150.269	22.540	0.2151	46
NSC1001+1933	150.275	19.558	0.1692	41
NSC1001+5059	150.292	50.989	0.1738	20
NSC1001+2010	150.317	20.167	0.2129	26
NSC1001+1852	150.323	18.873	0.1335	40
NSC1001+4857	150.361	48.951	0.1623	25
NSC1001+1945	150.372	19.747	0.2300	13
NSC1002+5001	150.410	50.018	0.1804	22
NSC1002+4921	150.474	49.343	0.2053	23
NSC1002+1908	150.474	19.127	0.1754	21
NSC1002+1749	150.529	17.823	0.0403	16
NSC1002+5159	150.589	51.982	0.1575	27
NSC1002+2030	150.607	20.499	0.3009	29
NSC1002+1843	150.624	18.717	0.1934	20
NSC1003+5051	150.665	50.842	0.1376	33
NSC1003+1951	150.751	19.851	0.2002	24
NSC1003+5629	150.818	56.483	0.2426	21
NSC1003+2116	150.865	21.265	0.1560	36
NSC1004+1931	150.882	19.510	0.2228	17
NSC1004+4407	150.915	44.123	0.1096	18
NSC1004+5138	150.998	51.627	0.1333	34
NSC1004+4530	151.063	45.497	0.1289	21
NSC1004+5056	151.077	50.932	0.2109	24
NSC1005+2052	151.154	20.862	0.2259	20
NSC1005+4856	151.167	48.933	0.2401	25
NSC1005+5626	151.194	56.428	0.1113	20
NSC1005+2104	151.206	21.074	0.2234	24
NSC1005+5012	151.256	50.204	0.1825	25
NSC1005+5060	151.309	50.999	0.2124	34
NSC1005+2057	151.326	20.945	0.2388	27
NSC1005+4639	151.335	46.644.	0.1762	32
NSC1005+2233	151.344	22.543	0.2273	13
NSC1006+1821	151.457	18.356	0.1007	28
NSC1006+4947	151.469	49.788	0.1874	28
NSC1006+4720	151.496	47.326	0.2327	32
NSC1006+4848	151.513	48.801	0.1697	30
NSC1006+5031	151.596	50.518	0.2094	29
NSC1006+1916	151.597	19.267	0.1996	25
NSC1006+5053	151.624	50.888	0.2622	19
NSC1007+2035	151.626	20.575	0.2084	23
NSC1007+1814	151.648	18.241	0.1338	21
NSC1007+2141	151.666	21.681	0.2115	32
NSC1007+1944	151.703	19.739	0.1822	21
NSC1007+5523	151.756	55.384	0.1391	36
NSC1007+2053	151.817	20.881	0.1390	19
NSC1007+5516	151.849	55.270	0.1185	35
NSC1007+2459	151.851	24.984	0.1829	23
NSC1007+4705	151.852	47.087	0.2567	29
NSC1008+1934	151.880	19.569	0.2174	30
NSC1008+2006	151.892	20.102	0.2255	22
NSC1008+4824	151.913	48.401	0.1809	26
NSC1008+5011	151.920	50.176	0.2107	23
NSC1008+2150	151.965	21.825	0.1897	15
NSC1008+4914	151.966	49.236	0.1977	29
NSC1008+4248	151.973	42.808	0.2158	27
NSC1008+5026	151.974	50.438	0.1703	46

Continued...

Table B.1 - NGP Robust, Continued

Name	RA	Dec	z_{phot}	N_{gal}
NSC1008+1838	151.976	18.637	0.1574	20
NSC1008+1823	152.010	18.385	0.1120	24
NSC1008+2132	152.036	21.541	0.1541	21
NSC1008+4630	152.046	46.496	0.1894	25
NSC1008+4801	152.048	48.018	0.2239	37
NSC1008+1936	152.055	19.602	0.2019	22
NSC1008+5018	152.124	50.293	0.1947	41
NSC1009+4930	152.170	49.495	0.1552	27
NSC1009+1901	152.187	19.023	0.1633	16
NSC1009+4251	152.190	42.843	0.1856	26
NSC1009+1950	152.222	19.835	0.1967	17
NSC1009+2133	152.258	21.542	0.1536	21
NSC1009+1845	152.290	18.745	0.1050	31
NSC1009+4814	152.310	48.227	0.2407	18
NSC1009+4433	152.333	44.552	0.1354	29
NSC1009+5507	152.350	55.110	0.1252	27
NSC1009+4956	152.368	49.941	0.1693	28
NSC1009+1825	152.371	18.418	0.1127	39
NSC1009+4444	152.372	44.730	0.1410	48
NSC1010+1815	152.430	18.251	0.2058	28
NSC1010+4551	152.452	45.854	0.1432	32
NSC1010+4251	152.482	42.857	0.2238	22
NSC1010+1742	152.512	17.693	0.2214	31
NSC1010+5429	152.524	54.480	0.0359	27
NSC1010+1835	152.536	18.590	0.1138	27
NSC1010+1859	152.556	18.982	0.1142	39
NSC1010+4757	152.579	47.947	0.1882	30
NSC1010+1847	152.592	18.776	0.1158	32
NSC1010+1738	152.622	17.633	0.1958	36
NSC1011+2137	152.631	21.621	0.2014	16
NSC1011+5639	152.649	56.654	0.1576	30
NSC1011+1755	152.675	17.923	0.1828	34
NSC1011+2557	152.758	25.954	0.2276	18
NSC1011+4349	152.774	43.820	0.1153	26
NSC1011+4641	152.774	46.685	0.1534	28
NSC1011+1746	152.780	17.759	0.1541	26
NSC1011+1914	152.789	19.240	0.1274	49
NSC1011+4802	152.809	48.032	0.2063	19
NSC1011+1949	152.839	19.814	0.1513	26
NSC1012+1931	152.928	19.525	0.1950	16
NSC1012+2053	152.942	20.884	0.1939	18
NSC1012+1915	152.960	19.258	0.1229	47
NSC1012+5737	152.971	57.619	0.1429	17
NSC1012+4559	153.013	45.987	0.1629	23
NSC1012+1939	153.058	19.645	0.1328	21
NSC1012+5043	153.079	50.721	0.2191	32
NSC1012+2350	153.091	23.834	0.2059	27
NSC1012+4735	153.098	47.586	0.1758	32
NSC1013+2204	153.157	22.064	0.2352	15
NSC1013+2315	153.162	23.242	0.2165	14
NSC1013+2520	153.186	25.339	0.1874	22
NSC1013+4809	153.220	48.154	0.2414	18
NSC1013+4625	153.246	46.422	0.1234	32
NSC1013+1507	153.255	15.109	0.1998	21
NSC1013+4317	153.260	43.289	0.0933	26
NSC1013+1542	153.263	15.696	0.1649	23
NSC1013+1515	153.273	15.245	0.1165	28
NSC1013+5713	153.319	57.209	0.1095	24
NSC1013+2358	153.344	23.965	0.2361	15
NSC1013+2450	153.362	24.839	0.2302	19
NSC1013+1321	153.370	13.348	0.1967	29
NSC1013+1413	153.370	14.219	0.1396	22
NSC1014+2033	153.391	20.555	0.2235	19
NSC1014+4934	153.404	49.558	0.1289	36
NSC1014+5505	153.414	55.080	0.1156	31
NSC1014+2005	153.424	20.080	0.1635	15
NSC1014+4747	153.426	47.776	0.1651	44
NSC1014+1944	153.452	19.732	0.1058	59
NSC1014+2053	153.516	20.880	0.1962	22
NSC1014+4547	153.531	45.784	0.1587	42
NSC1014+1849	153.575	18.823	0.1872	24
NSC1014+4951	153.610	49.856	0.1741	49
NSC1015+5705	153.665	57.089	0.1385	36
NSC1015+4450	153.668	44.827	0.1448	29
NSC1015+2148	153.689	21.800	0.1654	35
NSC1015+4927	153.734	49.453	0.1728	33
NSC1015+4714	153.753	47.226	0.1603	47
NSC1015+1853	153.755	18.890	0.1900	16
NSC1015+5302	153.759	53.034	0.1569	18
NSC1015+2107	153.771	21.116	0.2085	18
NSC1015+2221	153.771	22.347	0.2608	24
NSC1015+4859	153.774	48.980	0.0843	21
NSC1015+5312	153.848	53.208	0.1032	28
NSC1016+1557	153.895	15.943	0.1286	23
NSC1016+5645	153.947	56.748	0.1765	37
NSC1016+2104	153.988	21.064	0.1727	16
NSC1016+5256	154.005	52.938	0.1125	28

Continued...

Table B.1 - NGP Robust, Continued

Name	RA	Dec	z_{phot}	N_{gal}
NSC1016+5716	154.006	57.269	0.2170	22
NSC1016+2202	154.013	22.028	0.2275	22
NSC1016+4706	154.019	47.099	0.1633	44
NSC1016+1945	154.046	19.753	0.1749	25
NSC1016+1609	154.048	16.143	0.1344	22
NSC1016+2405	154.082	24.083	0.2103	19
NSC1016+2450	154.104	24.828	0.1450	37
NSC1016+4631	154.107	46.511	0.1556	25
NSC1016+5621	154.113	56.350	0.2059	34
NSC1017+1409	154.137	14.143	0.1819	29
NSC1017+4914	154.183	49.231	0.2342	18
NSC1017+1400	154.187	14.005	0.1225	35
NSC1017+1910	154.225	19.170	0.1935	23
NSC1017+1505	154.239	15.078	0.1750	20
NSC1017+5702	154.240	57.033	0.1979	21
NSC1017+5641	154.314	56.679	0.1990	29
NSC1017+1928	154.321	19.462	0.1249	30
NSC1017+2134	154.333	21.559	0.1987	24
NSC1017+1526	154.347	15.441	0.1820	20
NSC1018+1857	154.385	18.946	0.1430	28
NSC1018+2243	154.423	22.710	0.2076	23
NSC1018+2120	154.432	21.327	0.1677	18
NSC1018+1419	154.447	14.316	0.1693	24
NSC1018+1648	154.510	16.797	0.2073	22
NSC1018+2013	154.510	20.214	0.1320	30
NSC1018+4855	154.545	48.911	0.0900	29
NSC1018+1537	154.556	15.625	0.1712	23
NSC1018+2237	154.571	22.613	0.1983	22
NSC1018+4332	154.577	43.536	0.1288	40
NSC1018+5702	154.593	57.038	0.1228	41
NSC1018+2125	154.598	21.411	0.2049	25
NSC1018+4955	154.608	49.913	0.1202	50
NSC1018+1860	154.617	18.994	0.2464	18
NSC1018+2526	154.622	25.440	0.1856	18
NSC1019+1442	154.684	14.702	0.1298	29
NSC1019+4321	154.711	43.358	0.1131	47
NSC1019+1718	154.742	17.302	0.1149	35
NSC1019+1424	154.771	14.400	0.1522	21
NSC1019+1520	154.784	15.327	0.1454	23
NSC1019+2251	154.802	22.850	0.1684	24
NSC1019+4453	154.803	44.886	0.1174	31
NSC1019+4926	154.803	49.428	0.1765	16
NSC1019+2238	154.818	22.640	0.1154	38
NSC1019+5548	154.818	55.794	0.1810	22
NSC1019+1731	154.820	17.516	0.1613	28
NSC1019+1760	154.829	17.994	0.1301	29
NSC1019+4711	154.849	47.184	0.1604	30
NSC1019+1813	154.855	18.222	0.1557	28
NSC1020+4806	154.892	48.100	0.2097	34
NSC1020+1643	154.898	16.722	0.2091	21
NSC1020+1403	154.904	14.057	0.1394	61
NSC1020+2534	154.907	25.574	0.1298	22
NSC1020+2130	154.908	21.506	0.1901	21
NSC1020+4701	154.958	47.011	0.1761	33
NSC1020+4847	154.984	48.779	0.1794	28
NSC1020+1354	154.995	13.892	0.1742	32
NSC1020+5126	155.024	51.427	0.1758	23
NSC1020+2619	155.041	26.325	0.0082	3
NSC1020+1338	155.047	13.630	0.0735	27
NSC1020+4249	155.047	42.815	0.0895	36
NSC1020+1750	155.049	17.837	0.1844	42
NSC1020+4241	155.049	42.684	0.1012	49
NSC1020+2359	155.053	23.987	0.2119	23
NSC1020+4952	155.069	49.871	0.1225	44
NSC1020+1904	155.087	19.066	0.1465	39
NSC1020+1729	155.098	17.489	0.1974	22
NSC1020+2424	155.110	24.397	0.1746	18
NSC1021+1645	155.134	16.754	0.1710	17
NSC1021+2137	155.134	21.614	0.1443	16
NSC1021+1308	155.147	13.139	0.0642	15
NSC1021+4812	155.205	48.196	0.2111	20
NSC1021+1838	155.257	18.630	0.1367	30
NSC1021+1446	155.263	14.770	0.2386	32
NSC1021+4704	155.266	47.062	0.1228	31
NSC1021+4829	155.277	48.484	0.1421	33
NSC1021+2339	155.287	23.642	0.1097	21
NSC1021+1950	155.298	19.826	0.1517	22
NSC1021+2121	155.309	21.349	0.1761	22
NSC1021+2036	155.316	20.596	0.2294	25
NSC1021+1410	155.317	14.164	0.2166	36
NSC1021+2352	155.357	23.864	0.0564	32
NSC1021+2442	155.369	24.706	0.1492	32
NSC1021+5142	155.373	51.692	0.1029	26
NSC1022+1449	155.394	14.817	0.2325	22
NSC1022+1620	155.418	16.341	0.2423	18
NSC1022+1406	155.447	14.104	0.2001	54
NSC1022+5102	155.448	51.035	0.1856	39

Continued...

Table B.1 - NGP Robust, Continued

Name	RA	Dec	z_{phot}	N_{gal}
NSC1022+1334	155.461	13.559	0.1157	27
NSC1022+1529	155.474	15.491	0.1099	24
NSC1022+2335	155.486	23.585	0.1329	26
NSC1022+2114	155.507	21.241	0.2102	20
NSC1022+4910	155.526	49.166	0.1733	23
NSC1022+5218	155.530	52.298	0.1165	32
NSC1022+2519	155.530	25.316	0.1556	21
NSC1022+4848	155.542	48.795	0.1841	32
NSC1022+1812	155.560	18.198	0.1321	25
NSC1022+1854	155.561	18.905	0.1727	26
NSC1022+4937	155.562	49.609	0.2004	21
NSC1022+1342	155.574	13.701	0.1107	25
NSC1022+1921	155.621	19.356	0.2074	25
NSC1023+5007	155.658	50.116	0.1736	80
NSC1023+2028	155.703	20.464	0.0900	58
NSC1023+4740	155.706	47.669	0.1194	34
NSC1023+5046	155.714	50.766	0.1364	36
NSC1023+1324	155.715	13.396	0.1476	27
NSC1023+5203	155.719	52.052	0.1531	60
NSC1023+1509	155.722	15.158	0.2171	26
NSC1023+4753	155.729	47.885	0.1431	40
NSC1023+1537	155.741	15.622	0.1762	26
NSC1023+5111	155.744	51.186	0.1309	31
NSC1023+4624	155.758	46.393	0.2274	32
NSC1023+5019	155.783	50.320	0.1765	29
NSC1023+4803	155.805	48.051	0.1665	22
NSC1023+1252	155.810	12.873	0.0558	33
NSC1023+5035	155.856	50.584	0.1678	28
NSC1023+4725	155.859	47.419	0.1185	28
NSC1024+4909	155.880	49.147	0.1641	76
NSC1024+2206	155.893	22.096	0.0737	21
NSC1024+5206	155.912	52.097	0.2383	24
NSC1024+5224	155.948	52.408	0.1322	29
NSC1024+1407	155.968	14.124	0.1517	16
NSC1024+1711	156.028	17.189	0.0704	42
NSC1024+1639	156.055	16.657	0.1169	29
NSC1024+2408	156.058	24.134	0.1096	21
NSC1024+5138	156.060	51.629	0.1922	44
NSC1024+4824	156.081	48.398	0.1293	40
NSC1025+5058	156.126	50.971	0.2168	23
NSC1025+5011	156.179	50.184	0.1853	69
NSC1025+1727	156.181	17.453	0.1839	21
NSC1025+1541	156.187	15.676	0.1863	22
NSC1025+4639	156.191	46.657	0.1427	20
NSC1025+4954	156.255	49.896	0.1562	53
NSC1025+1959	156.284	19.991	0.1411	22
NSC1025+4810	156.292	48.164	0.1902	29
NSC1025+4749	156.303	47.822	0.0880	62
NSC1025+1557	156.335	15.950	0.1495	24
NSC1025+4701	156.369	47.020	0.2018	32
NSC1025+4930	156.372	49.507	0.1546	30
NSC1026+5102	156.395	51.032	0.1788	59
NSC1026+2240	156.399	22.674	0.0979	22
NSC1026+5028	156.420	50.467	0.1802	27
NSC1026+2216	156.441	22.267	0.0951	38
NSC1026+5636	156.450	56.603	0.1521	25
NSC1026+2154	156.458	21.892	0.2006	38
NSC1026+4720	156.483	47.334	0.1160	29
NSC1026+1637	156.483	16.613	0.2045	23
NSC1026+2125	156.494	21.421	0.1018	27
NSC1026+4253	156.511	42.890	0.1640	33
NSC1026+4925	156.554	49.418	0.2315	27
NSC1026+5154	156.588	51.900	0.1818	38
NSC1026+1829	156.589	18.483	0.2111	32
NSC1026+4827	156.595	48.444	0.1091	40
NSC1026+5138	156.618	51.634	0.1837	25
NSC1027+5307	156.708	53.122	0.1402	24
NSC1027+2723	156.753	27.384	0.1443	24
NSC1027+4944	156.778	49.730	0.2006	35
NSC1027+4512	156.779	45.192	0.1028	21
NSC1027+5530	156.822	55.498	0.1312	27
NSC1027+1851	156.842	18.844	0.1804	24
NSC1027+4757	156.845	47.951	0.1344	49
NSC1027+4255	156.869	42.911	0.1663	30
NSC1028+1650	156.893	16.839	0.1937	14
NSC1028+1428	156.915	14.467	0.1640	30
NSC1028+4644	156.925	46.733	0.1696	47
NSC1028+4353	156.955	43.886	0.0616	18
NSC1028+4320	156.972	43.325	0.0723	32
NSC1028+4922	156.999	49.360	0.1761	38
NSC1028+2123	157.006	21.390	0.1574	23
NSC1028+4956	157.009	49.941	0.1570	28
NSC1028+2243	157.012	22.715	0.1568	24
NSC1028+2444	157.013	24.732	0.1658	16
NSC1028+4703	157.016	47.046	0.2589	29
NSC1028+4525	157.030	45.413	0.1575	44
NSC1028+5118	157.032	51.304	0.1525	35

Continued...

Table B.1 - NGP Robust, Continued

Name	RA	Dec	z_{phot}	N_{gal}
NSC1028+1720	157.038	17.326	0.1878	22
NSC1028+4805	157.083	48.089	0.2588	18
NSC1028+1844	157.108	18.726	0.1583	32
NSC1029+4911	157.138	49.188	0.1451	32
NSC1029+1257	157.155	12.956	0.1644	30
NSC1029+4605	157.222	46.090	0.1770	28
NSC1029+1520	157.237	15.341	0.2027	23
NSC1029+2010	157.250	20.166	0.1022	23
NSC1029+5345	157.303	53.757	0.1635	30
NSC1029+4846	157.305	48.775	0.1085	35
NSC1029+2130	157.311	21.493	0.1931	24
NSC1029+5225	157.316	52.410	0.1784	26
NSC1029+4437	157.339	44.614	0.1714	25
NSC1029+4711	157.347	47.178	0.1163	49
NSC1029+2726	157.349	27.436	0.1321	36
NSC1029+4618	157.372	46.295	0.2023	25
NSC1029+4256	157.372	42.932	0.1970	26
NSC1030+1757	157.399	17.956	0.1264	38
NSC1030+2025	157.409	20.415	0.2534	22
NSC1030+2524	157.423	25.398	0.0000	3
NSC1030+4454	157.433	44.907	0.2215	36
NSC1030+2544	157.474	25.736	0.1602	18
NSC1030+4314	157.496	43.238	0.0775	44
NSC1030+5134	157.514	51.569	0.2106	20
NSC1030+1617	157.518	16.291	0.2336	23
NSC1030+4360	157.519	43.992	0.1387	40
NSC1030+5006	157.549	50.098	0.1732	23
NSC1030+1400	157.557	14.003	0.2264	23
NSC1030+2318	157.577	23.304	0.1853	24
NSC1030+5249	157.578	52.816	0.1574	30
NSC1031+4859	157.639	48.985	0.1880	28
NSC1031+1417	157.658	14.278	0.2232	26
NSC1031+5321	157.686	53.352	0.1837	44
NSC1031+4700	157.715	47.004	0.0994	44
NSC1031+4608	157.715	46.127	0.1412	38
NSC1031+1431	157.735	14.520	0.2109	15
NSC1031+4629	157.799	46.490	0.1330	46
NSC1031+1843	157.832	18.714	0.1945	33
NSC1031+1944	157.864	19.735	0.1710	34
NSC1031+4827	157.870	48.448	0.2119	23
NSC1032+4255	157.875	42.913	0.1800	27
NSC1032+2534	157.878	25.573	0.1753	21
NSC1032+1626	157.881	16.428	0.1094	18
NSC1032+2252	157.883	22.862	0.1455	17
NSC1032+5211	157.924	52.177	0.1258	24
NSC1032+5026	157.928	50.441	0.1773	36
NSC1032+2105	157.969	21.086	0.1504	26
NSC1032+4943	158.009	49.715	0.2262	31
NSC1032+1527	158.031	15.457	0.1792	23
NSC1032+5320	158.036	53.337	0.1467	49
NSC1032+1905	158.081	19.085	0.1176	24
NSC1032+1939	158.095	19.642	0.1293	29
NSC1033+1331	158.143	13.513	0.1388	22
NSC1033+5407	158.145	54.123	0.1514	31
NSC1033+4904	158.180	49.066	0.1206	35
NSC1033+2629	158.185	26.490	0.2333	18
NSC1033+2542	158.205	25.697	0.1552	23
NSC1033+4622	158.220	46.372	0.1828	30
NSC1033+1650	158.225	16.837	0.0884	22
NSC1033+1250	158.235	12.832	0.1522	34
NSC1033+4606	158.246	46.101	0.2106	18
NSC1033+5030	158.259	50.507	0.1249	27
NSC1033+1638	158.267	16.627	0.1164	30
NSC1033+1924	158.273	19.408	0.1614	26
NSC1033+4633	158.296	46.544	0.0969	33
NSC1033+2658	158.311	26.967	0.1917	20
NSC1033+1736	158.332	17.607	0.1592	23
NSC1033+5355	158.364	53.920	0.1514	26
NSC1034+1909	158.380	19.152	0.1313	26
NSC1034+1547	158.406	15.776	0.1874	33
NSC1034+1430	158.408	14.508	0.1630	22
NSC1034+5304	158.417	53.059	0.1601	34
NSC1034+1623	158.431	16.376	0.0664	30
NSC1034+5249	158.434	52.815	0.1391	53
NSC1034+4439	158.436	44.648	0.1937	28
NSC1034+2253	158.495	22.890	0.0914	25
NSC1034+5319	158.524	53.317	0.1667	29
NSC1034+1512	158.554	15.194	0.1092	34
NSC1034+4432	158.563	44.529	0.1049	32
NSC1034+1554	158.566	15.895	0.1583	37
NSC1034+1619	158.595	16.312	0.0851	41
NSC1034+4842	158.597	48.702	0.1651	25
NSC1034+1847	158.616	18.782	0.1642	26
NSC1034+4528	158.621	45.468	0.1429	48
NSC1034+5348	158.624	53.796	0.1650	22
NSC1034+2543	158.625	25.724	0.1255	31
NSC1035+4635	158.632	46.585	0.1903	30

Continued...

Table B.1 - NGP Robust, Continued

Name	RA	Dec	z_{phot}	N_{gal}
NSC1035+4537	158.636	45.623	0.2003	38
NSC1035+5442	158.643	54.705	0.1699	20
NSC1035+1823	158.677	18.384	0.1881	27
NSC1035+4723	158.686	47.388	0.1698	30
NSC1035+4708	158.690	47.140	0.2146	24
NSC1035+4259	158.692	42.983	0.1117	33
NSC1035+4610	158.708	46.163	0.1414	42
NSC1035+1944	158.721	19.732	0.1966	24
NSC1035+4504	158.743	45.059	0.1466	28
NSC1035+1318	158.837	13.299	0.2351	24
NSC1035+1350	158.847	13.831	0.1090	20
NSC1036+1948	158.892	19.804	0.1890	24
NSC1036+2540	158.892	25.660	0.1510	24
NSC1036+2426	158.900	24.435	0.1615	17
NSC1036+2125	158.946	21.419	0.2713	25
NSC1036+4614	158.949	46.226	0.1529	51
NSC1036+4959	158.961	49.983	0.1651	50
NSC1036+4557	158.963	45.955	0.1466	39
NSC1036+4356	158.966	43.929	0.1602	34
NSC1036+4738	158.984	47.638	0.1408	31
NSC1036+2615	158.994	26.254	0.2236	23
NSC1036+4523	159.032	45.382	0.1837	22
NSC1036+1908	159.063	19.139	0.1565	31
NSC1036+5123	159.069	51.386	0.2439	22
NSC1036+4510	159.071	45.159	0.1265	62
NSC1036+5424	159.072	54.392	0.1431	26
NSC1036+3049	159.084	30.815	0.1201	33
NSC1036+3157	159.096	31.957	0.2081	16
NSC1036+2805	159.106	28.087	0.1581	39
NSC1036+1952	159.121	19.863	0.1659	21
NSC1037+2349	159.134	23.815	0.2417	20
NSC1037+1540	159.156	15.664	0.0935	38
NSC1037+2637	159.161	26.618	0.1205	23
NSC1037+5348	159.203	53.800	0.1479	34
NSC1037+2536	159.212	25.608	0.1749	19
NSC1037+4449	159.222	44.818	0.1195	87
NSC1037+4306	159.225	43.106	0.1612	29
NSC1037+2408	159.232	24.136	0.1581	25
NSC1037+5008	159.257	50.129	0.1093	40
NSC1037+4612	159.266	46.197	0.1841	42
NSC1037+2906	159.298	29.094	0.1629	26
NSC1037+4344	159.330	43.728	0.1584	31
NSC1037+1808	159.331	18.131	0.1841	29
NSC1037+4240	159.332	42.659	0.1547	54
NSC1037+3043	159.335	30.715	0.1422	29
NSC1037+4833	159.351	48.550	0.1218	25
NSC1037+4749	159.356	47.813	0.1828	26
NSC1037+5238	159.371	52.625	0.1663	36
NSC1038+1909	159.382	19.145	0.1722	19
NSC1038+4407	159.386	44.117	0.1239	21
NSC1038+1358	159.408	13.966	0.1816	41
NSC1038+1254	159.419	12.893	0.1905	24
NSC1038+4706	159.425	47.095	0.1390	24
NSC1038+1540	159.454	15.667	0.1175	41
NSC1038+4511	159.479	45.178	0.1563	32
NSC1038+5726	159.491	57.438	0.2038	32
NSC1038+4809	159.495	48.158	0.1799	31
NSC1038+4150	159.531	41.830	0.1241	43
NSC1038+1853	159.548	18.882	0.1676	23
NSC1038+4750	159.549	47.833	0.1686	33
NSC1038+5047	159.574	50.777	0.1602	26
NSC1038+1513	159.583	15.223	0.1504	19
NSC1038+4819	159.600	48.310	0.1735	22
NSC1038+1841	159.620	18.682	0.1727	28
NSC1039+5011	159.627	50.186	0.1392	28
NSC1039+1742	159.639	17.707	0.2127	17
NSC1039+1728	159.640	17.469	0.1624	19
NSC1039+2842	159.651	28.707	0.2083	31
NSC1039+5358	159.655	53.972	0.2049	33
NSC1039+1552	159.661	15.864	0.1482	30
NSC1039+4724	159.687	47.397	0.1645	28
NSC1039+1414	159.725	14.230	0.1906	25
NSC1039+1320	159.736	13.326	0.1170	16
NSC1039+2648	159.750	26.806	0.1612	18
NSC1039+4850	159.762	48.828	0.2276	22
NSC1039+5427	159.766	54.448	0.1341	23
NSC1039+4445	159.775	44.747	0.1165	40
NSC1039+3947	159.785	39.790	0.0506	26
NSC1039+2715	159.815	27.243	0.2566	20
NSC1039+4459	159.818	44.977	0.1992	29
NSC1039+2504	159.829	25.073	0.1145	20
NSC1040+1843	159.946	18.725	0.2070	26
NSC1040+4251	159.966	42.855	0.1674	26
NSC1040+1427	159.970	14.448	0.2082	15
NSC1040+4860	159.977	48.998	0.1502	31
NSC1040+5318	160.106	53.301	0.1629	32
NSC1040+4720	160.116	47.331	0.1310	24

Continued...

Table B.1 - NGP Robust, Continued

Name	RA	Dec	z_{phot}	N_{gal}
NSC1040+4431	160.120	44.519	0.2216	33
NSC1041+2305	160.126	23.086	0.2187	19
NSC1041+4039	160.137	40.657	0.1813	24
NSC1041+4014	160.163	40.228	0.0826	33
NSC1041+2610	160.178	26.172	0.1561	17
NSC1041+3959	160.190	39.978	0.1658	41
NSC1041+5645	160.190	56.753	0.1911	33
NSC1041+2550	160.210	25.840	0.1749	25
NSC1041+5724	160.210	57.395	0.1285	23
NSC1041+5614	160.210	56.226	0.1695	19
NSC1041+4315	160.250	43.251	0.1768	28
NSC1041+5403	160.252	54.055	0.2119	18
NSC1041+1931	160.258	19.521	0.2074	21
NSC1041+2637	160.261	26.621	0.2192	19
NSC1041+2352	160.264	23.870	0.1774	23
NSC1041+1449	160.286	14.822	0.2027	26
NSC1041+2700	160.301	27.006	0.1994	25
NSC1041+3354	160.321	33.899	0.0453	22
NSC1042+4258	160.387	42.961	0.1644	30
NSC1042+1833	160.413	18.554	0.1828	24
NSC1042+2406	160.424	24.106	0.1574	22
NSC1042+3927	160.511	39.446	0.1124	45
NSC1042+5427	160.518	54.446	0.2496	25
NSC1042+2532	160.561	25.528	0.1143	24
NSC1042+2327	160.573	23.448	0.1825	18
NSC1042+4253	160.579	42.882	0.1471	37
NSC1042+5216	160.594	52.275	0.1377	30
NSC1042+5340	160.598	53.670	0.1761	23
NSC1042+4303	160.609	43.055	0.1757	34
NSC1042+5624	160.615	56.402	0.1449	22
NSC1043+1636	160.647	16.596	0.0785	33
NSC1043+1837	160.655	18.612	0.1477	28
NSC1043+4925	160.655	49.412	0.2190	25
NSC1043+3418	160.705	34.292	0.2175	29
NSC1043+5421	160.734	54.354	0.1749	27
NSC1043+3918	160.756	39.306	0.1074	26
NSC1043+2111	160.771	21.180	0.2097	23
NSC1043+3634	160.780	36.565	0.1474	31
NSC1043+5723	160.781	57.385	0.1188	45
NSC1043+4430	160.788	44.507	0.1092	25
NSC1043+4839	160.794	48.642	0.1777	16
NSC1043+1901	160.802	19.012	0.1177	41
NSC1043+5333	160.846	53.556	0.1755	36
NSC1043+4639	160.857	46.652	0.2193	36
NSC1043+2250	160.860	22.834	0.2142	14
NSC1044+2650	160.876	26.826	0.2498	21
NSC1044+4307	160.887	43.120	0.1875	25
NSC1044+4824	160.911	48.402	0.1722	22
NSC1044+2812	160.911	28.202	0.2557	18
NSC1044+4860	160.935	48.998	0.1566	30
NSC1044+5233	160.939	52.544	0.1959	22
NSC1044+3610	160.940	36.172	0.1921	32
NSC1044+1741	160.951	17.686	0.2510	28
NSC1044+1437	160.989	14.611	0.1712	29
NSC1044+1611	161.014	16.175	0.1028	23
NSC1044+2101	161.031	21.013	0.2098	24
NSC1044+5240	161.034	52.662	0.2076	32
NSC1044+3941	161.061	39.683	0.0617	28
NSC1044+3837	161.069	38.615	0.2075	23
NSC1044+4750	161.078	47.841	0.1511	30
NSC1044+1716	161.083	17.273	0.2081	19
NSC1044+4719	161.112	47.310	0.1502	33
NSC1045+4629	161.126	46.490	0.1999	60
NSC1045+1743	161.130	17.714	0.2265	36
NSC1045+3226	161.132	32.433	0.1645	24
NSC1045+1804	161.200	18.073	0.1351	24
NSC1045+2150	161.204	21.828	0.1997	24
NSC1045+3534	161.216	35.560	0.1076	51
NSC1045+5035	161.240	50.584	0.1212	26
NSC1045+5216	161.251	52.264	0.2004	21
NSC1045+1632	161.275	16.528	0.1675	32
NSC1045+2202	161.288	22.030	0.1075	26
NSC1045+4933	161.298	49.547	0.1640	40
NSC1045+4749	161.316	47.815	0.1235	31
NSC1045+2014	161.335	20.227	0.0920	24
NSC1045+1830	161.335	18.501	0.1225	23
NSC1045+1551	161.336	15.848	0.1322	18
NSC1045+2026	161.363	20.426	0.0736	30
NSC1046+1738	161.377	17.639	0.1650	37
NSC1046+4629	161.401	46.483	0.1761	28
NSC1046+4618	161.469	46.304	0.1438	27
NSC1046+2712	161.479	27.193	0.1631	19
NSC1046+4353	161.540	43.890	0.1907	30
NSC1046+4414	161.558	44.228	0.1859	21
NSC1046+1745	161.613	17.744	0.2170	25
NSC1047+3151	161.630	31.855	0.1311	24
NSC1047+3344	161.642	33.731	0.1925	23

Continued...

Table B.1 - NGP Robust, Continued

Name	RA	Dec	z_{phot}	N_{gal}
NSC1047+4506	161.696	45.097	0.1135	34
NSC1047+1646	161.721	16.769	0.1578	34
NSC1047+3141	161.752	31.687	0.2026	26
NSC1047+1804	161.777	18.069	0.1825	23
NSC1047+1732	161.795	17.534	0.1343	29
NSC1047+4239	161.870	42.656	0.1051	19
NSC1048+2718	161.898	27.304	0.1612	23
NSC1048+1752	161.909	17.862	0.1772	23
NSC1048+4348	161.913	43.805	0.1265	29
NSC1048+1951	161.922	19.843	0.0591	26
NSC1048+4443	161.937	44.713	0.1967	25
NSC1048+1516	161.963	15.261	0.2110	39
NSC1048+1643	161.999	16.721	0.1212	24
NSC1048+3130	162.024	31.494	0.1324	42
NSC1048+2148	162.064	21.793	0.1390	17
NSC1048+1620	162.094	16.330	0.1107	33
NSC1048+3855	162.107	38.914	0.1456	31
NSC1049+1852	162.130	18.862	0.1382	50
NSC1049+2804	162.143	28.061	0.2660	14
NSC1049+2215	162.168	22.249	0.0852	36
NSC1049+1736	162.205	17.608	0.1662	35
NSC1049+4422	162.214	44.365	0.2041	29
NSC1049+3122	162.219	31.371	0.0982	38
NSC1049+3448	162.234	34.805	0.1345	34
NSC1049+2434	162.292	24.568	0.1366	25
NSC1049+4349	162.293	43.818	0.1454	44
NSC1049+1322	162.299	13.370	0.1300	29
NSC1049+4446	162.371	44.764	0.2005	26
NSC1050+2227	162.379	22.452	0.2471	16
NSC1050+4739	162.400	47.652	0.1140	33
NSC1050+1818	162.413	18.299	0.0610	30
NSC1050+3222	162.431	32.360	0.1881	20
NSC1050+1908	162.448	19.136	0.1702	18
NSC1050+1749	162.457	17.821	0.1229	45
NSC1050+3413	162.469	34.212	0.1403	18
NSC1050+2211	162.473	22.182	0.1291	41
NSC1050+2330	162.476	23.503	0.1344	37
NSC1050+4433	162.484	44.545	0.2103	14
NSC1050+1829	162.488	18.485	0.0984	27
NSC1050+1612	162.490	16.204	0.1460	37
NSC1050+4420	162.504	44.341	0.2316	48
NSC1050+1741	162.517	17.689	0.1308	32
NSC1050+1530	162.533	15.495	0.1041	43
NSC1050+3141	162.542	31.690	0.1502	21
NSC1050+1340	162.554	13.673	0.0979	25
NSC1050+2158	162.555	21.963	0.1651	16
NSC1050+1657	162.570	16.943	0.2275	33
NSC1050+4713	162.583	47.217	0.1498	34
NSC1050+3712	162.602	37.193	0.1708	20
NSC1050+1719	162.602	17.320	0.1326	25
NSC1051+2051	162.626	20.854	0.1624	23
NSC1051+1647	162.636	16.779	0.2214	26
NSC1051+4517	162.658	45.278	0.1659	20
NSC1051+1443	162.666	14.720	0.2094	30
NSC1051+2134	162.666	21.568	0.1534	17
NSC1051+1835	162.677	18.587	0.2113	28
NSC1051+3153	162.720	31.890	0.1424	34
NSC1051+1726	162.721	17.436	0.1440	36
NSC1051+1810	162.753	18.174	0.1068	24
NSC1051+1631	162.753	16.513	0.1605	21
NSC1051+4434	162.768	44.559	0.2594	22
NSC1051+2953	162.789	29.879	0.1494	36
NSC1051+3738	162.790	37.634	0.1065	22
NSC1051+2204	162.800	22.070	0.1260	24
NSC1051+2857	162.817	28.953	0.1592	18
NSC1051+2010	162.824	20.164	0.1477	49
NSC1051+1846	162.829	18.775	0.1717	21
NSC1051+1759	162.831	17.981	0.2151	15
NSC1052+3018	162.880	30.295	0.1595	20
NSC1052+1632	162.880	16.533	0.2001	13
NSC1052+3337	162.911	33.615	0.2391	19
NSC1052+4530	162.912	45.502	0.1574	24
NSC1052+1710	162.920	17.166	0.1253	40
NSC1052+1822	162.948	18.371	0.1945	20
NSC1052+1409	162.957	14.148	0.1372	24
NSC1052+4002	162.958	40.027	0.1895	41
NSC1052+1650	162.958	16.828	0.1403	23
NSC1052+2303	162.959	23.054	0.1430	33
NSC1052+1851	162.984	18.848	0.1652	35
NSC1052+4541	162.989	45.691	0.1352	22
NSC1052+2406	162.991	24.102	0.2543	25
NSC1052+4708	163.002	47.136	0.1738	35
NSC1052+1746	163.018	17.764	0.1682	19
NSC1052+1910	163.038	19.167	0.2154	21
NSC1052+1813	163.040	18.224	0.2009	26
NSC1052+1730	163.054	17.495	0.1417	44
NSC1052+2535	163.073	25.578	0.1432	15

Continued...

Table B.1 - NGP Robust, Continued

Name	RA	Dec	z_{phot}	N_{gal}
NSC1052+1835	163.090	18.585	0.1481	31
NSC1052+1703	163.092	17.048	0.1440	42
NSC1052+2154	163.092	21.899	0.0403	18
NSC1052+1805	163.095	18.078	0.1491	24
NSC1053+1405	163.133	14.078	0.1623	28
NSC1053+1822	163.146	18.364	0.1603	33
NSC1053+2015	163.182	20.256	0.1726	35
NSC1053+3946	163.184	39.766	0.0632	31
NSC1053+1936	163.215	19.608	0.1867	23
NSC1053+2911	163.225	29.181	0.1672	22
NSC1053+4302	163.228	43.034	0.1083	30
NSC1053+4322	163.233	43.359	0.2110	26
NSC1053+2849	163.247	28.822	0.1195	16
NSC1053+1905	163.251	19.082	0.1868	24
NSC1053+3060	163.253	30.996	0.1856	19
NSC1053+3659	163.259	36.980	0.1146	32
NSC1053+1834	163.276	18.567	0.1317	28
NSC1053+1733	163.287	17.552	0.1791	59
NSC1053+2038	163.296	20.637	0.1635	23
NSC1053+3756	163.351	37.930	0.2210	27
NSC1053+1915	163.351	19.253	0.2042	26
NSC1053+4714	163.352	47.231	0.1453	41
NSC1053+1406	163.372	14.099	0.1124	40
NSC1053+1956	163.373	19.928	0.2614	28
NSC1054+3048	163.378	30.804	0.2337	29
NSC1054+1713	163.382	17.209	0.1568	30
NSC1054+4025	163.438	40.413	0.0807	31
NSC1054+1553	163.469	15.888	0.2177	26
NSC1054+1418	163.478	14.302	0.1772	34
NSC1054+1649	163.504	16.812	0.0993	87
NSC1054+1701	163.514	17.019	0.1041	68
NSC1054+3822	163.553	38.363	0.1857	44
NSC1054+1438	163.557	14.637	0.2481	31
NSC1054+1939	163.594	19.656	0.1898	39
NSC1054+3023	163.603	30.391	0.2170	14
NSC1054+2408	163.616	24.127	0.0202	3
NSC1054+1745	163.619	17.742	0.1674	20
NSC1055+3243	163.651	32.714	0.1823	20
NSC1055+1757	163.653	17.950	0.1770	24
NSC1055+1835	163.668	18.583	0.1933	31
NSC1055+2009	163.695	20.149	0.1643	21
NSC1055+1918	163.696	19.299	0.1832	27
NSC1055+1858	163.697	18.974	0.1466	39
NSC1055+2343	163.720	23.709	0.1016	29
NSC1055+4025	163.742	40.417	0.0865	43
NSC1055+1430	163.781	14.499	0.1316	22
NSC1055+1737	163.786	17.612	0.1780	25
NSC1055+2042	163.803	20.692	0.2095	21
NSC1055+1520	163.858	15.330	0.1834	18
NSC1055+3529	163.859	35.490	0.2765	19
NSC1055+1950	163.869	19.825	0.1193	22
NSC1056+4716	163.897	47.270	0.1387	45
NSC1056+4006	163.898	40.107	0.0980	27
NSC1056+2011	163.952	20.178	0.1473	19
NSC1056+1932	163.957	19.529	0.1711	26
NSC1056+3218	163.964	32.300	0.2257	17
NSC1056+1726	163.995	17.427	0.2306	20
NSC1056+3149	163.998	31.817	0.1134	24
NSC1056+4348	164.023	43.800	0.1939	27
NSC1056+1905	164.052	19.088	0.1180	19
NSC1056+1250	164.100	12.837	0.1965	29
NSC1056+1646	164.100	16.765	0.1751	31
NSC1056+2603	164.112	26.054	0.1751	25
NSC1057+2706	164.168	27.093	0.2990	30
NSC1057+2006	164.198	20.097	0.1725	19
NSC1057+4624	164.215	46.404	0.1858	19
NSC1057+4032	164.216	40.541	0.1070	39
NSC1057+3212	164.225	32.194	0.2182	38
NSC1057+4141	164.240	41.688	0.1587	32
NSC1057+2451	164.262	24.849	0.2033	31
NSC1057+3040	164.279	30.671	0.1913	19
NSC1057+3249	164.351	32.816	0.1518	27
NSC1058+1518	164.431	15.297	0.2194	23
NSC1058+1952	164.431	19.866	0.2844	15
NSC1058+2246	164.435	22.769	0.2214	16
NSC1058+4615	164.446	46.247	0.1612	30
NSC1058+1915	164.482	19.244	0.1076	18
NSC1058+1749	164.490	17.821	0.2750	15
NSC1058+2002	164.504	20.029	0.1564	33
NSC1058+2145	164.504	21.751	0.0430	23
NSC1058+4729	164.513	47.476	0.2167	25
NSC1058+4103	164.517	41.045	0.1385	65
NSC1058+2017	164.541	20.280	0.1257	31
NSC1058+3230	164.557	32.492	0.1733	25
NSC1058+1652	164.557	16.872	0.1225	29
NSC1058+4354	164.597	43.898	0.2734	19
NSC1058+2930	164.610	29.494	0.1298	20

Continued...

Table B.1 - NGP Robust, Continued

Name	RA	Dec	z_{phot}	N_{gal}
NSC1058+2048	164.618	20.798	0.1029	22
NSC1058+3260	164.619	32.995	0.1481	26
NSC1058+2253	164.624	22.881	0.2362	25
NSC1059+2501	164.680	25.012	0.1623	17
NSC1059+2624	164.701	26.408	0.1429	27
NSC1059+2160	164.703	21.998	0.1158	35
NSC1059+1642	164.713	16.702	0.1183	26
NSC1059+3226	164.715	32.429	0.1815	23
NSC1059+4219	164.729	42.317	0.2093	26
NSC1059+2744	164.738	27.737	0.1188	30
NSC1059+2218	164.748	22.293	0.2201	26
NSC1059+4117	164.779	41.290	0.1247	26
NSC1059+4432	164.779	44.529	0.1235	24
NSC1059+1946	164.796	19.774	0.1832	19
NSC1059+2953	164.832	29.889	0.1746	20
NSC1059+2106	164.841	21.099	0.1348	24
NSC1100+2557	164.925	25.948	0.2024	21
NSC1100+1742	164.948	17.698	0.1266	30
NSC1100+1915	164.963	19.254	0.2154	22
NSC1100+2409	165.012	24.157	0.1800	22
NSC1100+2241	165.039	22.682	0.1587	18
NSC1100+2007	165.119	20.116	0.1293	22
NSC1101+1805	165.141	18.085	0.1676	31
NSC1101+2259	165.185	22.986	0.1570	35
NSC1101+2623	165.202	26.385	0.2091	24
NSC1101+4010	165.264	40.164	0.1473	29
NSC1101+1858	165.296	18.968	0.2369	32
NSC1101+3443	165.300	34.724	0.1614	25
NSC1101+1544	165.302	15.727	0.0775	23
NSC1101+2526	165.317	25.434	0.1173	21
NSC1101+4133	165.356	41.549	0.1350	47
NSC1101+2826	165.361	28.428	0.1920	21
NSC1102+2354	165.444	23.899	0.1345	24
NSC1102+1643	165.446	16.719	0.0955	51
NSC1102+2913	165.458	29.217	0.1958	22
NSC1102+2702	165.503	27.038	0.2200	18
NSC1102+2243	165.531	22.717	0.2361	34
NSC1102+2431	165.556	24.518	0.1144	26
NSC1102+3258	165.601	32.966	0.1725	30
NSC1102+2721	165.603	27.345	0.2281	19
NSC1102+2644	165.607	26.735	0.2520	21
NSC1102+1409	165.612	14.142	0.1105	20
NSC1102+2657	165.618	26.945	0.1381	18
NSC1102+3334	165.624	33.570	0.1712	31
NSC1103+3140	165.634	31.674	0.2078	16
NSC1103+2238	165.662	22.630	0.1948	21
NSC1103+3230	165.692	32.505	0.2209	22
NSC1103+2916	165.747	29.259	0.1037	20
NSC1103+2748	165.762	27.800	0.1630	31
NSC1103+1912	165.790	19.206	0.1259	28
NSC1103+4207	165.793	42.121	0.1506	20
NSC1104+2854	165.896	28.894	0.2071	26
NSC1104+3805	165.898	38.091	0.1071	26
NSC1104+2837	165.952	28.622	0.2487	20
NSC1104+3206	165.973	32.093	0.2130	26
NSC1104+1747	165.978	17.791	0.1807	28
NSC1104+3306	166.001	33.101	0.1889	40
NSC1104+3143	166.048	31.725	0.1909	20
NSC1104+1912	166.053	19.194	0.1789	23
NSC1104+3514	166.097	35.239	0.0762	35
NSC1104+2829	166.098	28.491	0.2307	27
NSC1104+2241	166.123	22.685	0.1877	23
NSC1105+1335	166.134	13.589	0.1298	50
NSC1105+2647	166.142	26.791	0.1731	17
NSC1105+3214	166.143	32.231	0.1439	18
NSC1105+1750	166.163	17.841	0.1469	36
NSC1105+3435	166.181	34.586	0.1259	35
NSC1105+2214	166.216	22.226	0.1928	26
NSC1105+2320	166.231	23.328	0.1823	21
NSC1105+2816	166.247	28.263	0.1828	19
NSC1105+3140	166.302	31.670	0.2675	21
NSC1105+2658	166.316	26.975	0.2215	23
NSC1105+2909	166.367	29.149	0.2350	22
NSC1105+2427	166.368	24.458	0.1457	28
NSC1106+1252	166.377	12.864	0.1689	26
NSC1106+4107	166.398	41.108	0.1698	30
NSC1106+3106	166.448	31.104	0.2147	16
NSC1106+2536	166.452	25.597	0.2105	31
NSC1106+2150	166.473	21.826	0.1930	21
NSC1106+3122	166.479	31.374	0.1276	32
NSC1106+3232	166.490	32.535	0.1327	42
NSC1106+3245	166.501	32.758	0.1604	32
NSC1106+3441	166.537	34.683	0.1897	29
NSC1106+2622	166.548	26.370	0.2831	31
NSC1106+3154	166.615	31.904	0.2094	29
NSC1106+2317	166.617	23.287	0.1010	25
NSC1106+2406	166.619	24.103	0.1537	25

Continued...

Table B.1 - NGP Robust, Continued

Name	RA	Dec	z_{phot}	N_{gal}
NSC1106+2640	166.622	26.673	0.2069	33
NSC1107+1308	166.637	13.137	0.0973	47
NSC1107+2444	166.645	24.739	0.1417	24
NSC1107+2531	166.701	25.514	0.1866	34
NSC1107+1319	166.718	13.313	0.0953	39
NSC1107+3223	166.719	32.386	0.2092	26
NSC1107+2411	166.731	24.190	0.1870	24
NSC1107+3246	166.740	32.773	0.1857	26
NSC1107+3534	166.746	35.562	0.0370	20
NSC1107+2746	166.751	27.773	0.1725	23
NSC1107+1326	166.761	13.428	0.0869	30
NSC1107+1824	166.766	18.393	0.1648	22
NSC1107+2857	166.779	28.954	0.1863	36
NSC1107+1959	166.792	19.991	0.1142	20
NSC1107+1552	166.850	15.863	0.1065	51
NSC1107+2307	166.854	23.111	0.1577	18
NSC1108+2135	166.876	21.578	0.1516	27
NSC1108+1858	166.907	18.961	0.1357	24
NSC1108+2556	166.913	25.928	0.1716	26
NSC1108+2426	166.929	24.436	0.1940	24
NSC1108+2442	166.944	24.704	0.1243	42
NSC1108+2706	166.946	27.107	0.1861	31
NSC1108+3115	166.949	31.256	0.1095	44
NSC1108+2836	166.951	28.592	0.1507	34
NSC1108+1810	166.955	18.171	0.1069	22
NSC1108+3220	166.972	32.338	0.1883	17
NSC1108+2456	167.010	24.935	0.2316	26
NSC1108+2609	167.022	26.158	0.1913	32
NSC1108+2903	167.027	29.047	0.1893	20
NSC1108+1536	167.030	15.593	0.2477	30
NSC1108+4024	167.035	40.399	0.0563	29
NSC1108+2312	167.067	23.197	0.1580	24
NSC1108+1612	167.071	16.203	0.2090	27
NSC1108+2122	167.074	21.371	0.1782	19
NSC1108+4210	167.078	42.162	0.0857	23
NSC1108+2020	167.082	20.329	0.1777	29
NSC1108+3200	167.085	32.006	0.1453	33
NSC1108+2914	167.107	29.225	0.2005	17
NSC1108+2501	167.109	25.021	0.1961	23
NSC1108+1951	167.111	19.848	0.0581	13
NSC1109+3444	167.131	34.737	0.2741	19
NSC1109+3043	167.134	30.712	0.1861	21
NSC1109+2512	167.185	25.197	0.2150	27
NSC1109+3103	167.194	31.044	0.1710	19
NSC1109+2544	167.196	25.740	0.2302	34
NSC1109+2853	167.240	28.883	0.2242	26
NSC1109+1550	167.241	15.837	0.1819	27
NSC1109+4139	167.243	41.642	0.0812	51
NSC1109+3311	167.243	33.188	0.1544	50
NSC1109+3114	167.247	31.238	0.1140	43
NSC1109+1813	167.269	18.218	0.1817	19
NSC1109+1558	167.270	15.969	0.1809	22
NSC1109+2137	167.289	21.619	0.1167	60
NSC1109+3043	167.298	30.717	0.1618	23
NSC1109+2355	167.324	23.912	0.1296	43
NSC1109+2925	167.325	29.418	0.1715	42
NSC1109+2527	167.335	25.447	0.1228	43
NSC1109+2034	167.360	20.570	0.1172	45
NSC1110+2118	167.379	21.301	0.1858	28
NSC1110+3152	167.415	31.859	0.1461	40
NSC1110+2539	167.416	25.646	0.1758	31
NSC1110+1609	167.435	16.145	0.2417	23
NSC1110+3455	167.437	34.913	0.2081	29
NSC1110+3432	167.462	34.527	0.2307	25
NSC1110+3857	167.501	38.944	0.1440	24
NSC1110+2357	167.524	23.951	0.1177	54
NSC1110+1357	167.526	13.956	0.1556	34
NSC1110+1919	167.536	19.320	0.1205	26
NSC1110+3817	167.538	38.288	0.1397	22
NSC1110+2041	167.557	20.682	0.1604	46
NSC1110+1324	167.566	13.394	0.1961	29
NSC1110+1736	167.597	17.594	0.1772	24
NSC1110+2933	167.599	29.555	0.1701	28
NSC1110+2843	167.600	28.721	0.1269	56
NSC1111+3147	167.640	31.787	0.1950	26
NSC1111+2950	167.649	29.828	0.2039	21
NSC1111+2545	167.673	25.752	0.1945	24
NSC1111+1434	167.699	14.567	0.2231	25
NSC1111+3115	167.720	31.242	0.2009	23
NSC1111+4217	167.722	42.276	0.1560	38
NSC1111+2402	167.740	24.025	0.1250	32
NSC1111+1817	167.743	18.288	0.1907	32
NSC1111+3332	167.773	33.527	0.2187	26
NSC1111+3242	167.783	32.700	0.1401	29
NSC1111+2659	167.805	26.987	0.0953	18
NSC1111+1405	167.819	14.091	0.2018	35
NSC1111+2130	167.829	21.505	0.1764	64

Continued...

Table B.1 - NGP Robust, Continued

Name	RA	Dec	z_{phot}	N_{gal}
NSC1111+3008	167.830	30.129	0.2031	19
NSC1111+3934	167.833	39.569	0.0478	39
NSC1111+2602	167.847	26.033	0.2454	24
NSC1111+2116	167.853	21.262	0.1653	33
NSC1111+4231	167.857	42.514	0.1192	23
NSC1111+2509	167.860	25.148	0.1253	46
NSC1111+2057	167.864	20.956	0.1943	25
NSC1112+3232	167.877	32.541	0.2110	20
NSC1112+3131	167.881	31.523	0.1279	31
NSC1112+4052	167.903	40.866	0.0716	70
NSC1112+1641	167.912	16.688	0.1419	27
NSC1112+3301	167.917	33.015	0.1771	28
NSC1112+2811	167.941	28.179	0.1591	18
NSC1112+1655	167.953	16.921	0.1292	21
NSC1112+2141	167.962	21.685	0.1952	28
NSC1112+4033	167.967	40.543	0.0696	45
NSC1112+2557	168.007	25.948	0.1839	20
NSC1112+2736	168.013	27.595	0.0708	29
NSC1112+2850	168.018	28.839	0.2055	26
NSC1112+1636	168.027	16.595	0.2020	26
NSC1112+3039	168.033	30.656	0.1594	33
NSC1112+3941	168.034	39.690	0.0863	51
NSC1112+2351	168.042	23.849	0.2167	29
NSC1112+3342	168.045	33.708	0.1960	27
NSC1112+1940	168.048	19.668	0.1504	48
NSC1112+4232	168.060	42.536	0.1333	28
NSC1112+2929	168.073	29.490	0.1996	15
NSC1112+1251	168.114	12.857	0.2122	30
NSC1112+2006	168.116	20.106	0.1957	52
NSC1112+1811	168.118	18.180	0.2087	15
NSC1112+3022	168.120	30.359	0.1634	52
NSC1112+3055	168.125	30.911	0.2029	19
NSC1113+1405	168.140	14.077	0.1861	40
NSC1113+3628	168.165	36.470	0.0977	28
NSC1113+1428	168.202	14.459	0.1267	30
NSC1113+1301	168.207	13.013	0.1576	27
NSC1113+1326	168.217	13.431	0.1631	76
NSC1113+1347	168.300	13.791	0.1977	31
NSC1113+3248	168.310	32.803	0.0968	31
NSC1113+1734	168.329	17.562	0.2012	53
NSC1113+4013	168.340	40.211	0.0949	55
NSC1113+2141	168.342	21.683	0.2397	22
NSC1113+2208	168.350	22.142	0.1836	80
NSC1113+3923	168.351	39.383	0.0780	35
NSC1113+2025	168.352	20.410	0.2060	20
NSC1113+1423	168.361	14.390	0.1381	32
NSC1113+3603	168.361	36.045	0.0772	31
NSC1114+2941	168.378	29.691	0.1412	23
NSC1114+3722	168.391	37.374	0.0968	35
NSC1114+3047	168.417	30.784	0.2459	31
NSC1114+3214	168.424	32.236	0.1869	12
NSC1114+4019	168.431	40.312	0.0885	57
NSC1114+1641	168.436	16.676	0.1846	25
NSC1114+3347	168.437	33.779	0.1658	25
NSC1114+3406	168.506	34.098	0.1489	23
NSC1114+2254	168.532	22.904	0.1170	19
NSC1114+1417	168.543	14.288	0.1339	31
NSC1114+3124	168.546	31.404	0.2164	21
NSC1114+3054	168.548	30.908	0.2087	18
NSC1114+3257	168.554	32.943	0.1417	25
NSC1114+4051	168.581	40.843	0.1227	38
NSC1114+1941	168.606	19.677	0.1860	22
NSC1115+2115	168.634	21.243	0.1478	23
NSC1115+2447	168.654	24.783	0.0962	33
NSC1115+2435	168.675	24.585	0.1124	31
NSC1115+1644	168.709	16.736	0.1898	48
NSC1115+4210	168.722	42.164	0.1563	27
NSC1115+2554	168.726	25.900	0.0894	31
NSC1115+3202	168.774	32.036	0.2243	41
NSC1115+3614	168.779	36.232	0.1282	29
NSC1115+1339	168.793	13.654	0.1564	31
NSC1115+3214	168.848	32.237	0.1491	25
NSC1115+3148	168.850	31.806	0.1119	33
NSC1115+3506	168.858	35.094	0.2275	26
NSC1115+2426	168.870	24.438	0.2361	22
NSC1116+2054	168.911	20.908	0.2120	20
NSC1116+3121	168.957	31.354	0.2126	28
NSC1116+4043	168.963	40.717	0.0944	30
NSC1116+2621	169.009	26.357	0.1865	21
NSC1116+1657	169.046	16.951	0.1468	38
NSC1116+2915	169.123	29.245	0.0669	42
NSC1117+2436	169.158	24.606	0.1314	34
NSC1117+3236	169.167	32.604	0.0975	30
NSC1117+2141	169.205	21.684	0.1826	25
NSC1117+1309	169.206	13.151	0.1795	28
NSC1117+1908	169.242	19.129	0.1224	29
NSC1117+2720	169.260	27.329	0.1289	15

Continued...

Table B.1 - NGP Robust, Continued

Name	RA	Dec	z_{phot}	N_{gal}
NSC1117+3315	169.260	33.252	0.0916	27
NSC1117+1606	169.269	16.105	0.1925	22
NSC1117+2512	169.279	25.208	0.2171	18
NSC1117+2014	169.305	20.240	0.1185	29
NSC1117+1411	169.308	14.176	0.1330	44
NSC1117+2929	169.324	29.486	0.1386	24
NSC1117+2609	169.328	26.145	0.2612	22
NSC1117+2037	169.348	20.622	0.1664	26
NSC1117+2229	169.370	22.485	0.2139	15
NSC1118+1430	169.382	14.497	0.1219	45
NSC1118+2637	169.396	26.616	0.0955	24
NSC1118+2623	169.416	26.391	0.1740	28
NSC1118+2702	169.422	27.036	0.1884	21
NSC1118+1702	169.423	17.035	0.2073	38
NSC1118+2025	169.435	20.418	0.1505	25
NSC1118+1530	169.450	15.502	0.1962	23
NSC1118+3728	169.483	37.474	0.1748	30
NSC1118+1444	169.524	14.730	0.1847	27
NSC1118+2327	169.538	23.452	0.1300	22
NSC1118+2031	169.551	20.522	0.2125	21
NSC1118+1644	169.587	16.729	0.1605	64
NSC1118+3117	169.621	31.285	0.2207	29
NSC1118+3137	169.624	31.620	0.1532	26
NSC1119+1941	169.660	19.691	0.1810	19
NSC1119+1720	169.697	17.325	0.1948	28
NSC1119+3735	169.720	37.590	0.1708	21
NSC1119+2753	169.739	27.884	0.1139	35
NSC1119+2212	169.778	22.198	0.1993	23
NSC1119+3724	169.780	37.392	0.1575	33
NSC1119+3926	169.795	39.428	0.1204	23
NSC1119+2105	169.830	21.085	0.0658	26
NSC1119+3343	169.838	33.714	0.1013	25
NSC1119+1506	169.864	15.101	0.1555	37
NSC1120+3742	169.887	37.706	0.0900	27
NSC1120+2438	169.901	24.631	0.1880	24
NSC1120+2903	169.918	29.057	0.0953	34
NSC1120+1626	169.939	16.440	0.2366	35
NSC1120+1400	169.948	14.002	0.0997	33
NSC1120+1652	169.962	16.862	0.2023	21
NSC1120+3549	169.973	35.821	0.2412	14
NSC1120+1954	169.983	19.892	0.1702	27
NSC1120+3318	170.063	33.300	0.1206	33
NSC1120+2002	170.107	20.032	0.1862	23
NSC1120+4218	170.123	42.294	0.1129	28
NSC1121+3629	170.151	36.479	0.2438	23
NSC1121+1749	170.161	17.808	0.1743	28
NSC1121+2659	170.180	26.977	0.0636	22
NSC1121+1733	170.183	17.558	0.2336	24
NSC1121+2833	170.184	28.555	0.1586	18
NSC1121+1532	170.192	15.526	0.1374	29
NSC1121+3349	170.214	33.820	0.1624	37
NSC1121+1642	170.257	16.706	0.1548	21
NSC1121+2037	170.283	20.615	0.1618	24
NSC1121+1742	170.299	17.703	0.1224	38
NSC1121+2221	170.307	22.350	0.1426	34
NSC1121+4156	170.328	41.941	0.1313	20
NSC1121+2531	170.343	25.519	0.2149	28
NSC1121+3413	170.351	34.214	0.0586	38
NSC1121+3523	170.363	35.387	0.1165	38
NSC1122+2109	170.389	21.146	0.1459	24
NSC1122+2745	170.390	27.753	0.2438	15
NSC1122+3056	170.407	30.940	0.2361	17
NSC1122+1657	170.431	16.953	0.1932	34
NSC1122+2057	170.433	20.945	0.2124	30
NSC1122+1635	170.455	16.580	0.2052	31
NSC1122+1755	170.457	17.909	0.2022	41
NSC1122+1408	170.458	14.128	0.1595	23
NSC1122+1543	170.462	15.716	0.1848	28
NSC1122+3358	170.477	33.960	0.0657	43
NSC1122+3756	170.512	37.932	0.1319	34
NSC1122+1939	170.522	19.642	0.1417	48
NSC1122+2704	170.550	27.061	0.0896	37
NSC1122+4048	170.569	40.800	0.1137	25
NSC1122+2511	170.581	25.178	0.2158	25
NSC1122+1605	170.589	16.085	0.1727	30
NSC1122+2127	170.625	21.443	0.1756	65
NSC1123+2410	170.637	24.169	0.1802	29
NSC1123+2236	170.640	22.607	0.1684	24
NSC1123+1652	170.658	16.869	0.1480	47
NSC1123+2143	170.677	21.725	0.1654	27
NSC1123+2201	170.680	22.016	0.1873	27
NSC1123+1813	170.731	18.218	0.2045	31
NSC1123+3407	170.733	34.110	0.0463	51
NSC1123+2712	170.759	27.204	0.1534	35
NSC1123+3206	170.778	32.096	0.1525	30
NSC1123+1940	170.781	19.659	0.1317	75
NSC1123+1643	170.793	16.715	0.2016	26

Continued...

Table B.1 - NGP Robust, Continued

Name	RA	Dec	z_{phot}	N_{gal}
NSC1123+2019	170.793	20.313	0.1467	25
NSC1123+3456	170.803	34.936	0.1901	24
NSC1123+1659	170.803	16.977	0.1830	44
NSC1123+2453	170.815	24.876	0.1156	31
NSC1123+3620	170.833	36.326	0.2821	25
NSC1123+2060	170.870	20.995	0.1800	27
NSC1124+2227	170.913	22.454	0.1747	24
NSC1124+1718	170.929	17.308	0.1522	48
NSC1124+2031	170.931	20.519	0.1069	30
NSC1124+2239	170.941	22.649	0.2149	16
NSC1124+1959	170.951	19.986	0.1565	52
NSC1124+1823	170.964	18.390	0.1875	37
NSC1124+2129	170.987	21.486	0.2001	78
NSC1124+3560	170.995	35.993	0.1089	21
NSC1124+1808	171.009	18.137	0.1594	36
NSC1124+1510	171.052	15.170	0.1627	47
NSC1124+1738	171.062	17.631	0.1596	47
NSC1124+1524	171.068	15.397	0.1845	21
NSC1124+3219	171.069	32.314	0.1898	38
NSC1124+2731	171.102	27.514	0.1220	36
NSC1124+3514	171.106	35.241	0.1754	24
NSC1124+1902	171.108	19.027	0.1539	26
NSC1124+4025	171.115	40.424	0.1302	21
NSC1125+4157	171.134	41.943	0.2161	30
NSC1125+2007	171.137	20.115	0.1701	38
NSC1125+1637	171.137	16.621	0.1879	31
NSC1125+1731	171.161	17.521	0.1641	43
NSC1125+4015	171.199	40.246	0.1826	18
NSC1125+4231	171.208	42.523	0.2296	34
NSC1125+4141	171.208	41.685	0.1742	40
NSC1125+1934	171.227	19.563	0.1576	34
NSC1125+2227	171.337	22.450	0.2495	13
NSC1125+3328	171.349	33.459	0.1165	17
NSC1125+2104	171.357	21.067	0.1514	23
NSC1126+4127	171.405	41.442	0.1552	21
NSC1126+2127	171.410	21.457	0.1512	42
NSC1126+2156	171.436	21.926	0.1625	41
NSC1126+3726	171.451	37.425	0.1678	30
NSC1126+2216	171.451	22.266	0.1127	25
NSC1126+2456	171.458	24.926	0.1395	32
NSC1126+1708	171.463	17.132	0.2493	20
NSC1126+2528	171.502	25.468	0.1268	53
NSC1126+4205	171.510	42.075	0.2090	29
NSC1126+3229	171.518	32.475	0.1351	24
NSC1126+3153	171.538	31.879	0.2127	23
NSC1126+3521	171.577	35.349	0.1086	36
NSC1126+3025	171.597	30.412	0.2034	19
NSC1126+2956	171.599	29.941	0.2428	27
NSC1127+3337	171.640	33.621	0.1260	31
NSC1127+1447	171.650	14.777	0.1831	24
NSC1127+1705	171.651	17.091	0.1158	82
NSC1127+3710	171.689	37.165	0.1862	20
NSC1127+1641	171.690	16.690	0.1610	31
NSC1127+3529	171.780	35.480	0.1743	28
NSC1127+1333	171.781	13.557	0.1676	32
NSC1127+2519	171.798	25.321	0.1127	30
NSC1127+3634	171.800	36.560	0.1381	23
NSC1127+2455	171.809	24.914	0.1294	29
NSC1127+1915	171.826	19.255	0.0533	30
NSC1127+1343	171.834	13.715	0.2203	32
NSC1127+2133	171.834	21.550	0.1731	37
NSC1127+3944	171.851	39.726	0.0500	14
NSC1127+2448	171.866	24.797	0.1195	35
NSC1128+2230	171.877	22.499	0.2003	16
NSC1128+3404	171.877	34.059	0.1418	18
NSC1128+1652	171.887	16.866	0.1361	35
NSC1128+1632	171.894	16.537	0.2244	40
NSC1128+2002	171.899	20.031	0.1851	24
NSC1128+1943	171.903	19.724	0.1348	52
NSC1128+2011	171.921	20.177	0.1800	21
NSC1128+2657	171.937	26.954	0.0609	28
NSC1128+1951	171.957	19.846	0.1558	38
NSC1128+2128	171.985	21.462	0.1559	42
NSC1128+2055	171.986	20.915	0.1133	49
NSC1128+3635	172.003	36.588	0.1729	27
NSC1128+1440	172.017	14.661	0.1564	24
NSC1128+2737	172.026	27.624	0.1412	18
NSC1128+2613	172.036	26.214	0.1421	24
NSC1128+2549	172.052	25.819	0.2686	23
NSC1128+1548	172.060	15.808	0.1764	27
NSC1128+1337	172.068	13.612	0.1648	26
NSC1128+4132	172.080	41.540	0.1376	27
NSC1128+2354	172.091	23.898	0.1074	37
NSC1128+1457	172.099	14.953	0.1270	34
NSC1128+1421	172.100	14.355	0.1853	32
NSC1128+1641	172.105	16.679	0.1636	37
NSC1128+2013	172.116	20.225	0.2005	26

Continued...

Table B.1 - NGP Robust, Continued

Name	RA	Dec	z_{phot}	N_{gal}
NSC1128+3344	172.121	33.729	0.1706	25
NSC1128+1323	172.124	13.382	0.2155	20
NSC1129+1919	172.160	19.319	0.1914	29
NSC1129+2559	172.176	25.989	0.1766	27
NSC1129+1441	172.185	14.689	0.2045	23
NSC1129+1407	172.191	14.122	0.1749	21
NSC1129+2112	172.199	21.196	0.1448	41
NSC1129+2046	172.201	20.766	0.1055	53
NSC1129+3408	172.201	34.138	0.2512	28
NSC1129+3502	172.211	35.034	0.1988	20
NSC1129+3827	172.219	38.442	0.0978	24
NSC1129+2204	172.227	22.069	0.1550	23
NSC1129+2700	172.233	27.000	0.0774	21
NSC1129+3452	172.235	34.862	0.1789	28
NSC1129+1633	172.262	16.550	0.1394	26
NSC1129+3423	172.274	34.391	0.1295	35
NSC1129+3641	172.278	36.679	0.1041	44
NSC1129+3355	172.281	33.917	0.2215	25
NSC1129+2059	172.310	20.985	0.1234	69
NSC1129+2858	172.311	28.970	0.2183	25
NSC1129+2130	172.322	21.504	0.2055	34
NSC1129+1355	172.333	13.910	0.1252	40
NSC1129+4019	172.338	40.320	0.1798	16
NSC1130+2109	172.402	21.156	0.1205	54
NSC1130+1612	172.404	16.206	0.1362	22
NSC1130+1954	172.420	19.903	0.1139	66
NSC1130+2632	172.445	26.525	0.0760	29
NSC1130+1351	172.461	13.853	0.1279	38
NSC1130+3302	172.487	33.033	0.1899	30
NSC1130+1502	172.506	15.034	0.2494	17
NSC1130+2209	172.524	22.158	0.1897	33
NSC1130+1258	172.525	12.969	0.2011	62
NSC1130+2028	172.530	20.459	0.1184	111
NSC1130+1637	172.533	16.617	0.1447	41
NSC1130+2442	172.554	24.696	0.1645	37
NSC1130+3601	172.562	36.022	0.1829	17
NSC1130+3732	172.576	37.532	0.1816	24
NSC1130+3320	172.585	33.341	0.2020	33
NSC1130+2343	172.592	23.721	0.1548	46
NSC1130+2701	172.613	27.015	0.2221	25
NSC1130+2457	172.614	24.957	0.1100	26
NSC1130+1608	172.615	16.140	0.1455	30
NSC1130+1708	172.618	17.141	0.1932	23
NSC1130+2001	172.618	20.018	0.1289	41
NSC1130+3452	172.622	34.870	0.1730	33
NSC1131+3532	172.626	35.533	0.1701	28
NSC1131+2401	172.644	24.024	0.1278	36
NSC1131+3440	172.648	34.675	0.2454	25
NSC1131+3502	172.665	35.038	0.2113	27
NSC1131+1915	172.678	19.243	0.0595	20
NSC1131+2527	172.694	25.445	0.1475	26
NSC1131+3634	172.718	36.570	0.2231	18
NSC1131+1421	172.727	14.345	0.2307	26
NSC1131+2055	172.731	20.915	0.1417	26
NSC1131+2222	172.734	22.372	0.1619	39
NSC1131+3823	172.779	38.386	0.1337	39
NSC1131+1938	172.779	19.629	0.1405	31
NSC1131+2034	172.794	20.558	0.1866	28
NSC1131+2631	172.799	26.522	0.1633	20
NSC1131+3650	172.809	36.831	0.1728	30
NSC1131+1644	172.826	16.733	0.1292	38
NSC1131+1809	172.831	18.154	0.1917	43
NSC1131+3335	172.833	33.590	0.2460	28
NSC1131+3558	172.834	35.974	0.2523	20
NSC1131+2006	172.846	20.096	0.1765	32
NSC1131+3430	172.854	34.503	0.1631	33
NSC1131+1523	172.856	15.379	0.1293	44
NSC1131+2129	172.867	21.485	0.1246	44
NSC1131+1631	172.870	16.522	0.1405	35
NSC1132+3549	172.891	35.812	0.2366	35
NSC1132+1303	172.912	13.057	0.2107	21
NSC1132+2616	172.923	26.260	0.1701	27
NSC1132+1622	172.952	16.372	0.1790	31
NSC1132+1727	172.956	17.449	0.1339	35
NSC1132+4047	172.970	40.779	0.2305	26
NSC1132+3909	172.975	39.146	0.2566	40
NSC1132+2718	173.009	27.297	0.1789	27
NSC1132+1713	173.029	17.210	0.1598	37
NSC1132+2938	173.031	29.632	0.1365	23
NSC1132+1336	173.046	13.594	0.1757	21
NSC1132+2341	173.059	23.677	0.0932	32
NSC1132+3940	173.060	39.659	0.2604	22
NSC1132+3356	173.062	33.931	0.2577	41
NSC1132+3420	173.071	34.338	0.2515	28
NSC1132+2039	173.079	20.646	0.1001	33
NSC1132+3528	173.092	35.473	0.2477	23
NSC1132+3546	173.102	35.762	0.2567	35

Continued...

Table B.1 - NGP Robust, Continued

Name	RA	Dec	z_{phot}	N_{gal}
NSC1132+2011	173.111	20.185	0.1650	31
NSC1132+4039	173.117	40.644	0.1729	24
NSC1132+3624	173.123	36.405	0.1901	23
NSC1133+1952	173.130	19.861	0.1388	71
NSC1133+3508	173.134	35.133	0.2049	27
NSC1133+1517	173.136	15.287	0.2115	25
NSC1133+2230	173.145	22.506	0.0659	44
NSC1133+1540	173.156	15.670	0.2034	28
NSC1133+1433	173.165	14.545	0.1011	68
NSC1133+2448	173.184	24.800	0.1508	20
NSC1133+2147	173.197	21.781	0.1503	32
NSC1133+1406	173.213	14.104	0.2194	20
NSC1133+3445	173.221	34.752	0.2027	34
NSC1133+3956	173.230	39.931	0.1897	26
NSC1133+1552	173.243	15.869	0.2174	22
NSC1133+2337	173.243	23.617	0.0899	31
NSC1133+1726	173.287	17.433	0.1236	38
NSC1133+1503	173.296	15.048	0.1416	22
NSC1133+1920	173.303	19.331	0.2180	30
NSC1133+3901	173.319	39.020	0.2075	23
NSC1133+2851	173.325	28.857	0.1495	27
NSC1133+2250	173.334	22.833	0.1812	26
NSC1133+4033	173.346	40.555	0.2193	27
NSC1133+1439	173.354	14.649	0.1130	52
NSC1133+1346	173.359	13.770	0.1715	16
NSC1133+2522	173.368	25.373	0.1674	24
NSC1134+1527	173.379	15.444	0.2248	22
NSC1134+4127	173.392	41.445	0.1717	21
NSC1134+3553	173.410	35.879	0.2200	22
NSC1134+3417	173.440	34.277	0.2231	22
NSC1134+1543	173.468	15.716	0.0756	28
NSC1134+1645	173.472	16.753	0.1786	22
NSC1134+2219	173.476	22.322	0.1314	34
NSC1134+1953	173.483	19.880	0.2372	35
NSC1134+2535	173.487	25.583	0.1066	43
NSC1134+3952	173.488	39.871	0.2406	28
NSC1134+1706	173.497	17.108	0.1560	52
NSC1134+3833	173.540	38.554	0.1754	33
NSC1134+2116	173.552	21.270	0.1604	29
NSC1134+2057	173.560	20.957	0.0914	37
NSC1134+1928	173.573	19.466	0.2367	17
NSC1134+1729	173.574	17.478	0.1232	55
NSC1134+3851	173.592	38.852	0.1335	34
NSC1134+3343	173.598	33.724	0.2168	27
NSC1134+2220	173.618	22.328	0.1203	41
NSC1134+2949	173.625	29.817	0.1538	33
NSC1135+2458	173.633	24.960	0.1724	26
NSC1135+1825	173.634	18.418	0.0825	30
NSC1135+4046	173.635	40.771	0.2032	22
NSC1135+1612	173.661	16.206	0.1045	42
NSC1135+2228	173.689	22.462	0.0745	45
NSC1135+2042	173.691	20.698	0.1321	26
NSC1135+1929	173.733	19.486	0.1498	34
NSC1135+1255	173.740	12.916	0.1374	43
NSC1135+3333	173.744	33.548	0.1629	20
NSC1135+2257	173.759	22.958	0.0454	18
NSC1135+3612	173.782	36.197	0.1545	27
NSC1135+1537	173.800	15.621	0.1289	25
NSC1135+3044	173.812	30.736	0.1978	21
NSC1135+3723	173.818	37.389	0.1663	50
NSC1135+1451	173.822	14.847	0.1321	31
NSC1135+3101	173.834	31.009	0.1413	30
NSC1135+3540	173.838	35.666	0.2413	18
NSC1135+2104	173.847	21.069	0.1489	74
NSC1135+3901	173.850	39.013	0.1743	25
NSC1135+2230	173.858	22.497	0.0964	42
NSC1135+3153	173.869	31.891	0.2179	32
NSC1136+1348	173.877	13.806	0.1123	51
NSC1136+3618	173.891	36.300	0.1230	24
NSC1136+1825	173.895	18.415	0.0987	37
NSC1136+2456	173.897	24.940	0.1691	26
NSC1136+4120	173.901	41.330	0.2085	33
NSC1136+4053	173.912	40.880	0.2030	31
NSC1136+1340	173.914	13.673	0.1075	55
NSC1136+2055	173.917	20.913	0.1510	67
NSC1136+3011	173.925	30.189	0.1774	24
NSC1136+1447	173.933	14.783	0.1696	32
NSC1136+1513	173.948	15.223	0.1626	27
NSC1136+2643	173.951	26.722	0.1358	35
NSC1136+1419	173.980	14.319	0.2537	20
NSC1136+4002	173.981	40.025	0.2775	30
NSC1136+1328	174.070	13.472	0.1549	25
NSC1136+2240	174.073	22.674	0.1591	33
NSC1136+3851	174.076	38.856	0.1428	21
NSC1136+1704	174.088	17.066	0.2324	21
NSC1136+2217	174.090	22.282	0.1973	43
NSC1136+2556	174.092	25.937	0.0857	26

Continued...

Table B.1 - NGP Robust, Continued

Name	RA	Dec	z_{phot}	N_{gal}
NSC1136+2629	174.097	26.483	0.1414	36
NSC1136+2020	174.098	20.336	0.2484	33
NSC1136+1254	174.102	12.905	0.1607	29
NSC1136+3654	174.113	36.905	0.2437	25
NSC1137+2231	174.127	22.523	0.1064	36
NSC1137+1539	174.139	15.647	0.2443	37
NSC1137+1629	174.154	16.486	0.1305	33
NSC1137+3255	174.167	32.910	0.0874	44
NSC1137+1421	174.186	14.348	0.1172	31
NSC1137+1643	174.189	16.709	0.1284	34
NSC1137+3318	174.207	33.292	0.0846	58
NSC1137+3234	174.227	32.564	0.1644	31
NSC1137+2635	174.229	26.585	0.1606	51
NSC1137+1457	174.258	14.942	0.2496	17
NSC1137+4009	174.258	40.151	0.2295	19
NSC1137+1431	174.266	14.519	0.2629	17
NSC1137+1555	174.268	15.916	0.1084	20
NSC1137+1706	174.295	17.101	0.1457	26
NSC1137+2718	174.299	27.299	0.1051	35
NSC1137+1534	174.303	15.562	0.1557	27
NSC1137+2105	174.309	21.078	0.2371	26
NSC1137+1417	174.310	14.276	0.2001	24
NSC1137+1758	174.312	17.963	0.2708	28
NSC1137+4036	174.315	40.603	0.2533	21
NSC1137+1820	174.318	18.325	0.1065	36
NSC1137+3940	174.359	39.667	0.1588	25
NSC1138+3121	174.387	31.342	0.1200	32
NSC1138+3228	174.389	32.458	0.1020	43
NSC1138+2157	174.395	21.951	0.1692	30
NSC1138+2507	174.422	25.120	0.1979	35
NSC1138+1543	174.441	15.713	0.2297	20
NSC1138+1743	174.468	17.715	0.1607	31
NSC1138+1342	174.475	13.695	0.1417	41
NSC1138+2331	174.476	23.515	0.1526	28
NSC1138+3725	174.476	37.423	0.1605	48
NSC1138+1518	174.479	15.293	0.2276	28
NSC1138+3924	174.487	39.405	0.1772	18
NSC1138+1312	174.499	13.204	0.1468	18
NSC1138+2032	174.505	20.529	0.1434	50
NSC1138+2934	174.529	29.573	0.1470	21
NSC1138+2221	174.538	22.354	0.2301	41
NSC1138+2412	174.545	24.192	0.1579	21
NSC1138+3607	174.580	36.121	0.1563	30
NSC1138+1828	174.584	18.475	0.1898	23
NSC1138+2050	174.585	20.839	0.1288	25
NSC1138+3523	174.604	35.384	0.1617	18
NSC1139+2711	174.642	27.183	0.2378	18
NSC1139+1553	174.651	15.881	0.2062	28
NSC1139+1307	174.689	13.113	0.1148	18
NSC1139+2230	174.693	22.506	0.1424	27
NSC1139+3620	174.703	36.341	0.1339	28
NSC1139+3442	174.710	34.697	0.1787	21
NSC1139+2115	174.726	21.246	0.1409	32
NSC1139+3349	174.738	33.813	0.2148	30
NSC1139+1705	174.784	17.077	0.2194	28
NSC1139+2537	174.797	25.623	0.1931	28
NSC1139+1850	174.805	18.838	0.1205	33
NSC1139+1654	174.828	16.898	0.1282	40
NSC1139+1522	174.833	15.358	0.1256	33
NSC1139+2722	174.852	27.369	0.1433	29
NSC1139+1326	174.852	13.437	0.1347	31
NSC1139+3226	174.853	32.428	0.1213	55
NSC1140+2029	174.876	20.484	0.1697	28
NSC1140+2859	174.886	28.982	0.1517	25
NSC1140+3546	174.892	35.767	0.1691	27
NSC1140+2530	174.893	25.495	0.1943	26
NSC1140+1811	174.912	18.182	0.1472	45
NSC1140+2403	174.923	24.045	0.0992	35
NSC1140+1611	174.965	16.188	0.2192	15
NSC1140+2508	174.966	25.125	0.1546	24
NSC1140+1540	174.971	15.675	0.2106	21
NSC1140+1304	174.985	13.063	0.1156	35
NSC1140+2220	174.986	22.328	0.1652	34
NSC1140+1432	174.993	14.531	0.2433	29
NSC1140+2404	175.031	24.067	0.0918	35
NSC1140+1814	175.041	18.234	0.1182	49
NSC1140+2308	175.064	23.140	0.1161	24
NSC1140+3613	175.069	36.211	0.1085	29
NSC1140+2451	175.088	24.848	0.1678	36
NSC1141+1819	175.173	18.314	0.1610	48
NSC1141+2526	175.183	25.426	0.1950	25
NSC1141+2219	175.193	22.314	0.1576	24
NSC1141+1439	175.220	14.645	0.1317	33
NSC1141+2240	175.223	22.668	0.1741	25
NSC1141+2345	175.223	23.756	0.1631	21
NSC1141+1508	175.280	15.140	0.1931	37
NSC1141+2553	175.322	25.888	0.0798	26

Continued...

Table B.1 - NGP Robust, Continued

Name	RA	Dec	z_{phot}	N_{gal}
NSC1141+1753	175.326	17.882	0.1964	16
NSC1141+2457	175.329	24.958	0.2073	29
NSC1141+1540	175.356	15.670	0.1572	33
NSC1142+1718	175.389	17.299	0.1813	25
NSC1142+2433	175.395	24.553	0.1407	36
NSC1142+2310	175.397	23.161	0.1528	36
NSC1142+3541	175.415	35.685	0.1744	29
NSC1142+3452	175.447	34.871	0.1800	24
NSC1142+1307	175.462	13.120	0.0969	27
NSC1142+1845	175.482	18.744	0.1545	35
NSC1142+2504	175.496	25.075	0.2259	33
NSC1142+2444	175.503	24.728	0.1521	43
NSC1142+2242	175.506	22.705	0.1324	34
NSC1142+2837	175.509	28.610	0.1605	35
NSC1142+2146	175.530	21.768	0.1345	66
NSC1142+2633	175.535	26.542	0.1146	25
NSC1142+2407	175.544	24.122	0.1380	31
NSC1142+3604	175.544	36.059	0.2357	23
NSC1142+2742	175.551	27.698	0.2628	13
NSC1142+2226	175.558	22.438	0.2051	23
NSC1142+3441	175.568	34.690	0.1593	25
NSC1142+1523	175.583	15.377	0.2041	25
NSC1142+2806	175.602	28.107	0.1194	28
NSC1142+3218	175.605	32.304	0.1830	26
NSC1142+1533	175.619	15.550	0.1898	28
NSC1142+2528	175.621	25.474	0.1631	28
NSC1143+4117	175.642	41.288	0.2090	17
NSC1143+3332	175.649	33.541	0.1761	31
NSC1143+4150	175.682	41.831	0.2751	24
NSC1143+3911	175.690	39.187	0.2358	35
NSC1143+2455	175.704	24.921	0.1440	23
NSC1143+1256	175.709	12.931	0.1089	43
NSC1143+2330	175.731	23.501	0.0991	23
NSC1143+2303	175.739	23.057	0.1197	38
NSC1143+2811	175.743	28.187	0.1136	34
NSC1143+2647	175.745	26.783	0.1671	25
NSC1143+1306	175.748	13.098	0.1051	50
NSC1143+2547	175.776	25.783	0.1940	16
NSC1143+3452	175.790	34.872	0.2304	20
NSC1143+1522	175.795	15.358	0.1584	32
NSC1143+2156	175.800	21.927	0.1087	44
NSC1143+1358	175.821	13.972	0.1297	31
NSC1143+4110	175.826	41.164	0.2419	14
NSC1143+2140	175.828	21.667	0.1765	27
NSC1143+2640	175.863	26.671	0.1379	36
NSC1144+4014	175.881	40.238	0.1639	22
NSC1144+1549	175.889	15.820	0.1388	20
NSC1144+2949	175.931	29.817	0.1015	26
NSC1144+3402	175.932	34.030	0.1497	25
NSC1144+2428	175.965	24.459	0.2452	22
NSC1144+2230	175.966	22.500	0.1861	41
NSC1144+1536	175.976	15.592	0.1166	36
NSC1144+1713	175.976	17.223	0.2087	20
NSC1144+2217	176.010	22.281	0.1960	26
NSC1144+3602	176.012	36.037	0.2242	19
NSC1144+1255	176.020	12.924	0.2204	26
NSC1144+3937	176.040	39.609	0.1758	24
NSC1144+1648	176.047	16.798	0.2335	28
NSC1144+1519	176.065	15.311	0.2222	24
NSC1144+3804	176.067	38.064	0.1684	24
NSC1144+1946	176.072	19.762	0.0488	48
NSC1144+3110	176.085	31.160	0.1268	17
NSC1144+3053	176.090	30.878	0.0746	44
NSC1144+2238	176.114	22.633	0.2244	46
NSC1145+2340	176.130	23.659	0.1404	23
NSC1145+3713	176.144	37.224	0.0982	32
NSC1145+4219	176.153	42.321	0.1676	34
NSC1145+2434	176.163	24.559	0.1359	24
NSC1145+1556	176.167	15.938	0.2061	22
NSC1145+2305	176.182	23.080	0.0850	33
NSC1145+3545	176.195	35.745	0.2445	23
NSC1145+4136	176.202	41.594	0.1805	39
NSC1145+2459	176.218	24.980	0.1370	22
NSC1145+1538	176.233	15.625	0.1437	43
NSC1145+2143	176.263	21.714	0.2217	26
NSC1145+3329	176.274	33.488	0.1444	57
NSC1145+2942	176.274	29.699	0.1067	17
NSC1145+1458	176.309	14.959	0.1627	23
NSC1145+1721	176.319	17.358	0.2030	37
NSC1145+2126	176.328	21.427	0.1059	36
NSC1145+1529	176.340	15.482	0.0928	62
NSC1146+1542	176.395	15.702	0.1186	46
NSC1146+2236	176.417	22.597	0.2088	18
NSC1146+1423	176.429	14.387	0.2544	22
NSC1146+1602	176.430	16.029	0.1898	24
NSC1146+2543	176.473	25.716	0.1979	28
NSC1146+1442	176.482	14.705	0.1370	39

Continued...

Table B.1 - NGP Robust, Continued

Name	RA	Dec	z_{phot}	N_{gal}
NSC1146+2305	176.523	23.083	0.1832	21
NSC1146+3258	176.548	32.959	0.1824	18
NSC1146+4153	176.590	41.888	0.2249	27
NSC1146+2855	176.593	28.916	0.1362	31
NSC1146+1605	176.593	16.083	0.2487	17
NSC1146+3311	176.609	33.181	0.0950	44
NSC1146+1647	176.613	16.790	0.1900	21
NSC1147+2715	176.652	27.248	0.2030	21
NSC1147+2154	176.684	21.901	0.1400	35
NSC1147+2331	176.698	23.516	0.1767	25
NSC1147+2408	176.716	24.130	0.1172	28
NSC1147+2238	176.761	22.631	0.1873	36
NSC1147+4208	176.842	42.138	0.1501	22
NSC1147+3331	176.854	33.518	0.2085	30
NSC1147+2053	176.856	20.877	0.1095	49
NSC1148+2909	176.904	29.142	0.1114	20
NSC1148+2203	176.921	22.049	0.1751	28
NSC1148+2530	176.925	25.496	0.1080	79
NSC1148+2923	176.933	29.391	0.1874	18
NSC1148+2151	177.007	21.851	0.1503	41
NSC1148+3101	177.061	31.016	0.1563	26
NSC1148+2231	177.071	22.514	0.1857	40
NSC1148+2109	177.076	21.155	0.0948	30
NSC1148+3711	177.080	37.188	0.1443	38
NSC1148+3758	177.089	37.966	0.1888	31
NSC1148+4025	177.102	40.424	0.1216	39
NSC1148+4105	177.119	41.083	0.1849	18
NSC1149+2332	177.138	23.541	0.1798	40
NSC1149+2224	177.165	22.396	0.1806	47
NSC1149+1335	177.167	13.590	0.2443	19
NSC1149+3511	177.188	35.190	0.1856	26
NSC1149+2449	177.223	24.822	0.2212	16
NSC1149+3431	177.256	34.511	0.1964	26
NSC1149+2118	177.265	21.304	0.1481	17
NSC1149+2035	177.279	20.586	0.1673	26
NSC1149+1520	177.300	15.336	0.1199	31
NSC1149+1651	177.314	16.853	0.1592	37
NSC1149+1941	177.321	19.690	0.1898	31
NSC1149+2043	177.356	20.716	0.1666	22
NSC1149+3403	177.358	34.058	0.1927	25
NSC1150+3742	177.389	37.694	0.1411	34
NSC1150+2129	177.398	21.488	0.1425	27
NSC1150+2740	177.415	27.668	0.2109	36
NSC1150+3528	177.445	35.461	0.1947	28
NSC1150+3252	177.446	32.866	0.2455	22
NSC1150+3411	177.452	34.179	0.1936	27
NSC1150+2102	177.481	21.039	0.1517	26
NSC1150+2915	177.481	29.256	0.2144	14
NSC1150+1634	177.521	16.570	0.1318	22
NSC1150+1911	177.535	19.190	0.1471	34
NSC1150+2305	177.537	23.088	0.2454	25
NSC1150+2541	177.546	25.680	0.1433	31
NSC1150+3049	177.569	30.823	0.1579	20
NSC1150+2721	177.580	27.348	0.1311	26
NSC1150+1517	177.597	15.286	0.0795	29
NSC1150+1453	177.597	14.875	0.2550	23
NSC1150+2222	177.608	22.365	0.2629	31
NSC1150+4156	177.619	41.931	0.2855	17
NSC1151+3221	177.687	32.349	0.1451	28
NSC1151+2325	177.701	23.423	0.2414	31
NSC1151+2943	177.705	29.710	0.1635	27
NSC1151+1929	177.711	19.483	0.1221	33
NSC1151+2532	177.725	25.534	0.1702	29
NSC1151+4224	177.738	42.393	0.2437	32
NSC1151+4118	177.759	41.306	0.2117	24
NSC1151+1906	177.760	19.105	0.1633	29
NSC1151+2051	177.764	20.845	0.2046	29
NSC1151+2517	177.766	25.279	0.1582	30
NSC1151+2441	177.769	24.686	0.1449	32
NSC1151+2357	177.798	23.950	0.1507	34
NSC1151+2738	177.804	27.632	0.0672	26
NSC1151+2849	177.811	28.819	0.1617	20
NSC1151+2546	177.818	25.767	0.1541	32
NSC1151+3703	177.843	37.047	0.1839	22
NSC1151+2201	177.855	22.017	0.1559	46
NSC1151+3333	177.871	33.555	0.1788	35
NSC1152+1921	177.879	19.354	0.2806	25
NSC1152+3642	177.915	36.702	0.1801	30
NSC1152+3716	177.955	37.261	0.1446	77
NSC1152+2123	178.032	21.392	0.1446	27
NSC1152+1905	178.050	19.078	0.0845	22
NSC1152+2137	178.060	21.611	0.1262	30
NSC1152+2822	178.069	28.368	0.1713	40
NSC1152+1648	178.094	16.796	0.1504	25
NSC1152+1256	178.097	12.932	0.0636	58
NSC1152+3614	178.098	36.241	0.1265	20
NSC1152+2315	178.107	23.244	0.2434	21

Continued...

Table B.1 - NGP Robust, Continued

Name	RA	Dec	z_{phot}	N_{gal}
NSC1152+3716	178.107	37.268	0.1452	74
NSC1153+2332	178.132	23.527	0.1702	33
NSC1153+4229	178.137	42.490	0.2480	25
NSC1153+2718	178.155	27.307	0.1655	48
NSC1153+2009	178.163	20.152	0.1026	30
NSC1153+3516	178.164	35.264	0.1374	24
NSC1153+3405	178.175	34.080	0.2385	18
NSC1153+2152	178.183	21.872	0.1793	22
NSC1153+2206	178.211	22.108	0.1642	30
NSC1153+2413	178.217	24.213	0.1370	21
NSC1153+3214	178.221	32.230	0.2542	18
NSC1153+3621	178.291	36.344	0.1091	20
NSC1153+1256	178.309	12.939	0.0660	60
NSC1153+1745	178.311	17.755	0.1064	24
NSC1153+3055	178.327	30.920	0.1618	30
NSC1153+1955	178.335	19.914	0.1410	30
NSC1153+1353	178.338	13.876	0.1081	19
NSC1153+2244	178.343	22.728	0.0817	23
NSC1153+2327	178.362	23.451	0.2270	32
NSC1153+2209	178.363	22.142	0.1354	29
NSC1154+1451	178.385	14.855	0.2194	29
NSC1154+3229	178.391	32.491	0.1811	16
NSC1154+2124	178.396	21.406	0.1206	31
NSC1154+1527	178.400	15.451	0.0913	63
NSC1154+3126	178.409	31.435	0.1152	17
NSC1154+2219	178.416	22.315	0.1047	31
NSC1154+3714	178.455	37.237	0.1660	23
NSC1154+2113	178.458	21.219	0.1337	24
NSC1154+2750	178.458	27.829	0.1777	24
NSC1154+3322	178.462	33.374	0.1818	27
NSC1154+2101	178.466	21.019	0.1937	19
NSC1154+3241	178.482	32.681	0.1276	22
NSC1154+3744	178.509	37.725	0.1660	34
NSC1154+2916	178.553	29.264	0.2454	20
NSC1154+3047	178.567	30.785	0.1606	22
NSC1154+2110	178.581	21.162	0.1894	19
NSC1154+2207	178.581	22.123	0.1099	37
NSC1154+3414	178.581	34.237	0.1831	25
NSC1154+1908	178.586	19.140	0.0921	21
NSC1155+3429	178.638	34.483	0.1422	31
NSC1155+2257	178.639	22.952	0.1302	42
NSC1155+2157	178.641	21.958	0.2247	25
NSC1155+1531	178.662	15.510	0.0882	51
NSC1155+2454	178.680	24.894	0.1123	35
NSC1155+4209	178.681	42.144	0.2146	23
NSC1155+2128	178.685	21.475	0.1641	49
NSC1155+3518	178.704	35.305	0.2097	21
NSC1155+2146	178.704	21.771	0.2565	18
NSC1155+3552	178.708	35.860	0.1183	22
NSC1155+3331	178.780	33.509	0.1495	20
NSC1155+3721	178.806	37.353	0.1658	31
NSC1155+2325	178.818	23.423	0.1379	82
NSC1155+2746	178.829	27.765	0.1507	32
NSC1155+1619	178.848	16.309	0.1187	51
NSC1155+3605	178.856	36.086	0.1332	26
NSC1155+2630	178.864	26.502	0.1156	21
NSC1155+3005	178.865	30.084	0.1690	20
NSC1155+1407	178.869	14.125	0.1481	25
NSC1155+3537	178.874	35.625	0.1431	19
NSC1156+1448	178.890	14.794	0.1855	50
NSC1156+1905	178.915	19.079	0.1266	32
NSC1156+1311	178.940	13.190	0.0989	34
NSC1156+2123	178.960	21.380	0.1647	22
NSC1156+3440	178.993	34.674	0.2499	38
NSC1156+2717	179.008	27.285	0.1347	30
NSC1156+1454	179.015	14.907	0.1442	40
NSC1156+2812	179.017	28.205	0.1850	21
NSC1156+3432	179.019	34.533	0.2330	31
NSC1156+4231	179.044	42.522	0.2266	26
NSC1156+3319	179.061	33.317	0.1945	28
NSC1156+1307	179.070	13.125	0.1175	43
NSC1157+3112	179.136	31.200	0.2141	16
NSC1157+2222	179.139	22.371	0.0949	38
NSC1157+2608	179.149	26.137	0.1073	56
NSC1157+2048	179.156	20.793	0.2029	32
NSC1157+2020	179.160	20.326	0.1834	18
NSC1157+2115	179.162	21.257	0.1110	39
NSC1157+4005	179.174	40.077	0.2049	15
NSC1157+3631	179.179	36.511	0.1378	30
NSC1157+1631	179.200	16.512	0.1825	32
NSC1157+2702	179.202	27.038	0.0742	28
NSC1157+4221	179.206	42.354	0.1526	33
NSC1157+2835	179.207	28.578	0.2342	23
NSC1157+3657	179.216	36.945	0.1394	25
NSC1157+3607	179.221	36.119	0.2339	24
NSC1157+1342	179.225	13.699	0.1682	20
NSC1157+2323	179.232	23.388	0.1406	50

Continued...

Table B.1 - NGP Robust, Continued

Name	RA	Dec	z_{phot}	N_{gal}
NSC1157+2822	179.232	28.365	0.1853	23
NSC1157+2415	179.239	24.245	0.1362	36
NSC1157+1946	179.255	19.770	0.1442	35
NSC1157+2249	179.261	22.817	0.2355	27
NSC1157+1658	179.266	16.959	0.1811	22
NSC1157+1914	179.268	19.233	0.1513	14
NSC1157+2625	179.270	26.421	0.1613	33
NSC1157+3013	179.273	30.216	0.1319	27
NSC1157+2525	179.287	25.415	0.1520	38
NSC1157+2956	179.334	29.927	0.1657	32
NSC1157+1931	179.341	19.513	0.1503	20
NSC1157+4112	179.341	41.194	0.1554	18
NSC1157+3055	179.349	30.909	0.1619	22
NSC1157+2857	179.361	28.949	0.2661	17
NSC1157+2123	179.374	21.390	0.1836	36
NSC1158+4043	179.380	40.711	0.1694	32
NSC1158+2045	179.383	20.752	0.1260	29
NSC1158+3339	179.389	33.655	0.1314	72
NSC1158+3238	179.454	32.639	0.1013	23
NSC1158+3418	179.485	34.305	0.1963	41
NSC1158+2532	179.490	25.529	0.1581	28
NSC1158+3548	179.494	35.795	0.1479	21
NSC1158+3708	179.530	37.141	0.0925	26
NSC1158+3810	179.555	38.162	0.2575	23
NSC1158+2623	179.560	26.381	0.1323	63
NSC1158+3043	179.577	30.719	0.1164	40
NSC1158+1513	179.608	15.223	0.1276	30
NSC1159+2950	179.631	29.837	0.1874	33
NSC1159+2540	179.677	25.670	0.2217	23
NSC1159+2824	179.712	28.392	0.1545	38
NSC1159+3053	179.722	30.886	0.1037	35
NSC1159+2236	179.724	22.592	0.1096	32
NSC1159+3243	179.749	32.721	0.1494	27
NSC1159+3604	179.754	36.060	0.1278	22
NSC1159+3033	179.758	30.554	0.2061	19
NSC1159+3546	179.762	35.763	0.1766	29
NSC1159+2812	179.774	28.201	0.2161	18
NSC1159+3329	179.780	33.477	0.1902	24
NSC1159+3154	179.785	31.900	0.1608	27
NSC1159+3012	179.797	30.192	0.1680	37
NSC1159+3746	179.828	37.774	0.0799	24
NSC1200+1317	179.882	13.289	0.1343	25
NSC1200+3946	179.884	39.760	0.1803	18
NSC1200+1458	179.896	14.970	0.1003	32
NSC1200+4040	179.908	40.663	0.1388	32
NSC1200+2758	179.913	27.963	0.2268	26
NSC1200+2550	179.924	25.832	0.1979	46
NSC1200+2951	179.936	29.851	0.1631	42
NSC1200+1435	179.947	14.581	0.1728	36
NSC1200+2845	179.951	28.756	0.2475	20
NSC1200+3918	179.974	39.299	0.1073	23
NSC1200+2106	179.985	21.105	0.1577	28
NSC1200+1348	179.992	13.793	0.2581	19
NSC1200+2303	179.992	23.051	0.2545	22
NSC1200+2622	179.995	26.364	0.2314	23
NSC1200+1837	180.018	18.618	0.1091	22
NSC1200+1250	180.022	12.836	0.1955	22
NSC1200+3023	180.030	30.377	0.2112	34
NSC1200+3731	180.035	37.511	0.1569	20
NSC1200+1506	180.066	15.100	0.1968	23
NSC1200+1727	180.072	17.456	0.0589	22
NSC1200+2906	180.073	29.092	0.2042	29
NSC1200+3445	180.093	34.754	0.1231	25
NSC1200+2408	180.097	24.127	0.1325	22
NSC1201+4001	180.126	40.017	0.1746	22
NSC1201+1415	180.145	14.249	0.1463	29
NSC1201+3318	180.166	33.299	0.1676	19
NSC1201+3635	180.190	36.578	0.0149	3
NSC1201+2942	180.199	29.706	0.1860	37
NSC1201+3535	180.253	35.587	0.1414	36
NSC1201+2921	180.261	29.348	0.1902	22
NSC1201+3425	180.264	34.417	0.2086	28
NSC1201+1343	180.270	13.715	0.1322	29
NSC1201+1516	180.273	15.271	0.1288	50
NSC1201+3141	180.277	31.680	0.1762	29
NSC1201+1459	180.290	14.978	0.1969	20
NSC1201+1402	180.328	14.040	0.1522	29
NSC1201+4138	180.333	41.636	0.2255	19
NSC1201+2306	180.333	23.096	0.2629	36
NSC1201+3217	180.340	32.282	0.1491	24
NSC1201+3415	180.346	34.258	0.2156	29
NSC1201+2352	180.371	23.863	0.2004	35
NSC1201+4229	180.373	42.483	0.2248	13
NSC1202+2843	180.380	28.718	0.1672	21
NSC1202+2907	180.390	29.117	0.2192	20
NSC1202+3826	180.394	38.439	0.1167	27
NSC1202+3002	180.396	30.039	0.1603	41

Continued...

Table B.1 - NGP Robust, Continued

Name	RA	Dec	z_{phot}	N_{gal}
NSC1202+2115	180.405	21.258	0.2432	25
NSC1202+3258	180.414	32.964	0.1463	33
NSC1202+1407	180.446	14.123	0.1687	31
NSC1202+3812	180.461	38.196	0.1842	21
NSC1202+3746	180.469	37.764	0.0939	28
NSC1202+3159	180.474	31.984	0.1979	28
NSC1202+3042	180.481	30.708	0.1813	21
NSC1202+1350	180.490	13.832	0.1761	32
NSC1202+2422	180.495	24.373	0.1473	34
NSC1202+3724	180.496	37.397	0.0969	26
NSC1202+1430	180.497	14.493	0.2515	22
NSC1202+1615	180.514	16.249	0.0811	25
NSC1202+2058	180.526	20.969	0.2113	25
NSC1202+2019	180.542	20.319	0.1277	35
NSC1202+2350	180.543	23.834	0.1366	45
NSC1202+2750	180.544	27.828	0.2163	27
NSC1202+2930	180.546	29.504	0.2057	37
NSC1202+3512	180.553	35.198	0.1494	29
NSC1202+1447	180.606	14.790	0.1188	25
NSC1202+3328	180.608	33.460	0.2448	26
NSC1202+2730	180.617	27.505	0.1404	26
NSC1202+2708	180.619	27.131	0.2160	15
NSC1203+3312	180.625	33.195	0.1425	28
NSC1203+1643	180.626	16.711	0.1397	38
NSC1203+3946	180.649	39.768	0.1595	22
NSC1203+1410	180.652	14.163	0.1982	32
NSC1203+1846	180.664	18.760	0.1843	26
NSC1203+2045	180.676	20.744	0.2346	27
NSC1203+1433	180.681	14.550	0.1750	39
NSC1203+3935	180.681	39.582	0.1966	24
NSC1203+3248	180.682	32.803	0.1864	27
NSC1203+1713	180.691	17.222	0.1570	42
NSC1203+3221	180.701	32.342	0.1518	17
NSC1203+3104	180.706	31.067	0.2495	18
NSC1203+3927	180.710	39.443	0.2047	21
NSC1203+2340	180.737	23.665	0.1549	24
NSC1203+2836	180.756	28.596	0.1694	48
NSC1203+3513	180.767	35.209	0.2314	23
NSC1203+4012	180.771	40.206	0.1325	18
NSC1203+1306	180.779	13.094	0.1515	21
NSC1203+1452	180.797	14.859	0.1734	23
NSC1203+2959	180.826	29.976	0.2305	25
NSC1203+3343	180.835	33.721	0.1729	23
NSC1203+1323	180.844	13.390	0.1559	33
NSC1204+2757	180.886	27.949	0.1665	61
NSC1204+2202	180.888	22.035	0.1095	30
NSC1204+2348	180.892	23.794	0.1618	30
NSC1204+3527	180.906	35.446	0.1611	20
NSC1204+1655	180.923	16.917	0.1426	30
NSC1204+2812	180.957	28.205	0.1577	54
NSC1204+1506	180.966	15.102	0.1581	22
NSC1204+1443	181.032	14.709	0.2170	28
NSC1204+2919	181.048	29.308	0.1973	20
NSC1204+1338	181.054	13.637	0.1648	29
NSC1204+2002	181.080	20.028	0.0889	35
NSC1204+1309	181.081	13.142	0.2057	22
NSC1204+2147	181.097	21.791	0.1326	39
NSC1204+2800	181.104	28.006	0.1810	39
NSC1204+3516	181.105	35.269	0.2368	23
NSC1205+2424	181.133	24.396	0.2111	19
NSC1205+3005	181.151	30.081	0.1612	20
NSC1205+3222	181.166	32.365	0.1190	37
NSC1205+2338	181.178	23.636	0.0499	18
NSC1205+3720	181.179	37.328	0.1766	31
NSC1205+1503	181.181	15.056	0.1315	43
NSC1205+4232	181.214	42.526	0.1316	46
NSC1205+3759	181.215	37.981	0.2256	27
NSC1205+3524	181.217	35.395	0.1578	38
NSC1205+2235	181.219	22.581	0.2231	52
NSC1205+1927	181.244	19.447	0.1379	28
NSC1205+3206	181.254	32.093	0.1783	25
NSC1205+3121	181.318	31.350	0.2087	21
NSC1205+4225	181.319	42.411	0.1535	28
NSC1205+2139	181.329	21.646	0.2828	20
NSC1205+2725	181.332	27.418	0.2651	25
NSC1205+2409	181.334	24.154	0.1252	31
NSC1205+3360	181.339	33.999	0.1874	18
NSC1205+2247	181.343	22.778	0.1210	52
NSC1205+1944	181.349	19.725	0.0922	33
NSC1205+1528	181.359	15.462	0.1712	28
NSC1206+3806	181.384	38.103	0.2294	22
NSC1206+3045	181.412	30.756	0.1967	17
NSC1206+3556	181.418	35.925	0.1053	19
NSC1206+3741	181.423	37.682	0.2021	36
NSC1206+2941	181.445	29.688	0.1970	21
NSC1206+3349	181.446	33.822	0.2133	16
NSC1206+1432	181.454	14.527	0.1637	41

Continued...

Table B.1 - NGP Robust, Continued

Name	RA	Dec	z_{phot}	N_{gal}
NSC1206+2224	181.466	22.392	0.1020	39
NSC1206+3924	181.468	39.406	0.0915	37
NSC1206+3332	181.468	33.531	0.1774	21
NSC1206+1552	181.478	15.870	0.1106	40
NSC1206+4011	181.481	40.190	0.1424	22
NSC1206+1343	181.485	13.725	0.1532	43
NSC1206+2853	181.512	28.892	0.2308	28
NSC1206+3248	181.520	32.800	0.1927	25
NSC1206+2915	181.523	29.247	0.1831	23
NSC1206+1259	181.566	12.983	0.2220	25
NSC1206+2901	181.571	29.024	0.2458	21
NSC1206+3057	181.594	30.955	0.1994	22
NSC1206+1405	181.596	14.089	0.1934	21
NSC1206+2216	181.615	22.273	0.1127	46
NSC1206+3748	181.619	37.804	0.2193	32
NSC1207+3356	181.629	33.941	0.1628	16
NSC1207+2824	181.631	28.392	0.1692	24
NSC1207+1856	181.631	18.926	0.1961	29
NSC1207+2833	181.637	28.549	0.1915	22
NSC1207+2042	181.637	20.697	0.1005	35
NSC1207+3126	181.647	31.426	0.1827	29
NSC1207+3233	181.648	32.556	0.1935	23
NSC1207+2204	181.653	22.066	0.1923	49
NSC1207+2721	181.661	27.357	0.1835	19
NSC1207+3137	181.682	31.616	0.2123	24
NSC1207+4156	181.699	41.936	0.1681	19
NSC1207+1355	181.703	13.921	0.1959	27
NSC1207+3310	181.709	33.169	0.2057	29
NSC1207+4003	181.718	40.055	0.1987	21
NSC1207+1314	181.732	13.234	0.0509	27
NSC1207+3115	181.753	31.249	0.1979	34
NSC1207+3800	181.763	38.002	0.1488	28
NSC1207+1714	181.764	17.237	0.0906	23
NSC1207+3953	181.768	39.877	0.1672	33
NSC1207+1551	181.769	15.857	0.1751	25
NSC1207+2660	181.773	26.997	0.0487	23
NSC1207+1825	181.793	18.412	0.2210	14
NSC1207+1421	181.796	14.357	0.1700	35
NSC1207+2045	181.797	20.758	0.1516	24
NSC1207+2352	181.799	23.874	0.0965	48
NSC1207+1927	181.806	19.454	0.2490	25
NSC1207+1949	181.823	19.818	0.1055	20
NSC1207+3043	181.841	30.715	0.2223	23
NSC1207+3623	181.851	36.378	0.1993	18
NSC1207+2239	181.860	22.651	0.1928	21
NSC1207+2914	181.873	29.239	0.1733	26
NSC1208+2801	181.877	28.016	0.2112	19
NSC1208+1403	181.878	14.045	0.1606	35
NSC1208+1513	181.884	15.216	0.1613	32
NSC1208+2902	181.908	29.026	0.1748	25
NSC1208+2815	181.914	28.242	0.2250	20
NSC1208+2725	181.923	27.413	0.1317	29
NSC1208+2739	181.932	27.645	0.2022	25
NSC1208+2422	181.939	24.365	0.1477	24
NSC1208+3051	181.961	30.848	0.1985	19
NSC1208+3006	181.972	30.104	0.2205	24
NSC1208+2541	181.978	25.679	0.0383	21
NSC1208+1459	182.012	14.978	0.1898	58
NSC1208+1254	182.049	12.901	0.1358	30
NSC1208+4022	182.063	40.366	0.1434	38
NSC1208+3128	182.077	31.470	0.1803	25
NSC1208+1409	182.092	14.145	0.1715	29
NSC1208+1728	182.113	17.470	0.1906	22
NSC1208+2845	182.120	28.755	0.1810	24
NSC1209+4107	182.128	41.117	0.1389	46
NSC1209+1621	182.133	16.346	0.1958	22
NSC1209+2939	182.135	29.649	0.1285	19
NSC1209+2743	182.142	27.710	0.1001	34
NSC1209+1335	182.162	13.588	0.1814	23
NSC1209+3259	182.166	32.991	0.1164	21
NSC1209+1556	182.174	15.930	0.1292	38
NSC1209+4117	182.176	41.285	0.0943	45
NSC1209+3101	182.187	31.012	0.1787	27
NSC1209+3606	182.201	36.096	0.1703	20
NSC1209+3646	182.212	36.765	0.0859	30
NSC1209+2733	182.236	27.548	0.1134	27
NSC1209+2721	182.284	27.343	0.1515	24
NSC1209+1615	182.294	16.254	0.1853	25
NSC1209+4037	182.296	40.621	0.2354	33
NSC1209+3025	182.303	30.424	0.1463	22
NSC1209+1418	182.303	14.294	0.1482	26
NSC1209+4053	182.314	40.884	0.2100	18
NSC1209+2901	182.344	29.014	0.1748	31
NSC1209+2939	182.355	29.646	0.2064	20
NSC1209+2422	182.359	24.364	0.2059	27
NSC1209+2218	182.369	22.294	0.1024	44
NSC1210+4208	182.375	42.132	0.1705	21

Continued...

Table B.1 - NGP Robust, Continued

Name	RA	Dec	z_{phot}	N_{gal}
NSC1210+1849	182.389	18.810	0.1567	31
NSC1210+4141	182.389	41.686	0.1983	18
NSC1210+2146	182.417	21.764	0.1838	28
NSC1210+1734	182.425	17.559	0.1618	25
NSC1210+1304	182.435	13.063	0.1593	34
NSC1210+3201	182.487	32.016	0.1298	40
NSC1210+4131	182.510	41.515	0.2006	23
NSC1210+1329	182.514	13.483	0.1340	55
NSC1210+3808	182.548	38.135	0.2082	24
NSC1210+1756	182.568	17.934	0.1876	23
NSC1210+1308	182.575	13.126	0.1479	30
NSC1210+2804	182.592	28.067	0.2537	18
NSC1210+3924	182.605	39.399	0.1425	26
NSC1210+3619	182.613	36.318	0.1339	26
NSC1210+1910	182.617	19.168	0.0948	23
NSC1211+2938	182.628	29.635	0.2457	17
NSC1211+3637	182.633	36.617	0.0819	25
NSC1211+2436	182.652	24.594	0.1481	24
NSC1211+1539	182.680	15.646	0.1642	28
NSC1211+1846	182.689	18.769	0.2148	19
NSC1211+4042	182.694	40.707	0.1940	34
NSC1211+1452	182.714	14.874	0.1212	23
NSC1211+3052	182.724	30.862	0.1019	44
NSC1211+1556	182.760	15.928	0.1121	63
NSC1211+3753	182.761	37.885	0.2037	28
NSC1211+2823	182.795	28.384	0.2659	21
NSC1211+1713	182.812	17.218	0.1699	37
NSC1211+3520	182.816	35.332	0.2067	40
NSC1211+1411	182.825	14.187	0.1766	28
NSC1211+3814	182.834	38.237	0.1384	34
NSC1211+1320	182.838	13.332	0.1249	41
NSC1211+2204	182.846	22.062	0.1687	27
NSC1211+2507	182.849	25.121	0.0556	19
NSC1212+2938	182.901	29.630	0.2268	22
NSC1212+2723	182.903	27.389	0.1366	38
NSC1212+1851	182.904	18.849	0.1666	23
NSC1212+1810	182.913	18.174	0.1866	25
NSC1212+1751	182.915	17.856	0.2624	21
NSC1212+2958	182.936	29.971	0.2293	47
NSC1212+4012	182.959	40.201	0.1969	22
NSC1212+1447	182.963	14.784	0.2302	24
NSC1212+1941	182.968	19.677	0.1691	31
NSC1212+2713	182.983	27.215	0.1270	30
NSC1212+1345	182.995	13.758	0.1666	50
NSC1212+3541	183.001	35.688	0.1441	25
NSC1212+3756	183.018	37.938	0.1587	25
NSC1212+3059	183.027	30.977	0.1618	23
NSC1212+3834	183.035	38.569	0.1931	25
NSC1212+4047	183.058	40.786	0.1091	19
NSC1212+1340	183.074	13.675	0.1909	40
NSC1212+3035	183.075	30.591	0.1319	38
NSC1212+2732	183.079	27.541	0.2312	21
NSC1212+1609	183.083	16.148	0.1398	23
NSC1212+1941	183.100	19.677	0.1784	27
NSC1213+1834	183.126	18.575	0.1540	36
NSC1213+4104	183.132	41.065	0.2326	30
NSC1213+4139	183.138	41.645	0.1632	14
NSC1213+2940	183.141	29.667	0.2161	19
NSC1213+3627	183.150	36.455	0.2358	16
NSC1213+1254	183.154	12.907	0.1285	33
NSC1213+3352	183.213	33.869	0.1917	28
NSC1213+2727	183.213	27.457	0.1719	36
NSC1213+3410	183.221	34.164	0.2629	35
NSC1213+1531	183.242	15.509	0.1962	38
NSC1213+1345	183.270	13.743	0.1875	30
NSC1213+2912	183.273	29.194	0.1300	64
NSC1213+2033	183.310	20.547	0.1585	27
NSC1213+2356	183.314	23.932	0.2076	28
NSC1213+3547	183.322	35.786	0.1990	22
NSC1213+2139	183.324	21.654	0.0680	25
NSC1213+1606	183.368	16.103	0.1865	26
NSC1213+3230	183.368	32.503	0.1766	25
NSC1214+2915	183.383	29.247	0.1374	61
NSC1214+3158	183.431	31.965	0.1789	33
NSC1214+2408	183.435	24.135	0.1912	25
NSC1214+2701	183.440	27.013	0.2296	13
NSC1214+1752	183.468	17.868	0.1612	23
NSC1214+2638	183.488	26.633	0.1581	37
NSC1214+1813	183.492	18.225	0.1723	17
NSC1214+2360	183.508	23.994	0.2082	28
NSC1214+2735	183.512	27.585	0.1430	19
NSC1214+1918	183.532	19.295	0.1744	25
NSC1214+2856	183.532	28.938	0.1430	27
NSC1214+1834	183.560	18.569	0.2311	19
NSC1214+3141	183.583	31.683	0.1420	47
NSC1214+1408	183.588	14.127	0.1281	40
NSC1214+3016	183.591	30.274	0.1050	37

Continued...

Table B.1 - NGP Robust, Continued

Name	RA	Dec	z_{phot}	N_{gal}
NSC1214+4109	183.602	41.155	0.1930	21
NSC1214+1753	183.607	17.888	0.1696	25
NSC1215+1342	183.631	13.699	0.1209	49
NSC1215+2130	183.653	21.503	0.1988	31
NSC1215+1621	183.732	16.346	0.1271	33
NSC1215+2550	183.762	25.827	0.1458	31
NSC1215+3808	183.776	38.129	0.1681	26
NSC1215+1819	183.786	18.308	0.1653	41
NSC1215+1612	183.805	16.200	0.1717	29
NSC1215+1723	183.808	17.380	0.1931	16
NSC1215+1744	183.813	17.731	0.1448	33
NSC1215+2854	183.816	28.899	0.1749	36
NSC1215+4054	183.817	40.899	0.2065	20
NSC1215+2732	183.826	27.538	0.1493	38
NSC1215+3653	183.834	36.888	0.2261	25
NSC1215+1535	183.849	15.577	0.2317	21
NSC1215+2628	183.862	26.473	0.1457	28
NSC1215+1554	183.864	15.902	0.1357	29
NSC1216+1423	183.887	14.387	0.1516	29
NSC1216+1839	183.894	18.644	0.1661	41
NSC1216+1930	183.899	19.508	0.1207	33
NSC1216+3148	183.900	31.804	0.2196	27
NSC1216+2838	183.900	28.628	0.0861	29
NSC1216+1519	183.924	15.319	0.2389	22
NSC1216+1912	183.935	19.195	0.1394	28
NSC1216+1244	183.936	12.740	0.2404	33
NSC1216+1815	183.939	18.244	0.1687	40
NSC1216+1736	183.944	17.607	0.1766	24
NSC1216+1625	183.951	16.423	0.1442	22
NSC1216+2115	183.998	21.245	0.1136	36
NSC1216+1727	184.002	17.451	0.1832	30
NSC1216+4119	184.009	41.313	0.1639	27
NSC1216+3707	184.015	37.109	0.2103	21
NSC1216+1716	184.028	17.259	0.1552	28
NSC1216+2724	184.072	27.395	0.1216	26
NSC1216+3543	184.079	35.711	0.2786	18
NSC1216+2958	184.102	29.970	0.0893	23
NSC1217+2709	184.129	27.149	0.2608	28
NSC1217+4204	184.131	42.068	0.1658	22
NSC1217+1953	184.141	19.890	0.1359	23
NSC1217+1535	184.146	15.589	0.1520	35
NSC1217+1644	184.153	16.737	0.2136	29
NSC1217+1908	184.172	19.132	0.1379	38
NSC1217+2111	184.188	21.181	0.1114	37
NSC1217+3518	184.246	35.293	0.2408	27
NSC1217+4047	184.315	40.787	0.1182	26
NSC1217+1838	184.320	18.631	0.1666	21
NSC1217+2036	184.322	20.594	0.1772	27
NSC1217+3252	184.324	32.862	0.2349	17
NSC1217+4108	184.339	41.139	0.1529	23
NSC1218+2258	184.392	22.962	0.1265	34
NSC1218+1734	184.410	17.572	0.1876	26
NSC1218+1321	184.414	13.344	0.1662	30
NSC1218+3911	184.430	39.180	0.2100	18
NSC1218+2547	184.433	25.787	0.2827	22
NSC1218+2021	184.460	20.347	0.1433	30
NSC1218+2038	184.495	20.639	0.2041	46
NSC1218+3417	184.495	34.290	0.1907	26
NSC1218+2958	184.497	29.972	0.0951	37
NSC1218+1855	184.535	18.919	0.1309	38
NSC1218+3334	184.596	33.572	0.1937	23
NSC1218+3234	184.605	32.564	0.1575	24
NSC1218+1825	184.623	18.420	0.1887	37
NSC1219+3808	184.663	38.129	0.1695	22
NSC1219+2757	184.689	27.953	0.1008	44
NSC1219+1322	184.714	13.362	0.2003	32
NSC1219+1845	184.738	18.748	0.1293	39
NSC1219+2104	184.756	21.066	0.1354	21
NSC1219+3532	184.757	35.527	0.1968	38
NSC1219+1615	184.767	16.245	0.1828	25
NSC1219+2219	184.769	22.311	0.1285	33
NSC1219+3611	184.770	36.190	0.2682	20
NSC1219+3702	184.774	37.036	0.2001	29
NSC1219+2655	184.805	26.912	0.0538	27
NSC1219+3336	184.806	33.594	0.2385	22
NSC1219+3039	184.815	30.654	0.2055	29
NSC1219+3505	184.832	35.091	0.2437	23
NSC1219+1753	184.847	17.891	0.1825	32
NSC1219+3832	184.859	38.531	0.2522	19
NSC1219+2437	184.859	24.612	0.1320	18
NSC1220+3653	184.901	36.887	0.1844	23
NSC1220+1958	184.904	19.963	0.1198	30
NSC1220+2219	184.952	22.320	0.1247	42
NSC1220+1625	184.978	16.416	0.1388	24
NSC1220+1313	184.987	13.210	0.1605	27
NSC1220+1709	184.999	17.147	0.2449	25
NSC1220+3522	185.001	35.372	0.1646	25

Continued...

Table B.1 - NGP Robust, Continued

Name	RA	Dec	z_{phot}	N_{gal}
NSC1220+3433	185.018	34.544	0.2609	30
NSC1220+1328	185.029	13.470	0.1936	24
NSC1220+3719	185.031	37.322	0.2119	27
NSC1220+2721	185.039	27.344	0.1833	22
NSC1220+3606	185.060	36.105	0.2083	28
NSC1220+3927	185.086	39.447	0.2103	18
NSC1220+2343	185.099	23.712	0.1917	24
NSC1221+3254	185.164	32.896	0.2256	30
NSC1221+1936	185.166	19.599	0.1512	33
NSC1221+1356	185.250	13.926	0.2471	21
NSC1221+2514	185.258	25.235	0.2216	19
NSC1221+4150	185.276	41.838	0.0848	15
NSC1221+1913	185.288	19.217	0.2361	21
NSC1221+3158	185.296	31.971	0.2033	24
NSC1221+1960	185.319	19.999	0.2066	23
NSC1221+1720	185.339	17.340	0.1914	30
NSC1221+1701	185.344	17.025	0.1287	37
NSC1221+1930	185.349	19.506	0.1534	30
NSC1222+3560	185.400	35.996	0.2522	15
NSC1222+1345	185.432	13.754	0.0992	69
NSC1222+4019	185.437	40.323	0.2548	31
NSC1222+2701	185.453	27.014	0.0648	30
NSC1222+3533	185.456	35.558	0.2641	19
NSC1222+2356	185.481	23.925	0.1301	27
NSC1222+1843	185.488	18.714	0.2664	17
NSC1222+3822	185.489	38.359	0.1480	32
NSC1222+2135	185.493	21.579	0.2120	24
NSC1222+2104	185.557	21.067	0.1729	30
NSC1222+2032	185.573	20.539	0.2375	22
NSC1222+1346	185.573	13.765	0.1201	54
NSC1222+1258	185.597	12.964	0.1667	33
NSC1222+2725	185.604	27.419	0.1949	30
NSC1223+1946	185.635	19.771	0.1938	21
NSC1223+2048	185.647	20.807	0.1346	34
NSC1223+1910	185.684	19.160	0.1766	25
NSC1223+1656	185.701	16.940	0.1354	36
NSC1223+1957	185.742	19.956	0.1034	45
NSC1223+1350	185.752	13.841	0.2069	28
NSC1223+3713	185.753	37.224	0.1950	26
NSC1223+2501	185.785	25.022	0.1504	35
NSC1223+1300	185.817	13.002	0.2313	20
NSC1223+2446	185.843	24.761	0.2139	21
NSC1223+2022	185.861	20.374	0.1430	27
NSC1224+1901	185.887	19.022	0.2100	24
NSC1224+3107	185.907	31.118	0.0462	18
NSC1224+2344	185.908	23.740	0.2006	23
NSC1224+4030	185.920	40.493	0.1560	21
NSC1224+2721	185.951	27.345	0.0859	26
NSC1224+1407	185.962	14.122	0.2059	24
NSC1224+2007	185.973	20.124	0.1468	32
NSC1224+3208	186.038	32.130	0.1087	34
NSC1224+2045	186.057	20.756	0.1440	51
NSC1224+2021	186.070	20.344	0.1539	36
NSC1224+2714	186.125	27.230	0.0990	27
NSC1225+3158	186.160	31.970	0.0894	44
NSC1225+1402	186.175	14.026	0.1227	32
NSC1225+3604	186.207	36.065	0.2287	18
NSC1225+2028	186.261	20.472	0.1028	42
NSC1225+3126	186.274	31.427	0.0396	24
NSC1225+1957	186.274	19.956	0.1347	22
NSC1225+3213	186.311	32.211	0.1231	43
NSC1225+3159	186.326	31.991	0.0991	43
NSC1225+2050	186.334	20.827	0.1390	26
NSC1225+3738	186.344	37.633	0.1355	27
NSC1225+1928	186.349	19.473	0.1686	45
NSC1226+2529	186.381	25.488	0.0771	41
NSC1226+3638	186.404	36.632	0.1412	26
NSC1226+4015	186.407	40.242	0.2070	33
NSC1226+1618	186.428	16.306	0.2148	29
NSC1226+4051	186.494	40.855	0.2796	31
NSC1226+2611	186.533	26.185	0.1388	29
NSC1226+2127	186.560	21.451	0.2181	22
NSC1226+3157	186.569	31.957	0.2239	26
NSC1226+2018	186.584	20.307	0.1823	32
NSC1226+1351	186.599	13.852	0.2396	18
NSC1226+1719	186.607	17.320	0.2162	28
NSC1226+2515	186.622	25.242	0.1543	19
NSC1227+1924	186.659	19.399	0.1506	28
NSC1227+1952	186.667	19.860	0.2300	38
NSC1227+1707	186.672	17.118	0.1715	32
NSC1227+3354	186.683	33.906	0.1451	21
NSC1227+1443	186.688	14.714	0.1720	25
NSC1227+3315	186.702	33.249	0.2234	26
NSC1227+3244	186.765	32.725	0.2075	19
NSC1227+4007	186.805	40.117	0.2216	20
NSC1227+2748	186.830	27.797	0.0466	13
NSC1227+1358	186.845	13.962	0.2474	29

Continued...

Table B.1 - NGP Robust, Continued

Name	RA	Dec	z_{phot}	N_{gal}
NSC1227+2511	186.857	25.183	0.1486	28
NSC1227+2231	186.869	22.520	0.2005	21
NSC1228+1939	186.881	19.651	0.1626	33
NSC1228+3255	186.913	32.918	0.1887	26
NSC1228+3022	186.936	30.374	0.1357	38
NSC1228+3341	186.938	33.677	0.1705	17
NSC1228+1419	186.972	14.312	0.2665	22
NSC1228+1329	187.011	13.476	0.1995	28
NSC1228+3448	187.015	34.801	0.2549	21
NSC1228+1914	187.045	19.228	0.1422	50
NSC1228+3036	187.048	30.608	0.0806	34
NSC1228+1944	187.073	19.740	0.2043	16
NSC1228+2643	187.083	26.711	0.1484	49
NSC1228+1845	187.094	18.758	0.1731	23
NSC1228+2133	187.121	21.545	0.2121	22
NSC1229+2055	187.135	20.925	0.1608	25
NSC1229+3248	187.137	32.804	0.2002	24
NSC1229+2718	187.138	27.305	0.0803	29
NSC1229+2814	187.138	28.240	0.1940	22
NSC1229+2503	187.166	25.057	0.1158	30
NSC1229+2151	187.189	21.844	0.2148	23
NSC1229+1833	187.200	18.556	0.1303	41
NSC1229+1923	187.212	19.388	0.1584	61
NSC1229+2727	187.229	27.457	0.0915	33
NSC1229+1626	187.239	16.434	0.1906	35
NSC1229+1733	187.258	17.555	0.2550	19
NSC1229+3141	187.270	31.682	0.1532	18
NSC1229+1814	187.277	18.231	0.1724	25
NSC1229+1246	187.290	12.763	0.1996	65
NSC1229+2858	187.293	28.973	0.0838	41
NSC1229+2160	187.362	21.997	0.1495	27
NSC1229+2757	187.371	27.946	0.0431	16
NSC1230+2220	187.392	22.330	0.2069	23
NSC1230+3644	187.428	36.735	0.1615	35
NSC1230+2134	187.437	21.568	0.1632	41
NSC1230+3345	187.445	33.744	0.1629	19
NSC1230+2120	187.456	21.335	0.1746	38
NSC1230+1910	187.469	19.167	0.1403	27
NSC1230+1806	187.474	18.099	0.1596	44
NSC1230+1629	187.483	16.489	0.2315	35
NSC1230+2244	187.518	22.741	0.1454	21
NSC1230+3631	187.519	36.523	0.1361	35
NSC1230+3421	187.560	34.355	0.1933	22
NSC1230+1458	187.570	14.961	0.2041	24
NSC1230+1617	187.570	16.281	0.2283	30
NSC1230+3721	187.578	37.355	0.2771	21
NSC1231+2456	187.658	24.928	0.1547	32
NSC1231+3407	187.666	34.122	0.2747	25
NSC1231+3503	187.682	35.053	0.1266	26
NSC1231+2944	187.684	29.725	0.1271	30
NSC1231+1853	187.743	18.879	0.1446	25
NSC1231+2416	187.755	24.270	0.1362	34
NSC1231+1556	187.756	15.937	0.1824	45
NSC1231+2855	187.766	28.914	0.0773	32
NSC1231+1811	187.768	18.184	0.1859	29
NSC1231+2107	187.827	21.119	0.1913	22
NSC1231+3722	187.831	37.373	0.2332	19
NSC1231+2404	187.845	24.062	0.1646	23
NSC1231+1733	187.851	17.550	0.0927	25
NSC1231+1251	187.861	12.858	0.1655	18
NSC1231+4042	187.863	40.699	0.1909	33
NSC1231+4212	187.871	42.196	0.1829	22
NSC1232+3410	187.900	34.168	0.1910	21
NSC1232+1704	187.935	17.069	0.2249	23
NSC1232+3730	187.940	37.505	0.1720	26
NSC1232+1317	187.989	13.275	0.2379	21
NSC1232+2423	188.058	24.386	0.0513	16
NSC1232+4225	188.097	42.413	0.1957	21
NSC1232+2118	188.103	21.293	0.1126	17
NSC1232+4103	188.108	41.043	0.1910	24
NSC1232+3307	188.124	33.114	0.2133	26
NSC1233+3428	188.171	34.469	0.1646	22
NSC1233+2607	188.185	26.113	0.2153	23
NSC1233+4053	188.259	40.891	0.1763	22
NSC1233+2637	188.269	26.621	0.1346	28
NSC1233+1721	188.281	17.343	0.1727	57
NSC1233+1930	188.291	19.497	0.2392	32
NSC1233+1702	188.291	17.033	0.2307	29
NSC1233+2319	188.300	23.323	0.2183	21
NSC1233+4005	188.303	40.081	0.1967	25
NSC1233+2207	188.312	22.122	0.1891	31
NSC1233+1902	188.313	19.034	0.1460	21
NSC1233+2545	188.324	25.752	0.1838	19
NSC1233+2001	188.354	20.017	0.1661	26
NSC1234+1318	188.380	13.303	0.1541	25
NSC1234+1841	188.381	18.683	0.1228	27
NSC1234+1527	188.452	15.453	0.2512	42

Continued...

Table B.1 - NGP Robust, Continued

Name	RA	Dec	z_{phot}	N_{gal}
NSC1234+2834	188.466	28.561	0.1987	21
NSC1234+4230	188.473	42.507	0.1921	29
NSC1234+1922	188.492	19.369	0.1668	16
NSC1234+4109	188.510	41.147	0.1513	61
NSC1234+1727	188.537	17.453	0.2328	28
NSC1234+3735	188.542	37.583	0.1466	23
NSC1234+2527	188.559	25.443	0.2131	17
NSC1234+1513	188.568	15.224	0.2487	50
NSC1234+1329	188.579	13.487	0.1919	33
NSC1234+2751	188.608	27.845	0.2087	30
NSC1234+4060	188.616	40.993	0.1606	42
NSC1235+2811	188.639	28.190	0.1192	24
NSC1235+4213	188.644	42.209	0.2349	29
NSC1235+1632	188.674	16.534	0.1169	58
NSC1235+2831	188.687	28.517	0.1379	26
NSC1235+3810	188.687	38.164	0.2272	21
NSC1235+4126	188.690	41.434	0.2633	22
NSC1235+2540	188.703	25.667	0.1551	36
NSC1235+4233	188.748	42.556	0.1663	30
NSC1235+3420	188.764	34.337	0.1677	25
NSC1235+3959	188.766	39.980	0.2080	23
NSC1235+1515	188.769	15.248	0.2697	28
NSC1235+1609	188.782	16.156	0.1571	27
NSC1235+3944	188.790	39.731	0.1885	25
NSC1235+1637	188.795	16.615	0.1461	39
NSC1235+1914	188.799	19.240	0.2027	38
NSC1235+4119	188.801	41.311	0.2201	41
NSC1235+2735	188.817	27.579	0.0802	24
NSC1235+3521	188.865	35.353	0.0567	14
NSC1236+4142	188.877	41.694	0.1711	35
NSC1236+1311	188.882	13.177	0.2303	23
NSC1236+1721	188.884	17.345	0.1455	33
NSC1236+1655	188.890	16.912	0.2335	21
NSC1236+4128	188.939	41.467	0.2033	42
NSC1236+2704	188.970	27.074	0.1094	29
NSC1236+1345	188.980	13.752	0.2357	15
NSC1236+3808	189.014	38.128	0.1985	27
NSC1236+2642	189.025	26.694	0.2260	34
NSC1236+1529	189.038	15.476	0.2221	30
NSC1236+2900	189.051	29.000	0.2306	24
NSC1236+1633	189.076	16.558	0.0971	79
NSC1236+2051	189.077	20.858	0.1466	27
NSC1236+1619	189.085	16.311	0.1359	34
NSC1236+1948	189.087	19.804	0.1481	50
NSC1236+3752	189.094	37.869	0.1825	25
NSC1236+1740	189.104	17.659	0.1376	40
NSC1236+1829	189.114	18.484	0.1860	23
NSC1237+2213	189.146	22.218	0.1907	24
NSC1237+1908	189.160	19.132	0.2155	26
NSC1237+4013	189.163	40.221	0.2632	20
NSC1237+2550	189.229	25.841	0.1734	41
NSC1237+2537	189.235	25.616	0.2141	18
NSC1237+4134	189.253	41.565	0.2905	34
NSC1237+3653	189.260	36.890	0.2581	25
NSC1237+1525	189.280	15.421	0.1421	26
NSC1237+3427	189.296	34.453	0.1677	27
NSC1237+2649	189.302	26.821	0.1949	32
NSC1237+2622	189.318	26.361	0.2409	25
NSC1237+4156	189.345	41.931	0.1712	29
NSC1237+1932	189.363	19.531	0.2505	23
NSC1237+1542	189.374	15.705	0.2651	16
NSC1238+4232	189.442	42.533	0.1524	23
NSC1238+1516	189.469	15.264	0.1038	38
NSC1238+2548	189.498	25.799	0.1787	30
NSC1238+4011	189.549	40.184	0.2084	18
NSC1238+3738	189.554	37.635	0.2034	31
NSC1238+1558	189.558	15.963	0.2027	29
NSC1238+1823	189.562	18.376	0.2240	26
NSC1238+1637	189.570	16.616	0.1079	35
NSC1238+2314	189.590	23.237	0.1947	19
NSC1238+3637	189.625	36.623	0.1914	15
NSC1239+1439	189.659	14.656	0.1778	19
NSC1239+4135	189.690	41.585	0.1125	25
NSC1239+1716	189.694	17.260	0.1125	45
NSC1239+4029	189.698	40.483	0.2494	27
NSC1239+1702	189.716	17.027	0.1837	27
NSC1239+2550	189.716	25.830	0.2198	23
NSC1239+1936	189.733	19.594	0.2014	19
NSC1239+1458	189.758	14.967	0.1881	22
NSC1239+1549	189.759	15.815	0.2192	26
NSC1239+2438	189.764	24.641	0.2086	16
NSC1239+3645	189.768	36.758	0.1811	23
NSC1239+3812	189.785	38.199	0.1865	17
NSC1239+1847	189.786	18.785	0.2587	40
NSC1239+1640	189.791	16.660	0.0923	38
NSC1239+1518	189.794	15.308	0.1727	22
NSC1239+1743	189.799	17.712	0.1202	41

Continued...

Table B.1 - NGP Robust, Continued

Name	RA	Dec	z_{phot}	N_{gal}
NSC1239+1409	189.810	14.149	0.2208	21
NSC1239+1622	189.864	16.363	0.1876	36
NSC1240+1534	189.894	15.563	0.1108	29
NSC1240+4046	189.942	40.767	0.2318	25
NSC1240+3312	189.954	33.206	0.1025	21
NSC1240+3425	189.958	34.416	0.1744	29
NSC1240+3446	189.995	34.766	0.1708	19
NSC1240+3626	189.996	36.428	0.1585	21
NSC1240+3746	190.001	37.775	0.2258	41
NSC1240+1722	190.117	17.363	0.2133	21
NSC1241+4135	190.149	41.591	0.1544	31
NSC1241+1659	190.157	16.983	0.1187	31
NSC1241+1625	190.163	16.412	0.2360	20
NSC1241+1733	190.163	17.547	0.1510	22
NSC1241+3825	190.216	38.416	0.1777	24
NSC1241+1919	190.222	19.309	0.1590	29
NSC1241+3301	190.247	33.011	0.2359	21
NSC1241+2004	190.286	20.058	0.1661	26
NSC1241+2735	190.286	27.579	0.1732	32
NSC1241+3600	190.311	36.007	0.1720	24
NSC1241+1835	190.327	18.586	0.0975	98
NSC1241+3736	190.348	37.595	0.1331	22
NSC1241+3612	190.363	36.206	0.2264	23
NSC1242+2945	190.415	29.757	0.2295	29
NSC1242+1629	190.419	16.477	0.1683	21
NSC1242+3250	190.436	32.827	0.2467	28
NSC1242+3517	190.443	35.283	0.1237	25
NSC1242+2736	190.467	27.598	0.1723	29
NSC1242+3814	190.472	38.231	0.1864	24
NSC1242+1733	190.497	17.546	0.1450	25
NSC1242+3322	190.498	33.373	0.1424	25
NSC1242+2927	190.517	29.450	0.2308	18
NSC1242+4202	190.520	42.032	0.1800	26
NSC1242+1946	190.529	19.760	0.2209	59
NSC1242+2055	190.530	20.924	0.1075	25
NSC1242+2613	190.553	26.212	0.1960	24
NSC1242+4217	190.554	42.276	0.0957	38
NSC1242+3725	190.567	37.414	0.1791	25
NSC1242+1926	190.605	19.438	0.2017	23
NSC1243+3529	190.627	35.476	0.2691	20
NSC1243+3817	190.635	38.289	0.2165	29
NSC1243+2208	190.637	22.141	0.1952	30
NSC1243+2906	190.647	29.106	0.2110	36
NSC1243+2848	190.648	28.797	0.2262	24
NSC1243+4021	190.653	40.346	0.2328	26
NSC1243+1902	190.715	19.035	0.1151	47
NSC1243+3746	190.721	37.762	0.2068	22
NSC1243+2115	190.763	21.257	0.1798	21
NSC1243+3211	190.763	32.180	0.1819	22
NSC1243+3504	190.788	35.067	0.2510	17
NSC1243+3735	190.800	37.590	0.2119	20
NSC1243+2132	190.803	21.538	0.2484	19
NSC1243+3319	190.814	33.324	0.1757	23
NSC1243+3949	190.829	39.810	0.1807	26
NSC1243+2718	190.849	27.295	0.2247	25
NSC1244+2744	190.878	27.741	0.2133	34
NSC1244+2803	190.894	28.049	0.2095	23
NSC1244+4052	190.907	40.871	0.1691	23
NSC1244+3148	190.909	31.806	0.1375	17
NSC1244+2622	190.921	26.360	0.1718	25
NSC1244+3113	190.927	31.221	0.2192	18
NSC1244+3933	190.946	39.549	0.1201	32
NSC1244+1848	190.948	18.807	0.1751	27
NSC1244+2856	190.982	28.936	0.2404	37
NSC1244+4207	190.989	42.115	0.1317	30
NSC1244+4028	191.032	40.461	0.1974	13
NSC1244+1429	191.047	14.482	0.2433	29
NSC1244+1650	191.099	16.833	0.1894	26
NSC1244+4104	191.111	41.066	0.2172	24
NSC1245+1930	191.149	19.504	0.1561	21
NSC1245+2831	191.150	28.513	0.2214	28
NSC1245+3757	191.154	37.956	0.1860	21
NSC1245+1921	191.163	19.346	0.1992	24
NSC1245+3316	191.168	33.267	0.1310	31
NSC1245+2028	191.172	20.472	0.2175	19
NSC1245+2256	191.178	22.925	0.2228	17
NSC1245+4205	191.180	42.091	0.1956	30
NSC1245+2938	191.188	29.625	0.1329	20
NSC1245+1814	191.192	18.241	0.1445	33
NSC1245+3140	191.196	31.669	0.2257	27
NSC1245+4005	191.204	40.081	0.2036	21
NSC1245+1725	191.216	17.411	0.2208	32
NSC1245+1843	191.298	18.720	0.2502	30
NSC1245+2048	191.321	20.804	0.2115	31
NSC1245+3118	191.338	31.301	0.2245	16
NSC1245+3155	191.338	31.918	0.2095	23
NSC1245+4108	191.349	41.126	0.1672	32

Continued...

Table B.1 - NGP Robust, Continued

Name	RA	Dec	z_{phot}	N_{gal}
NSC1246+2020	191.375	20.330	0.1152	20
NSC1246+3217	191.383	32.285	0.1873	26
NSC1246+3031	191.386	30.515	0.2279	18
NSC1246+3323	191.388	33.385	0.1417	49
NSC1246+4004	191.410	40.064	0.1757	21
NSC1246+2928	191.429	29.461	0.2130	32
NSC1246+1760	191.502	17.997	0.0543	16
NSC1246+1706	191.510	17.107	0.1304	30
NSC1246+1732	191.512	17.527	0.2257	21
NSC1246+3018	191.530	30.306	0.2037	21
NSC1246+1851	191.531	18.848	0.1571	38
NSC1246+2851	191.546	28.845	0.1678	25
NSC1246+2308	191.556	23.137	0.1946	20
NSC1246+3254	191.559	32.897	0.1318	23
NSC1246+3602	191.566	36.037	0.1194	31
NSC1246+3526	191.609	35.441	0.2351	20
NSC1246+1715	191.610	17.249	0.1485	32
NSC1246+2628	191.614	26.466	0.0940	46
NSC1247+2340	191.634	23.672	0.2006	20
NSC1247+2515	191.656	25.246	0.1088	26
NSC1247+1723	191.704	17.377	0.1403	30
NSC1247+2648	191.712	26.794	0.1988	19
NSC1247+3003	191.726	30.043	0.1365	54
NSC1247+2856	191.764	28.940	0.1893	20
NSC1247+3549	191.793	35.814	0.2307	21
NSC1247+2915	191.793	29.253	0.1534	16
NSC1247+2753	191.801	27.882	0.1392	16
NSC1247+1832	191.809	18.532	0.2107	43
NSC1247+1854	191.809	18.908	0.1533	63
NSC1247+3622	191.821	36.372	0.1399	33
NSC1247+3533	191.871	35.547	0.1647	48
NSC1248+2456	191.881	24.928	0.1569	20
NSC1248+4009	191.917	40.143	0.1629	21
NSC1248+1825	191.976	18.412	0.2011	21
NSC1248+2057	192.014	20.958	0.2137	22
NSC1248+3732	192.016	37.532	0.1725	20
NSC1248+3514	192.019	35.226	0.1281	31
NSC1248+3847	192.066	38.791	0.1458	22
NSC1248+2947	192.116	29.784	0.0983	27
NSC1249+1546	192.163	15.764	0.2651	18
NSC1249+2928	192.239	29.472	0.2136	26
NSC1249+1923	192.267	19.383	0.2248	25
NSC1249+3008	192.268	30.125	0.1355	35
NSC1249+2834	192.317	28.559	0.2664	29
NSC1249+3940	192.328	39.674	0.1859	23
NSC1249+1349	192.363	13.818	0.1839	26
NSC1249+2712	192.368	27.193	0.1678	11
NSC1249+2847	192.370	28.783	0.2470	28
NSC1250+3448	192.385	34.805	0.2074	23
NSC1250+3307	192.401	33.113	0.1566	29
NSC1250+3354	192.402	33.894	0.1229	26
NSC1250+3810	192.431	38.173	0.1288	25
NSC1250+2453	192.447	24.876	0.2013	18
NSC1250+1929	192.455	19.475	0.2089	24
NSC1250+1850	192.455	18.829	0.2179	21
NSC1250+1904	192.466	19.071	0.2105	33
NSC1250+2658	192.476	26.975	0.1783	21
NSC1250+1606	192.517	16.105	0.2437	19
NSC1250+3034	192.539	30.561	0.1202	20
NSC1250+1303	192.556	13.042	0.1289	31
NSC1250+2951	192.600	29.855	0.2191	17
NSC1250+3122	192.604	31.366	0.2605	38
NSC1251+3344	192.644	33.742	0.1987	22
NSC1251+1543	192.706	15.725	0.2567	20
NSC1251+1933	192.734	19.556	0.2500	15
NSC1251+2840	192.735	28.668	0.2027	37
NSC1251+1639	192.740	16.654	0.2199	36
NSC1251+1815	192.748	18.245	0.1878	37
NSC1251+1346	192.756	13.771	0.1861	27
NSC1251+1831	192.759	18.509	0.1896	24
NSC1251+3022	192.765	30.367	0.1959	20
NSC1251+1407	192.796	14.124	0.2369	20
NSC1251+1855	192.801	18.915	0.1819	26
NSC1251+3104	192.871	31.058	0.2103	18
NSC1252+1841	192.892	18.681	0.1816	34
NSC1252+3317	192.904	33.284	0.1376	23
NSC1252+1312	192.923	13.198	0.2133	21
NSC1252+3519	192.932	35.325	0.1859	26
NSC1252+3119	192.957	31.323	0.2831	14
NSC1252+3053	192.970	30.882	0.2036	21
NSC1252+1853	192.998	18.891	0.2137	26
NSC1252+3539	193.010	35.650	0.1831	24
NSC1252+1808	193.068	18.139	0.2148	29
NSC1252+1818	193.083	18.296	0.1776	30
NSC1252+2859	193.116	28.984	0.2196	19
NSC1253+2842	193.155	28.706	0.2098	22
NSC1253+3449	193.158	34.818	0.2429	18

Continued...

Table B.1 - NGP Robust, Continued

Name	RA	Dec	z_{phot}	N_{gal}
NSC1253+1906	193.191	19.103	0.2704	49
NSC1253+1411	193.215	14.179	0.2071	25
NSC1253+3328	193.223	33.466	0.1443	28
NSC1253+1515	193.236	15.258	0.2320	27
NSC1253+2850	193.247	28.826	0.1804	26
NSC1253+1919	193.269	19.318	0.2696	28
NSC1253+1819	193.321	18.313	0.2073	32
NSC1253+1727	193.338	17.453	0.1782	23
NSC1254+2208	193.407	22.128	0.1821	30
NSC1254+3032	193.435	30.532	0.1796	23
NSC1254+1744	193.446	17.738	0.2101	26
NSC1254+3622	193.455	36.364	0.1967	29
NSC1254+3052	193.470	30.865	0.1144	35
NSC1254+3604	193.484	36.061	0.1936	22
NSC1254+3936	193.488	39.608	0.1255	18
NSC1254+1718	193.576	17.302	0.1346	28
NSC1254+1810	193.596	18.173	0.2724	23
NSC1254+3023	193.622	30.390	0.1812	17
NSC1255+2526	193.634	25.427	0.2236	22
NSC1255+1755	193.634	17.913	0.2046	22
NSC1255+1858	193.638	18.960	0.1159	60
NSC1255+2547	193.675	25.787	0.1379	34
NSC1255+2820	193.700	28.331	0.2160	24
NSC1255+1308	193.707	13.135	0.3040	25
NSC1255+1838	193.727	18.634	0.2178	27
NSC1255+3537	193.732	35.623	0.2337	14
NSC1255+3603	193.756	36.047	0.1766	31
NSC1255+2930	193.777	29.500	0.1948	21
NSC1255+2418	193.778	24.308	0.1647	24
NSC1255+3521	193.821	35.345	0.1974	30
NSC1255+1817	193.846	18.276	0.2656	21
NSC1256+2846	193.892	28.765	0.2348	24
NSC1256+3633	193.898	36.546	0.2375	18
NSC1256+3457	193.901	34.945	0.2241	28
NSC1256+1747	193.926	17.776	0.2461	27
NSC1256+1826	193.942	18.436	0.2447	48
NSC1256+2830	193.951	28.501	0.1383	51
NSC1256+1359	193.956	13.991	0.1856	22
NSC1256+2758	193.970	27.959	0.1914	22
NSC1256+2026	193.971	20.442	0.2025	20
NSC1256+1535	193.982	15.588	0.1835	30
NSC1256+2909	194.016	29.157	0.1954	18
NSC1256+1949	194.041	19.820	0.1351	17
NSC1256+1328	194.064	13.468	0.2144	22
NSC1256+3542	194.066	35.702	0.1564	34
NSC1256+1613	194.100	16.211	0.2118	26
NSC1256+2051	194.112	20.849	0.2583	18
NSC1256+2422	194.119	24.362	0.1540	28
NSC1256+2951	194.121	29.850	0.1711	25
NSC1256+1841	194.125	18.684	0.1768	40
NSC1257+2921	194.135	29.347	0.2606	27
NSC1257+2544	194.136	25.726	0.2247	28
NSC1257+1816	194.139	18.269	0.1671	42
NSC1257+1414	194.144	14.228	0.1923	18
NSC1257+4204	194.197	42.067	0.2062	16
NSC1257+3637	194.205	36.618	0.2604	33
NSC1257+1830	194.229	18.499	0.2127	34
NSC1257+1924	194.234	19.399	0.1946	21
NSC1257+4026	194.254	40.434	0.1447	33
NSC1257+3335	194.256	33.578	0.1284	25
NSC1257+3042	194.256	30.701	0.1136	24
NSC1257+1441	194.273	14.676	0.2092	20
NSC1257+1415	194.302	14.255	0.1661	26
NSC1257+2628	194.308	26.472	0.1299	23
NSC1257+3629	194.329	36.491	0.1972	26
NSC1257+1755	194.331	17.914	0.1263	32
NSC1257+1847	194.341	18.779	0.1566	20
NSC1257+1741	194.358	17.681	0.2251	16
NSC1257+2008	194.362	20.133	0.2067	45
NSC1258+1832	194.434	18.527	0.1803	28
NSC1258+1610	194.453	16.163	0.1464	17
NSC1258+3712	194.478	37.196	0.1890	21
NSC1258+1935	194.492	19.590	0.1633	34
NSC1258+2508	194.494	25.138	0.1507	24
NSC1258+2749	194.515	27.822	0.0816	75
NSC1258+3650	194.536	36.838	0.2414	28
NSC1258+1322	194.593	13.369	0.2282	20
NSC1258+1929	194.598	19.483	0.1369	30
NSC1258+2832	194.619	28.527	0.1689	15
NSC1259+3318	194.650	33.302	0.1898	27
NSC1259+1255	194.677	12.912	0.1940	29
NSC1259+3715	194.679	37.255	0.1735	38
NSC1259+3049	194.694	30.818	0.1815	22
NSC1259+2944	194.724	29.736	0.2327	18
NSC1259+1334	194.725	13.572	0.2117	21
NSC1259+3504	194.731	35.064	0.1948	25
NSC1259+2360	194.743	23.997	0.1332	30

Continued...

Table B.1 - NGP Robust, Continued

Name	RA	Dec	z_{phot}	N_{gal}
NSC1259+3005	194.750	30.081	0.1345	37
NSC1259+1947	194.773	19.781	0.2505	21
NSC1259+2827	194.821	28.454	0.1165	32
NSC1259+3640	194.825	36.660	0.2699	23
NSC1259+2715	194.864	27.243	0.1324	27
NSC1259+1730	194.867	17.499	0.1523	23
NSC1259+4033	194.871	40.558	0.1102	29
NSC1300+1938	194.886	19.640	0.1524	60
NSC1300+3851	194.901	38.844	0.0798	17
NSC1300+1810	194.905	18.166	0.1433	55
NSC1300+2227	194.905	22.453	0.1910	26
NSC1300+2907	194.910	29.120	0.1551	22
NSC1300+4012	194.922	40.194	0.1589	18
NSC1300+3120	194.925	31.341	0.0760	30
NSC1300+1755	194.926	17.909	0.1575	23
NSC1300+3412	194.931	34.200	0.2531	24
NSC1300+1841	194.963	18.683	0.1697	27
NSC1300+3614	194.972	36.230	0.2371	24
NSC1300+1934	194.981	19.566	0.2057	51
NSC1300+3042	195.000	30.708	0.2003	26
NSC1300+1634	195.002	16.568	0.1557	22
NSC1300+1522	195.028	15.367	0.1752	20
NSC1300+2555	195.032	25.922	0.2638	28
NSC1300+3028	195.040	30.470	0.1731	19
NSC1300+1922	195.056	19.370	0.2496	27
NSC1300+1956	195.059	19.933	0.1443	29
NSC1300+2648	195.059	26.795	0.1482	23
NSC1300+2423	195.064	24.381	0.1175	44
NSC1300+2358	195.066	23.971	0.1517	37
NSC1300+1908	195.081	19.132	0.1230	28
NSC1300+2946	195.113	29.775	0.2409	20
NSC1301+2157	195.140	21.944	0.2207	25
NSC1301+3051	195.143	30.857	0.2224	29
NSC1301+2658	195.145	26.970	0.1481	19
NSC1301+1434	195.152	14.561	0.2489	18
NSC1301+3419	195.192	34.317	0.1530	22
NSC1301+3312	195.193	33.195	0.1389	19
NSC1301+2429	195.198	24.480	0.1644	24
NSC1301+2218	195.198	22.293	0.1561	29
NSC1301+4018	195.225	40.292	0.0634	26
NSC1301+1847	195.239	18.788	0.1246	39
NSC1301+2438	195.250	24.628	0.1973	27
NSC1301+2740	195.266	27.666	0.0904	44
NSC1301+1752	195.277	17.865	0.1520	24
NSC1301+1927	195.282	19.442	0.2495	21
NSC1301+2931	195.286	29.512	0.1724	22
NSC1301+1406	195.289	14.102	0.1867	26
NSC1301+3545	195.303	35.755	0.1766	23
NSC1301+3939	195.312	39.652	0.1192	23
NSC1301+2359	195.339	23.991	0.1958	31
NSC1301+3018	195.342	30.296	0.1669	26
NSC1301+2701	195.347	27.024	0.1702	28
NSC1302+1813	195.376	18.216	0.1849	37
NSC1302+2412	195.383	24.195	0.2257	20
NSC1302+3636	195.384	36.596	0.1674	31
NSC1302+2813	195.385	28.212	0.1126	37
NSC1302+2839	195.401	28.657	0.2334	18
NSC1302+2907	195.402	29.122	0.2107	37
NSC1302+1915	195.409	19.248	0.1246	70
NSC1302+2502	195.429	25.035	0.2193	17
NSC1302+3326	195.467	33.441	0.2487	38
NSC1302+1449	195.470	14.812	0.1803	33
NSC1302+2654	195.495	26.898	0.1675	30
NSC1302+3354	195.502	33.903	0.2342	18
NSC1302+3550	195.508	35.831	0.1927	17
NSC1302+3803	195.515	38.052	0.1330	21
NSC1302+3618	195.553	36.301	0.1181	30
NSC1302+2935	195.559	29.583	0.1877	29
NSC1302+1312	195.581	13.197	0.1600	23
NSC1303+2402	195.642	24.034	0.2204	28
NSC1303+1652	195.652	16.867	0.1935	19
NSC1303+1434	195.658	14.564	0.1965	23
NSC1303+2419	195.682	24.312	0.2662	21
NSC1303+2641	195.683	26.685	0.2499	26
NSC1303+2610	195.724	26.160	0.1933	24
NSC1303+1905	195.724	19.089	0.1125	44
NSC1303+2949	195.729	29.817	0.1667	21
NSC1303+1720	195.756	17.326	0.1969	23
NSC1303+3350	195.763	33.840	0.2108	30
NSC1303+2020	195.764	20.326	0.1737	36
NSC1303+2817	195.805	28.278	0.1739	27
NSC1303+1810	195.819	18.167	0.1558	27
NSC1303+4160	195.820	41.995	0.2465	21
NSC1303+3148	195.820	31.807	0.1742	47
NSC1303+3249	195.868	32.821	0.1674	29
NSC1303+2758	195.868	27.975	0.1540	34
NSC1303+3439	195.870	34.651	0.2593	11

Continued...

Table B.1 - NGP Robust, Continued

Name	RA	Dec	z_{phot}	N_{gal}
NSC1304+3231	195.880	32.514	0.1470	19
NSC1304+1400	195.887	14.002	0.2041	21
NSC1304+1918	195.926	19.302	0.0996	65
NSC1304+2929	195.960	29.490	0.1821	26
NSC1304+2747	195.998	27.780	0.1428	16
NSC1304+1830	196.010	18.503	0.1353	37
NSC1304+1856	196.016	18.925	0.1796	30
NSC1304+2019	196.029	20.323	0.1965	46
NSC1304+1909	196.031	19.146	0.1525	55
NSC1304+3336	196.031	33.596	0.2080	30
NSC1304+2053	196.054	20.879	0.1625	34
NSC1304+4211	196.087	42.176	0.2469	22
NSC1304+3415	196.113	34.244	0.1972	22
NSC1304+1929	196.114	19.478	0.0859	48
NSC1305+1950	196.134	19.835	0.2602	21
NSC1305+1627	196.138	16.458	0.1884	24
NSC1305+3158	196.144	31.960	0.1303	24
NSC1305+4006	196.147	40.107	0.1938	32
NSC1305+1743	196.148	17.709	0.1930	38
NSC1305+3145	196.174	31.750	0.2166	13
NSC1305+1757	196.212	17.954	0.1457	37
NSC1305+1700	196.227	17.008	0.1975	26
NSC1305+4227	196.253	42.446	0.2593	18
NSC1305+4156	196.264	41.939	0.2112	17
NSC1305+2012	196.285	20.198	0.1902	27
NSC1305+4011	196.298	40.183	0.1389	35
NSC1305+2912	196.301	29.203	0.1654	28
NSC1305+3007	196.303	30.115	0.2242	19
NSC1305+3915	196.304	39.247	0.0345	5
NSC1305+3423	196.317	34.377	0.2024	26
NSC1305+3435	196.324	34.577	0.1796	37
NSC1305+2043	196.352	20.716	0.2288	27
NSC1305+1819	196.366	18.322	0.1069	30
NSC1305+3215	196.368	32.242	0.1925	19
NSC1306+1807	196.393	18.117	0.2015	23
NSC1306+3055	196.426	30.910	0.1719	22
NSC1306+3411	196.454	34.180	0.2317	38
NSC1306+1758	196.491	17.967	0.1060	32
NSC1306+2030	196.585	20.494	0.1790	31
NSC1306+3422	196.621	34.366	0.2399	29
NSC1307+2052	196.633	20.871	0.1196	26
NSC1307+3147	196.640	31.786	0.1910	36
NSC1307+1800	196.643	18.001	0.0935	32
NSC1307+3948	196.645	39.798	0.1000	37
NSC1307+3932	196.666	39.528	0.1133	22
NSC1307+1426	196.676	14.432	0.1512	21
NSC1307+2920	196.679	29.327	0.1551	21
NSC1307+3123	196.729	31.389	0.1794	27
NSC1307+1842	196.734	18.704	0.0964	22
NSC1307+1917	196.743	19.280	0.1136	37
NSC1307+3416	196.747	34.270	0.2335	27
NSC1307+1742	196.751	17.698	0.1062	32
NSC1307+2856	196.763	28.932	0.1621	25
NSC1307+3557	196.821	35.955	0.1644	25
NSC1307+1341	196.837	13.687	0.1432	28
NSC1307+2058	196.855	20.961	0.1852	26
NSC1308+2048	196.883	20.796	0.1599	24
NSC1308+1434	196.941	14.560	0.2795	22
NSC1308+1249	196.962	12.814	0.1430	49
NSC1308+1946	197.065	19.761	0.1520	25
NSC1308+1543	197.065	15.712	0.1790	22
NSC1308+3955	197.081	39.911	0.1357	27
NSC1308+4213	197.104	42.213	0.1881	20
NSC1308+3619	197.111	36.323	0.1668	22
NSC1308+1305	197.111	13.089	0.1639	29
NSC1309+1922	197.147	19.369	0.2139	28
NSC1309+2220	197.154	22.334	0.1986	31
NSC1309+1348	197.169	13.795	0.1034	32
NSC1309+3604	197.173	36.072	0.2253	16
NSC1309+2054	197.203	20.895	0.1352	32
NSC1309+1418	197.204	14.294	0.2424	22
NSC1309+4002	197.218	40.030	0.1194	26
NSC1309+1316	197.241	13.262	0.1778	24
NSC1309+3446	197.283	34.774	0.1874	25
NSC1309+3244	197.291	32.726	0.1565	21
NSC1310+1305	197.435	13.091	0.1752	40
NSC1310+3755	197.435	37.910	0.1537	29
NSC1310+1320	197.470	13.325	0.1997	24
NSC1310+1536	197.471	15.593	0.2534	23
NSC1310+3929	197.473	39.486	0.1404	24
NSC1310+3246	197.515	32.768	0.1452	19
NSC1310+1358	197.550	13.973	0.1090	29
NSC1310+1426	197.576	14.429	0.2462	25
NSC1310+4015	197.577	40.246	0.0247	7
NSC1310+1415	197.592	14.245	0.1748	29
NSC1310+3147	197.620	31.778	0.1581	27
NSC1311+3200	197.668	32.005	0.1350	21

Continued...

Table B.1 - NGP Robust, Continued

Name	RA	Dec	z_{phot}	N_{gal}
NSC1311+1346	197.671	13.770	0.1215	29
NSC1311+1549	197.702	15.817	0.2083	25
NSC1311+3039	197.706	30.647	0.1337	19
NSC1311+1448	197.761	14.798	0.1649	23
NSC1311+3917	197.825	39.288	0.0846	51
NSC1311+3233	197.855	32.542	0.2150	22
NSC1311+3306	197.864	33.105	0.1994	23
NSC1312+1305	197.875	13.088	0.1338	21
NSC1312+3359	197.879	33.992	0.2108	26
NSC1312+3139	197.892	31.648	0.1689	20
NSC1312+3130	197.937	31.496	0.1972	21
NSC1312+4024	197.940	40.401	0.0992	20
NSC1312+1411	197.949	14.183	0.2252	19
NSC1312+2933	198.079	29.556	0.1602	25
NSC1312+3508	198.097	35.139	0.1921	22
NSC1313+4112	198.127	41.193	0.2041	20
NSC1313+3240	198.149	32.668	0.2036	23
NSC1313+3217	198.188	32.290	0.2440	16
NSC1313+3901	198.220	39.020	0.1359	26
NSC1313+2922	198.296	29.365	0.2316	20
NSC1313+3612	198.314	36.194	0.1818	27
NSC1314+3153	198.396	31.890	0.1747	15
NSC1314+3146	198.401	31.764	0.2083	23
NSC1314+3130	198.409	31.500	0.1472	38
NSC1314+2849	198.417	28.823	0.2385	20
NSC1314+3028	198.421	30.473	0.1556	21
NSC1314+3852	198.422	38.872	0.1371	32
NSC1314+3206	198.459	32.093	0.2268	25
NSC1314+4124	198.576	41.408	0.2025	40
NSC1314+3327	198.610	33.453	0.2140	24
NSC1315+3842	198.648	38.698	0.1678	16
NSC1315+3015	198.654	30.247	0.1880	23
NSC1315+2844	198.669	28.727	0.1558	29
NSC1315+2751	198.690	27.851	0.1096	30
NSC1315+3834	198.712	38.559	0.2690	16
NSC1315+3030	198.738	30.493	0.1744	35
NSC1315+3208	198.748	32.141	0.2236	19
NSC1315+3658	198.756	36.966	0.1681	21
NSC1315+4118	198.759	41.293	0.1796	32
NSC1315+2908	198.867	29.129	0.1516	26
NSC1315+3619	198.875	36.322	0.1862	24
NSC1316+3944	198.891	39.728	0.1524	16
NSC1316+2826	198.930	28.426	0.1558	23
NSC1316+2751	198.946	27.843	0.1952	22
NSC1316+3108	198.951	31.137	0.2138	15
NSC1316+2937	199.049	29.611	0.2126	14
NSC1316+2909	199.053	29.143	0.1514	28
NSC1316+3333	199.082	33.547	0.1493	17
NSC1316+3354	199.085	33.906	0.2077	21
NSC1316+3218	199.092	32.304	0.1592	40
NSC1316+2855	199.107	28.922	0.2220	20
NSC1317+3723	199.167	37.388	0.1169	36
NSC1317+3124	199.283	31.407	0.2107	17
NSC1317+3620	199.342	36.330	0.2714	25
NSC1317+3302	199.365	33.037	0.2339	22
NSC1318+4116	199.413	41.263	0.1253	17
NSC1318+3150	199.469	31.831	0.2067	25
NSC1318+3534	199.472	35.559	0.2248	20
NSC1318+3007	199.511	30.111	0.1817	21
NSC1318+3338	199.544	33.631	0.2139	33
NSC1318+2936	199.582	29.601	0.2118	19
NSC1319+3622	199.630	36.362	0.2216	17
NSC1319+3844	199.630	38.733	0.1746	22
NSC1319+3314	199.636	33.236	0.2086	22
NSC1319+2922	199.686	29.375	0.1758	31
NSC1319+3431	199.742	34.520	0.1532	33
NSC1319+3642	199.763	36.705	0.1538	19
NSC1319+3103	199.790	31.055	0.1469	31
NSC1319+3152	199.848	31.870	0.1830	38
NSC1319+3948	199.860	39.808	0.1346	22
NSC1320+3052	199.922	30.874	0.2242	26
NSC1320+2851	199.923	28.844	0.1952	23
NSC1320+4241	199.932	42.684	0.1227	47
NSC1320+3320	199.999	33.325	0.2174	26
NSC1320+4105	200.061	41.078	0.1898	22
NSC1320+3703	200.073	37.047	0.1468	36
NSC1320+3406	200.075	34.108	0.1826	28
NSC1320+3747	200.080	37.789	0.1519	31
NSC1320+2839	200.086	28.647	0.1474	36
NSC1320+3306	200.098	33.094	0.1904	32
NSC1321+3327	200.160	33.446	0.2824	31
NSC1321+3116	200.162	31.273	0.1423	27
NSC1321+3219	200.167	32.309	0.2136	14
NSC1321+3209	200.167	32.145	0.2077	18
NSC1321+2823	200.182	28.382	0.1841	26
NSC1321+4129	200.195	41.483	0.1905	33
NSC1321+2915	200.203	29.252	0.1820	29

Continued...

Table B.1 - NGP Robust, Continued

Name	RA	Dec	z_{phot}	N_{gal}
NSC1321+3354	200.235	33.907	0.2243	37
NSC1321+3235	200.258	32.589	0.2306	20
NSC1321+4200	200.262	42.005	0.1652	22
NSC1321+3826	200.269	38.437	0.2438	24
NSC1321+3251	200.275	32.849	0.1839	28
NSC1321+3727	200.308	37.449	0.1460	28
NSC1321+3716	200.356	37.259	0.1398	30
NSC1321+4236	200.369	42.595	0.1102	25
NSC1322+4150	200.395	41.831	0.2297	20
NSC1322+4114	200.403	41.242	0.1744	26
NSC1322+3227	200.501	32.446	0.2619	37
NSC1322+3457	200.537	34.949	0.2387	18
NSC1322+3130	200.538	31.498	0.2351	21
NSC1322+3644	200.558	36.740	0.2069	21
NSC1322+3711	200.559	37.187	0.0889	41
NSC1322+4126	200.559	41.437	0.1721	24
NSC1323+2915	200.639	29.252	0.2800	18
NSC1323+3636	200.651	36.597	0.1545	22
NSC1323+3238	200.667	32.628	0.1112	30
NSC1323+3139	200.686	31.648	0.2877	38
NSC1323+3033	200.719	30.551	0.2320	22
NSC1323+3743	200.770	37.718	0.1704	13
NSC1323+3217	200.774	32.278	0.2285	25
NSC1323+3532	200.843	35.540	0.2030	19
NSC1324+3048	200.875	30.800	0.1708	27
NSC1324+3253	200.881	32.876	0.1662	22
NSC1324+3009	200.899	30.145	0.2074	21
NSC1324+2924	200.945	29.393	0.2620	12
NSC1324+2842	200.962	28.699	0.2213	16
NSC1324+4132	200.990	41.534	0.2108	24
NSC1324+3101	200.994	31.022	0.2038	26
NSC1324+3151	201.020	31.848	0.2174	24
NSC1324+3223	201.065	32.390	0.2373	20
NSC1324+3735	201.083	37.581	0.2115	22
NSC1325+3108	201.127	31.131	0.1753	26
NSC1325+3310	201.159	33.168	0.1822	16
NSC1325+3052	201.183	30.874	0.1416	27
NSC1325+4109	201.220	41.143	0.2064	16
NSC1325+3957	201.280	39.953	0.1724	22
NSC1325+3419	201.294	34.319	0.1786	23
NSC1326+3302	201.383	33.039	0.2047	21
NSC1326+3650	201.486	36.830	0.1904	17
NSC1326+4142	201.495	41.702	0.1918	40
NSC1326+2801	201.516	28.011	0.2172	33
NSC1326+2926	201.537	29.441	0.1545	29
NSC1326+2849	201.572	28.814	0.2303	15
NSC1326+3233	201.611	32.545	0.1940	23
NSC1326+3853	201.614	38.891	0.1153	23
NSC1327+3221	201.699	32.358	0.1924	19
NSC1327+3210	201.702	32.170	0.2048	27
NSC1327+3443	201.762	34.716	0.2020	24
NSC1327+3503	201.796	35.058	0.2033	30
NSC1327+3150	201.804	31.836	0.1846	34
NSC1327+3141	201.823	31.690	0.1326	36
NSC1327+4134	201.830	41.560	0.1570	21
NSC1327+3127	201.852	31.454	0.1815	21
NSC1328+3324	201.888	33.400	0.2234	19
NSC1328+3048	201.910	30.803	0.2361	15
NSC1328+3529	201.926	35.487	0.2547	31
NSC1328+3423	202.005	34.392	0.2355	27
NSC1328+4147	202.114	41.786	0.2212	18
NSC1329+3209	202.131	32.146	0.1576	27
NSC1329+3848	202.169	38.792	0.1210	30
NSC1329+3651	202.173	36.849	0.2014	17
NSC1329+2840	202.175	28.665	0.1906	14
NSC1329+3133	202.217	31.546	0.2253	22
NSC1329+2753	202.220	27.886	0.1347	23
NSC1329+3228	202.242	32.460	0.1214	28
NSC1329+3124	202.254	31.397	0.2072	26
NSC1329+3738	202.320	37.639	0.0757	44
NSC1330+3118	202.397	31.298	0.2082	26
NSC1330+3730	202.448	37.507	0.1117	42
NSC1330+3129	202.507	31.487	0.1766	24
NSC1330+3254	202.528	32.892	0.2324	19
NSC1330+3044	202.536	30.730	0.2638	22
NSC1330+3011	202.584	30.178	0.1972	23
NSC1330+3201	202.591	32.022	0.2519	25
NSC1330+3853	202.617	38.876	0.2232	31
NSC1331+3818	202.639	38.307	0.0901	17
NSC1331+3108	202.642	31.125	0.1656	28
NSC1331+3452	202.647	34.859	0.1437	24
NSC1331+4054	202.650	40.898	0.1372	24
NSC1331+3643	202.668	36.715	0.2091	22
NSC1331+3148	202.680	31.796	0.1913	39
NSC1331+3908	202.691	39.138	0.1261	25
NSC1331+3321	202.788	33.354	0.1685	25
NSC1331+3205	202.814	32.078	0.2305	24

Continued...

Table B.1 - NGP Robust, Continued

Name	RA	Dec	z_{phot}	N_{gal}
NSC1332+3103	202.907	31.045	0.2280	23
NSC1332+3730	202.985	37.494	0.2165	21
NSC1332+4104	203.014	41.073	0.2607	17
NSC1332+3756	203.026	37.928	0.1233	33
NSC1332+3115	203.111	31.249	0.1416	22
NSC1333+3902	203.145	39.026	0.1582	36
NSC1333+3135	203.156	31.587	0.1434	26
NSC1333+3302	203.188	33.031	0.1700	27
NSC1333+2955	203.222	29.912	0.2203	17
NSC1333+3745	203.229	37.752	0.2040	29
NSC1333+3253	203.232	32.890	0.2041	21
NSC1334+3942	203.461	39.697	0.1712	16
NSC1334+3921	203.464	39.354	0.1047	26
NSC1334+3858	203.498	38.968	0.1370	26
NSC1334+2808	203.588	28.126	0.1937	20
NSC1334+4123	203.614	41.376	0.1895	26
NSC1334+3127	203.619	31.451	0.0838	33
NSC1335+3136	203.635	31.592	0.1570	27
NSC1335+3442	203.635	34.708	0.2638	19
NSC1335+3328	203.639	33.473	0.1862	29
NSC1335+3543	203.659	35.719	0.2250	24
NSC1335+3822	203.678	38.371	0.0773	27
NSC1335+3251	203.690	32.853	0.2206	32
NSC1335+3057	203.735	30.944	0.2455	21
NSC1335+4101	203.806	41.022	0.2434	61
NSC1335+3558	203.821	35.975	0.1510	20
NSC1335+3832	203.850	38.540	0.1152	32
NSC1336+3220	203.878	32.330	0.2242	22
NSC1336+3001	203.887	30.011	0.1761	25
NSC1336+3324	203.887	33.397	0.1843	41
NSC1336+3051	203.887	30.842	0.2612	26
NSC1336+3552	203.972	35.864	0.0731	28
NSC1336+3235	203.983	32.577	0.2209	26
NSC1336+3121	204.015	31.358	0.1613	29
NSC1336+3850	204.015	38.842	0.1342	22
NSC1336+3837	204.084	38.624	0.2059	23
NSC1336+3422	204.089	34.370	0.2533	32
NSC1336+3640	204.089	36.663	0.2177	28
NSC1336+4111	204.123	41.184	0.1590	31
NSC1337+3609	204.147	36.156	0.1947	25
NSC1337+3523	204.157	35.378	0.1256	28
NSC1337+3451	204.175	34.845	0.0787	32
NSC1337+2930	204.191	29.502	0.1334	27
NSC1337+3352	204.208	33.874	0.2222	15
NSC1337+2750	204.208	27.838	0.1829	22
NSC1337+3631	204.212	36.509	0.1857	33
NSC1337+3226	204.225	32.428	0.1647	34
NSC1337+3954	204.300	39.894	0.1892	18
NSC1337+3327	204.303	33.451	0.2643	27
NSC1337+3938	204.329	39.626	0.1548	29
NSC1338+2752	204.376	27.871	0.1911	32
NSC1338+3050	204.401	30.836	0.1325	20
NSC1338+3834	204.451	38.561	0.1966	33
NSC1338+3857	204.458	38.950	0.2111	27
NSC1338+3504	204.511	35.060	0.2327	23
NSC1338+3247	204.530	32.786	0.2399	26
NSC1339+3643	204.690	36.713	0.2210	25
NSC1339+3346	204.722	33.761	0.2294	28
NSC1339+3315	204.776	33.257	0.2186	31
NSC1339+2750	204.823	27.834	0.1517	44
NSC1339+3908	204.871	39.139	0.2316	17
NSC1340+3824	204.904	38.398	0.1509	22
NSC1340+2922	204.927	29.362	0.1764	30
NSC1340+3342	204.975	33.705	0.2295	22
NSC1340+4228	204.997	42.472	0.1732	25
NSC1340+3901	205.046	39.015	0.1833	28
NSC1340+4117	205.100	41.291	0.2068	32
NSC1340+2852	205.119	28.869	0.1581	34
NSC1341+3720	205.239	37.328	0.2035	26
NSC1341+2918	205.243	29.308	0.1224	42
NSC1341+3848	205.271	38.800	0.1530	25
NSC1341+3734	205.274	37.569	0.1817	28
NSC1341+4001	205.284	40.020	0.2140	55
NSC1341+3706	205.291	37.103	0.1945	26
NSC1341+2949	205.331	29.823	0.0639	56
NSC1341+4223	205.335	42.387	0.2640	19
NSC1341+2841	205.354	28.690	0.0942	230
NSC1341+3321	205.359	33.346	0.1808	24
NSC1341+2853	205.367	28.877	0.1636	23
NSC1342+2820	205.416	28.339	0.0950	279
NSC1342+3941	205.480	39.680	0.1994	25
NSC1342+3249	205.491	32.809	0.2485	18
NSC1342+2829	205.602	28.488	0.0972	242
NSC1343+2949	205.627	29.821	0.0939	45
NSC1343+3905	205.637	39.089	0.1593	21
NSC1343+3937	205.652	39.608	0.1547	33
NSC1343+3342	205.681	33.695	0.1956	26

Continued...

Table B.1 - NGP Robust, Continued

Name	RA	Dec	z_{phot}	N_{gal}
NSC1343+2819	205.687	28.312	0.1119	262
NSC1343+3311	205.721	33.176	0.1727	21
NSC1343+3630	205.757	36.503	0.2502	17
NSC1343+3238	205.759	32.635	0.2584	22
NSC1343+3809	205.825	38.152	0.1896	28
NSC1343+3928	205.834	39.468	0.1751	32
NSC1343+2804	205.855	28.063	0.2392	40
NSC1343+4006	205.872	40.106	0.2187	33
NSC1344+3232	205.982	32.530	0.2364	21
NSC1344+3244	205.989	32.741	0.3081	34
NSC1344+3753	205.993	37.879	0.2096	23
NSC1344+3207	205.998	32.123	0.1585	19
NSC1344+3640	206.048	36.671	0.1711	26
NSC1344+3019	206.064	30.317	0.1896	28
NSC1344+3923	206.081	39.376	0.2739	26
NSC1345+3039	206.132	30.652	0.1782	28
NSC1345+3333	206.140	33.544	0.2038	17
NSC1345+3810	206.179	38.173	0.1788	54
NSC1345+2942	206.181	29.695	0.0961	41
NSC1345+2921	206.185	29.358	0.1898	24
NSC1345+2838	206.186	28.632	0.2790	31
NSC1345+3709	206.205	37.147	0.1793	27
NSC1345+3639	206.244	36.650	0.2044	22
NSC1345+4048	206.262	40.795	0.2412	21
NSC1345+3250	206.291	32.833	0.2372	19
NSC1345+2746	206.311	27.774	0.1539	28
NSC1345+3948	206.311	39.794	0.1839	20
NSC1345+3628	206.355	36.473	0.1569	19
NSC1345+3343	206.374	33.709	0.2263	23
NSC1346+3105	206.394	31.081	0.1990	22
NSC1346+3701	206.407	37.024	0.1470	25
NSC1346+3545	206.414	35.743	0.2260	24
NSC1346+3114	206.448	31.239	0.2076	25
NSC1346+2822	206.470	28.362	0.2355	22
NSC1346+3649	206.474	36.817	0.2765	28
NSC1346+3940	206.531	39.669	0.2192	28
NSC1346+3709	206.535	37.143	0.2401	16
NSC1346+3855	206.560	38.919	0.1705	23
NSC1347+2752	206.650	27.859	0.1804	32
NSC1347+2837	206.702	28.619	0.1751	26
NSC1347+3112	206.730	31.193	0.2333	25
NSC1347+3616	206.737	36.261	0.1999	33
NSC1347+2857	206.770	28.942	0.1933	22
NSC1347+3021	206.784	30.342	0.2002	23
NSC1347+2956	206.802	29.931	0.2259	26
NSC1347+2818	206.848	28.293	0.1161	29
NSC1347+4105	206.859	41.083	0.2223	21
NSC1348+3202	206.907	32.033	0.1207	37
NSC1348+3414	206.908	34.230	0.1629	21
NSC1348+3254	206.920	32.892	0.2135	32
NSC1348+3506	206.945	35.099	0.1762	26
NSC1348+3643	206.948	36.717	0.1625	24
NSC1348+3051	206.979	30.845	0.2497	35
NSC1348+3557	207.004	35.943	0.2147	30
NSC1348+3823	207.007	38.381	0.1812	30
NSC1348+2844	207.028	28.741	0.2174	17
NSC1348+3219	207.057	32.315	0.1071	72
NSC1348+2857	207.091	28.952	0.2729	16
NSC1349+2935	207.162	29.585	0.2657	15
NSC1349+3607	207.167	36.118	0.1590	24
NSC1349+3729	207.174	37.477	0.2248	19
NSC1349+3051	207.242	30.843	0.1687	29
NSC1349+3914	207.273	39.238	0.1430	32
NSC1349+3004	207.301	30.059	0.2619	23
NSC1349+2830	207.318	28.500	0.1529	34
NSC1349+2943	207.331	29.724	0.1665	33
NSC1349+3137	207.333	31.623	0.1313	33
NSC1349+2804	207.365	28.061	0.0856	78
NSC1350+3530	207.384	35.505	0.2471	38
NSC1350+3844	207.408	38.727	0.0932	42
NSC1350+3017	207.444	30.283	0.2632	33
NSC1350+3259	207.450	32.980	0.1808	29
NSC1350+2956	207.492	29.930	0.1359	26
NSC1350+3617	207.502	36.276	0.2221	21
NSC1350+2947	207.503	29.785	0.2330	23
NSC1350+2817	207.526	28.285	0.1258	61
NSC1350+3043	207.574	30.713	0.2084	21
NSC1350+2910	207.579	29.172	0.1029	42
NSC1351+3842	207.675	38.698	0.1876	23
NSC1351+3053	207.781	30.885	0.2476	28
NSC1351+3620	207.785	36.336	0.2052	26
NSC1351+2752	207.796	27.872	0.1839	26
NSC1351+3003	207.824	30.048	0.1304	28
NSC1352+3340	207.878	33.667	0.1292	22
NSC1352+2937	207.940	29.611	0.1674	46
NSC1352+2926	207.948	29.427	0.0908	46
NSC1352+3238	207.959	32.627	0.2382	24

Continued...

Table B.1 - NGP Robust, Continued

Name	RA	Dec	z_{phot}	N_{gal}
NSC1352+3042	207.959	30.699	0.2097	19
NSC1352+3134	208.042	31.565	0.1707	25
NSC1352+2857	208.056	28.958	0.1598	28
NSC1352+3559	208.060	35.989	0.1918	24
NSC1352+3260	208.111	32.993	0.2225	19
NSC1352+3731	208.113	37.521	0.1351	25
NSC1353+3419	208.132	34.321	0.1725	28
NSC1353+3111	208.154	31.186	0.1800	38
NSC1353+3616	208.158	36.266	0.1679	51
NSC1353+2854	208.176	28.896	0.1414	30
NSC1353+3228	208.176	32.469	0.2176	25
NSC1353+3306	208.237	33.093	0.1247	26
NSC1353+3933	208.253	39.547	0.1665	28
NSC1353+3543	208.285	35.714	0.1574	23
NSC1353+3740	208.298	37.672	0.1528	41
NSC1353+3002	208.318	30.027	0.1990	22
NSC1353+4000	208.334	40.005	0.1109	31
NSC1353+3501	208.348	35.019	0.2050	19
NSC1353+3707	208.363	37.110	0.2127	19
NSC1354+3633	208.379	36.543	0.1796	16
NSC1354+3530	208.392	35.496	0.1174	39
NSC1354+3056	208.410	30.925	0.1762	22
NSC1354+3149	208.427	31.812	0.1528	31
NSC1354+3620	208.430	36.334	0.1785	29
NSC1354+3647	208.454	36.790	0.1526	26
NSC1354+3258	208.473	32.974	0.1814	18
NSC1354+2942	208.477	29.706	0.1678	31
NSC1354+3335	208.494	33.583	0.1606	17
NSC1354+3906	208.532	39.095	0.2302	22
NSC1354+3355	208.546	33.913	0.2168	25
NSC1354+3604	208.552	36.062	0.1487	21
NSC1354+2853	208.569	28.881	0.2549	26
NSC1354+2904	208.581	29.071	0.1701	25
NSC1354+2916	208.581	29.271	0.2243	21
NSC1354+2811	208.587	28.179	0.0993	49
NSC1354+3409	208.594	34.152	0.2142	20
NSC1354+2833	208.594	28.549	0.1874	54
NSC1355+3528	208.651	35.469	0.1586	26
NSC1355+3321	208.653	33.354	0.1923	24
NSC1355+2939	208.678	29.645	0.1818	29
NSC1355+3131	208.691	31.523	0.2090	27
NSC1355+2920	208.698	29.333	0.2568	20
NSC1355+3624	208.725	36.406	0.1835	29
NSC1355+2960	208.828	29.998	0.2515	19
NSC1355+3236	208.855	32.599	0.2159	34
NSC1355+3038	208.859	30.628	0.1082	29
NSC1355+2835	208.860	28.584	0.1904	26
NSC1355+3913	208.866	39.209	0.1750	19
NSC1356+3522	208.878	35.375	0.1382	20
NSC1356+3311	208.892	33.181	0.2273	20
NSC1356+3054	208.965	30.900	0.1838	37
NSC1356+2833	209.033	28.545	0.1468	29
NSC1356+3036	209.086	30.607	0.1522	35
NSC1356+3511	209.088	35.183	0.1817	22
NSC1356+3127	209.097	31.454	0.1436	49
NSC1356+3830	209.105	38.497	0.1271	18
NSC1357+3821	209.148	38.343	0.1504	18
NSC1357+3114	209.160	31.238	0.1420	28
NSC1357+3309	209.215	33.151	0.2321	17
NSC1357+3138	209.372	31.641	0.1022	14
NSC1358+3310	209.386	33.164	0.1784	16
NSC1358+2949	209.405	29.822	0.2769	18
NSC1358+3038	209.432	30.627	0.1816	64
NSC1358+2827	209.465	28.449	0.1160	40
NSC1358+3600	209.497	36.008	0.1379	26
NSC1358+2850	209.506	28.837	0.1474	40
NSC1358+3325	209.511	33.422	0.2729	26
NSC1358+3821	209.513	38.344	0.1477	35
NSC1358+3523	209.625	35.385	0.1331	21
NSC1359+3927	209.641	39.451	0.0746	18
NSC1359+2948	209.700	29.792	0.2227	32
NSC1359+2758	209.770	27.974	0.0977	142
NSC1359+3115	209.775	31.251	0.2147	20
NSC1359+2934	209.785	29.561	0.1801	52
NSC1359+2917	209.800	29.279	0.2605	21
NSC1359+3030	209.808	30.499	0.2216	39
NSC1400+2857	209.950	28.948	0.2540	25
NSC1400+2832	210.016	28.532	0.1210	57
NSC1400+3310	210.052	33.160	0.1988	19
NSC1400+4102	210.065	41.033	0.2578	39
NSC1400+3010	210.068	30.169	0.1425	31
NSC1400+2933	210.108	29.549	0.1665	42
NSC1401+2954	210.150	29.893	0.2050	22
NSC1401+2912	210.155	29.203	0.1425	32
NSC1401+3211	210.328	32.191	0.1773	18
NSC1401+2832	210.332	28.538	0.1249	59
NSC1401+2748	210.353	27.796	0.1170	31

Continued...

Table B.1 - NGP Robust, Continued

Name	RA	Dec	z_{phot}	N_{gal}
NSC1401+2853	210.369	28.884	0.1806	25
NSC1402+2924	210.376	29.402	0.1858	29
NSC1402+3034	210.387	30.574	0.1496	43
NSC1402+2911	210.433	29.192	0.2059	20
NSC1402+3015	210.444	30.246	0.1954	23
NSC1402+4113	210.521	41.221	0.1997	16
NSC1402+4229	210.597	42.476	0.2383	22
NSC1403+2752	210.658	27.866	0.1112	52
NSC1403+2807	210.680	28.120	0.1007	37
NSC1403+3013	210.845	30.219	0.2103	37
NSC1403+3851	210.860	38.853	0.1496	25
NSC1404+2929	210.887	29.490	0.2346	31
NSC1404+3102	211.013	31.030	0.1912	40
NSC1404+2819	211.067	28.325	0.1873	20
NSC1405+3015	211.291	30.253	0.1338	19
NSC1405+2925	211.354	29.419	0.0922	21
NSC1406+4006	211.378	40.102	0.1533	21
NSC1406+2750	211.388	27.840	0.1652	21
NSC1406+2950	211.403	29.826	0.2581	20
NSC1406+3453	211.417	34.884	0.2273	17
NSC1406+4159	211.518	41.979	0.2388	26
NSC1406+4054	211.571	40.893	0.1760	20
NSC1406+4225	211.586	42.411	0.2335	24
NSC1406+3117	211.588	31.278	0.1989	21
NSC1406+2943	211.602	29.721	0.2602	21
NSC1407+3333	211.682	33.545	0.1930	22
NSC1407+2836	211.724	28.608	0.1651	32
NSC1407+2751	211.858	27.842	0.1787	54
NSC1407+3831	211.869	38.522	0.1664	25
NSC1408+3820	212.007	38.332	0.1495	30
NSC1408+3160	212.008	32.000	0.2084	20
NSC1408+4140	212.014	41.665	0.1597	18
NSC1408+2801	212.045	28.017	0.1869	29
NSC1408+3446	212.045	34.761	0.2622	22
NSC1408+3725	212.067	37.418	0.1433	19
NSC1408+3302	212.089	33.032	0.2148	22
NSC1408+2813	212.121	28.217	0.2160	31
NSC1409+3823	212.145	38.387	0.1430	30
NSC1409+3322	212.172	33.368	0.1937	20
NSC1409+3459	212.212	34.983	0.2109	23
NSC1409+3110	212.270	31.162	0.2008	41
NSC1409+3708	212.277	37.133	0.1691	33
NSC1409+2928	212.298	29.466	0.2133	25
NSC1409+4015	212.361	40.256	0.1783	20
NSC1409+3523	212.361	35.386	0.1896	21
NSC1409+3053	212.375	30.889	0.1752	27
NSC1410+4133	212.378	41.555	0.2286	15
NSC1410+3753	212.428	37.876	0.1480	26
NSC1410+3442	212.450	34.698	0.2461	24
NSC1410+2934	212.450	29.559	0.1985	21
NSC1410+2915	212.466	29.248	0.1711	33
NSC1410+4145	212.482	41.747	0.1435	33
NSC1410+3304	212.490	33.062	0.2451	22
NSC1410+3703	212.496	37.044	0.2205	15
NSC1410+3856	212.581	38.937	0.0953	16
NSC1410+2951	212.607	29.851	0.2394	23
NSC1411+3510	212.651	35.163	0.2119	19
NSC1411+4113	212.652	41.221	0.1467	24
NSC1411+3014	212.712	30.236	0.1626	27
NSC1411+4138	212.718	41.638	0.1494	19
NSC1411+2957	212.731	29.949	0.1902	35
NSC1411+3022	212.773	30.366	0.1268	35
NSC1411+2913	212.789	29.216	0.1372	32
NSC1411+4014	212.794	40.226	0.1438	20
NSC1411+2944	212.853	29.739	0.2004	23
NSC1412+2810	212.877	28.171	0.0837	32
NSC1412+3859	212.879	38.991	0.1800	16
NSC1412+3632	212.953	36.534	0.2375	24
NSC1412+3740	212.983	37.660	0.1795	27
NSC1412+3645	213.003	36.745	0.2475	25
NSC1412+2857	213.064	28.954	0.1975	20
NSC1412+3934	213.103	39.559	0.1309	16
NSC1413+3358	213.173	33.968	0.2323	16
NSC1413+4108	213.173	41.128	0.1480	26
NSC1413+2755	213.188	27.923	0.1402	26
NSC1413+3926	213.201	39.433	0.1509	16
NSC1413+2913	213.240	29.214	0.2481	44
NSC1413+4057	213.277	40.955	0.2081	18
NSC1414+2815	213.378	28.250	0.1494	24
NSC1414+3501	213.388	35.020	0.1833	20
NSC1415+4049	213.655	40.813	0.1971	31
NSC1415+3549	213.686	35.820	0.1649	19
NSC1415+4233	213.799	42.555	0.1359	15
NSC1415+4103	213.817	41.052	0.2106	19
NSC1415+2911	213.854	29.181	0.0489	19
NSC1415+2825	213.865	28.415	0.2210	19
NSC1416+3927	213.943	39.457	0.2408	18

Continued...

Table B.1 - NGP Robust, Continued

Name	RA	Dec	z_{phot}	N_{gal}
NSC1416+2926	213.945	29.435	0.0934	38
NSC1416+3856	213.948	38.929	0.0489	11
NSC1416+4049	213.954	40.808	0.1660	22
NSC1416+3509	214.030	35.149	0.1876	22
NSC1416+2811	214.062	28.192	0.1844	26
NSC1417+3045	214.144	30.749	0.1725	53
NSC1417+2837	214.258	28.623	0.1168	27
NSC1417+3554	214.270	35.896	0.2202	20
NSC1417+3440	214.330	34.671	0.2308	21
NSC1418+3410	214.389	34.160	0.1953	18
NSC1418+2803	214.429	28.052	0.1444	57
NSC1418+3751	214.470	37.857	0.1937	23
NSC1418+3609	214.482	36.154	0.1858	18
NSC1418+3722	214.526	37.371	0.1742	25
NSC1418+4110	214.588	41.164	0.1862	16
NSC1419+3750	214.704	37.825	0.1289	35
NSC1419+3957	214.730	39.951	0.2648	18
NSC1419+4145	214.789	41.752	0.1917	16
NSC1419+3937	214.821	39.623	0.2536	19
NSC1420+4111	214.881	41.176	0.2009	17
NSC1420+4129	214.885	41.486	0.2518	18
NSC1420+3504	214.893	35.065	0.1436	28
NSC1420+3206	214.899	32.106	0.2196	22
NSC1420+3611	214.912	36.184	0.1750	31
NSC1420+2756	214.918	27.937	0.1233	48
NSC1420+2851	214.949	28.852	0.0780	28
NSC1420+3541	214.992	35.681	0.1724	35
NSC1420+3112	215.007	31.204	0.1368	29
NSC1420+3923	215.033	39.380	0.1604	33
NSC1420+3413	215.088	34.217	0.2236	15
NSC1420+2907	215.118	29.124	0.1551	25
NSC1421+3513	215.197	35.209	0.1275	43
NSC1421+4020	215.294	40.332	0.1335	34
NSC1421+3603	215.295	36.058	0.1789	42
NSC1421+3817	215.340	38.290	0.2200	19
NSC1421+4134	215.366	41.561	0.1718	25
NSC1422+3732	215.418	37.534	0.1730	21
NSC1422+3715	215.430	37.253	0.1892	63
NSC1422+4012	215.435	40.197	0.1443	28
NSC1422+3535	215.437	35.582	0.1430	37
NSC1422+4222	215.451	42.367	0.2034	27
NSC1422+3407	215.473	34.114	0.1408	21
NSC1423+3848	215.640	38.792	0.1094	25
NSC1423+3818	215.663	38.301	0.1761	21
NSC1423+3520	215.671	35.326	0.1895	29
NSC1423+3503	215.697	35.043	0.1792	29
NSC1423+4233	215.727	42.556	0.2132	19
NSC1423+3337	215.729	33.621	0.1797	15
NSC1423+3400	215.731	34.007	0.2528	20
NSC1423+3413	215.755	34.208	0.2318	19
NSC1423+3207	215.810	32.117	0.1851	25
NSC1423+3939	215.868	39.654	0.1686	31
NSC1424+3514	215.942	35.239	0.1898	30
NSC1424+4013	215.948	40.224	0.1467	35
NSC1424+3329	215.997	33.486	0.2051	17
NSC1424+2937	216.030	29.613	0.1029	38
NSC1424+2811	216.042	28.177	0.1615	25
NSC1424+3857	216.105	38.956	0.2026	39
NSC1425+3709	216.236	37.154	0.1945	19
NSC1425+3757	216.264	37.955	0.1567	24
NSC1425+3844	216.265	38.734	0.1320	27
NSC1425+3332	216.323	33.535	0.1469	30
NSC1425+2943	216.352	29.713	0.1428	23
NSC1425+3935	216.361	39.576	0.1059	28
NSC1426+3257	216.395	32.956	0.2136	20
NSC1426+3323	216.425	33.378	0.2205	17
NSC1426+4035	216.460	40.577	0.2153	21
NSC1426+3737	216.495	37.621	0.1727	25
NSC1426+2801	216.514	28.019	0.1419	15
NSC1426+3750	216.514	37.833	0.1640	50
NSC1426+3442	216.613	34.694	0.1728	23
NSC1427+3213	216.656	32.213	0.2663	33
NSC1427+3230	216.670	32.508	0.1570	22
NSC1427+2935	216.703	29.576	0.1184	24
NSC1427+4205	216.732	42.086	0.1498	25
NSC1427+3413	216.748	34.211	0.1801	40
NSC1427+3248	216.802	32.792	0.2255	31
NSC1427+4235	216.865	42.577	0.1427	19
NSC1428+3847	216.910	38.782	0.1803	19
NSC1428+2932	216.994	29.529	0.1976	21
NSC1428+4051	217.073	40.851	0.1761	18
NSC1429+3455	217.130	34.922	0.1712	23
NSC1429+3422	217.169	34.374	0.1497	26
NSC1429+3510	217.188	35.174	0.1825	18
NSC1429+3239	217.194	32.645	0.1140	48
NSC1429+3146	217.231	31.770	0.1736	23
NSC1429+3251	217.300	32.857	0.1798	21

Continued...

Table B.1 - NGP Robust, Continued

Name	RA	Dec	z_{phot}	N_{gal}
NSC1430+3015	217.382	30.251	0.1315	36
NSC1430+3402	217.421	34.031	0.1537	28
NSC1430+3256	217.559	32.938	0.2276	17
NSC1430+3047	217.601	30.777	0.2137	21
NSC1431+3133	217.715	31.558	0.2272	23
NSC1431+2809	217.739	28.149	0.1736	23
NSC1431+3507	217.798	35.109	0.2501	30
NSC1431+4232	217.798	42.540	0.1405	26
NSC1431+3235	217.807	32.575	0.2423	18
NSC1431+3349	217.826	33.813	0.1896	19
NSC1431+3607	217.854	36.121	0.1916	15
NSC1431+3432	217.855	34.536	0.2179	22
NSC1432+3534	217.892	35.570	0.1503	19
NSC1432+3441	217.959	34.681	0.2017	17
NSC1432+2935	218.015	29.576	0.2437	41
NSC1432+4047	218.023	40.791	0.1781	16
NSC1432+3422	218.038	34.373	0.2069	26
NSC1432+4003	218.091	40.057	0.1612	15
NSC1432+3457	218.108	34.951	0.1830	21
NSC1432+3431	218.124	34.523	0.2354	19
NSC1433+3546	218.135	35.762	0.1551	21
NSC1433+3135	218.180	31.575	0.1342	42
NSC1433+3030	218.209	30.507	0.2065	27
NSC1433+3014	218.214	30.235	0.1507	31
NSC1433+3407	218.217	34.123	0.1399	21
NSC1433+3005	218.220	30.079	0.1631	26
NSC1433+3448	218.251	34.804	0.2297	22
NSC1433+4023	218.278	40.384	0.2056	24
NSC1433+4232	218.280	42.540	0.2483	23
NSC1433+2958	218.349	29.968	0.1706	18
NSC1434+2929	218.378	29.479	0.2429	58
NSC1434+3349	218.391	33.817	0.1471	21
NSC1434+4047	218.399	40.787	0.1878	16
NSC1434+2836	218.428	28.608	0.1429	31
NSC1434+2813	218.475	28.210	0.1119	27
NSC1434+2753	218.479	27.878	0.2074	22
NSC1434+3012	218.490	30.206	0.1544	25
NSC1434+2955	218.540	29.924	0.1606	34
NSC1434+4016	218.566	40.271	0.1610	25
NSC1435+3330	218.678	33.504	0.1802	15
NSC1435+3542	218.681	35.694	0.1515	23
NSC1435+4225	218.757	42.425	0.2219	20
NSC1435+2848	218.758	28.807	0.1837	23
NSC1435+2822	218.818	28.375	0.1699	25
NSC1435+4010	218.857	40.170	0.1824	17
NSC1435+2952	218.859	29.859	0.1819	16
NSC1435+2755	218.871	27.913	0.2023	29
NSC1436+2812	218.912	28.192	0.1588	36
NSC1436+2847	218.956	28.785	0.1938	27
NSC1436+3144	219.016	31.732	0.2232	17
NSC1436+4236	219.032	42.605	0.2639	21
NSC1436+3326	219.041	33.430	0.2552	20
NSC1436+3029	219.100	30.483	0.1441	28
NSC1436+3350	219.102	33.830	0.2880	20
NSC1436+2903	219.106	29.053	0.2256	23
NSC1436+3257	219.123	32.957	0.1509	23
NSC1437+3615	219.150	36.249	0.2190	18
NSC1437+2839	219.155	28.648	0.2548	28
NSC1437+3419	219.284	34.322	0.2255	25
NSC1437+2909	219.309	29.146	0.2169	21
NSC1438+3104	219.390	31.068	0.1481	19
NSC1438+3010	219.396	30.159	0.2576	33
NSC1438+3846	219.431	38.760	0.2250	13
NSC1438+3027	219.434	30.447	0.1862	51
NSC1438+4016	219.463	40.271	0.2122	41
NSC1438+3930	219.484	39.501	0.2396	33
NSC1438+4037	219.572	40.612	0.2047	25
NSC1439+3834	219.644	38.572	0.2236	19
NSC1439+2846	219.693	28.772	0.2301	20
NSC1439+2903	219.797	29.047	0.2156	29
NSC1439+3054	219.850	30.893	0.1282	25
NSC1440+3315	219.938	33.248	0.1517	21
NSC1440+3046	219.952	30.767	0.1420	33
NSC1440+3447	219.964	34.785	0.1456	18
NSC1440+3706	219.988	37.094	0.1236	41
NSC1440+2849	219.995	28.815	0.2538	24
NSC1441+4023	220.155	40.383	0.2139	14
NSC1441+3628	220.156	36.472	0.1680	18
NSC1441+3856	220.167	38.932	0.1680	18
NSC1441+3346	220.192	33.768	0.2408	23
NSC1441+3309	220.219	33.150	0.2492	21
NSC1441+3008	220.238	30.131	0.1700	21
NSC1441+2837	220.255	28.617	0.2021	39
NSC1441+3506	220.285	35.103	0.1395	26
NSC1441+4111	220.285	41.190	0.1901	14
NSC1442+2915	220.409	29.254	0.2203	20
NSC1442+2959	220.427	29.991	0.2276	17

Continued...

Table B.1 - NGP Robust, Continued

Name	RA	Dec	z_{phot}	N_{gal}
NSC1442+3018	220.438	30.303	0.1352	29
NSC1442+3916	220.455	39.259	0.2006	26
NSC1442+3132	220.467	31.534	0.1905	28
NSC1442+3034	220.504	30.559	0.1593	25
NSC1442+2830	220.513	28.500	0.1720	45
NSC1442+2902	220.540	29.025	0.2116	23
NSC1442+3527	220.542	35.446	0.1798	15
NSC1442+3401	220.562	34.019	0.1348	20
NSC1442+3450	220.566	34.837	0.1569	18
NSC1442+2946	220.573	29.771	0.2852	28
NSC1442+2925	220.604	29.415	0.2129	26
NSC1442+3216	220.605	32.273	0.2055	21
NSC1443+3234	220.631	32.567	0.2309	37
NSC1443+3849	220.637	38.812	0.1625	20
NSC1443+3058	220.643	30.972	0.1207	25
NSC1443+3349	220.679	33.822	0.1303	24
NSC1443+3144	220.697	31.729	0.1909	36
NSC1443+3805	220.775	38.080	0.1785	19
NSC1443+3058	220.802	30.971	0.2139	34
NSC1443+3112	220.805	31.202	0.2211	19
NSC1443+3130	220.825	31.501	0.1695	37
NSC1444+2753	220.888	27.881	0.2613	31
NSC1444+2918	220.985	29.305	0.2083	16
NSC1444+4112	220.993	41.197	0.2228	16
NSC1444+3838	220.997	38.636	0.1680	23
NSC1444+2905	220.998	29.086	0.1448	21
NSC1444+3555	221.055	35.919	0.2580	17
NSC1444+4050	221.077	40.838	0.1854	23
NSC1444+3421	221.115	34.352	0.2287	26
NSC1445+3113	221.127	31.220	0.2488	43
NSC1445+3314	221.142	33.236	0.1793	17
NSC1445+3336	221.176	33.606	0.1593	21
NSC1445+3618	221.210	36.302	0.2048	21
NSC1445+3002	221.222	30.032	0.1869	36
NSC1445+3130	221.244	31.494	0.2329	40
NSC1445+3627	221.300	36.443	0.2669	21
NSC1445+3834	221.300	38.564	0.2360	15
NSC1445+3529	221.301	35.483	0.1996	19
NSC1445+3704	221.316	37.067	0.1410	35
NSC1445+4239	221.369	42.645	0.2224	20
NSC1446+4204	221.411	42.060	0.2097	26
NSC1446+3136	221.421	31.608	0.2596	20
NSC1446+3402	221.455	34.039	0.1587	26
NSC1446+3102	221.496	31.040	0.2352	29
NSC1446+3013	221.514	30.215	0.1425	36
NSC1446+3519	221.522	35.315	0.2391	20
NSC1446+4041	221.563	40.686	0.2115	20
NSC1446+3458	221.566	34.962	0.1502	37
NSC1446+3817	221.571	38.291	0.2186	17
NSC1446+3803	221.604	38.045	0.2446	18
NSC1446+3603	221.610	36.043	0.1465	18
NSC1447+4238	221.633	42.631	0.1718	26
NSC1447+3749	221.636	37.823	0.2135	30
NSC1447+3222	221.643	32.362	0.2148	26
NSC1447+2945	221.649	29.751	0.1562	30
NSC1447+2819	221.652	28.310	0.1532	40
NSC1447+3320	221.667	33.328	0.1032	29
NSC1447+4145	221.686	41.745	0.1942	13
NSC1447+3152	221.703	31.871	0.2655	28
NSC1447+2832	221.716	28.537	0.2192	27
NSC1447+3330	221.739	33.499	0.1351	19
NSC1447+3405	221.749	34.084	0.2107	19
NSC1447+3105	221.771	31.090	0.2388	21
NSC1447+3208	221.778	32.126	0.1998	20
NSC1447+3026	221.795	30.441	0.1442	28
NSC1447+2741	221.808	27.681	0.2102	23
NSC1447+3305	221.864	33.084	0.1297	44
NSC1448+3233	221.921	32.554	0.1470	21
NSC1448+3003	221.934	30.048	0.1629	26
NSC1448+4235	221.940	42.581	0.2185	24
NSC1448+2850	221.975	28.830	0.1667	28
NSC1448+3143	222.021	31.710	0.1900	24
NSC1448+2936	222.057	29.602	0.1074	28
NSC1448+4114	222.120	41.233	0.2527	23
NSC1449+3039	222.143	30.658	0.1666	45
NSC1449+4242	222.153	42.704	0.1991	32
NSC1449+3002	222.177	30.026	0.2320	14
NSC1449+2910	222.200	29.173	0.2433	19
NSC1449+3235	222.212	32.576	0.1646	23
NSC1449+3338	222.254	33.636	0.1923	27
NSC1449+3645	222.294	36.746	0.1464	17
NSC1449+2856	222.316	28.937	0.2101	25
NSC1449+4046	222.320	40.770	0.2302	23
NSC1449+4100	222.322	41.007	0.1792	19
NSC1449+3226	222.322	32.438	0.2420	25
NSC1449+2804	222.342	28.065	0.1709	34
NSC1450+4225	222.381	42.424	0.2328	20

Continued...

Table B.1 - NGP Robust, Continued

Name	RA	Dec	z_{phot}	N_{gal}
NSC1450+3824	222.409	38.397	0.2055	19
NSC1450+3047	222.471	30.779	0.1895	42
NSC1450+4003	222.476	40.057	0.2695	22
NSC1450+3422	222.483	34.368	0.1154	23
NSC1450+4138	222.492	41.625	0.1809	23
NSC1450+4039	222.522	40.658	0.2157	19
NSC1450+4129	222.542	41.483	0.2265	26
NSC1450+3353	222.582	33.882	0.1413	43
NSC1450+3406	222.583	34.096	0.1195	21
NSC1450+3457	222.611	34.943	0.2297	22
NSC1450+3513	222.614	35.212	0.1726	29
NSC1451+2947	222.643	29.789	0.1908	28
NSC1451+3429	222.647	34.484	0.1490	30
NSC1451+3309	222.678	33.144	0.1122	23
NSC1451+2809	222.698	28.151	0.1897	22
NSC1451+3118	222.724	31.302	0.1943	61
NSC1451+3043	222.755	30.717	0.1520	57
NSC1451+3013	222.762	30.215	0.2058	28
NSC1451+2749	222.775	27.814	0.2291	25
NSC1451+3224	222.817	32.396	0.1513	32
NSC1451+3425	222.844	34.415	0.1665	20
NSC1451+3024	222.860	30.408	0.2266	39
NSC1452+3610	222.904	36.170	0.1557	21
NSC1452+3244	222.915	32.741	0.2227	28
NSC1452+3133	222.923	31.555	0.1134	31
NSC1452+2943	222.941	29.721	0.1687	27
NSC1452+4233	222.966	42.547	0.2351	28
NSC1452+4050	222.997	40.834	0.2475	23
NSC1452+3753	223.003	37.882	0.2530	37
NSC1452+3857	223.047	38.946	0.1394	18
NSC1452+3445	223.064	34.756	0.2575	24
NSC1452+3041	223.075	30.678	0.1506	33
NSC1452+3104	223.077	31.067	0.1082	30
NSC1452+3616	223.107	36.260	0.2187	15
NSC1452+2758	223.109	27.959	0.1609	46
NSC1453+2953	223.139	29.888	0.1232	30
NSC1453+3128	223.143	31.467	0.1363	20
NSC1453+3640	223.152	36.673	0.1142	21
NSC1453+3814	223.178	38.232	0.1757	28
NSC1453+3521	223.196	35.355	0.1981	17
NSC1453+2933	223.200	29.542	0.2171	18
NSC1453+3140	223.203	31.665	0.1587	31
NSC1453+4217	223.205	42.287	0.2256	21
NSC1453+2816	223.205	28.271	0.1702	23
NSC1453+3355	223.221	33.918	0.2254	17
NSC1453+4131	223.240	41.525	0.2817	33
NSC1453+3303	223.245	33.054	0.2265	15
NSC1453+3223	223.255	32.378	0.1621	33
NSC1453+4232	223.276	42.527	0.2494	26
NSC1453+3846	223.290	38.771	0.2117	17
NSC1453+3020	223.351	30.335	0.2095	26
NSC1453+3450	223.354	34.838	0.1343	29
NSC1454+3649	223.394	36.814	0.1931	23
NSC1454+4209	223.440	42.145	0.1997	18
NSC1454+4119	223.448	41.321	0.1685	16
NSC1454+2806	223.458	28.107	0.2324	36
NSC1454+3434	223.473	34.565	0.1911	25
NSC1454+3359	223.488	33.987	0.2070	22
NSC1454+3629	223.505	36.485	0.1815	21
NSC1454+2827	223.512	28.456	0.2758	24
NSC1454+4109	223.555	41.147	0.1995	18
NSC1454+3248	223.555	32.803	0.1931	21
NSC1454+3808	223.607	38.136	0.2007	20
NSC1454+2841	223.608	28.684	0.1516	21
NSC1455+3031	223.630	30.520	0.2168	23
NSC1455+3240	223.674	32.672	0.1785	25
NSC1455+3109	223.686	31.145	0.1761	30
NSC1455+3056	223.725	30.937	0.1293	31
NSC1455+3838	223.739	38.631	0.2403	19
NSC1455+3141	223.786	31.676	0.1450	38
NSC1455+3330	223.822	33.498	0.1625	20
NSC1455+3345	223.836	33.745	0.2374	21
NSC1455+4240	223.846	42.667	0.2745	20
NSC1456+3403	223.887	34.051	0.1921	21
NSC1456+3602	223.890	36.028	0.2235	18
NSC1456+3454	223.909	34.907	0.1645	21
NSC1456+2926	223.922	29.425	0.1584	23
NSC1456+3022	223.936	30.367	0.1964	21
NSC1456+2903	223.937	29.049	0.1612	27
NSC1456+3239	223.961	32.646	0.1273	30
NSC1456+3424	223.984	34.395	0.1785	17
NSC1456+2822	223.993	28.373	0.1781	17
NSC1456+3639	223.994	36.645	0.1432	19
NSC1456+3305	224.001	33.080	0.1111	27
NSC1456+2849	224.073	28.823	0.1262	37
NSC1456+3727	224.110	37.446	0.2156	19
NSC1457+2801	224.125	28.020	0.2349	27

Continued...

Table B.1 - NGP Robust, Continued

Name	RA	Dec	z_{phot}	N_{gal}
NSC1457+4141	224.130	41.676	0.1995	19
NSC1457+3036	224.136	30.608	0.1962	28
NSC1457+3736	224.245	37.598	0.1621	15
NSC1457+3324	224.260	33.408	0.2999	17
NSC1457+3314	224.302	33.233	0.2005	21
NSC1457+2746	224.304	27.768	0.2322	18
NSC1458+4240	224.397	42.668	0.2286	21
NSC1458+4143	224.406	41.715	0.1869	15
NSC1458+3708	224.411	37.132	0.1455	24
NSC1458+3435	224.449	34.575	0.1940	23
NSC1458+2938	224.495	29.640	0.1341	28
NSC1458+3409	224.537	34.146	0.1217	37
NSC1458+4040	224.559	40.662	0.2134	21
NSC1459+3312	224.632	33.201	0.1638	26
NSC1459+2904	224.635	29.064	0.2366	25
NSC1459+3617	224.648	36.280	0.2366	20
NSC1459+2750	224.654	27.833	0.1496	66
NSC1459+3758	224.657	37.968	0.1965	56
NSC1459+2931	224.677	29.519	0.1986	22
NSC1459+4240	224.678	42.663	0.2339	19
NSC1459+2917	224.759	29.282	0.2302	15
NSC1459+3737	224.809	37.618	0.1259	35
NSC1459+2757	224.816	27.952	0.2123	43
NSC1459+4209	224.842	42.155	0.2549	17
NSC1500+3022	224.886	30.360	0.2589	27
NSC1500+3331	224.897	33.517	0.1551	21
NSC1500+4225	224.901	42.414	0.2658	28
NSC1500+2821	224.917	28.347	0.2331	23
NSC1500+3348	224.923	33.797	0.1608	21
NSC1500+2942	224.929	29.695	0.1587	22
NSC1500+2903	224.931	29.056	0.1752	24
NSC1500+4239	224.971	42.649	0.2684	28
NSC1500+4107	224.972	41.114	0.1916	33
NSC1500+3456	225.051	34.934	0.2287	14
NSC1500+3643	225.055	36.711	0.1841	17
NSC1500+3728	225.056	37.464	0.1569	31
NSC1500+4119	225.072	41.314	0.1745	27
NSC1500+2816	225.074	28.269	0.1885	28
NSC1500+2853	225.104	28.877	0.1519	33
NSC1500+2943	225.106	29.724	0.1651	33
NSC1501+3714	225.126	37.236	0.1503	36
NSC1501+2907	225.135	29.111	0.1259	27
NSC1501+3628	225.166	36.468	0.1501	33
NSC1501+3211	225.209	32.191	0.1108	41
NSC1501+2814	225.307	28.233	0.2115	24
NSC1501+3742	225.344	37.702	0.1563	36
NSC1502+2847	225.395	28.787	0.1280	27
NSC1502+3756	225.400	37.930	0.1585	19
NSC1502+3213	225.409	32.215	0.1369	31
NSC1502+3803	225.458	38.055	0.1622	30
NSC1502+3642	225.464	36.697	0.1570	28
NSC1502+3120	225.472	31.332	0.1219	33
NSC1502+2804	225.558	28.067	0.2082	21
NSC1502+3747	225.600	37.780	0.1568	27
NSC1503+3547	225.637	35.775	0.1393	30
NSC1503+4035	225.661	40.582	0.1816	23
NSC1503+2860	225.672	28.995	0.1472	27
NSC1503+3810	225.721	38.171	0.1570	31
NSC1503+3553	225.747	35.876	0.1284	38
NSC1503+3359	225.778	33.989	0.1527	26
NSC1503+3717	225.786	37.278	0.1123	34
NSC1503+3609	225.800	36.148	0.1328	31
NSC1503+3452	225.825	34.867	0.2432	22
NSC1503+2806	225.832	28.102	0.1549	23
NSC1504+3740	225.876	37.668	0.0861	54
NSC1504+2900	225.876	29.005	0.1374	28
NSC1504+2754	225.885	27.904	0.1586	45
NSC1504+3243	225.911	32.721	0.2071	21
NSC1504+2917	226.064	29.286	0.1845	40
NSC1504+4034	226.082	40.564	0.1838	22
NSC1504+3028	226.090	30.471	0.1328	25
NSC1504+3556	226.105	35.942	0.0636	56
NSC1505+3534	226.215	35.569	0.0937	44
NSC1505+2827	226.216	28.456	0.1162	62
NSC1505+2935	226.232	29.589	0.1649	28
NSC1505+3605	226.240	36.086	0.0766	43
NSC1505+2851	226.264	28.844	0.1762	19
NSC1505+2811	226.272	28.181	0.2338	26
NSC1505+3856	226.284	38.938	0.1482	25
NSC1505+3652	226.302	36.869	0.0701	27
NSC1505+4144	226.312	41.725	0.1409	25
NSC1505+4230	226.333	42.502	0.1717	32
NSC1505+2917	226.345	29.279	0.1415	36
NSC1505+4214	226.357	42.229	0.1479	31
NSC1506+2859	226.411	28.990	0.1695	25
NSC1506+3347	226.435	33.784	0.2048	19
NSC1506+5311	226.512	53.185	0.1855	26

Continued...

Table B.1 - NGP Robust, Continued

Name	RA	Dec	z_{phot}	N_{gal}
NSC1506+4200	226.609	42.008	0.2297	18
NSC1507+2750	226.646	27.841	0.2397	18
NSC1507+3224	226.672	32.395	0.1777	30
NSC1507+2835	226.684	28.577	0.1935	28
NSC1507+3054	226.706	30.898	0.2437	23
NSC1507+3430	226.709	34.495	0.1842	61
NSC1508+2811	226.896	28.178	0.2465	15
NSC1508+4242	226.897	42.700	0.2031	44
NSC1508+3256	226.913	32.934	0.2398	25
NSC1508+3931	226.930	39.522	0.1007	28
NSC1508+2847	226.932	28.787	0.1971	25
NSC1508+3821	226.988	38.342	0.2070	24
NSC1508+3436	227.021	34.593	0.1736	32
NSC1508+2914	227.033	29.239	0.1622	48
NSC1508+4236	227.037	42.602	0.2180	27
NSC1508+3607	227.053	36.110	0.0742	43
NSC1508+2858	227.085	28.964	0.1750	25
NSC1508+2936	227.091	29.604	0.1162	50
NSC1508+3619	227.118	36.310	0.0977	36
NSC1509+3258	227.159	32.967	0.2387	40
NSC1509+2746	227.177	27.761	0.1640	26
NSC1509+4109	227.203	41.145	0.2130	21
NSC1509+2814	227.224	28.240	0.2174	28
NSC1509+4209	227.239	42.153	0.2170	21
NSC1509+3015	227.239	30.249	0.1801	47
NSC1509+3042	227.245	30.705	0.1893	22
NSC1509+2951	227.267	29.851	0.1387	26
NSC1509+2924	227.285	29.401	0.1707	31
NSC1509+3458	227.295	34.971	0.1671	37
NSC1509+3860	227.300	38.999	0.1614	24
NSC1509+4024	227.309	40.395	0.2269	25
NSC1509+3106	227.363	31.104	0.1668	17
NSC1510+4106	227.376	41.108	0.1645	16
NSC1510+3422	227.378	34.367	0.1817	30
NSC1510+3719	227.398	37.308	0.2103	32
NSC1510+2753	227.401	27.877	0.1677	39
NSC1510+3351	227.405	33.853	0.2649	16
NSC1510+3646	227.447	36.763	0.1528	46
NSC1510+3431	227.488	34.512	0.2057	28
NSC1510+3329	227.515	33.490	0.1225	129
NSC1510+3714	227.603	37.240	0.1743	22
NSC1511+3942	227.628	39.697	0.2206	18
NSC1511+3348	227.629	33.800	0.1782	29
NSC1511+2810	227.639	28.170	0.2491	18
NSC1511+4058	227.642	40.960	0.2916	13
NSC1511+3402	227.643	34.040	0.2160	27
NSC1511+4142	227.649	41.697	0.1722	25
NSC1511+3649	227.651	36.810	0.1628	45
NSC1511+2925	227.654	29.419	0.1305	28
NSC1511+3240	227.712	32.672	0.1774	40
NSC1511+3636	227.806	36.602	0.1690	43
NSC1511+4232	227.810	42.537	0.1961	17
NSC1511+3704	227.837	37.069	0.1347	65
NSC1512+4220	227.882	42.334	0.1459	25
NSC1512+4143	227.897	41.721	0.2496	34
NSC1512+3449	227.912	34.818	0.2115	35
NSC1512+4031	227.923	40.511	0.1693	18
NSC1512+3418	227.962	34.304	0.2975	13
NSC1512+2807	227.964	28.123	0.1695	23
NSC1512+2756	227.964	27.927	0.1531	18
NSC1512+3656	228.000	36.941	0.1974	40
NSC1512+3503	228.032	35.044	0.1828	37
NSC1512+3052	228.037	30.870	0.1135	24
NSC1512+2750	228.066	27.835	0.1335	21
NSC1512+3551	228.094	35.858	0.2258	29
NSC1512+2936	228.123	29.604	0.2046	25
NSC1513+3711	228.126	37.191	0.1585	19
NSC1513+3525	228.145	35.421	0.1453	48
NSC1513+3518	228.154	35.302	0.2103	32
NSC1513+3642	228.154	36.706	0.2253	32
NSC1513+4318	228.179	43.297	0.1965	28
NSC1513+3727	228.237	37.446	0.2079	32
NSC1513+3445	228.241	34.746	0.1705	35
NSC1513+3020	228.242	30.326	0.2021	18
NSC1513+3058	228.286	30.968	0.1746	17
NSC1513+4330	228.288	43.499	0.2229	28
NSC1513+3359	228.349	33.977	0.1278	29
NSC1513+3602	228.350	36.033	0.1434	40
NSC1514+2803	228.399	28.049	0.1871	29
NSC1514+3537	228.414	35.623	0.1173	35
NSC1514+3738	228.433	37.636	0.1646	32
NSC1514+3526	228.471	35.431	0.1894	24
NSC1514+4138	228.485	41.629	0.1427	30
NSC1514+3618	228.488	36.307	0.1419	39
NSC1514+5445	228.508	54.749	0.1434	29
NSC1514+4336	228.525	43.598	0.2234	22
NSC1514+3007	228.531	30.125	0.1536	16

Continued...

Table B.1 - NGP Robust, Continued

Name	RA	Dec	z_{phot}	N_{gal}
NSC1514+3658	228.580	36.973	0.1962	24
NSC1515+4140	228.666	41.667	0.1676	20
NSC1515+2856	228.676	28.930	0.1668	26
NSC1515+3618	228.710	36.294	0.1403	39
NSC1515+3626	228.741	36.429	0.1517	33
NSC1515+3032	228.749	30.531	0.2403	37
NSC1515+5417	228.790	54.283	0.1726	18
NSC1515+3945	228.793	39.748	0.1482	21
NSC1515+4341	228.797	43.683	0.2096	25
NSC1515+4121	228.810	41.356	0.1849	27
NSC1515+5532	228.851	55.525	0.1307	34
NSC1515+3541	228.852	35.678	0.1812	29
NSC1515+3149	228.861	31.824	0.1388	34
NSC1515+3723	228.869	37.378	0.1927	55
NSC1515+2845	228.870	28.746	0.1622	25
NSC1516+4545	228.890	45.742	0.1927	19
NSC1516+4348	228.901	43.793	0.1587	24
NSC1516+2800	228.929	28.003	0.1386	21
NSC1516+5620	228.968	56.330	0.1472	52
NSC1516+3444	228.979	34.730	0.1395	28
NSC1516+4126	228.996	41.431	0.1908	22
NSC1516+3831	229.016	38.514	0.2041	25
NSC1516+2938	229.060	29.635	0.3002	19
NSC1516+4160	229.078	41.996	0.2768	16
NSC1516+4846	229.091	48.772	0.1712	24
NSC1516+4315	229.102	43.254	0.2117	20
NSC1516+2827	229.107	28.455	0.1447	27
NSC1516+3119	229.125	31.311	0.1494	21
NSC1517+5421	229.131	54.355	0.1605	21
NSC1517+3012	229.132	30.196	0.1877	15
NSC1517+3557	229.141	35.952	0.1748	28
NSC1517+3613	229.167	36.210	0.2036	32
NSC1517+2922	229.185	29.364	0.1765	30
NSC1517+5553	229.228	55.891	0.2068	20
NSC1517+3312	229.248	33.202	0.1318	52
NSC1517+3104	229.264	31.067	0.2106	15
NSC1517+3322	229.266	33.363	0.1194	57
NSC1517+4416	229.285	44.260	0.1428	24
NSC1517+3116	229.294	31.272	0.2305	23
NSC1517+3351	229.295	33.854	0.1029	32
NSC1517+2841	229.320	28.683	0.2202	19
NSC1517+4329	229.325	43.483	0.1624	28
NSC1517+3531	229.335	35.518	0.2014	20
NSC1518+5321	229.392	53.355	0.1955	28
NSC1518+2753	229.395	27.888	0.1305	43
NSC1518+3622	229.398	36.365	0.1296	25
NSC1518+3244	229.403	32.740	0.2039	20
NSC1518+5050	229.433	50.836	0.1828	16
NSC1518+4401	229.455	44.024	0.1568	29
NSC1518+5330	229.459	53.495	0.2254	33
NSC1518+2952	229.491	29.861	0.2022	15
NSC1518+2849	229.499	28.823	0.2097	24
NSC1518+3635	229.503	36.583	0.1923	38
NSC1518+3311	229.528	33.190	0.1283	39
NSC1518+4146	229.529	41.759	0.1174	17
NSC1518+3549	229.546	35.816	0.2238	35
NSC1518+5609	229.552	56.147	0.1450	37
NSC1518+3117	229.555	31.291	0.1655	27
NSC1518+3517	229.561	35.288	0.2075	22
NSC1518+3716	229.574	37.264	0.1417	30
NSC1518+5056	229.618	50.926	0.1522	21
NSC1519+3538	229.690	35.632	0.1880	29
NSC1519+2843	229.730	28.722	0.1655	38
NSC1519+4346	229.785	43.775	0.1683	18
NSC1519+2820	229.794	28.333	0.1032	57
NSC1519+4505	229.799	45.078	0.1039	24
NSC1519+2900	229.854	29.004	0.1281	45
NSC1520+4424	229.880	44.405	0.1066	20
NSC1520+2747	229.895	27.779	0.1081	29
NSC1520+3135	229.902	31.580	0.1885	22
NSC1520+4113	229.911	41.209	0.2115	28
NSC1520+3542	229.927	35.701	0.2116	34
NSC1520+3612	229.958	36.200	0.1874	25
NSC1520+4354	229.991	43.906	0.1913	20
NSC1520+5120	229.995	51.337	0.1381	21
NSC1520+3107	230.037	31.115	0.1203	28
NSC1520+3245	230.038	32.757	0.0975	55
NSC1520+4130	230.056	41.506	0.2269	32
NSC1520+4335	230.066	43.588	0.1940	32
NSC1520+4825	230.073	48.411	0.2043	21
NSC1520+3537	230.094	35.612	0.2531	27
NSC1520+2851	230.112	28.845	0.1212	61
NSC1521+4608	230.183	46.126	0.1491	28
NSC1521+3323	230.192	33.384	0.2149	47
NSC1521+3548	230.201	35.799	0.2503	20
NSC1521+3525	230.210	35.411	0.2199	25
NSC1521+4345	230.223	43.758	0.1329	34

Continued...

Table B.1 - NGP Robust, Continued

Name	RA	Dec	z_{phot}	N_{gal}
NSC1521+3650	230.256	36.829	0.2003	27
NSC1521+4840	230.306	48.660	0.1057	52
NSC1521+3040	230.327	30.665	0.0994	94
NSC1521+2806	230.332	28.101	0.1362	69
NSC1521+3619	230.338	36.320	0.1529	29
NSC1521+2834	230.342	28.558	0.1458	31
NSC1521+2927	230.365	29.443	0.1478	43
NSC1522+3208	230.397	32.140	0.1161	68
NSC1522+3351	230.434	33.851	0.2128	35
NSC1522+3714	230.496	37.233	0.0953	29
NSC1522+3729	230.536	37.486	0.2533	26
NSC1522+3701	230.540	37.022	0.0981	32
NSC1522+4832	230.548	48.535	0.1394	29
NSC1522+3114	230.565	31.226	0.1728	25
NSC1522+4338	230.586	43.640	0.2455	23
NSC1522+3132	230.595	31.529	0.1201	28
NSC1522+2828	230.619	28.466	0.1116	47
NSC1522+2749	230.621	27.811	0.0813	151
NSC1523+3144	230.637	31.738	0.1834	16
NSC1523+2959	230.648	29.990	0.1111	41
NSC1523+3642	230.651	36.693	0.1087	35
NSC1523+4217	230.655	42.276	0.1376	26
NSC1523+3823	230.662	38.379	0.1577	21
NSC1523+4051	230.673	40.851	0.2454	18
NSC1523+3542	230.694	35.693	0.1442	35
NSC1523+5741	230.697	57.682	0.0325	5
NSC1523+3506	230.803	35.104	0.2641	20
NSC1523+3059	230.810	30.991	0.1270	62
NSC1523+3216	230.823	32.260	0.1622	26
NSC1524+3306	230.891	33.097	0.1988	22
NSC1524+2816	230.893	28.259	0.1782	33
NSC1524+2908	230.901	29.130	0.1448	23
NSC1524+3613	230.911	36.209	0.1879	35
NSC1524+3137	230.919	31.619	0.1597	16
NSC1524+4348	230.923	43.795	0.1283	28
NSC1524+2844	230.946	28.732	0.1106	38
NSC1524+4134	230.980	41.563	0.1371	23
NSC1524+4414	231.001	44.235	0.1939	35
NSC1524+4750	231.004	47.827	0.1559	18
NSC1524+4325	231.029	43.424	0.2296	23
NSC1524+2955	231.070	29.919	0.1347	79
NSC1524+3245	231.088	32.754	0.1460	34
NSC1524+2748	231.109	27.798	0.1116	55
NSC1524+3528	231.117	35.464	0.2396	34
NSC1524+3518	231.120	35.294	0.2279	48
NSC1525+3135	231.156	31.576	0.2200	19
NSC1525+3700	231.218	37.008	0.2026	52
NSC1525+4838	231.266	48.639	0.2093	14
NSC1525+3327	231.272	33.458	0.1779	34
NSC1525+4545	231.314	45.756	0.2116	27
NSC1525+4359	231.322	43.982	0.2030	25
NSC1525+3534	231.324	35.561	0.2256	30
NSC1525+4129	231.337	41.484	0.1460	23
NSC1526+3210	231.382	32.167	0.1748	23
NSC1526+4722	231.385	47.362	0.1761	26
NSC1526+2829	231.390	28.477	0.1469	49
NSC1526+3510	231.452	35.174	0.2297	25
NSC1526+4260	231.455	42.997	0.1380	15
NSC1526+3057	231.463	30.952	0.2008	23
NSC1526+3532	231.489	35.526	0.1598	28
NSC1526+3752	231.510	37.869	0.1434	36
NSC1526+3635	231.547	36.590	0.1796	20
NSC1526+2843	231.547	28.716	0.1897	21
NSC1526+3621	231.582	36.345	0.0897	49
NSC1526+2818	231.606	28.304	0.1404	27
NSC1526+2956	231.609	29.939	0.1048	37
NSC1526+5424	231.620	54.392	0.1409	20
NSC1527+3551	231.659	35.857	0.1127	24
NSC1527+2939	231.666	29.643	0.0984	44
NSC1527+3319	231.678	33.323	0.0897	38
NSC1527+5138	231.690	51.626	0.1572	33
NSC1527+3309	231.705	33.156	0.0803	38
NSC1527+3457	231.755	34.953	0.1617	27
NSC1527+2821	231.790	28.348	0.1398	34
NSC1527+3621	231.870	36.342	0.2366	23
NSC1528+3521	231.904	35.354	0.0754	43
NSC1528+4147	231.909	41.785	0.1898	52
NSC1528+3458	231.926	34.967	0.2041	23
NSC1528+2848	231.957	28.794	0.1219	67
NSC1528+3041	231.957	30.689	0.2157	24
NSC1528+4129	231.964	41.489	0.1805	35
NSC1528+4106	232.003	41.101	0.1677	34
NSC1528+3358	232.020	33.971	0.1977	21
NSC1528+3030	232.086	30.497	0.1166	34
NSC1528+3642	232.093	36.695	0.1413	40
NSC1528+4352	232.100	43.862	0.0840	25
NSC1529+2818	232.134	28.305	0.0982	40

Continued...

Table B.1 - NGP Robust, Continued

Name	RA	Dec	z_{phot}	N_{gal}
NSC1529+3751	232.136	37.843	0.2286	19
NSC1529+3306	232.153	33.097	0.0401	25
NSC1529+2933	232.154	29.548	0.1215	31
NSC1529+2904	232.157	29.062	0.1639	38
NSC1529+2830	232.168	28.498	0.1455	22
NSC1529+4259	232.185	42.984	0.1877	29
NSC1529+3430	232.201	34.497	0.1497	28
NSC1529+3616	232.201	36.261	0.2081	18
NSC1529+3537	232.212	35.609	0.1750	27
NSC1529+3049	232.250	30.809	0.1274	34
NSC1529+4242	232.252	42.703	0.1598	32
NSC1529+5252	232.331	52.872	0.0880	35
NSC1529+3458	232.356	34.963	0.1822	25
NSC1529+3124	232.372	31.395	0.2577	23
NSC1530+5310	232.394	53.173	0.1048	23
NSC1530+5532	232.417	55.540	0.1449	23
NSC1530+3043	232.437	30.710	0.1846	39
NSC1530+4402	232.449	44.039	0.2319	23
NSC1530+2903	232.477	29.043	0.1408	47
NSC1530+2821	232.495	28.342	0.1784	30
NSC1530+3517	232.548	35.288	0.1971	43
NSC1530+4304	232.555	43.070	0.1218	35
NSC1530+3540	232.589	35.670	0.1532	35
NSC1530+5028	232.601	50.465	0.1221	25
NSC1530+3212	232.608	32.199	0.2009	24
NSC1530+3710	232.621	37.172	0.0840	25
NSC1531+3326	232.627	33.429	0.0874	31
NSC1531+3046	232.643	30.762	0.1235	24
NSC1531+3253	232.719	32.880	0.1314	34
NSC1531+2756	232.726	27.935	0.1546	36
NSC1531+3137	232.737	31.614	0.1871	17
NSC1531+5057	232.752	50.945	0.1044	28
NSC1531+2931	232.788	29.509	0.2069	23
NSC1531+2856	232.792	28.934	0.1086	37
NSC1531+3856	232.839	38.931	0.1508	36
NSC1531+3317	232.857	33.281	0.0911	31
NSC1531+3201	232.865	32.014	0.2185	28
NSC1531+5157	232.866	51.956	0.1828	20
NSC1531+3427	232.872	34.443	0.1489	35
NSC1532+3845	232.901	38.749	0.1735	31
NSC1532+4420	232.902	44.333	0.0436	19
NSC1532+3704	232.917	37.066	0.1750	25
NSC1532+3355	232.934	33.914	0.1543	39
NSC1532+3125	232.995	31.425	0.2109	19
NSC1532+3501	233.008	35.014	0.1999	17
NSC1532+2830	233.013	28.497	0.2398	22
NSC1532+3019	233.031	30.309	0.2054	17
NSC1532+4340	233.047	43.669	0.1324	22
NSC1532+3051	233.078	30.854	0.1303	29
NSC1532+5131	233.094	51.518	0.2049	22
NSC1532+3901	233.105	39.017	0.2178	27
NSC1533+2804	233.140	28.070	0.1078	54
NSC1533+3221	233.156	32.351	0.2279	28
NSC1533+4049	233.156	40.815	0.1984	34
NSC1533+3603	233.159	36.056	0.0703	19
NSC1533+4306	233.165	43.102	0.1530	33
NSC1533+3434	233.224	34.572	0.1592	30
NSC1533+4350	233.246	43.837	0.1913	31
NSC1533+3412	233.250	34.194	0.2501	24
NSC1533+4943	233.261	49.711	0.1822	28
NSC1533+3812	233.263	38.195	0.1357	32
NSC1533+4918	233.271	49.302	0.1567	22
NSC1533+3341	233.296	33.685	0.0834	32
NSC1533+3704	233.333	37.066	0.1366	33
NSC1533+3425	233.343	34.418	0.1340	29
NSC1533+3241	233.346	32.677	0.2134	20
NSC1533+3111	233.349	31.179	0.1151	51
NSC1534+3143	233.405	31.713	0.1518	29
NSC1534+3034	233.436	30.573	0.0912	31
NSC1534+2924	233.451	29.399	0.1455	33
NSC1534+4343	233.452	43.716	0.1913	25
NSC1534+3613	233.478	36.212	0.0824	24
NSC1534+4508	233.503	45.130	0.0000	3
NSC1534+4618	233.503	46.298	0.1602	22
NSC1534+3123	233.538	31.378	0.1133	41
NSC1534+3456	233.550	34.936	0.1482	34
NSC1534+3335	233.552	33.582	0.1757	35
NSC1534+3705	233.571	37.077	0.1381	60
NSC1534+3214	233.592	32.227	0.1773	33
NSC1534+3054	233.603	30.902	0.1818	15
NSC1534+2827	233.624	28.447	0.1280	22
NSC1535+2857	233.654	28.948	0.1988	18
NSC1535+2920	233.667	29.340	0.1734	23
NSC1535+4533	233.668	45.551	0.1923	15
NSC1535+3650	233.670	36.839	0.1783	35
NSC1535+3143	233.689	31.711	0.1609	29
NSC1535+4031	233.696	40.515	0.2106	45

Continued...

Table B.1 - NGP Robust, Continued

Name	RA	Dec	z_{phot}	N_{gal}
NSC1535+2930	233.710	29.493	0.2097	19
NSC1535+2910	233.733	29.170	0.1886	27
NSC1535+3455	233.767	34.910	0.1850	23
NSC1535+3202	233.782	32.031	0.2113	25
NSC1535+4347	233.799	43.791	0.1917	23
NSC1535+4144	233.801	41.732	0.0876	34
NSC1535+3624	233.804	36.395	0.1692	23
NSC1535+3422	233.811	34.368	0.2241	37
NSC1535+3221	233.824	32.349	0.1718	29
NSC1535+3918	233.830	39.304	0.1427	23
NSC1535+3722	233.839	37.369	0.1234	102
NSC1536+3332	233.889	33.538	0.1269	43
NSC1536+3836	233.897	38.600	0.1575	26
NSC1536+3802	233.906	38.030	0.1924	31
NSC1536+3016	233.936	30.263	0.2315	18
NSC1536+3642	233.958	36.708	0.2017	23
NSC1536+5127	233.985	51.443	0.1596	23
NSC1536+3235	234.013	32.575	0.1468	23
NSC1536+2756	234.020	27.941	0.1297	28
NSC1536+3456	234.025	34.930	0.1645	29
NSC1536+3532	234.052	35.533	0.1638	32
NSC1536+3106	234.089	31.099	0.1804	19
NSC1536+3738	234.116	37.636	0.1261	96
NSC1537+5348	234.130	53.801	0.1915	17
NSC1537+5220	234.130	52.335	0.1711	24
NSC1537+3130	234.145	31.494	0.1920	21
NSC1537+3359	234.146	33.980	0.1731	24
NSC1537+3118	234.153	31.305	0.1665	23
NSC1537+3634	234.179	36.565	0.1882	31
NSC1537+5123	234.208	51.375	0.1219	23
NSC1537+4931	234.213	49.512	0.2229	16
NSC1537+3751	234.216	37.848	0.1239	75
NSC1537+3454	234.216	34.906	0.1838	36
NSC1537+3202	234.235	32.027	0.2296	20
NSC1537+3827	234.239	38.443	0.1734	19
NSC1537+2933	234.255	29.548	0.1841	18
NSC1537+3253	234.287	32.891	0.1096	27
NSC1537+3102	234.292	31.029	0.1310	19
NSC1538+3209	234.388	32.157	0.1686	20
NSC1538+3931	234.393	39.516	0.2363	26
NSC1538+3822	234.415	38.366	0.1392	30
NSC1538+5136	234.415	51.592	0.1808	23
NSC1538+2754	234.466	27.896	0.0360	13
NSC1538+4548	234.535	45.797	0.1738	17
NSC1538+4354	234.548	43.900	0.1200	15
NSC1538+3155	234.557	31.915	0.2184	22
NSC1538+4305	234.569	43.085	0.1571	18
NSC1538+5323	234.594	53.377	0.2208	32
NSC1539+3209	234.685	32.143	0.0786	21
NSC1539+5455	234.718	54.922	0.1724	18
NSC1539+3338	234.728	33.639	0.1648	61
NSC1539+4611	234.732	46.191	0.1604	28
NSC1539+3053	234.746	30.883	0.1215	26
NSC1539+3751	234.792	37.851	0.1498	38
NSC1539+4627	234.805	46.456	0.1936	23
NSC1539+3401	234.835	34.011	0.0813	28
NSC1539+2958	234.846	29.959	0.1830	19
NSC1539+4532	234.866	45.534	0.1613	28
NSC1539+4942	234.868	49.697	0.2212	21
NSC1540+5309	234.916	53.142	0.1686	21
NSC1540+3421	234.934	34.346	0.2035	67
NSC1540+3547	234.948	35.777	0.1105	39
NSC1540+3907	234.982	39.113	0.1938	26
NSC1540+3043	235.026	30.724	0.1105	53
NSC1540+3213	235.061	32.218	0.2502	20
NSC1540+5155	235.069	51.925	0.1471	32
NSC1540+4300	235.072	43.007	0.1932	29
NSC1540+3321	235.084	33.354	0.0998	37
NSC1540+3459	235.120	34.976	0.1878	34
NSC1541+3432	235.172	34.525	0.1808	29
NSC1541+3409	235.185	34.142	0.1840	30
NSC1541+4223	235.200	42.386	0.0935	22
NSC1541+3119	235.226	31.312	0.1546	25
NSC1541+4545	235.230	45.750	0.2068	27
NSC1541+3342	235.247	33.705	0.1502	31
NSC1541+4634	235.272	46.573	0.1650	20
NSC1541+4725	235.353	47.417	0.1932	27
NSC1541+3427	235.363	34.448	0.1579	30
NSC1541+5141	235.371	51.676	0.1771	35
NSC1542+3410	235.377	34.172	0.2115	21
NSC1542+3348	235.386	33.795	0.1463	36
NSC1542+3454	235.405	34.896	0.2057	17
NSC1542+4826	235.429	48.431	0.1150	25
NSC1542+3554	235.454	35.892	0.1748	25
NSC1542+4336	235.454	43.601	0.1597	25
NSC1542+3302	235.464	33.025	0.1562	30
NSC1542+3221	235.476	32.351	0.1038	25

Continued...

Table B.1 - NGP Robust, Continued

Name	RA	Dec	z_{phot}	N_{gal}
NSC1542+4810	235.485	48.162	0.2080	44
NSC1542+2954	235.505	29.902	0.1608	25
NSC1542+3643	235.512	36.721	0.1785	35
NSC1542+2816	235.514	28.271	0.0534	37
NSC1542+5449	235.528	54.823	0.2271	25
NSC1542+4232	235.548	42.539	0.1668	22
NSC1542+3621	235.552	36.349	0.0464	23
NSC1542+4246	235.583	42.761	0.2054	38
NSC1542+5304	235.593	53.059	0.1338	18
NSC1542+4757	235.596	47.943	0.1709	21
NSC1542+4348	235.604	43.800	0.2443	24
NSC1543+4149	235.652	41.820	0.1292	68
NSC1543+2751	235.655	27.848	0.1546	20
NSC1543+3225	235.689	32.419	0.1644	25
NSC1543+3208	235.690	32.131	0.1938	25
NSC1543+3501	235.693	35.008	0.1339	38
NSC1543+3536	235.702	35.596	0.1705	33
NSC1543+3321	235.732	33.352	0.0813	18
NSC1543+3310	235.781	33.169	0.0618	35
NSC1543+4211	235.795	42.178	0.1188	29
NSC1543+3625	235.808	36.422	0.0754	39
NSC1543+3239	235.859	32.658	0.1583	21
NSC1543+3553	235.871	35.884	0.1374	34
NSC1544+3413	235.893	34.217	0.1059	28
NSC1544+3720	235.898	37.335	0.1637	19
NSC1544+3434	235.903	34.562	0.1252	54
NSC1544+4644	235.969	46.733	0.2208	26
NSC1544+5120	235.992	51.329	0.1922	36
NSC1544+3613	236.018	36.210	0.1145	54
NSC1544+3330	236.070	33.493	0.1221	27
NSC1544+4731	236.099	47.510	0.1963	29
NSC1544+5128	236.114	51.473	0.2000	39
NSC1544+4751	236.124	47.856	0.1262	24
NSC1545+5345	236.125	53.755	0.1156	26
NSC1545+3442	236.147	34.694	0.0933	62
NSC1545+4128	236.164	41.469	0.1023	31
NSC1545+4626	236.182	46.437	0.1494	47
NSC1545+3250	236.228	32.830	0.1891	24
NSC1545+3607	236.233	36.113	0.0854	78
NSC1545+5441	236.235	54.681	0.1954	18
NSC1545+3525	236.242	35.418	0.1064	37
NSC1545+3234	236.246	32.573	0.2074	23
NSC1545+3624	236.260	36.407	0.2318	22
NSC1545+4819	236.299	48.314	0.1541	26
NSC1545+4913	236.308	49.221	0.1846	21
NSC1545+3324	236.329	33.406	0.0637	27
NSC1545+3547	236.338	35.785	0.1143	55
NSC1545+3260	236.343	32.993	0.1630	30
NSC1545+4612	236.345	46.196	0.2133	30
NSC1546+3407	236.381	34.117	0.0880	47
NSC1546+5328	236.398	53.468	0.2069	24
NSC1546+4427	236.412	44.456	0.1119	25
NSC1546+5056	236.467	50.935	0.1833	22
NSC1546+3449	236.484	34.822	0.1741	23
NSC1546+4738	236.499	47.640	0.1381	24
NSC1546+4848	236.513	48.806	0.1433	24
NSC1546+3402	236.520	34.035	0.0882	47
NSC1546+2826	236.523	28.436	0.1691	23
NSC1546+4816	236.565	48.269	0.2119	19
NSC1546+3237	236.567	32.609	0.1718	19
NSC1546+4751	236.598	47.856	0.2281	19
NSC1546+4907	236.613	49.119	0.2423	23
NSC1546+3025	236.617	30.414	0.0464	23
NSC1547+5505	236.649	55.078	0.2170	26
NSC1547+3658	236.680	36.967	0.1213	10
NSC1547+5026	236.690	50.436	0.2101	21
NSC1547+3307	236.690	33.113	0.1028	54
NSC1547+2811	236.709	28.183	0.1025	42
NSC1547+3539	236.738	35.655	0.1193	46
NSC1547+2928	236.741	29.460	0.0921	36
NSC1547+4308	236.761	43.125	0.0127	3
NSC1547+2918	236.782	29.295	0.1031	27
NSC1547+4056	236.788	40.931	0.1895	28
NSC1547+2758	236.819	27.973	0.0782	48
NSC1547+4745	236.874	47.757	0.1430	38
NSC1548+4526	236.889	45.439	0.1855	24
NSC1548+3319	236.927	33.316	0.0968	61
NSC1548+4922	236.942	49.371	0.2302	18
NSC1548+5442	236.986	54.699	0.1582	27
NSC1548+3636	236.992	36.595	0.2361	41
NSC1548+3452	236.999	34.875	0.1430	35
NSC1548+3552	237.011	35.865	0.1919	22
NSC1548+2857	237.038	28.943	0.1420	22
NSC1548+2754	237.046	27.900	0.0900	45
NSC1548+2908	237.066	29.131	0.1093	17
NSC1548+5514	237.077	55.234	0.1903	25
NSC1548+3627	237.120	36.443	0.1201	28

Continued...

Table B.1 - NGP Robust, Continued

Name	RA	Dec	z_{phot}	N_{gal}
NSC1549+5110	237.132	51.168	0.1729	25
NSC1549+3605	237.143	36.076	0.2275	38
NSC1549+3433	237.163	34.546	0.1074	27
NSC1549+3314	237.188	33.233	0.1325	38
NSC1549+3328	237.199	33.462	0.1799	28
NSC1549+4507	237.217	45.124	0.0550	11
NSC1549+5550	237.238	55.836	0.1621	30
NSC1549+3029	237.298	30.477	0.1809	20
NSC1549+3355	237.324	33.918	0.1886	36
NSC1549+3217	237.329	32.287	0.1421	23
NSC1549+3155	237.342	31.912	0.1350	24
NSC1550+3208	237.414	32.128	0.1398	31
NSC1550+3331	237.414	33.509	0.1328	36
NSC1550+3620	237.429	36.327	0.1940	46
NSC1550+2835	237.439	28.578	0.1110	49
NSC1550+2910	237.472	29.159	0.0873	57
NSC1550+3313	237.474	33.213	0.2378	17
NSC1550+5126	237.484	51.428	0.1419	29
NSC1550+3826	237.545	38.428	0.1154	23
NSC1550+2836	237.622	28.599	0.0916	67
NSC1551+3337	237.631	33.610	0.1564	26
NSC1551+3622	237.660	36.374	0.1621	40
NSC1551+3030	237.665	30.494	0.1783	18
NSC1551+4735	237.674	47.590	0.1532	28
NSC1551+2850	237.709	28.830	0.1532	34
NSC1551+5027	237.743	50.447	0.1529	30
NSC1551+4327	237.772	43.454	0.2053	22
NSC1551+2823	237.773	28.389	0.1019	43
NSC1551+3331	237.792	33.517	0.1304	39
NSC1551+3253	237.807	32.878	0.1140	34
NSC1551+2807	237.814	28.111	0.1785	23
NSC1551+3232	237.839	32.534	0.1586	20
NSC1552+5325	237.884	53.420	0.0812	34
NSC1552+3437	237.892	34.622	0.0822	19
NSC1552+4534	237.922	45.573	0.1156	45
NSC1552+3112	237.926	31.203	0.2220	22
NSC1552+3627	237.936	36.456	0.1779	30
NSC1552+2753	237.981	27.877	0.0929	56
NSC1552+3332	238.063	33.526	0.1901	41
NSC1552+3647	238.110	36.782	0.1552	19
NSC1552+3555	238.119	35.923	0.1262	35
NSC1553+4620	238.141	46.340	0.1626	25
NSC1553+3404	238.145	34.066	0.0702	46
NSC1553+4309	238.174	43.143	0.1469	24
NSC1553+3437	238.180	34.623	0.1088	23
NSC1553+4160	238.196	41.993	0.1187	30
NSC1553+3225	238.228	32.417	0.1822	20
NSC1553+2760	238.303	27.998	0.1004	26
NSC1553+4730	238.350	47.503	0.1606	29
NSC1554+3149	238.399	31.823	0.0458	25
NSC1554+5107	238.407	51.113	0.1950	26
NSC1554+3228	238.414	32.460	0.1422	31
NSC1554+3246	238.436	32.766	0.1187	29
NSC1554+3333	238.467	33.550	0.1684	47
NSC1554+4015	238.526	40.244	0.0710	21
NSC1554+5625	238.530	56.416	0.1362	31
NSC1554+3625	238.530	36.421	0.1498	27
NSC1554+3946	238.561	39.764	0.0513	23
NSC1554+3347	238.585	33.788	0.1303	36
NSC1554+3605	238.587	36.088	0.0944	35
NSC1554+4840	238.617	48.674	0.2557	21
NSC1555+4103	238.658	41.046	0.0970	19
NSC1555+4755	238.660	47.912	0.0315	22
NSC1555+3305	238.676	33.089	0.1091	29
NSC1555+3223	238.685	32.391	0.2299	23
NSC1555+3257	238.695	32.957	0.1317	32
NSC1555+5311	238.744	53.189	0.0577	20
NSC1555+4047	238.745	40.789	0.0667	25
NSC1555+3615	238.795	36.246	0.1219	60
NSC1555+4817	238.810	48.279	0.1203	31
NSC1555+4606	238.822	46.103	0.1655	21
NSC1555+2900	238.846	29.008	0.0627	61
NSC1555+3336	238.866	33.594	0.0927	64
NSC1556+4133	238.881	41.555	0.0683	40
NSC1556+2812	238.906	28.205	0.1501	51
NSC1556+3509	238.909	35.156	0.0833	28
NSC1556+4045	238.985	40.746	0.0672	16
NSC1556+2750	239.028	27.831	0.1248	20
NSC1556+2848	239.063	28.794	0.0766	55
NSC1556+5059	239.077	50.976	0.1275	31
NSC1556+2836	239.102	28.595	0.1058	39
NSC1557+2926	239.149	29.436	0.1338	26
NSC1557+2906	239.162	29.096	0.1024	39
NSC1557+4844	239.180	48.732	0.1841	23
NSC1557+2951	239.205	29.843	0.0867	26
NSC1557+3454	239.211	34.894	0.0698	58
NSC1557+4622	239.212	46.368	0.1338	26

Continued...

Table B.1 - NGP Robust, Continued

Name	RA	Dec	z_{phot}	N_{gal}
NSC1557+3257	239.216	32.958	0.1524	46
NSC1557+3151	239.232	31.845	0.1477	30
NSC1557+3344	239.233	33.741	0.1041	38
NSC1557+4520	239.239	45.327	0.2257	33
NSC1557+4429	239.241	44.489	0.1481	24
NSC1557+3226	239.248	32.440	0.2269	26
NSC1557+3547	239.329	35.782	0.1555	36
NSC1557+3107	239.346	31.119	0.1309	30
NSC1557+3354	239.349	33.905	0.1052	43
NSC1557+2812	239.370	28.200	0.1674	28
NSC1558+2748	239.415	27.806	0.1017	54
NSC1558+3216	239.422	32.270	0.1565	20
NSC1558+3123	239.437	31.381	0.1433	35
NSC1558+3530	239.471	35.494	0.1521	88
NSC1558+5626	239.474	56.432	0.2394	19
NSC1558+2850	239.493	28.828	0.0885	55
NSC1558+3311	239.513	33.182	0.1733	23
NSC1558+3401	239.543	34.022	0.1406	34
NSC1558+5355	239.562	53.915	0.1009	27
NSC1558+3729	239.563	37.491	0.1948	34
NSC1558+3110	239.578	31.172	0.1712	21
NSC1558+5209	239.615	52.147	0.0124	3
NSC1559+3048	239.635	30.803	0.2108	19
NSC1559+3243	239.638	32.720	0.2242	30
NSC1559+4441	239.652	44.690	0.1560	25
NSC1559+4002	239.669	40.028	0.0806	24
NSC1559+5335	239.670	53.575	0.0412	40
NSC1559+3229	239.682	32.490	0.1749	23
NSC1559+4901	239.791	49.024	0.1498	22
NSC1559+3335	239.826	33.581	0.1626	30
NSC1559+5443	239.827	54.720	0.1769	25
NSC1559+5013	239.870	50.216	0.2345	25
NSC1600+3944	239.875	39.731	0.0586	22
NSC1600+3524	239.910	35.395	0.1436	45
NSC1600+4451	239.948	44.846	0.1956	22
NSC1600+3357	240.002	33.956	0.1340	38
NSC1600+4235	240.007	42.577	0.0429	13
NSC1600+3436	240.010	34.607	0.1189	68
NSC1600+3039	240.067	30.653	0.1619	31
NSC1600+5417	240.082	54.285	0.1145	33
NSC1600+4443	240.093	44.723	0.1868	17
NSC1600+4356	240.096	43.936	0.2073	14
NSC1600+3312	240.119	33.198	0.1323	111
NSC1600+3415	240.122	34.256	0.1009	28
NSC1601+3012	240.162	30.195	0.1630	21
NSC1601+3227	240.185	32.450	0.1660	28
NSC1601+5656	240.201	56.936	0.2132	17
NSC1601+3509	240.251	35.145	0.1784	34
NSC1601+4852	240.272	48.864	0.1010	25
NSC1601+4924	240.274	49.393	0.2062	19
NSC1601+3039	240.308	30.652	0.1373	23
NSC1601+5318	240.323	53.303	0.0884	36
NSC1601+5336	240.334	53.602	0.0716	60
NSC1601+4358	240.343	43.964	0.1795	22
NSC1601+4601	240.352	46.019	0.1521	17
NSC1601+3803	240.358	38.058	0.1230	35
NSC1601+3332	240.359	33.525	0.0954	41
NSC1601+5353	240.367	53.889	0.1143	95
NSC1602+4732	240.390	47.535	0.2235	20
NSC1602+4618	240.410	46.300	0.1675	43
NSC1602+5228	240.436	52.475	0.0766	30
NSC1602+4342	240.448	43.693	0.1724	20
NSC1602+3410	240.474	34.171	0.1737	34
NSC1602+4439	240.490	44.649	0.2093	29
NSC1602+2941	240.558	29.685	0.1687	20
NSC1602+5324	240.565	53.404	0.0548	46
NSC1602+5034	240.579	50.574	0.2023	34
NSC1603+3252	240.629	32.866	0.1709	51
NSC1603+3329	240.637	33.480	0.1301	29
NSC1603+5611	240.637	56.176	0.1967	26
NSC1603+2957	240.716	29.948	0.1495	28
NSC1603+3944	240.776	39.737	0.1300	37
NSC1603+2837	240.782	28.616	0.2301	20
NSC1603+4223	240.819	42.386	0.1180	30
NSC1603+3739	240.840	37.647	0.2500	30
NSC1603+4659	240.845	46.987	0.1173	25
NSC1603+3013	240.857	30.209	0.1777	24
NSC1604+4755	240.894	47.921	0.1264	33
NSC1604+3339	240.905	33.657	0.2150	29
NSC1604+2857	240.908	28.945	0.2363	28
NSC1604+5524	240.940	55.405	0.1063	15
NSC1604+3032	240.940	30.541	0.1455	23
NSC1604+2924	240.948	29.406	0.1112	28
NSC1604+3126	240.954	31.437	0.1008	36
NSC1604+4455	240.971	44.913	0.1985	19
NSC1604+2759	240.982	27.989	0.1431	24
NSC1604+2817	240.992	28.280	0.1329	20

Continued...

Table B.1 - NGP Robust, Continued

Name	RA	Dec	z_{phot}	N_{gal}
NSC1604+5360	241.016	53.993	0.1422	18
NSC1604+3720	241.024	37.340	0.2058	37
NSC1604+4255	241.026	42.913	0.1762	29
NSC1604+2746	241.029	27.768	0.2454	24
NSC1604+3814	241.051	38.234	0.1163	30
NSC1604+4838	241.054	48.636	0.2008	28
NSC1604+2914	241.062	29.235	0.2048	23
NSC1604+3009	241.072	30.151	0.1733	29
NSC1604+2938	241.110	29.632	0.1216	28
NSC1604+3826	241.119	38.426	0.1587	19
NSC1605+3317	241.127	33.283	0.1168	65
NSC1605+3433	241.150	34.548	0.1589	20
NSC1605+2844	241.156	28.736	0.1484	32
NSC1605+3345	241.181	33.747	0.1757	29
NSC1605+5435	241.214	54.583	0.2220	26
NSC1605+2905	241.228	29.090	0.1836	39
NSC1605+5050	241.241	50.836	0.0755	22
NSC1605+2813	241.255	28.212	0.1140	28
NSC1605+4707	241.258	47.118	0.1429	23
NSC1605+5538	241.259	55.631	0.1867	28
NSC1605+3258	241.287	32.971	0.1598	33
NSC1605+3328	241.293	33.461	0.1054	60
NSC1605+2825	241.295	28.411	0.1727	29
NSC1605+3151	241.329	31.850	0.0784	32
NSC1605+5258	241.354	52.972	0.1604	25
NSC1605+3717	241.366	37.290	0.1326	36
NSC1606+2751	241.383	27.853	0.2101	24
NSC1606+5313	241.407	53.211	0.0994	34
NSC1606+5347	241.412	53.779	0.1643	29
NSC1606+4318	241.412	43.294	0.1879	24
NSC1606+5447	241.414	54.781	0.2443	31
NSC1606+2904	241.461	29.061	0.1354	20
NSC1606+4010	241.516	40.163	0.0916	33
NSC1606+3934	241.516	39.561	0.0945	21
NSC1606+3257	241.538	32.955	0.1481	41
NSC1606+4254	241.557	42.907	0.2135	30
NSC1606+4307	241.573	43.115	0.1637	27
NSC1606+3521	241.611	35.356	0.2144	30
NSC1607+3802	241.633	38.031	0.1232	27
NSC1607+4813	241.650	48.221	0.2104	23
NSC1607+3317	241.660	33.277	0.0804	52
NSC1607+3744	241.693	37.731	0.1248	32
NSC1607+2831	241.698	28.517	0.1967	21
NSC1607+5241	241.699	52.682	0.2262	19
NSC1607+3143	241.701	31.712	0.1573	20
NSC1607+2913	241.702	29.217	0.2193	31
NSC1607+2800	241.724	28.008	0.1796	52
NSC1607+2821	241.740	28.344	0.1626	26
NSC1607+3713	241.757	37.222	0.0584	26
NSC1607+2750	241.781	27.830	0.2021	20
NSC1607+3256	241.784	32.937	0.1757	29
NSC1607+2850	241.790	28.828	0.1387	37
NSC1607+4016	241.801	40.259	0.1799	23
NSC1607+3208	241.809	32.130	0.1814	41
NSC1607+4756	241.835	47.938	0.2200	37
NSC1607+4816	241.863	48.273	0.1334	30
NSC1607+3331	241.869	33.510	0.1661	28
NSC1608+2838	241.937	28.626	0.2270	23
NSC1608+5320	241.947	53.325	0.1485	41
NSC1608+2826	241.973	28.431	0.1694	35
NSC1608+3303	241.984	33.045	0.1065	24
NSC1608+4339	242.000	43.644	0.2395	20
NSC1608+2817	242.006	28.282	0.1977	25
NSC1608+3632	242.040	36.529	0.1327	29
NSC1608+5336	242.045	53.606	0.1296	29
NSC1608+3050	242.045	30.825	0.1349	37
NSC1608+4303	242.049	43.043	0.1547	33
NSC1608+3856	242.049	38.938	0.0727	28
NSC1608+4846	242.061	48.760	0.0992	20
NSC1608+3025	242.068	30.411	0.1427	66
NSC1608+3745	242.096	37.752	0.0643	33
NSC1608+4824	242.124	48.407	0.1726	26
NSC1609+5212	242.125	52.192	0.1007	23
NSC1609+2859	242.139	28.991	0.1108	28
NSC1609+3149	242.160	31.819	0.1402	23
NSC1609+3439	242.164	34.654	0.0717	37
NSC1609+4150	242.170	41.835	0.1223	35
NSC1609+2909	242.180	29.157	0.1715	28
NSC1609+5528	242.236	55.459	0.1206	44
NSC1609+3715	242.247	37.248	0.0535	29
NSC1609+3301	242.264	33.012	0.1538	28
NSC1609+2845	242.270	28.746	0.1838	29
NSC1609+3242	242.271	32.704	0.1280	30
NSC1609+3111	242.272	31.189	0.1366	25
NSC1609+3331	242.296	33.521	0.1643	33
NSC1609+3839	242.305	38.646	0.2066	24
NSC1609+3142	242.345	31.696	0.1422	22

Continued...

Table B.1 - NGP Robust, Continued

Name	RA	Dec	z_{phot}	N_{gal}
NSC1609+4554	242.350	45.907	0.1916	23
NSC1609+4319	242.371	43.313	0.2038	20
NSC1610+5304	242.385	53.062	0.1051	46
NSC1610+5348	242.398	53.793	0.1316	51
NSC1610+3231	242.401	32.517	0.1549	35
NSC1610+4733	242.419	47.550	0.2284	19
NSC1610+3722	242.459	37.375	0.0729	36
NSC1610+3150	242.518	31.835	0.2312	30
NSC1610+2819	242.534	28.324	0.1467	53
NSC1610+4414	242.557	44.229	0.1773	21
NSC1610+5335	242.558	53.583	0.1044	45
NSC1610+3221	242.579	32.351	0.1619	26
NSC1610+5347	242.593	53.780	0.1155	57
NSC1611+5324	242.634	53.404	0.1166	36
NSC1611+2931	242.665	29.518	0.1213	52
NSC1611+3005	242.672	30.085	0.1363	25
NSC1611+4003	242.681	40.053	0.1003	29
NSC1611+4319	242.735	43.322	0.1829	17
NSC1611+5227	242.752	52.456	0.0753	70
NSC1611+3833	242.756	38.557	0.1217	26
NSC1611+3241	242.764	32.684	0.1424	28
NSC1611+3932	242.776	39.525	0.1322	31
NSC1611+5618	242.778	56.299	0.2241	24
NSC1611+4507	242.786	45.120	0.1620	16
NSC1611+4719	242.798	47.315	0.1238	17
NSC1611+5540	242.837	55.668	0.1531	27
NSC1611+4837	242.849	48.618	0.1357	24
NSC1611+3230	242.853	32.506	0.1549	23
NSC1611+2956	242.853	29.935	0.1893	39
NSC1611+2858	242.857	28.970	0.1969	22
NSC1611+4133	242.859	41.557	0.1519	39
NSC1611+5206	242.860	52.092	0.1113	62
NSC1611+4611	242.862	46.179	0.1622	25
NSC1611+3700	242.874	37.000	0.0769	48
NSC1612+2936	242.906	29.607	0.1060	49
NSC1612+2810	242.910	28.171	0.1178	35
NSC1612+5420	242.922	54.329	0.2616	24
NSC1612+4518	242.935	45.308	0.1995	18
NSC1612+3156	242.942	31.937	0.2077	27
NSC1612+4346	242.949	43.758	0.1124	18
NSC1612+4803	242.954	48.054	0.1509	23
NSC1612+2924	242.957	29.398	0.2286	34
NSC1612+4052	242.957	40.864	0.1610	16
NSC1612+2910	242.984	29.172	0.1724	42
NSC1612+5322	243.013	53.371	0.0783	26
NSC1612+3103	243.014	31.047	0.0927	42
NSC1612+2828	243.036	28.473	0.1253	33
NSC1612+4756	243.046	47.939	0.1057	32
NSC1612+2748	243.049	27.800	0.2701	28
NSC1612+2934	243.053	29.569	0.1146	57
NSC1612+5301	243.086	53.020	0.1254	27
NSC1612+5345	243.103	53.747	0.1773	29
NSC1612+3207	243.118	32.118	0.1021	32
NSC1612+5444	243.123	54.726	0.1976	24
NSC1613+4312	243.135	43.205	0.2561	22
NSC1613+2813	243.166	28.222	0.1386	35
NSC1613+2956	243.212	29.926	0.1054	48
NSC1613+5410	243.255	54.167	0.1572	52
NSC1613+4135	243.278	41.581	0.0940	29
NSC1613+5628	243.289	56.475	0.1586	29
NSC1613+3327	243.290	33.451	0.2542	26
NSC1613+4829	243.295	48.485	0.1710	25
NSC1613+2946	243.298	29.772	0.1842	28
NSC1613+3054	243.312	30.899	0.0675	67
NSC1613+2909	243.312	29.145	0.1296	40
NSC1613+4355	243.329	43.913	0.1301	26
NSC1613+4411	243.336	44.191	0.1680	21
NSC1613+3305	243.348	33.082	0.1769	28
NSC1613+5241	243.365	52.688	0.1830	34
NSC1614+5129	243.379	51.478	0.0643	30
NSC1614+4317	243.398	43.288	0.2260	26
NSC1614+2937	243.422	29.625	0.2126	20
NSC1614+4907	243.426	49.111	0.0988	52
NSC1614+4242	243.434	42.705	0.0819	30
NSC1614+3239	243.444	32.658	0.1706	34
NSC1614+4330	243.458	43.493	0.1490	28
NSC1614+5021	243.468	50.346	0.0714	28
NSC1614+5601	243.504	56.023	0.1716	34
NSC1614+4603	243.523	46.047	0.2263	25
NSC1614+5444	243.536	54.738	0.2798	24
NSC1614+5332	243.542	53.535	0.1882	21
NSC1614+3656	243.544	36.941	0.0734	28
NSC1614+3458	243.546	34.965	0.1695	29
NSC1614+2947	243.548	29.781	0.2423	19
NSC1614+4346	243.557	43.761	0.1722	24
NSC1614+2758	243.564	27.974	0.2493	37
NSC1614+2808	243.570	28.133	0.1946	33

Continued...

Table B.1 - NGP Robust, Continued

Name	RA	Dec	z_{phot}	N_{gal}
NSC1614+4639	243.595	46.651	0.1043	24
NSC1614+5029	243.596	50.486	0.0810	32
NSC1614+3824	243.602	38.400	0.1525	46
NSC1615+4143	243.641	41.711	0.1448	27
NSC1615+4828	243.649	48.462	0.2199	20
NSC1615+3751	243.655	37.854	0.1494	25
NSC1615+5427	243.672	54.458	0.2079	31
NSC1615+4941	243.694	49.682	0.2027	27
NSC1615+3021	243.705	30.355	0.1305	36
NSC1615+2816	243.740	28.262	0.1365	25
NSC1615+2929	243.800	29.492	0.2078	14
NSC1615+5743	243.802	57.713	0.0103	3
NSC1615+2960	243.803	29.997	0.1384	32
NSC1615+4316	243.859	43.266	0.1465	22
NSC1616+2805	243.941	28.076	0.1555	38
NSC1616+5405	243.964	54.084	0.1026	31
NSC1616+2748	243.985	27.805	0.1566	32
NSC1616+3300	243.986	33.004	0.0909	34
NSC1616+3829	244.002	38.489	0.1074	23
NSC1616+3930	244.006	39.496	0.1241	22
NSC1616+4405	244.045	44.086	0.1603	33
NSC1616+4418	244.049	44.293	0.1674	25
NSC1616+4916	244.056	49.273	0.1343	19
NSC1616+5025	244.062	50.413	0.2311	16
NSC1616+4304	244.080	43.062	0.1384	19
NSC1616+5038	244.107	50.626	0.2286	25
NSC1616+4953	244.118	49.878	0.2148	36
NSC1617+2814	244.133	28.234	0.1361	29
NSC1617+3858	244.134	38.963	0.1931	14
NSC1617+4226	244.135	42.430	0.1463	49
NSC1617+4806	244.181	48.102	0.1540	27
NSC1617+3320	244.202	33.333	0.0608	18
NSC1617+5114	244.203	51.227	0.2459	17
NSC1617+4455	244.206	44.919	0.1512	20
NSC1617+3441	244.207	34.681	0.0464	47
NSC1617+5621	244.213	56.351	0.1101	17
NSC1617+5503	244.226	55.047	0.1404	31
NSC1617+3009	244.239	30.147	0.2020	28
NSC1617+4639	244.267	46.653	0.1702	29
NSC1617+2938	244.283	29.635	0.1455	20
NSC1617+5045	244.298	50.756	0.2159	31
NSC1617+2752	244.320	27.873	0.1972	33
NSC1617+5012	244.322	50.193	0.2403	16
NSC1617+5234	244.343	52.568	0.2083	30
NSC1617+5649	244.363	56.824	0.1297	58
NSC1618+3054	244.381	30.905	0.1066	24
NSC1618+2956	244.401	29.934	0.1383	38
NSC1618+5218	244.401	52.294	0.1363	34
NSC1618+4232	244.409	42.537	0.2582	33
NSC1618+5020	244.416	50.341	0.2173	41
NSC1618+4412	244.448	44.202	0.1977	29
NSC1618+4510	244.451	45.164	0.2306	17
NSC1618+3307	244.467	33.112	0.1571	29
NSC1618+3851	244.474	38.842	0.1665	18
NSC1618+3923	244.487	39.385	0.1422	16
NSC1618+2758	244.494	27.959	0.1487	24
NSC1618+4309	244.500	43.156	0.1104	36
NSC1618+3808	244.518	38.132	0.0839	28
NSC1618+2807	244.532	28.121	0.1788	35
NSC1618+4603	244.537	46.055	0.1260	24
NSC1618+3001	244.568	30.016	0.1357	42
NSC1618+3509	244.581	35.154	0.0406	46
NSC1618+4956	244.591	49.930	0.2146	20
NSC1618+5323	244.613	53.384	0.0870	29
NSC1618+2911	244.615	29.180	0.1742	31
NSC1618+4713	244.616	47.216	0.1380	20
NSC1618+4306	244.624	43.099	0.0987	35
NSC1619+3012	244.628	30.205	0.1437	38
NSC1619+3137	244.638	31.621	0.1068	31
NSC1619+4407	244.650	44.121	0.1768	20
NSC1619+4436	244.702	44.606	0.1748	28
NSC1619+4731	244.727	47.520	0.2251	24
NSC1619+3827	244.744	38.457	0.1934	26
NSC1619+3218	244.763	32.301	0.2375	18
NSC1619+3731	244.785	37.525	0.1839	35
NSC1619+2751	244.804	27.856	0.2506	23
NSC1619+4326	244.805	43.435	0.1766	18
NSC1619+5408	244.837	54.138	0.1018	45
NSC1619+4249	244.841	42.821	0.1901	31
NSC1619+5210	244.851	52.174	0.1432	41
NSC1620+3828	244.920	38.474	0.1550	24
NSC1620+3119	244.940	31.324	0.1991	22
NSC1620+5030	244.959	50.497	0.2381	31
NSC1620+4549	244.995	45.813	0.1731	24
NSC1620+5235	245.022	52.589	0.1354	39
NSC1620+4229	245.049	42.480	0.1530	49
NSC1620+4741	245.066	47.691	0.2321	46

Continued...

Table B.1 - NGP Robust, Continued

Name	RA	Dec	z_{phot}	N_{gal}
NSC1620+5048	245.074	50.797	0.2208	25
NSC1620+3734	245.077	37.561	0.0922	43
NSC1620+3913	245.087	39.215	0.1462	28
NSC1620+4556	245.093	45.941	0.2197	23
NSC1620+4520	245.115	45.330	0.2291	20
NSC1621+5745	245.156	57.750	0.0000	3
NSC1621+5104	245.159	51.071	0.2022	17
NSC1621+5549	245.192	55.812	0.2104	21
NSC1621+2953	245.194	29.891	0.1301	90
NSC1621+4441	245.225	44.684	0.2139	36
NSC1621+4007	245.227	40.108	0.1793	23
NSC1621+4235	245.256	42.585	0.1553	23
NSC1621+5017	245.302	50.281	0.2036	45
NSC1621+3049	245.315	30.811	0.1546	19
NSC1621+4257	245.318	42.947	0.1946	30
NSC1621+5602	245.323	56.026	0.1165	24
NSC1621+5002	245.345	50.027	0.2122	25
NSC1621+5536	245.351	55.593	0.1224	29
NSC1622+4432	245.391	44.526	0.1541	37
NSC1622+4733	245.398	47.546	0.1886	19
NSC1622+5552	245.434	55.865	0.1809	22
NSC1622+4245	245.439	42.753	0.1431	41
NSC1622+4307	245.458	43.116	0.2331	20
NSC1622+5154	245.466	51.896	0.1995	35
NSC1622+4905	245.474	49.084	0.1087	26
NSC1622+3800	245.475	38.007	0.1734	13
NSC1622+3336	245.483	33.604	0.1398	38
NSC1622+2829	245.518	28.488	0.2360	25
NSC1622+5121	245.560	51.347	0.2247	27
NSC1622+4342	245.577	43.696	0.1055	25
NSC1622+4034	245.612	40.563	0.1276	24
NSC1623+3059	245.638	30.989	0.2213	19
NSC1623+4711	245.663	47.188	0.1524	18
NSC1623+5555	245.671	55.922	0.0760	28
NSC1623+4132	245.688	41.535	0.0975	24
NSC1623+4434	245.702	44.559	0.2074	33
NSC1623+4356	245.709	43.927	0.1340	24
NSC1623+3706	245.719	37.099	0.0872	16
NSC1623+5211	245.720	52.187	0.1712	27
NSC1623+5222	245.791	52.368	0.2177	31
NSC1623+5357	245.803	53.952	0.0935	34
NSC1623+3648	245.808	36.794	0.1596	23
NSC1623+2844	245.821	28.732	0.1225	24
NSC1623+5413	245.828	54.223	0.1641	28
NSC1623+2814	245.843	28.226	0.2088	19
NSC1623+3101	245.844	31.013	0.2193	21
NSC1623+5142	245.874	51.699	0.1182	20
NSC1624+4143	245.879	41.721	0.1044	35
NSC1624+2855	245.892	28.916	0.1756	16
NSC1624+3013	245.909	30.219	0.1904	20
NSC1624+4503	245.933	45.044	0.1947	38
NSC1624+4115	245.958	41.245	0.1718	35
NSC1624+4759	245.966	47.977	0.2006	50
NSC1624+4547	245.976	45.790	0.1177	18
NSC1624+4409	245.977	44.154	0.1768	26
NSC1624+5710	245.996	57.175	0.1640	20
NSC1624+3760	246.001	37.992	0.1097	31
NSC1624+5458	246.004	54.961	0.1437	40
NSC1624+4608	246.018	46.132	0.1204	24
NSC1624+3618	246.022	36.292	0.1441	21
NSC1624+3915	246.035	39.249	0.0638	49
NSC1624+3352	246.059	33.861	0.1794	24
NSC1624+5449	246.094	54.816	0.1189	43
NSC1624+4357	246.105	43.956	0.1689	17
NSC1624+4835	246.122	48.592	0.1470	43
NSC1625+5725	246.159	57.415	0.0958	19
NSC1625+4019	246.168	40.323	0.2363	18
NSC1625+4457	246.175	44.954	0.1175	36
NSC1625+3944	246.203	39.741	0.2126	26
NSC1625+3321	246.215	33.344	0.1132	32
NSC1625+2757	246.227	27.958	0.2408	17
NSC1625+3341	246.245	33.679	0.1301	40
NSC1625+2833	246.267	28.550	0.2174	30
NSC1625+3826	246.292	38.437	0.1000	37
NSC1625+3345	246.307	33.747	0.1193	40
NSC1625+3312	246.318	33.196	0.1164	27
NSC1625+3610	246.326	36.162	0.1143	18
NSC1625+3510	246.345	35.164	0.0677	21
NSC1625+4105	246.359	41.091	0.2398	19
NSC1626+4152	246.381	41.863	0.1131	35
NSC1626+5151	246.382	51.854	0.2695	24
NSC1626+3105	246.401	31.090	0.1961	20
NSC1626+4121	246.405	41.356	0.1317	28
NSC1626+2813	246.420	28.225	0.2260	22
NSC1626+3336	246.449	33.605	0.1343	29
NSC1626+4358	246.465	43.963	0.1459	36
NSC1626+5714	246.465	57.232	0.1717	33

Continued...

Table B.1 - NGP Robust, Continued

Name	RA	Dec	z_{phot}	N_{gal}
NSC1626+4437	246.528	44.616	0.1497	36
NSC1626+4250	246.531	42.830	0.1782	40
NSC1626+3352	246.537	33.868	0.1125	44
NSC1626+4347	246.551	43.781	0.1810	29
NSC1626+4623	246.564	46.377	0.1205	19
NSC1626+2757	246.565	27.957	0.1616	28
NSC1626+3920	246.574	39.327	0.1491	22
NSC1626+4550	246.603	45.836	0.1274	25
NSC1626+4534	246.608	45.567	0.1982	29
NSC1626+4334	246.609	43.575	0.1174	33
NSC1627+3800	246.633	38.000	0.1092	28
NSC1627+3345	246.659	33.752	0.1152	36
NSC1627+5100	246.659	51.000	0.1968	24
NSC1627+3315	246.682	33.245	0.1232	27
NSC1627+4828	246.687	48.462	0.1909	50
NSC1627+3622	246.696	36.371	0.1927	20
NSC1627+5110	246.700	51.161	0.1631	25
NSC1627+5530	246.711	55.496	0.1272	59
NSC1627+4423	246.748	44.384	0.1418	22
NSC1627+5554	246.749	55.906	0.1027	24
NSC1627+3124	246.751	31.398	0.2198	18
NSC1627+3549	246.784	35.823	0.1113	23
NSC1627+4132	246.802	41.540	0.1554	55
NSC1627+4214	246.823	42.227	0.1438	20
NSC1627+5411	246.862	54.184	0.2275	27
NSC1628+3001	246.880	30.022	0.2589	18
NSC1628+3939	246.893	39.643	0.0897	46
NSC1628+3957	246.899	39.948	0.1452	24
NSC1628+5344	246.902	53.739	0.2045	19
NSC1628+5148	246.905	51.797	0.1433	32
NSC1628+3258	246.909	32.964	0.1591	23
NSC1628+4652	246.919	46.866	0.2914	16
NSC1628+3020	246.937	30.326	0.2566	17
NSC1628+4409	246.948	44.142	0.1629	29
NSC1628+3911	246.959	39.183	0.1202	31
NSC1628+4838	246.959	48.641	0.2569	16
NSC1628+4820	246.968	48.335	0.1710	27
NSC1628+4115	246.982	41.246	0.1729	23
NSC1628+3609	246.987	36.152	0.1819	28
NSC1628+3350	247.008	33.827	0.1184	46
NSC1628+4613	247.014	46.223	0.1507	21
NSC1628+4353	247.025	43.882	0.2774	36
NSC1628+5424	247.056	54.401	0.1179	25
NSC1628+4253	247.065	42.880	0.1271	42
NSC1628+3831	247.094	38.517	0.2220	22
NSC1628+5314	247.105	53.231	0.2074	24
NSC1628+3203	247.111	32.046	0.2568	17
NSC1629+3454	247.186	34.897	0.1085	20
NSC1629+3130	247.193	31.502	0.1788	22
NSC1629+4847	247.201	48.779	0.1732	36
NSC1629+4431	247.228	44.516	0.1239	37
NSC1629+4350	247.248	43.829	0.1152	26
NSC1629+3948	247.268	39.808	0.0692	63
NSC1629+5034	247.271	50.572	0.1649	27
NSC1629+4710	247.294	47.175	0.1846	24
NSC1629+4011	247.309	40.181	0.2404	16
NSC1629+4135	247.326	41.576	0.1138	27
NSC1629+4935	247.326	49.578	0.2099	25
NSC1629+3529	247.357	35.479	0.1507	45
NSC1629+2809	247.366	28.151	0.2079	50
NSC1630+3918	247.380	39.295	0.1601	16
NSC1630+3342	247.431	33.701	0.1501	28
NSC1630+4556	247.432	45.937	0.2157	16
NSC1630+3935	247.441	39.582	0.0827	78
NSC1630+3231	247.445	32.522	0.2780	20
NSC1630+5560	247.462	56.000	0.2470	28
NSC1630+5427	247.489	54.445	0.2217	41
NSC1630+4915	247.514	49.254	0.1943	26
NSC1630+5016	247.535	50.273	0.2537	23
NSC1630+3612	247.554	36.200	0.1044	36
NSC1630+4649	247.575	46.822	0.1732	20
NSC1630+4341	247.576	43.681	0.2545	25
NSC1630+4731	247.581	47.510	0.2137	22
NSC1630+5718	247.607	57.298	0.1901	22
NSC1630+4441	247.613	44.689	0.2120	25
NSC1630+3108	247.619	31.125	0.2336	22
NSC1630+5528	247.624	55.461	0.1035	36
NSC1631+5514	247.635	55.237	0.1201	39
NSC1631+3536	247.642	35.599	0.1799	34
NSC1631+4322	247.651	43.362	0.1967	38
NSC1631+4622	247.689	46.362	0.2524	21
NSC1631+4118	247.705	41.298	0.0912	52
NSC1631+3140	247.736	31.660	0.1713	18
NSC1631+3543	247.760	35.715	0.1264	25
NSC1631+3744	247.770	37.738	0.1607	22
NSC1631+3429	247.773	34.491	0.1357	23
NSC1631+3908	247.774	39.130	0.0855	12

Continued...

Table B.1 - NGP Robust, Continued

Name	RA	Dec	z_{phot}	N_{gal}
NSC1631+2813	247.790	28.218	0.2209	19
NSC1631+4645	247.801	46.754	0.2096	24
NSC1631+4718	247.816	47.297	0.1828	30
NSC1631+3944	247.826	39.737	0.0487	30
NSC1631+4109	247.851	41.143	0.2015	31
NSC1631+3439	247.853	34.653	0.1377	27
NSC1631+5001	247.865	50.015	0.2179	18
NSC1632+3129	247.882	31.480	0.2016	28
NSC1632+4321	247.886	43.356	0.1915	32
NSC1632+4444	247.893	44.733	0.1546	15
NSC1632+4132	247.902	41.526	0.0945	46
NSC1632+4840	247.961	48.666	0.1973	19
NSC1632+3403	247.972	34.054	0.1731	25
NSC1632+3736	247.979	37.604	0.1640	21
NSC1632+3244	248.076	32.726	0.2216	27
NSC1632+4431	248.083	44.525	0.1161	22
NSC1632+3634	248.104	36.563	0.0610	28
NSC1633+4641	248.166	46.685	0.2596	18
NSC1633+4313	248.182	43.220	0.1541	24
NSC1633+3759	248.201	37.975	0.1023	21
NSC1633+5206	248.207	52.099	0.2414	39
NSC1633+3445	248.213	34.747	0.1149	18
NSC1633+5237	248.231	52.610	0.2548	36
NSC1633+4221	248.270	42.351	0.0392	23
NSC1633+3611	248.278	36.181	0.1674	26
NSC1633+5711	248.280	57.178	0.1130	25
NSC1633+4230	248.280	42.496	0.1352	16
NSC1633+2948	248.289	29.798	0.1978	22
NSC1633+3342	248.302	33.704	0.1619	19
NSC1633+5032	248.315	50.526	0.1037	80
NSC1633+4857	248.315	48.948	0.1359	31
NSC1633+4017	248.333	40.283	0.1736	28
NSC1633+4917	248.350	49.288	0.1877	39
NSC1633+3233	248.360	32.551	0.2138	30
NSC1634+5025	248.411	50.422	0.1149	67
NSC1634+4355	248.425	43.912	0.1450	29
NSC1634+4305	248.440	43.082	0.1876	32
NSC1634+3918	248.464	39.292	0.1107	15
NSC1634+4102	248.476	41.030	0.1102	35
NSC1634+5330	248.493	53.497	0.1259	39
NSC1634+3321	248.499	33.346	0.1296	22
NSC1634+5612	248.500	56.198	0.0902	21
NSC1634+3016	248.518	30.265	0.1983	24
NSC1634+5246	248.522	52.774	0.1779	25
NSC1634+3252	248.537	32.870	0.1683	34
NSC1634+4320	248.558	43.338	0.1757	24
NSC1634+4939	248.586	49.656	0.2151	26
NSC1634+3539	248.589	35.653	0.1842	25
NSC1634+3948	248.602	39.799	0.1394	25
NSC1635+5041	248.637	50.691	0.2416	35
NSC1635+4916	248.666	49.262	0.1722	35
NSC1635+2831	248.749	28.521	0.2035	21
NSC1635+3214	248.767	32.239	0.2158	19
NSC1635+3735	248.768	37.586	0.0868	28
NSC1635+5131	248.775	51.511	0.1480	24
NSC1635+4111	248.785	41.184	0.1396	22
NSC1635+4751	248.814	47.856	0.2104	24
NSC1635+3423	248.815	34.390	0.2211	22
NSC1635+4251	248.821	42.858	0.1507	39
NSC1635+4308	248.822	43.135	0.1993	33
NSC1635+3757	248.827	37.957	0.1757	13
NSC1635+4856	248.848	48.925	0.1910	19
NSC1636+4530	248.887	45.504	0.2262	16
NSC1636+5049	248.891	50.817	0.1946	18
NSC1636+5037	248.899	50.613	0.2454	24
NSC1636+5341	248.900	53.677	0.1528	28
NSC1636+4016	249.009	40.270	0.1049	33
NSC1636+5323	249.010	53.390	0.1663	40
NSC1636+3834	249.013	38.563	0.1264	23
NSC1636+3310	249.022	33.174	0.1393	25
NSC1636+4709	249.026	47.157	0.1723	22
NSC1636+2836	249.041	28.592	0.2189	29
NSC1636+4915	249.055	49.251	0.1416	37
NSC1636+4820	249.057	48.338	0.1891	22
NSC1636+5016	249.060	50.265	0.2431	31
NSC1636+2910	249.102	29.169	0.2051	27
NSC1636+2923	249.123	29.381	0.1404	22
NSC1636+3731	249.125	37.525	0.2064	15
NSC1637+2943	249.127	29.710	0.2193	27
NSC1637+2851	249.138	28.846	0.2342	16
NSC1637+4114	249.141	41.240	0.1777	44
NSC1637+2820	249.168	28.331	0.1972	30
NSC1637+3624	249.185	36.404	0.1421	24
NSC1637+5042	249.193	50.700	0.2640	25
NSC1637+4209	249.211	42.155	0.1537	24
NSC1637+2901	249.223	29.010	0.2335	22
NSC1637+5104	249.236	51.074	0.2022	20

Continued...

Table B.1 - NGP Robust, Continued

Name	RA	Dec	z_{phot}	N_{gal}
NSC1637+5325	249.254	53.423	0.1664	26
NSC1637+4955	249.317	49.913	0.2222	26
NSC1637+5649	249.321	56.812	0.2073	23
NSC1637+5342	249.333	53.700	0.1478	37
NSC1637+4140	249.364	41.661	0.1707	24
NSC1638+3523	249.385	35.389	0.1664	19
NSC1638+5348	249.408	53.800	0.1143	41
NSC1638+4911	249.428	49.180	0.1980	29
NSC1638+4801	249.463	48.024	0.2219	59
NSC1638+4008	249.474	40.128	0.0947	14
NSC1638+3754	249.486	37.897	0.1629	38
NSC1638+5315	249.494	53.242	0.1862	20
NSC1638+2858	249.527	28.967	0.2678	22
NSC1638+2917	249.537	29.286	0.1795	17
NSC1638+5530	249.592	55.503	0.1130	23
NSC1638+3251	249.594	32.853	0.1679	26
NSC1638+2751	249.604	27.851	0.1382	42
NSC1638+3308	249.616	33.136	0.1934	20
NSC1639+3233	249.633	32.547	0.1627	29
NSC1639+2816	249.682	28.274	0.1921	30
NSC1639+3720	249.685	37.327	0.1247	26
NSC1639+5244	249.687	52.725	0.1498	28
NSC1639+3501	249.691	35.010	0.1800	16
NSC1639+4137	249.735	41.615	0.2094	24
NSC1639+5154	249.776	51.902	0.2128	24
NSC1639+3339	249.783	33.655	0.2015	22
NSC1639+5401	249.784	54.015	0.0891	38
NSC1639+5255	249.802	52.918	0.2110	28
NSC1639+3612	249.830	36.198	0.1470	20
NSC1639+3904	249.834	39.059	0.2221	20
NSC1639+5213	249.847	52.219	0.1729	35
NSC1639+5132	249.854	51.530	0.1736	38
NSC1639+4119	249.862	41.310	0.1758	17
NSC1639+3803	249.863	38.049	0.1861	18
NSC1639+2948	249.863	29.794	0.1297	48
NSC1640+3351	249.878	33.848	0.1344	24
NSC1640+3314	249.889	33.235	0.1821	21
NSC1640+5032	249.946	50.525	0.2193	23
NSC1640+3637	249.950	36.611	0.1604	30
NSC1640+5347	249.961	53.790	0.1360	48
NSC1640+2820	249.989	28.334	0.1697	42
NSC1640+3825	249.991	38.425	0.1547	24
NSC1640+2753	249.993	27.884	0.1982	23
NSC1640+5358	250.016	53.968	0.1055	50
NSC1640+5228	250.021	52.473	0.1627	35
NSC1640+4159	250.048	41.976	0.0873	24
NSC1640+5252	250.086	52.873	0.1720	25
NSC1640+4816	250.090	48.261	0.2666	21
NSC1640+3207	250.097	32.117	0.1409	25
NSC1640+5559	250.103	55.981	0.2056	32
NSC1641+4853	250.135	48.879	0.2506	18
NSC1641+3933	250.136	39.557	0.1162	26
NSC1641+4828	250.171	48.467	0.2015	38
NSC1641+2753	250.174	27.890	0.1452	61
NSC1641+3215	250.174	32.253	0.1247	19
NSC1641+2926	250.194	29.428	0.1730	28
NSC1641+3950	250.201	39.836	0.1248	20
NSC1641+3816	250.231	38.259	0.2041	19
NSC1641+4023	250.233	40.391	0.1190	21
NSC1641+3249	250.249	32.820	0.1568	42
NSC1641+5226	250.262	52.431	0.2119	34
NSC1641+3628	250.276	36.459	0.0721	270
NSC1641+3001	250.303	30.018	0.1791	17
NSC1641+2852	250.335	28.864	0.0831	28
NSC1641+3858	250.337	38.970	0.1793	20
NSC1641+3744	250.338	37.729	0.2086	24
NSC1641+5134	250.342	51.560	0.2367	22
NSC1641+2904	250.349	29.065	0.0585	38
NSC1641+2817	250.349	28.278	0.1736	20
NSC1641+5014	250.371	50.235	0.2202	25
NSC1642+3636	250.382	36.600	0.0707	312
NSC1642+3802	250.390	38.025	0.1580	53
NSC1642+3835	250.390	38.585	0.1553	37
NSC1642+3237	250.391	32.612	0.2327	21
NSC1642+3722	250.397	37.367	0.1610	44
NSC1642+2759	250.415	27.979	0.1529	38
NSC1642+5644	250.430	56.736	0.1801	31
NSC1642+3225	250.449	32.415	0.2047	21
NSC1642+4941	250.469	49.676	0.1888	36
NSC1642+3937	250.488	39.615	0.2277	23
NSC1642+4917	250.542	49.279	0.2107	21
NSC1642+3730	250.578	37.506	0.1779	18
NSC1642+3029	250.583	30.482	0.1629	38
NSC1642+4008	250.589	40.131	0.1583	24
NSC1642+5124	250.600	51.394	0.1855	39
NSC1642+2903	250.623	29.043	0.0753	30
NSC1643+3917	250.644	39.290	0.1983	27

Continued...

Table B.1 - NGP Robust, Continued

Name	RA	Dec	z_{phot}	N_{gal}
NSC1643+2754	250.651	27.893	0.0708	32
NSC1643+3256	250.670	32.927	0.2269	24
NSC1643+3215	250.681	32.256	0.1682	21
NSC1643+2814	250.689	28.228	0.1258	32
NSC1643+3755	250.703	37.914	0.1958	21
NSC1643+3345	250.707	33.752	0.1616	23
NSC1643+2954	250.721	29.897	0.1350	33
NSC1643+4753	250.747	47.887	0.1678	28
NSC1643+3927	250.750	39.451	0.1846	19
NSC1643+3040	250.768	30.669	0.2184	24
NSC1643+3233	250.798	32.558	0.1398	34
NSC1643+5052	250.829	50.869	0.2152	37
NSC1643+5114	250.830	51.234	0.2242	45
NSC1643+4802	250.832	48.025	0.2572	30
NSC1643+3718	250.835	37.297	0.1728	41
NSC1643+3755	250.864	37.918	0.1639	19
NSC1643+5255	250.865	52.916	0.2189	22
NSC1643+3134	250.872	31.574	0.1695	20
NSC1644+3107	250.906	31.123	0.1835	32
NSC1644+3322	250.915	33.362	0.2307	21
NSC1644+3020	250.917	30.326	0.1843	29
NSC1644+3532	250.942	35.528	0.1334	22
NSC1644+3050	250.950	30.828	0.1701	31
NSC1644+3116	250.969	31.270	0.1839	24
NSC1644+2926	251.010	29.441	0.1393	29
NSC1644+2901	251.021	29.023	0.1671	30
NSC1644+3007	251.059	30.122	0.1319	26
NSC1644+3820	251.067	38.338	0.2215	20
NSC1644+3729	251.073	37.490	0.1104	32
NSC1644+3229	251.083	32.478	0.1662	28
NSC1645+2811	251.155	28.176	0.1338	23
NSC1645+3755	251.173	37.915	0.1440	16
NSC1645+3857	251.176	38.949	0.1683	17
NSC1645+2937	251.201	29.610	0.1883	33
NSC1645+3020	251.204	30.334	0.1775	24
NSC1645+2856	251.215	28.926	0.1481	26
NSC1645+3713	251.218	37.220	0.1477	18
NSC1645+4003	251.231	40.045	0.2111	17
NSC1645+3519	251.284	35.322	0.0951	28
NSC1645+3532	251.309	35.532	0.1403	35
NSC1645+3838	251.327	38.626	0.1863	24
NSC1645+3045	251.340	30.752	0.1634	27
NSC1645+3952	251.349	39.868	0.1625	32
NSC1645+2810	251.358	28.166	0.1794	24
NSC1645+2935	251.363	29.591	0.1266	43
NSC1646+3312	251.393	33.208	0.1477	26
NSC1646+2747	251.406	27.787	0.1467	20
NSC1646+3217	251.439	32.286	0.1690	18
NSC1646+3801	251.474	38.025	0.1230	18
NSC1646+4238	251.481	42.634	0.1590	27
NSC1646+4010	251.494	40.173	0.0599	33
NSC1646+2855	251.498	28.918	0.1105	36
NSC1646+3242	251.500	32.706	0.1882	24
NSC1646+3108	251.508	31.131	0.1275	28
NSC1646+3040	251.583	30.667	0.1524	29
NSC1647+2835	251.694	28.590	0.1211	29
NSC1647+3021	251.709	30.354	0.2002	25
NSC1647+4235	251.711	42.579	0.2039	25
NSC1647+3104	251.745	31.072	0.1262	26
NSC1647+3234	251.755	32.563	0.1577	23
NSC1647+3850	251.759	38.834	0.0952	35
NSC1647+3623	251.764	36.387	0.2222	15
NSC1647+3035	251.813	30.578	0.1555	24
NSC1647+2814	251.841	28.234	0.1402	39
NSC1648+3432	251.894	34.531	0.0929	32
NSC1648+3301	251.901	33.022	0.1956	24
NSC1648+3238	251.924	32.640	0.2143	18
NSC1648+2956	251.929	29.935	0.1009	60
NSC1648+2913	251.950	29.223	0.1303	69
NSC1648+3903	251.952	39.054	0.0740	32
NSC1648+3556	251.967	35.938	0.1192	25
NSC1648+3626	251.968	36.441	0.1616	23
NSC1648+3342	251.977	33.706	0.2170	19
NSC1648+3103	252.000	31.043	0.1737	20
NSC1648+3126	252.008	31.430	0.2233	16
NSC1648+2944	252.010	29.731	0.1772	27
NSC1648+3153	252.017	31.891	0.2532	18
NSC1648+3332	252.029	33.532	0.1885	17
NSC1648+3959	252.076	39.978	0.1391	30
NSC1648+3118	252.107	31.294	0.1335	23
NSC1649+3628	252.136	36.471	0.1522	31
NSC1649+4054	252.139	40.906	0.1778	22
NSC1649+3209	252.140	32.146	0.1780	33
NSC1649+3033	252.212	30.547	0.1971	26
NSC1649+3837	252.215	38.623	0.2057	38
NSC1649+3754	252.219	37.893	0.1177	38
NSC1649+2924	252.224	29.406	0.1199	39

Continued...

Table B.1 - NGP Robust, Continued

Name	RA	Dec	z_{phot}	N_{gal}
NSC1649+3914	252.248	39.240	0.1932	23
NSC1649+3340	252.273	33.669	0.1301	28
NSC1649+2752	252.302	27.865	0.1708	30
NSC1649+3329	252.305	33.478	0.1925	24
NSC1649+3551	252.311	35.856	0.2095	17
NSC1649+3024	252.323	30.400	0.1471	35
NSC1649+3726	252.362	37.429	0.1559	37
NSC1650+3750	252.385	37.837	0.1423	33
NSC1650+2802	252.407	28.040	0.1706	32
NSC1650+3309	252.431	33.157	0.1669	21
NSC1650+2834	252.482	28.570	0.1657	30
NSC1650+3051	252.543	30.853	0.1753	16
NSC1650+3321	252.595	33.355	0.1809	28
NSC1650+3854	252.595	38.899	0.0473	27
NSC1650+2849	252.597	28.824	0.1384	51
NSC1651+3117	252.667	31.285	0.1967	23
NSC1651+2811	252.672	28.188	0.2120	27
NSC1651+4126	252.701	41.427	0.1608	25
NSC1651+3258	252.739	32.959	0.1360	29
NSC1651+3909	252.763	39.145	0.1386	22
NSC1651+3821	252.769	38.357	0.2207	25
NSC1651+2858	252.827	28.971	0.1786	21
NSC1651+3746	252.832	37.764	0.1582	34
NSC1651+3027	252.846	30.450	0.1602	24
NSC1651+3344	252.853	33.739	0.1137	24
NSC1651+2908	252.855	29.135	0.1781	28
NSC1651+3044	252.860	30.740	0.2041	19
NSC1651+3135	252.863	31.580	0.2456	24
NSC1652+4020	252.924	40.335	0.1640	21
NSC1652+3544	252.956	35.736	0.1369	22
NSC1652+2749	252.961	27.814	0.2539	31
NSC1652+3156	253.001	31.930	0.2326	25
NSC1652+3316	253.019	33.272	0.1636	40
NSC1652+4138	253.020	41.641	0.1748	22
NSC1652+3740	253.047	37.672	0.1556	17
NSC1652+3345	253.076	33.748	0.1325	39
NSC1652+3408	253.111	34.128	0.2085	15
NSC1652+3117	253.118	31.287	0.1622	26
NSC1653+2745	253.142	27.758	0.1349	40
NSC1653+2801	253.155	28.015	0.2252	25
NSC1653+2947	253.194	29.779	0.1685	29
NSC1653+3247	253.203	32.788	0.1288	28
NSC1653+4216	253.207	42.270	0.1329	28
NSC1653+3658	253.214	36.960	0.1769	20
NSC1653+3012	253.218	30.199	0.1587	29
NSC1653+4009	253.219	40.156	0.1861	34
NSC1653+2830	253.222	28.504	0.2216	30
NSC1653+4141	253.240	41.680	0.1859	16
NSC1653+3836	253.246	38.602	0.1621	25
NSC1653+2911	253.276	29.177	0.1698	57
NSC1653+3254	253.320	32.907	0.1566	32
NSC1653+3419	253.334	34.312	0.1767	19
NSC1653+3760	253.358	37.994	0.1616	30
NSC1653+3026	253.363	30.436	0.2087	30
NSC1653+3236	253.367	32.599	0.1578	16
NSC1654+3614	253.393	36.237	0.1462	23
NSC1654+3817	253.403	38.289	0.1635	27
NSC1654+3715	253.447	37.250	0.2240	20
NSC1654+3324	253.466	33.404	0.2169	20
NSC1654+3924	253.473	39.405	0.1687	34
NSC1654+3020	253.487	30.337	0.1726	24
NSC1654+3135	253.522	31.576	0.1366	38
NSC1654+3309	253.528	33.145	0.1424	28
NSC1654+3125	253.537	31.416	0.1614	44
NSC1654+2929	253.548	29.484	0.1698	36
NSC1654+3739	253.580	37.653	0.1600	22
NSC1654+3103	253.591	31.044	0.1293	20
NSC1654+4012	253.591	40.194	0.1781	35
NSC1654+4056	253.597	40.941	0.2045	23
NSC1654+2747	253.604	27.786	0.2480	35
NSC1654+3806	253.607	38.104	0.1345	28
NSC1654+2820	253.612	28.339	0.1684	27
NSC1655+2921	253.649	29.347	0.1598	51
NSC1655+4107	253.652	41.119	0.2411	14
NSC1655+3017	253.699	30.279	0.1663	26
NSC1655+4001	253.717	40.025	0.1617	53
NSC1655+4128	253.724	41.468	0.1542	39
NSC1655+3250	253.731	32.835	0.1767	43
NSC1655+3712	253.753	37.204	0.1387	34
NSC1655+3032	253.764	30.527	0.1476	41
NSC1655+3752	253.768	37.860	0.1584	33
NSC1655+3140	253.782	31.660	0.2427	20
NSC1655+2819	253.802	28.320	0.1835	39
NSC1655+4052	253.809	40.869	0.2295	25
NSC1655+3725	253.826	37.411	0.1698	38
NSC1655+3610	253.840	36.162	0.1949	28
NSC1655+3659	253.847	36.982	0.1669	27

Continued...

Table B.1 - NGP Robust, Continued

Name	RA	Dec	z_{phot}	N_{gal}
NSC1656+2757	253.889	27.956	0.1957	37
NSC1656+3804	253.894	38.062	0.1050	53
NSC1656+2808	253.923	28.134	0.1602	34
NSC1656+3735	253.926	37.578	0.2346	29
NSC1656+4225	253.929	42.413	0.2147	22
NSC1656+3122	253.941	31.368	0.1754	21
NSC1656+3833	253.944	38.558	0.1310	27
NSC1656+3441	253.946	34.676	0.2100	18
NSC1656+3211	253.963	32.183	0.1127	47
NSC1656+3557	253.985	35.944	0.1565	14
NSC1656+3918	253.990	39.306	0.1895	33
NSC1656+4155	254.026	41.919	0.1601	25
NSC1656+4141	254.043	41.687	0.1784	33
NSC1656+4019	254.053	40.322	0.2111	17
NSC1656+3530	254.058	35.494	0.1427	27
NSC1656+3238	254.061	32.641	0.1683	28
NSC1656+4127	254.068	41.442	0.1285	33
NSC1656+3131	254.085	31.520	0.1669	20
NSC1656+3115	254.086	31.255	0.1580	22
NSC1656+3632	254.099	36.530	0.1675	26
NSC1656+3303	254.120	33.058	0.1164	31
NSC1657+3001	254.129	30.010	0.1086	23
NSC1657+4031	254.136	40.509	0.2570	16
NSC1657+3324	254.171	33.392	0.1926	27
NSC1657+3037	254.178	30.619	0.1870	24
NSC1657+3843	254.230	38.717	0.1482	19
NSC1657+3615	254.257	36.248	0.1434	21
NSC1657+3923	254.266	39.386	0.1479	70
NSC1657+4136	254.271	41.606	0.1959	20
NSC1657+3725	254.306	37.423	0.1989	36
NSC1657+2807	254.310	28.122	0.1629	31
NSC1657+2759	254.371	27.976	0.0946	58
NSC1658+3226	254.376	32.437	0.1240	32
NSC1658+3129	254.385	31.485	0.1464	43
NSC1658+3034	254.395	30.570	0.1763	41
NSC1658+3901	254.396	39.012	0.1494	42
NSC1658+2926	254.401	29.428	0.1848	30
NSC1658+3715	254.409	37.242	0.1555	48
NSC1658+3354	254.418	33.896	0.1240	23
NSC1658+3529	254.418	35.478	0.1120	18
NSC1658+3139	254.448	31.646	0.1679	35
NSC1658+4134	254.468	41.559	0.1640	24
NSC1658+3252	254.490	32.871	0.2310	39
NSC1658+3838	254.521	38.626	0.1884	24
NSC1658+2857	254.522	28.956	0.1748	26
NSC1658+2804	254.527	28.074	0.1671	32
NSC1658+3204	254.567	32.072	0.1723	26
NSC1658+3708	254.602	37.128	0.1586	42
NSC1658+3512	254.612	35.205	0.2153	22
NSC1659+3156	254.656	31.935	0.1583	44
NSC1659+4055	254.695	40.918	0.1576	18
NSC1659+2748	254.697	27.798	0.1140	51
NSC1659+3906	254.700	39.092	0.1704	57
NSC1659+3605	254.704	36.077	0.2018	25
NSC1659+2803	254.730	28.053	0.1575	35
NSC1659+4026	254.791	40.438	0.1137	29
NSC1659+3517	254.800	35.280	0.1651	18
NSC1659+4146	254.800	41.772	0.1105	34
NSC1659+4042	254.801	40.701	0.1991	22
NSC1659+2854	254.801	28.892	0.1197	55
NSC1659+3724	254.805	37.393	0.1702	31
NSC1659+3111	254.808	31.191	0.1910	23
NSC1659+2844	254.816	28.738	0.1343	44
NSC1659+3149	254.831	31.824	0.2232	20
NSC1659+4156	254.833	41.941	0.1245	31
NSC1659+3618	254.854	36.306	0.1854	24
NSC1700+3318	254.876	33.308	0.2511	28
NSC1700+3412	254.911	34.201	0.1398	17
NSC1700+4238	254.919	42.635	0.1982	24
NSC1700+3732	254.950	37.530	0.1471	47
NSC1700+3936	254.955	39.605	0.2004	19
NSC1700+3308	254.963	33.139	0.2319	22
NSC1700+3517	254.973	35.278	0.2067	33
NSC1700+3532	254.985	35.530	0.1930	26
NSC1700+2760	254.986	27.993	0.1127	49
NSC1700+3349	255.010	33.819	0.1604	29
NSC1700+3848	255.010	38.807	0.1622	24
NSC1700+3252	255.012	32.867	0.1501	37
NSC1700+4003	255.028	40.053	0.2145	23
NSC1700+2909	255.042	29.156	0.1302	25
NSC1700+3834	255.066	38.575	0.1880	15
NSC1700+3823	255.066	38.382	0.1465	23
NSC1700+3714	255.079	37.227	0.1495	35
NSC1700+4216	255.079	42.267	0.1750	27
NSC1700+3403	255.091	34.049	0.1381	26
NSC1700+3237	255.106	32.609	0.1351	53
NSC1701+3814	255.165	38.240	0.2182	25

Continued...

Table B.1 - NGP Robust, Continued

Name	RA	Dec	z_{phot}	N_{gal}
NSC1701+2753	255.179	27.881	0.0968	53
NSC1701+3943	255.230	39.712	0.1679	17
NSC1701+3357	255.233	33.951	0.1789	36
NSC1701+2806	255.272	28.107	0.0677	60
NSC1701+3551	255.299	35.853	0.1490	27
NSC1701+4031	255.313	40.512	0.2326	21
NSC1701+3636	255.316	36.604	0.1646	27
NSC1701+3741	255.317	37.684	0.0931	42
NSC1701+4120	255.322	41.330	0.1694	37
NSC1701+3913	255.356	39.224	0.1654	24
NSC1701+3831	255.371	38.520	0.1657	17
NSC1702+3726	255.381	37.441	0.1324	31
NSC1702+3759	255.416	37.991	0.1685	23
NSC1702+4001	255.417	40.010	0.1064	26
NSC1702+3646	255.440	36.765	0.1731	32
NSC1702+4158	255.452	41.959	0.1514	31
NSC1702+3504	255.476	35.061	0.1202	61
NSC1702+2816	255.482	28.265	0.1582	39
NSC1702+3548	255.494	35.793	0.1993	26
NSC1702+3604	255.511	36.070	0.1506	26
NSC1702+4048	255.532	40.797	0.1389	40
NSC1702+4149	255.574	41.821	0.1828	32
NSC1702+4131	255.596	41.509	0.1820	24
NSC1702+3254	255.608	32.905	0.1490	45
NSC1702+3106	255.614	31.098	0.1712	29
NSC1702+3518	255.619	35.292	0.1046	55
NSC1703+3128	255.665	31.469	0.1862	24
NSC1703+3822	255.670	38.363	0.1559	28
NSC1703+3803	255.689	38.052	0.1924	38
NSC1703+4237	255.697	42.625	0.2329	24
NSC1703+3717	255.707	37.288	0.1492	32
NSC1703+3403	255.708	34.046	0.1237	126
NSC1703+4125	255.726	41.413	0.1617	26
NSC1703+4006	255.735	40.106	0.1757	28
NSC1703+3656	255.750	36.931	0.1901	16
NSC1703+3004	255.762	30.064	0.1426	26
NSC1703+2825	255.784	28.422	0.1124	39
NSC1703+3243	255.791	32.721	0.1751	22
NSC1703+2847	255.797	28.781	0.1409	31
NSC1703+3332	255.818	33.535	0.0955	90
NSC1703+3031	255.821	30.513	0.1067	41
NSC1703+3920	255.823	39.340	0.2127	35
NSC1703+3604	255.834	36.063	0.1403	37
NSC1703+4022	255.834	40.371	0.1505	34
NSC1703+2950	255.841	29.837	0.1754	20
NSC1703+3843	255.842	38.715	0.2303	22
NSC1703+2803	255.867	28.057	0.1343	45
NSC1704+2833	255.937	28.556	0.1548	33
NSC1704+4136	255.938	41.593	0.1866	33
NSC1704+2933	255.953	29.543	0.1922	19
NSC1704+3742	255.966	37.702	0.1426	31
NSC1704+3856	255.998	38.930	0.1319	29
NSC1704+3759	256.000	37.986	0.1939	20
NSC1704+3353	256.009	33.891	0.1137	46
NSC1704+4151	256.010	41.853	0.1895	33
NSC1704+3257	256.013	32.955	0.1315	49
NSC1704+4223	256.032	42.383	0.2393	25
NSC1704+3722	256.033	37.370	0.1533	32
NSC1704+3713	256.043	37.220	0.1540	27
NSC1704+2750	256.052	27.837	0.2440	22
NSC1704+3825	256.053	38.417	0.1846	25
NSC1704+4040	256.054	40.674	0.1804	17
NSC1704+3021	256.075	30.357	0.1495	44
NSC1704+3907	256.086	39.123	0.1750	26
NSC1704+4137	256.099	41.621	0.1826	26
NSC1704+2905	256.101	29.087	0.1851	38
NSC1704+3935	256.109	39.576	0.1358	14
NSC1704+4103	256.117	41.045	0.1643	21
NSC1704+2957	256.123	29.954	0.2273	22
NSC1705+3035	256.175	30.580	0.2372	25
NSC1705+3625	256.229	36.419	0.1597	24
NSC1705+2816	256.230	28.270	0.1456	54
NSC1705+3759	256.235	37.986	0.2217	25
NSC1705+3659	256.247	36.991	0.1532	33
NSC1705+2923	256.249	29.376	0.1541	23
NSC1705+3840	256.250	38.665	0.1583	36
NSC1705+3544	256.261	35.739	0.1617	18
NSC1705+3427	256.274	34.445	0.1779	22
NSC1705+3921	256.354	39.349	0.2081	27
NSC1706+4227	256.377	42.448	0.2725	17
NSC1706+2825	256.416	28.415	0.1197	40
NSC1706+3722	256.423	37.363	0.1718	36
NSC1706+3329	256.424	33.478	0.2015	38
NSC1706+4144	256.432	41.739	0.1573	34
NSC1706+4200	256.435	42.003	0.2245	19
NSC1706+4006	256.441	40.101	0.1271	42
NSC1706+3542	256.452	35.700	0.1511	31

Continued...

Table B.1 - NGP Robust, Continued

Name	RA	Dec	z_{phot}	N_{gal}
NSC1706+4126	256.455	41.434	0.2412	19
NSC1706+3906	256.468	39.100	0.1675	29
NSC1706+3532	256.469	35.532	0.1409	25
NSC1706+3702	256.479	37.029	0.2153	41
NSC1706+3636	256.492	36.600	0.2445	30
NSC1706+3950	256.499	39.834	0.1214	32
NSC1706+3141	256.501	31.691	0.1423	32
NSC1706+3503	256.518	35.046	0.1451	32
NSC1706+3747	256.520	37.790	0.1620	26
NSC1706+3618	256.539	36.308	0.1780	25
NSC1706+3830	256.558	38.504	0.1678	28
NSC1706+3124	256.564	31.408	0.1275	66
NSC1706+3417	256.593	34.285	0.1874	26
NSC1706+3348	256.603	33.792	0.0808	54
NSC1706+3015	256.610	30.258	0.1603	31
NSC1706+4145	256.616	41.752	0.1967	25
NSC1706+2904	256.616	29.066	0.2184	17
NSC1707+3337	256.670	33.622	0.0771	52
NSC1707+4229	256.671	42.483	0.1085	41
NSC1707+3552	256.704	35.861	0.1315	22
NSC1707+3140	256.745	31.673	0.1489	43
NSC1707+4203	256.752	42.048	0.1665	23
NSC1707+3456	256.762	34.937	0.1631	21
NSC1707+3533	256.779	35.556	0.1730	43
NSC1707+3416	256.787	34.269	0.1435	28
NSC1707+3343	256.790	33.725	0.1275	40
NSC1707+3923	256.794	39.387	0.1398	29
NSC1707+3436	256.808	34.606	0.2319	27
NSC1707+3611	256.871	36.181	0.1946	36
NSC1708+3249	256.893	32.811	0.1755	29
NSC1708+3907	256.915	39.114	0.1236	33
NSC1708+3541	256.926	35.681	0.1787	28
NSC1708+3630	256.935	36.507	0.2102	31
NSC1708+4116	256.945	41.268	0.1725	20
NSC1708+2946	256.966	29.762	0.1390	33
NSC1708+3332	256.972	33.533	0.2592	25
NSC1708+3920	257.013	39.330	0.1693	29
NSC1708+3804	257.016	38.066	0.2129	34
NSC1708+4014	257.039	40.232	0.2067	22
NSC1708+3615	257.048	36.247	0.1401	48
NSC1708+3702	257.066	37.037	0.1586	32
NSC1708+3355	257.087	33.916	0.1646	38
NSC1708+3001	257.111	30.013	0.1708	20
NSC1709+2909	257.147	29.156	0.2146	31
NSC1709+3960	257.160	39.999	0.1265	29
NSC1709+3944	257.185	39.729	0.1133	26
NSC1709+3844	257.229	38.733	0.1335	38
NSC1709+4148	257.261	41.792	0.1394	25
NSC1709+2757	257.278	27.947	0.1976	40
NSC1709+3529	257.320	35.484	0.1611	20
NSC1709+3200	257.324	32.008	0.1874	31
NSC1710+2854	257.386	28.905	0.2079	33
NSC1710+3209	257.408	32.142	0.1794	26
NSC1710+4127	257.431	41.451	0.2132	18
NSC1710+3429	257.435	34.475	0.0927	125
NSC1710+2932	257.464	29.533	0.1828	33
NSC1710+3840	257.468	38.669	0.1657	22
NSC1710+3632	257.471	36.530	0.1380	47
NSC1710+4228	257.509	42.464	0.1591	29
NSC1710+3336	257.513	33.598	0.1439	45
NSC1710+3928	257.515	39.475	0.0949	52
NSC1710+3745	257.526	37.750	0.1780	29
NSC1710+2945	257.550	29.758	0.2152	25
NSC1711+2748	257.629	27.799	0.1578	37
NSC1711+2807	257.629	28.122	0.1739	24
NSC1711+2851	257.641	28.857	0.2009	37
NSC1711+4132	257.650	41.525	0.2190	30
NSC1711+3619	257.651	36.312	0.1633	33
NSC1711+3307	257.652	33.125	0.1872	36
NSC1711+4115	257.654	41.251	0.1196	24
NSC1711+3255	257.655	32.919	0.2073	38
NSC1711+3913	257.665	39.212	0.1435	27
NSC1711+2922	257.676	29.368	0.2068	35
NSC1711+3412	257.696	34.200	0.1767	32
NSC1711+3007	257.726	30.113	0.1583	33
NSC1711+2956	257.730	29.935	0.2560	21
NSC1711+4155	257.731	41.914	0.1970	24
NSC1711+4241	257.752	42.690	0.1853	34
NSC1711+3456	257.753	34.937	0.1853	32
NSC1711+3939	257.780	39.655	0.0910	89
NSC1711+3608	257.789	36.129	0.1429	27
NSC1711+3750	257.791	37.840	0.1825	26
NSC1711+2828	257.794	28.467	0.2043	18
NSC1711+3552	257.844	35.864	0.2010	23
NSC1711+3815	257.852	38.253	0.1418	21
NSC1711+3641	257.862	36.682	0.1593	21
NSC1712+3534	257.890	35.572	0.2040	24

Continued...

Table B.1 - NGP Robust, Continued

Name	RA	Dec	z_{phot}	N_{gal}
NSC1712+2921	257.896	29.358	0.2196	24
NSC1712+4020	257.915	40.327	0.1410	54
NSC1712+3710	257.929	37.166	0.2094	18
NSC1712+3505	257.941	35.086	0.2627	20
NSC1712+2948	257.969	29.806	0.1745	26
NSC1712+3332	257.988	33.526	0.1827	38
NSC1712+3355	258.007	33.923	0.1732	19
NSC1712+2857	258.017	28.943	0.2352	23
NSC1712+3757	258.022	37.944	0.2091	20
NSC1712+2811	258.041	28.191	0.2025	24
NSC1712+3111	258.044	31.176	0.1752	26
NSC1712+2827	258.047	28.454	0.2143	23
NSC1712+3458	258.066	34.968	0.1585	24
NSC1712+4203	258.105	42.047	0.2154	20
NSC1713+4028	258.141	40.474	0.1481	50
NSC1713+3540	258.147	35.673	0.1358	23
NSC1713+2917	258.176	29.290	0.1710	40
NSC1713+4112	258.183	41.205	0.1892	19
NSC1713+3619	258.215	36.318	0.1431	40
NSC1713+3913	258.221	39.224	0.1249	26
NSC1713+2937	258.247	29.620	0.2457	40
NSC1713+3844	258.282	38.732	0.1126	30
NSC1713+3142	258.318	31.697	0.2111	36
NSC1713+2813	258.324	28.223	0.1919	21
NSC1713+3944	258.329	39.737	0.1369	31
NSC1713+4015	258.331	40.243	0.1777	24
NSC1713+2750	258.352	27.834	0.2067	43
NSC1714+4219	258.375	42.317	0.1850	23
NSC1714+2944	258.378	29.737	0.2116	37
NSC1714+3804	258.414	38.062	0.1353	23
NSC1714+4030	258.438	40.506	0.1487	21
NSC1714+2857	258.451	28.956	0.2192	34
NSC1714+4244	258.460	42.730	0.1114	27
NSC1714+2841	258.473	28.684	0.2482	21
NSC1714+3639	258.480	36.651	0.1676	34
NSC1714+3160	258.481	31.995	0.1390	25
NSC1714+4055	258.514	40.913	0.1968	20
NSC1714+4235	258.519	42.587	0.1259	20
NSC1714+4149	258.531	41.810	0.0958	23
NSC1714+3305	258.536	33.081	0.2225	25
NSC1714+2948	258.541	29.807	0.2034	31
NSC1714+2908	258.554	29.137	0.2782	28
NSC1714+3729	258.562	37.479	0.1883	20
NSC1714+3745	258.571	37.755	0.1546	25
NSC1714+3603	258.584	36.045	0.1925	38
NSC1714+3439	258.592	34.658	0.2830	19
NSC1714+4132	258.596	41.535	0.1199	24
NSC1714+4200	258.602	42.008	0.0901	37
NSC1714+3518	258.619	35.297	0.1946	22
NSC1714+4042	258.620	40.701	0.1393	21
NSC1715+3930	258.640	39.502	0.1469	27
NSC1715+3153	258.649	31.883	0.1254	48
NSC1715+3955	258.665	39.913	0.2091	21
NSC1715+3917	258.679	39.278	0.2332	25
NSC1715+3851	258.702	38.850	0.1565	36
NSC1715+3805	258.702	38.078	0.1017	21
NSC1715+3812	258.705	38.196	0.0998	33
NSC1715+2847	258.727	28.791	0.2294	25
NSC1715+4236	258.769	42.600	0.1544	45
NSC1715+4010	258.773	40.165	0.1743	39
NSC1715+3527	258.775	35.449	0.1310	17
NSC1715+3730	258.790	37.492	0.1755	20
NSC1715+3222	258.792	32.362	0.1591	22
NSC1715+3610	258.830	36.172	0.2169	26
NSC1715+4217	258.872	42.284	0.2203	19
NSC1716+3947	258.877	39.786	0.1143	15
NSC1716+3926	258.878	39.434	0.1742	22
NSC1716+3839	258.879	38.658	0.1241	64
NSC1716+2806	258.882	28.096	0.2442	35
NSC1716+3817	258.908	38.276	0.1067	25
NSC1716+3748	258.937	37.799	0.2274	27
NSC1716+3509	258.941	35.143	0.1214	32
NSC1716+2905	258.942	29.084	0.1799	33
NSC1716+3657	258.971	36.951	0.2078	24
NSC1716+3138	258.976	31.634	0.2357	24
NSC1716+2754	258.985	27.895	0.1897	43
NSC1716+3459	258.986	34.983	0.1517	28
NSC1716+3338	259.018	33.633	0.1946	27
NSC1716+3050	259.022	30.829	0.1241	53
NSC1716+3717	259.027	37.286	0.2257	22
NSC1716+4052	259.032	40.859	0.0956	54
NSC1716+3855	259.057	38.912	0.1602	34
NSC1716+3823	259.071	38.382	0.1246	27
NSC1716+3412	259.086	34.200	0.2570	40
NSC1716+3258	259.099	32.968	0.2526	36
NSC1716+3139	259.110	31.654	0.1666	29
NSC1716+3904	259.119	39.060	0.0932	50

Continued...

Table B.1 - NGP Robust, Continued

Name	RA	Dec	z_{phot}	N_{gal}
NSC1716+4009	259.121	40.157	0.1694	26
NSC1717+2918	259.126	29.294	0.2906	32
NSC1717+4231	259.149	42.521	0.1698	47
NSC1717+3513	259.154	35.221	0.2418	33
NSC1717+3812	259.159	38.199	0.1325	15
NSC1717+3351	259.166	33.855	0.1916	29
NSC1717+3606	259.186	36.099	0.1498	35
NSC1717+2823	259.188	28.387	0.2406	26
NSC1717+3019	259.214	30.322	0.2143	20
NSC1717+4242	259.232	42.701	0.1226	30
NSC1717+3633	259.245	36.557	0.1870	39
NSC1717+3251	259.245	32.842	0.1953	50
NSC1717+4022	259.247	40.362	0.1540	35
NSC1717+3544	259.270	35.730	0.2629	25
NSC1717+3216	259.272	32.267	0.1488	46
NSC1717+4221	259.292	42.357	0.1659	66
NSC1717+3828	259.302	38.464	0.2324	17
NSC1717+2951	259.307	29.853	0.2513	27
NSC1717+3335	259.329	33.586	0.1197	39
NSC1717+2931	259.337	29.510	0.2245	34
NSC1717+4036	259.344	40.608	0.1798	22
NSC1718+3630	259.389	36.496	0.2424	37
NSC1718+3408	259.413	34.141	0.1595	29
NSC1718+4017	259.450	40.285	0.1600	36
NSC1718+3028	259.452	30.466	0.2550	29
NSC1718+3743	259.456	37.723	0.1010	31
NSC1718+4136	259.459	41.603	0.1648	19
NSC1718+4150	259.478	41.826	0.1131	24
NSC1718+3234	259.486	32.564	0.1204	113
NSC1718+3703	259.531	37.051	0.2849	20
NSC1718+3444	259.542	34.727	0.1347	39
NSC1718+4232	259.548	42.527	0.1603	37
NSC1718+3935	259.548	39.580	0.1215	30
NSC1718+3038	259.551	30.633	0.1621	28
NSC1718+3830	259.553	38.492	0.1946	29
NSC1718+3001	259.572	30.024	0.2476	32
NSC1718+2937	259.587	29.616	0.2706	35
NSC1718+3510	259.610	35.164	0.2211	30
NSC1718+2921	259.623	29.349	0.2276	32
NSC1719+4000	259.663	40.008	0.1631	32
NSC1719+3144	259.667	31.733	0.1990	43
NSC1719+3208	259.685	32.127	0.1719	38
NSC1719+4248	259.685	42.805	0.1828	38
NSC1719+3347	259.710	33.785	0.2294	17
NSC1719+4217	259.729	42.278	0.1508	25
NSC1719+3310	259.740	33.161	0.1325	36
NSC1719+3045	259.808	30.742	0.2540	38
NSC1719+2748	259.821	27.797	0.2125	30
NSC1719+4017	259.821	40.286	0.1419	37
NSC1719+3552	259.870	35.874	0.2621	21
NSC1720+3253	259.886	32.887	0.1492	47
NSC1720+4120	259.886	41.338	0.1772	28
NSC1720+3406	259.897	34.101	0.1100	51
NSC1720+4030	259.920	40.502	0.1307	30
NSC1720+3459	259.934	34.983	0.2292	23
NSC1720+2920	259.942	29.328	0.2063	23
NSC1720+2931	259.947	29.522	0.2036	31
NSC1720+3508	260.000	35.126	0.1985	31
NSC1720+2946	260.019	29.766	0.1815	37
NSC1720+2812	260.036	28.199	0.1665	28
NSC1720+3043	260.062	30.709	0.1651	28
NSC1720+3538	260.086	35.634	0.2733	40
NSC1720+3327	260.113	33.448	0.1426	23
NSC1720+3448	260.117	34.799	0.1768	22
NSC1720+3412	260.117	34.201	0.1692	31
NSC1720+3125	260.118	31.413	0.2183	33
NSC1721+4033	260.150	40.556	0.2110	25
NSC1721+2754	260.164	27.905	0.1925	26
NSC1721+2955	260.193	29.910	0.2227	35
NSC1721+2910	260.203	29.173	0.2444	31
NSC1721+3336	260.209	33.594	0.1692	30
NSC1721+3309	260.232	33.151	0.2326	27
NSC1721+3256	260.236	32.928	0.1961	43
NSC1721+3513	260.290	35.218	0.2543	32
NSC1721+4149	260.300	41.809	0.1828	20
NSC1721+3707	260.319	37.122	0.2559	22
NSC1721+3102	260.321	31.040	0.1862	32
NSC1721+2942	260.361	29.696	0.2061	56
NSC1722+3744	260.387	37.727	0.2144	18
NSC1722+3356	260.394	33.940	0.1879	28
NSC1722+3042	260.405	30.695	0.1322	64
NSC1722+3443	260.406	34.713	0.2046	39
NSC1722+3529	260.414	35.483	0.2415	20
NSC1722+3616	260.419	36.267	0.2111	30
NSC1722+3016	260.459	30.275	0.2490	30
NSC1722+3459	260.481	34.988	0.1230	44
NSC1722+3146	260.495	31.770	0.1989	29

Continued...

Table B.1 - NGP Robust, Continued

Name	RA	Dec	z_{phot}	N_{gal}
NSC1722+3635	260.504	36.579	0.1946	22
NSC1722+2759	260.525	27.988	0.1958	31
NSC1722+3114	260.534	31.237	0.2440	21
NSC1722+2924	260.550	29.397	0.1799	35
NSC1722+3337	260.555	33.609	0.1542	29
NSC1722+4026	260.564	40.426	0.2113	22
NSC1722+3727	260.571	37.445	0.1903	22
NSC1722+3050	260.574	30.826	0.1187	69
NSC1722+4236	260.590	42.608	0.2293	16
NSC1722+3308	260.615	33.128	0.1064	63
NSC1722+3835	260.616	38.577	0.1405	31
NSC1722+3700	260.620	37.007	0.1559	19
NSC1723+2825	260.637	28.424	0.2531	31
NSC1723+3438	260.654	34.637	0.2106	22
NSC1723+3938	260.656	39.632	0.1629	22
NSC1723+3210	260.678	32.174	0.2438	57
NSC1723+2951	260.683	29.844	0.1996	37
NSC1723+4106	260.700	41.094	0.2513	23
NSC1723+3512	260.725	35.207	0.2202	22
NSC1723+3359	260.763	33.983	0.2438	26
NSC1723+3042	260.764	30.695	0.2160	34
NSC1723+3821	260.802	38.344	0.1995	18
NSC1723+4226	260.820	42.441	0.1785	26
NSC1723+3601	260.824	36.019	0.1808	46
NSC1723+3523	260.841	35.391	0.2272	32
NSC1723+2755	260.858	27.922	0.2594	29
NSC1724+3232	260.884	32.541	0.2862	30
NSC1724+2926	260.889	29.437	0.2267	40
NSC1724+3008	260.891	30.142	0.2186	35
NSC1724+3460	260.892	34.995	0.2225	26
NSC1724+3416	260.896	34.260	0.1936	36
NSC1724+3259	260.922	32.981	0.1711	47
NSC1724+2841	260.959	28.691	0.1674	49
NSC1724+2824	260.972	28.400	0.2058	26
NSC1724+3508	260.978	35.135	0.2790	21
NSC1724+3041	260.979	30.686	0.1573	33
NSC1724+2910	260.991	29.161	0.1896	50
NSC1724+3356	261.022	33.941	0.1448	19
NSC1724+3006	261.036	30.104	0.1909	34
NSC1724+3611	261.039	36.181	0.1519	43
NSC1724+3536	261.043	35.605	0.1461	48
NSC1724+4015	261.048	40.251	0.1794	30
NSC1724+3445	261.077	34.742	0.1244	24
NSC1724+3960	261.101	39.995	0.1185	43
NSC1724+3148	261.125	31.806	0.1516	57
NSC1725+4151	261.135	41.856	0.2016	22
NSC1725+4240	261.139	42.659	0.2198	20
NSC1725+3747	261.163	37.785	0.1624	32
NSC1725+3201	261.187	32.024	0.2051	66
NSC1725+3412	261.218	34.194	0.1392	37
NSC1725+3501	261.281	35.021	0.1853	17
NSC1725+3935	261.281	39.578	0.1761	37
NSC1725+2758	261.282	27.959	0.2067	38
NSC1725+4148	261.288	41.805	0.2022	18
NSC1725+3601	261.289	36.021	0.1170	34
NSC1725+3527	261.299	35.448	0.2935	29
NSC1725+3636	261.311	36.592	0.1778	28
NSC1725+3429	261.315	34.481	0.1931	26
NSC1725+3357	261.317	33.948	0.1670	31
NSC1725+3438	261.322	34.625	0.1222	34
NSC1725+3021	261.338	30.345	0.1905	24
NSC1726+3118	261.407	31.305	0.1275	48
NSC1726+3149	261.443	31.816	0.1358	31
NSC1726+3952	261.452	39.875	0.1864	34
NSC1726+4005	261.455	40.090	0.1972	26
NSC1726+4211	261.459	42.178	0.1628	43
NSC1726+2751	261.460	27.849	0.2319	30
NSC1726+3135	261.494	31.586	0.1212	79
NSC1726+4231	261.523	42.516	0.2043	24
NSC1726+2831	261.536	28.510	0.2431	25
NSC1726+2812	261.539	28.206	0.1998	32
NSC1726+2937	261.546	29.622	0.1922	49
NSC1726+4241	261.547	42.681	0.2265	26
NSC1726+3108	261.559	31.135	0.1436	37
NSC1726+2901	261.569	29.024	0.2957	26
NSC1726+4017	261.575	40.286	0.1610	21
NSC1726+3851	261.599	38.857	0.2124	28
NSC1726+3242	261.623	32.705	0.1822	35
NSC1727+3759	261.649	37.977	0.1456	24
NSC1727+4107	261.650	41.119	0.1813	31
NSC1727+3011	261.654	30.182	0.2264	32
NSC1727+3924	261.655	39.395	0.1689	36
NSC1727+4159	261.661	41.987	0.1483	29
NSC1727+3025	261.665	30.413	0.2221	27
NSC1727+2955	261.671	29.911	0.2240	37
NSC1727+2809	261.740	28.151	0.1770	33
NSC1727+3946	261.742	39.770	0.1772	33

Continued...

Table B.1 - NGP Robust, Continued

Name	RA	Dec	z_{phot}	N_{gal}
NSC1727+3837	261.754	38.624	0.1555	32
NSC1727+4046	261.766	40.772	0.1399	42
NSC1727+2927	261.770	29.458	0.2033	29
NSC1727+3802	261.799	38.027	0.1923	20
NSC1727+4139	261.810	41.649	0.2836	31
NSC1727+3139	261.851	31.656	0.2020	23
NSC1727+4224	261.855	42.399	0.1943	22
NSC1727+3158	261.873	31.974	0.2313	35
NSC1728+2820	261.887	28.329	0.2041	27
NSC1728+3108	261.895	31.127	0.1876	32
NSC1728+3927	261.900	39.451	0.1201	38
NSC1728+4119	261.902	41.314	0.1679	18
NSC1728+3235	261.907	32.591	0.1564	23
NSC1728+3015	261.913	30.249	0.2123	25
NSC1728+4144	261.926	41.736	0.2145	21
NSC1728+3123	261.934	31.389	0.1999	25
NSC1728+3044	261.948	30.729	0.1791	30
NSC1728+4029	261.993	40.489	0.1355	31
NSC1728+3909	262.000	39.158	0.1552	26
NSC1728+3833	262.006	38.548	0.1548	30
NSC1728+4047	262.022	40.778	0.1618	35
NSC1728+4222	262.064	42.373	0.1482	19
NSC1729+4057	262.158	40.957	0.1836	40
NSC1729+4200	262.181	42.002	0.1589	24
NSC1729+4003	262.229	40.042	0.2039	26
NSC1729+3945	262.279	39.756	0.1850	24
NSC1729+4020	262.317	40.329	0.1516	35
NSC1729+4145	262.351	41.751	0.2125	25
NSC1729+3806	262.363	38.104	0.1713	33
NSC1729+3927	262.371	39.453	0.1563	36
NSC1730+4105	262.375	41.075	0.2181	25
NSC1730+4235	262.402	42.587	0.1659	28
NSC1730+3904	262.419	39.065	0.1276	26
NSC1730+4204	262.425	42.073	0.1489	21
NSC1730+3834	262.498	38.570	0.2098	26
NSC1730+4050	262.515	40.836	0.2295	17
NSC1730+4118	262.559	41.306	0.1666	32
NSC1730+4103	262.580	41.043	0.2341	18
NSC1730+4131	262.580	41.524	0.1727	25
NSC1730+4032	262.625	40.532	0.2054	18
NSC1731+3804	262.648	38.067	0.1469	39
NSC1731+4204	262.707	42.074	0.2324	27
NSC1731+3755	262.721	37.922	0.1540	31
NSC1732+3912	262.917	39.204	0.2335	18
NSC1732+3956	262.952	39.935	0.1560	52
NSC1732+3754	262.964	37.904	0.1926	18
NSC1732+4100	262.968	41.008	0.2245	20
NSC1732+4209	262.990	42.151	0.2211	20
NSC1732+4034	263.003	40.572	0.1666	59
NSC1732+4133	263.010	41.552	0.2207	20
NSC1732+4015	263.024	40.256	0.1430	38
NSC1732+3922	263.028	39.371	0.2249	21
NSC1732+3935	263.082	39.585	0.1690	21
NSC1732+4244	263.085	42.733	0.1951	34
NSC1733+3846	263.130	38.774	0.1898	29
NSC1733+3826	263.134	38.441	0.1639	25
NSC1733+4128	263.144	41.464	0.1594	34
NSC1733+4151	263.154	41.848	0.1676	24
NSC1733+4112	263.204	41.205	0.1698	32
NSC1733+3803	263.226	38.058	0.1622	22
NSC1733+3860	263.228	38.993	0.1649	20
NSC1733+4042	263.296	40.697	0.1480	88
NSC1733+4205	263.313	42.083	0.1728	36
NSC1733+3937	263.332	39.610	0.1927	20
NSC1734+3817	263.411	38.286	0.2455	30
NSC1734+4224	263.433	42.400	0.1934	38
NSC1734+4149	263.464	41.818	0.1366	28
NSC1734+4009	263.475	40.152	0.2017	32
NSC1734+3758	263.502	37.973	0.1482	35

Table B.2 - SGP Robust Candidate Galaxy Clusters

Name	RA	Dec	z_{phot}	N_{gal}
NSC0000+1300	0.002	13.002	0.1791	29
NSC0000+0042	0.003	0.699	0.1774	37
NSC0000+0856	0.011	8.937	0.2068	29
NSC0000+1930	0.024	19.506	0.2036	20
NSC0000+1551	0.031	15.855	0.1692	22
NSC0000+2433	0.033	24.545	0.0883	23
NSC0000+1526	0.034	15.439	0.1395	46
NSC0000+1754	0.037	17.894	0.1816	22
NSC0000+1038	0.053	10.635	0.1840	25
NSC0000+1203	0.068	12.051	0.1324	44
NSC0000+0645	0.069	6.748	0.1299	50
NSC0000+1544	0.085	15.727	0.1017	22
NSC0000+0445	0.086	4.745	0.2212	29
NSC0000+2155	0.103	21.918	0.1913	44
NSC0000+1431	0.117	14.520	0.1176	53
NSC0000+0630	0.124	6.500	0.1899	16
NSC0001+0554	0.145	5.904	0.1712	30
NSC0001+0658	0.153	6.968	0.1272	29
NSC0001+0528	0.155	5.466	0.2029	22
NSC0001+0721	0.189	7.349	0.2005	19
NSC0001+0047	0.213	0.778	0.2013	22
NSC0001+0646	0.213	6.767	0.2146	15
NSC0001+0537	0.227	5.617	0.1414	22
NSC0001+1415	0.228	14.257	0.0798	35
NSC0001+1524	0.242	15.393	0.1602	35
NSC0001+1259	0.244	12.978	0.1400	34
NSC0001+0234	0.257	2.559	0.1235	35
NSC0001+0617	0.272	6.279	0.1546	27
NSC0001+0552	0.335	5.861	0.0874	44
NSC0001+1813	0.366	18.224	0.1377	37
NSC0002+0806	0.414	8.099	0.2196	16
NSC0002+1038	0.436	10.626	0.2303	14
NSC0002+0745	0.443	7.751	0.1616	19
NSC0002+1203	0.469	12.057	0.2134	53
NSC0002+2526	0.477	25.438	0.1277	23
NSC0002+0604	0.478	6.071	0.1937	26
NSC0002+0543	0.481	5.717	0.2433	23
NSC0002+1245	0.513	12.757	0.1150	42
NSC0002+1920	0.533	19.328	0.1480	28
NSC0002+1526	0.545	15.432	0.1171	42
NSC0002+2443	0.558	24.725	0.1729	24
NSC0002+2009	0.578	20.148	0.0972	32
NSC0002+0756	0.593	7.935	0.1495	20
NSC0002+0524	0.602	5.404	0.1726	17
NSC0002+1306	0.605	13.107	0.1063	37
NSC0003+0646	0.653	6.764	0.2301	16
NSC0003+0039	0.657	0.651	0.2507	27
NSC0003+2230	0.660	22.504	0.1653	25
NSC0003+0031	0.661	0.521	0.1714	34
NSC0003+1245	0.680	12.745	0.1349	49
NSC0003+0555	0.684	5.920	0.2239	23
NSC0003+0620	0.695	6.337	0.1566	25
NSC0003+0426	0.706	4.426	0.1784	23
NSC0003+0659	0.732	6.984	0.2255	22
NSC0003+0610	0.734	6.165	0.1870	22
NSC0003+1533	0.770	15.556	0.1266	32
NSC0003+0520	0.791	5.329	0.2246	21
NSC0003+0106	0.813	1.100	0.1358	26
NSC0003+1331	0.836	13.521	0.1364	29
NSC0003+0133	0.839	1.550	0.1750	25
NSC0003+0437	0.844	4.613	0.1360	39
NSC0003+0054	0.850	0.903	0.1552	36
NSC0003+0713	0.861	7.225	0.2215	27
NSC0003+0214	0.872	2.241	0.1685	21
NSC0003+0837	0.872	8.616	0.1341	13
NSC0004+1006	0.892	10.092	0.1946	14
NSC0004+1128	0.901	11.460	0.1697	19
NSC0004+0855	0.914	8.911	0.0887	33
NSC0004+1360	0.915	13.997	0.1047	28
NSC0004+0522	0.925	5.368	0.2207	28
NSC0004+0730	0.945	7.494	0.2120	25
NSC0004+1016	0.945	10.274	0.1500	25
NSC0004+0205	0.957	2.077	0.1472	39
NSC0004+0030	0.984	0.498	0.1325	27
NSC0004+0757	0.988	7.954	0.1598	20
NSC0004+1033	1.033	10.554	0.1686	12
NSC0004+0043	1.073	0.709	0.1960	31
NSC0004+1051	1.077	10.849	0.2126	21
NSC0004+0611	1.079	6.188	0.1522	38
NSC0004+1737	1.091	17.621	0.1329	42
NSC0004+0349	1.097	3.822	0.1254	20
NSC0004+1431	1.112	14.511	0.1371	33
NSC0004+0530	1.124	5.498	0.1935	19
NSC0005+2408	1.128	24.127	0.1751	20
NSC0005+0144	1.200	1.729	0.2099	16
NSC0005+0453	1.207	4.881	0.1706	19
NSC0005+1551	1.207	15.854	0.1074	40
NSC0005+0058	1.238	0.959	0.1709	28
NSC0005+0644	1.242	6.741	0.1656	16

Continued...

Table B.2 - SGP Robust, Continued

Name	RA	Dec	z_{phot}	N_{gal}
NSC0005+0022	1.249	0.367	0.1335	32
NSC0005+1214	1.313	12.229	0.1844	18
NSC0005+0728	1.324	7.466	0.2169	15
NSC0005+0448	1.331	4.792	0.1423	28
NSC0005+1848	1.342	18.800	0.2021	19
NSC0005+1050	1.346	10.828	0.2008	14
NSC0005+1613	1.365	16.216	0.1122	75
NSC0006+0433	1.375	4.554	0.1535	22
NSC0006+1138	1.377	11.636	0.1184	31
NSC0006+1129	1.381	11.488	0.1768	28
NSC0006+1541	1.449	15.691	0.1307	52
NSC0006+1038	1.453	10.627	0.1956	15
NSC0006+1111	1.466	11.186	0.1438	41
NSC0006+1554	1.475	15.895	0.1216	59
NSC0006+1141	1.511	11.677	0.2241	21
NSC0006+2622	1.512	26.365	0.2228	17
NSC0006+1049	1.604	10.817	0.2202	33
NSC0006+0635	1.623	6.576	0.2001	20
NSC0006+1343	1.623	13.711	0.1248	44
NSC0007+1132	1.639	11.537	0.1785	23
NSC0007+2505	1.684	25.084	0.1774	39
NSC0007+0506	1.784	5.108	0.2141	16
NSC0007+1036	1.788	10.595	0.1968	24
NSC0007+2635	1.795	26.590	0.2187	30
NSC0007+0405	1.819	4.076	0.1374	23
NSC0007+0036	1.857	0.592	0.1956	22
NSC0007+1630	1.862	16.500	0.0993	68
NSC0008+2320	1.885	23.337	0.1473	32
NSC0008+0213	1.897	2.218	0.2160	30
NSC0008+1448	1.915	14.806	0.0960	25
NSC0008+0709	1.926	7.158	0.1299	36
NSC0008+1257	1.943	12.947	0.1869	21
NSC0008+2447	1.968	24.784	0.0903	22
NSC0008+1012	1.976	10.197	0.1658	25
NSC0008+1431	1.976	14.518	0.1598	22
NSC0008+0723	1.982	7.376	0.1410	28
NSC0008+0544	2.023	5.739	0.2303	15
NSC0008+1043	2.044	10.711	0.1858	19
NSC0009+0734	2.130	7.571	0.0962	44
NSC0009+2030	2.134	20.499	0.1508	22
NSC0009+0608	2.137	6.132	0.2382	26
NSC0009+1320	2.145	13.332	0.1116	25
NSC0009+1145	2.155	11.757	0.2149	15
NSC0009+0744	2.177	7.734	0.2037	24
NSC0009+0324	2.276	3.401	0.1681	15
NSC0009+1839	2.278	18.656	0.1544	27
NSC0009+0646	2.306	6.772	0.2527	35
NSC0009+1048	2.328	10.796	0.1796	22
NSC0009+0703	2.356	7.049	0.1520	17
NSC0009+0360	2.357	3.992	0.1420	43
NSC0009+0211	2.366	2.185	0.2057	29
NSC0010+0533	2.384	5.555	0.1888	31
NSC0010+0951	2.422	9.846	0.1928	26
NSC0010+1133	2.433	11.547	0.1756	18
NSC0010+1958	2.519	19.973	0.2399	21
NSC0010+1218	2.537	12.305	0.2117	34
NSC0010+1745	2.549	17.748	0.1332	44
NSC0010+0609	2.550	6.149	0.2143	19
NSC0010+1009	2.562	10.150	0.1730	17
NSC0010+0321	2.578	3.356	0.1050	25
NSC0010+0640	2.580	6.670	0.2702	26
NSC0010+0700	2.597	7.006	0.2173	27
NSC0010+0921	2.621	9.352	0.1528	31
NSC0010+1505	2.624	15.084	0.1055	25
NSC0011+1133	2.679	11.554	0.1269	49
NSC0011+1056	2.694	10.927	0.1743	23
NSC0011+1243	2.696	12.725	0.1670	28
NSC0011+0626	2.725	6.441	0.2450	24
NSC0011+2418	2.764	24.292	0.1995	21
NSC0011+0615	2.769	6.244	0.1756	24
NSC0011+1229	2.771	12.486	0.1333	37
NSC0011+2728	2.786	27.461	0.1582	15
NSC0011+1350	2.823	13.840	0.1205	33
NSC0012+1119	2.895	11.323	0.1318	30
NSC0012+0919	2.910	9.311	0.1301	26
NSC0012+1149	2.916	11.816	0.1472	27
NSC0012+1201	2.926	12.019	0.1444	19
NSC0012+1236	2.956	12.597	0.1877	33
NSC0012+2754	2.971	27.903	0.1247	21
NSC0012+0849	2.974	8.824	0.2030	13
NSC0012+1139	3.006	11.651	0.1672	18
NSC0012+0927	3.019	9.458	0.1434	63
NSC0012+2633	3.101	26.546	0.1274	26
NSC0013+2217	3.148	22.288	0.2051	24
NSC0013+1930	3.177	19.506	0.1418	47
NSC0013+0020	3.205	0.341	0.1408	32
NSC0013+2001	3.274	20.024	0.1506	24

Continued...

Table B.2 - SGP Robust, Continued

Name	RA	Dec	z_{phot}	N_{gal}
NSC0013+1431	3.286	14.511	0.2038	16
NSC0013+2728	3.330	27.468	0.1362	23
NSC0013+2431	3.334	24.520	0.1948	25
NSC0013+0248	3.342	2.798	0.1228	27
NSC0014+0042	3.412	0.699	0.1102	25
NSC0014+2346	3.538	23.765	0.1904	23
NSC0014+2003	3.573	20.052	0.1812	19
NSC0014+1945	3.598	19.745	0.1631	25
NSC0015+1819	3.652	18.325	0.1524	30
NSC0015+2444	3.668	24.727	0.1733	32
NSC0015+2432	3.724	24.526	0.2505	19
NSC0015+2118	3.775	21.295	0.1667	26
NSC0015+2452	3.804	24.873	0.2033	29
NSC0015+2154	3.809	21.907	0.1918	22
NSC0015+2655	3.816	26.915	0.1856	24
NSC0015+1650	3.845	16.832	0.1446	18
NSC0015+1914	3.847	19.227	0.1527	42
NSC0015+2503	3.861	25.051	0.2334	21
NSC0016+1820	3.887	18.338	0.1339	43
NSC0016+1441	3.897	14.676	0.1090	39
NSC0016+2439	4.053	24.651	0.1661	33
NSC0016+0247	4.081	2.776	0.1913	24
NSC0017+1606	4.137	16.101	0.1274	28
NSC0017+1626	4.161	16.428	0.0941	27
NSC0017+1757	4.179	17.950	0.1968	20
NSC0017+1822	4.192	18.366	0.1457	66
NSC0017+1919	4.208	19.315	0.1337	30
NSC0017+2432	4.353	24.527	0.2420	23
NSC0018+1504	4.379	15.064	0.1768	21
NSC0018+2245	4.485	22.754	0.1602	34
NSC0018+1836	4.486	18.598	0.1353	30
NSC0018+2640	4.510	26.662	0.1682	21
NSC0018+2316	4.515	23.269	0.1237	20
NSC0018+1810	4.555	18.168	0.1242	34
NSC0018+0201	4.584	2.010	0.2384	16
NSC0019+1850	4.663	18.835	0.1293	32
NSC0019+1714	4.740	17.240	0.1233	29
NSC0019+1932	4.784	19.530	0.1054	23
NSC0019+0129	4.794	1.478	0.2216	15
NSC0019+2615	4.801	26.247	0.1831	21
NSC0019+2507	4.818	25.119	0.2628	14
NSC0020+2519	4.903	25.312	0.2228	35
NSC0020+1440	4.906	14.673	0.1836	31
NSC0020+0122	4.961	1.371	0.1569	27
NSC0020+1728	5.019	17.462	0.1732	19
NSC0020+1819	5.042	18.320	0.2364	21
NSC0020+0006	5.066	0.098	0.2096	44
NSC0020+2321	5.068	23.342	0.0990	43
NSC0020+0040	5.075	0.672	0.1895	19
NSC0021+1625	5.155	16.424	0.1285	25
NSC0021+0203	5.162	2.055	0.2595	23
NSC0021+2346	5.166	23.772	0.1824	30
NSC0021+0133	5.174	1.556	0.2313	27
NSC0021+2604	5.191	26.066	0.1241	35
NSC0021+2241	5.224	22.682	0.1608	33
NSC0021+0009	5.228	0.157	0.2095	34
NSC0021+1950	5.262	19.837	0.1344	25
NSC0022+1723	5.427	17.376	0.1976	23
NSC0022+2253	5.474	22.886	0.1715	27
NSC0022+2430	5.478	24.496	0.1482	36
NSC0022+2319	5.524	23.312	0.1161	114
NSC0022+2411	5.550	24.175	0.1239	49
NSC0022+2754	5.583	27.892	0.1156	50
NSC0022+2002	5.601	20.030	0.1152	30
NSC0022+2343	5.617	23.717	0.1024	53
NSC0023+0016	5.646	0.259	0.1432	36
NSC0023+2624	5.711	26.399	0.1521	22
NSC0023+1414	5.740	14.232	0.1126	28
NSC0023+2515	5.770	25.246	0.1127	49
NSC0023+0010	5.802	0.159	0.2333	25
NSC0024+0139	5.877	1.658	0.1877	31
NSC0024+1715	5.909	17.255	0.1207	23
NSC0024+2526	6.033	25.428	0.1062	28
NSC0025+1334	6.171	13.574	0.1190	26
NSC0025+2531	6.298	25.523	0.1238	35
NSC0025+2305	6.305	23.091	0.1196	37
NSC0025+1829	6.330	18.481	0.1459	22
NSC0025+2442	6.330	24.702	0.1879	22
NSC0026+2335	6.382	23.591	0.1303	33
NSC0026+2635	6.418	26.580	0.2098	31
NSC0026+0135	6.460	1.580	0.2361	21
NSC0026+1743	6.545	17.710	0.1507	27
NSC0026+2347	6.580	23.778	0.0978	42
NSC0027+2640	6.628	26.663	0.2521	20
NSC0027+0030	6.641	0.498	0.1247	25
NSC0027+1723	6.643	17.387	0.1268	23
NSC0027+0113	6.652	1.213	0.1819	31

Continued...

Table B.2 - SGP Robust, Continued

Name	RA	Dec	z_{phot}	N_{gal}
NSC0027+0141	6.668	1.677	0.1526	24
NSC0027+1943	6.673	19.722	0.1146	45
NSC0027+2659	6.680	26.986	0.1290	28
NSC0027+2240	6.783	22.661	0.1372	68
NSC0027+0032	6.787	0.537	0.1966	22
NSC0027+0225	6.796	2.412	0.1650	39
NSC0027+2753	6.821	27.883	0.1136	37
NSC0027+1327	6.845	13.445	0.1776	27
NSC0028+1733	6.893	17.558	0.1463	30
NSC0028+1711	6.921	17.175	0.1601	25
NSC0028+2418	6.945	24.303	0.1910	22
NSC0028+2516	7.036	25.264	0.2350	21
NSC0028+1355	7.062	13.911	0.1453	44
NSC0029+0042	7.179	0.692	0.1971	25
NSC0029+2630	7.187	26.503	0.2116	19
NSC0029+1727	7.189	17.444	0.1481	39
NSC0029+0018	7.204	0.294	0.1831	32
NSC0029+1744	7.210	17.733	0.1038	72
NSC0029+1627	7.236	16.446	0.1346	54
NSC0029+1819	7.243	18.309	0.1630	45
NSC0029+2360	7.288	23.997	0.1897	24
NSC0029+2624	7.359	26.396	0.1453	41
NSC0029+1643	7.370	16.718	0.1812	27
NSC0030+1824	7.396	18.402	0.1559	71
NSC0030+2417	7.476	24.285	0.1913	26
NSC0030+1450	7.482	14.839	0.2091	28
NSC0030+1510	7.507	15.158	0.1384	26
NSC0030+2724	7.552	27.404	0.1591	27
NSC0030+1328	7.554	13.474	0.1426	40
NSC0030+1845	7.620	18.745	0.1640	47
NSC0031+1828	7.656	18.467	0.1175	77
NSC0031+2316	7.662	23.262	0.1574	16
NSC0031+2025	7.780	20.422	0.1127	20
NSC0031+2612	7.785	26.203	0.1171	28
NSC0031+1443	7.813	14.721	0.1877	34
NSC0031+0227	7.834	2.452	0.1310	36
NSC0031+1843	7.858	18.713	0.1582	33
NSC0031+1855	7.862	18.922	0.1904	23
NSC0032+0128	7.899	1.468	0.1496	25
NSC0032+0015	7.908	0.243	0.2036	25
NSC0032+2202	7.972	22.036	0.1594	26
NSC0032+0236	8.003	2.604	0.1501	35
NSC0032+0020	8.008	0.329	0.1345	24
NSC0032+2245	8.013	22.753	0.2157	32
NSC0032+1752	8.025	17.868	0.1471	30
NSC0032+1428	8.041	14.459	0.1833	30
NSC0032+0121	8.066	1.354	0.1477	30
NSC0032+1831	8.123	18.509	0.1468	41
NSC0033+1419	8.145	14.319	0.1700	21
NSC0033+2246	8.164	22.763	0.1317	46
NSC0033+0504	8.170	5.073	0.1431	36
NSC0033+2005	8.220	20.088	0.1250	26
NSC0033+1814	8.221	18.234	0.1798	28
NSC0033+1213	8.224	12.209	0.1793	42
NSC0033+0359	8.240	3.980	0.2350	30
NSC0033+1748	8.281	17.803	0.0848	32
NSC0033+2611	8.295	26.175	0.0923	43
NSC0033+1111	8.300	11.189	0.2080	21
NSC0034+0120	8.411	1.335	0.1672	27
NSC0034+0534	8.442	5.571	0.1079	17
NSC0034+1832	8.453	18.527	0.1430	36
NSC0034+1357	8.458	13.955	0.2689	23
NSC0034+1912	8.474	19.196	0.2244	24
NSC0034+1822	8.476	18.364	0.1536	48
NSC0034+1948	8.476	19.798	0.1855	27
NSC0034+1738	8.481	17.628	0.1931	22
NSC0034+0620	8.495	6.338	0.1214	43
NSC0034+2644	8.495	26.731	0.2638	26
NSC0034+0050	8.555	0.836	0.2091	27
NSC0034+2518	8.559	25.306	0.1368	33
NSC0034+1249	8.560	12.812	0.2378	25
NSC0034+1456	8.615	14.928	0.1408	19
NSC0035+1756	8.644	17.934	0.2524	21
NSC0035+2633	8.659	26.547	0.1597	31
NSC0035+1218	8.687	12.299	0.1279	29
NSC0035+1835	8.699	18.576	0.2627	19
NSC0035+1248	8.700	12.797	0.2125	23
NSC0035+0142	8.825	1.701	0.0830	47
NSC0035+2554	8.830	25.899	0.2011	35
NSC0035+2026	8.832	20.427	0.1606	57
NSC0035+2328	8.839	23.467	0.1308	35
NSC0035+1820	8.852	18.330	0.1768	28
NSC0035+1407	8.866	14.123	0.2486	21
NSC0036+1257	8.880	12.951	0.2125	30
NSC0036+2140	8.895	21.662	0.1538	36
NSC0036+2219	8.901	22.315	0.2337	24
NSC0036+1840	8.936	18.659	0.1475	31

Continued...

Table B.2 - SGP Robust, Continued

Name	RA	Dec	z_{phot}	N_{gal}
NSC0036+2046	8.993	20.773	0.1526	34
NSC0036+2657	9.014	26.954	0.1007	21
NSC0036+0438	9.022	4.626	0.1634	34
NSC0036+0236	9.046	2.593	0.1351	31
NSC0036+2631	9.056	26.516	0.1444	25
NSC0036+2555	9.061	25.923	0.1838	20
NSC0036+2212	9.094	22.197	0.1806	34
NSC0036+1824	9.113	18.405	0.1762	23
NSC0037+0632	9.130	6.541	0.1105	28
NSC0037+1854	9.144	18.901	0.1720	39
NSC0037+0031	9.166	0.514	0.1528	24
NSC0037+1905	9.237	19.081	0.1651	44
NSC0037+1751	9.251	17.857	0.1698	17
NSC0037+2133	9.255	21.545	0.2177	26
NSC0037+2201	9.271	22.022	0.1446	23
NSC0037+0909	9.279	9.156	0.2588	25
NSC0037+2514	9.294	25.228	0.1604	36
NSC0037+1919	9.325	19.310	0.1317	57
NSC0037+0006	9.366	0.095	0.1689	37
NSC0038+1316	9.392	13.272	0.2043	26
NSC0038+1808	9.412	18.134	0.1363	55
NSC0038+1822	9.425	18.366	0.1235	54
NSC0038+1847	9.451	18.784	0.1688	33
NSC0038+1423	9.461	14.387	0.1369	21
NSC0038+0930	9.563	9.494	0.2546	27
NSC0038+0706	9.572	7.093	0.2088	18
NSC0038+2039	9.574	20.645	0.1539	22
NSC0039+1909	9.627	19.152	0.1037	46
NSC0039+2544	9.643	25.736	0.1228	39
NSC0039+2053	9.686	20.878	0.1658	26
NSC0039+1134	9.727	11.573	0.1365	27
NSC0039+1831	9.783	18.515	0.1416	36
NSC0039+2407	9.792	24.111	0.1499	28
NSC0039+1402	9.798	14.027	0.1428	32
NSC0039+0344	9.820	3.736	0.1134	23
NSC0039+1714	9.832	17.227	0.1374	21
NSC0039+1839	9.861	18.655	0.1679	27
NSC0040+2144	9.877	21.730	0.1718	35
NSC0040+1930	9.894	19.501	0.1944	22
NSC0040+0718	9.909	7.296	0.1738	16
NSC0040+2052	9.915	20.868	0.1451	23
NSC0040+2653	9.940	26.881	0.1995	22
NSC0040+0331	9.952	3.509	0.0899	29
NSC0040+0647	9.971	6.787	0.0583	48
NSC0040+1907	9.983	19.112	0.1696	36
NSC0040+1336	10.024	13.607	0.1821	19
NSC0040+2551	10.055	25.857	0.1791	36
NSC0040+2233	10.086	22.543	0.2100	18
NSC0040+1123	10.100	11.383	0.1942	22
NSC0040+2532	10.122	25.530	0.1363	47
NSC0041+1307	10.129	13.109	0.1972	19
NSC0041+2159	10.136	21.976	0.1766	17
NSC0041+2649	10.145	26.821	0.1984	36
NSC0041+1829	10.153	18.482	0.1533	28
NSC0041+1702	10.163	17.032	0.1428	37
NSC0041+1809	10.163	18.143	0.1540	42
NSC0041+1603	10.188	16.052	0.2146	22
NSC0041+2458	10.190	24.970	0.1673	38
NSC0041+1427	10.201	14.454	0.2276	31
NSC0041+2015	10.216	20.254	0.1228	23
NSC0041+2128	10.219	21.467	0.1198	47
NSC0041+1945	10.220	19.758	0.1078	36
NSC0041+2217	10.220	22.281	0.1543	46
NSC0041+0233	10.239	2.544	0.1474	31
NSC0041+1537	10.240	15.616	0.2119	33
NSC0041+2523	10.260	25.383	0.1299	91
NSC0041+1902	10.268	19.033	0.1885	33
NSC0041+0844	10.296	8.727	0.2436	18
NSC0041+2654	10.324	26.902	0.1457	24
NSC0041+2235	10.330	22.578	0.2069	27
NSC0041+2512	10.357	25.202	0.1176	62
NSC0041+1401	10.372	14.022	0.2443	38
NSC0042+1934	10.426	19.573	0.1437	18
NSC0042+0905	10.429	9.076	0.1454	15
NSC0042+1803	10.429	18.046	0.2436	18
NSC0042+2127	10.433	21.443	0.1223	82
NSC0042+2060	10.486	20.993	0.1898	32
NSC0042+1521	10.488	15.355	0.1137	34
NSC0042+2047	10.540	20.785	0.1967	23
NSC0042+2524	10.610	25.401	0.1411	54
NSC0042+2023	10.620	20.381	0.1017	34
NSC0042+2437	10.621	24.622	0.1783	26
NSC0043+1609	10.641	16.153	0.2031	27
NSC0043+1315	10.654	13.256	0.1744	22
NSC0043+1825	10.657	18.421	0.2561	30
NSC0043+2155	10.658	21.916	0.1628	29
NSC0043+2306	10.680	23.099	0.1517	33

Continued...

Table B.2 - SGP Robust, Continued

Name	RA	Dec	z_{phot}	N_{gal}
NSC0043+1459	10.720	14.985	0.2091	23
NSC0043+2418	10.720	24.302	0.1109	37
NSC0043+1517	10.739	15.286	0.1246	49
NSC0043+0013	10.771	0.216	0.1573	27
NSC0043+1954	10.807	19.908	0.1637	26
NSC0043+2401	10.841	24.016	0.1924	25
NSC0044+1811	10.884	18.189	0.1466	44
NSC0044+0101	10.901	1.019	0.0768	30
NSC0044+2042	10.933	20.695	0.2104	34
NSC0044+0211	10.939	2.188	0.1111	41
NSC0044+2423	10.941	24.390	0.1102	53
NSC0044+2001	10.942	20.015	0.1217	33
NSC0044+2748	10.946	27.793	0.1495	25
NSC0044+0007	10.965	0.113	0.1970	29
NSC0044+1037	10.986	10.609	0.1979	35
NSC0044+2656	11.010	26.941	0.1438	41
NSC0044+0111	11.017	1.189	0.0640	36
NSC0044+2135	11.017	21.589	0.1346	25
NSC0044+0455	11.036	4.915	0.1712	23
NSC0044+2247	11.041	22.788	0.1807	21
NSC0044+1534	11.108	15.569	0.1886	29
NSC0044+1627	11.119	16.455	0.2357	23
NSC0045+0322	11.142	3.361	0.1552	40
NSC0045+1739	11.193	17.652	0.1718	23
NSC0045+1108	11.219	11.136	0.2391	22
NSC0045+0547	11.241	5.788	0.1148	27
NSC0045+0159	11.248	1.979	0.1101	30
NSC0045+2523	11.287	25.381	0.1865	21
NSC0045+1529	11.293	15.476	0.2593	21
NSC0045+0504	11.298	5.069	0.0979	26
NSC0045+0841	11.299	8.686	0.2445	29
NSC0045+1446	11.304	14.772	0.2076	20
NSC0045+2455	11.305	24.915	0.1592	31
NSC0045+1547	11.312	15.781	0.2062	17
NSC0045+1940	11.328	19.666	0.1827	14
NSC0045+1007	11.346	10.121	0.1867	34
NSC0045+2746	11.346	27.774	0.1373	20
NSC0046+1560	11.402	15.993	0.2362	33
NSC0046+2238	11.407	22.631	0.2081	20
NSC0046+0923	11.423	9.382	0.2119	24
NSC0046+0539	11.431	5.653	0.1022	30
NSC0046+1527	11.433	15.449	0.1749	25
NSC0046+2015	11.455	20.244	0.1448	32
NSC0046+0903	11.476	9.056	0.1854	27
NSC0046+2707	11.495	27.111	0.1779	38
NSC0046+0059	11.512	0.978	0.1208	26
NSC0046+1933	11.538	19.547	0.1279	40
NSC0046+1628	11.548	16.465	0.2419	27
NSC0046+0005	11.561	0.076	0.1367	33
NSC0046+2032	11.583	20.540	0.1323	120
NSC0046+2448	11.605	24.793	0.1736	27
NSC0047+1752	11.631	17.872	0.2035	25
NSC0047+1539	11.647	15.655	0.1552	33
NSC0047+0916	11.671	9.262	0.1420	23
NSC0047+1530	11.758	15.497	0.1515	22
NSC0047+1850	11.784	18.841	0.1867	27
NSC0047+2226	11.800	22.440	0.2368	26
NSC0047+1803	11.838	18.055	0.1999	20
NSC0048+2225	11.967	22.425	0.1791	23
NSC0048+0043	12.038	0.718	0.1484	18
NSC0048+1738	12.058	17.637	0.2215	25
NSC0048+2360	12.070	23.998	0.1549	23
NSC0048+2328	12.073	23.465	0.1847	31
NSC0048+0122	12.099	1.362	0.0997	40
NSC0049+0129	12.168	1.490	0.0822	54
NSC0049+2424	12.174	24.392	0.0988	29
NSC0049+2348	12.193	23.807	0.1572	33
NSC0049+2256	12.233	22.929	0.1888	34
NSC0049+2145	12.273	21.755	0.1547	15
NSC0049+2608	12.294	26.127	0.2266	21
NSC0049+2344	12.353	23.727	0.1574	35
NSC0049+0149	12.361	1.819	0.1937	21
NSC0049+1729	12.362	17.487	0.2576	17
NSC0050+0207	12.379	2.116	0.1840	23
NSC0050+1341	12.384	13.682	0.2154	19
NSC0050+0101	12.442	1.011	0.1981	21
NSC0050+2616	12.460	26.263	0.2745	22
NSC0050+2429	12.514	24.486	0.1256	78
NSC0050+1401	12.516	14.019	0.2315	15
NSC0050+2135	12.568	21.588	0.1410	32
NSC0050+1346	12.572	13.766	0.1461	18
NSC0050+1541	12.579	15.682	0.1649	34
NSC0050+1729	12.602	17.491	0.2529	23
NSC0050+1557	12.615	15.944	0.1309	43
NSC0051+1809	12.637	18.151	0.1485	31
NSC0051+2403	12.640	24.046	0.1920	36
NSC0051+1554	12.746	15.895	0.1076	50

Continued...

Table B.2 - SGP Robust, Continued

Name	RA	Dec	z_{phot}	N_{gal}
NSC0051+2621	12.747	26.345	0.2210	42
NSC0051+0125	12.826	1.419	0.1468	20
NSC0051+2408	12.873	24.133	0.2500	34
NSC0052+1729	12.907	17.476	0.2144	21
NSC0052+1742	12.946	17.702	0.1977	21
NSC0052+0814	12.957	8.229	0.1352	24
NSC0052+2423	12.969	24.377	0.1334	58
NSC0052+1629	13.040	16.487	0.2360	18
NSC0052+2217	13.112	22.279	0.1779	47
NSC0052+1841	13.120	18.688	0.1211	22
NSC0053+0202	13.151	2.026	0.2118	19
NSC0053+1547	13.198	15.778	0.1562	26
NSC0053+1957	13.212	19.950	0.2102	17
NSC0053+2201	13.217	22.009	0.1559	22
NSC0053+2419	13.235	24.309	0.1273	61
NSC0053+0607	13.236	6.121	0.1624	40
NSC0053+1042	13.244	10.702	0.1680	30
NSC0053+1609	13.269	16.158	0.1109	31
NSC0053+2653	13.308	26.884	0.1977	27
NSC0053+1929	13.311	19.476	0.1787	20
NSC0053+0151	13.325	1.853	0.1592	28
NSC0054+1716	13.383	17.265	0.1843	25
NSC0054+2016	13.506	20.259	0.2538	29
NSC0054+2719	13.522	27.311	0.1063	37
NSC0054+0629	13.531	6.486	0.1256	25
NSC0054+2034	13.557	20.571	0.1584	19
NSC0054+1927	13.562	19.448	0.1589	20
NSC0055+2318	13.662	23.292	0.1815	34
NSC0055+1815	13.671	18.248	0.0718	22
NSC0055+2023	13.712	20.377	0.1531	44
NSC0055+0546	13.757	5.761	0.1506	39
NSC0055+0634	13.768	6.560	0.1225	21
NSC0055+0204	13.858	2.072	0.0854	21
NSC0055+2456	13.866	24.931	0.1517	20
NSC0056+0514	13.962	5.227	0.1373	29
NSC0056+2513	13.977	25.224	0.1542	24
NSC0056+2625	13.983	26.414	0.1752	76
NSC0056+0038	13.998	0.631	0.1425	50
NSC0056+2549	14.057	25.816	0.1367	44
NSC0056+2123	14.073	21.378	0.2133	31
NSC0056+0815	14.121	8.248	0.1390	33
NSC0057+1844	14.153	18.741	0.1238	55
NSC0057+1516	14.229	15.261	0.0930	40
NSC0057+1117	14.292	11.279	0.1556	23
NSC0057+0003	14.309	0.055	0.1566	22
NSC0057+1448	14.328	14.799	0.1129	26
NSC0057+0808	14.331	8.133	0.0825	33
NSC0058+2157	14.451	21.956	0.2831	20
NSC0058+1452	14.493	14.868	0.0931	35
NSC0058+1356	14.557	13.933	0.1701	20
NSC0058+0541	14.594	5.684	0.0955	21
NSC0058+1441	14.606	14.686	0.0968	34
NSC0058+0356	14.612	3.930	0.1859	17
NSC0059+0855	14.638	8.917	0.0790	19
NSC0059+0940	14.655	9.670	0.2086	18
NSC0059+1246	14.677	12.762	0.1099	48
NSC0059+2134	14.759	21.571	0.2014	18
NSC0059+2703	14.763	27.049	0.0789	62
NSC0059+1914	14.796	19.231	0.2414	19
NSC0059+1115	14.798	11.242	0.1771	20
NSC0059+0410	14.823	4.162	0.2052	25
NSC0059+1853	14.868	18.879	0.1731	29
NSC0059+2630	14.874	26.496	0.1637	20
NSC0100+2144	14.877	21.737	0.2341	26
NSC0100+0914	14.888	9.236	0.1722	25
NSC0100+2247	14.925	22.787	0.1286	14
NSC0100+2347	14.961	23.791	0.1413	40
NSC0100+1419	14.976	14.313	0.1682	42
NSC0100+1340	15.065	13.658	0.1521	22
NSC0100+2237	15.094	22.613	0.2091	22
NSC0101+0833	15.159	8.542	0.1853	22
NSC0101+2519	15.160	25.312	0.1500	22
NSC0101+2246	15.166	22.772	0.1930	20
NSC0101+2035	15.192	20.587	0.1574	37
NSC0101+1206	15.210	12.094	0.2133	22
NSC0101+0139	15.228	1.652	0.2170	30
NSC0101+2539	15.251	25.658	0.0889	27
NSC0101+0030	15.282	0.502	0.1646	29
NSC0101+2152	15.315	21.867	0.1821	28
NSC0101+1353	15.319	13.889	0.1664	28
NSC0101+1540	15.332	15.665	0.1628	21
NSC0101+0849	15.371	8.810	0.2249	17
NSC0102+0045	15.378	0.753	0.2352	26
NSC0102+0560	15.392	5.992	0.1324	29
NSC0102+2420	15.451	24.334	0.1808	12
NSC0102+2503	15.490	25.047	0.1941	29
NSC0102+2658	15.493	26.971	0.1218	35

Continued...

Table B.2 - SGP Robust, Continued

Name	RA	Dec	z_{phot}	N_{gal}
NSC0102+2622	15.515	26.364	0.2325	21
NSC0102+1549	15.578	15.816	0.2099	22
NSC0102+1340	15.580	13.668	0.2128	25
NSC0102+1451	15.583	14.858	0.1572	38
NSC0102+1952	15.601	19.868	0.2046	18
NSC0103+2156	15.633	21.930	0.1491	51
NSC0103+2523	15.655	25.377	0.1404	40
NSC0103+0109	15.672	1.147	0.1570	46
NSC0103+0010	15.697	0.163	0.2412	23
NSC0103+0825	15.721	8.421	0.1677	26
NSC0103+2400	15.722	24.006	0.2011	24
NSC0103+2703	15.743	27.048	0.2200	33
NSC0103+2128	15.758	21.474	0.1735	43
NSC0103+1321	15.803	13.344	0.1657	21
NSC0103+1446	15.818	14.767	0.1840	17
NSC0103+2648	15.822	26.804	0.1370	35
NSC0103+2518	15.828	25.293	0.1563	38
NSC0103+0019	15.843	0.312	0.2342	22
NSC0103+1549	15.871	15.822	0.2172	18
NSC0104+1959	15.885	19.983	0.2134	22
NSC0104+1532	15.916	15.536	0.1805	27
NSC0104+2327	15.918	23.447	0.1810	27
NSC0104+2532	15.926	25.527	0.1030	35
NSC0104+0133	15.934	1.549	0.1541	27
NSC0104+2708	15.953	27.126	0.2452	27
NSC0104+2627	15.959	26.454	0.1724	45
NSC0104+0852	15.971	8.870	0.1284	30
NSC0104+1448	15.976	14.794	0.1960	26
NSC0104+2237	15.985	22.615	0.2390	20
NSC0104+2601	15.992	26.015	0.1571	31
NSC0104+0417	15.996	4.281	0.1293	18
NSC0104+2215	16.006	22.257	0.2289	25
NSC0104+0638	16.015	6.629	0.1416	20
NSC0104+1525	16.052	15.412	0.1555	35
NSC0104+2507	16.060	25.116	0.1862	47
NSC0104+2719	16.064	27.325	0.1689	28
NSC0104+2348	16.102	23.805	0.2218	15
NSC0104+2106	16.108	21.099	0.1424	28
NSC0104+2230	16.125	22.503	0.1812	29
NSC0105+1405	16.145	14.087	0.1563	24
NSC0105+2642	16.160	26.694	0.1468	46
NSC0105+1746	16.168	17.764	0.1245	17
NSC0105+2542	16.179	25.700	0.1541	54
NSC0105+2438	16.192	24.637	0.2332	19
NSC0105+2216	16.227	22.273	0.2036	21
NSC0105+2559	16.230	25.984	0.1413	38
NSC0105+0004	16.231	0.060	0.2756	38
NSC0105+0201	16.233	2.022	0.1610	112
NSC0105+0657	16.238	6.954	0.1954	15
NSC0105+1542	16.241	15.695	0.2045	22
NSC0105+0210	16.263	2.159	0.1636	113
NSC0105+0719	16.265	7.310	0.1262	27
NSC0105+2319	16.279	23.322	0.1776	19
NSC0105+0239	16.339	2.652	0.1715	24
NSC0105+2611	16.361	26.189	0.1223	29
NSC0105+1516	16.374	15.259	0.1605	26
NSC0106+2749	16.379	27.811	0.2230	27
NSC0106+0005	16.441	0.088	0.2142	26
NSC0106+2459	16.448	24.983	0.1725	32
NSC0106+1535	16.450	15.575	0.1659	35
NSC0106+0727	16.492	7.449	0.0740	39
NSC0106+1333	16.511	13.545	0.1481	22
NSC0106+0945	16.512	9.747	0.2383	18
NSC0106+2528	16.524	25.473	0.1953	22
NSC0106+0334	16.526	3.561	0.1033	28
NSC0106+0036	16.533	0.595	0.1553	27
NSC0106+0052	16.542	0.861	0.2423	21
NSC0106+1431	16.548	14.515	0.1782	24
NSC0106+0110	16.551	1.171	0.2240	23
NSC0106+0007	16.589	0.121	0.2389	27
NSC0106+0421	16.591	4.351	0.1274	28
NSC0107+2450	16.635	24.834	0.1806	19
NSC0107+1500	16.643	15.001	0.1989	18
NSC0107+0017	16.659	0.287	0.2185	35
NSC0107+0954	16.666	9.903	0.1533	20
NSC0107+2613	16.678	26.218	0.1819	47
NSC0107+0104	16.701	1.065	0.2359	29
NSC0107+0038	16.728	0.633	0.1304	43
NSC0107+1918	16.738	19.306	0.2293	25
NSC0107+1546	16.746	15.762	0.1951	29
NSC0107+0731	16.813	7.523	0.1014	27
NSC0107+2148	16.817	21.808	0.2410	27
NSC0107+2210	16.844	22.167	0.2239	18
NSC0107+1416	16.852	14.267	0.1159	62
NSC0107+0904	16.864	9.061	0.1429	27
NSC0108+0850	16.876	8.837	0.1577	23
NSC0108+2438	16.925	24.626	0.1876	27

Continued...

Table B.2 - SGP Robust, Continued

Name	RA	Dec	z_{phot}	N_{gal}
NSC0108+0042	16.937	0.705	0.1443	23
NSC0108+0459	16.947	4.979	0.2416	15
NSC0108+2450	16.951	24.825	0.2024	21
NSC0108+2653	16.956	26.882	0.2217	24
NSC0108+0022	16.981	0.358	0.1436	26
NSC0108+1829	16.996	18.487	0.2203	23
NSC0108+2727	17.000	27.457	0.1524	32
NSC0108+2701	17.011	27.013	0.2029	26
NSC0108+2743	17.012	27.723	0.1717	25
NSC0108+1843	17.016	18.718	0.2212	20
NSC0108+2125	17.017	21.415	0.2226	17
NSC0108+2531	17.035	25.509	0.1646	27
NSC0108+0217	17.043	2.283	0.0613	46
NSC0108+1312	17.043	13.198	0.2252	19
NSC0108+2756	17.105	27.936	0.2452	25
NSC0109+0257	17.142	2.954	0.2516	20
NSC0109+0406	17.172	4.098	0.2174	15
NSC0109+2522	17.180	25.363	0.1606	36
NSC0109+2454	17.205	24.907	0.2169	25
NSC0109+2747	17.230	27.778	0.1863	15
NSC0109+2151	17.238	21.847	0.1687	30
NSC0109+1327	17.243	13.458	0.1559	30
NSC0109+1310	17.290	13.161	0.0987	61
NSC0109+1453	17.336	14.890	0.1639	40
NSC0110+0654	17.387	6.893	0.1296	26
NSC0110+0516	17.398	5.264	0.1619	57
NSC0110+2704	17.456	27.075	0.1885	26
NSC0110+2711	17.468	27.182	0.1632	16
NSC0110+1360	17.485	13.994	0.0983	40
NSC0110+2507	17.495	25.123	0.1124	40
NSC0110+1101	17.508	11.020	0.2563	23
NSC0110+2723	17.520	27.390	0.1859	18
NSC0110+0802	17.555	8.031	0.1146	39
NSC0110+0825	17.566	8.410	0.1399	29
NSC0110+1749	17.572	17.811	0.0769	75
NSC0110+0842	17.584	8.693	0.1831	26
NSC0110+1614	17.595	16.233	0.1165	41
NSC0111+1733	17.630	17.547	0.0813	73
NSC0111+1030	17.633	10.505	0.1223	36
NSC0111+0103	17.665	1.045	0.1837	24
NSC0111+2744	17.671	27.740	0.1797	26
NSC0111+1653	17.674	16.877	0.0904	48
NSC0111+1358	17.682	13.962	0.2121	26
NSC0111+1137	17.699	11.615	0.1383	38
NSC0111+2027	17.731	20.458	0.2534	14
NSC0111+0911	17.776	9.187	0.1558	35
NSC0111+1814	17.783	18.226	0.2017	19
NSC0111+2652	17.793	26.873	0.1493	38
NSC0111+0854	17.811	8.907	0.2078	27
NSC0111+1856	17.812	18.934	0.2272	27
NSC0111+2627	17.821	26.450	0.1389	27
NSC0111+2254	17.842	22.903	0.1678	23
NSC0111+1736	17.843	17.601	0.0832	75
NSC0111+2456	17.843	24.925	0.1416	45
NSC0111+0658	17.847	6.963	0.1257	22
NSC0111+2043	17.871	20.718	0.2415	22
NSC0112+1142	17.908	11.700	0.2041	20
NSC0112+0829	17.912	8.491	0.1986	34
NSC0112+1843	17.915	18.723	0.2234	24
NSC0112+1714	17.922	17.228	0.1086	38
NSC0112+0502	17.928	5.040	0.1947	28
NSC0112+1654	17.938	16.899	0.1096	57
NSC0112+1004	17.952	10.064	0.1585	38
NSC0112+1116	17.954	11.269	0.1613	19
NSC0112+2057	17.960	20.947	0.2185	18
NSC0112+2427	17.965	24.444	0.1484	46
NSC0112+0954	17.977	9.902	0.1825	25
NSC0112+2747	17.988	27.791	0.1420	56
NSC0112+2658	17.989	26.965	0.1100	30
NSC0112+1724	18.002	17.393	0.1436	39
NSC0112+0943	18.033	9.716	0.1363	41
NSC0112+2434	18.048	24.563	0.1479	47
NSC0112+2425	18.087	24.411	0.1937	44
NSC0112+1620	18.092	16.327	0.0707	45
NSC0112+2029	18.097	20.483	0.2371	20
NSC0112+1835	18.112	18.583	0.1521	33
NSC0113+1252	18.138	12.871	0.1900	26
NSC0113+2460	18.152	24.999	0.1168	42
NSC0113+0513	18.165	5.211	0.2192	20
NSC0113+2722	18.214	27.361	0.1667	23
NSC0113+2230	18.232	22.504	0.2341	21
NSC0113+2513	18.244	25.219	0.1579	44
NSC0113+1129	18.258	11.484	0.1327	41
NSC0113+2003	18.268	20.045	0.1806	26
NSC0113+1604	18.278	16.071	0.0952	58
NSC0113+1412	18.285	14.208	0.1287	22
NSC0113+2730	18.288	27.508	0.1656	32

Continued...

Table B.2 - SGP Robust, Continued

Name	RA	Dec	z_{phot}	N_{gal}
NSC0113+1530	18.297	15.499	0.0753	56
NSC0113+1013	18.323	10.209	0.1266	31
NSC0113+2209	18.326	22.143	0.2713	18
NSC0113+1553	18.334	15.875	0.0933	40
NSC0113+1706	18.340	17.103	0.1226	36
NSC0113+0127	18.367	1.458	0.1385	32
NSC0113+1619	18.369	16.313	0.1007	34
NSC0114+2359	18.400	23.981	0.1671	30
NSC0114+1303	18.422	13.049	0.1543	38
NSC0114+2024	18.448	20.395	0.1521	19
NSC0114+2738	18.480	27.636	0.2542	23
NSC0114+2321	18.511	23.358	0.1513	23
NSC0114+1804	18.520	18.066	0.1295	39
NSC0114+2248	18.562	22.797	0.1665	24
NSC0114+0254	18.587	2.901	0.1577	37
NSC0114+1247	18.617	12.787	0.1848	25
NSC0114+1034	18.621	10.572	0.0968	24
NSC0114+1946	18.623	19.764	0.1306	40
NSC0115+2538	18.643	25.627	0.1743	29
NSC0115+2442	18.645	24.708	0.1897	48
NSC0115+1959	18.679	19.976	0.1968	42
NSC0115+2232	18.691	22.542	0.1835	21
NSC0115+2748	18.741	27.802	0.2267	26
NSC0115+1858	18.759	18.962	0.1785	21
NSC0115+1525	18.802	15.410	0.1310	31
NSC0115+0017	18.821	0.277	0.0828	46
NSC0115+2431	18.822	24.517	0.1764	47
NSC0115+0916	18.864	9.274	0.1588	33
NSC0115+1831	18.867	18.511	0.2023	17
NSC0116+0247	18.881	2.782	0.2139	27
NSC0116+2523	18.918	25.387	0.1672	23
NSC0116+1458	18.951	14.959	0.1698	24
NSC0116+2228	18.961	22.471	0.1510	33
NSC0116+0533	18.973	5.545	0.1593	28
NSC0116+1955	19.006	19.924	0.2011	19
NSC0116+1305	19.019	13.091	0.1682	52
NSC0116+2247	19.020	22.790	0.2013	23
NSC0116+1105	19.025	11.088	0.1863	18
NSC0116+2743	19.051	27.713	0.2264	36
NSC0116+0705	19.061	7.086	0.1241	30
NSC0117+2201	19.127	22.025	0.2069	25
NSC0117+0322	19.143	3.369	0.0599	30
NSC0117+1925	19.149	19.418	0.1854	18
NSC0117+1156	19.172	11.926	0.1748	32
NSC0117+2131	19.186	21.518	0.1759	22
NSC0117+2322	19.214	23.369	0.1839	32
NSC0117+2737	19.217	27.611	0.2197	25
NSC0117+2233	19.232	22.552	0.1941	22
NSC0117+1140	19.245	11.674	0.1673	23
NSC0117+2027	19.283	20.453	0.1984	27
NSC0117+2203	19.289	22.051	0.2210	19
NSC0117+1615	19.292	16.250	0.0988	59
NSC0117+0310	19.294	3.160	0.1138	29
NSC0117+1501	19.297	15.018	0.2184	44
NSC0117+1250	19.310	12.825	0.1742	24
NSC0117+2332	19.311	23.536	0.1007	36
NSC0117+2013	19.339	20.211	0.2708	15
NSC0117+2257	19.346	22.942	0.1859	30
NSC0117+2235	19.371	22.583	0.2028	18
NSC0118+2527	19.376	25.458	0.2330	18
NSC0118+1308	19.410	13.132	0.2283	30
NSC0118+0954	19.413	9.905	0.0954	37
NSC0118+1718	19.420	17.299	0.0824	49
NSC0118+1959	19.468	19.990	0.2171	24
NSC0118+1250	19.473	12.826	0.1587	25
NSC0118+2220	19.504	22.332	0.1870	16
NSC0118+1646	19.508	16.765	0.1319	31
NSC0118+1537	19.514	15.609	0.1197	39
NSC0118+1626	19.530	16.428	0.1412	25
NSC0118+1941	19.556	19.683	0.1768	21
NSC0118+2319	19.558	23.320	0.1049	20
NSC0118+2248	19.591	22.802	0.2194	22
NSC0118+2739	19.593	27.657	0.1929	31
NSC0119+2423	19.680	24.387	0.1364	34
NSC0119+2651	19.739	26.848	0.1334	19
NSC0119+0257	19.766	2.947	0.1179	23
NSC0119+2122	19.766	21.359	0.2102	23
NSC0119+2509	19.766	25.153	0.2132	27
NSC0119+1121	19.799	11.347	0.1873	21
NSC0119+1441	19.805	14.688	0.1035	53
NSC0119+0536	19.807	5.600	0.1289	25
NSC0119+1616	19.834	16.258	0.1441	37
NSC0119+2045	19.835	20.749	0.1894	23
NSC0119+1938	19.852	19.640	0.2598	23
NSC0119+1239	19.856	12.654	0.0935	41
NSC0120+2435	19.876	24.585	0.1681	34
NSC0120+2659	19.900	26.981	0.1345	20

Continued...

Table B.2 - SGP Robust, Continued

Name	RA	Dec	z_{phot}	N_{gal}
NSC0120+2452	19.910	24.874	0.1162	35
NSC0120+1454	19.932	14.900	0.1135	94
NSC0120+1644	19.933	16.736	0.2024	34
NSC0120+2754	19.933	27.906	0.2828	23
NSC0120+2154	19.983	21.893	0.2281	15
NSC0120+2253	20.016	22.880	0.1669	17
NSC0120+1220	20.022	12.331	0.1007	24
NSC0120+2133	20.027	21.549	0.1643	29
NSC0120+1045	20.028	10.751	0.1244	26
NSC0120+1954	20.049	19.899	0.2074	18
NSC0120+1621	20.079	16.354	0.1971	25
NSC0120+2111	20.091	21.185	0.2218	28
NSC0121+2151	20.145	21.842	0.2184	18
NSC0121+1409	20.167	14.142	0.2251	17
NSC0121+2014	20.180	20.230	0.1904	28
NSC0121+1007	20.234	10.109	0.1659	24
NSC0121+2031	20.257	20.511	0.2269	18
NSC0121+2253	20.349	22.888	0.1532	24
NSC0121+2055	20.369	20.909	0.2093	27
NSC0122+1033	20.378	10.558	0.1656	28
NSC0122+2159	20.389	21.979	0.1580	48
NSC0122+2146	20.394	21.763	0.2307	36
NSC0122+2007	20.402	20.124	0.2062	52
NSC0122+1342	20.414	13.702	0.1990	29
NSC0122+1951	20.417	19.846	0.1904	29
NSC0122+2028	20.428	20.461	0.1581	27
NSC0122+0303	20.523	3.051	0.1640	32
NSC0122+1505	20.555	15.089	0.1579	19
NSC0122+0021	20.559	0.355	0.1915	43
NSC0122+1055	20.580	10.918	0.2096	30
NSC0122+1942	20.587	19.697	0.1666	37
NSC0123+0339	20.629	3.647	0.0469	20
NSC0123+0940	20.647	9.668	0.1514	65
NSC0123+0444	20.650	4.738	0.1336	31
NSC0123+1931	20.660	19.518	0.1484	50
NSC0123+1358	20.677	13.972	0.1589	38
NSC0123+1301	20.699	13.019	0.2663	37
NSC0123+2155	20.718	21.918	0.2360	25
NSC0123+2120	20.727	21.339	0.1744	20
NSC0123+1317	20.729	13.279	0.2000	20
NSC0123+1513	20.757	15.214	0.1550	19
NSC0123+1904	20.771	19.068	0.1495	36
NSC0123+1827	20.791	18.450	0.1637	29
NSC0123+2002	20.794	20.035	0.2534	23
NSC0123+2208	20.812	22.134	0.1368	32
NSC0123+1808	20.825	18.139	0.2132	20
NSC0123+1219	20.858	12.310	0.1943	24
NSC0123+0136	20.868	1.605	0.1302	44
NSC0124+1459	20.929	14.980	0.1232	28
NSC0124+2230	20.941	22.497	0.1516	26
NSC0124+1535	20.994	15.587	0.1874	22
NSC0124+2035	21.015	20.592	0.2064	16
NSC0124+1820	21.047	18.325	0.2031	23
NSC0125+2116	21.156	21.274	0.1790	29
NSC0125+2054	21.157	20.905	0.2223	21
NSC0125+1229	21.168	12.483	0.1379	26
NSC0125+1815	21.175	18.252	0.2516	21
NSC0125+1941	21.202	19.687	0.2456	19
NSC0125+1440	21.209	14.659	0.1464	30
NSC0125+0231	21.220	2.516	0.2005	23
NSC0125+1703	21.223	17.052	0.1776	23
NSC0125+1953	21.241	19.885	0.1669	17
NSC0125+2154	21.252	21.904	0.1672	28
NSC0125+0842	21.272	8.706	0.0474	68
NSC0125+2135	21.303	21.586	0.2238	17
NSC0125+2054	21.307	20.902	0.2118	25
NSC0125+2127	21.347	21.450	0.1939	27
NSC0125+2203	21.348	22.046	0.2489	27
NSC0125+1557	21.352	15.944	0.1330	23
NSC0126+1015	21.412	10.254	0.2079	28
NSC0126+1842	21.426	18.695	0.2267	24
NSC0126+0114	21.452	1.236	0.2051	24
NSC0126+1134	21.459	11.569	0.1033	23
NSC0126+0031	21.460	0.522	0.1810	28
NSC0126+0959	21.481	9.984	0.1380	31
NSC0126+1936	21.490	19.605	0.2141	25
NSC0126+1038	21.523	10.630	0.2145	44
NSC0126+0059	21.553	0.991	0.1563	32
NSC0126+1241	21.557	12.688	0.1829	27
NSC0126+1648	21.590	16.796	0.2301	17
NSC0127+1330	21.639	13.495	0.2012	21
NSC0127+1200	21.648	12.003	0.1748	26
NSC0127+1908	21.677	19.127	0.1909	26
NSC0127+0128	21.686	1.472	0.1943	18
NSC0127+2107	21.708	21.116	0.2540	21
NSC0127+0944	21.716	9.734	0.1335	26
NSC0127+1517	21.761	15.277	0.1971	33

Continued...

Table B.2 - SGP Robust, Continued

Name	RA	Dec	z_{phot}	N_{gal}
NSC0127+2212	21.779	22.207	0.1939	20
NSC0127+0156	21.787	1.931	0.1599	25
NSC0127+0133	21.820	1.554	0.1980	20
NSC0127+2057	21.824	20.946	0.2504	17
NSC0127+2117	21.824	21.286	0.2394	29
NSC0127+1624	21.832	16.392	0.2453	21
NSC0128+1213	21.926	12.222	0.0928	27
NSC0128+0716	21.949	7.271	0.1213	34
NSC0128+1529	21.949	15.479	0.1734	35
NSC0128+2249	21.950	22.822	0.2214	28
NSC0128+1508	21.960	15.125	0.1254	52
NSC0128+0148	21.974	1.800	0.1698	34
NSC0128+1156	22.007	11.932	0.0977	25
NSC0128+1633	22.016	16.556	0.0977	42
NSC0128+2159	22.045	21.976	0.2252	31
NSC0128+0441	22.047	4.687	0.0907	28
NSC0128+1237	22.050	12.613	0.1795	22
NSC0128+0550	22.081	5.839	0.0799	22
NSC0128+2010	22.086	20.167	0.2179	24
NSC0128+2219	22.104	22.325	0.2249	29
NSC0128+2117	22.115	21.279	0.2543	19
NSC0128+1612	22.117	16.201	0.1743	38
NSC0129+1825	22.167	18.424	0.1572	24
NSC0129+1651	22.178	16.850	0.1281	34
NSC0129+0156	22.187	1.927	0.1929	25
NSC0129+1252	22.187	12.871	0.1500	33
NSC0129+2229	22.206	22.483	0.2495	27
NSC0129+1560	22.296	15.996	0.2454	34
NSC0129+1316	22.303	13.274	0.2548	24
NSC0129+0617	22.305	6.292	0.1366	18
NSC0129+0606	22.346	6.093	0.1164	24
NSC0130+2234	22.378	22.563	0.1777	19
NSC0130+1957	22.384	19.949	0.2052	29
NSC0130+1159	22.452	11.989	0.0951	31
NSC0130+0916	22.556	9.268	0.1528	25
NSC0130+2138	22.589	21.634	0.2586	15
NSC0130+0533	22.614	5.553	0.1122	34
NSC0131+1936	22.645	19.599	0.1777	23
NSC0131+0832	22.681	8.541	0.1442	26
NSC0131+2029	22.681	20.487	0.2394	19
NSC0131+2157	22.682	21.943	0.1688	25
NSC0131+1551	22.687	15.857	0.1592	24
NSC0131+0034	22.741	0.565	0.1655	23
NSC0131+2251	22.750	22.855	0.1770	16
NSC0131+1448	22.786	14.800	0.2293	24
NSC0131+0820	22.791	8.325	0.1332	29
NSC0131+0632	22.861	6.537	0.1660	24
NSC0131+0513	22.863	5.214	0.2259	20
NSC0131+0410	22.872	4.162	0.1728	20
NSC0132+0033	22.879	0.549	0.1020	40
NSC0132+0651	22.881	6.853	0.1255	35
NSC0132+0040	22.913	0.671	0.1381	36
NSC0132+1928	22.917	19.471	0.2417	22
NSC0132+0500	22.919	5.003	0.1215	25
NSC0132+0834	23.091	8.574	0.2155	22
NSC0133+1423	23.125	14.388	0.2353	18
NSC0133+1449	23.146	14.823	0.2307	17
NSC0133+0059	23.267	0.978	0.1104	28
NSC0133+1208	23.304	12.135	0.2450	20
NSC0133+1360	23.306	13.998	0.2451	19
NSC0133+1309	23.372	13.152	0.1677	40
NSC0134+1907	23.403	19.118	0.2008	29
NSC0134+2244	23.412	22.726	0.2146	33
NSC0134+1342	23.433	13.703	0.2236	22
NSC0134+0325	23.435	3.416	0.1024	19
NSC0134+0624	23.458	6.402	0.1630	21
NSC0134+1402	23.486	14.029	0.2379	20
NSC0134+1113	23.489	11.211	0.1224	20
NSC0134+2219	23.527	22.320	0.2191	25
NSC0134+0532	23.542	5.532	0.2265	27
NSC0134+1624	23.563	16.395	0.1198	34
NSC0134+0604	23.580	6.073	0.0619	16
NSC0134+1431	23.589	14.519	0.1563	26
NSC0134+0432	23.597	4.538	0.2306	18
NSC0134+1344	23.600	13.741	0.2222	20
NSC0134+0408	23.616	4.139	0.1577	28
NSC0134+2257	23.621	22.957	0.2537	19
NSC0134+1601	23.622	16.012	0.1641	18
NSC0135+1612	23.627	16.200	0.1088	48
NSC0135+1955	23.646	19.914	0.1769	30
NSC0135+1746	23.685	17.767	0.2218	24
NSC0135+0022	23.774	0.360	0.1802	25
NSC0135+1337	23.778	13.624	0.2551	16
NSC0135+1748	23.816	17.806	0.2316	24
NSC0135+1520	23.828	15.335	0.1266	27
NSC0135+2037	23.859	20.620	0.1961	38
NSC0135+2235	23.870	22.578	0.1730	21

Continued...

Table B.2 - SGP Robust, Continued

Name	RA	Dec	z_{phot}	N_{gal}
NSC0136+1453	23.876	14.882	0.1800	32
NSC0136+1402	23.929	14.029	0.2368	16
NSC0136+0911	23.955	9.178	0.2578	23
NSC0136+1312	24.047	13.201	0.1783	25
NSC0136+0826	24.056	8.435	0.1834	36
NSC0136+1331	24.067	13.515	0.2925	26
NSC0136+1759	24.076	17.989	0.2291	21
NSC0136+2209	24.120	22.143	0.2141	16
NSC0137+1252	24.126	12.866	0.1272	33
NSC0137+2250	24.135	22.839	0.2302	25
NSC0137+2236	24.138	22.594	0.2011	19
NSC0137+2014	24.159	20.231	0.2239	28
NSC0137+1811	24.199	18.186	0.2205	26
NSC0137+2258	24.249	22.963	0.1366	27
NSC0137+1317	24.296	13.287	0.1571	24
NSC0137+1945	24.306	19.747	0.2646	18
NSC0137+1617	24.328	16.287	0.1701	24
NSC0137+0912	24.334	9.198	0.1955	37
NSC0137+0256	24.360	2.937	0.1088	28
NSC0137+1718	24.360	17.294	0.2184	25
NSC0137+1518	24.361	15.303	0.2193	22
NSC0138+0935	24.388	9.582	0.2091	23
NSC0138+2023	24.484	20.378	0.1602	17
NSC0138+0856	24.485	8.940	0.1407	28
NSC0138+1540	24.496	15.675	0.1464	21
NSC0138+1809	24.515	18.153	0.1866	35
NSC0138+1152	24.540	11.859	0.1488	42
NSC0138+1344	24.546	13.732	0.2085	26
NSC0138+0834	24.550	8.569	0.1477	20
NSC0138+2055	24.562	20.925	0.1728	19
NSC0138+1313	24.566	13.223	0.1086	23
NSC0138+0847	24.586	8.783	0.1807	21
NSC0138+1325	24.603	13.420	0.1968	26
NSC0139+2202	24.754	22.039	0.2083	29
NSC0139+1913	24.770	19.215	0.2732	22
NSC0139+0959	24.787	9.980	0.1307	32
NSC0139+1850	24.821	18.830	0.1715	38
NSC0139+1833	24.825	18.543	0.2011	17
NSC0139+1750	24.846	17.827	0.1860	23
NSC0140+0910	24.905	9.162	0.1439	25
NSC0140+0121	24.923	1.351	0.1280	31
NSC0140+1811	24.941	18.188	0.2151	34
NSC0140+1326	25.002	13.431	0.1972	17
NSC0140+1229	25.112	12.483	0.1608	28
NSC0141+1521	25.131	15.351	0.2279	15
NSC0141+1247	25.166	12.782	0.2252	25
NSC0141+1432	25.191	14.537	0.2228	17
NSC0141+1854	25.195	18.898	0.2151	42
NSC0141+1301	25.202	13.025	0.2182	17
NSC0141+1909	25.221	19.157	0.1758	18
NSC0141+2013	25.258	20.212	0.2434	28
NSC0141+2746	25.287	27.761	0.1581	28
NSC0141+1531	25.290	15.512	0.2386	16
NSC0141+1215	25.300	12.243	0.1996	34
NSC0141+0010	25.304	0.164	0.0857	22
NSC0141+1120	25.306	11.329	0.1656	21
NSC0141+0524	25.321	5.400	0.1679	19
NSC0141+1524	25.355	15.403	0.2401	24
NSC0141+1209	25.372	12.145	0.2132	25
NSC0142+1010	25.454	10.159	0.1727	33
NSC0142+1649	25.482	16.820	0.2406	41
NSC0142+0737	25.490	7.610	0.0866	58
NSC0142+2002	25.497	20.036	0.1349	40
NSC0142+1303	25.511	13.045	0.1748	30
NSC0142+2131	25.512	21.517	0.2575	29
NSC0142+0924	25.514	9.397	0.2211	17
NSC0142+1909	25.516	19.148	0.1686	24
NSC0143+1040	25.628	10.675	0.1541	27
NSC0143+1421	25.689	14.354	0.2388	22
NSC0143+2446	25.723	24.762	0.1815	21
NSC0143+1160	25.760	11.999	0.1668	23
NSC0143+1301	25.785	13.013	0.2147	21
NSC0143+1959	25.817	19.990	0.2143	32
NSC0143+1217	25.867	12.280	0.1513	47
NSC0144+0612	25.876	6.197	0.0996	29
NSC0144+0945	25.887	9.757	0.1801	27
NSC0144+1205	25.911	12.086	0.1717	23
NSC0144+2606	25.929	26.103	0.1863	16
NSC0144+1307	25.977	13.113	0.1951	37
NSC0144+0624	25.988	6.407	0.0699	35
NSC0144+2059	25.990	20.977	0.2317	28
NSC0144+1118	26.018	11.307	0.2346	26
NSC0144+0901	26.021	9.009	0.2425	15
NSC0144+1322	26.039	13.361	0.2477	18
NSC0144+1830	26.057	18.499	0.2061	49
NSC0144+1601	26.067	16.010	0.1571	16
NSC0144+1355	26.071	13.924	0.2496	26

Continued...

Table B.2 - SGP Robust, Continued

Name	RA	Dec	z_{phot}	N_{gal}
NSC0144+0947	26.073	9.783	0.2064	36
NSC0144+1338	26.077	13.639	0.1823	22
NSC0144+1524	26.078	15.404	0.2187	26
NSC0144+1542	26.091	15.697	0.2418	19
NSC0144+1226	26.114	12.438	0.1647	29
NSC0144+0212	26.123	2.207	0.1659	24
NSC0145+0329	26.146	3.475	0.1217	22
NSC0145+1217	26.149	12.281	0.1677	28
NSC0145+0544	26.162	5.730	0.0840	38
NSC0145+1243	26.177	12.711	0.1625	38
NSC0145+0040	26.185	0.663	0.1190	24
NSC0145+1413	26.188	14.216	0.2713	21
NSC0145+1736	26.188	17.594	0.2226	18
NSC0145+1934	26.219	19.573	0.2425	21
NSC0145+1649	26.229	16.817	0.1994	19
NSC0145+1813	26.238	18.221	0.2116	15
NSC0145+1458	26.271	14.975	0.2198	22
NSC0145+2305	26.300	23.080	0.1370	26
NSC0145+1330	26.329	13.503	0.2461	22
NSC0145+1739	26.365	17.642	0.2014	37
NSC0146+1845	26.396	18.757	0.1785	20
0.1146	26.400	0.000	0.0000	0
NSC0146+2329	26.439	23.479	0.0714	31
NSC0146+1706	26.465	17.104	0.1336	35
NSC0146+1923	26.469	19.387	0.1946	20
NSC0146+1135	26.482	11.586	0.1459	30
NSC0146+1613	26.546	16.211	0.2016	28
NSC0146+1935	26.547	19.589	0.1957	22
NSC0147+1312	26.638	13.197	0.2129	37
NSC0147+1348	26.644	13.803	0.2305	21
NSC0147+1449	26.644	14.818	0.2353	20
NSC0147+2408	26.651	24.138	0.2168	21
NSC0147+1338	26.672	13.625	0.2212	17
NSC0147+2040	26.675	20.667	0.2229	20
NSC0147+2348	26.706	23.806	0.1595	22
NSC0147+1325	26.714	13.415	0.2499	24
NSC0147+2003	26.717	20.051	0.1810	31
NSC0147+1622	26.724	16.370	0.2089	22
NSC0147+1709	26.768	17.155	0.1424	30
NSC0147+1738	26.782	17.634	0.2412	18
NSC0147+1949	26.820	19.825	0.1664	25
NSC0147+1412	26.868	14.203	0.2849	15
NSC0147+1324	26.869	13.402	0.2489	18
NSC0148+2038	26.947	20.629	0.2414	36
NSC0148+2004	26.961	20.062	0.2266	37
NSC0148+2606	26.975	26.095	0.2486	18
NSC0148+1402	26.991	14.029	0.2037	34
NSC0148+0018	27.039	0.296	0.1684	20
NSC0148+1207	27.044	12.109	0.2181	29
NSC0148+1256	27.048	12.930	0.1544	54
NSC0148+1735	27.058	17.575	0.1737	33
NSC0148+1347	27.098	13.785	0.2437	26
NSC0149+2302	27.201	23.035	0.2048	26
NSC0149+0941	27.223	9.685	0.1811	21
NSC0149+1037	27.237	10.611	0.1244	23
NSC0149+1322	27.250	13.370	0.2271	31
NSC0149+1358	27.285	13.961	0.1453	60
NSC0149+1441	27.357	14.676	0.2189	24
NSC0150+0842	27.402	8.707	0.0901	18
NSC0150+1448	27.445	14.803	0.2317	16
NSC0150+1343	27.475	13.725	0.2056	38
NSC0150+2327	27.505	23.443	0.0613	29
NSC0150+1434	27.544	14.559	0.2210	17
NSC0150+1746	27.558	17.766	0.1636	26
NSC0150+0847	27.562	8.779	0.1123	26
NSC0151+1557	27.634	15.958	0.2447	25
NSC0151+1441	27.641	14.678	0.2443	30
NSC0151+2713	27.659	27.211	0.1908	26
NSC0151+2050	27.662	20.833	0.1516	20
NSC0151+1002	27.691	10.027	0.2253	26
NSC0151+0937	27.743	9.623	0.1311	21
NSC0151+1356	27.749	13.931	0.2222	37
NSC0152+1338	27.928	13.627	0.2474	20
NSC0152+0152	27.943	1.874	0.1513	23
NSC0152+0713	27.977	7.224	0.0898	11
NSC0152+2716	28.010	27.265	0.1865	15
NSC0152+0132	28.046	1.532	0.1634	30
NSC0152+1513	28.061	15.217	0.1869	18
NSC0152+1337	28.116	13.612	0.2356	37
NSC0152+2019	28.122	20.308	0.1903	15
NSC0153+1605	28.180	16.085	0.1652	23
NSC0153+0102	28.210	1.027	0.2180	38
NSC0153+2407	28.251	24.123	0.1443	31
NSC0153+1519	28.258	15.314	0.2636	26
NSC0153+0038	28.354	0.631	0.0888	17
NSC0153+1012	28.362	10.194	0.1117	21
NSC0154+1404	28.430	14.062	0.1786	24

Continued...

Table B.2 - SGP Robust, Continued

Name	RA	Dec	z_{phot}	N_{gal}
NSC0154+0140	28.520	1.665	0.0667	38
NSC0154+2259	28.541	22.979	0.1770	19
NSC0154+1151	28.558	11.852	0.1528	20
NSC0155+0906	28.630	9.100	0.1141	42
NSC0155+0109	28.637	1.143	0.1007	22
NSC0155+1811	28.663	18.185	0.1276	22
NSC0155+2004	28.665	20.072	0.1701	31
NSC0155+2136	28.691	21.592	0.2072	36
NSC0155+0928	28.753	9.469	0.1119	18
NSC0155+1616	28.780	16.260	0.1352	23
NSC0155+0228	28.791	2.473	0.0699	15
NSC0155+1337	28.839	13.622	0.2273	26
NSC0155+1652	28.872	16.860	0.0686	26
NSC0156+1441	28.943	14.681	0.2045	33
NSC0156+1915	28.962	19.246	0.1912	29
NSC0156+1450	28.968	14.838	0.1521	50
NSC0156+0759	28.972	7.987	0.1613	30
NSC0156+1114	28.975	11.228	0.1207	25
NSC0156+1803	28.979	18.054	0.2178	21
NSC0156+1903	29.031	19.054	0.2069	18
NSC0156+0104	29.081	1.073	0.1124	58
NSC0156+0727	29.099	7.449	0.1617	25
NSC0157+2234	29.132	22.560	0.1528	28
NSC0157+0050	29.150	0.841	0.1860	31
NSC0157+1743	29.153	17.715	0.1953	21
NSC0157+2719	29.158	27.320	0.1606	26
NSC0157+1620	29.179	16.334	0.1604	29
NSC0157+0314	29.197	3.238	0.1491	30
NSC0157+1828	29.248	18.462	0.2152	13
NSC0157+1312	29.258	13.201	0.1465	36
NSC0157+0024	29.310	0.398	0.1511	17
NSC0157+1058	29.323	10.970	0.1015	24
NSC0157+1548	29.345	15.792	0.1739	21
NSC0157+1840	29.359	18.659	0.2227	12
NSC0157+2220	29.366	22.329	0.2808	19
NSC0158+1746	29.408	17.758	0.1706	22
NSC0158+2139	29.411	21.651	0.2084	32
NSC0158+1153	29.437	11.890	0.2286	20
NSC0158+1649	29.460	16.813	0.2149	29
NSC0158+0925	29.483	9.412	0.1711	25
NSC0158+1824	29.501	18.398	0.2487	17
NSC0158+2007	29.554	20.116	0.1738	33
NSC0159+2442	29.750	24.707	0.2262	23
NSC0159+2536	29.753	25.608	0.1384	21
NSC0159+2653	29.757	26.876	0.1268	33
NSC0159+0817	29.829	8.281	0.1750	32
NSC0200+1326	29.917	13.435	0.1888	26
NSC0200+0953	29.922	9.880	0.1590	25
NSC0200+2531	29.939	25.511	0.1701	25
NSC0200+2513	29.976	25.209	0.1799	18
NSC0200+2343	29.983	23.724	0.0765	17
NSC0200+0333	30.030	3.542	0.1354	36
NSC0200+0959	30.035	9.985	0.1117	42
NSC0200+1016	30.050	10.274	0.0802	18
NSC0200+1159	30.057	11.980	0.1855	25
NSC0200+0930	30.059	9.503	0.1664	35
NSC0201+0035	30.137	0.581	0.1431	30
NSC0201+2758	30.213	27.963	0.1859	24
NSC0201+0339	30.214	3.643	0.1428	46
NSC0201+2641	30.254	26.689	0.1216	32
NSC0201+1125	30.326	11.418	0.0661	17
NSC0201+1151	30.366	11.853	0.1622	28
NSC0201+0812	30.370	8.198	0.1021	32
NSC0202+0346	30.460	3.760	0.1384	65
NSC0202+0840	30.599	8.672	0.2175	25
NSC0202+0528	30.601	5.474	0.2010	32
NSC0203+2736	30.641	27.602	0.1460	22
NSC0203+2421	30.655	24.358	0.1707	26
NSC0203+0831	30.656	8.511	0.1663	26
NSC0203+2458	30.743	24.960	0.1222	25
NSC0203+2624	30.771	26.405	0.1326	28
NSC0203+2438	30.797	24.636	0.1499	29
NSC0203+1154	30.799	11.900	0.1210	44
NSC0203+0403	30.843	4.046	0.1493	21
NSC0203+2306	30.858	23.107	0.2099	16
NSC0204+0518	30.899	5.306	0.1393	25
NSC0204+1137	31.014	11.617	0.1772	30
NSC0204+0326	31.020	3.440	0.1337	22
NSC0205+1547	31.137	15.781	0.1712	26
NSC0205+0020	31.146	0.327	0.1582	29
NSC0205+1755	31.162	17.911	0.2122	26
NSC0205+1330	31.235	13.494	0.1591	28
NSC0205+0946	31.250	9.760	0.1469	63
NSC0205+0304	31.293	3.065	0.1982	18
NSC0205+0320	31.307	3.333	0.1772	22
NSC0205+0352	31.331	3.874	0.2121	15
NSC0205+1756	31.332	17.940	0.2049	42

Continued...

Table B.2 - SGP Robust, Continued

Name	RA	Dec	z_{phot}	N_{gal}
NSC0206+1456	31.445	14.932	0.1926	25
NSC0206+1031	31.460	10.519	0.1895	26
NSC0206+0445	31.509	4.753	0.1278	31
NSC0206+0529	31.528	5.479	0.1230	28
NSC0206+1127	31.534	11.443	0.1922	24
NSC0206+1156	31.593	11.934	0.1997	19
NSC0206+0431	31.605	4.511	0.1287	39
NSC0206+1120	31.618	11.334	0.1550	23
NSC0207+0522	31.627	5.362	0.2243	29
NSC0207+1043	31.664	10.709	0.1159	27
NSC0207+1020	31.700	10.326	0.1877	32
NSC0207+1625	31.733	16.419	0.1857	19
NSC0207+1446	31.737	14.773	0.1946	25
NSC0207+1140	31.763	11.672	0.1420	39
NSC0207+0537	31.803	5.615	0.1982	29
NSC0207+0459	31.806	4.980	0.1793	26
NSC0207+2314	31.822	23.230	0.2225	14
NSC0207+2522	31.823	25.365	0.1746	30
NSC0207+0856	31.851	8.936	0.1955	24
NSC0207+1040	31.869	10.675	0.2232	22
NSC0208+0912	31.932	9.197	0.2218	22
NSC0208+2655	31.951	26.912	0.1679	20
NSC0208+2314	31.953	23.235	0.1477	33
NSC0208+1158	31.981	11.959	0.1212	36
NSC0208+1027	31.997	10.448	0.2049	56
NSC0208+0344	32.009	3.726	0.1635	23
NSC0208+1438	32.019	14.629	0.2254	29
NSC0208+1331	32.026	13.520	0.2506	20
NSC0208+2738	32.053	27.631	0.0677	34
NSC0208+1428	32.070	14.460	0.2157	22
NSC0208+2707	32.070	27.124	0.1032	23
NSC0208+0920	32.104	9.331	0.2451	21
NSC0208+2304	32.105	23.062	0.1623	24
NSC0208+0859	32.118	8.985	0.1704	27
NSC0209+1129	32.135	11.478	0.1409	24
NSC0209+0526	32.136	5.436	0.1848	33
NSC0209+0303	32.149	3.047	0.1931	40
NSC0209+1225	32.172	12.415	0.0870	50
NSC0209+2647	32.205	26.776	0.1008	23
NSC0209+0411	32.217	4.190	0.2301	28
NSC0209+0334	32.310	3.564	0.1957	19
NSC0209+1005	32.314	10.079	0.1572	25
NSC0209+1043	32.331	10.713	0.1584	35
NSC0209+1028	32.335	10.459	0.1102	31
NSC0209+1338	32.338	13.638	0.2035	27
NSC0209+0907	32.360	9.123	0.2172	19
NSC0209+0949	32.365	9.816	0.1184	57
NSC0210+0923	32.377	9.380	0.2033	43
NSC0210+0452	32.415	4.867	0.1476	43
NSC0210+2321	32.418	23.344	0.1255	45
NSC0210+1523	32.426	15.385	0.1883	30
NSC0210+2635	32.428	26.583	0.1432	34
NSC0210+1018	32.454	10.302	0.1652	22
NSC0210+0431	32.471	4.515	0.1195	34
NSC0210+0253	32.500	2.889	0.1608	60
NSC0210+0551	32.512	5.843	0.1242	41
NSC0210+0809	32.531	8.144	0.1722	31
NSC0210+1728	32.552	17.461	0.2245	29
NSC0210+1006	32.553	10.096	0.1693	21
NSC0210+1040	32.554	10.665	0.1422	50
NSC0210+2718	32.604	27.299	0.1804	27
NSC0210+1414	32.616	14.227	0.2080	19
NSC0211+0948	32.634	9.793	0.1844	26
NSC0211+1107	32.641	11.120	0.1478	23
NSC0211+2630	32.672	26.500	0.1337	36
NSC0211+2712	32.686	27.207	0.1675	28
NSC0211+1801	32.741	18.025	0.2187	22
NSC0211+1117	32.746	11.284	0.2047	21
NSC0211+1458	32.789	14.960	0.2017	22
NSC0211+0920	32.797	9.333	0.2012	15
NSC0211+2406	32.812	24.098	0.1821	32
NSC0211+1300	32.813	13.002	0.1125	40
NSC0211+1320	32.837	13.336	0.2086	32
NSC0211+0511	32.842	5.183	0.2276	25
NSC0211+1736	32.870	17.601	0.2562	26
NSC0212+1205	32.894	12.079	0.2159	41
NSC0212+1445	32.905	14.748	0.2275	18
NSC0212+0023	32.933	0.384	0.2250	22
NSC0212+1407	32.946	14.119	0.2240	30
NSC0212+1143	32.962	11.713	0.2194	15
NSC0212+1310	32.991	13.174	0.1975	24
NSC0212+1750	32.994	17.831	0.2228	21
NSC0212+1051	33.005	10.856	0.1953	12
NSC0212+0922	33.030	9.365	0.2780	24
NSC0212+1453	33.083	14.884	0.2180	17
NSC0212+1419	33.092	14.324	0.2139	35
NSC0212+2751	33.123	27.851	0.1316	26

Continued...

Table B.2 - SGP Robust, Continued

Name	RA	Dec	z_{phot}	N_{gal}
NSC0213+0011	33.134	0.190	0.2095	24
NSC0213+0027	33.171	0.451	0.1803	33
NSC0213+2652	33.175	26.864	0.1210	33
NSC0213+2446	33.198	24.773	0.1493	29
NSC0213+2626	33.223	26.439	0.1058	45
NSC0213+2521	33.232	25.345	0.2002	36
NSC0213+2307	33.322	23.112	0.1870	30
NSC0214+1728	33.410	17.473	0.1536	43
NSC0214+0729	33.432	7.487	0.1232	57
NSC0214+2437	33.448	24.610	0.1716	31
NSC0214+0029	33.459	0.476	0.2239	25
NSC0214+1513	33.466	15.217	0.1212	31
NSC0214+2610	33.533	26.168	0.0926	25
NSC0214+1319	33.573	13.316	0.0986	33
NSC0214+0749	33.610	7.817	0.1242	44
NSC0214+2306	33.621	23.106	0.1662	38
NSC0215+1640	33.713	16.664	0.1421	30
NSC0215+0057	33.813	0.957	0.1606	33
NSC0215+0235	33.828	2.582	0.1591	21
NSC0215+1323	33.832	13.377	0.2108	15
NSC0216+2703	33.879	27.049	0.1809	18
NSC0216+0710	34.024	7.160	0.1126	35
NSC0216+0015	34.058	0.243	0.2471	20
NSC0217+1727	34.157	17.450	0.1868	33
NSC0217+1649	34.182	16.817	0.1328	64
NSC0217+1748	34.226	17.807	0.1464	48
NSC0217+2428	34.242	24.473	0.1765	19
NSC0217+0722	34.249	7.360	0.1509	27
NSC0217+0017	34.311	0.283	0.1642	16
NSC0217+2753	34.316	27.891	0.1647	31
NSC0217+1456	34.320	14.934	0.1484	36
NSC0217+1543	34.324	15.719	0.2144	30
NSC0217+2745	34.338	27.747	0.1400	37
NSC0218+1734	34.480	17.565	0.1516	62
NSC0218+2522	34.509	25.364	0.1002	25
NSC0218+0755	34.511	7.910	0.1963	19
NSC0218+1503	34.541	15.056	0.2147	17
NSC0218+1704	34.558	17.061	0.0935	33
NSC0218+1530	34.572	15.506	0.2125	33
NSC0218+1517	34.606	15.284	0.1688	36
NSC0219+0719	34.638	7.314	0.2062	20
NSC0219+1437	34.687	14.624	0.1295	36
NSC0219+1545	34.785	15.751	0.1847	27
NSC0219+0610	34.853	6.169	0.2454	25
NSC0219+2712	34.862	27.197	0.1503	27
NSC0220+2522	34.877	25.373	0.1064	24
NSC0220+1331	34.903	13.518	0.2385	17
NSC0220+1410	34.954	14.162	0.1489	37
NSC0220+0245	34.970	2.743	0.2486	39
NSC0220+1723	35.001	17.376	0.1076	54
NSC0220+2055	35.036	20.923	0.1645	18
NSC0220+1555	35.045	15.913	0.1198	52
NSC0220+2631	35.089	26.517	0.0864	35
NSC0220+2737	35.095	27.619	0.1280	19
NSC0220+2355	35.102	23.919	0.1086	27
NSC0221+1722	35.256	17.373	0.1283	51
NSC0221+1820	35.296	18.326	0.1520	25
NSC0221+2445	35.303	24.745	0.1603	41
NSC0221+2306	35.310	23.100	0.2295	20
NSC0221+1335	35.362	13.591	0.1289	42
NSC0222+2123	35.412	21.390	0.1578	84
NSC0222+0153	35.446	1.883	0.1889	31
NSC0222+2230	35.461	22.499	0.1825	35
NSC0222+1725	35.499	17.409	0.0911	43
NSC0222+2639	35.517	26.654	0.1027	36
NSC0222+1849	35.527	18.818	0.1340	67
NSC0222+2625	35.550	26.418	0.1593	51
NSC0222+0412	35.551	4.198	0.1324	28
NSC0222+0454	35.551	4.898	0.1931	21
NSC0222+2139	35.570	21.643	0.1636	22
NSC0222+0118	35.592	1.297	0.2102	23
NSC0223+0144	35.672	1.732	0.2373	16
NSC0223+2642	35.676	26.703	0.1456	30
NSC0223+2525	35.710	25.412	0.1363	43
NSC0223+1847	35.730	18.789	0.1724	25
NSC0223+2620	35.744	26.341	0.1845	46
NSC0223+1750	35.758	17.833	0.1070	52
NSC0223+1717	35.784	17.290	0.0926	81
NSC0223+1837	35.784	18.611	0.1239	32
NSC0223+1413	35.796	14.221	0.1676	26
NSC0223+2126	35.840	21.439	0.1265	42
NSC0223+1347	35.847	13.777	0.1175	34
NSC0223+0641	35.867	6.689	0.1592	33
NSC0223+1359	35.867	13.988	0.1577	31
NSC0223+1732	35.870	17.530	0.0939	63
NSC0224+1829	35.907	18.490	0.1121	37
NSC0224+0619	35.915	6.314	0.1869	21

Continued...

Table B.2 - SGP Robust, Continued

Name	RA	Dec	z_{phot}	N_{gal}
NSC0224+2634	35.922	26.567	0.0652	58
NSC0224+2745	35.933	27.753	0.2221	20
NSC0224+0105	35.946	1.080	0.2480	21
NSC0224+2523	35.959	25.382	0.1373	41
NSC0224+2556	35.972	25.928	0.1233	52
NSC0224+2108	36.022	21.125	0.1104	37
NSC0224+2536	36.068	25.606	0.1105	55
NSC0224+1858	36.081	18.961	0.1665	20
NSC0224+2626	36.092	26.425	0.0669	58
NSC0224+1324	36.120	13.399	0.0644	23
NSC0225+1350	36.128	13.841	0.1754	26
NSC0225+0122	36.190	1.359	0.2083	23
NSC0225+1719	36.217	17.317	0.1465	41
NSC0225+2351	36.241	23.846	0.1192	19
NSC0225+2625	36.284	26.410	0.0768	46
NSC0225+1739	36.298	17.648	0.1018	38
NSC0225+1358	36.313	13.968	0.1452	33
NSC0225+0628	36.345	6.473	0.2269	18
NSC0225+1513	36.362	15.222	0.1500	24
NSC0225+2605	36.366	26.091	0.0800	48
NSC0226+2752	36.413	27.873	0.2251	21
NSC0226+0119	36.438	1.319	0.1807	28
NSC0226+2522	36.440	25.361	0.1644	36
NSC0226+2458	36.479	24.973	0.1168	45
NSC0226+1340	36.493	13.674	0.1537	35
NSC0226+2738	36.522	27.629	0.1466	29
NSC0226+1545	36.537	15.743	0.0602	16
NSC0226+1727	36.603	17.446	0.0897	49
NSC0226+2528	36.604	25.465	0.1541	33
NSC0227+1341	36.637	13.687	0.1408	33
NSC0227+1407	36.743	14.124	0.1335	41
NSC0227+2446	36.804	24.773	0.0902	37
NSC0227+0654	36.832	6.893	0.1895	16
NSC0227+0601	36.858	6.008	0.2280	24
NSC0228+1515	36.891	15.258	0.1345	32
NSC0228+2130	36.896	21.503	0.1641	29
NSC0228+1435	36.898	14.585	0.1441	23
NSC0228+0258	36.951	2.958	0.2103	26
NSC0228+0105	36.954	1.088	0.1455	30
NSC2240+0605	340.047	6.083	0.1119	36
NSC2240+2657	340.055	26.943	0.2180	27
NSC2240+0636	340.069	6.594	0.1049	35
NSC2240+1217	340.106	12.284	0.1670	51
NSC2241+0130	340.168	1.503	0.1247	33
NSC2241+1715	340.185	17.248	0.1253	42
NSC2241+2659	340.190	26.989	0.1354	25
NSC2241+2114	340.242	21.226	0.1723	19
NSC2241+2615	340.253	26.245	0.1809	38
NSC2241+0543	340.280	5.715	0.1693	26
NSC2241+1621	340.319	16.352	0.1675	18
NSC2241+0144	340.329	1.737	0.0878	30
NSC2241+1846	340.342	18.759	0.1726	18
NSC2241+2605	340.349	26.083	0.1860	21
NSC2241+2541	340.361	25.691	0.2285	17
NSC2242+1031	340.397	10.516	0.1055	39
NSC2242+0716	340.458	7.271	0.1257	21
NSC2242+0830	340.498	8.501	0.1320	44
NSC2242+1733	340.503	17.545	0.1968	19
NSC2242+0723	340.548	7.386	0.0755	25
NSC2242+1538	340.558	15.629	0.2491	20
NSC2242+0109	340.567	1.147	0.1099	65
NSC2242+2651	340.594	26.856	0.1300	32
NSC2242+0310	340.607	3.160	0.1478	21
NSC2242+0930	340.618	9.506	0.1608	26
NSC2243+1309	340.636	13.152	0.1299	60
NSC2243+1515	340.659	15.249	0.2221	26
NSC2243+0730	340.660	7.505	0.1918	34
NSC2243+1034	340.712	10.560	0.1365	23
NSC2243+0825	340.730	8.421	0.1483	32
NSC2243+0059	340.754	0.981	0.1534	34
NSC2243+1351	340.777	13.847	0.1400	26
NSC2243+1308	340.853	13.133	0.1608	27
NSC2243+2437	340.869	24.616	0.1942	23
NSC2244+0020	340.918	0.327	0.1320	30
NSC2244+2516	340.921	25.274	0.1017	43
NSC2244+2715	340.932	27.252	0.1747	33
NSC2244+2457	340.937	24.943	0.1043	36
NSC2244+1402	340.967	14.033	0.1731	27
NSC2244+0500	340.999	5.002	0.1022	30
NSC2244+0713	341.013	7.215	0.2133	23
NSC2244+0515	341.026	5.253	0.1539	24
NSC2244+2529	341.048	25.491	0.1846	13
NSC2244+1025	341.080	10.419	0.1880	32
NSC2244+2253	341.110	22.881	0.2219	28
NSC2245+0111	341.163	1.188	0.1335	61
NSC2245+0033	341.165	0.543	0.1231	66
NSC2245+2619	341.187	26.312	0.1483	25

Continued...

Table B.2 - SGP Robust, Continued

Name	RA	Dec	z_{phot}	N_{gal}
NSC2245+1036	341.200	10.592	0.1246	34
NSC2245+1057	341.204	10.945	0.2774	43
NSC2245+0823	341.237	8.376	0.2625	31
NSC2245+2628	341.250	26.471	0.1112	21
NSC2245+1712	341.259	17.201	0.2492	13
NSC2245+2438	341.270	24.630	0.1164	36
NSC2245+0549	341.271	5.818	0.0936	41
NSC2245+2756	341.334	27.939	0.1341	50
NSC2245+2658	341.342	26.963	0.1733	24
NSC2246+1003	341.412	10.050	0.2092	26
NSC2246+2554	341.457	25.905	0.1621	33
NSC2246+1031	341.493	10.509	0.1815	45
NSC2246+1521	341.506	15.358	0.1572	37
NSC2246+2544	341.514	25.735	0.1772	30
NSC2246+0131	341.531	1.523	0.1405	27
NSC2246+2726	341.570	27.438	0.1284	34
NSC2246+2049	341.581	20.811	0.1082	18
NSC2246+1633	341.582	16.543	0.0943	31
NSC2246+1735	341.590	17.585	0.1116	23
NSC2246+1136	341.597	11.595	0.1165	17
NSC2246+2633	341.610	26.555	0.2387	30
NSC2247+2751	341.632	27.856	0.1563	25
NSC2247+0854	341.668	8.899	0.1329	33
NSC2247+0928	341.696	9.461	0.0994	21
NSC2247+1841	341.703	18.679	0.1689	22
NSC2247+1558	341.729	15.972	0.1928	23
NSC2247+0141	341.733	1.691	0.1273	48
NSC2247+0805	341.744	8.090	0.1902	18
NSC2247+0217	341.757	2.289	0.1242	21
NSC2247+0155	341.773	1.921	0.1140	34
NSC2247+0126	341.811	1.440	0.1234	32
NSC2247+2516	341.825	25.261	0.1269	35
NSC2247+0501	341.827	5.010	0.1365	27
NSC2247+1528	341.847	15.461	0.1030	44
NSC2247+2743	341.857	27.714	0.1882	60
NSC2248+1614	341.887	16.233	0.1767	32
NSC2248+1320	341.917	13.340	0.1412	35
NSC2248+0224	341.921	2.398	0.1366	36
NSC2248+2419	341.943	24.315	0.2412	20
NSC2248+1542	341.946	15.708	0.1663	23
NSC2248+1402	341.984	14.035	0.1234	45
NSC2248+0126	341.993	1.437	0.1040	35
NSC2248+0801	342.001	8.014	0.1572	20
NSC2248+0006	342.012	0.092	0.0931	17
NSC2248+1641	342.012	16.679	0.1839	35
NSC2248+2722	342.018	27.364	0.1260	40
NSC2248+0504	342.087	5.072	0.0959	27
NSC2248+1344	342.110	13.735	0.1301	46
NSC2249+1201	342.125	12.025	0.1346	42
NSC2249+1907	342.133	19.108	0.0832	47
NSC2249+2240	342.141	22.666	0.1145	31
NSC2249+1606	342.147	16.098	0.2164	34
NSC2249+1939	342.159	19.646	0.1779	33
NSC2249+1709	342.197	17.152	0.1662	20
NSC2249+0551	342.199	5.848	0.1900	15
NSC2249+2229	342.215	22.478	0.2427	22
NSC2249+0440	342.217	4.666	0.1358	27
NSC2249+1348	342.229	13.797	0.0977	44
NSC2249+0606	342.240	6.103	0.2249	28
NSC2249+2733	342.298	27.551	0.1780	40
NSC2249+1121	342.302	11.344	0.1570	28
NSC2249+1727	342.309	17.449	0.1971	27
NSC2249+0643	342.334	6.715	0.1701	26
NSC2249+1432	342.340	14.541	0.1994	21
NSC2249+1852	342.356	18.872	0.1003	31
NSC2249+1802	342.362	18.037	0.2268	16
NSC2250+1841	342.386	18.686	0.1625	36
NSC2250+1605	342.388	16.087	0.1894	28
NSC2250+2626	342.429	26.426	0.1505	42
NSC2250+0112	342.448	1.205	0.1595	24
NSC2250+1113	342.466	11.224	0.0654	25
NSC2250+1140	342.467	11.670	0.1073	99
NSC2250+2715	342.482	27.248	0.1557	40
NSC2250+2756	342.497	27.935	0.2145	34
NSC2250+0712	342.508	7.196	0.2106	23
NSC2250+0818	342.513	8.292	0.2290	25
NSC2250+2519	342.517	25.317	0.1271	33
NSC2250+0439	342.549	4.643	0.0848	90
NSC2250+1636	342.554	16.600	0.2186	25
NSC2250+1055	342.585	10.911	0.2865	21
NSC2250+1616	342.588	16.264	0.1648	48
NSC2250+2118	342.594	21.300	0.1671	26
NSC2250+0851	342.594	8.858	0.1629	26
NSC2250+0508	342.612	5.133	0.1417	20
NSC2251+1830	342.630	18.493	0.1857	35
NSC2251+1353	342.633	13.881	0.2250	36
NSC2251+2008	342.635	20.140	0.1572	28

Continued...

Table B.2 - SGP Robust, Continued

Name	RA	Dec	z_{phot}	N_{gal}
NSC2251+2244	342.639	22.727	0.1720	25
NSC2251+2749	342.639	27.818	0.1458	64
NSC2251+1414	342.659	14.240	0.1459	53
NSC2251+1548	342.668	15.806	0.1356	54
NSC2251+0820	342.676	8.336	0.1495	26
NSC2251+1107	342.686	11.120	0.1270	23
NSC2251+1020	342.743	10.326	0.1438	25
NSC2251+2636	342.748	26.593	0.1796	30
NSC2251+1342	342.767	13.708	0.1152	26
NSC2251+1751	342.774	17.855	0.1304	48
NSC2251+1028	342.803	10.473	0.1111	68
NSC2251+1517	342.830	15.284	0.1668	44
NSC2251+1042	342.830	10.697	0.0973	64
NSC2251+1149	342.838	11.820	0.2199	27
NSC2251+2031	342.865	20.522	0.2285	19
NSC2251+1108	342.870	11.130	0.2475	20
NSC2252+1718	342.922	17.302	0.1592	27
NSC2252+0606	342.925	6.099	0.2364	23
NSC2252+1031	342.968	10.524	0.2368	27
NSC2252+1423	342.973	14.377	0.1959	22
NSC2252+2609	342.982	26.149	0.1235	46
NSC2252+2643	343.005	26.718	0.2009	25
NSC2252+2508	343.006	25.137	0.1626	33
NSC2252+2739	343.030	27.642	0.1403	33
NSC2252+2753	343.033	27.886	0.1178	42
NSC2252+0521	343.040	5.343	0.0753	25
NSC2252+1113	343.041	11.217	0.1584	27
NSC2252+1503	343.109	15.051	0.2307	34
NSC2253+1136	343.126	11.594	0.1946	21
NSC2253+0835	343.141	8.583	0.1906	22
NSC2253+2403	343.150	24.044	0.1599	24
NSC2253+0530	343.177	5.506	0.0902	18
NSC2253+0508	343.198	5.128	0.1708	29
NSC2253+1037	343.212	10.614	0.2220	25
NSC2253+0859	343.240	8.990	0.2173	23
NSC2253+0650	343.255	6.838	0.2325	37
NSC2253+2340	343.260	23.674	0.2286	16
NSC2253+2459	343.262	24.985	0.1211	27
NSC2253+1718	343.268	17.306	0.2114	35
NSC2253+1525	343.294	15.418	0.1357	29
NSC2253+0804	343.301	8.073	0.2040	12
NSC2253+2202	343.304	22.034	0.0876	34
NSC2253+0518	343.332	5.303	0.1772	31
NSC2254+1021	343.384	10.343	0.1624	33
NSC2254+0045	343.392	0.748	0.1457	37
NSC2254+0344	343.410	3.734	0.1327	42
NSC2254+1302	343.414	13.040	0.1520	40
NSC2254+1231	343.427	12.514	0.1446	26
NSC2254+1519	343.460	15.311	0.1572	33
NSC2254+1805	343.477	18.085	0.1234	34
NSC2254+2311	343.477	23.182	0.2047	27
NSC2254+1529	343.501	15.488	0.1558	21
NSC2254+2648	343.517	26.807	0.1578	30
NSC2254+1310	343.520	13.163	0.1424	34
NSC2254+2752	343.537	27.870	0.1304	31
NSC2254+2726	343.567	27.431	0.1611	33
NSC2254+0727	343.583	7.456	0.2002	25
NSC2254+0511	343.584	5.182	0.1922	18
NSC2254+1846	343.593	18.772	0.1327	33
NSC2254+2624	343.623	26.404	0.1965	27
NSC2255+1031	343.637	10.524	0.2128	31
NSC2255+0455	343.648	4.914	0.1508	40
NSC2255+2249	343.665	22.820	0.1391	40
NSC2255+0657	343.669	6.945	0.1303	43
NSC2255+1319	343.687	13.312	0.1771	26
NSC2255+1253	343.720	12.886	0.1886	26
NSC2255+0735	343.735	7.579	0.2047	22
NSC2255+2648	343.755	26.808	0.1364	28
NSC2255+0345	343.803	3.756	0.1744	27
NSC2255+1826	343.821	18.430	0.1375	27
NSC2255+1036	343.825	10.601	0.1531	23
NSC2255+1441	343.825	14.684	0.1812	26
NSC2256+2450	343.903	24.828	0.1206	25
NSC2256+1249	343.905	12.814	0.1159	29
NSC2256+2532	343.905	25.536	0.1386	45
NSC2256+1011	343.923	10.191	0.2185	12
NSC2256+1841	343.924	18.676	0.1638	22
NSC2256+1326	343.927	13.429	0.2091	22
NSC2256+2756	343.959	27.925	0.1557	26
NSC2256+2608	343.978	26.125	0.1315	30
NSC2256+2128	344.000	21.459	0.1978	20
NSC2256+1105	344.006	11.083	0.2185	31
NSC2256+2720	344.035	27.331	0.1108	58
NSC2256+1653	344.048	16.880	0.1425	40
NSC2256+1718	344.056	17.292	0.2295	24
NSC2256+1124	344.057	11.399	0.1989	27
NSC2256+1312	344.077	13.194	0.1801	23

Continued...

Table B.2 - SGP Robust, Continued

Name	RA	Dec	z_{phot}	N_{gal}
NSC2256+0441	344.077	4.680	0.1495	30
NSC2256+1452	344.096	14.875	0.1701	27
NSC2256+0753	344.117	7.881	0.2232	30
NSC2257+0730	344.143	7.495	0.2117	21
NSC2257+0710	344.151	7.163	0.1714	24
NSC2257+1614	344.163	16.240	0.2324	24
NSC2257+0531	344.181	5.509	0.1262	28
NSC2257+2448	344.185	24.797	0.1330	58
NSC2257+1322	344.201	13.373	0.2246	26
NSC2257+2605	344.204	26.084	0.2220	22
NSC2257+2455	344.225	24.916	0.1446	74
NSC2257+0813	344.225	8.211	0.2396	27
NSC2257+2617	344.272	26.288	0.1275	70
NSC2257+0602	344.290	6.032	0.1804	28
NSC2257+1302	344.316	13.032	0.1341	27
NSC2257+1152	344.359	11.872	0.1241	44
NSC2257+0618	344.363	6.308	0.2003	21
NSC2257+1113	344.369	11.222	0.1832	25
NSC2257+0848	344.372	8.802	0.1347	32
NSC2257+1432	344.375	14.530	0.2014	23
NSC2258+1001	344.402	10.008	0.0800	22
NSC2258+1252	344.408	12.868	0.1818	22
NSC2258+2436	344.416	24.599	0.1391	47
NSC2258+0911	344.419	9.180	0.1699	29
NSC2258+2630	344.447	26.506	0.1900	25
NSC2258+1409	344.492	14.149	0.1001	49
NSC2258+0110	344.504	1.164	0.1053	25
NSC2258+1328	344.522	13.468	0.0844	66
NSC2258+0014	344.528	0.241	0.1386	30
NSC2258+0502	344.555	5.035	0.0996	44
NSC2258+0030	344.560	0.502	0.1069	60
NSC2258+0702	344.564	7.039	0.1315	36
NSC2258+2654	344.565	26.901	0.2293	24
NSC2258+0637	344.574	6.615	0.1966	33
NSC2258+2645	344.582	26.751	0.1242	28
NSC2259+1728	344.633	17.466	0.2003	30
NSC2259+1414	344.667	14.231	0.1827	47
NSC2259+2637	344.703	26.611	0.1123	45
NSC2259+2109	344.718	21.150	0.2502	18
NSC2259+1329	344.736	13.480	0.0894	61
NSC2259+2720	344.758	27.337	0.1708	49
NSC2259+2540	344.784	25.672	0.0837	68
NSC2259+1437	344.809	14.619	0.1777	20
NSC2259+0931	344.822	9.521	0.2625	20
NSC2259+2613	344.842	26.221	0.2142	45
NSC2259+2135	344.854	21.582	0.1666	24
NSC2259+1523	344.860	15.379	0.1021	45
NSC2300+0940	344.875	9.673	0.1620	28
NSC2300+0017	344.906	0.285	0.2052	19
NSC2300+1635	344.911	16.587	0.1014	30
NSC2300+1008	344.913	10.134	0.2039	20
NSC2300+0733	344.941	7.551	0.1654	26
NSC2300+0829	344.979	8.477	0.1620	27
NSC2300+0758	344.985	7.963	0.1606	23
NSC2300+0814	344.996	8.241	0.1795	37
NSC2300+0901	344.997	9.011	0.1038	27
NSC2300+1836	345.004	18.599	0.2162	15
NSC2300+0739	345.015	7.650	0.1510	27
NSC2300+1041	345.022	10.677	0.1054	24
NSC2300+1540	345.032	15.664	0.1028	75
NSC2300+0920	345.052	9.333	0.0909	48
NSC2300+2445	345.054	24.751	0.1219	34
NSC2300+0654	345.073	6.894	0.1259	44
NSC2300+0718	345.077	7.308	0.2104	18
NSC2300+2653	345.078	26.890	0.1204	62
NSC2300+1617	345.088	16.287	0.2254	43
NSC2301+2749	345.126	27.816	0.1961	18
NSC2301+1245	345.136	12.747	0.1773	24
NSC2301+0814	345.141	8.228	0.1645	49
NSC2301+0144	345.143	1.735	0.1051	44
NSC2301+2315	345.158	23.247	0.0888	53
NSC2301+1153	345.168	11.881	0.1306	36
NSC2301+1560	345.172	15.997	0.2542	22
NSC2301+2506	345.188	25.106	0.1554	25
NSC2301+1430	345.190	14.497	0.1301	55
NSC2301+1400	345.191	14.004	0.2235	23
NSC2301+2452	345.194	24.875	0.1855	28
NSC2301+0643	345.196	6.710	0.1843	31
NSC2301+0737	345.208	7.619	0.1803	25
NSC2301+0926	345.232	9.426	0.1548	40
NSC2301+1056	345.234	10.940	0.2197	21
NSC2301+2710	345.246	27.171	0.1426	42
NSC2301+1114	345.252	11.237	0.1198	46
NSC2301+2754	345.253	27.908	0.1382	78
NSC2301+1009	345.258	10.145	0.1327	27
NSC2301+2232	345.264	22.534	0.0940	87
NSC2301+2618	345.265	26.295	0.1897	21

Continued...

Table B.2 - SGP Robust, Continued

Name	RA	Dec	z_{phot}	N_{gal}
NSC2301+0936	345.267	9.606	0.1667	24
NSC2301+2143	345.276	21.715	0.2163	34
NSC2301+2737	345.284	27.610	0.2246	18
NSC2301+0618	345.287	6.302	0.1943	28
NSC2301+2157	345.294	21.944	0.2053	16
NSC2301+0348	345.296	3.808	0.1279	34
NSC2301+0650	345.312	6.830	0.1008	40
NSC2301+1058	345.340	10.966	0.1116	36
NSC2301+1843	345.354	18.720	0.1664	31
NSC2302+0750	345.436	7.828	0.0873	41
NSC2302+0457	345.438	4.949	0.1688	19
NSC2302+0243	345.450	2.713	0.1750	36
NSC2302+0448	345.450	4.795	0.1998	18
NSC2302+1707	345.457	17.112	0.1758	18
NSC2302+2548	345.471	25.800	0.1107	56
NSC2302+1403	345.491	14.049	0.1778	21
NSC2302+0944	345.508	9.736	0.1911	22
NSC2302+0011	345.510	0.190	0.2507	17
NSC2302+2445	345.513	24.742	0.0897	55
NSC2302+1152	345.527	11.874	0.2189	30
NSC2302+1756	345.541	17.930	0.2635	17
NSC2302+2639	345.541	26.650	0.1760	27
NSC2302+2748	345.572	27.806	0.1693	30
NSC2302+2235	345.586	22.585	0.1965	16
NSC2302+1105	345.591	11.080	0.0975	33
NSC2302+1225	345.613	12.412	0.2132	15
NSC2303+2424	345.632	24.394	0.1461	24
NSC2303+2714	345.653	27.232	0.0945	47
NSC2303+2248	345.654	22.798	0.1719	27
NSC2303+1211	345.657	12.190	0.1676	23
NSC2303+0905	345.660	9.089	0.1045	58
NSC2303+1415	345.676	14.254	0.1868	19
NSC2303+1945	345.676	19.754	0.2306	27
NSC2303+1350	345.684	13.829	0.1790	19
NSC2303+2511	345.685	25.177	0.0936	37
NSC2303+1541	345.688	15.680	0.1766	33
NSC2303+2344	345.688	23.731	0.0829	61
NSC2303+1154	345.712	11.901	0.0814	48
NSC2303+2702	345.745	27.038	0.0880	74
NSC2303+2330	345.747	23.506	0.0671	51
NSC2303+2452	345.751	24.868	0.1322	58
NSC2303+1743	345.758	17.720	0.1553	22
NSC2303+1554	345.762	15.894	0.1391	42
NSC2303+2623	345.768	26.386	0.1337	30
NSC2303+0423	345.776	4.380	0.1590	30
NSC2303+0702	345.777	7.030	0.1698	25
NSC2303+2737	345.782	27.622	0.2757	44
NSC2303+1830	345.784	18.508	0.1136	53
NSC2303+2548	345.785	25.800	0.1242	55
NSC2303+1449	345.786	14.822	0.2451	18
NSC2303+1409	345.786	14.142	0.1683	16
NSC2303+1103	345.787	11.050	0.1603	18
NSC2303+1710	345.829	17.166	0.2330	30
NSC2303+1652	345.829	16.862	0.2101	28
NSC2303+1257	345.839	12.954	0.1442	26
NSC2303+0757	345.844	7.957	0.1350	34
NSC2303+2751	345.864	27.843	0.2618	11
NSC2303+2226	345.867	22.429	0.2381	26
NSC2304+1208	345.883	12.134	0.1252	26
NSC2304+1521	345.908	15.345	0.1501	23
NSC2304+1912	345.911	19.204	0.1404	29
NSC2304+1813	345.914	18.216	0.1963	34
NSC2304+1636	345.937	16.594	0.1884	27
NSC2304+1123	345.939	11.379	0.1971	17
NSC2304+1429	345.940	14.488	0.1449	42
NSC2304+1023	345.940	10.386	0.1017	48
NSC2304+0916	345.942	9.270	0.1283	35
NSC2304+1624	345.943	16.402	0.1197	19
NSC2304+1933	345.948	19.557	0.1280	53
NSC2304+0048	345.955	0.796	0.2021	27
NSC2304+1956	345.985	19.929	0.0880	53
NSC2304+2632	345.990	26.531	0.2316	34
NSC2304+2246	345.995	22.765	0.2325	20
NSC2304+1144	346.010	11.734	0.2552	25
NSC2304+2004	346.034	20.073	0.1898	19
NSC2304+1156	346.059	11.926	0.0864	32
NSC2304+1059	346.060	10.983	0.2821	31
NSC2304+1541	346.063	15.690	0.1130	65
NSC2304+2115	346.068	21.258	0.1758	23
NSC2304+2300	346.071	23.001	0.1628	25
NSC2304+2217	346.108	22.280	0.1682	39
NSC2304+2727	346.113	27.456	0.2160	30
NSC2305+1351	346.144	13.848	0.1262	69
NSC2305+2327	346.146	23.456	0.1691	37
NSC2305+1337	346.150	13.616	0.1818	30
NSC2305+2416	346.161	24.270	0.2456	22
NSC2305+1011	346.186	10.176	0.1494	31

Continued...

Table B.2 - SGP Robust, Continued

Name	RA	Dec	z_{phot}	N_{gal}
NSC2305+1911	346.190	19.187	0.2449	32
NSC2305+2338	346.202	23.625	0.1803	26
NSC2305+2751	346.205	27.845	0.1095	43
NSC2305+1601	346.211	16.023	0.2089	43
NSC2305+1549	346.212	15.811	0.1613	34
NSC2305+1857	346.224	18.943	0.1019	66
NSC2305+1245	346.234	12.751	0.1282	64
NSC2305+2402	346.259	24.031	0.2132	18
NSC2305+1534	346.276	15.574	0.2396	13
NSC2305+0805	346.297	8.082	0.1450	30
NSC2305+0756	346.304	7.930	0.2163	21
NSC2305+0921	346.311	9.357	0.2333	21
NSC2305+2103	346.328	21.055	0.1504	52
NSC2305+1120	346.339	11.333	0.1775	38
NSC2305+0845	346.340	8.753	0.1777	18
NSC2305+2460	346.355	24.999	0.1288	50
NSC2305+2412	346.373	24.194	0.2084	22
NSC2306+1050	346.380	10.838	0.2287	27
NSC2306+1606	346.380	16.096	0.1505	24
NSC2306+2306	346.389	23.094	0.1402	44
NSC2306+0534	346.401	5.562	0.1278	27
NSC2306+1545	346.401	15.754	0.2398	21
NSC2306+1953	346.404	19.882	0.1052	49
NSC2306+1846	346.416	18.761	0.1666	26
NSC2306+0520	346.417	5.331	0.2121	18
NSC2306+2635	346.422	26.578	0.2455	24
NSC2306+1153	346.429	11.886	0.1868	41
NSC2306+1937	346.457	19.614	0.1547	41
NSC2306+2318	346.473	23.306	0.1638	25
NSC2306+2732	346.501	27.541	0.1447	43
NSC2306+0801	346.508	8.012	0.0917	65
NSC2306+1409	346.514	14.149	0.0884	67
NSC2306+2346	346.555	23.771	0.1055	48
NSC2306+1157	346.562	11.954	0.2223	40
NSC2306+1620	346.575	16.340	0.1205	39
NSC2306+0918	346.579	9.293	0.1446	34
NSC2306+1429	346.595	14.481	0.1180	32
NSC2306+1452	346.607	14.873	0.2241	25
NSC2307+2614	346.631	26.239	0.2565	21
NSC2307+1643	346.658	16.711	0.1751	30
NSC2307+1132	346.659	11.529	0.1609	23
NSC2307+2629	346.659	26.489	0.1134	38
NSC2307+2750	346.663	27.827	0.2220	26
NSC2307+2013	346.664	20.217	0.1296	45
NSC2307+2515	346.685	25.255	0.1975	20
NSC2307+1519	346.690	15.318	0.2233	21
NSC2307+1706	346.709	17.105	0.1936	74
NSC2307+1612	346.710	16.194	0.1300	30
NSC2307+2131	346.719	21.519	0.0972	26
NSC2307+1555	346.736	15.908	0.1340	45
NSC2307+2437	346.739	24.616	0.2519	20
NSC2307+1635	346.754	16.587	0.1407	39
NSC2307+0934	346.767	9.559	0.1683	23
NSC2307+2700	346.767	27.001	0.1979	22
NSC2307+1158	346.768	11.970	0.1835	26
NSC2307+1543	346.778	15.718	0.2206	18
NSC2307+2645	346.778	26.742	0.1538	41
NSC2307+2417	346.799	24.280	0.1965	20
NSC2307+1503	346.817	15.055	0.1475	44
NSC2307+0921	346.824	9.343	0.1628	37
NSC2307+2346	346.836	23.767	0.2605	16
NSC2307+1924	346.843	19.404	0.1326	35
NSC2308+0828	346.906	8.460	0.0981	72
NSC2308+2724	346.907	27.402	0.1284	35
NSC2308+2633	346.919	26.544	0.1937	28
NSC2308+1524	346.921	15.395	0.1531	23
NSC2308+0535	346.949	5.578	0.2508	21
NSC2308+1622	346.960	16.366	0.2076	28
NSC2308+0657	346.981	6.957	0.1637	49
NSC2308+2509	346.990	25.157	0.1196	54
NSC2308+1643	347.046	16.710	0.1920	22
NSC2308+1133	347.073	11.558	0.1339	53
NSC2308+2610	347.084	26.160	0.1507	40
NSC2308+0812	347.090	8.198	0.1725	33
NSC2308+0346	347.093	3.770	0.1100	47
NSC2309+0929	347.131	9.480	0.1557	30
NSC2309+1701	347.138	17.011	0.1317	40
NSC2309+1201	347.203	12.017	0.1522	30
NSC2309+1852	347.211	18.872	0.1634	25
NSC2309+0744	347.225	7.729	0.2318	17
NSC2309+2447	347.243	24.780	0.1175	19
NSC2309+2318	347.260	23.292	0.1359	76
NSC2309+1232	347.267	12.534	0.1200	31
NSC2309+1646	347.275	16.764	0.1174	54
NSC2309+0442	347.279	4.697	0.1009	25
NSC2309+2601	347.287	26.009	0.2181	17
NSC2309+2736	347.288	27.602	0.2023	26

Continued...

Table B.2 - SGP Robust, Continued

Name	RA	Dec	z_{phot}	N_{gal}
NSC2309+1144	347.294	11.731	0.1890	28
NSC2309+1511	347.300	15.191	0.1572	26
NSC2309+2710	347.303	27.165	0.1877	19
NSC2309+1912	347.332	19.203	0.1311	27
NSC2309+0545	347.363	5.756	0.2058	33
NSC2309+2038	347.367	20.635	0.1170	43
NSC2309+2150	347.372	21.832	0.2037	29
NSC2310+1221	347.386	12.345	0.1121	39
NSC2310+0937	347.436	9.608	0.1670	24
NSC2310+1313	347.469	13.212	0.1772	15
NSC2310+1023	347.477	10.376	0.2129	20
NSC2310+0538	347.490	5.634	0.1299	66
NSC2310+1657	347.490	16.942	0.2568	13
NSC2310+1909	347.493	19.149	0.1890	21
NSC2310+0902	347.504	9.038	0.1754	33
NSC2310+0526	347.516	5.430	0.2224	29
NSC2310+2745	347.522	27.746	0.1520	22
NSC2310+1820	347.525	18.327	0.2113	21
NSC2310+2555	347.552	25.920	0.1179	25
NSC2310+1127	347.556	11.452	0.1185	37
NSC2310+2641	347.584	26.686	0.1569	26
NSC2310+2146	347.600	21.770	0.1922	21
NSC2311+2122	347.688	21.367	0.2148	29
NSC2311+1925	347.693	19.413	0.1532	21
NSC2311+2613	347.742	26.215	0.1784	28
NSC2311+0750	347.745	7.841	0.1777	22
NSC2311+1138	347.758	11.641	0.1256	43
NSC2311+0701	347.762	7.020	0.1236	43
NSC2311+1219	347.800	12.315	0.1747	36
NSC2311+0621	347.801	6.348	0.1223	40
NSC2311+0740	347.819	7.661	0.1482	39
NSC2311+1348	347.825	13.808	0.1205	31
NSC2311+1256	347.838	12.939	0.1943	30
NSC2311+1006	347.845	10.103	0.2637	24
NSC2311+2635	347.856	26.578	0.0779	35
NSC2312+2755	347.880	27.916	0.2075	22
NSC2312+0340	347.892	3.669	0.1701	36
NSC2312+2042	347.897	20.700	0.1837	42
NSC2312+2218	347.898	22.295	0.1610	20
NSC2312+0728	347.927	7.464	0.1434	31
NSC2312+1135	347.927	11.590	0.1238	45
NSC2312+1237	347.930	12.616	0.1718	25
NSC2312+0411	347.955	4.182	0.1592	30
NSC2312+2047	348.042	20.778	0.1393	47
NSC2312+1008	348.044	10.128	0.2047	32
NSC2312+1610	348.047	16.174	0.1484	58
NSC2312+1043	348.103	10.717	0.2003	24
NSC2313+1205	348.147	12.079	0.2417	24
NSC2313+2029	348.148	20.478	0.1657	47
NSC2313+1022	348.161	10.368	0.2482	30
NSC2313+2629	348.176	26.479	0.1895	17
NSC2313+0926	348.183	9.434	0.1950	20
NSC2313+1360	348.212	13.995	0.2933	26
NSC2313+2723	348.263	27.390	0.2175	17
NSC2313+1015	348.265	10.247	0.2238	19
NSC2313+1541	348.308	15.691	0.0702	55
NSC2313+0421	348.315	4.347	0.2022	21
NSC2313+2743	348.318	27.718	0.1711	27
NSC2313+1258	348.359	12.975	0.1501	32
NSC2313+1604	348.359	16.063	0.1981	26
NSC2313+1614	348.363	16.238	0.1847	27
NSC2313+1654	348.368	16.907	0.1349	23
NSC2313+1023	348.369	10.378	0.1158	62
NSC2314+1354	348.377	13.893	0.1395	35
NSC2314+1501	348.393	15.024	0.1916	56
NSC2314+1139	348.415	11.652	0.1246	46
NSC2314+1448	348.415	14.796	0.2544	21
NSC2314+0642	348.428	6.694	0.1165	55
NSC2314+1840	348.428	18.660	0.1902	25
NSC2314+1701	348.481	17.018	0.2443	20
NSC2314+2655	348.481	26.920	0.1497	31
NSC2314+1250	348.526	12.838	0.2014	15
NSC2314+1308	348.565	13.129	0.1670	25
NSC2314+1925	348.583	19.414	0.1698	46
NSC2314+1027	348.584	10.443	0.1099	29
NSC2314+2745	348.587	27.755	0.2501	25
NSC2314+0644	348.622	6.726	0.1755	27
NSC2314+1446	348.623	14.767	0.1459	41
NSC2315+2319	348.658	23.309	0.0936	41
NSC2315+2735	348.661	27.575	0.1406	31
NSC2315+1408	348.667	14.134	0.1574	28
NSC2315+2522	348.667	25.373	0.1868	31
NSC2315+0523	348.671	5.381	0.2736	24
NSC2315+1221	348.688	12.354	0.1509	26
NSC2315+2151	348.697	21.847	0.2011	27
NSC2315+1014	348.699	10.241	0.1793	17
NSC2315+2645	348.716	26.750	0.1204	47

Continued...

Table B.2 - SGP Robust, Continued

Name	RA	Dec	z_{phot}	N_{gal}
NSC2315+1931	348.734	19.524	0.2038	20
NSC2315+1521	348.780	15.347	0.1714	28
NSC2316+1241	348.880	12.687	0.1922	20
NSC2316+2602	348.897	26.032	0.1996	28
NSC2316+1001	348.918	10.017	0.0842	57
NSC2316+1027	348.944	10.445	0.1380	73
NSC2316+1434	348.955	14.563	0.1076	28
NSC2316+1445	348.962	14.742	0.1437	56
NSC2316+1733	348.963	17.556	0.1485	37
NSC2316+2415	349.003	24.249	0.2112	32
NSC2316+0604	349.010	6.059	0.1615	32
NSC2316+1353	349.017	13.881	0.1668	36
NSC2316+2724	349.022	27.394	0.1846	32
NSC2316+0703	349.039	7.045	0.2237	26
NSC2316+1616	349.053	16.271	0.1772	29
NSC2316+1910	349.064	19.166	0.1499	33
NSC2316+1835	349.067	18.586	0.2056	19
NSC2316+1515	349.074	15.254	0.1588	20
NSC2316+0159	349.088	1.977	0.2478	28
NSC2317+2703	349.137	27.053	0.1737	17
NSC2317+2600	349.159	26.001	0.1440	31
NSC2317+2233	349.210	22.555	0.1948	25
NSC2317+1048	349.226	10.803	0.2073	31
NSC2317+2251	349.248	22.850	0.1721	30
NSC2317+1855	349.271	18.924	0.1779	36
NSC2317+1933	349.283	19.550	0.1870	22
NSC2317+0801	349.285	8.024	0.1553	33
NSC2317+2437	349.306	24.622	0.2238	24
NSC2317+2555	349.315	25.918	0.2437	26
NSC2317+2413	349.334	24.224	0.1739	42
NSC2317+1133	349.343	11.555	0.1968	16
NSC2317+2526	349.351	25.432	0.1321	40
NSC2317+2317	349.356	23.275	0.2440	27
NSC2317+1222	349.369	12.362	0.2222	27
NSC2318+1058	349.380	10.960	0.2229	27
NSC2318+1026	349.391	10.438	0.1878	21
NSC2318+1538	349.396	15.631	0.1484	29
NSC2318+1834	349.397	18.573	0.1354	33
NSC2318+1307	349.397	13.118	0.1822	19
NSC2318+0255	349.408	2.919	0.2122	23
NSC2318+2443	349.419	24.719	0.1993	31
NSC2318+2641	349.421	26.681	0.1256	45
NSC2318+0731	349.422	7.517	0.0897	48
NSC2318+1145	349.428	11.755	0.1768	31
NSC2318+0818	349.430	8.305	0.1846	25
NSC2318+0602	349.456	6.030	0.1595	19
NSC2318+0717	349.465	7.276	0.2575	19
NSC2318+1352	349.482	13.868	0.2755	21
NSC2318+1513	349.517	15.213	0.1719	47
NSC2318+0159	349.549	1.980	0.0995	20
NSC2318+1342	349.564	13.692	0.2161	20
NSC2318+0958	349.570	9.975	0.1528	23
NSC2318+1816	349.607	18.267	0.1648	43
NSC2318+0646	349.608	6.766	0.2503	22
NSC2318+1837	349.623	18.621	0.1635	30
NSC2319+1227	349.656	12.453	0.1317	40
NSC2319+1959	349.659	19.977	0.1830	31
NSC2319+2523	349.662	25.382	0.2031	20
NSC2319+0423	349.671	4.378	0.1799	33
NSC2319+2656	349.672	26.927	0.1652	30
NSC2319+0725	349.677	7.409	0.2064	36
NSC2319+1515	349.697	15.244	0.1673	24
NSC2319+0740	349.701	7.670	0.2473	20
NSC2319+2226	349.728	22.438	0.1527	26
NSC2319+0639	349.743	6.646	0.1407	29
NSC2319+1114	349.760	11.231	0.1811	33
NSC2319+1000	349.815	10.004	0.1765	22
NSC2319+1938	349.827	19.630	0.0663	19
NSC2319+2643	349.848	26.723	0.1610	34
NSC2319+0235	349.870	2.591	0.1678	20
NSC2320+1224	349.886	12.400	0.2216	31
NSC2320+2207	349.906	22.123	0.1534	30
NSC2320+1927	349.917	19.456	0.2053	20
NSC2320+1550	349.920	15.841	0.1514	21
NSC2320+1237	349.933	12.609	0.2047	30
NSC2320+0722	349.936	7.368	0.2078	19
NSC2320+1809	349.984	18.145	0.1583	44
NSC2320+2249	350.041	22.810	0.1657	25
NSC2320+1943	350.043	19.711	0.2024	24
NSC2320+2716	350.057	27.265	0.1277	44
NSC2320+2411	350.079	24.180	0.1472	37
NSC2320+1157	350.115	11.946	0.1414	65
NSC2321+0831	350.154	8.523	0.1970	27
NSC2321+0957	350.162	9.946	0.1198	33
NSC2321+1210	350.190	12.164	0.0857	47
NSC2321+2230	350.199	22.508	0.1624	21
NSC2321+0031	350.215	0.514	0.1862	28

Continued...

Table B.2 - SGP Robust, Continued

Name	RA	Dec	z_{phot}	N_{gal}
NSC2321+2213	350.217	22.216	0.1372	27
NSC2321+2445	350.224	24.745	0.1960	18
NSC2321+0114	350.226	1.237	0.1956	23
NSC2321+0741	350.229	7.689	0.1986	37
NSC2321+1826	350.258	18.441	0.2182	12
NSC2321+2245	350.267	22.756	0.1441	38
NSC2321+1926	350.281	19.438	0.1311	26
NSC2321+1137	350.298	11.620	0.2012	18
NSC2321+1902	350.318	19.041	0.2360	7
NSC2321+1616	350.320	16.275	0.1757	49
NSC2321+0949	350.371	9.812	0.1187	27
NSC2322+2150	350.399	21.835	0.1765	24
NSC2322+0730	350.408	7.502	0.2824	33
NSC2322+1504	350.409	15.071	0.1893	25
NSC2322+1052	350.416	10.860	0.0908	15
NSC2322+0606	350.418	6.099	0.1680	21
NSC2322+1605	350.430	16.084	0.2061	44
NSC2322+0919	350.441	9.318	0.2618	22
NSC2322+0253	350.443	2.877	0.1006	33
NSC2322+2734	350.478	27.565	0.1476	34
NSC2322+0659	350.482	6.982	0.2058	38
NSC2322+2249	350.483	22.818	0.2096	18
NSC2322+1936	350.499	19.608	0.0994	41
NSC2322+1855	350.507	18.912	0.1022	34
NSC2322+1951	350.513	19.856	0.1750	21
NSC2322+2721	350.516	27.352	0.1617	43
NSC2322+0617	350.526	6.280	0.1828	28
NSC2322+0746	350.528	7.759	0.1686	37
NSC2322+1913	350.532	19.217	0.1916	51
NSC2322+0842	350.545	8.707	0.1877	26
NSC2322+1035	350.567	10.585	0.2227	28
NSC2322+0822	350.577	8.361	0.2109	30
NSC2322+1621	350.587	16.350	0.1392	23
NSC2322+0137	350.590	1.612	0.1013	52
NSC2322+0105	350.594	1.082	0.1069	36
NSC2322+2446	350.601	24.768	0.1531	31
NSC2322+0545	350.625	5.745	0.2257	22
NSC2323+2515	350.641	25.242	0.1434	67
NSC2323+0957	350.642	9.954	0.1910	22
NSC2323+1154	350.654	11.899	0.0810	26
NSC2323+0920	350.671	9.330	0.1538	51
NSC2323+0653	350.675	6.880	0.2124	23
NSC2323+0558	350.676	5.966	0.2438	23
NSC2323+0642	350.687	6.699	0.1751	22
NSC2323+1529	350.690	15.483	0.1579	17
NSC2323+0754	350.727	7.893	0.2334	28
NSC2323+2744	350.761	27.741	0.1366	28
NSC2323+2323	350.768	23.384	0.0637	59
NSC2323+1813	350.773	18.212	0.1757	27
NSC2323+0059	350.775	0.987	0.2717	25
NSC2323+2424	350.801	24.407	0.1581	25
NSC2323+0617	350.812	6.290	0.2014	33
NSC2323+0856	350.820	8.928	0.1415	37
NSC2323+1618	350.837	16.305	0.1501	33
NSC2323+1101	350.837	11.024	0.1736	35
NSC2323+0810	350.840	8.168	0.2371	31
NSC2323+0031	350.851	0.522	0.1135	33
NSC2323+0630	350.863	6.503	0.2054	24
NSC2323+0705	350.863	7.078	0.2179	31
NSC2323+0722	350.867	7.372	0.2206	14
NSC2324+1643	350.875	16.724	0.1088	32
NSC2324+2736	350.875	27.594	0.1735	31
NSC2324+0551	350.877	5.858	0.2097	12
NSC2324+0253	350.878	2.888	0.1706	43
NSC2324+0829	350.889	8.477	0.2415	21
NSC2324+0911	350.895	9.188	0.1060	34
NSC2324+0925	350.922	9.411	0.1701	42
NSC2324+1311	350.922	13.186	0.1360	31
NSC2324+1632	350.929	16.527	0.1183	25
NSC2324+0559	350.964	5.988	0.1155	36
NSC2324+2038	350.966	20.634	0.1998	19
NSC2324+1647	350.988	16.788	0.2031	35
NSC2324+2231	351.005	22.518	0.1790	13
NSC2324+0902	351.027	9.034	0.2159	44
NSC2324+1500	351.033	15.002	0.1758	21
NSC2324+1451	351.034	14.845	0.1240	47
NSC2324+0127	351.040	1.458	0.1725	36
NSC2324+2339	351.040	23.653	0.2075	29
NSC2324+1936	351.049	19.605	0.2207	21
NSC2324+0702	351.054	7.029	0.1862	31
NSC2324+1713	351.063	17.215	0.1499	29
NSC2324+0019	351.065	0.313	0.1370	27
NSC2324+1813	351.065	18.210	0.0917	66
NSC2324+0205	351.070	2.081	0.1745	24
NSC2324+0824	351.074	8.400	0.2101	41
NSC2324+0651	351.089	6.857	0.1749	20
NSC2324+0805	351.090	8.091	0.1718	31

Continued...

Table B.2 - SGP Robust, Continued

Name	RA	Dec	z_{phot}	N_{gal}
NSC2324+1414	351.097	14.227	0.2369	29
NSC2324+1755	351.105	17.923	0.1698	29
NSC2324+1438	351.113	14.639	0.1925	22
NSC2324+1358	351.118	13.975	0.1099	38
NSC2325+0216	351.131	2.271	0.1011	25
NSC2325+2745	351.136	27.745	0.0845	31
NSC2325+2631	351.147	26.516	0.1796	18
NSC2325+1550	351.159	15.825	0.1109	31
NSC2325+1723	351.164	17.389	0.1976	35
NSC2325+0926	351.190	9.433	0.1942	23
NSC2325+2313	351.213	23.224	0.1205	34
NSC2325+0512	351.219	5.195	0.1580	33
NSC2325+2621	351.229	26.344	0.1288	26
NSC2325+1534	351.238	15.572	0.1171	65
NSC2325+0802	351.252	8.040	0.1684	26
NSC2325+1755	351.262	17.909	0.1060	25
NSC2325+0737	351.270	7.620	0.1280	38
NSC2325+1733	351.270	17.547	0.1528	45
NSC2325+1646	351.288	16.773	0.1114	33
NSC2325+1443	351.303	14.722	0.1421	36
NSC2325+2042	351.311	20.698	0.2368	15
NSC2325+1928	351.319	19.471	0.1402	32
NSC2325+1258	351.320	12.965	0.1713	45
NSC2325+1630	351.327	16.507	0.1919	23
NSC2325+2440	351.337	24.665	0.1341	38
NSC2325+0503	351.340	5.058	0.1514	40
NSC2325+1842	351.342	18.693	0.1471	22
NSC2325+0622	351.344	6.366	0.2332	42
NSC2325+0858	351.348	8.964	0.1590	28
NSC2326+0702	351.374	7.032	0.1770	43
NSC2326+2455	351.388	24.920	0.1056	53
NSC2326+0635	351.416	6.585	0.1409	27
NSC2326+1937	351.454	19.615	0.1521	37
NSC2326+0611	351.465	6.188	0.1998	34
NSC2326+1713	351.471	17.223	0.1604	33
NSC2326+2435	351.485	24.581	0.1775	25
NSC2326+1656	351.497	16.934	0.2064	34
NSC2326+2014	351.499	20.241	0.1162	49
NSC2326+2724	351.501	27.400	0.2411	23
NSC2326+1533	351.515	15.546	0.1360	29
NSC2326+1960	351.528	19.993	0.2096	23
NSC2326+0707	351.538	7.117	0.1757	36
NSC2326+0802	351.561	8.036	0.0958	38
NSC2326+2645	351.570	26.745	0.0997	45
NSC2326+2529	351.572	25.489	0.1706	34
NSC2326+1752	351.582	17.862	0.2411	30
NSC2327+0457	351.633	4.947	0.1951	26
NSC2327+2120	351.637	21.332	0.1650	46
NSC2327+0541	351.645	5.689	0.0827	70
NSC2327+0627	351.658	6.457	0.0772	89
NSC2327+1943	351.660	19.718	0.1637	18
NSC2327+0654	351.664	6.905	0.1976	33
NSC2327+1344	351.672	13.737	0.0985	45
NSC2327+1647	351.681	16.781	0.1740	24
NSC2327+0904	351.702	9.061	0.2039	19
NSC2327+0822	351.704	8.372	0.1793	23
NSC2327+1051	351.709	10.857	0.1952	27
NSC2327+0520	351.712	5.336	0.1968	25
NSC2327+1718	351.713	17.307	0.0839	48
NSC2327+1901	351.735	19.013	0.2204	15
NSC2327+1704	351.739	17.059	0.1286	25
NSC2327+0606	351.740	6.103	0.2168	16
NSC2327+2622	351.742	26.364	0.1059	24
NSC2327+1148	351.773	11.800	0.1326	63
NSC2327+1926	351.775	19.431	0.1928	47
NSC2327+0815	351.788	8.246	0.1389	29
NSC2327+1823	351.802	18.380	0.1718	29
NSC2327+1454	351.811	14.897	0.1645	21
NSC2327+2633	351.842	26.558	0.1935	13
NSC2328+2242	351.880	22.708	0.1608	41
NSC2328+0409	351.881	4.152	0.1999	22
NSC2328+2654	351.901	26.907	0.2501	25
NSC2328+0846	351.906	8.767	0.1649	26
NSC2328+0421	351.928	4.358	0.1870	21
NSC2328+0818	351.961	8.298	0.2116	28
NSC2328+0450	351.976	4.832	0.1104	28
NSC2328+0902	352.011	9.041	0.1679	26
NSC2328+1935	352.024	19.588	0.1442	31
NSC2328+1903	352.065	19.044	0.2197	40
NSC2328+2422	352.101	24.363	0.1348	41
NSC2328+2406	352.115	24.107	0.1511	51
NSC2328+1444	352.118	14.741	0.1997	26
NSC2328+2511	352.119	25.178	0.1843	36
NSC2328+2709	352.121	27.157	0.1539	45
NSC2328+2746	352.124	27.767	0.1904	27
NSC2329+1345	352.132	13.753	0.2789	14
NSC2329+0830	352.136	8.506	0.2118	40

Continued...

Table B.2 - SGP Robust, Continued

Name	RA	Dec	z_{phot}	N_{gal}
NSC2329+1248	352.147	12.800	0.1210	25
NSC2329+0734	352.148	7.560	0.1342	36
NSC2329+0942	352.158	9.695	0.1298	31
NSC2329+1645	352.200	16.744	0.1161	55
NSC2329+2319	352.228	23.320	0.2044	23
NSC2329+0515	352.257	5.247	0.1265	25
NSC2329+0745	352.271	7.747	0.2166	23
NSC2329+2608	352.278	26.139	0.1916	24
NSC2329+0503	352.290	5.057	0.2296	24
NSC2329+0916	352.303	9.269	0.1635	32
NSC2329+2208	352.314	22.140	0.1491	29
NSC2329+0713	352.316	7.216	0.1159	34
NSC2329+2137	352.327	21.614	0.1512	33
NSC2329+0528	352.335	5.458	0.1227	28
NSC2329+1121	352.365	11.355	0.1084	27
NSC2329+1620	352.370	16.338	0.2192	31
NSC2330+1247	352.385	12.780	0.1284	38
NSC2330+0431	352.427	4.515	0.1364	58
NSC2330+2120	352.431	21.326	0.2290	21
NSC2330+1115	352.437	11.246	0.1950	21
NSC2330+0837	352.446	8.617	0.1195	54
NSC2330+2751	352.487	27.856	0.2192	25
NSC2330+2702	352.510	27.032	0.1399	37
NSC2330+2316	352.535	23.271	0.1793	40
NSC2330+0540	352.538	5.673	0.1070	50
NSC2330+2417	352.546	24.288	0.1438	24
NSC2330+0818	352.555	8.301	0.1852	49
NSC2330+2507	352.583	25.119	0.0871	35
NSC2330+1718	352.587	17.306	0.1326	38
NSC2330+2007	352.601	20.118	0.1838	20
NSC2330+2041	352.603	20.679	0.1760	27
NSC2330+1354	352.608	13.897	0.1760	32
NSC2330+2223	352.611	22.378	0.2249	19
NSC2331+0721	352.638	7.352	0.1338	46
NSC2331+1647	352.642	16.779	0.2197	22
NSC2331+0411	352.658	4.192	0.1709	18
NSC2331+1122	352.668	11.366	0.1697	16
NSC2331+1438	352.669	14.627	0.1639	26
NSC2331+1333	352.707	13.545	0.1666	28
NSC2331+2734	352.708	27.565	0.1151	51
NSC2331+0921	352.721	9.355	0.1657	23
NSC2331+1930	352.724	19.507	0.1024	21
NSC2331+0738	352.740	7.641	0.2300	17
NSC2331+1001	352.742	10.021	0.1080	39
NSC2331+2123	352.773	21.379	0.1976	29
NSC2331+0823	352.789	8.380	0.1330	24
NSC2331+1744	352.793	17.727	0.1146	29
NSC2331+0401	352.813	4.018	0.1280	44
NSC2331+2711	352.830	27.186	0.2165	23
NSC2331+2614	352.856	26.238	0.0802	27
NSC2331+2055	352.870	20.909	0.1972	23
NSC2331+1903	352.871	19.058	0.1077	58
NSC2331+2508	352.873	25.135	0.1117	40
NSC2332+2658	352.903	26.975	0.1392	43
NSC2332+0809	352.911	8.149	0.1633	42
NSC2332+2341	352.915	23.686	0.1880	16
NSC2332+1150	352.931	11.839	0.1925	26
NSC2332+0945	352.967	9.756	0.1487	29
NSC2332+2353	352.972	23.885	0.1748	39
NSC2332+0832	352.972	8.534	0.2106	34
NSC2332+1845	352.983	18.751	0.1241	28
NSC2332+0843	353.015	8.719	0.1166	37
NSC2332+2326	353.031	23.431	0.1668	31
NSC2332+2516	353.040	25.270	0.1823	26
NSC2332+0909	353.055	9.152	0.1558	21
NSC2332+2313	353.091	23.214	0.2644	37
NSC2332+2606	353.095	26.098	0.1215	32
NSC2332+1146	353.103	11.768	0.1725	26
NSC2333+1924	353.142	19.393	0.1688	35
NSC2333+2610	353.212	26.160	0.1928	36
NSC2333+0903	353.220	9.057	0.1321	32
NSC2333+2457	353.234	24.943	0.1129	29
NSC2333+2144	353.234	21.729	0.2135	20
NSC2333+0731	353.245	7.510	0.1291	30
NSC2333+1924	353.284	19.397	0.1637	23
NSC2333+2557	353.288	25.955	0.1514	34
NSC2333+1805	353.319	18.082	0.1463	34
NSC2333+2324	353.324	23.399	0.1439	21
NSC2333+0807	353.341	8.125	0.1535	25
NSC2333+0147	353.344	1.784	0.1553	24
NSC2333+1948	353.367	19.797	0.1758	44
NSC2333+2026	353.368	20.438	0.1514	24
NSC2334+0538	353.377	5.629	0.1291	30
NSC2334+0926	353.378	9.430	0.2039	28
NSC2334+2142	353.381	21.698	0.2050	21
NSC2334+0549	353.392	5.824	0.2095	20
NSC2334+0818	353.404	8.300	0.1062	51

Continued...

Table B.2 - SGP Robust, Continued

Name	RA	Dec	z_{phot}	N_{gal}
NSC2334+2301	353.409	23.010	0.1619	23
NSC2334+2554	353.412	25.892	0.1802	21
NSC2334+1816	353.418	18.270	0.1213	30
NSC2334+2356	353.432	23.928	0.2857	35
NSC2334+1855	353.438	18.916	0.0943	36
NSC2334+2502	353.440	25.030	0.2282	31
NSC2334+2040	353.447	20.670	0.1620	31
NSC2334+2717	353.464	27.279	0.1964	21
NSC2334+2610	353.479	26.162	0.1301	47
NSC2334+0704	353.495	7.061	0.1507	60
NSC2334+2201	353.508	22.012	0.1403	21
NSC2334+0720	353.524	7.327	0.2425	44
NSC2334+2544	353.541	25.732	0.0882	32
NSC2334+1953	353.582	19.881	0.0821	97
NSC2334+2051	353.586	20.852	0.1259	60
NSC2334+0652	353.588	6.870	0.1773	29
NSC2335+1933	353.630	19.554	0.2007	25
NSC2335+0507	353.647	5.115	0.2062	26
NSC2335+2554	353.668	25.898	0.2211	23
NSC2335+0832	353.669	8.526	0.0710	19
NSC2335+0760	353.685	7.993	0.2066	30
NSC2335+0537	353.739	5.619	0.1337	24
NSC2335+1921	353.779	19.354	0.1099	33
NSC2335+0857	353.785	8.952	0.1799	16
NSC2335+2720	353.787	27.334	0.1789	25
NSC2335+1510	353.793	15.164	0.1235	28
NSC2335+2152	353.799	21.860	0.0826	26
NSC2335+1809	353.800	18.145	0.1001	41
NSC2335+0352	353.801	3.862	0.1874	55
NSC2335+1842	353.810	18.694	0.2352	22
NSC2335+0104	353.818	1.059	0.2513	41
NSC2335+2044	353.821	20.739	0.2286	20
NSC2335+2311	353.834	23.187	0.2200	15
NSC2335+2546	353.837	25.769	0.1057	63
NSC2335+2604	353.845	26.067	0.1948	33
NSC2336+0144	353.902	1.729	0.0732	35
NSC2336+2242	353.914	22.705	0.1842	31
NSC2336+0625	353.916	6.415	0.2156	20
NSC2336+2635	353.929	26.581	0.1218	48
NSC2336+0536	353.938	5.604	0.1340	30
NSC2336+1955	353.944	19.913	0.2298	23
NSC2336+1901	353.948	19.012	0.1667	19
NSC2336+0443	353.950	4.722	0.2594	25
NSC2336+2058	353.984	20.975	0.1979	37
NSC2336+0513	353.998	5.216	0.1976	35
NSC2336+0421	354.037	4.343	0.1740	20
NSC2336+0612	354.040	6.195	0.1034	25
NSC2336+1918	354.041	19.297	0.1484	65
NSC2336+2033	354.045	20.551	0.0913	39
NSC2336+2129	354.051	21.489	0.1744	26
NSC2336+2228	354.078	22.468	0.1015	35
NSC2336+0603	354.100	6.049	0.1341	38
NSC2336+1809	354.115	18.153	0.2309	17
NSC2336+1603	354.117	16.042	0.2403	20
NSC2336+2511	354.122	25.190	0.2080	30
NSC2336+2355	354.124	23.924	0.1225	38
NSC2336+2112	354.125	21.199	0.1101	35
NSC2337+1617	354.139	16.289	0.1339	36
NSC2337+0828	354.147	8.473	0.1250	31
NSC2337+0856	354.200	8.930	0.2385	36
NSC2337+0647	354.202	6.781	0.2049	23
NSC2337+0445	354.219	4.757	0.2242	14
NSC2337+0459	354.240	4.990	0.0972	35
NSC2337+2053	354.251	20.886	0.1303	25
NSC2337+2310	354.265	23.162	0.1117	36
NSC2337+2432	354.287	24.528	0.1572	23
NSC2337+1551	354.309	15.854	0.1947	18
NSC2337+2610	354.352	26.173	0.0680	21
NSC2337+2704	354.353	27.068	0.1879	22
NSC2338+0507	354.404	5.117	0.2469	25
NSC2338+0016	354.408	0.274	0.1483	27
NSC2338+2630	354.412	26.496	0.2432	23
NSC2338+0535	354.427	5.582	0.1409	35
NSC2338+1554	354.447	15.906	0.1322	68
NSC2338+2135	354.454	21.583	0.1239	22
NSC2338+2550	354.488	25.827	0.0990	65
NSC2338+1311	354.489	13.188	0.1683	40
NSC2338+2144	354.492	21.739	0.1637	33
NSC2338+0352	354.504	3.873	0.1142	24
NSC2338+0835	354.516	8.588	0.1131	26
NSC2338+1927	354.519	19.447	0.0768	51
NSC2338+2455	354.531	24.922	0.1741	30
NSC2338+2715	354.556	27.256	0.2094	25
NSC2338+0642	354.564	6.707	0.1905	29
NSC2338+1805	354.565	18.088	0.2165	25
NSC2338+2753	354.567	27.889	0.2097	22
NSC2338+0552	354.571	5.868	0.1475	24

Continued...

Table B.2 - SGP Robust, Continued

Name	RA	Dec	z_{phot}	N_{gal}
NSC2338+1621	354.596	16.343	0.1652	29
NSC2338+2205	354.602	22.089	0.1078	74
NSC2338+0456	354.604	4.927	0.1580	27
NSC2339+2740	354.641	27.674	0.0991	32
NSC2339+2548	354.645	25.799	0.1034	28
NSC2339+0342	354.655	3.693	0.1663	27
NSC2339+0719	354.682	7.324	0.1176	28
NSC2339+2525	354.692	25.412	0.1572	27
NSC2339+1521	354.700	15.356	0.2599	18
NSC2339+2342	354.721	23.694	0.1179	73
NSC2339+0531	354.737	5.520	0.2222	20
NSC2339+0602	354.742	6.035	0.1863	26
NSC2339+2642	354.750	26.705	0.0968	27
NSC2339+2129	354.753	21.484	0.1590	21
NSC2339+0650	354.757	6.835	0.1130	80
NSC2339+0743	354.769	7.715	0.1320	45
NSC2339+2755	354.772	27.911	0.1647	61
NSC2339+0608	354.795	6.136	0.2465	16
NSC2339+2256	354.827	22.940	0.2011	17
NSC2339+2705	354.863	27.083	0.1368	35
NSC2339+0824	354.870	8.400	0.1047	38
NSC2339+2043	354.870	20.720	0.1103	18
NSC2340+2534	354.879	25.569	0.1613	22
NSC2340+2423	354.903	24.386	0.1605	34
NSC2340+2509	354.915	25.158	0.2105	25
NSC2340+2012	354.915	20.199	0.2314	26
NSC2340+2330	354.928	23.505	0.2613	19
NSC2340+1429	354.936	14.477	0.1918	26
NSC2340+2554	354.974	25.901	0.1909	32
NSC2340+2625	354.977	26.422	0.2028	32
NSC2340+0420	355.020	4.326	0.1769	25
NSC2340+2360	355.027	23.994	0.1565	28
NSC2340+0336	355.040	3.598	0.1626	21
NSC2340+0452	355.047	4.866	0.2020	23
NSC2340+0837	355.056	8.619	0.2003	27
NSC2340+1531	355.084	15.517	0.1012	31
NSC2340+1938	355.087	19.635	0.2054	16
NSC2340+0259	355.102	2.990	0.1739	32
NSC2340+0902	355.107	9.025	0.1153	33
NSC2340+2158	355.111	21.968	0.2006	23
NSC2340+1034	355.113	10.568	0.1037	28
NSC2340+2510	355.120	25.167	0.1092	27
NSC2341+2348	355.129	23.803	0.2135	28
NSC2341+2634	355.145	26.573	0.1929	39
NSC2341+1741	355.154	17.677	0.1233	22
NSC2341+0523	355.183	5.390	0.1316	40
NSC2341+2131	355.207	21.524	0.1786	27
NSC2341+0006	355.210	0.098	0.1219	28
NSC2341+2520	355.240	25.338	0.2068	25
NSC2341+2621	355.243	26.344	0.1161	61
NSC2341+1544	355.265	15.727	0.1614	24
NSC2341+2030	355.276	20.503	0.1126	36
NSC2341+1927	355.285	19.449	0.2218	19
NSC2341+0424	355.293	4.400	0.1590	25
NSC2341+0336	355.308	3.607	0.1142	60
NSC2341+1626	355.311	16.438	0.2495	16
NSC2341+2039	355.315	20.652	0.1923	19
NSC2341+2550	355.339	25.829	0.1345	27
NSC2341+2442	355.350	24.701	0.1820	22
NSC2341+2747	355.357	27.779	0.1120	40
NSC2341+2604	355.370	26.070	0.1625	26
NSC2342+2738	355.376	27.632	0.2119	30
NSC2342+0760	355.408	7.999	0.1244	27
NSC2342+1508	355.412	15.128	0.1273	19
NSC2342+2101	355.458	21.021	0.1172	35
NSC2342+1546	355.471	15.759	0.0929	40
NSC2342+0216	355.484	2.263	0.1271	40
NSC2342+2645	355.486	26.748	0.0722	34
NSC2342+2131	355.491	21.523	0.1708	45
NSC2342+2654	355.506	26.906	0.1821	27
NSC2342+1929	355.522	19.475	0.1429	24
NSC2342+0430	355.568	4.505	0.1280	24
NSC2342+0804	355.585	8.059	0.2054	22
NSC2342+2146	355.604	21.768	0.2019	28
NSC2343+2353	355.638	23.889	0.1553	31
NSC2343+1510	355.649	15.169	0.2481	28
NSC2343+2709	355.670	27.157	0.2112	24
NSC2343+0823	355.703	8.389	0.1167	33
NSC2343+2320	355.705	23.332	0.1705	44
NSC2343+2643	355.717	26.724	0.1367	30
NSC2343+0717	355.732	7.284	0.1161	35
NSC2343+2539	355.737	25.643	0.2316	22
NSC2343+0739	355.743	7.643	0.1991	14
NSC2343+1420	355.757	14.327	0.1355	39
NSC2343+0433	355.801	4.543	0.1065	28
NSC2343+2044	355.807	20.730	0.1452	45
NSC2343+1934	355.842	19.560	0.1333	28

Continued...

Table B.2 - SGP Robust, Continued

Name	RA	Dec	z_{phot}	N_{gal}
NSC2343+2058	355.855	20.972	0.1471	25
NSC2343+2659	355.855	26.980	0.2370	22
NSC2343+0414	355.866	4.234	0.2092	18
NSC2344+2745	355.885	27.742	0.1440	29
NSC2344+1742	355.891	17.695	0.0990	58
NSC2344+2730	355.908	27.508	0.1550	34
NSC2344+1916	355.913	19.261	0.1362	24
NSC2344+0018	355.917	0.306	0.1430	19
NSC2344+1419	355.941	14.315	0.1600	58
NSC2344+1831	355.993	18.512	0.2528	21
NSC2344+2649	356.000	26.821	0.1982	24
NSC2344+2537	356.001	25.620	0.1701	30
NSC2344+1409	356.003	14.157	0.2733	25
NSC2344+0703	356.006	7.048	0.1214	31
NSC2344+2023	356.011	20.376	0.1352	33
NSC2344+2346	356.012	23.775	0.1275	40
NSC2344+2530	356.015	25.501	0.1114	39
NSC2344+1158	356.017	11.969	0.1614	52
NSC2344+0500	356.044	5.001	0.2045	25
NSC2344+0426	356.085	4.433	0.1877	37
NSC2344+2110	356.087	21.166	0.1851	28
NSC2344+1550	356.113	15.837	0.1976	18
NSC2344+0307	356.115	3.114	0.1345	35
NSC2345+1616	356.127	16.263	0.1531	23
NSC2345+0911	356.174	9.181	0.1659	18
NSC2345+0728	356.176	7.473	0.1559	34
NSC2345+2745	356.182	27.755	0.1245	53
NSC2345+0108	356.210	1.135	0.2887	21
NSC2345+1651	356.217	16.856	0.2224	21
NSC2345+0408	356.244	4.133	0.1577	23
NSC2345+1929	356.276	19.488	0.2294	23
NSC2345+1950	356.286	19.841	0.1237	34
NSC2345+0802	356.287	8.037	0.1678	29
NSC2345+2158	356.318	21.966	0.1749	22
NSC2345+2237	356.371	22.616	0.0936	34
NSC2346+0447	356.409	4.788	0.1812	23
NSC2346+0317	356.462	3.286	0.1537	22
NSC2346+2440	356.501	24.660	0.1605	36
NSC2346+2703	356.509	27.044	0.2603	25
NSC2346+2201	356.510	22.013	0.1217	26
NSC2346+0829	356.513	8.487	0.1455	27
NSC2346+1430	356.526	14.502	0.1703	30
NSC2346+0432	356.540	4.530	0.1022	38
NSC2346+0057	356.549	0.953	0.0955	40
NSC2346+2231	356.562	22.511	0.1438	40
NSC2346+1234	356.571	12.573	0.1510	34
NSC2346+1410	356.580	14.167	0.1882	24
NSC2346+2559	356.582	25.980	0.1322	51
NSC2346+2221	356.592	22.349	0.2146	21
NSC2346+0811	356.600	8.181	0.1497	21
NSC2346+0046	356.623	0.760	0.1167	42
NSC2347+2657	356.636	26.942	0.1432	25
NSC2347+0651	356.647	6.851	0.1334	37
NSC2347+0424	356.661	4.396	0.1217	34
NSC2347+1809	356.711	18.144	0.1033	14
NSC2347+0706	356.719	7.097	0.1064	40
NSC2347+2758	356.731	27.965	0.1671	26
NSC2347+0902	356.769	9.039	0.1321	23
NSC2347+2246	356.773	22.760	0.1953	21
NSC2347+2634	356.777	26.566	0.1489	25
NSC2347+1439	356.783	14.644	0.1237	56
NSC2347+0411	356.790	4.179	0.1876	33
NSC2347+1252	356.810	12.868	0.1118	31
NSC2347+2135	356.817	21.591	0.1185	55
NSC2347+1534	356.834	15.564	0.1797	25
NSC2348+2658	356.899	26.963	0.2093	23
NSC2348+2158	356.953	21.968	0.1939	21
NSC2348+1441	356.960	14.690	0.1200	36
NSC2348+0347	357.041	3.781	0.1744	28
NSC2348+0536	357.042	5.602	0.1676	35
NSC2349+2701	357.143	27.014	0.1724	21
NSC2349+2711	357.249	27.187	0.1395	26
NSC2349+1809	357.288	18.146	0.2715	26
NSC2349+0441	357.303	4.689	0.1671	29
NSC2349+1515	357.327	15.243	0.1272	51
NSC2349+0951	357.360	9.844	0.1904	25
NSC2349+1630	357.367	16.499	0.1229	25
NSC2350+1041	357.422	10.675	0.1160	66
NSC2350+0230	357.457	2.507	0.0930	33
NSC2350+0005	357.492	0.083	0.1677	23
NSC2350+0337	357.520	3.613	0.2416	26
NSC2350+0956	357.528	9.933	0.0894	29
NSC2350+0244	357.544	2.734	0.1766	18
NSC2350+0324	357.555	3.405	0.1231	23
NSC2350+0841	357.557	8.689	0.1695	27
NSC2350+2334	357.577	23.568	0.1783	24
NSC2350+0728	357.595	7.469	0.1413	19

Continued...

Table B.2 - SGP Robust, Continued

Name	RA	Dec	z_{phot}	N_{gal}
NSC2350+0315	357.616	3.251	0.1720	25
NSC2351+1459	357.634	14.989	0.1338	31
NSC2351+2656	357.649	26.930	0.1751	17
NSC2351+2434	357.656	24.571	0.1822	33
NSC2351+0608	357.712	6.135	0.1173	46
NSC2351+2425	357.724	24.411	0.1470	28
NSC2351+1249	357.736	12.819	0.1801	21
NSC2351+2443	357.756	24.709	0.2557	28
NSC2351+1055	357.768	10.916	0.1103	31
NSC2351+2742	357.774	27.707	0.1783	15
NSC2351+0710	357.815	7.174	0.1478	21
NSC2351+2507	357.831	25.112	0.1348	33
NSC2351+0537	357.843	5.611	0.1418	25
NSC2352+2545	357.899	25.747	0.2336	20
NSC2352+1634	357.994	16.572	0.1792	22
NSC2352+2218	357.996	22.297	0.2519	19
NSC2352+2335	358.008	23.577	0.1308	26
NSC2352+2113	358.023	21.212	0.1966	38
NSC2352+1647	358.045	16.776	0.1235	34
NSC2352+2452	358.056	24.865	0.2533	35
NSC2352+0546	358.059	5.772	0.2431	23
NSC2352+1404	358.061	14.062	0.1095	34
NSC2352+1246	358.084	12.763	0.1082	41
NSC2352+1733	358.098	17.544	0.2234	20
NSC2352+2505	358.110	25.078	0.1398	25
NSC2352+2519	358.125	25.323	0.1403	25
NSC2353+0652	358.222	6.874	0.2525	23
NSC2353+1043	358.233	10.709	0.1640	22
NSC2353+2653	358.245	26.884	0.1887	17
NSC2353+2457	358.250	24.952	0.2101	30
NSC2353+1837	358.252	18.611	0.0945	33
NSC2353+1125	358.257	11.413	0.2274	23
NSC2353+1703	358.275	17.049	0.1596	35
NSC2353+1346	358.276	13.770	0.1756	25
NSC2353+0133	358.282	1.555	0.1448	31
NSC2353+0046	358.285	0.771	0.1811	17
NSC2353+0814	358.319	8.239	0.1251	44
NSC2353+0852	358.329	8.873	0.1509	31
NSC2353+1022	358.344	10.373	0.1287	32
NSC2353+2526	358.344	25.427	0.2295	16
NSC2354+0234	358.385	2.559	0.1384	40
NSC2354+1223	358.385	12.378	0.1739	23
NSC2354+2534	358.433	25.571	0.2411	28
NSC2354+1111	358.471	11.189	0.1614	23
NSC2354+2757	358.471	27.952	0.1315	31
NSC2354+2654	358.482	26.895	0.1835	20
NSC2354+0546	358.497	5.766	0.1934	17
NSC2354+0352	358.504	3.874	0.1234	27
NSC2354+1051	358.551	10.853	0.2180	39
NSC2354+2621	358.558	26.351	0.1694	25
NSC2354+0333	358.572	3.547	0.2287	19
NSC2354+1628	358.603	16.467	0.1271	39
NSC2355+0220	358.639	2.334	0.0998	27
NSC2355+1354	358.643	13.902	0.1737	17
NSC2355+0211	358.661	2.190	0.2090	33
NSC2355+1606	358.664	16.104	0.0979	19
NSC2355+0323	358.674	3.381	0.2339	31
NSC2355+0157	358.730	1.953	0.1016	27
NSC2355+2012	358.736	20.204	0.1033	17
NSC2355+2157	358.763	21.955	0.1824	20
NSC2355+0217	358.791	2.278	0.1093	26
NSC2355+2734	358.815	27.570	0.1907	25
NSC2355+1342	358.824	13.706	0.1185	44
NSC2355+2627	358.825	26.443	0.1686	19
NSC2355+1926	358.835	19.434	0.2021	24
NSC2355+0527	358.847	5.447	0.1388	33
NSC2355+0147	358.868	1.780	0.2614	18
NSC2356+1121	358.918	11.354	0.1365	37
NSC2356+1136	358.941	11.595	0.2516	33
NSC2356+1552	358.942	15.869	0.2210	15
NSC2356+0437	358.972	4.622	0.1097	29
NSC2356+0604	358.978	6.069	0.1131	47
NSC2356+0505	358.980	5.081	0.1852	28
NSC2356+0403	358.990	4.044	0.2172	14
NSC2356+2534	358.996	25.570	0.1457	34
NSC2356+2339	359.032	23.652	0.1055	29
NSC2356+2406	359.037	24.094	0.1524	19
NSC2356+2134	359.038	21.561	0.2125	14
NSC2356+2450	359.075	24.833	0.1223	38
NSC2356+0507	359.092	5.117	0.1510	22
NSC2356+2636	359.109	26.594	0.2021	15
NSC2357+2526	359.126	25.432	0.0992	25
NSC2357+2514	359.169	25.235	0.2286	23
NSC2357+2008	359.196	20.127	0.1693	28
NSC2357+1919	359.203	19.317	0.2977	14
NSC2357+2755	359.220	27.909	0.1448	26
NSC2357+0041	359.223	0.686	0.2443	25

Continued...

Table B.2 - SGP Robust, Continued

Name	RA	Dec	z_{phot}	N_{gal}
NSC2357+2641	359.242	26.688	0.1147	26
NSC2357+2546	359.258	25.774	0.2203	21
NSC2357+0629	359.269	6.490	0.1568	28
NSC2357+2450	359.281	24.837	0.1770	28
NSC2357+1904	359.306	19.065	0.1151	26
NSC2357+0532	359.328	5.534	0.1491	32
NSC2358+2552	359.382	25.875	0.1595	19
NSC2358+1509	359.386	15.148	0.1740	20
NSC2358+2051	359.394	20.847	0.1416	22
NSC2358+1401	359.401	14.012	0.1864	30
NSC2358+0129	359.404	1.480	0.1483	15
NSC2358+0011	359.410	0.179	0.1973	24
NSC2358+0923	359.422	9.389	0.1453	26
NSC2358+2104	359.432	21.061	0.1235	20
NSC2358+1451	359.437	14.849	0.2572	22
NSC2358+2042	359.453	20.699	0.1496	24
NSC2358+2534	359.460	25.567	0.1835	15
NSC2358+0116	359.469	1.275	0.1582	31
NSC2358+1203	359.496	12.045	0.2070	17
NSC2358+1529	359.541	15.482	0.1749	47
NSC2358+0931	359.551	9.515	0.1641	36
NSC2358+0406	359.558	4.107	0.1251	33
NSC2358+0511	359.561	5.183	0.1380	43
NSC2358+1512	359.576	15.202	0.1640	26
NSC2358+1914	359.586	19.229	0.1142	30
NSC2358+0045	359.591	0.747	0.1478	29
NSC2359+0316	359.648	3.265	0.0895	28
NSC2359+1407	359.725	14.113	0.1701	35
NSC2359+0447	359.769	4.788	0.1078	40
NSC2359+0015	359.799	0.251	0.1653	26
NSC2359+0460	359.839	4.994	0.1998	16
NSC2359+1445	359.842	14.758	0.2061	24
NSC2359+0545	359.848	5.750	0.1258	35
NSC2359+1548	359.873	15.804	0.1796	37
NSC0000+2323	359.892	23.387	0.1849	31
NSC0000+1343	359.901	13.708	0.1335	32
NSC0000+1203	359.932	12.056	0.2195	27
NSC0000+0734	359.949	7.567	0.1119	30
NSC0000+1320	359.962	13.339	0.2117	24
NSC0000+0518	359.999	5.306	0.2526	17

Table B.3 - Photometric Redshifts for Abell Clusters

Abell	CCD	$(g-r)_{med}$	g_{mean}	E(B − V)	z_{phot}	Error	z_{spec}
21	13	0.56984	19.1749	0.03911	0.0881	0.0243	0.0946
26	13	0.68976	19.8172	0.06752	0.1448	0.0243	0.1449
31	16	0.62472	19.9006	0.03836	0.1452	0.0289	0.1596
31	16	0.65092	19.7028	0.03686	0.1498	0.0289	0.1596
54	13	0.75757	20.4157	0.04703	0.1947	0.0245	–
59	13	0.71243	20.1403	0.05342	0.1660	0.0245	–
60	13	0.97409	19.9467	0.04778	0.2061	0.0250	–
62	16	0.50123	19.4658	0.03938	0.0933	0.0289	–
65	16	0.78512	20.0763	0.06377	0.2026	0.0287	0.1206
68	13	1.11481	20.5031	0.09476	0.2233	0.0250	0.2546
69	13	0.64688	20.1062	0.05788	0.1415	0.0243	0.1454
69	16	0.84825	19.2846	0.05788	0.1899	0.0292	0.1454
73	13	1.05318	20.3368	0.09367	0.2244	0.0250	–
79	16	0.69633	19.7945	0.08488	0.1676	0.0292	0.0927
82	13	0.64521	19.4615	0.03514	0.1181	0.0243	–
83	16	0.80527	20.2038	0.08388	0.2119	0.0287	–
98	13	0.57916	19.7885	0.04508	0.1073	0.0243	0.1050
98	16	0.58635	19.0310	0.04508	0.1136	0.0289	0.1050
110	13	0.49108	19.4000	0.04784	0.0715	0.0243	–
115	16	0.90548	19.3913	0.05764	0.1995	0.0292	0.1971
136	16	0.90075	20.5781	0.05666	0.2418	0.0287	0.1569
137	16	0.58929	19.6325	0.06651	0.1264	0.0289	–
142	16	1.19339	20.3110	0.02611	0.1846	0.0292	–
143	16	0.64219	20.2976	0.07644	0.1617	0.0292	–
152	13	0.51463	18.8969	0.03561	0.0679	0.0243	0.0581
153	13	0.61917	20.1015	0.03076	0.1313	0.0243	0.1279
153	13	0.64632	19.4959	0.03076	0.1196	0.0243	0.1279
154	13	0.50904	19.1955	0.06283	0.0722	0.0243	0.0624
163	16	0.62553	20.2190	0.05280	0.1532	0.0292	–
165	13	0.60361	19.7734	0.05807	0.1149	0.0243	–
167	16	0.68404	20.3669	0.05187	0.1795	0.0292	–
175	13	0.47655	18.6362	0.05604	0.0549	0.0243	0.1292
175	13	0.60273	19.8184	0.05604	0.1160	0.0243	0.1292
184	13	0.90874	20.8581	0.03488	0.2598	0.0306	–
184	16	0.82114	20.6201	0.03484	0.2306	0.0287	–
191	13	0.90729	20.6865	0.06023	0.2477	0.0250	–
196	13	0.91350	20.1011	0.07062	0.2117	0.0250	–
219	13	0.70417	18.9628	0.07354	0.1182	0.0243	–
227	13	0.67306	20.0422	0.07266	0.1482	0.0243	0.1768
234	13	0.67408	20.3887	0.06394	0.1634	0.0245	0.1731
245	13	0.47259	19.1110	0.05571	0.0616	0.0243	0.0790
246	13	0.53622	18.6123	0.06930	0.0677	0.0243	0.0700
247	16	0.70622	19.9252	0.05394	0.1745	0.0292	–
249	13	0.69410	20.6258	0.07400	0.1824	0.0245	–
249	13	0.85473	20.4095	0.07359	0.2208	0.0250	–
253	13	1.05273	19.1403	0.09358	0.1617	0.0245	–
257	16	0.61246	19.6717	0.05504	0.1355	0.0289	0.0703
258	13	0.09506	18.7597	0.10749	0.0111	0.0244	–
258	13	0.15118	18.8687	0.10749	0.0075	0.0244	–
260	13	0.48142	19.2192	0.04944	0.0656	0.0243	0.0369
262	13	0.52546	18.2927	0.09019	0.0598	0.0243	0.0163
272	13	0.57489	19.7996	0.04788	0.1062	0.0243	0.0877
275	16	0.86527	20.2964	0.05229	0.2268	0.0287	–
278	13	0.56409	19.7509	0.05465	0.1013	0.0243	0.0891
288	13	0.70207	19.6760	0.06845	0.1430	0.0243	–
288	13	0.71702	19.5644	0.06845	0.1431	0.0243	–
300	16	0.72066	20.2539	0.05813	0.1890	0.0292	–
307	13	1.94115	19.4678	0.09527	0.0051	0.0244	–
311	13	0.49321	18.2959	0.16897	0.0533	0.0243	0.0649
318	13	0.65820	19.8653	0.06498	0.1363	0.0243	0.1320
320	13	0.91160	20.1860	0.08404	0.2165	0.0250	–
330	13	0.58288	20.2481	0.09242	0.1231	0.0243	–
333	16	0.70736	19.9606	0.09204	0.1759	0.0292	–
345	13	0.61722	19.2636	0.16864	0.1038	0.0243	–
347	13	1.09518	17.3148	0.05747	0.0950	0.0243	0.0184
349	13	0.57984	19.3553	0.06075	0.0955	0.0243	–
360	13	0.85185	20.2633	0.07576	0.2116	0.0250	0.2205
364	13	0.66718	20.1751	0.16586	0.1516	0.0245	0.1800
372	13	0.64544	19.8768	0.09561	0.1324	0.0243	0.1073
373	13	0.63530	19.4034	0.15390	0.1486	0.0243	–
373	13	0.66272	20.1405	0.15390	0.1133	0.0243	–
374	13	0.61523	19.3218	0.05121	0.1049	0.0243	0.0757
376	13	0.49633	18.3979	0.07008	0.0554	0.0243	0.0481
377	13	0.74239	19.7053	0.14500	0.1937	0.0245	–
377	13	0.75779	20.3970	0.14423	0.1560	0.0245	–
382	13	0.57552	19.7137	0.05816	0.1040	0.0243	–
384	16	0.97386	20.3809	0.04618	0.2356	0.0287	–
397	13	0.40766	18.5634	0.15054	0.0405	0.0244	0.0327
399	13	0.45026	19.8261	0.16449	0.0686	0.0243	0.0724
408	13	0.65978	19.6092	0.22645	0.1275	0.0243	–
410	13	0.42726	19.1095	0.10081	0.0512	0.0243	0.0897
411	16	0.51087	19.3963	0.08243	0.0953	0.0289	0.1567
421	13	0.50475	18.5584	0.36592	0.0597	0.0243	–
421	13	0.57261	19.1531	0.34166	0.0884	0.0243	–
426	16	0.60447	19.4184	0.17631	0.1273	0.0289	0.0179
427	13	0.69380	19.5394	0.19721	0.1354	0.0243	–
429	13	0.66930	19.2705	0.36639	0.1189	0.0243	–
429	13	0.72971	18.8353	0.36639	0.1201	0.0243	–
436	13	0.52151	18.4605	0.27183	0.0617	0.0243	–

Continued...

Table B.3 - Abell Cluster Photometric Redshifts, Continued

Abell	CCD	$(g-r)_{med}$	g_{mean}	$E(B-V)$	z_{phot}	Error	z_{spec}
437	13	0.55318	19.4990	0.04673	0.0913	0.0243	0.0847
439	13	0.63436	18.9645	0.18273	0.1002	0.0243	0.1068
444	13	0.56523	19.1289	0.15907	0.0858	0.0243	–
452	13	0.74202	20.1905	0.17141	0.1781	0.0245	–
461	13	0.94078	19.9688	0.09804	0.2063	0.0250	–
465	13	0.65280	19.7421	0.26737	0.1300	0.0243	0.1300
468	13	0.55633	18.9604	0.18108	0.0796	0.0243	0.1325
468	13	0.73595	18.7085	0.18108	0.1174	0.0243	0.1325
477	13	0.92203	20.5368	0.19900	0.2394	0.0250	–
477	13	1.13313	20.2364	0.19900	0.2033	0.0250	–
478	13	0.59300	18.9106	0.50950	0.0880	0.0243	0.0881
485	13	0.73114	19.6791	0.19952	0.1517	0.0245	–
497	13	0.53389	18.8471	0.33775	0.0716	0.0243	–
498	13	0.54786	18.3495	0.40129	0.0655	0.0243	–
501	13	0.53564	19.8623	0.20177	0.0952	0.0243	0.1517
502	13	0.47876	17.9946	0.16282	0.0465	0.0244	–
504	13	0.53734	19.0054	0.13891	0.0757	0.0243	–
508	13	0.61470	19.6654	0.13706	0.1151	0.0243	0.1479
509	13	0.68490	20.2419	0.14506	0.1609	0.0245	0.0836
515	13	0.44215	18.3532	0.09844	0.0443	0.0244	–
520	13	0.71559	19.9856	0.04703	0.1601	0.0245	0.1990
523	13	0.60029	18.8808	0.14601	0.0891	0.0243	0.1000
525	13	0.67672	19.8333	0.13798	0.1412	0.0243	–
526	13	0.54725	19.4433	0.09844	0.0882	0.0243	0.0835
529	13	0.52781	19.1887	0.08734	0.0770	0.0243	–
530	13	0.71692	18.6154	0.07989	0.1103	0.0243	–
532	13	0.66377	19.3781	0.21411	0.1209	0.0243	–
537	13	0.83142	20.5565	0.13948	0.2244	0.0250	–
539	13	0.31046	18.2052	0.16181	0.0232	0.0244	0.0284
541	13	1.44808	17.8569	0.19176	0.0496	0.0244	–
546	13	0.83132	19.8455	0.19558	0.1847	0.0245	–
549	13	0.99926	20.4647	0.14110	0.2371	0.0250	–
553	13	0.46492	19.2178	0.15635	0.0615	0.0243	0.0664
554	13	0.54244	19.0158	0.10251	0.0772	0.0243	–
556	13	0.65611	18.8411	0.09980	0.1024	0.0243	–
557	13	1.37318	19.9090	0.10900	0.1117	0.0243	–
558	13	0.17091	18.2115	0.10936	0.0846	0.0243	–
558	13	0.57205	19.0006	0.10936	0.0105	0.0244	–
567	13	0.59490	19.8080	0.11074	0.1131	0.0243	–
567	13	0.60708	20.1740	0.11074	0.1295	0.0243	–
569	13	0.61141	19.0390	0.07308	0.0961	0.0243	0.0201
574	13	0.96262	20.3645	0.03163	0.2309	0.0250	0.1740
579	16	0.60821	19.5383	0.06854	0.1311	0.0289	–
580	13	0.47746	19.7908	0.07691	0.0756	0.0243	–
583	16	0.66862	20.0568	0.06291	0.1651	0.0292	–
586	16	0.67197	19.9786	0.05758	0.1642	0.0292	0.1710
587	13	0.55457	19.9488	0.06260	0.1038	0.0243	0.1680
590	13	0.53404	20.0988	0.05466	0.1010	0.0243	–
611	13	0.61826	20.3126	0.04781	0.1388	0.0243	0.2880
630	13	0.69993	20.6623	0.04882	0.1865	0.0245	–
635	13	0.46777	19.3110	0.04504	0.0638	0.0243	–
647	13	0.86745	20.5141	0.02353	0.2299	0.0250	–
657	13	0.06363	19.7952	0.02951	0.0080	0.0244	–
657	13	0.59567	19.3910	0.02951	0.1011	0.0243	–
658	13	0.57290	19.8568	0.03135	0.1073	0.0243	0.0917
659	13	0.62426	19.4196	0.05547	0.1105	0.0243	–
660	13	0.68376	20.5299	0.04733	0.1736	0.0245	–
665	13	0.36927	19.8699	0.04360	0.0487	0.0244	0.1819
668	13	0.55004	19.6021	0.05564	0.1621	0.0245	0.1588
677	13	0.70330	21.1855	0.04541	0.2430	0.0250	–
677	13	1.10518	20.7766	0.04360	0.2168	0.0250	–
687	13	0.94758	20.5253	0.02483	0.2407	0.0250	–
688	13	0.66148	19.9358	0.02399	0.1401	0.0243	–
696	13	0.66665	20.2914	0.02464	0.1563	0.0245	–
699	13	0.50383	19.2307	0.05015	0.0716	0.0243	0.0851
706	13	0.68127	20.7678	0.05126	0.1843	0.0245	–
710	13	0.82540	20.8878	0.03391	0.2441	0.0250	–
715	13	0.70071	20.9068	0.03819	0.1998	0.0245	0.1685
720	13	1.03609	20.8913	0.03034	0.2635	0.0306	0.1329
724	16	0.53159	18.5909	0.02975	0.0895	0.0289	0.0933
732	13	0.64268	20.5079	0.04848	0.1637	0.0245	0.2030
732	13	0.68154	20.3330	0.04848	0.1563	0.0245	0.2030
734	13	0.81491	20.6592	0.03223	0.2264	0.0250	0.0719
741	16	0.87969	19.7788	0.02001	0.2102	0.0287	–
749	13	0.69543	20.0636	0.04477	0.1568	0.0245	–
750	13	0.69561	20.2390	0.04248	0.1583	0.0245	0.1800
750	13	0.70324	20.0379	0.04248	0.1646	0.0245	0.1800
752	13	0.63009	20.6341	0.02153	0.1565	0.0245	–
752	13	0.91807	20.1178	0.02630	0.2131	0.0250	–
759	16	0.94435	20.0263	0.01980	0.2228	0.0287	–
779	13	0.95300	20.9636	0.01599	0.2717	0.0306	0.0229
781	13	1.02474	20.9976	0.02206	0.2725	0.0306	0.2980
791	13	0.79105	20.1921	0.03118	0.1929	0.0245	–
795	13	0.54773	20.0723	0.02871	0.1050	0.0243	0.1359
795	13	0.62135	19.9541	0.02962	0.1269	0.0243	0.1359
815	13	0.90653	20.5706	0.01982	0.2399	0.0250	–
835	13	0.62725	20.1492	0.03356	0.1360	0.0243	–

Continued...

Table B.3 - Abell Cluster Photometric Redshifts, Continued

Abell	CCD	$(g-r)_{med}$	g_{mean}	$E(B-V)$	z_{phot}	Error	z_{spec}
850	13	0.61231	20.1526	0.03610	0.1307	0.0243	–
851	16	1.26743	20.9694	0.01711	0.1746	0.0292	0.4069
891	13	0.75560	20.4164	0.01970	0.1940	0.0245	–
898	16	0.90464	20.6850	0.01030	0.2464	0.0287	–
937	13	0.56146	19.9056	0.04112	0.1048	0.0243	–
942	13	0.58843	20.1755	0.01418	0.1227	0.0243	–
954	16	0.59112	19.3193	0.03458	0.1207	0.0289	0.0932
957	16	0.87561	19.4017	0.03351	0.1971	0.0292	0.0450
967	16	0.84000	20.1400	0.01359	0.2169	0.0287	–
969	16	0.50442	18.8411	0.03372	0.0852	0.0289	–
986	13	0.85127	20.6757	0.04148	0.2368	0.0250	–
1015	13	1.29165	20.5934	0.01384	0.1684	0.0245	–
1019	16	0.72710	20.3242	0.01938	0.1934	0.0292	–
1030	16	0.85723	20.3117	0.01841	0.2261	0.0287	0.1780
1034	13	0.72808	20.0985	0.03329	0.1692	0.0245	–
1050	16	0.58565	19.3148	0.01948	0.1188	0.0289	0.1208
1062	13	0.76750	20.5136	0.03201	0.2033	0.0250	–
1063	13	0.68803	20.2837	0.04027	0.1639	0.0245	–
1081	13	0.57394	20.0114	0.01671	0.1123	0.0243	0.1585
1095	13	0.69758	20.4506	0.02989	0.1752	0.0245	0.2108
1095	13	0.73707	20.2775	0.02989	0.1808	0.0245	0.2108
1101	16	0.92782	20.3118	0.01740	0.2331	0.0287	0.2322
1114	13	0.47207	20.1248	0.02872	0.0811	0.0243	0.0140
1120	13	0.79550	20.9401	0.02972	0.2383	0.0250	0.2218
1140	13	1.17952	20.9944	0.01990	0.2347	0.0250	–
1299	13	0.41872	20.1729	0.02565	0.0661	0.0243	0.2247
1345	13	0.50007	19.9364	0.04435	0.0856	0.0243	0.1095
1356	13	0.44753	20.0358	0.04992	0.0718	0.0243	0.0698
1413	13	0.57322	19.6151	0.02308	0.1005	0.0243	0.1427
1441	13	0.56523	19.5451	0.01963	0.0961	0.0243	–
1445	13	0.60697	20.4888	0.02511	0.1411	0.0243	0.1694
1475	13	0.71660	20.7940	0.03053	0.2002	0.0250	–
1481	13	0.46412	20.1934	0.03169	0.0801	0.0243	–
1487	13	0.80138	20.7258	0.01770	0.2265	0.0250	0.2111
1489	13	1.03265	19.9782	0.02366	0.2055	0.0250	0.2060
1495	13	0.59984	20.0652	0.02300	0.1231	0.0243	0.1429
1497	13	0.65830	20.3739	0.02513	0.1567	0.0245	0.1669
1499	13	0.60883	20.1277	0.03933	0.1285	0.0243	0.1569
1526	13	0.52537	19.6862	0.04942	0.0875	0.0243	0.0800
1551	16	0.70359	19.6431	0.01295	0.1658	0.0292	–
1577	13	0.59981	19.8800	0.02463	0.1170	0.0243	0.1409
1578	16	0.63441	19.1858	0.02452	0.1323	0.0289	–
1592	16	0.86737	20.3286	0.01626	0.2283	0.0287	–
1608	16	0.73723	19.3522	0.01494	0.1678	0.0292	0.1319
1613	16	0.67606	19.7880	0.01833	0.1606	0.0292	0.1608
1620	13	0.45548	19.8524	0.02533	0.0705	0.0243	0.0821
1647	16	0.78172	19.9377	0.02458	0.1972	0.0292	–
1656	13	0.42058	18.5126	0.00840	0.0423	0.0244	0.0231
1657	16	0.77811	19.6795	0.02757	0.1881	0.0292	–
1661	16	0.66630	19.6312	0.01671	0.1532	0.0292	0.1690
1661	16	0.68407	19.1141	0.01671	0.1463	0.0289	0.1690
1670	16	1.19250	19.5283	0.02222	0.1627	0.0292	–
1677	16	0.87111	19.1111	0.00942	0.1875	0.0292	0.1820
1680	13	0.48350	19.8260	0.01743	0.0781	0.0243	–
1694	16	0.82213	19.9190	0.01146	0.2058	0.0287	–
1711	13	0.46982	19.7342	0.02744	0.0723	0.0243	–
1712	16	1.01113	20.7184	0.01231	0.2457	0.0287	–
1714	16	0.96882	20.6158	0.01342	0.2242	0.0287	–
1714	16	1.09522	20.5804	0.01342	0.2450	0.0287	–
1717	13	0.64266	20.0143	0.01437	0.1365	0.0243	–
1719	13	1.01227	19.7564	0.00958	0.1947	0.0245	–
1728	13	0.44244	18.8809	0.02792	0.0513	0.0243	–
1739	16	0.56328	19.5497	0.01693	0.1157	0.0289	–
1746	13	0.74077	20.3378	0.00950	0.1850	0.0245	–
1752	13	0.53579	20.5101	0.01115	0.1137	0.0243	–
1759	16	1.09547	19.6304	0.02935	0.1919	0.0292	0.1680
1760	16	0.61888	19.5574	0.02926	0.1352	0.0289	0.1711
1785	13	0.60443	20.1930	0.01169	0.1292	0.0243	0.2136
1795	16	0.57284	19.9279	0.01240	0.1266	0.0289	0.0631
1799	13	0.91528	20.7716	0.01594	0.2546	0.0306	0.2451
1810	16	0.68330	19.5209	0.01207	0.1561	0.0292	–
1813	16	0.54633	19.0667	0.01668	0.1015	0.0289	0.0947
1820	13	0.81117	20.6951	0.02743	0.2275	0.0250	–
1821	16	0.61573	19.3145	0.01523	0.1289	0.0289	–
1826	16	0.86756	19.8284	0.01636	0.2104	0.0287	–
1856	13	0.56361	20.5709	0.01695	0.1267	0.0243	0.1854
1874	16	0.73527	19.2227	0.01704	0.1638	0.0292	–
1889	16	0.43053	19.5939	0.01446	0.0730	0.0289	0.1860
1900	16	0.73368	19.3106	0.01198	0.1657	0.0292	0.1718
1905	13	0.90926	20.5457	0.01967	0.2386	0.0250	0.3392
1909	13	0.26985	18.7493	0.02100	0.0217	0.0244	0.1456
1914	13	0.70911	19.9440	0.02253	0.1562	0.0245	0.1712
1917	13	0.65653	20.7987	0.03411	0.1753	0.0245	–
1926	13	0.45225	19.0446	0.03235	0.0558	0.0243	0.1338
1934	13	0.81717	20.5205	0.01296	0.2185	0.0250	0.2194
1954	13	0.49161	20.5259	0.01765	0.0976	0.0243	0.1810
1965	16	1.33724	20.8859	0.01321	0.1213	0.0289	–

Continued...

Table B.3 - Abell Cluster Photometric Redshifts, Continued

Abell	CCD	$(g-r)_{med}$	g_{mean}	$E(B-V)$	z_{phot}	Error	z_{spec}
1965	16	1.39209	21.0136	0.01321	0.1420	0.0289	–
1965	16	1.52184	20.8693	0.01321	0.0707	0.0289	–
1979	13	0.69590	19.8762	0.01644	0.1491	0.0243	0.1687
1987	16	0.60901	19.0374	0.01949	0.1210	0.0289	–
1990	13	0.83691	20.4901	0.02416	0.2217	0.0250	0.1269
2005	16	0.65914	19.1451	0.02643	0.1393	0.0289	0.1234
2008	13	0.75044	20.3750	0.05147	0.1902	0.0245	0.1810
2016	13	0.65029	20.2297	0.04019	0.1477	0.0243	–
2017	13	0.62659	20.1667	0.04933	0.1364	0.0243	0.1187
2034	16	0.68979	18.7973	0.01520	0.1405	0.0289	0.1130
2042	16	0.59510	19.7934	0.01658	0.1319	0.0289	0.2353
2063	13	0.66303	19.9529	0.03458	0.1412	0.0243	0.0353
2065	16	0.39157	19.3454	0.04122	0.0595	0.0289	0.0726
2069	16	0.50431	19.3059	0.02346	0.0918	0.0289	0.1160
2110	16	0.51463	19.0823	0.02508	0.0917	0.0289	0.0980
2111	16	0.97285	20.2236	0.02595	0.2296	0.0287	0.2290
2116	13	1.29418	20.4549	0.03000	0.1611	0.0245	–
2126	13	0.71284	20.4204	0.06225	0.1793	0.0245	0.1656
2129	13	0.74726	20.3378	0.05130	0.1872	0.0245	–
2141	16	0.60366	20.0573	0.02138	0.1410	0.0289	0.1584
2141	16	0.79995	19.6468	0.02125	0.1923	0.0292	0.1584
2147	13	0.48392	19.8084	0.03332	0.0727	0.0243	0.0350
2147	13	0.48680	19.5180	0.03332	0.0779	0.0243	0.0350
2152	13	0.41326	19.6833	0.04018	0.0565	0.0243	0.0410
2155	13	1.17570	20.4862	0.06581	0.2054	0.0250	0.2465
2157	13	1.02867	21.0270	0.01809	0.2743	0.0306	–
2160	16	0.80138	20.2053	0.03127	0.2110	0.0287	–
2162	13	0.43867	20.1324	0.03728	0.0711	0.0243	0.0322
2170	13	0.49221	19.2521	0.08171	0.0690	0.0243	0.1030
2173	13	0.61042	20.2919	0.06308	0.1350	0.0243	–
2177	13	0.67667	20.4227	0.03891	0.1659	0.0245	0.1610
2178	16	0.53237	19.8593	0.05602	0.1105	0.0289	0.0928
2188	16	0.47539	20.1565	0.02184	0.0952	0.0289	–
2192	16	0.61924	20.2626	0.01013	0.1519	0.0292	0.1875
2193	13	0.45168	20.0398	0.04102	0.0731	0.0243	–
2195	13	0.86845	20.3751	0.01547	0.2215	0.0250	–
2196	16	0.52552	19.8127	0.00573	0.1072	0.0289	0.1339
2197	13	0.46110	18.2195	0.00777	0.0461	0.0244	0.0308
2198	13	0.90143	20.8216	0.00694	0.2562	0.0306	0.0798
2199	13	0.61377	19.3977	0.01070	0.1067	0.0243	0.0299
2199	16	0.56860	19.0855	0.01070	0.1089	0.0289	0.0299
2200	13	0.70059	20.0345	0.06997	0.1573	0.0245	–
2205	13	0.52694	19.8040	0.05611	0.0909	0.0243	0.0876
2215	13	0.83647	20.6864	0.02702	0.2339	0.0250	–
2217	16	0.67713	19.6565	0.05380	0.1575	0.0292	–
2219	13	0.97399	20.2862	0.02349	0.2262	0.0250	0.2256
2221	13	0.75515	20.2772	0.01248	0.1866	0.0245	0.1019
2228	13	0.62752	19.6874	0.04829	0.1200	0.0243	0.1013
2229	13	0.75386	20.3148	0.02118	0.1882	0.0245	–
2238	13	0.67963	20.1779	0.01715	0.1562	0.0245	–
2240	13	0.74809	20.7689	0.04179	0.2110	0.0250	0.1380
2241	16	0.51370	19.5172	0.03004	0.0982	0.0289	–
2243	13	0.63968	20.1087	0.02133	0.1390	0.0243	–
2244	13	0.57937	19.8780	0.02313	0.1100	0.0243	0.0968
2246	13	1.03852	20.8495	0.02377	0.2602	0.0306	0.2250
2251	16	0.72084	20.1940	0.04985	0.1873	0.0292	–
2252	13	0.79111	20.6880	0.01414	0.2210	0.0250	0.1147
2254	13	0.70617	20.2366	0.05330	0.1682	0.0245	0.1780
2255	13	0.68960	19.6058	0.02622	0.1366	0.0243	0.0806
2256	13	0.53847	19.2448	0.04982	0.0811	0.0243	0.0581
2257	13	0.62971	19.4428	0.04085	0.1128	0.0243	0.1054
2261	16	0.56827	20.2002	0.04453	0.1306	0.0289	0.2240
2262	13	0.91988	20.5466	0.05507	0.2399	0.0250	–
2262	16	0.89261	20.1596	0.05507	0.2251	0.0287	–
2263	13	0.60642	20.2462	0.04994	0.1319	0.0243	0.1051
2266	16	0.71157	20.3038	0.04183	0.1875	0.0292	0.1671
2267	13	0.86400	20.5473	0.02297	0.2313	0.0250	–
2268	13	0.73229	20.4696	0.03480	0.1888	0.0245	–
2269	13	1.16571	21.0218	0.03386	0.2415	0.0250	–
2270	16	0.78089	20.7234	0.03440	0.2240	0.0287	0.2377
2272	13	0.62073	20.2334	0.05035	0.1368	0.0243	0.1329
2273	13	1.01048	20.7064	0.03138	0.2527	0.0306	–
2274	13	1.02068	19.8009	0.03767	0.1966	0.0245	–
2275	13	0.52463	19.7815	0.04312	0.0896	0.0243	0.1029
2278	13	0.73838	20.6429	0.03667	0.2003	0.0250	–
2279	13	0.65266	19.8254	0.07495	0.1330	0.0243	–
2285	16	0.43095	19.1077	0.02784	0.0675	0.0289	–
2286	13	0.53359	19.6268	0.04234	0.0886	0.0243	–
2288	13	0.48939	19.3434	0.06314	0.0700	0.0243	–
2289	13	0.88125	20.6091	0.04916	0.2385	0.0250	0.2276
2291	13	0.81070	19.9702	0.05685	0.1864	0.0245	0.1810
2292	13	0.64847	18.9927	0.04306	0.1047	0.0243	0.1190
2297	13	0.50607	20.0410	0.03817	0.0901	0.0243	–
2297	13	0.74219	20.3259	0.04254	0.1849	0.0245	–
2298	13	0.80612	20.0823	0.05148	0.1911	0.0245	–
2299	13	0.55541	20.0556	0.03908	0.1515	0.0245	–
2299	13	0.69345	19.9546	0.05563	0.1071	0.0243	–

Continued...

Table B.3 - Abell Cluster Photometric Redshifts, Continued

Abell	CCD	$(g-r)_{med}$	g_{mean}	$E(B-V)$	z_{phot}	Error	z_{spec}
2300	13	0.64421	19.5768	0.07032	0.1216	0.0243	–
2310	13	0.63194	19.3633	0.07897	0.1111	0.0243	–
2311	13	0.52620	18.9747	0.06498	0.0722	0.0243	0.0890
2314	13	0.86960	20.0638	0.07862	0.2035	0.0250	–
2315	13	0.52220	19.0739	0.08541	0.0732	0.0243	0.0894
2316	13	0.99357	20.4234	0.09037	0.2346	0.0250	0.2147
2317	13	0.89940	20.4905	0.06625	0.2337	0.0250	0.2110
2318	13	0.60557	20.1790	0.06819	0.1291	0.0243	0.1405
2319	13	0.54066	19.3494	0.11363	0.0841	0.0243	0.0557
2320	13	0.62367	19.0166	0.17918	0.0988	0.0243	0.1710
2321	13	0.66613	20.2440	0.16135	0.1541	0.0245	–
2322	13	0.69446	19.7792	0.25078	0.1447	0.0243	–
2323	13	0.66152	19.7576	0.09939	0.1334	0.0243	–
2326	13	0.65102	19.4072	0.48845	0.1181	0.0243	–
2327	13	0.61473	19.8558	0.08081	0.1213	0.0243	–
2349	16	0.38086	19.0358	0.04782	0.0540	0.0289	–
2349	16	0.58182	20.0422	0.04858	0.1324	0.0289	–
2353	13	0.52112	19.2298	0.05477	0.0761	0.0243	0.1210
2355	13	1.04350	20.6513	0.06633	0.2458	0.0250	0.1244
2355	16	0.59421	20.4228	0.06633	0.1459	0.0289	0.1244
2356	16	0.54219	19.3538	0.06931	0.1050	0.0289	0.1161
2359	13	0.73060	20.3196	0.08706	0.1807	0.0245	–
2373	13	0.80311	20.8274	0.05509	0.2335	0.0250	–
2379	13	0.68978	19.8457	0.11891	0.1459	0.0243	–
2381	13	0.83569	20.2282	0.05782	0.2061	0.0250	0.0726
2386	13	0.56365	19.9434	0.07340	0.1067	0.0243	–
2386	13	0.73147	20.4833	0.06705	0.1893	0.0245	–
2387	13	0.80581	19.0725	0.14370	0.1449	0.0243	0.1450
2388	13	0.46280	17.7167	0.05006	0.0405	0.0244	0.0615
2390	16	0.74397	20.4617	0.11311	0.2034	0.0287	0.2280
2390	16	0.81282	20.4291	0.11562	0.2216	0.0287	0.2280
2392	16	0.83911	20.1990	0.07231	0.2189	0.0287	–
2395	13	0.72047	20.0539	0.04946	0.1647	0.0245	0.1508
2396	13	0.56837	19.7775	0.07442	0.1035	0.0243	0.1946
2397	13	0.81644	20.4615	0.05322	0.2149	0.0250	0.2240
2397	16	0.91703	20.0800	0.05322	0.2240	0.0287	0.2240
2406	16	0.79625	20.4579	0.06294	0.2186	0.0287	–
2407	13	0.62568	19.5082	0.05697	0.1136	0.0243	–
2407	13	0.65888	19.8073	0.05697	0.1344	0.0243	–
2408	13	0.72784	20.4625	0.05279	0.1869	0.0245	–
2409	13	0.67936	20.2982	0.10835	0.1613	0.0245	0.1479
2413	13	0.64357	20.3016	0.08163	0.1480	0.0243	–
2414	13	0.54429	19.6266	0.05859	0.1143	0.0243	–
2414	13	0.66671	19.1478	0.05859	0.0918	0.0243	–
2419	13	0.65240	20.2949	0.05203	0.1511	0.0245	0.0456
2422	16	0.98668	20.5918	0.12078	0.2430	0.0287	–
2423	16	0.53334	19.5092	0.08588	0.1046	0.0289	–
2424	13	0.74243	20.2355	0.06700	0.1804	0.0245	0.1510
2425	13	0.81797	20.7676	0.09094	0.2341	0.0250	–
2425	16	1.13616	20.2419	0.09307	0.2011	0.0287	–
2429	16	0.78587	20.3804	0.06104	0.2131	0.0287	–
2429	16	1.10455	20.6698	0.06104	0.2250	0.0287	–
2431	16	0.63601	20.2324	0.06324	0.1576	0.0292	–
2431	16	0.70041	20.0241	0.06324	0.1754	0.0292	–
2432	13	0.68740	20.2438	0.09827	0.1619	0.0245	–
2435	16	0.73958	20.1356	0.06413	0.1915	0.0292	–
2437	13	0.69214	20.2262	0.08662	0.1628	0.0245	–
2439	16	0.70738	20.2025	0.06611	0.1830	0.0292	–
2440	16	0.57093	19.7181	0.08757	0.1216	0.0289	0.0906
2443	13	0.64240	19.8860	0.06173	0.1317	0.0243	0.1080
2445	13	0.64582	20.3701	0.05318	0.1517	0.0245	–
2447	13	0.44196	19.2650	0.09851	0.0568	0.0243	–
2447	13	0.62960	20.3519	0.09851	0.1447	0.0243	–
2449	13	0.49500	19.6080	0.05987	0.1072	0.0243	–
2449	13	0.58114	19.7637	0.05987	0.0768	0.0243	–
2454	13	0.65046	20.2845	0.13473	0.1500	0.0243	0.1590
2454	16	0.61853	19.8051	0.13443	0.1407	0.0289	0.1590
2454	16	0.65777	19.9817	0.13443	0.1592	0.0292	0.1590
2457	16	0.50568	19.0917	0.08380	0.0891	0.0289	0.0597
2458	16	0.55545	19.8929	0.04334	0.1195	0.0289	–
2471	13	0.66070	20.0663	0.10078	0.1449	0.0243	0.1078
2471	16	0.78578	19.8804	0.10078	0.1964	0.0292	0.1078
2472	13	1.08891	21.0285	0.04027	0.2643	0.0306	–
2475	13	0.82174	20.5048	0.11083	0.2188	0.0250	–
2483	16	0.52421	19.9429	0.06316	0.1090	0.0289	–
2491	16	0.69385	20.2091	0.06395	0.1784	0.0292	–
2494	13	0.68420	19.4728	0.11406	0.1301	0.0243	–
2495	13	0.52068	19.2362	0.07727	0.1030	0.0243	0.0775
2495	13	0.57994	19.6307	0.07727	0.0761	0.0243	0.0775
2503	13	0.44194	19.5523	0.06396	0.0615	0.0243	0.0827
2505	13	0.44775	20.4853	0.06581	0.0813	0.0243	–
2506	13	0.65002	20.5516	0.05708	0.1612	0.0245	0.0289
2507	13	0.76623	20.1576	0.09621	0.1840	0.0245	0.1960
2512	13	0.58753	20.1112	0.08314	0.1202	0.0243	0.1603
2513	13	0.74724	20.5557	0.09173	0.1987	0.0245	0.0250
2515	13	0.84587	20.0317	0.07771	0.1974	0.0245	–
2516	13	0.64835	20.2746	0.10313	0.1488	0.0243	0.0793

Continued...

Table B.3 - Abell Cluster Photometric Redshifts, Continued

Abell	CCD	$(g-r)_{med}$	g_{mean}	$E(B-V)$	z_{phot}	Error	z_{spec}
2516	16	0.64359	20.3556	0.10313	0.1638	0.0292	0.0793
2517	13	0.76274	19.5212	0.11367	0.1537	0.0245	–
2522	13	0.66416	20.4527	0.09737	0.1624	0.0245	0.1562
2530	13	0.56802	19.7513	0.11501	0.1026	0.0243	–
2532	13	0.69960	20.4157	0.08593	0.1742	0.0245	–
2535	13	0.66319	19.5869	0.14319	0.1278	0.0243	–
2545	13	0.76899	19.8956	0.07205	0.1720	0.0245	–
2551	13	0.50094	20.1173	0.07791	0.0903	0.0243	–
2552	16	0.68599	20.2365	0.05088	0.1764	0.0292	0.1330
2562	13	0.80266	19.7829	0.06523	0.2218	0.0250	–
2562	13	0.90301	20.2926	0.06446	0.1753	0.0245	–
2570	13	0.53636	18.9403	0.04200	0.0741	0.0243	–
2571	16	0.54843	19.5510	0.04538	0.1105	0.0289	0.1084
2574	16	0.53587	20.3121	0.05075	0.1203	0.0289	–
2582	16	0.60813	19.8203	0.04932	0.1373	0.0289	–
2584	13	0.58608	20.3071	0.11019	0.1263	0.0243	0.1200
2590	16	0.68153	20.2835	0.03588	0.1762	0.0292	0.0790
2594	13	0.64749	20.4907	0.09116	0.1575	0.0245	–
2602	13	0.66981	20.0542	0.07331	0.1476	0.0243	–
2607	13	0.59903	19.9719	0.05932	0.1197	0.0243	0.1201
2610	13	0.69146	20.2495	0.04707	0.1636	0.0245	–
2616	13	0.67396	20.1020	0.06841	0.1510	0.0245	0.1832
2616	16	0.70984	19.9135	0.06841	0.1753	0.0292	0.1832
2617	16	0.68110	20.3109	0.06647	0.1768	0.0292	0.1630
2620	13	1.14380	20.9492	0.07324	0.2439	0.0250	0.1911
2621	13	0.97878	20.6458	0.06112	0.2496	0.0250	–
2622	13	0.52331	19.0075	0.05718	0.0722	0.0243	0.0621
2623	13	0.84819	20.3273	0.06631	0.2146	0.0250	0.1784
2624	13	0.89365	20.6794	0.07054	0.2452	0.0250	–
2627	13	0.58119	20.1524	0.07086	0.1193	0.0243	0.1255
2631	13	1.09759	20.7569	0.03792	0.2434	0.0250	0.2730
2631	16	0.98491	20.6245	0.03859	0.2445	0.0287	0.2730
2633	16	0.60596	19.7828	0.05176	0.1356	0.0289	–
2639	16	0.74011	19.8492	0.05066	0.1829	0.0292	–
2649	13	0.50078	19.5811	0.07831	0.0779	0.0243	–
2650	13	0.73413	19.3363	0.06955	0.1389	0.0243	–
2657	13	0.46187	18.4020	0.12911	0.0486	0.0244	0.0402
2666	13	0.39746	18.4351	0.03879	0.0374	0.0244	0.0272
2668	16	0.46489	19.5665	0.03653	0.0831	0.0289	–
2668	16	0.57262	19.6900	0.03718	0.1217	0.0289	–
2671	13	0.67403	20.5999	0.05555	0.1731	0.0245	0.1799
2672	13	0.66410	19.2755	0.04222	0.1176	0.0243	0.2412
2675	16	0.58614	19.5086	0.07751	0.1228	0.0289	0.0713
2695	16	0.53040	19.3407	0.03076	0.1008	0.0289	–
2696	13	0.56125	19.3736	0.03027	0.0906	0.0243	0.0844
2698	16	0.64731	19.5626	0.02219	0.1451	0.0289	0.0979
2706	16	0.57138	19.4338	0.08982	0.1163	0.0289	–
2711	13	0.74385	20.1832	0.04961	0.1783	0.0245	–

Appendix C

Imaging of Candidate Galaxy Clusters

This apppendix contains color images of cluster candidates generated from Palomar 60″ imaging. The Gunn *gri* filters have been mapped to RGB output; red galaxies therefore appear yellow. Additionally, the corresponding $g - r$ *vs.* r color-magnitude diagram is plotted for each candidate.

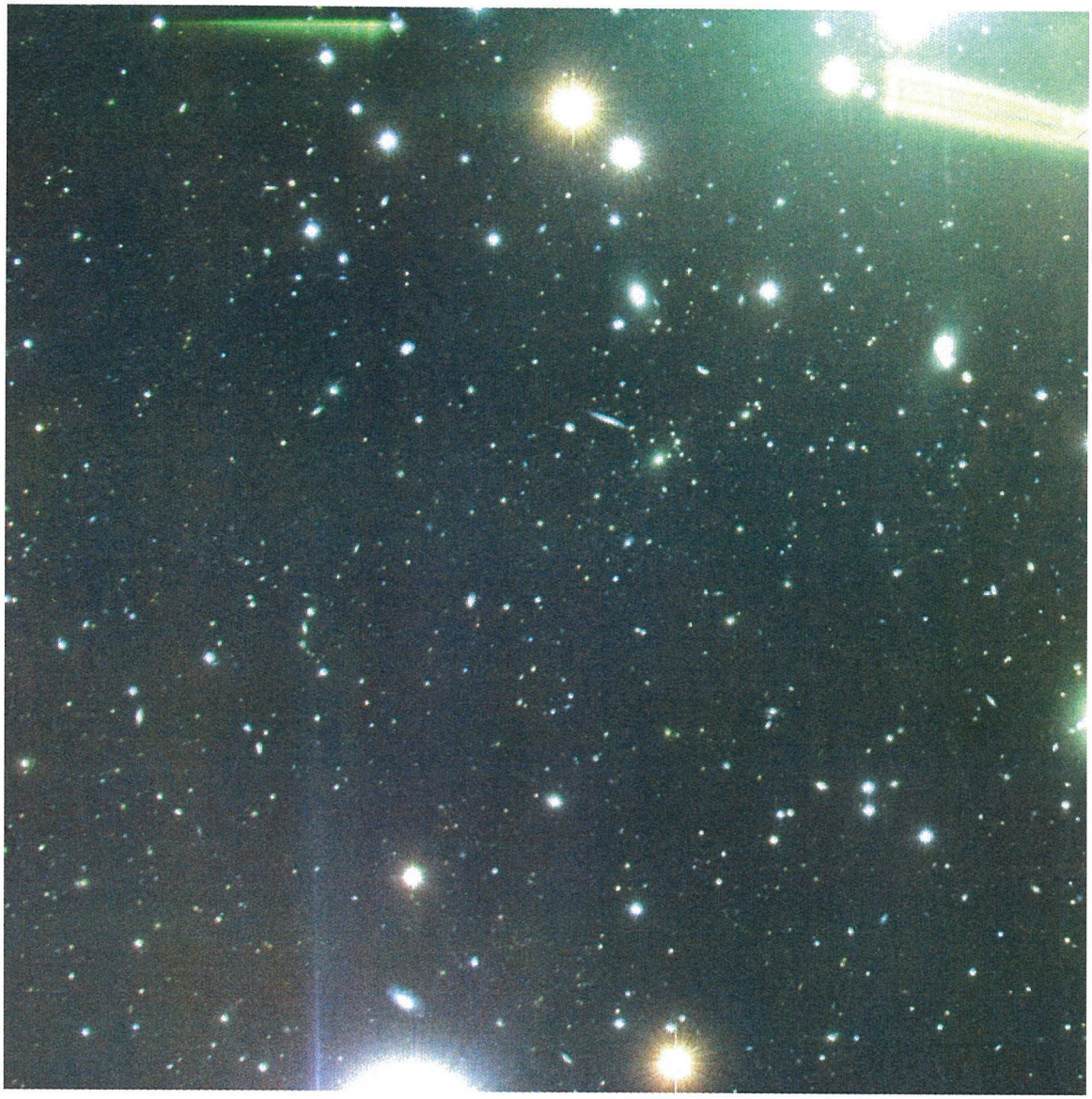

Figure C.1: Candidate NSC0104+2627.

Figure C.2: Candidate NSC0103+2703.

Figure C.3: Candidate NSC0118+2248.

Figure C.4: Candidate NSC0105+2438.

Figure C.5: Candidate NSC0112+2427.

Figure C.6: Candidate NSC0104+2230.

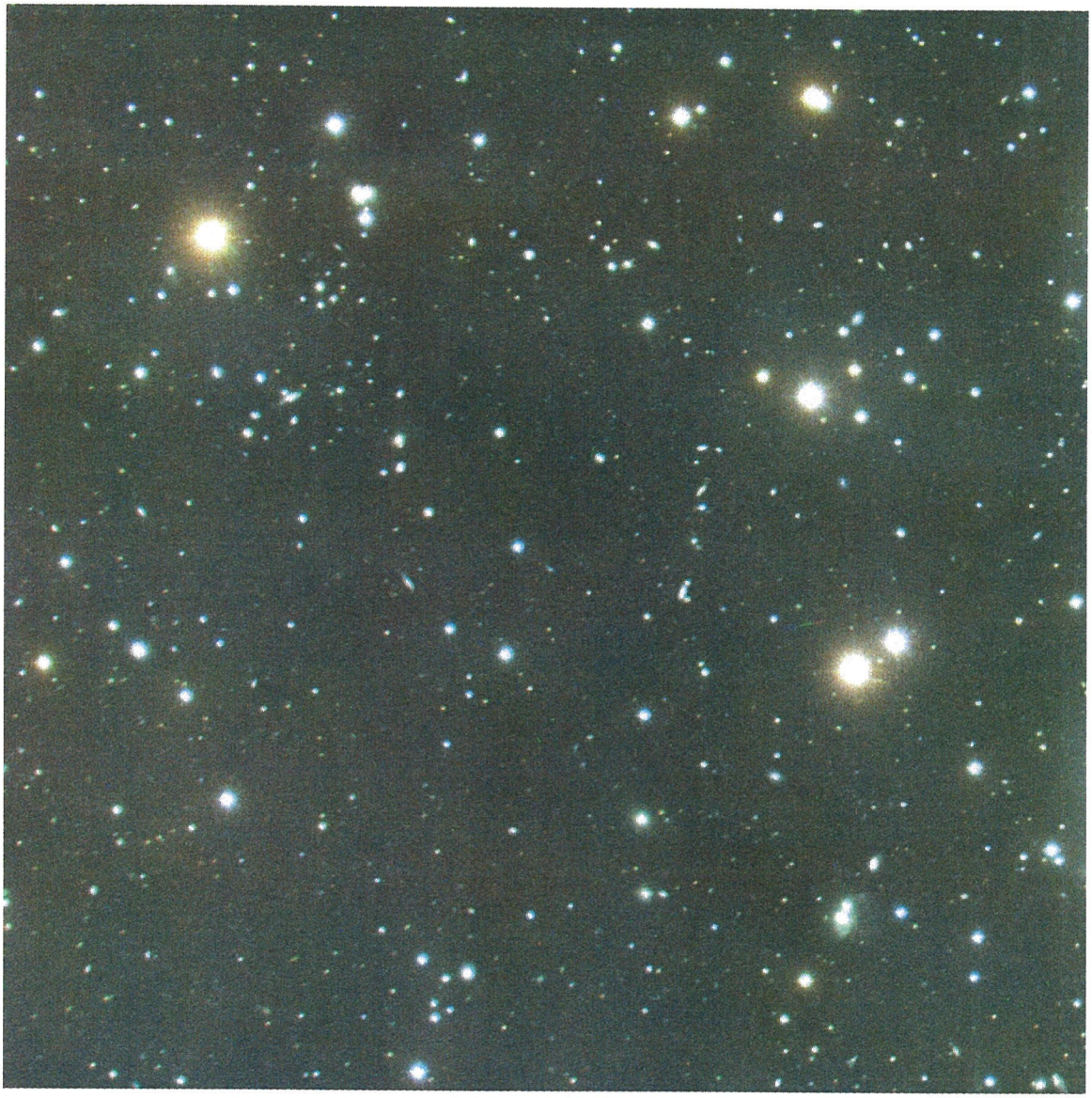

Figure C.7: Candidate NSC0120+2452.

Figure C.8: Candidate NSC0104+2719.

Figure C.9: Candidate NSC0108+2653.

Figure C.10: Candidate NSC0108+2438.

Figure C.11: Candidate NSC0106+2459.

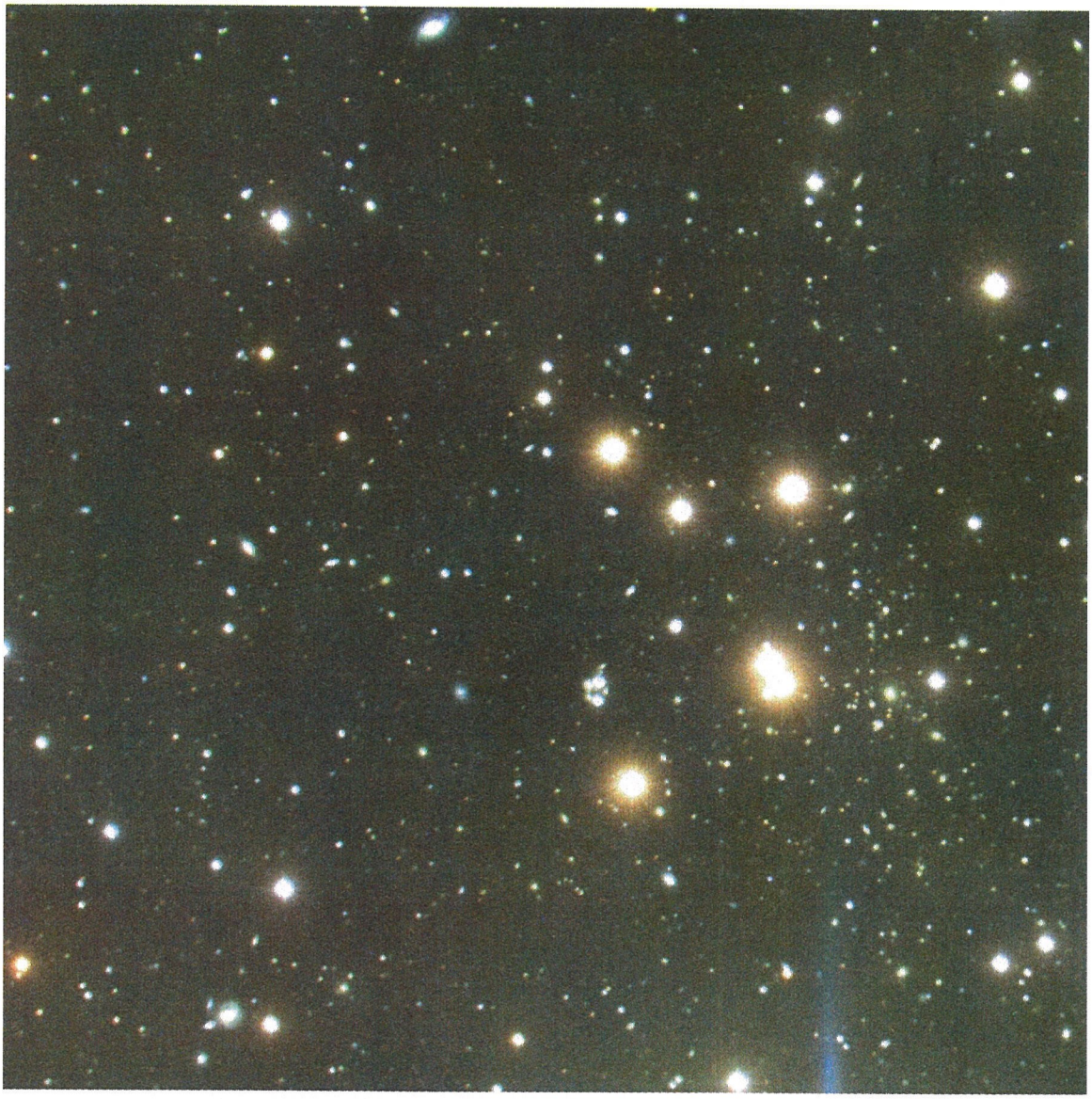

Figure C.12: Candidate NSC0102+2503.

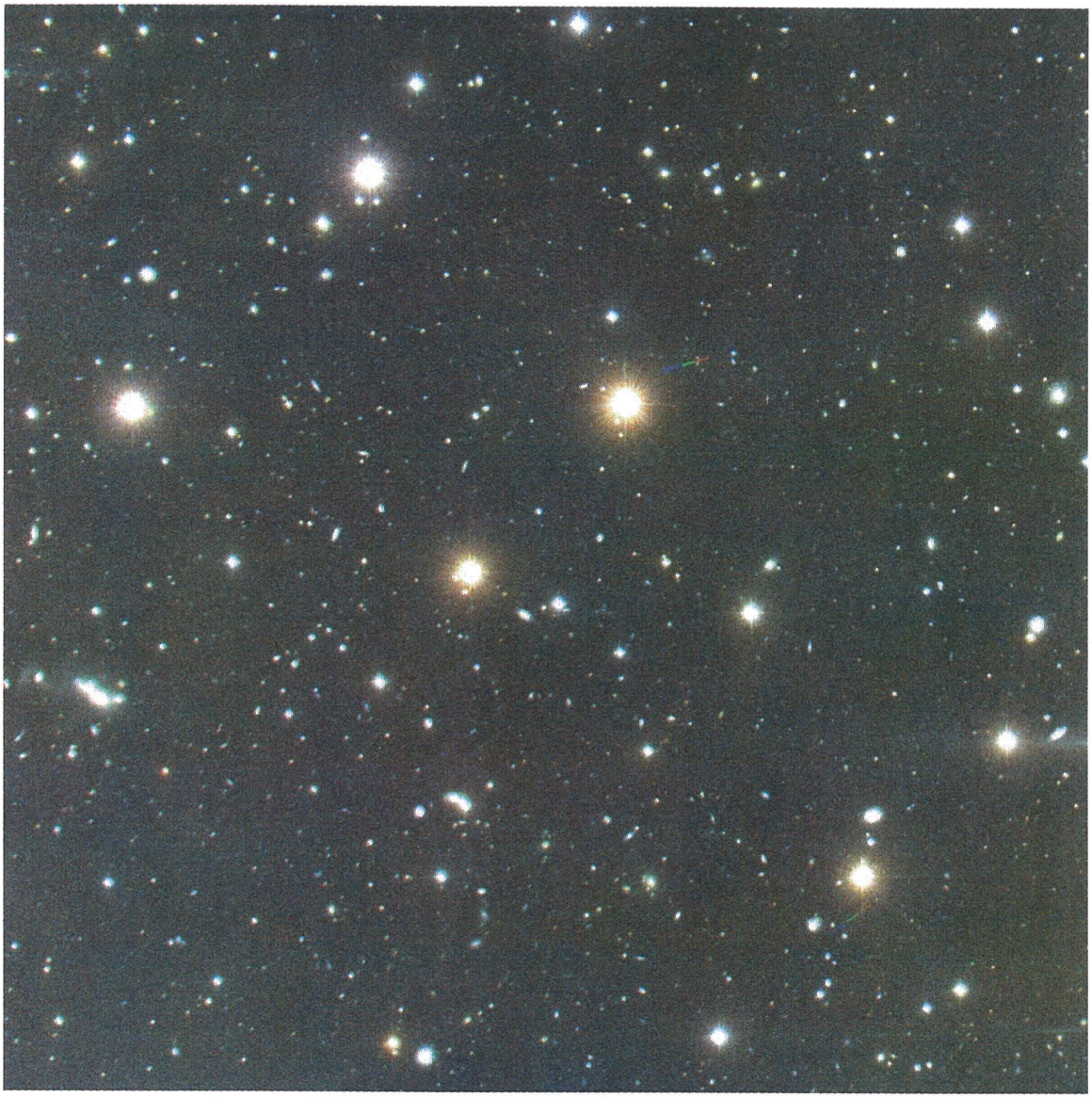

Figure C.13: Candidate NSC0110+2507.

Figure C.14: Candidate NSC0113+2513.

Figure C.15: Candidate NSC0112+2747.